

COMPUTATIONAL INVESTIGATION OF TURBULENT,  
NON-NEWTONIAN FLOW IN HEART VALVE CONDUITS

by

GEOFFREY DOUGLAS TANSLEY B.Sc., AMIMechE, MBES

Thesis submitted to the Council for National  
Academic Awards in partial fulfilment of the  
requirements for the degree of Doctor of  
Philosophy

Research conducted at the Department of  
Mechanical Engineering, Trent Polytechnic,  
Nottingham in collaboration with Killingbeck  
Hospital, Leeds.

February 1988

ProQuest Number: 10290060

All rights reserved

INFORMATION TO ALL USERS

The quality of this reproduction is dependent upon the quality of the copy submitted.

In the unlikely event that the author did not send a complete manuscript and there are missing pages, these will be noted. Also, if material had to be removed, a note will indicate the deletion.



ProQuest 10290060

Published by ProQuest LLC (2017). Copyright of the Dissertation is held by the Author.

All rights reserved.

This work is protected against unauthorized copying under Title 17, United States Code  
Microform Edition © ProQuest LLC.

ProQuest LLC.  
789 East Eisenhower Parkway  
P.O. Box 1346  
Ann Arbor, MI 48106 – 1346

COMPUTATIONAL INVESTIGATION OF TURBULENT,  
NON-NEWTONIAN FLOW IN HEART VALVE CONDUITS

by

Geoffrey Douglas Tansley

ABSTRACT

Heart valve conduit prosthesis design has, to date, simply incorporated an existing aortic or mitral valve prosthesis into a length of cylindrical graft tubing. However, as these valves are developed to control flow between the large chambers of the heart, their use in conduits ignores the potential benefits that might be afforded by a "purpose-built" conduit valve.

The purpose of this thesis is to describe the design and assessment of haemodynamics of such a valve, aided via the application of computational fluid Mechanics (CFM).

First a computational model of blood flow was developed which was based on a  $k - \epsilon$  model of turbulence coupled with a constitutive equation to describe the non-Newtonian flow behaviour of blood. This was applied to a ball valve conduit with a diverging/converging form, and appraisal was made of pressure drop, flow fields, occluder stability and shear components. Behavioural differences between blood analogue solution and blood were limited, thereby endorsing the use of analogues for in-vitro experiments.

The valve finally developed exhibited excellent pressure/flow characteristics, in particular a pressure drop less than half that of an ideal annulus-mounted valve. Furthermore the computational technique allows it to be sized to minimise the thromboembolic and haemolytic potentials (based on predicted shear rate and shear stresses) for any individual patient, rather than simply to fit an annulus.

The major conclusions are:

- i) the additional flow parameter information, especially thromboembolic and haemolytic potentials, gained from applying CFM at the design stage of valve development is invaluable
- ii) employment of a realistic constitutive function for non-Newtonian modelling of blood flow provides the standard against which other flow models should be compared
- iii) greatly improved flow characteristics may be realised with purpose built valved conduits.

To him who is able to keep you from falling and to present you before his glorious presence without fault and with great joy - to the only God our saviour be glory, majesty, power and authority, through Jesus Christ our Lord, before all ages, now and for evermore!

Jude 17: 24-25

## ACKNOWLEDGEMENTS

Firstly, I would like to express my sincere gratitude to Dr. C.R. Gentle, my supervisor and Director of Studies, he has provided a great deal of guidance, direction for my ideas, encouragement during the times I felt no progress was being made and understanding (of my all too frequent crises). I much appreciate the effort and time he has devoted to me over the past three years, enabling me to develop and eventually present my work in its present form.

Special thanks are also due to Professor B.L. Button, Head of Department of Mechanical Engineering and my second supervisor, for his guidance and insight into the processes of researching a Ph.D. I am grateful also for the support Professor Button has given in easing the procurement of laboratory space, equipment, technical support and finances.

I am most grateful to to Mr Alan Crisp, Senior Technician, and the technician staff for first rate technical support, most specifically, Mr Bob Oreszczyn for assistance in experimentation, Messers Keith Adams and Tony Maides for the manufacture of test equipment, Mr Ken Elmer and Mr Keith Rickers for the manufacture of electronic monitoring equipment and Mr John Cooper for photographic processing.

My thanks also go to Jim Cortlett, Engineering Librarian, Tricia Deane, Senior Library Assistant and all the Library staff for their help in locating the many obscure works I required, and for their excellent support over the years.

I am grateful to Mr Alban Davies, Cardiac Surgeon, and Mr Duncan Walker, Director of Cardiovascular Research, Killingbeck Hospital, Leeds for their collaboration and assistance in allowing me to attend heart valve replacement operations.

To my colleagues:

Ms Shirley Ashforth, Mr Brian Dobbins, Mr Richard Edwards, Mr Shabir Kapasi, Dr Mehran Pasdari, Dr Chris Saluja, Mr Faramarz Shemirani, Dr Ali Uzel, Mr Dave York, and Mr Sharokh Zangeneh. I extend my thanks to them all, as in day-to-day contact, they individually and corporately made an excellent sounding board for ideas, provided a wealth of information and hours of entertainment!. Special thanks go to Simon Leefe, a former colleague who shared many academic interests and with whom I published two papers: to Richard , with whom I co-authored two papers: and to Shabir for his help with hardware and software design.

I would like to thank Mrs Trish Wise for the time, skill and patience she has applied to the word processing and typing of this thesis.

Thanks must go to my family and friends who have supported me, both emotionally and financially, especially Maurice, my father and Doreen, my mother. I thank them especially, because without their support, love and encouragement this thesis would never have been written.

Many thanks are given to my wife, Ela; her love has never failed through all the hours of loneliness. Ela's encouragement has been considerable as have her efforts in looking after my welfare and in the help she has given in the preparation of this work.

I also acknowledge, with thanks the financial support of the Science and Engineering Research Council who funded this project.

This work is dedicated to Christ Jesus, but for whose grace this work would not have been completed.

## AIMS

The objectives of this thesis were several:

- i) to assess the usefulness of Computational Fluid Mechanics to the evaluation of prosthetic heart valve flow. To this end, a commercially available computer code was employed allowing a more rapid commencement of modelling than would be possible if 'in-house' coding had been written
- ii) to establish critical blood flow characteristics such as shear rates and shear stresses for use in the analysis of prosthetic valve thromboembolic and haemolytic potentials
- iii) the development of computational grid geometry closely representing geometries into which a conduit might be implanted
- iv) the inclusion of a constitutive equation, describing blood's shear/viscosity relationship, into CFM solution routines in an attempt to model conduit flow in a situation more closely allied to that in-vivo
- v) final haemodynamic design of a ball occluded heart valve conduit
- vi) analysis of final conduit design to assess possible clinical acceptability.

## TABLE OF CONTENTS

<u>Section</u>	<u>Description</u>	<u>Page</u>
	<u>Abstract</u>	i
	<u>Dedication</u>	ii
	<u>Acknowledgements</u>	iii
	<u>Aims</u>	vi
	<u>Table of Contents</u>	vii
	<u>List of Figures</u>	xi
	<u>Nomenclature</u>	xix
	<u>Valve Geometry Nomenclature</u>	xxv
1.0	<u>Chapter One: Introduction</u>	
1.1	General Introduction	1
1.2	The History of Heart Valve flow Visualisation	8
1.3	In-vitro Measurement Techniques	9
1.4	Haemodynamic Quantities	20
1.5	Computational Fluid Dynamics	24
1.6	Prototype Nomenclature	28
2.0	<u>Chapter Two: Experimental Investigation</u>	
2.1	Introduction	32
2.2	Static Pressure Measurement	32
2.3	Streak Photography	37

3.0	<u>Chapter Three: The Rheology of Blood and its Mathematical Description</u>	
3.1	Introduction	49
3.2	Whole Blood	49
3.3	Plasma Rheology	54
3.4	Yield Stress	55
3.5	Experimentally Derived Blood Viscosity Data/Relationships	57
3.6	Blood Models	60
4.0	<u>Chapter Four: Computational Modelling of Blood and Analogue Flow</u>	
4.1	Computational Fluid Mechanics	76
4.2	A Blood Viscosity Model for CFM	80
4.3	The Development of a Computational Model	82
4.4	Laminar Flow	83
4.5	Blood Flow	84
4.6	Turbulence Modelling	85
4.7	Geometrical Considerations	88
4.8	Regime Definition	92
5.0	<u>Chapter Five: Initial Development of a Prosthetic Heart Valve Conduit</u>	
5.1	Design Philosophy	95
5.2	Conduit Performance: First Prototype (SISO)	102
5.3	Conduit Performance: Second Prototype (SICO)	106
6.0	<u>Chapter Six: Results- an Analysis of PHOENICS</u>	
6.1	Introduction	116
6.2	Grid Dependency	119

6.3	Momentum in Orthogonally Modelled Grids - Simple Pipe	140
6.4	Momentum in Orthogonally Modelled Grids - Valve Geometry	144
6.5	Momentum Predictions in Curvilinear Grids	144
6.6	Convergence, Convection/Diffusion and Continuity	153
6.7	Pressure Predictions	158
6.8	Shear Stress and Shear Rate	166
6.9	Prediction of Occluder Instability	168
6.10	Blood Model	173
7.0	<u>Chapter Seven: Conduit Re-design</u>	
7.1	Introduction	175
7.2	Best Valve Profile	175
7.3	Finalisation of Design for Blood Flow	202
7.4	Assessment of Final Design	208
7.5	Recommendations as to Application	230
8.0	<u>Chapter Eight: Discussion</u>	
8.1	Functionality of CFM	231
8.2	Effectiveness of the Blood Model	233
8.3	A Further Example of CFM Applied to Heart Valves - Backflow	236
8.4	Performance of the Final Conduit Design	237
8.5	Confidence in Computational Predictions	241
8.6	Continuation of CFM Study of Heart Valves	242
8.7	Further Work on the Ceramic Conduit Designs	243
9.0	<u>Chapter Nine: Conclusions</u>	247
11.0	<u>References</u>	253

A.0	<u>Appendices</u>	
A.1	Appendix one : Derivation of velocity profile for non-Newtonian pipe flow	A1.1
A.2	Appendix Two : Geometry generation coding for the LRR series of valve prototypes	A2.1
A.3	Appendix Three : PHOENICS 'Q1' input file for blood or analogue solution flow in conduits	A3.1
A.4	Appendix Four : Statistical analysis of radial shear stress variation for turbulent pipe flow	A4.1
A.5	Appendix five: Gorlin- Gorlin analysis applied to finalised LRRSICO conduit	A5.1
A.6	Appendix six: Changes to Fortran 'GROUND' and GREX1 coding to introduce blood flow model etc.	A6.1
A.7	Published papers and Presentations	A7.1

## LIST OF FIGURES

<u>Figure</u>	<u>Description</u>	<u>Page</u>
<u>Chapter One</u>		
1.1	Starr - Edwards ball valve in mitral position	3
1.2	Valved conduit in apicoaortic shunt application	4
1.3	Schematic of an LDA system	12
1.4	LDA Control volume interference fringe pattern	13
1.5	Doppler burst signals	14
1.6	Finite element and finite difference grids	29
1.7	Valve prototype geometry designations	30
<u>Chapter Two</u>		
2.1	Experimental valve sections with single pressure tappings on inlet and outlet sections	34
2.2	Pressure measurement equipment and experimental SICO valve with multi pressure tappings	35
2.3	Schematic of experimental rig	36
2.4	Photograph of experimental rig	38
2.5	Schema of optics for laser illumination of a plane; for flow visualisation	39
2.6	Photograph of optics for illumination of a plane; for flow visualisation	40
2.7	Diagram of SICO test section with integral correcting optics	44
2.8	Photograph of SICO test section with integral correcting optics	45
2.9	Streamlines produced by flow visualisation of SISO valve	47
2.10	Streamlines produced by flow visualisation of SICO valve	48

### Chapter Three

3.1	Apparent viscosity/shear rate curve for blood	50
3.2	Velocity profile of fully developed laminar flow of blood in large bore tube ( $>0.5\text{mm}$ )	51
3.3	The usefulness of Chmiel and Walitza's constitutive equation in shear rates $0.1 - 10\text{s}^{-1}$	69
3.4	The usefulness of Chmiel and Walitza's constitutive equation in shear rates $0.01 - 100\text{s}^{-1}$	70
3.5	Comparison of constitutive equations for blood of 45 haematocrit: $x$ versus $\ln(d)$	73
3.6	Comparison of constitutive equations for blood of 45 haematocrit: $\sigma_a$ versus $\ln(d)$	74

### Chapter Four

4.1	Grid axis definition	89
-----	----------------------	----

### Chapter Five

5.1	Commercial tilting disk valved conduit in part section	96
5.2	Jet issue from a tilting disk valve mounted into a conduit	98
5.3	SISO valve: five sections of constant flow area	101
5.4	Pressure/flow characteristics of several conduits in water flow	104
5.5	Pressure/flow characteristics of several conduits in blood analogue solution flow	105
5.6	Gorlin - Gorlin analysis of several valved conduits in water flow	107
5.7	Gorlin - Gorlin analysis of several valved conduits in blood analogue solution flow	108
5.8	Pressure/flow characteristics of several valved conduits in water flow: $E_u$ versus $Re_d$	109
5.9	Pressure/flow characteristics of several valved conduits in analogue solution flow: $E_u$ versus $Re_d$	110
5.10	Mathematical description of SICO valve outflow tract	112

5.11	Comparison of pressure/flow characteristics of SISO and SICO valves: experimentally derived	114
 <u>Chapter Six</u>		
6.1	Orthogonal grid for SISO valve	117
6.2	Orthogonal grid for SICO valve	118
6.3	Grid independence: pressure gradient versus central flow region grid density	120
6.4	Grid independence: centreline pressure versus central flow region grid density	122
6.5	Grid independence: centreline shear stress versus central flow region grid density	123
6.6	Grid independence: wall shear rate versus central flow region grid density	124
6.7	Grid independence: wall shear stress versus central flow region grid density	125
6.8	Grid independence: streamwise occluder force versus wall-cell centre distance	126
6.9	Grid independence: pressure gradient versus wall-cell centre distance	127
6.10	Grid independence: dimensionless pressure gradient versus $y^+$ for different $Re_a$	128
6.11	Solution dependence on $y^+$ at wall-cell centre: $y^+$ at conduit wall for water flow rate of 7 l/min	129
6.12	Solution dependence on $y^+$ at wall-cell centre: $y^+$ at ball surface for water flow rate of 7 l/min	130
6.13	Solution dependence on $y^+$ at wall-cell centre: $y^+$ at conduit wall for water flow rate of 21 l/min	132
6.14	Solution dependence on $y^+$ at wall-cell centre: $y^+$ at ball surface for water flow rate of 21 l/min	133
6.15	$y^+$ at wall-cell centres on conduit surface, for varying water flow rates in SISO valve	134
6.16	$y^+$ at wall-cell centres on occluder surface, for varying water flow rates in SISO valve	135
6.17	$y^+$ at wall-cell centres on conduit surface, for varying water flow rates in SICO valve	136

6.18	$y^+$ at wall-cell centres on occluder surface, for varying water flow rates in SICO valve	137
6.19	$y^+$ at wall-cell centres on conduit wall, for varying blood flow rates in LRRSICO valve	138
6.20	$y^+$ at wall-cell centres on occluder surface, for varying water flow rates in LRRSICO valve	139
6.21	Comparison of analytical and numerical predictions of laminar, Newtonian pipe flow development length	141
6.22	Comparison of analytical and numerical predictions of maximum laminar pipe flow velocity	142
6.23	Numerically predicted turbulent pipe flow velocity profile	143
6.24	Streamline plots for water flow through SISO valve, modelled onto an orthogonal grid	145
6.25	Streamline plots for water flow through SICO valve, modelled onto an orthogonal grid	146
6.26	Velocity vector plot, $y^+$ at wall-cell centres = 3.18	147
6.27	Velocity vector plot, $y^+$ at wall-cell centres = 6.82	148
6.28	Velocity vector plot, $y^+$ at wall-cell centres = 9.1	149
6.29	Velocity vector plot, $y^+$ at wall-cell centres = 20.7	150
6.30	SISO valve modelled non-orthogonally	154
6.31	SICO valve modelled non-orthogonally	155
6.32	LRRSICO valve with 30mm blending radius modelled non-orthogonally	156
6.33	Comparison of analytical and numerical predictions of pressure gradients for water flow in a pipe	159
6.34	Comparison of analytical and numerical predictions of pressure gradients for water flow through SISO valve	160
6.35	Dependence of pressure gradient prediction on the location of pressure monitoring planes	162

6.36	Dependence of pressure gradient prediction across the SISO valve on the development length	163
6.37	Analysis of the effect of entry length on pressure gradients across the SISO valve	165
6.38	Comparison of analytical and numerical predictions of shear stress profile in laminar pipe flow	167
6.39	Comparison of numerical turbulent shear stress profile with the findings of Laufer (1954)	169
6.40	Grid independence: streamwise force on the ball versus central flow region cell density (for SISO)	171
6.41	Grid independence: streamwise force on the ball versus wall-cell centre position	172
6.42	Comparison of analytical and numerical predictions of non-Newtonian pipe flow velocity profile	174

#### Chapter Seven

7.1	SICO valve with blending radius added at outflow section	176
7.2	Full field shear stress contours in SISO valve	178
7.3	Full field shear stress contours in SICO valve	179
7.4	Full field shear stress contours in SICO valve with added 45mm blending radius	180
7.5	The effect of blending radius on pressure gradient	181
7.6	The effect of blending radius on streamwise force on the ball	182
7.7	CICO valve geometry	183
7.8	Comparison of shear stresses at conduit wall in SISO, SICO and LRRSICO (with 20mm rad) valves in water flow of rate 7l/min	184
7.9	Comparison of shear stresses at centreline in SISO, SICO and LRRSICO (with 20mm rad) valves in water flow of rate 7l/min	185
7.10	Comparison of shear stresses at conduit wall in SISO, SICO and LRRSICO (with 20mm rad) valves in water flow of rate 30l/min	186

7.11	Comparison of shear stresses at centreline in SISO, SICO and LRRSICO (with 20mm rad) valves in water flow of rate 30l/min	187
7.12	LRR series valve geometry designation	189
7.13	LRRSICO valve geometry with 30mm blending radius	190
7.14	Streamwise force at each cell on the ball surface as influenced by blending radius	191
7.15	Pressure at each cell on the ball surface as influenced by blending radius	192
7.16	Shear rate at each cell on the conduit wall as influenced by blending radius	193
7.17	Comparison of pressure/flow characteristics of SISO, SICO and LRRSICO (with 20mm rad) valves in water flow	195
7.18	Predicted occluder stability for SISO, SICO and LRRSICO (with 20mm rad) valves in varying water flow rates	196
7.19	Comparison of pressure at each cell on the ball surface: SISO, SICO and LRRSICO (with 20mm rad) valves in 30l/min water flow	197
7.20	Comparison of force at each cell on the ball surface: SISO, SICO and LRRSICO (with 20mm rad) valves in 7l/min water flow	198
7.21	Comparison of force at each cell on the ball surface: SISO, SICO and LRRSICO (with 20mm rad) valves in 30l/min water flow	199
7.22	$y^+$ at the conduit wall for varying blending radii	200
7.23	$y^+$ at the ball surface for varying blending radii	201
7.24	The effects of blending radius on occluder stability SISO, SICO and LRRSICO in varying flow media	203
7.25	The effects of blending radius on pressure drop in SISO, SICO and LRRSICO in varying flow media	204
7.26	The influence of blending radius on shear stress at flow impingement point in the LRRSICO valve	205
7.27	Centreline shear stress in LRRSICO valve for varying media and blending radii	206

7.28	Conduit wall shear stress in LRRSICO valve for varying media and blending radii	207
7.29	Centreline shear rate in LRRSICO valve for varying media and blending radii	209
7.30	Conduit wall shear rate in LRRSICO valve for varying media and blending radii	210
7.31	$y^+$ at the ball surface in LRRSICO valve for varying media and blending radii	211
7.32	$y^+$ at the conduit surface in LRRSICO valve for varying media and blending radii	212
7.33	Pressure/flow characteristics of LRRSICO valve with 30mm blending radius for varying conduit size	213
7.34	Pressure/flow characteristics of LRRSICO valve with 30mm blending radius in varying flow rates	214
7.35	Gorlin - Gorlin analysis of pressure/flow characteristics of LRRSICO valve with 30mm radius	216
7.36	Streamwise force on the ball of LRRSICO valve with 30mm blending radius for varying conduit sizes	219
7.37	Streamwise force on the ball of LRRSICO valve with 30mm blending radius in varying flow rates	220
7.38	$y^+$ at wall-cell centres at ball surface of LRRSICO valve for varying blood flow rates	221
7.39	Maximum shear stress versus size of LRRSICO valve with 30mm blending radius	222
7.40	Maximum shear stress in LRRSICO valve with 30mm blending radius for varying blood flow rate	223
7.41	Shear stress distribution along conduit wall of LRRSICO valve (30mm radius) with varying flow rate	224
7.42	Shear stress distribution along occluder surface of LRRSICO valve (30mm radius) with varying flow rate	225
7.43	Total shear stress contours in blood flow for LRRSICO valve with 30mm blending radius	226
7.44	Minimum shear rates contours for blood flow through LRRSICO valve with varying conduit diameter	228
7.45	Minimum shear rates contours for blood flow through LRRSICO valve with varying flow rate	229

## Chapter Eight

8.1	Geometry for computational modelling of backflow through Gentle's twin flap mitral valve	238
8.2	Prediction of laminarisation of backflow in a twin flap mitral valve	239
8.3	shear stress contours for backflow through a twin flap mitral valve	240
8.4	suggested method of assembly of LRRSICO conduit valve with single-piece body casting	264

## Appendices

A1.1	Element of fluid in fully developed laminar pipe flow	A1.2
------	---	------

## NOMENCLATURE

<u>Symbol</u>	<u>Meaning</u>	<u>Unit</u>
a	geometrical constant used in BFC grids Weltmann and Green's (1943) constant general constant	Pa
A	flow area through valved conduits stress constant (Merrill et al 1963)	m <sup>2</sup> (Pa) <sup>1/3</sup>
A <sub>p</sub>	occluder surface area perpendicular to flow axis	m <sup>2</sup>
A(γ)	function of shear rate and blood sample (Andrade)	Pa s
b	geometrical constant used in BFC grids Weltmann and Green's (1943) constant general constant	
c	geometrical constant used in BFC grids linear regression Y-axis intercept general constant	
C <sub>1</sub>	empirical constant of k - ε model = 1.44 constant from Walburn and Schneck's BTVM [3.7]	Pa s
C <sub>2</sub>	empirical constant of k - ε model = 1.92 constant from Walburn and Schneck's BTVM [3.7]	
C <sub>3</sub>	constant from Walburn and Schneck's BTVM [3.7]	
C <sub>4</sub>	constant from BTVM/B3VM [3.7, 3.8]	
C <sub>4a</sub>	constant from BTVM/B3VM [3.7, 3.8]	
C <sub>μ</sub>	empirical constant of k - ε model = 0.5478	

$C_D$	empirical constant of $k - \epsilon$ model = 0.1634	
$d$	diameter of conduit/pipe	m
	general constant	
$E$	van Dreist's constant, for smooth wall = 9.0	
	activation energy	J/mole
$Eu$	Euler number = $\Delta / .5 \rho w^2$	
$f$	friction factor defined by equation [4.2]	
$F_p$	streamwise force on the occluder due to pressure acting over an area [6.4]	
$F_v$	streamwise force on the occluder due to viscous shear	
$g$	constant of gravitational acceleration = 9.81	m/s <sup>2</sup>
$H$	haematocrit expressed as a percentage	
$H_m$	haematocrit below which shear stress is not evident ( $\approx 5\%$ )	
$h_f$	friction head defined by equation [4.1]	m fluid
$k$	kinetic energy of turbulence (in $k - \epsilon$ model)	
	blood characteristic coefficient Quemada (1976a,b) equation [3.14]	Pa s <sup>1/2</sup>
$k$	power law equation constant	
$l$	length (generally along Z-axis)	m
$l$	mixing length	
$m$	linear regression slope constant	
$n$	power law constant	
$N_X$	number of cells along X-axis	

NY	number of cells along Y-axis	
NZ	number of cells along Z-axis	
P	pressure	Pa, mmHg
Q	flow rate of working fluid	l/min
r	elemental radius	m
	radial direction in polar cylindrical geometry	
R	outer radius of pipe	m
	volume fraction	
	gas constant	J/kg K
R <sup>2</sup>	statistical value denoting quality of fit of linear regression	
Rb	radius of ball occluder	m
Ro	outer radius of conduit profiling	m
Rea	Reynolds' Number based on pipe/conduit diameter	
Re <sub>w</sub>	local, near-wall Reynolds number = $w\delta\rho/\mu_L$	
s	constant used in Casson equation [3.10]	(Pa s) <sup>1/2</sup>
S <sub>φ</sub>	generalised friction factor; equation [4.8]	
t	time	s
T	absolute temperature	K
TPMA	Total plasma minus albumin; constant used in Walburn and Schneck's B3VM [3.8]	kg/l
u	velocity in the 'X' (circumferential) direction	m/s
U <sub>τ</sub>	friction velocity	

$u'$	maximum instantaneous velocity in X direction	m/s
$u$	time averaged turbulent velocity in X direction	m/s
$v$	velocity in the 'Y' (radial) direction	m/s
$v'$	maximum instantaneous velocity in Y direction	m/s
$v$	time averaged turbulent velocity in Y direction	m/s
$w$	velocity in the 'Z' (axial/streamwise) direction	m/s
$w'$	maximum instantaneous velocity in Z direction	m/s
$w$	time averaged turbulent velocity in Z direction	m/s
$w_{ave}$	radially averaged velocity in X direction	m/s
$w_{max}$	maximum X direction velocity at a radial plane	m/s
$x$	Distance along Cartesian ordinate X-axis	m
$X$	Pertaining to Cartesian ordinate	
$IX$	development length	m
$X_1, X_2, X_3$	haematocrit, fibrinogen and globulin used by Begg and Hearn (1966)	
$y$	Distance along Cartesian ordinate Y-axis	m
$Y$	Pertaining to Cartesian ordinate	
	$\ln(\Psi)$ Begg and Hearn (1966)	$\ln s^{-1}$
$y^+$	non-dimensional wall distance $y^+ = \delta U_{\tau} / \nu$	
$z$	Distance along Cartesian ordinate Z-axis	m
$Z$	Pertaining to Cartesian ordinate	
	Direction of steamwise dominance	
$\partial$	partial differential	
$\alpha_0$	$\Psi_c^{-1/2}$ (Quemada 1976a,b) see $\Psi_c$ below	$s^{1/2}$

$\delta$	distance from wall to first cell centre	m
$\Delta$	denotes a difference or gradient	
$\dot{\gamma}$	shear rate (production rate)	$s^{-1}$
$\dot{\gamma}_c$	critical shear rate, above which non-Newtonian concentrate disperse systems act in a Newtonian manner (Quemada 1976a,b)	$s^{-1}$
$\epsilon$	turbulence dissipation rate	
$\kappa$	Von Karman's constant for smooth wall = 0.435	
$\theta$	angle	$^\circ$
	temperature	$^\circ C$
$\mu$	dynamic viscosity	Pa s
$\mu_0$	Intrinsic viscosity at zero shear Quemada (1976a,b)	Pa s
$\mu_a$	apparent viscosity of non-Newtonian fluid	
$\mu_L$	laminar (intrinsic) viscosity	Pa s
$\mu_p$	viscosity of plasma	Pa s
$\mu_r$	viscosity of blood relative to water	
$\mu_T$	turbulent viscosity	Pa s
$\mu_{eff}$	effective viscosity, $\mu_{eff} = \mu_L + \mu_T$	Pa s
$\mu_{\infty}$	Intrinsic viscosity at infinite shear Quemada (1976a,b)	Pa s
$\sigma_\epsilon$	empirical constant used in k - $\epsilon$ model = 1.314	
$\sigma_k$	empirical constant used in k - $\epsilon$ model = 1.0	
$\tau$	elemental shear stress	Pa
$\tau_0$	'pseudo yield stress' (Quemada 1976a,b)	Pa
$\tau_w$	shear stress at the wall	Pa

$\tau_y$  shear stress at flow yield of non-Newtonian fluid Pa  
 $\nu$  kinematic viscosity;  $\nu = \mu/\rho$   
 $\pi$  Pythagoras' constant  
 $\rho$  density kg/m<sup>3</sup>

Subscripts

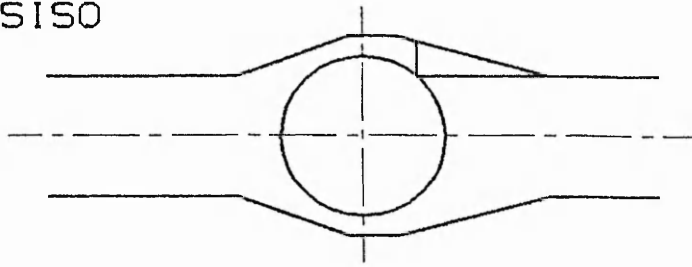
in referring to inlet conditions

## VALVE GEOMETRY NOMENCLATURE

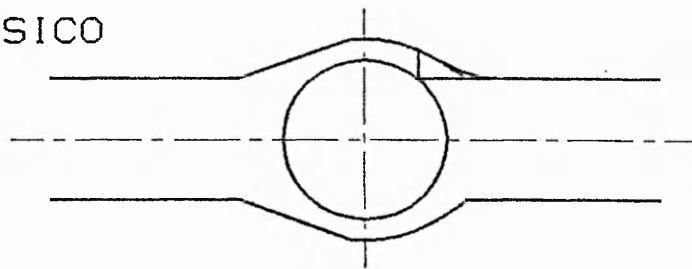
The valve names below are derived from the first letters of the words describing the inlet and outlet sections of each prototype, and the ratio of ball radius to conduit radius. These nomenclatures are shown in diagrammatic form, on the following page.

- SISO            Valved conduit featuring divergent/convergent conical inlet and outlet sections of straight profile, hence Straight Inlet Straight Outlet.
- SICO            valved conduit with the outlet section altered to a curved profile of the form given by equation 5.1, hence Straight Inlet Curved Outlet
- CICO            Inlet and outlet profiles of this valve are similar, ie Curved Inlet Curved Outlet
- LRR series     In this series of valves the diameter of occluding ball was reduced with respect to the conduit radius, hence "Low Radius Ratio" (LRR)

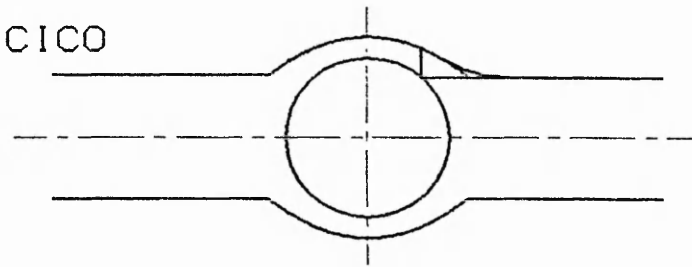
SISO



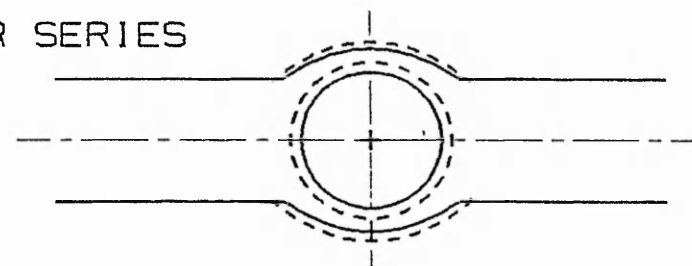
SICO



CICO



LRR SERIES



GENETIC VARIATIONS OF CONDUIT  
VALVE DESIGN: DESIGNATIONS

CHAPTER ONE

INTRODUCTION

## 1.1 General Introduction

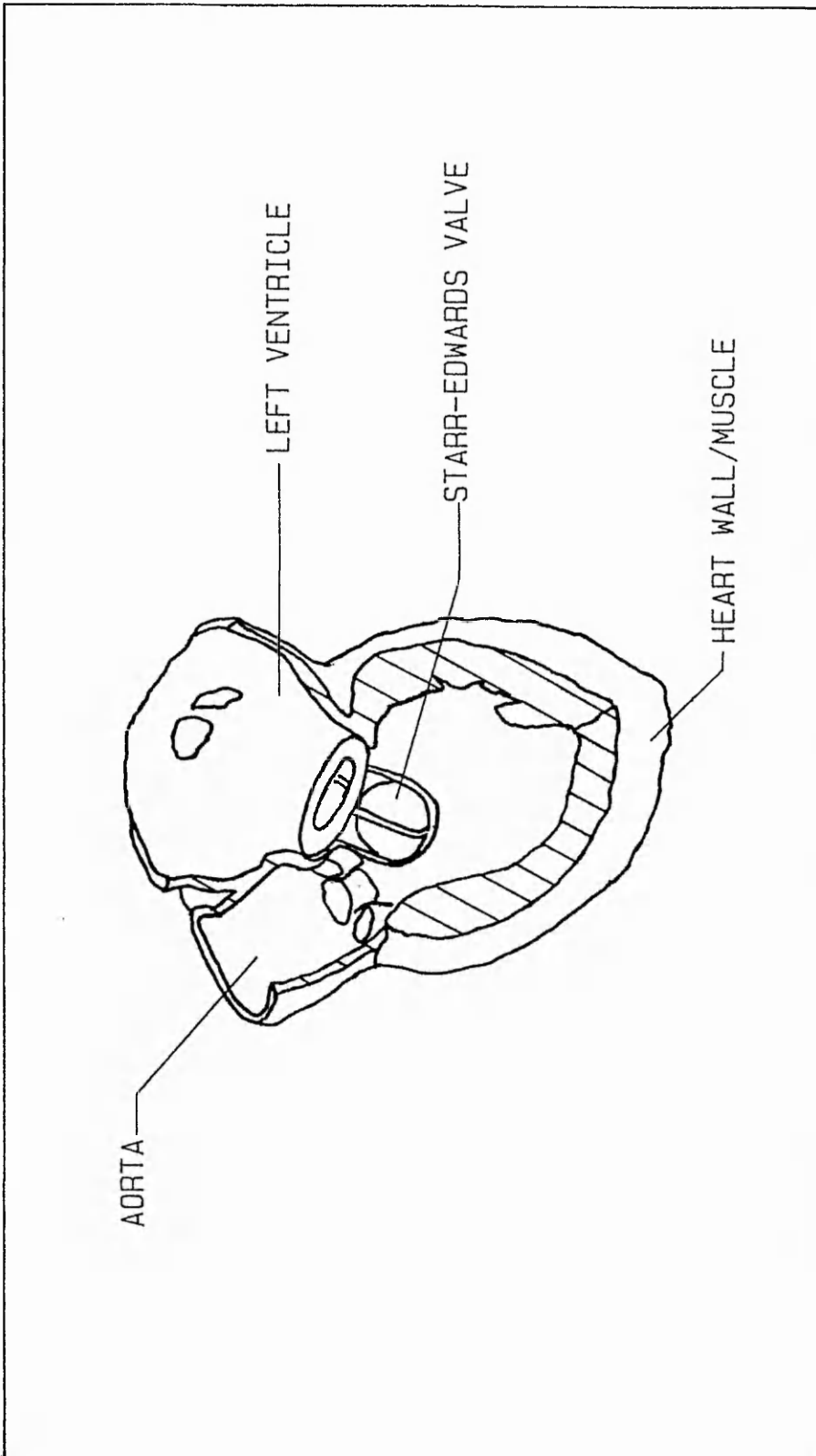
Heart valve replacement is today a common place surgical technique, the number of heart valve manufacturers, let alone prosthetic valve models, being an indication of the size of the market in valves. Like most markets, designs are sold on effectiveness of the product, which in the case of heart valves means improvement of quality of patient life. In furtherance of valve design and because of the consequences of valve failure, each valve manufacturer stringently tests every valve design. The amount of information about a valve's clinical and haemodynamic performance is further increased by the battery of comparative tests performed by other interested parties. This is in an effort to improve further the state-of-the-art of valve design, to quantify a valve's mode of failure, or simply perhaps as an academic exercise.

Because of the success of valve replacements in the case of acquired heart valve disease, there have been attempts more recently to use them in reconstructive surgery. These attempts have mostly involved inserting a valve along with a length of tubing to build, for example, a new aorta. To reduce operating time, manufacturers started to provide what have come to be known as valved conduits.

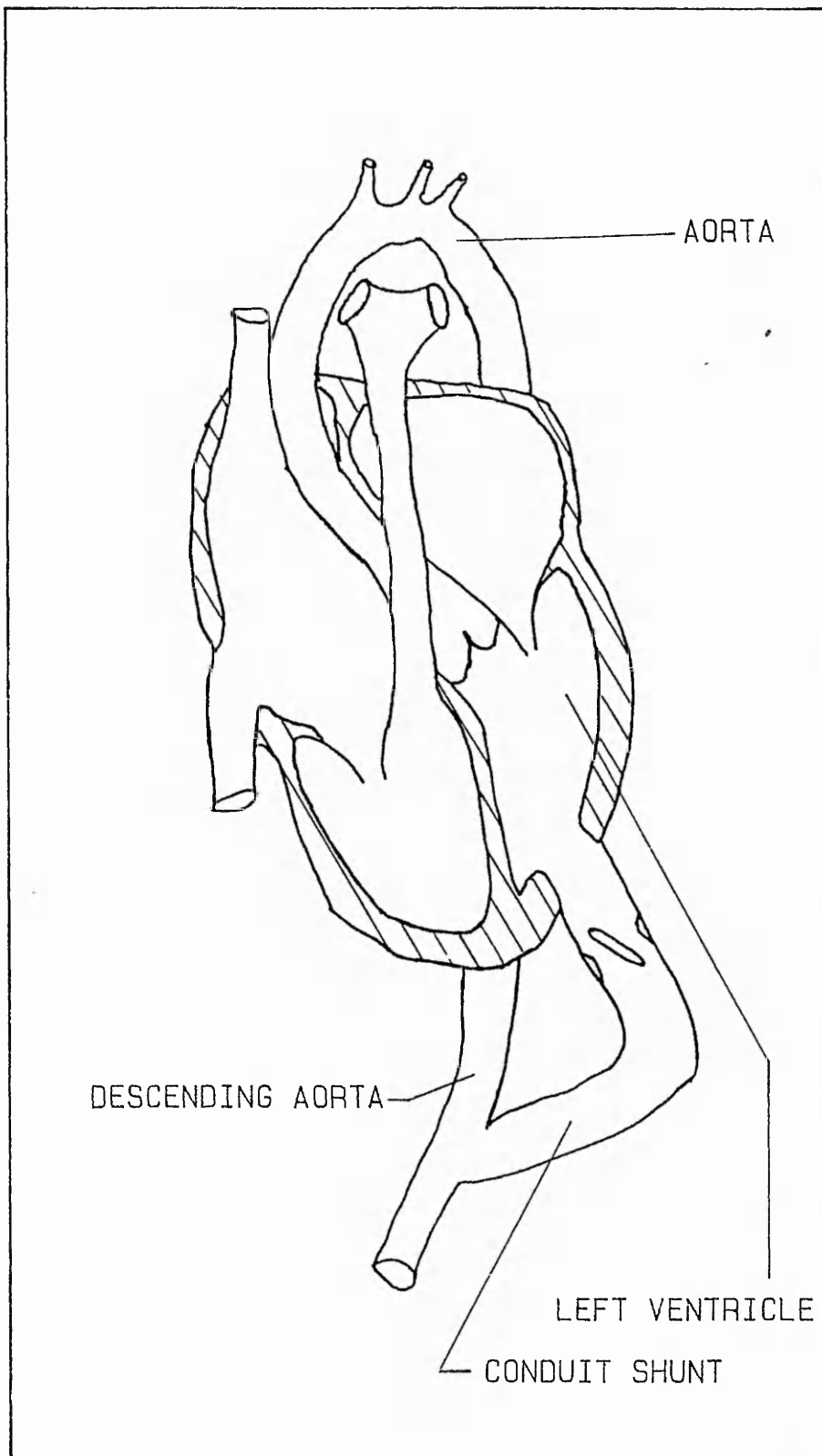
To date, commercially available conduits comprise an aortic or mitral valve mounted into a section of graft tubing. Most popular are bioprosthetic valve conduits, such as Polystan's VPC Porcine valved pulmonary grafts, and Hancock Laboratories or Edwards' Porcine valved conduits. Of the mechanical valves, the

Björk-Shiley tilting disk (AGV/GVP) has found the greatest favour in conduit application. However, each of these valves was designed to be fitted to a tissue annulus in place of an excised natural valve (figure 1.1), and as such they are not wholly suited to conduit application. Although such valved conduits perform satisfactorily, they do not take advantage of the improved haemodynamic characteristics that might be afforded a purpose built device. Furthermore, the number of different conduit designs is small and the development time expended on conduits is disproportionately lower than for traditional valves, so it is unlikely that designs are optimised. This state of affairs is probably driven by market forces, as the number of conduits implanted annually is only a small fraction of the number of aortic/mitral valve implantations, the areas of application being limited now to surgical techniques in acquired disease such as the replacement of degenerating ascending aorta and aortic valve and apicoaortic shunts (figure 1.2) and for reconstruction in congenital heart diseases, eg asplenia syndrome, tetralogy of Fallot, transposition of the major vessels and double outletting ventricles.

Market forces aside, the need to design a superior conduit valve must surely present a challenge, bearing in mind that conduit prostheses are more commonly used in paediatrics. Here prostheses should not only boast an increased longevity of acceptable mechanical function, but should remain suited to the recipient for a normal life span and be free from the need for anticoagulation. The ramifications of this are that conduits, even the smaller sizes, have to have exceptional pressure/flow characteristics so that a valve implanted into an infant might



CAGED BALL PROSTHETIC HEART VALVE  
IN SITE OF EXCISED MITRAL VALVE



APPLICATION OF A VALVED CONDUIT AS AN APICOAORTIC SHUNT

remain suitable in adult life. Such improved valved conduits might find application in a greater range of clinical situations, for example the replacement of aortic valves facilitated by the removal of a section of aorta, even where aortic degeneration is absent. This would allow the implantation of valves of large flow areas incorporated into conduits of diameter equal to that of the heart annulus. However, allowance would be necessary in the conduit for coronary artery outflow.

The above highlights the need for more development of conduit valves. However, such development is traditionally time consuming and very expensive. Techniques commonly applied to the assessment of valve function, for example Laser Doppler Anemometry and static pressure measurement techniques, yield good analyses of flow field information and pressure flow characteristics, but fall short of the ability to predict the more important clinical problems of thromboembolism and haemolysis. These parameters at present are assessed by conducting animal trials, which themselves are expensive and yield data of dubious clinical value. The optimisation of valve design which minimises thromboembolic and haemolytic potential is difficult to achieve if repeated animal trials are needed for each design change. Recent research has enabled critical analysis of thromboembolic and haemolytic potentials based on shear stresses and shear rates induced by a prosthesis. Although this analysis falls short of the ideal, it does improve the potential for valve design. Unfortunately, none of the present day experimental techniques is capable of yielding sufficient information, so other techniques must be sought to do so. Further limitations to experimental techniques might be

introduced by a reliance on the use of Newtonian analogue solutions to produce flow in-vitro. Such solutions are chosen to exhibit viscosities and densities comparable to the properties of bulk blood flow, but a full understanding of the differences between the flow of blood and analogue fluids has not been available and this casts additional doubt on the validity of such experimental tests.

One possible improvement to modelling is via the application of Computational Fluid Mechanics (CFM). Theoretically it is possible to computationally predict all the relevant flow parameters using blood as the working fluid. This could lead to a greater correlation between the flow analysed "through the valve" during the design stage, and the actual flow in-vivo. If such modelling were successful a complete and accurate picture of haemodynamic parameters, such as shear stress and therefore haemolysis would be achieved. However, computational modelling itself is not without its difficulties; present day computers are incapable of solving the Navier-Stokes equations in turbulent flow. The problem lies in the excessive storage and computational time requirements needed to solve such spacially and temporally dense flow fields. The solution is instead approached by the use of a turbulence model which predicts time averaged turbulence flow parameters. Further limitations are the need for a constitutive equation for the description of blood viscosity variation with shear rate, brought about by an incomplete knowledge of the physics of flow of concentrate disperse systems.

This thesis aims to integrate all the above areas by describing the Computer Aided Design of a ball occluded heart valve conduit, paying particular attention to the thromboembolic and haemolytic potentials of the valves by modelling in blood flow. It describes a research project which aimed to design a "purpose built" conduit valve capable of displaying considerably enhanced pressure flow characteristics and reduced thromboembolic and haemolytic potentials. The steps taken to accomplish this design were:

- i) Critical flow parameters were identified against which the completed design could be assessed
- ii) A turbulent, non-Newtonian blood flow model was developed for introduction into a proprietary finite difference package
- iii) A series of valves was developed based on a coherent development plan, each valve being assessed for excellence of pressure/flow characteristics and thromboembolic and haemolytic potentials.

Firstly however, there follows a brief discussion of the history of valve flow visualisation, an introduction to present day experimental techniques applied to valve flow analysis, a discussion of critical haemodynamic parameters and a brief and very general introduction to computational fluid mechanics.

## 1.2 The History of Heart Valve Flow Visualisation

Flow visualisation studies are, generally, very simple to perform and the basic principle of monitoring the passage of seeding particles has been widely applied in a multitude of areas of hydrodynamics over the last fifty years or so. A brief summary of such techniques is given by Clayton and Massey (1967). Heart valve flow studies have been performed since the late 1960's when Weiting (1969) and Duff (1970) applied flow visualisation techniques to the assessment of the flow characteristics of several models of prosthetic heart valves. Since these first flow visualisation studies in heart valves, this method of analysis has become common place and many works present qualitative results from such studies (refs: Modi and Akutsu 1980, Swanson and Clark 1980, Reul et al 1981, Woo et al 1983 and Benjamin 1986). In recent years the techniques of flow visualisation have diversified, making possible quantitative, unambiguous analysis of flow fields, by the application of stroboscopic lighting in a similar manner to that employed by Hampshire (1984), or by particle tracking via multiple exposure. Even greater potential, though as yet unrealised, is offered by the implementation of Partical Image Velocimetry or Laser Speckle Velocimetry as described by Meynart and Lourenco (1984) and Lourenco and Krothapalli (1987).

Laser Doppler Anemometry has been applied by many researchers to the evaluation of flow fields in prosthetic heart valves. Some of these studies present the most simple usage of LDA, namely steady flow velocity fields (Yoganathan et al 1979a and 1979b) while other LDA studies address the problems of pulsatile flow, via the

employment of pulsed Doppler techniques (Bruss et al 1983, Chandran et al 1985a,b, Giersiepen et al 1986 and Tiederman et al, 1986). LDA is also capable of yielding stress information, an ability which has been exploited in several studies (Tiederman et al 1986, Woo et al 1983, Akutsu and Modi 1982). These studies have all assumed isotropic turbulence and have utilised only one or two dimensional doppler measurement. Furthermore, all these studies have used blood analogue fluids as the flow medium because of the difficulties presented by LDA measurements in blood as a working fluid.

Further advances in the field of heart valve flow visualisation are promised by the relatively recent technique of Ultrasound Doppler, as described by Mann et al (1987). Although this technique offers the researcher the option of using blood as a working fluid, problems are still presented by the opaqueness of the valve and by the limited spatial resolution of the technique.

### 1.3 In-Vitro Measurement Techniques

Most of the common experimental liquid flow techniques are employed in the field of heart valve flow analysis. However, each of the techniques has limitations when applied to blood flow experimentation. The major problem is due to the nature of the blood, which is opaque and difficult to handle because of its clotting functions, let alone its scarcity. In order to elaborate further, the following sections briefly discuss the methods, limitations and capabilities of the applicable experimental techniques:

t) Flow Visualisation

**The Techniques:** There are several flow visualisation techniques. These basically all consist of small tracer particles (powders, emulsions, gas bubbles or beads) being added to the bulk fluid. As the tracers pass through an illuminated section the paths they prescribe are captured on a recording medium - generally photographic film or video. The data yielded is generally only qualitative, showing streamlines, but by using stroboscopic lighting with unequal ratios of illumination and extinction and then by mapping the length of streak obtained in a known film exposure time, a quantitative description of the velocity field can be gained. A recent development in flow visualisation techniques is Particle Image Velocimetry (PIV), where a high concentration of very small particles (10 $\mu$ m diameter) is used to seed the flow. Multiple exposures of the particles passing through a thin sheet of laser light are taken in rapid succession. Velocity vectors are yielded by the interrogation, by laser, of the contact printed positive transparency of the particle images. Velocity vector magnitude is inversely proportional to the Young's fringe spacing set up by the interrogation and vector direction is perpendicular to the lay of the fringes.

**Advantages/Capabilities:** The several techniques vary not only in the amount of data they can yield but in the difficulty of application, generally the more complex techniques being the most expensive but yielding the most information. Geometrical constraints are not so stringent as for LDA and implementation of a simpler working system is

not time consuming. None of the different forms of the technique is intrusive and all give full flow field information.

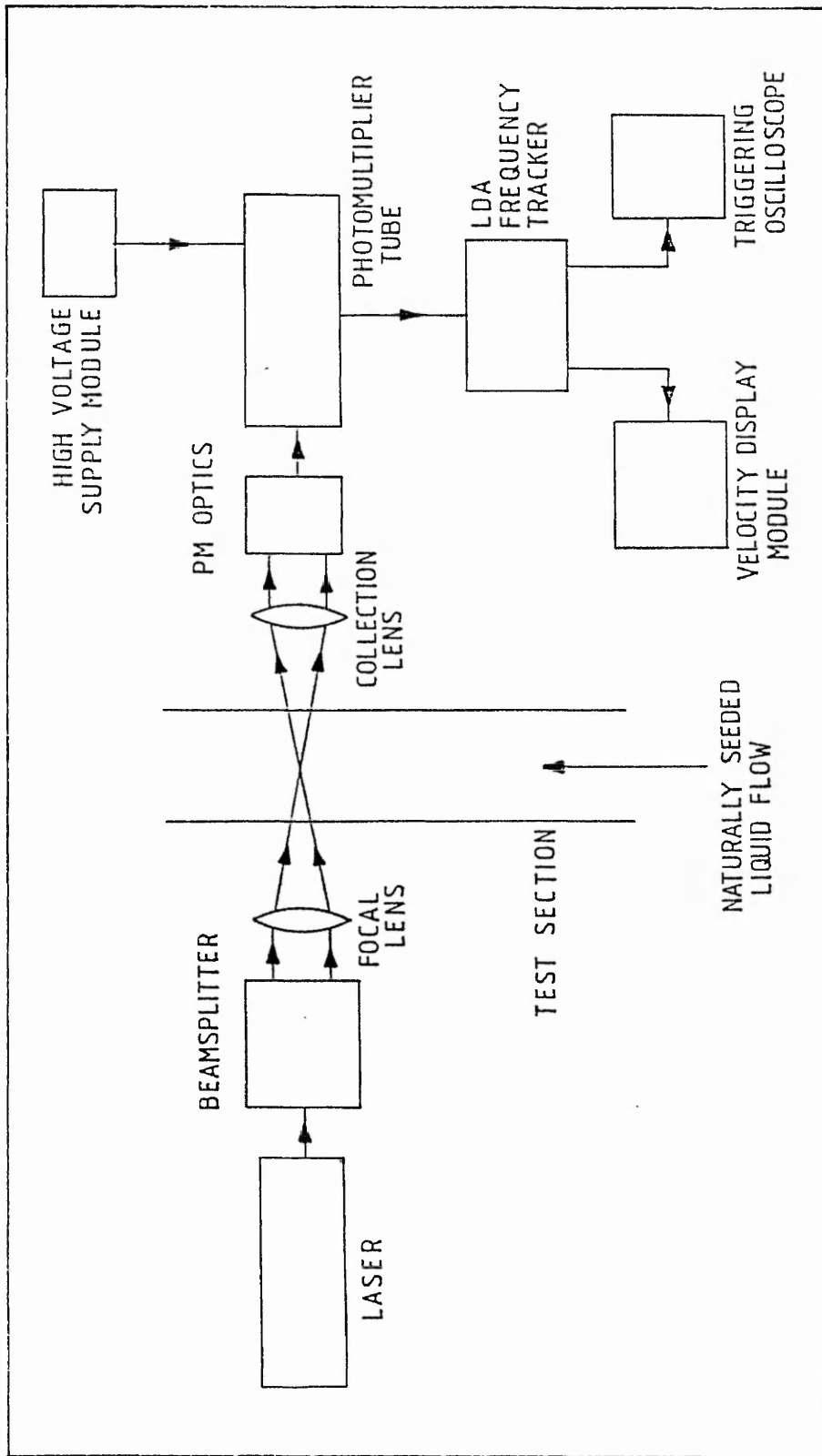
Disadvantages/Limitations: Most flow visualisation techniques are only qualitative and therefore only give limited understanding of a flow regime. Quantitative flow visualisation techniques require a large input of time in the analysis of photographic recordings and the installation of PIV for the analysis of turbulent flow is very expensive and not an established technique.

ii) Laser Doppler Anemometry (LDA)

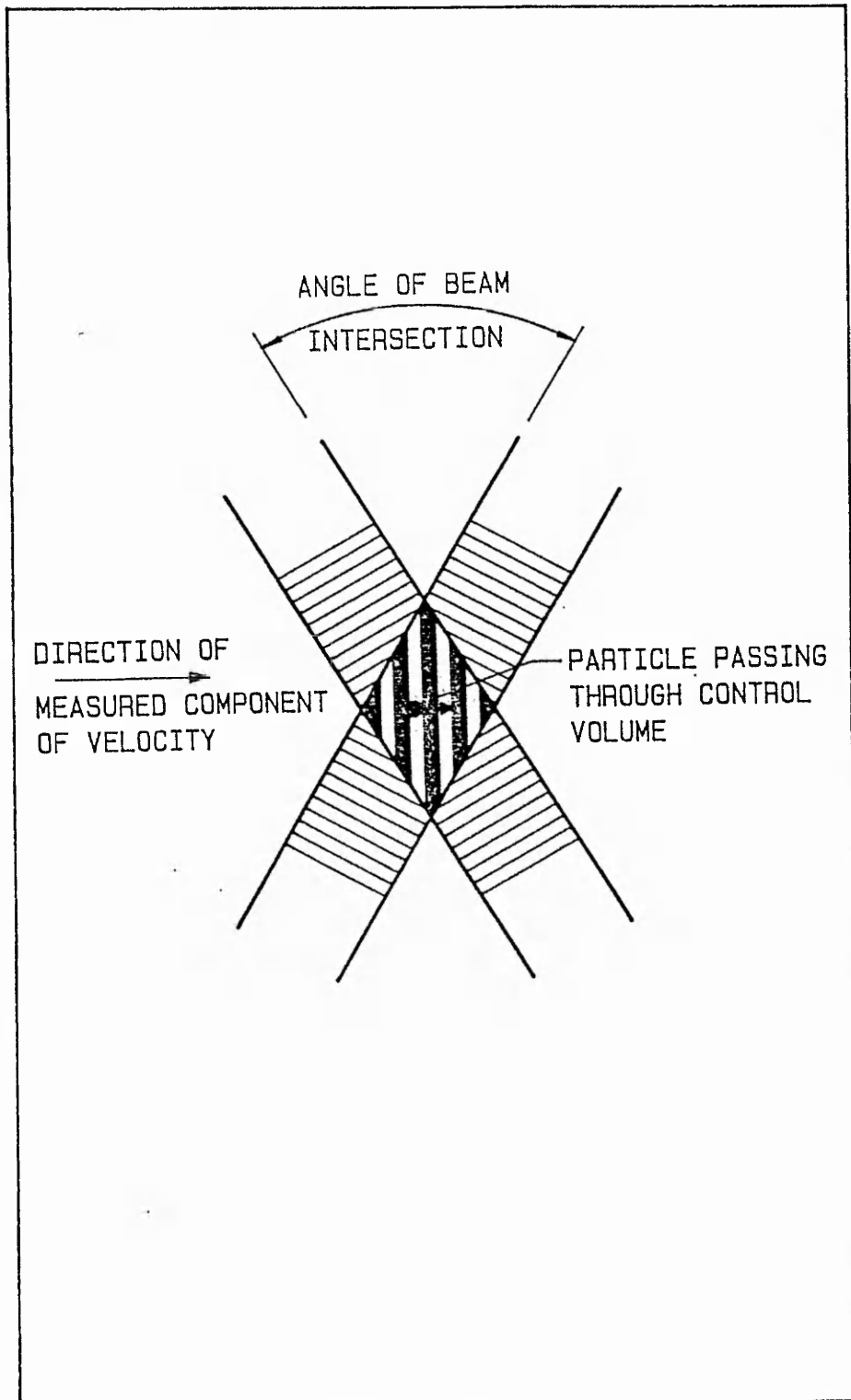
The Technique: A laser beam is bifurcated or trifurcated by diffraction gratings or acousto-optic/electro-optic modulators and brought together again at predescribed angles to form a control volume (see figure 1.3), the path lengths being equal. In the control volume an interference pattern is set up (as in figure 1.4) and any particle crossing this pattern will reflect a "Doppler burst" of light (figure 1.5) which is detected by photo-multipliers. By quantifying the periodic frequency of the burst, the velocity of the particle can be deduced.

Capabilities/Advantages: This technique is well established and non-intrusive and so does not disturb the flow field. The spatial resolution is high, which is important in such small geometries as valves. Absolute velocities are measured alleviating the need for calibration.

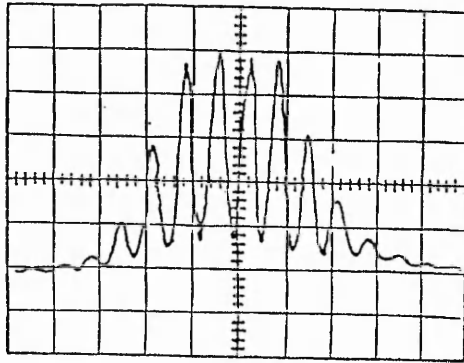
Directionally unambiguous velocities and turbulence



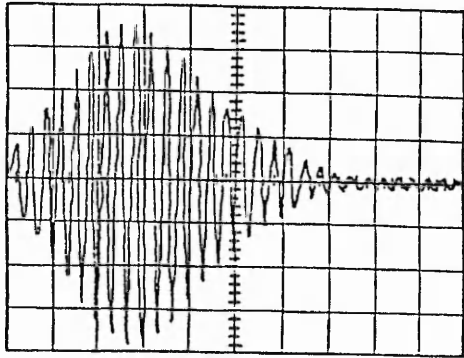
SCHEMATIC OF AN LDA SYSTEM



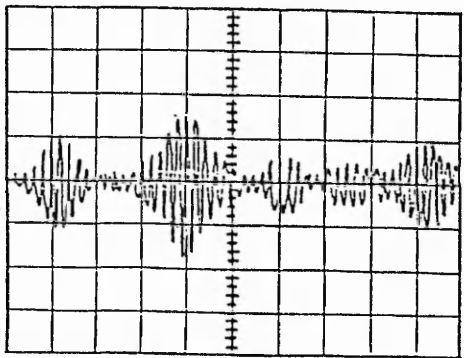
LDA CONTROL VOLUME INTERFERENCE  
FRINGE PATTERN



Doppler Burst - Detector Signal



Doppler Burst - Band-pass  
Filtered Signal



Multiple-particle Signal

TYPICAL LDA SIGNALS

intensities can be established in three dimensions as can Reynolds' stresses, though with limitations. LDA can also be used in a pulsed mode for the analysis of pulsatile flow fields.

Disadvantages/Limitations: LDA cannot easily be used to map fluid velocities in opaque media (Stern 1985) and therefore has not seen widespread application to the analysis of blood flow. The geometry of the test section can cause untold problems because of inaccessibility both of the control volume and of the photo-multipliers. Distortion of the control volume by refractive index mismatching can occur leading either to measuring in the wrong place or, even worse, a distortion of the control volume and consequently a velocity offset error (Bicen 1982). This technique also suffers because of its inability to obtain data close to walls and blockages.

### iii) Ultrasound Doppler

The Technique: Like LDA this method of analysing velocities relies on the Doppler principle: as particles (in this case normally blood cells) cross the reference beam a Doppler shift is introduced in the reflected beam. The magnitude of this shift is proportional to the velocity of the particles. Ultrasound Doppler differs from LDA in that the beam is not of laser light, but of ultrasound waves, to which soft body tissues and blood are translucent.

Advantage/Capabilities: The ability of Ultrasound Doppler to see through body tissues allows the positioning of the

control volume in places such as the ascending aorta or within the ventricles and thus yielding information about heart valve flow in-vivo. The use of Ultrasound Doppler in-vitro allows the measurement of velocity (Mann et al 1987) and Reynolds' stresses in blood-filled test sections thus eliminating the need to model using transparent solutions.

Disadvantages/Limitations: Two dimensionality of measurement is possibly the major drawback of the technique. In-vivo there is no solution to this problem as three dimensional measurement is not practicable, but in-vitro a three beam setup could do away with this problem. The size of the control volume is large and difficult to control due to the spreading out of the ultrasound waves, which means that a lot of the smaller scale turbulence information can not be assessed.

iv) Hot film anemometry

The Technique: An electrical current is caused to flow through and heat a film of high electrical resistivity. The film which is either probe or wall mounted is placed into a moving fluid where the conduction of heat away from the probe is dependent upon the velocity of fluid passing over it. The current drawn in maintaining the probe at a constant temperature is proportional to the cooling effect on the probe. Consequently, by monitoring the current necessary to maintain the probe temperature, the velocity of the fluid passing over it can be deduced following calibration against a known fluid velocity.

Advantages/Capabilities: Hot film anemometry is very well established, widely accepted and relatively cheap to install. It is a very simple technique to use and can be used in opaque media. The technique will yield velocity and Reynolds' stress information and shear stresses at a wall (Tillmann et al 1984).

Disadvantages/Limitations: The use of probe based anemometry necessarily complicates the test section geometry because of the need to place a probe into the flow. Probably the factor that most restricts hot film anemometry is the intrusive nature of the probes themselves. This makes meaningless any velocity data recovered from recirculative flow because of the interaction of the probe and mount on the flow. The probes, because of their size, have a limited spatial resolution of application and cannot be used in very close proximity to walls and obstructions though film can be wall mounted to yield information about boundary layer flow. Velocity information gleaned from statically mounted probes is directionally ambiguous.

v) Pitot tube measurements

The Technique: Static and dynamic pressures are obtained by a probe, having perpendicularly opposed pressure tapings, which is placed into the flow field. The difference between these two pressures is proportional to  $1/2 \rho w^2$  - knowing the density of the fluid, the velocity can be determined.

Advantages/Capabilities: The technique is very simple, yielding velocities and static pressures, its cost is very

low and analysis of results is straight forward.

Disadvantages/Limitations: Pitot tube measurements can only be applied successfully to streamwise dominant flow and have limited spatial resolution, due to the dimensions of the probe. This also limits near-wall measurements. Flow sections are necessarily complicated to allow for probe intrusion.

vi) Static pressure measurements

The Technique: A small pressure tapping is made in the side of the test section wall, generally one before the valve and one after. A pressure measuring device ("U-tube", variable reluctance transducer or similar) is connected to the taps to measure either differential pressures across the valve, or gauge pressures above atmospheric. Energy loss measurements are effected by gathering Pressure drops and Flow Rates throughout a series of complete heart cycles, although recent analysis (Leefe and Gentle 1987) has shown that this is by no means as simple as is currently supposed.

Advantages/Capabilities: This form of measurement is very simple and cheap to achieve, yielding static pressure gradients and pressure recovery information. For a long time the technique has been used almost as the definitive classifier of valve haemodynamic performance.

Disadvantages/Limitations: Static pressure measured in the above way is very prone to inaccuracies because of the assumption that the pressure distribution will be the same

throughout the radial plane. This is not the case in flows where streamlines are strongly curved - the flow regime that is dominant in most cases of heart valve flow.

vii) Flow metering

**The Methods:** There are two very popular flow meter types applied to prosthetic heart valve flow measurement; electro-magnetic and turbine. The electro-magnetic meter works by the Hall effect where an electrically conducting fluid passing through a field of magnetic flux induces an EMF. The magnitude of this induced voltage is directly proportional to the flow velocity. The turbine flow meter relies on the movement of a turbine inserted into the flow. The movement of the turbine causes a small current to be developed in an attached generator indicating flow rate.

**Advantages/Capabilities:** Both methods of measuring flow rate are relatively inexpensive and easily applied in-vitro. Signal conditioning and analysis are straight forward and quick, accuracy can be high but is dependent on conditions such as flow symmetry and working fluid. Directionally unambiguous flow data is yielded, along with energy losses when used in conjunction with pressure measurement methods.

**Disadvantages/Limitations:** Turbine meters can be slow to react to small variations in flow rate due to their inertia and consequently can lag behind the fluid, or completely miss small fluctuations. Electro-magnetic flow meters do not suffer from inertia problems as there are no moving parts, but deviations of the flow profile away from symmetry

will cause errors. This also occurs, though much less significantly, in turbine meters. Electro-magnetic flow meters can also be affected by electrical noise and by the choice of working fluid, one particular problem being the formation of oxides on the sensors of the probe, introducing a zero offset error.

#### 1.4 Haemodynamic Quantities

The associations between poor haemodynamics and clinical complications have been well discussed over the last thirty years or so, since Ross et al (1954) first reported on haemolysis caused by prosthetic heart valves. Here then, only a brief outline to the clinical complications that are related to fluid flow are presented. The aim is to establish critical limits to flow parameters of interest when assessing flow via techniques such as LDA or CFM. Five clinical conditions dependent on bulk blood flow (ie not material or mechanically related etc.) have been identified as being potential causes of failure of heart valve prostheses:

##### i) Haemolysis due to high in-bulk shear stress

To predict the destruction of erythrocytes in bulk flow the dependence of haemolysis on the magnitude and duration of high in-bulk shear stress needs to be established. Leverett et al (1972) summarise the findings of various researchers: Rooney (1970), Blackshear (1972), Williams (1970), Shapiro and Williams (1970), etc. and estimate, graphically, a relationship between the threshold shear and exposure time. Later, Hellums and Brown (1975) concluded that the levels of

shear stress sufficient to cause in-bulk haemolysis are present in normally functioning prosthetic valves. This statement was based on a discussion of data presented by Roschke et al (1975) who gave conservative estimates of shear stress based on wall shear stresses in boundary layer flow. Hellums and Brown use as their threshold for haemolysis a stress magnitude and duration of  $500\text{N/m}^2$  and  $1 \times 10^{-3}$  seconds respectively, this, they argue is representative of the "flight time" of a blood cell through a valve prosthesis.

ii) Shear stress related haemolysis at the blood/prosthesis interface

There is no doubt that haemolysis occurs at the wall of a prosthesis in shear stresses much lower than those needed in the above case (below  $150\text{N/m}^2$ ), however, the precise mechanics of this haemolysis are not fully understood. There have been several approaches to the investigation of surface induced haemolysis including analysis of: the role of surface roughness (Bacher and Williams 1970), haemolysis at wall contact (Wielogorski et al 1976, Solen et al 1978, 1981), and the material forming the prosthetic surface (Lampert and Williams 1972, Solen et al 1978 and Monroe et al 1980) and the surface/volume ratio (Beissinger and Williams 1984). One cause, argues Blackshear (1972), is that additional stresses are encountered by erythrocytes as they adhere to and are subsequently torn from the prosthetic surface. This is not a problem that can be solved by a fluid dynamic analysis and therefore will not be discussed here. What is of fluid dynamic interest is the reduction of

this occurrence brought about by decreasing shear stresses and levels of turbulence near to the wall: Blackshear (1972) suggests that high shear stresses near to a prosthetic surface lead to the increased probability of cell contact with the wall and hence an increase in haemolysis via this mechanism. This is exacerbated by the excitation of clotting agents due to limited releases by erythrocytes in the elevated stress regions (Johnson 1970 and Blackshear 1972). For a more complete reference see Blackshear and Blackshear (1987).

iii) Damage to endothelial linings due to jet impingement

Several studies - eg Figliola and Mueller (1981) and Fry (1968, 1969), have discussed the possibility of damage to the endothelial lining of the aorta due to the implantation of prosthetic heart valves. This damage is reported by Fry (1968,1969) to occur in shear stresses as low as  $40\text{N/m}^2$ . This phenomenon is highly dependent upon the direction of blood issuing through the orifices of a prosthetic heart valve, particularly around a ball or disc occluder or through the minor orifice of a tilting disc valve, but is especially sensitive to the magnitude of the shear stress impingent on the wall.

iv) Valve dysfunction due to thrombus formation at hinge points

Possibly a more important cause of valve unacceptability is dysfunction due to occluder immobilization by the formation of thrombus at critical sites, especially the hinge points of twin flap or tilting disk valves. There is ample clinical documentation of the occurrence of such problems

(refs : Narducci et al 1986, Nunez et al 1980, Aston and Mulder 1971, Roshcke et al 1977, etc.). Clots are known to form in areas of haemostasis or low shear, the mechanisms being discussed by Dintenfass (1964a,b) who presents data on the time related aspects of clotting under differing shear rate conditions. Dintenfass (1962, 1964a,b) also presents, as it were, a critical lower shear rate (of order of magnitude of  $7s^{-1}$ ) where clotting due to the low shear mechanism is accelerated by up to one thousand fold. Thrombosis can also be caused by higher shear rates as the aggregation of cells takes place in eddies and in an environment of the contents of damaged erythrocytes (in a similar manner to that discussed earlier). These mechanisms are further exacerbated by the complex, non-Newtonian viscosity of blood which, as it starts to slow down, is further slowed by the increase of viscosity - see Whitmore (1968) for a more complete discussion of blood viscosity.

v) Thromboembolism

This final category of bulk fluid related prosthetic heart valve failure is caused by the same mechanisms as the previous, ie low shear rates at stasis points or higher rates close by, but the sites may be different, and valve dysfunction does not necessarily occur. Thrombus can form both upstream and downstream of the valve, as well as at the occluder and may be apparent at any point where low shear rates occur - some possibilities being close to the sewing ring, upstream of the occluder and shielded from a washing action by the occluder, or at the apex of a ball valve cage. Thrombosis in itself in these areas is not of great concern

(if stenosis does not ensue because of it), but the mobilization of the thrombus leading to thromboembolism at a downstream site cannot be tolerated.

Summarising, the aim of the above discussion is to emphasise the need to know the magnitudes of shear stress and shear rate that exist in any valve flow condition, in order that one might avoid known critical values, and thus reduce the thrombotic and haemolytic potentials of a prosthesis at the onset of its design. Having established the importance of haemodynamic occurrences to clinical performance one is left to ascertain the actual values of these parameters existent in a particular valve. This, for obvious reasons, is generally done in-vitro, but such modelling opens itself to all manner of problems - primarily those of selecting the methods of flow study to be employed along with the analysis techniques.

#### 1.5 Computational Fluid Dynamics

Due to the complex nature of the Navier-Stokes' partial differential equations describing fluid flow, a purely analytical solution is only possible for simple configurations in laminar, steady, fully developed regimes. As such flow situations do not occur in the cardiovascular system close to the heart, or indeed in prosthetic valve flow, which can be either undeveloped laminar or turbulent, the use of analytical methods in heart valve design is very restricted. Hence a numerical approach must be adopted if relevant flows are to be analysed non-experimentally. In its simplest form computational analysis will be the solution of the parabolised Navier-Stokes equations, yielding information about

boundary layer type flows (Launder and Spalding 1972). If the flow has areas of streamwise separation or impingement, or if downstream events are likely to influence upstream parameters, then the full (elliptic) form of the Navier-Stokes equations must be invoked.

Computational numerical methods in the form of finite difference or finite element approximation procedures offer solutions to differential equations and have been of immense value for some time in the fields of mechanical stress and vibration analysis. Unfortunately, standard computational numerical methods cannot be applied to the solution of turbulent fluid flow because the requirements of excessive storage space and run time make it impractical on existing computers. This is due to the nature of turbulent flow: inherently three dimensional, non-linear and with a very high spatial and temporal density of occurrence of important turbulent processes (ie processes taking place in short distances and time periods). In order to overcome the problems of solving turbulent flow, time-averaged properties of turbulence are considered, thus eliminating the necessity for an extremely fine grid, but this requires a model to describe the transport of momentum by the turbulent motions. The reasons for the onset of turbulence are complex, but generally turbulence occurs when flow is sufficiently disturbed at relatively high Reynolds' numbers, though this is very geometry dependent. Numerous attempts to describe turbulence physically in terms of calculable properties have been made and can be classified into two concepts; turbulent (eddy) viscosity and turbulent stress. Here, only on the most widely used and accepted model which utilises the turbulent viscosity concept and is known as the  $k - \epsilon$  model (Jones and

Launder 1972) will be considered. This two equation procedure calculates the quantities:  $k$ , the kinetic energy and  $\epsilon$ , its dissipation rate, to yield a time averaged description of turbulence. The local turbulent viscosity  $\mu_T$  is then found from:

$$\mu_T = C_\mu \rho \frac{k^2}{\epsilon}$$

where:  $C_\mu$  is a constant of turbulence

$\rho$  is the density of the working fluid.

An effective viscosity  $\mu_{eff}$  can then be obtained from:

$$\mu_{eff} = \mu_L + \mu_T$$

where  $\mu_L$  is the laminar (intrinsic) viscosity of the fluid.

This facilitates the calculation of turbulent stresses from:

$$\tau = \mu_{eff} du/dz$$

When the flow is purely laminar, the turbulent solver is suppressed and the laminar form of the Navier-Stokes equations are solved, then simply:

$$\mu_{eff} = \mu_L$$

To obtain  $k$  and  $\epsilon$ , empirical constants are required by the model and these have been established in free turbulent flows. Such constants were the failure of earlier models, due to their values varying so greatly for differing flow situations. Launder and Spalding (1974) reported the establishment of a universally applicable  $k - \epsilon$  model of reasonable accuracy both in near wall and free stream analysis. However, Abujelula and Lilley (1984) discussed the limitations of the empirical constants of the  $k - \epsilon$  model and concluded that modifications were required in certain flows but that, in general, realistic predictions could be obtained with the standard model. However, modelling turbulence in unsteady (pulsatile) flow situations is highly complex with

much to be completed before standard models can be applied with confidence. At the present time empirically derived modifications to existing models relating to a particular flow geometry will have to be made in order to numerically describe transient flow. Morain (1982) and Metha and Lomax (1982) provide some insight into the current state-of-the-art in turbulence modelling and conclude that current research is working towards a catalogue of models which have been established in particular areas of fluid flow. Bearing in mind that serious research in the modelling of turbulence has only taken place over the last sixteen years and that there is a vast amount yet to do, it is still a matter of speculation as to whether a uniquely acceptable turbulence model will exist before the availability of computers with sufficient storage capability to make turbulence modelling redundant.

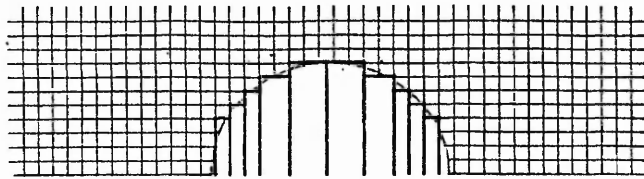
Because of the special requirements of turbulence models in solution algorithms, finite difference techniques are utilised significantly more than finite element methods. In particular, finite element methods need parameter values at nodal points within individual elements, whereas such values are assumed constant with the volume domain in finite difference methods. However, recent developments in finite element techniques have enabled their application to the modelling of both turbulent flows (Autret et al 1987) and non-Newtonian flows (Gartling 1986). Although finite element solution algorithms generally obtain convergence more slowly than finite difference methods, they have been favoured in the majority of mathematically modelled fields. The primary reason for this is the inherent obtrusiveness of finite difference grids in non-orthogonal

geometries (figure 1.6) which is responsible for large inaccuracies at discontinuities in the solution domain. It was such inadequacies in finite difference grids which gave birth to finite elements, in order to analyse stress fields in airframes. Considerable effort has been made to enable non-interfering grid generation and it has only been in the last five years that non-interfering grids have become commercially available in finite difference solution algorithms, in the form of Body Fitted Coordinates. This significant break-through has importance in areas of research such as prosthetics where the vast majority of geometries are non-orthogonal. State-of-the-art finite difference solvers can now boast flexibility in grid generation as well as a choice of turbulence models. Such solution procedures are becoming commonplace in aircraft and automotive aerodynamics, petroleum research, weather prediction and nuclear engineering.

## 1.6 Prototype Nomenclature

The grids used were necessarily changed with each new valve modelled, and with more than twenty or so differing geometries, it became necessary to assign a name to each, as after a while generation numbers became meaningless. To aid in the reading of this thesis the nomenclature of the grids is defined below, in order of generation. The letters used in designation are taken from geometrical features, namely the inlet and outlet profiles, and the ratio of ball diameter to conduit diameter. Each of the valve sections below is shown in figure 1.7.

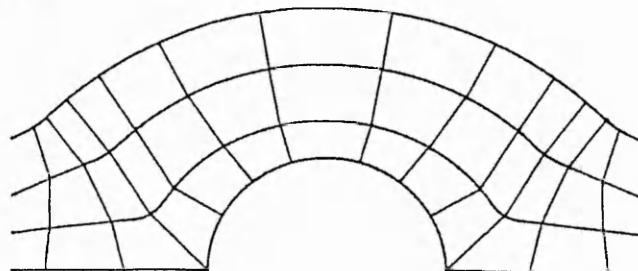
- i) SISO: this is the name assigned to Benjamin's original valve



ORTHOGONAL FINITE DIFFERENCE GRID

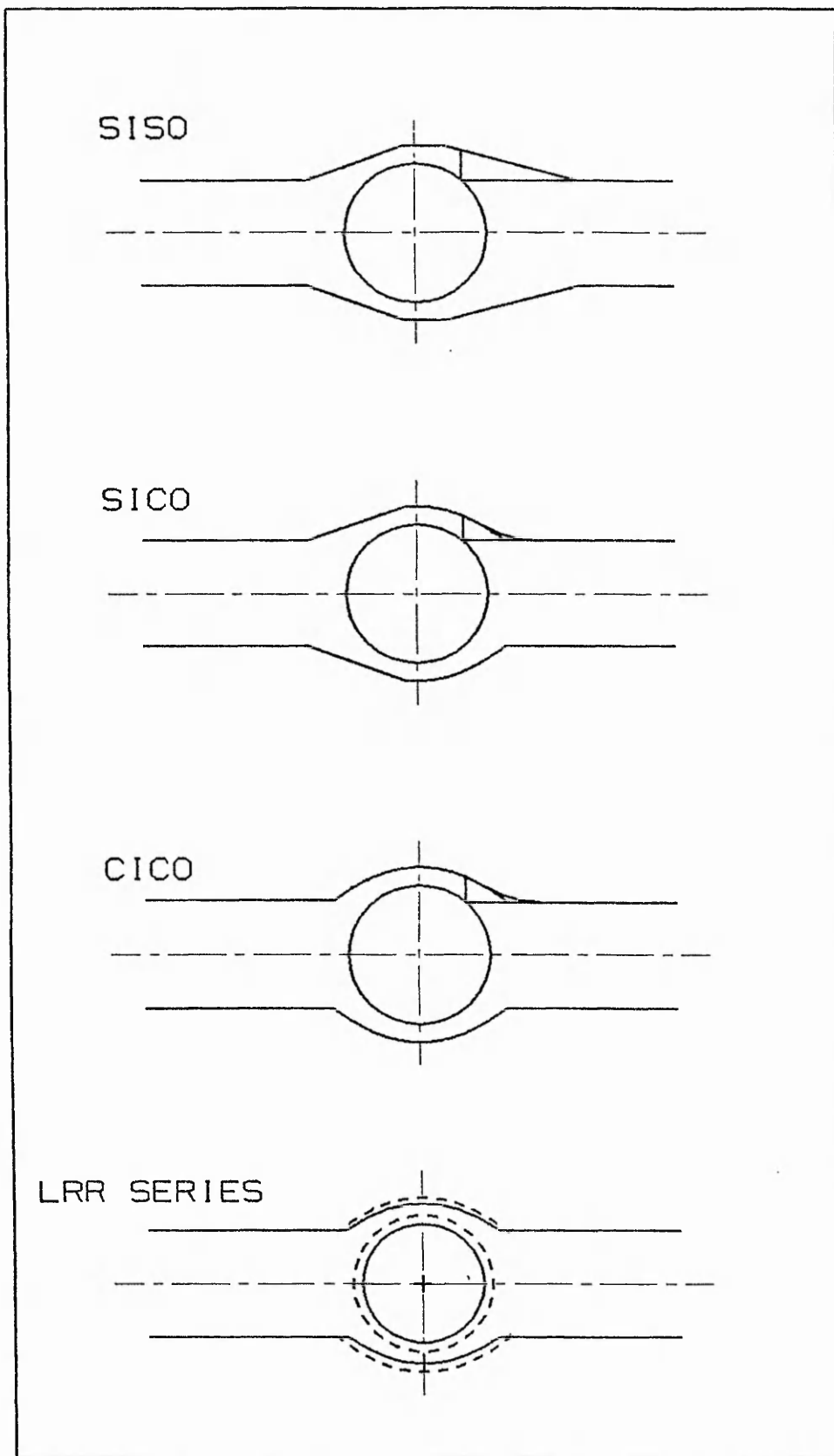


NON-ORTHOGONAL FINITE DIFFERENCE GRID  
(BFC GRID)



FINITE ELEMENT GRID

EXAMPLES OF FINITE ELEMENT  
AND FINITE DIFFERENCE GRIDS



GENETIC VARIATIONS OF CONDUIT VALVE DESIGN: DESIGNATIONS

which sported Straight Inlet and Straight Outlet cones.

- ii) SICO: was the second prototype generated, the outlet section having been changed from a straight one to a curved one following the relationship of equation [5.1], hence Straight Inlet Curved Outlet.
- iii) CICO: differed from SICO in as far as the diverging inlet and converging outlet profiles were modelled in a similar manner to the outlet of the above SICO valve, hence Curved Inlet Curved Outlet.
- iv) LRR: this range of valve sections with various inlet and outlet profiles differed from the previous range in so far as the radius of conduit was decreased with respect to the ball radius, and hence "Low Radius Ratio" was used as a prefix to designate the range.

CHAPTER TWO

EXPERIMENTAL INVESTIGATION

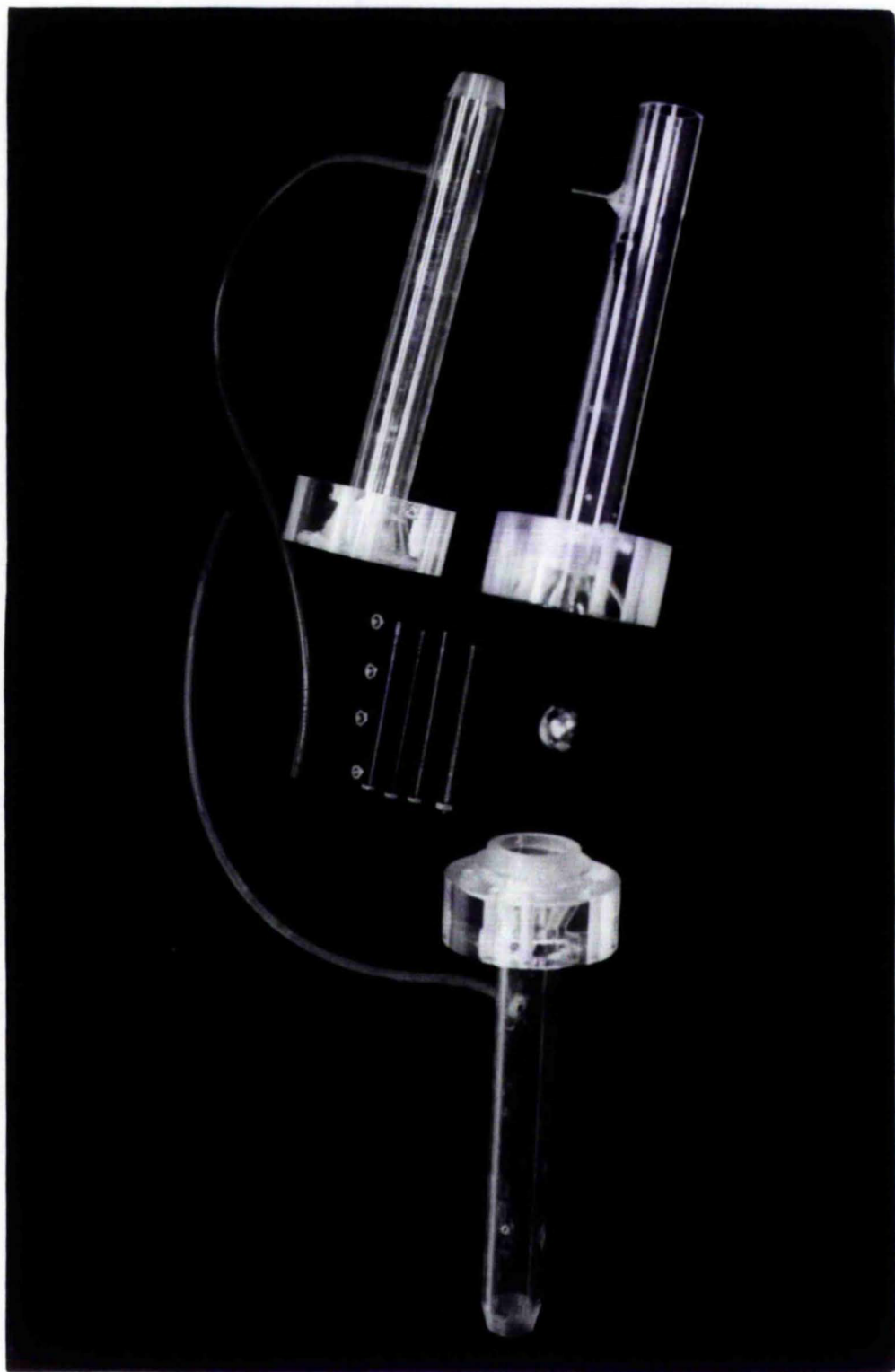
## 2.1 Introduction

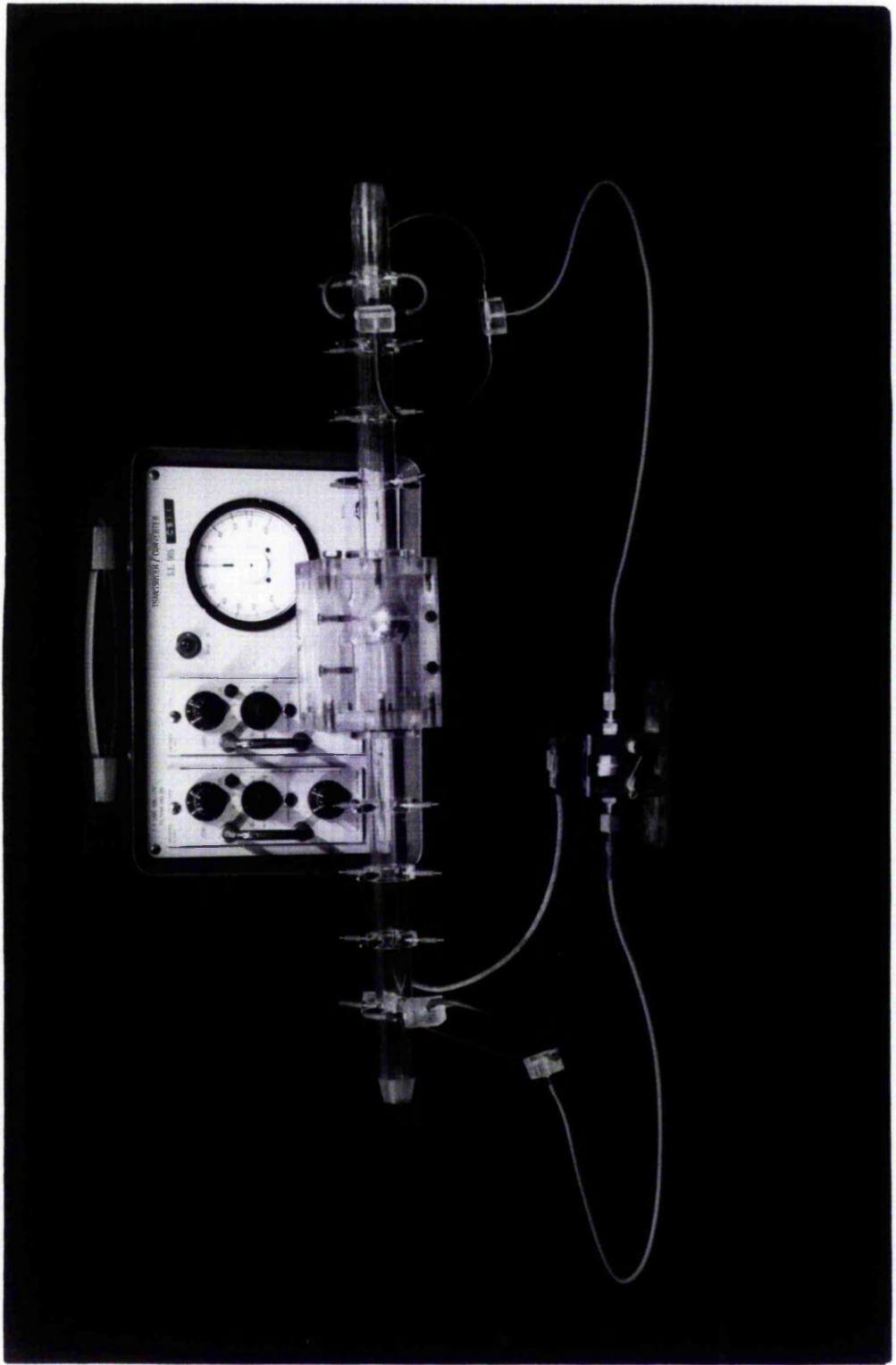
The amount of experimental work carried out as part of this thesis was limited, with emphasis being placed on the verification of numerical predictions and not on establishing complete flow characteristics of the valves tested. Of primary concern was the examination of stationary flow fields and static pressure gradients across the valve sections. Further reasons for conducting an experimental investigation were cautionary, ie flow conditions might be apparent experimentally that might not have been accounted for in a numerical study. Such an example was the occluder instability witnessed during steady forward flow tests. This problem is unlikely to have been foreseen or noticed in a purely numerical investigation and could well have lead to the final design being unsuitable for clinical application, even though pressure/flow characteristics were good.

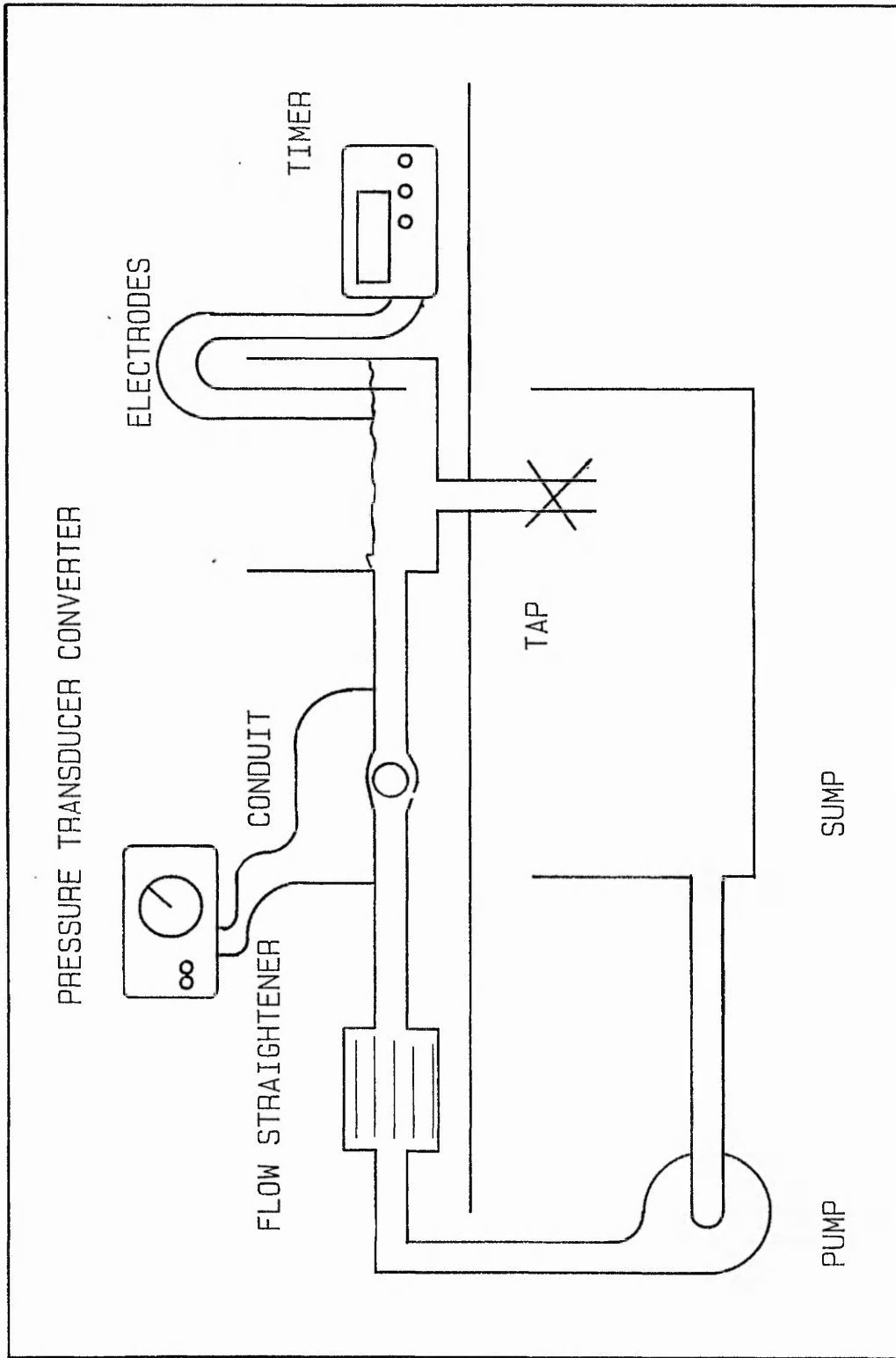
## 2.2 Static Pressure Measurement

The obvious first step in a static pressure measurement study is the location of pressure tapings, as discussed by Swanson (1984). The location of tapings can have a marked influence on the final results. The inlet pressure tapings were placed greater than two diameters upstream of the ball occluder. If the tapings were located closer to the ball then flow curvature effects caused by the ball would be likely to increase static pressure measurements. Swanson suggests that 3% or above of the dynamic pressure head might be monitored by tapings in this region. The downstream tapings were constrained similarly, and were located 7 diameters downstream, greater than the 4-5

diameters minimum recommended by Swanson. The location of the single inlet and outlet pressure tapping were made to coincide with Benjamin's (1986). The valve sections tested experimentally corresponded to 16mm versions of the SISO and SICO conduits (described briefly in Chapter one and in detail in later chapters). Figure 2.1 shows these valve sections with a single pressure tapping at outlet and inlet. The rigid inlet and outlet lengths incorporated into these prototypes were made similar to those used by Benjamin, the development lengths afforded by which were a constant 10 diameters upstream and downstream. A flow straightener and long section of straightened flexible feed tubing were used upstream to aid development. Further rigid inlet and outlet sections were manufactured with pressure tappings constructed in accordance with the recommendations of British Standard BS 5317: part 2 (1977). Four pressure tappings, of equal radial disposition were located at four different axial planes along these inlet and outlet sections, and pressures at each of the four radial stations was averaged by interconnecting the tappings, as per the above British Standard. Pressure differentials were established using an S.E.1150/D variable reluctance differential pressure transducer supported by a S.E. 905 transducer converter, this pressure measurement arrangement is shown in figure 2.2. Flow rates were measured by electrically monitoring the time taken for a volume of working fluid to pass through the valved test section, and into a receiver. A contact was made, and timing begun, when the fluid reached a pair of electrodes suspended into the receiver, passing current between the electrodes. Timing ceased upon the fluid level reaching a second pair of electrodes. The test rig and monitoring equipment is shown in diagrammatic form in figure 2.3 and photographically







SCHEMATIC OF EXPERIMENTAL TEST RIG

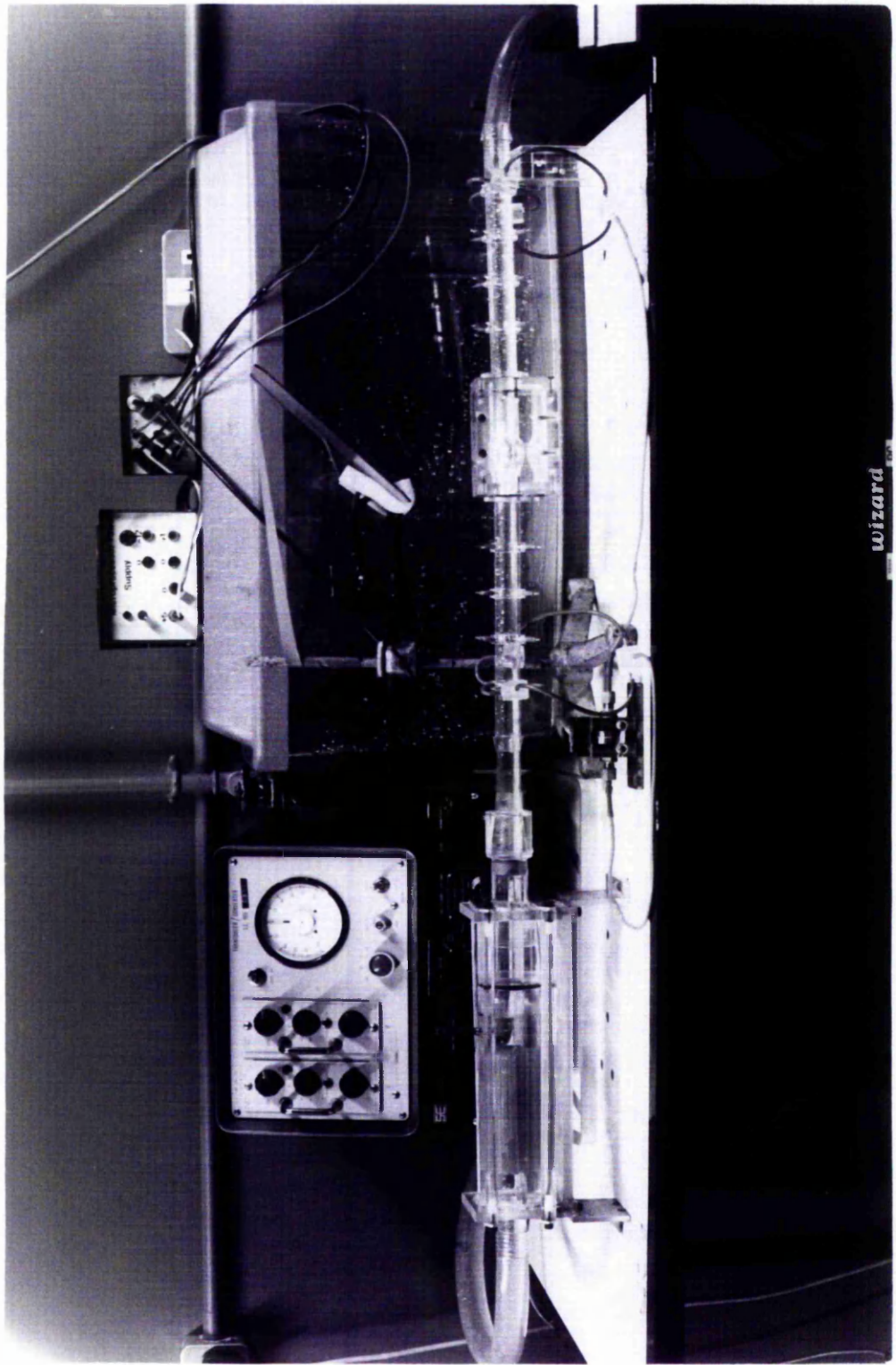
by figure 2.4.

The occluder of the SISO valve was seen to be unstable in water flow rates exceeding 5l/min (Tansley et al 1986) and in order to avoid damage to the perspex prototype valve, by the Stellite ball, it was necessary to fix the occluder in its fully open position. Occluder instability was not evident at any flow rate in the SICO valve.

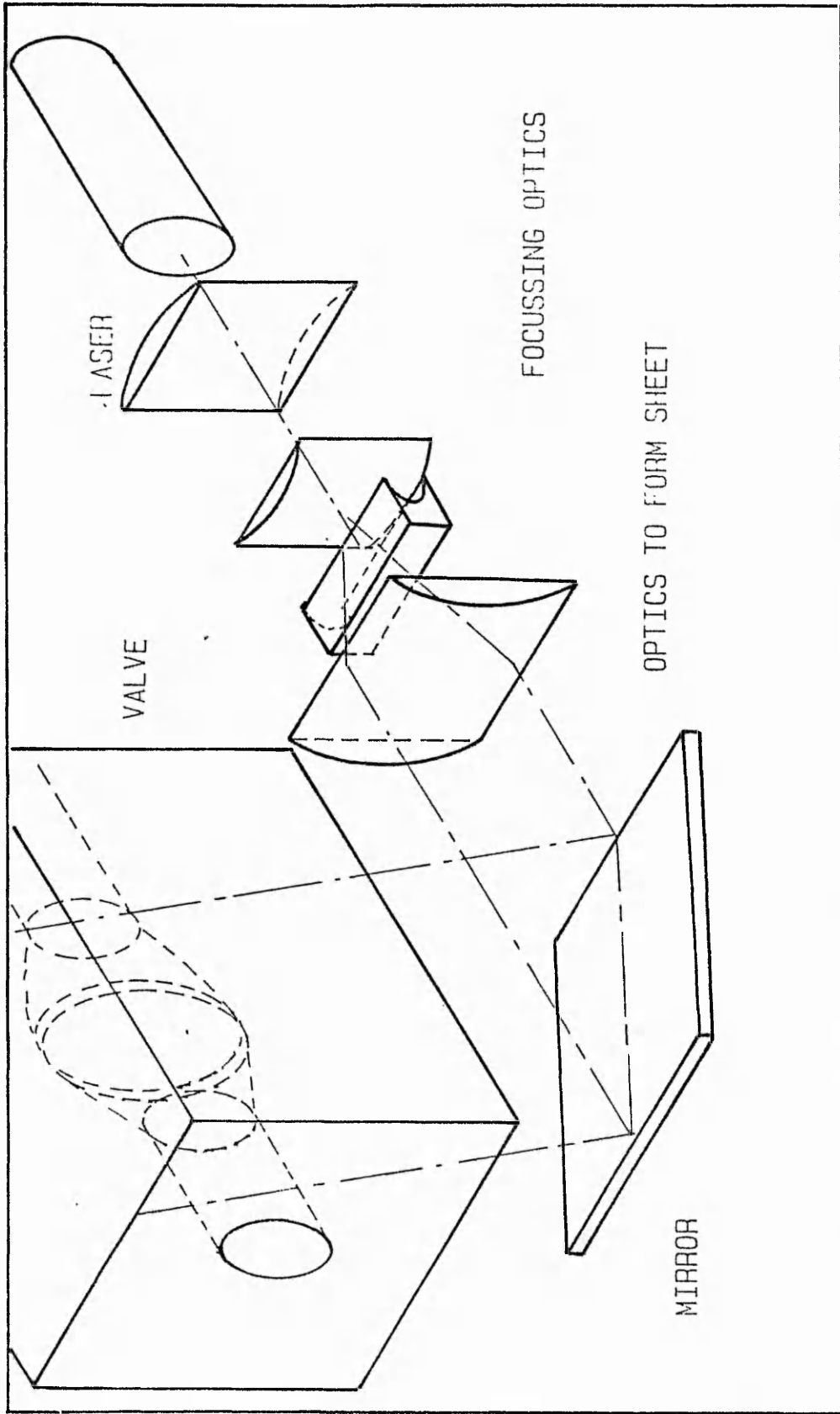
The results of pressure measurement tests, which matched those of Benjamin, for the original (SISO) valve, are shown in a comparison with results of the second prototype (SICO) valve in figure 5.11. More complete discussion of results is given in chapter five. Pressure measurements at a point were not significantly altered when the original single tapped inlet and outlet sections were replaced by the multi-tapped sections.

### 2.3 Streak Photography

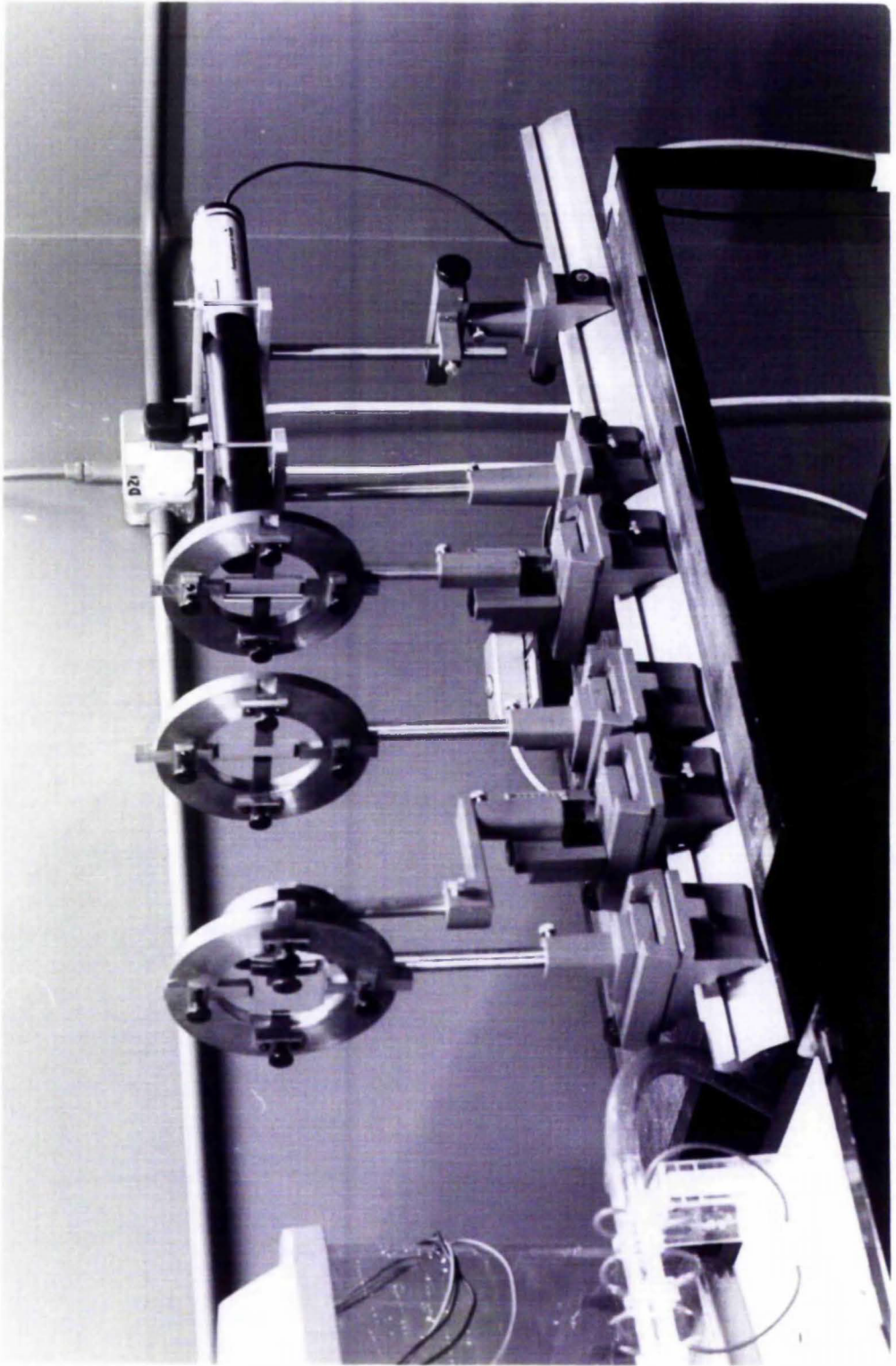
Flow visualisation was carried out using a 10mW Helium-Neon Laser as the light source. The output from the laser was focused to a plane 0.8mm thick, by two plano-cylindrical lenses. The width of the plane was increased by passing the light through a second series of two lenses which diverged the plane to 30mm wide, and then re-collimated the light to form a sheet of dimensions 0.8mm x 30mm. This optical arrangement is shown in figure 2.5 and photographically in figure 2.6. The light sheet was passed through the perspex valve test section and attempts were made to chop the light at irregular intervals to facilitate quantitative flow visualisation by stroboscopic streak photography, in a



Wizard



SCHEMATIC OF OPTICS TO FORM SHEET OF LASER LIGHT FOR FLOW VISUALISATION



manner similar to that employed by Hampshire (1984). The chopping device consisted of a micro computer controlled stepper motor with a flag mounted onto the spindle. Chopping was effected by the flag moving between the laser and correcting/focusing optics.

The fluid medium was seeded with small particles from which the light could be reflected in a side-scatter mode. Selection of the best particles involved surveying those which were neutrally buoyant in the flow medium. Fifteen different particle materials were tried including lobelia and poppy seeds, ground pea, melamine, polyester, impact resistant polystyrene and clear polystyrene. The plastics were milled into sizes ranging from 1.18mm down to 0.063mm mesh size. Particle selection was based on four factors:

- i) nearness to neutral buoyancy in analogue fluid: this was assessed by simply monitoring the time taken for the particles to sink to the bottom of a flask full of blood analogue solution. If particles sank too quickly during flow visualisation studies the monitoring of radial velocity ( $dv/dt$ ) would have been disturbed.
- ii) light scattering ability: Some materials had obviously better light scattering ability in the side scatter mode than others. This was assessed, during particle selection, by monitoring each seeding materials image reflected onto a photographic film. It was necessary to maximise the intensity of light emitted to the recording plane, as this would allow increased velocities to be analysed by reducing

necessary exposure times

- iii) size: light scattering ability generally is enhanced with increasing particle size, but if any density mis-match occurred between flow media and seeding particles then the seeding would lag behind the fluid and not faithfully represent fluid velocities, further high concentrations of relatively large particles would change the flow characteristics of the fluid
- iv) quality of dispersion: It was found that some materials were not suited to being used as seeding particles, as they conglomerated into large groups of particles

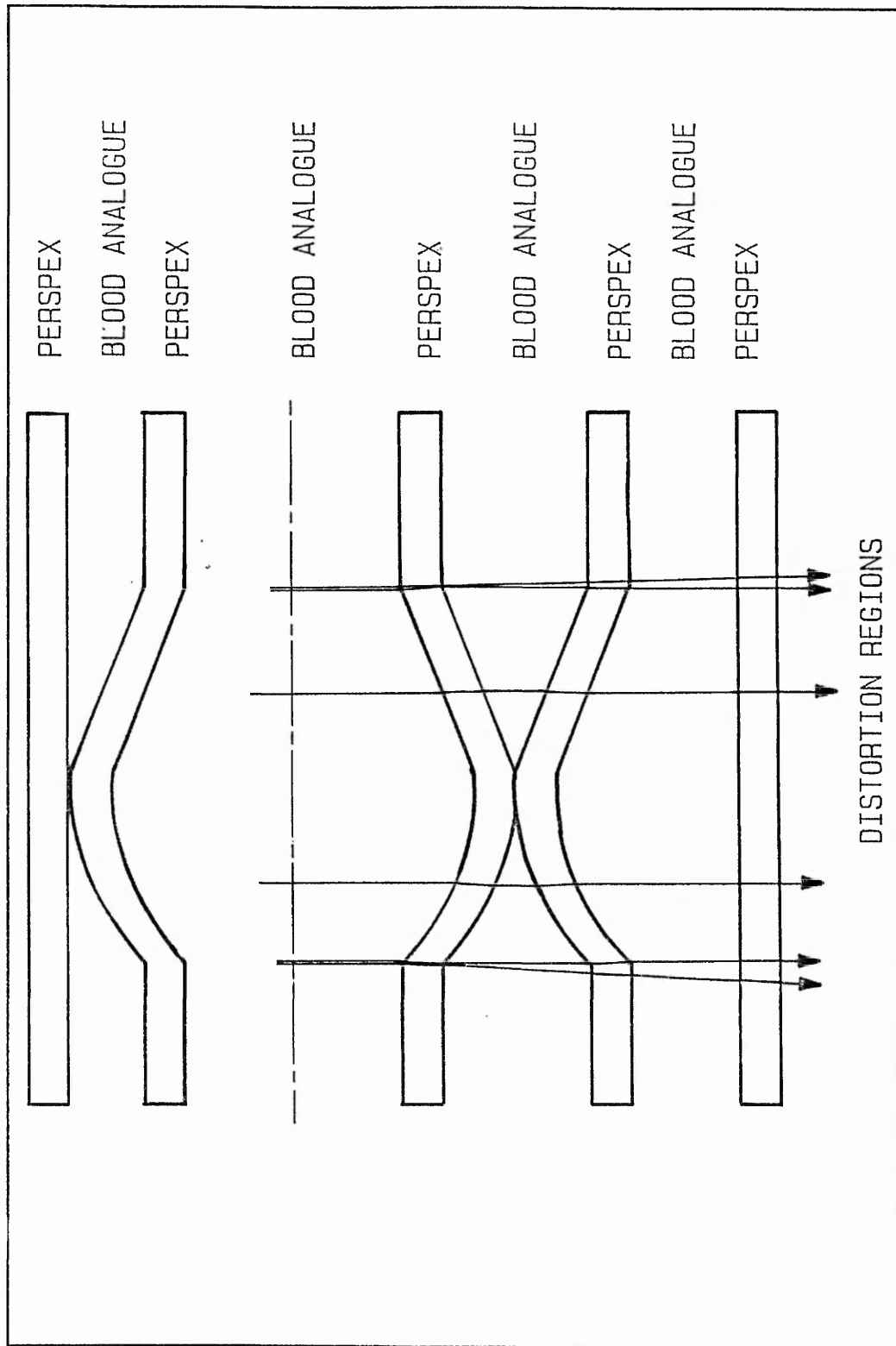
The particles finally chosen were 0.425mm diameter clear polystyrene of density  $1.050\text{kg/m}^3$  as these exhibited the best light scattering properties for small particle size, and the density closely matched that of the analogue fluid, the density of which was  $1.107\text{kg/m}^3$ .

Optical test section design was carried out to account for refraction of light as it traversed the perspex and flow medium. A SICO valve section incorporating correcting lenses was designed to allow for flow visualisation away from the flow axis, to which visualisation was confined in the original SISO valve. Further optical design was carried out to correct distortion in the axial and radial planes, this would allow for the direct measurement of axial and radial velocities without the introduction of errors in streak length due to optical distortion. By filling the lenses and voids with the working fluid, distortion could be controlled

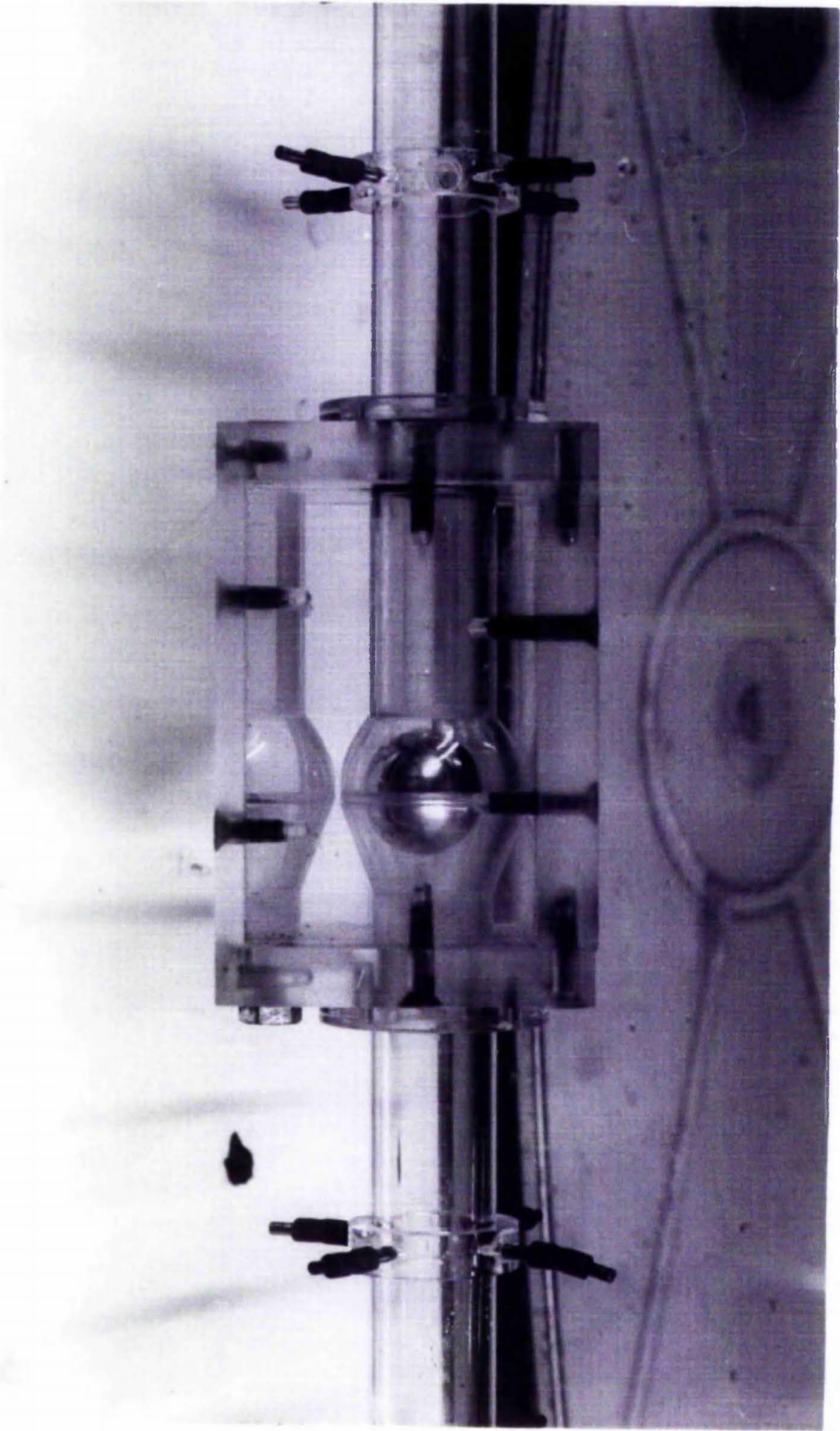
for any transparent flow medium, thus allowing for water and blood analogue solution flow studies. This optical design is shown in figure 2.7 and photographically in figure 2.8.

The recording film, Kodak Panchromatic 2475, was chosen as it displayed extended sensitivity to far-red light radiation. This suited its application to recording light scattered from a Helium-Neon laser which radiated at  $0.633\mu\text{m}$  wavelength. Further advantages of this film were a relatively small grain size for such a high film speed (approximately ASA 1 000/ 31 DIN), high stability of the ester based film and good contrast between in low light conditions.

Results of the flow visualisation studies were disappointing and were necessarily limited to qualitative analysis. This was because the film could not be satisfactorily exposed by the short durations of illumination when the laser beam was chopped, as the light intensities reflected by the particles in this side scatter mode were relatively low. This problem was compounded by poor optical efficiency of the perspex body of the valve prototype and lenses, which had to be omitted to allow for qualitative flow visualisation. The lack of availability of a more powerful laser, finally meant that quantitative studies could not successfully be carried out. Qualitative results were also hampered by these same mechanisms, and in the higher physiological flow rates reflected light intensities were not sufficient to expose the recording film, but intensities were sufficient for manual visualisation. Throughout the range of physiological flow rates of blood analogue solution, recirculation was not apparent in either the SISO or SICO valves.



SCHEMATIC OF SECTION THROUGH SICO  
VALVE WITH CORRECTING LENSES



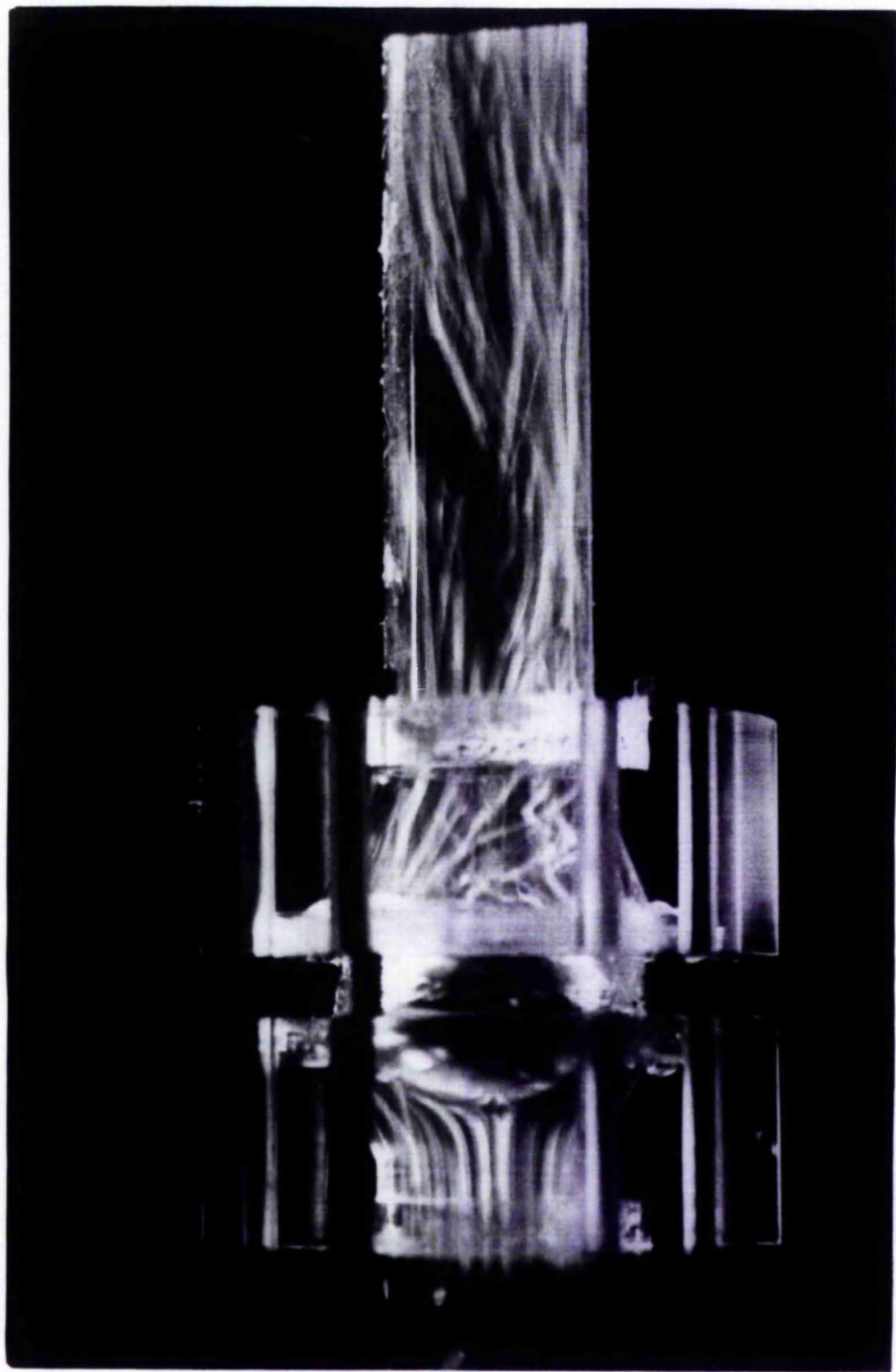
Figures 2.9 and 2.10 show representative streak photographs for blood analogue flow through each of these valves respectively.

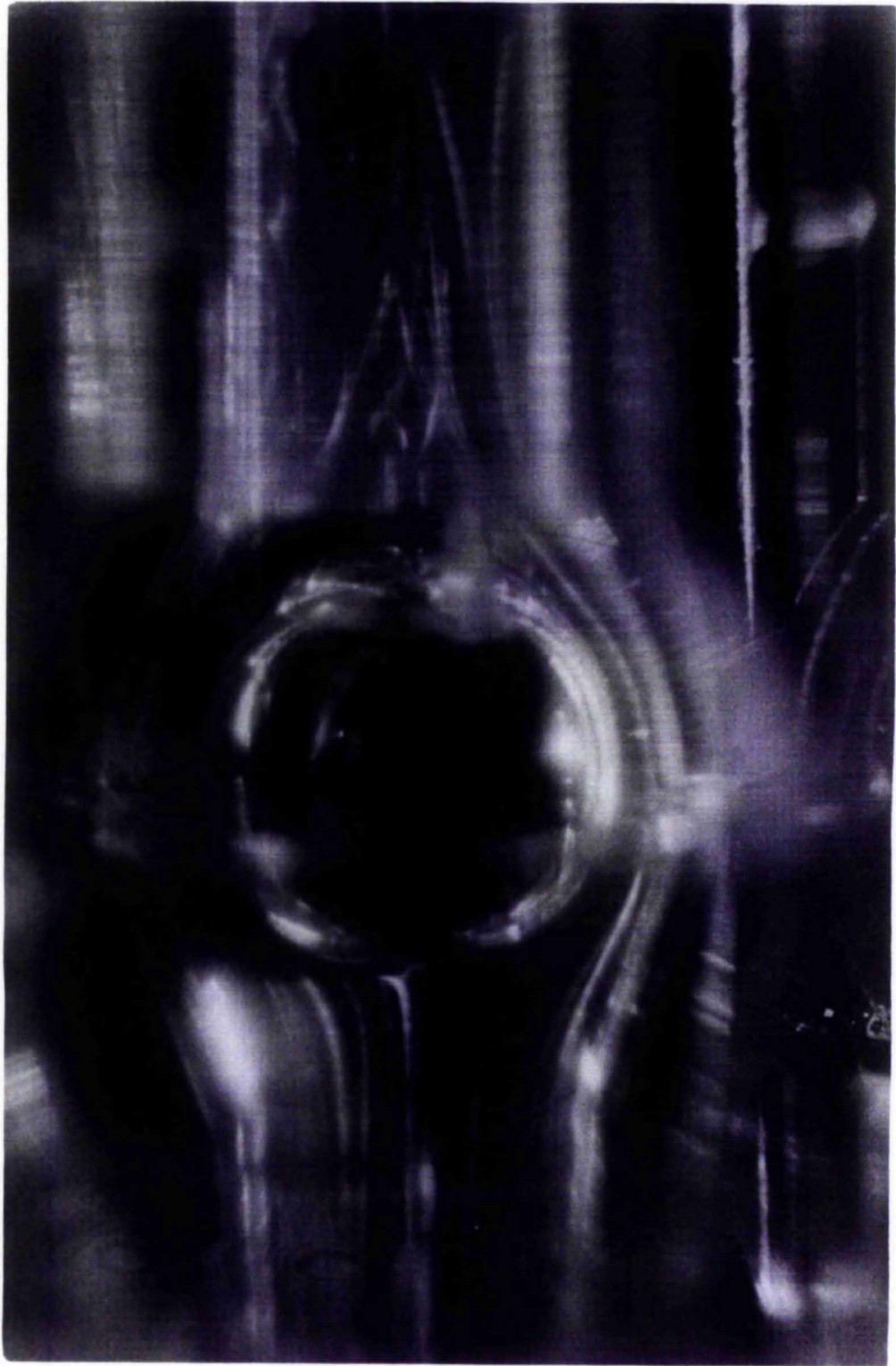
The results of pressure/flow testing are presented and discussed in the relevant sections of chapters five, six and seven later in the thesis.

### In Conclusion

Pressure/flow characteristics of the valve were assessed fully, and agreement with Benjamin (1986) was good, these results were used to verify pressure gradients predicted numerically.

Streak photography results were poor but yielded sufficient information to verify numerically predicted flow fields (chapter six)





CHAPTER THREE

THE RHEOLOGY OF BLOOD AND ITS MATHEMATICAL DESCRIPTION

### 3.1 Introduction

This chapter briefly discusses the general rheological behaviour of blood. Emphasis is placed on mathematical models which best describe the relationship between shear rate and shear stress, and which are capable of incorporation into computational studies. A typical shear rate/viscosity curve for blood is shown in figure 3.1. Many researchers have reasoned that blood may be realistically represented by a Newtonian analogue fluid, as average in-vivo blood shear rates exceed  $100\text{s}^{-1}$ , a value above which blood flow is almost Newtonian (Whitmore 1963). However, shear rates in a cylindrical flow section will vary radially from a maximum close to the wall to almost zero at the flow axis. This means that viscosity will also vary radially, giving rise to a significant variation of velocity profiles between blood and Newtonian fluids (see figure 3.2).

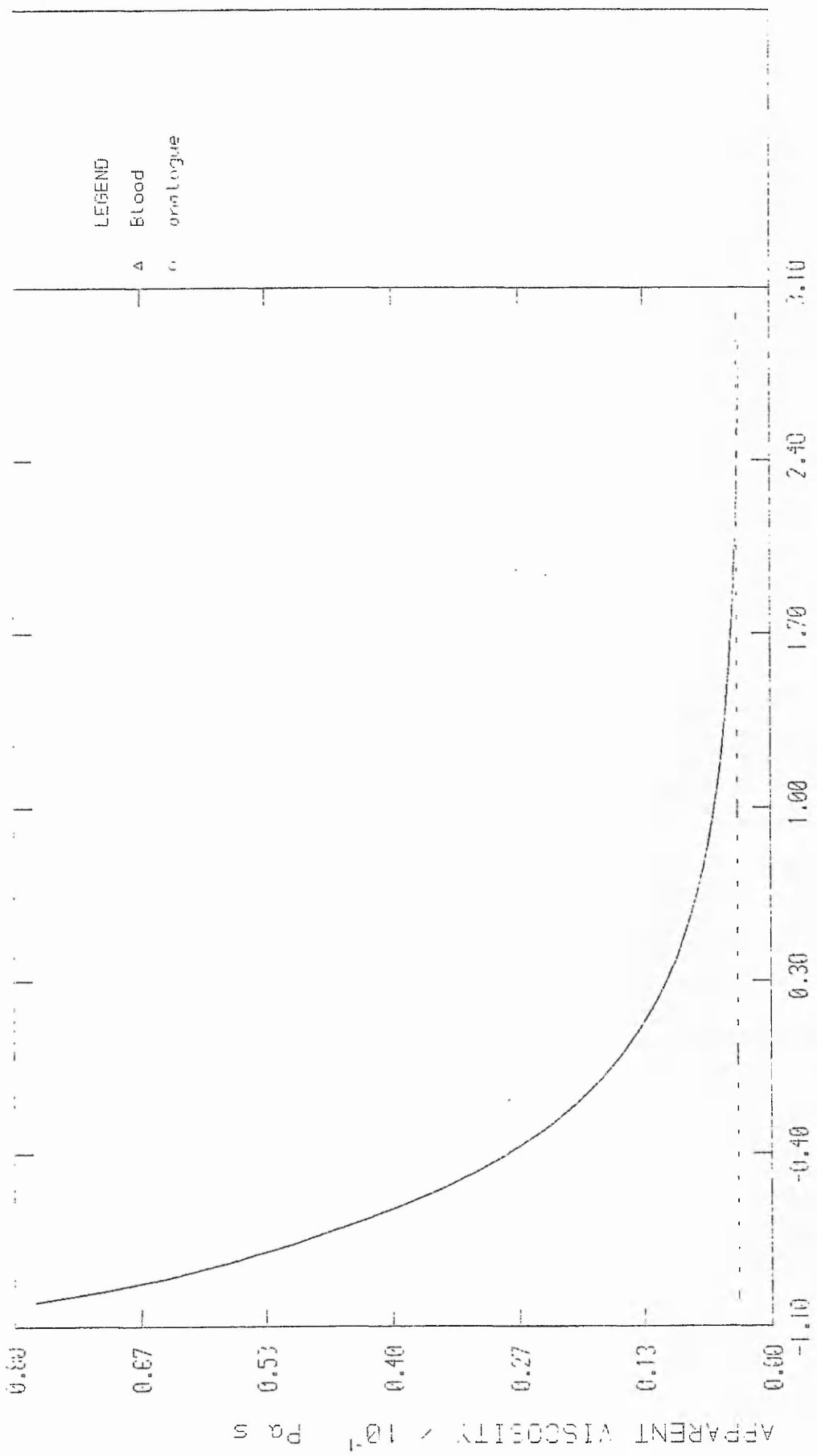
Throughout the chapter blood is generally assumed to be a continuum for the purposes of mathematical modelling and its mean rheological properties are taken to be universally applicable.

### 3.2 Whole Blood

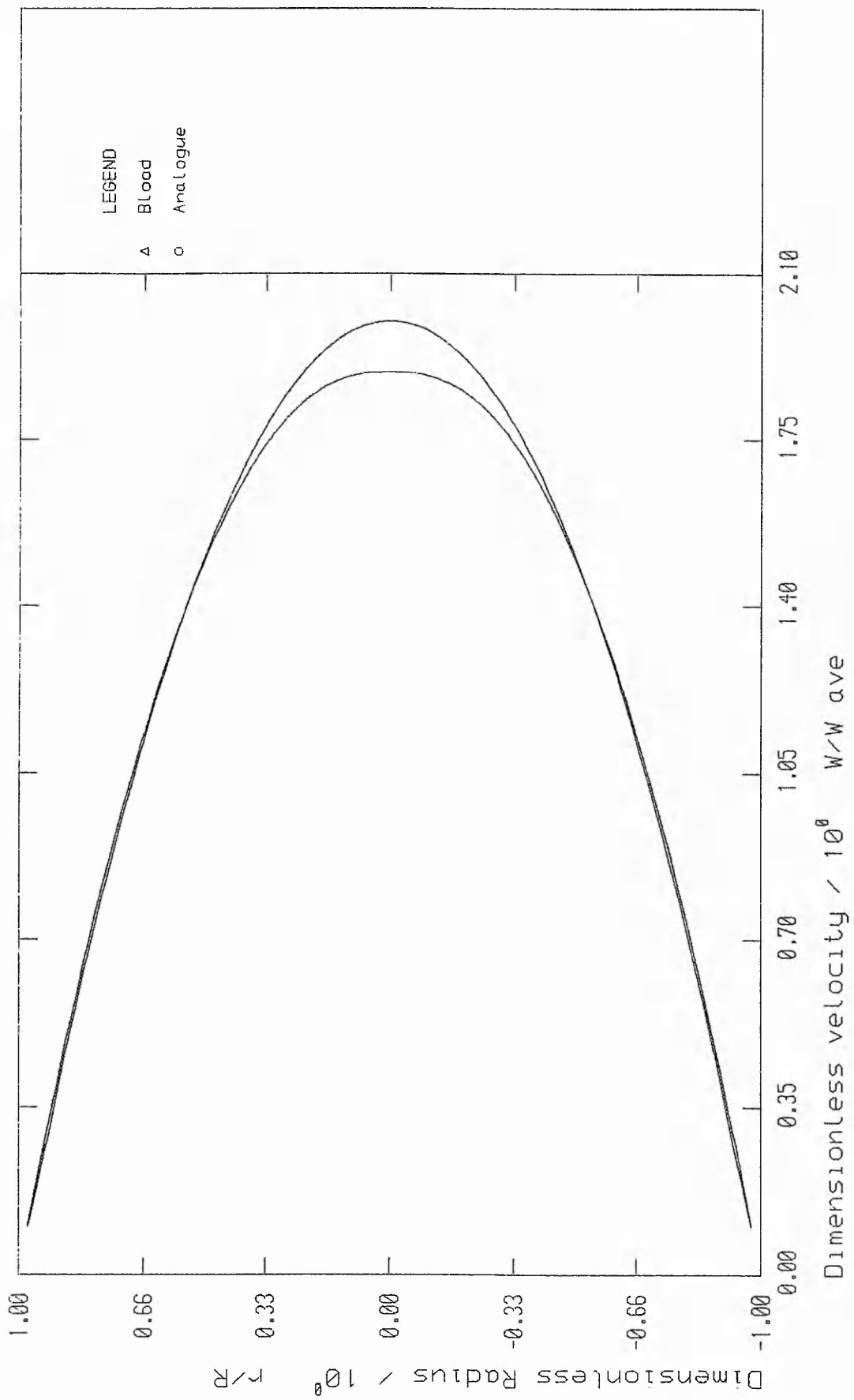
Blood is a non-Newtonian fluid comprising cells and protein in a plasma base:

#### Red Blood Cells (RBCs)

RBCs form the bulk of the blood cells (about 97% of the total cell volume). Their primary function is to carry oxygen suspended in haemoglobin, which forms the contents of the flexible membrane of



NON-NEWTONIAN VISCOSITY DEPENDENCE OF BLOOD WITH INCREASING SHEAR RATE



A COMPARISON BETWEEN VELOCITY GRADIENTS FOR LAMINAR ANALOGUE AND BLOOD PIPE FLOW OF CONSTANT RATE

the RBC. These cells are biconcave discoid in shape and their size is approximately  $8\mu\text{m} \times 2\mu\text{m}$ . Their life cycle starts in the bone marrow where from haemocytoblast cells they undergo several metamorphic changes and are released into the blood as reticulocytes. Within two days they become mature red cells known as erythrocytes. Their life cycle normally ends about 120 days later. The proportion of reticulocytes to erythrocytes is approximately 1%. The concentration of RBCs (erythrocytes) is approximately  $5 \times 10^{12}/\text{l}$  of blood. Expressed as a percentage by volume of whole blood, the haematocrit or packed cell volume is typically 42-45%, though this varies even in healthy people depending on many factors, eg altitude and sex (generally haematocrit is one or two percent lower in women than in men). In unhealthy people the haematocrit can be seen to vary much more, ranging from 20% in severe sickle-cell anaemia to 75% in polycythaemia. Because of the predominance of erythrocytes, heterogeneous models often consider blood to be a suspension purely of these cells as they have a greater influence on the blood viscosity than any other constituent. Another factor that may influence blood viscosity is the formation of rouleaux of erythrocytes, which are aggregates of normally 6 - 10 cells. Secondary aggregation, ie the aggregation of several rouleaux, also occurs and it is argued by many (eg Merrill et al 1963 and Schmid-Schönbien et al 1973) that it is the breakdown of such aggregations that causes the non-Newtonian behaviour of blood. Other researchers, eg Chmiel and Walitza (1980) disagree with this hypothesis, giving as an alternative explanation for the non-Newtonian aspects of blood flow, the changes in viscosity due to absorption of energy by erythrocytes as they deform. They point out that shear thinning is very much reduced in suspensions of

hardened cells. The most likely explanation of viscosity changes, and that adopted by many authors, eg Chien (1971), Cokelet (1978) and Gupta et al (1982) embraces both mechanisms of shear thinning; aggregation of cells at low shear rates, and cell deformation at higher shear rates.

### Leukocytes

leukocytes or white blood corpuscles constitute such a small fraction of total blood cells that their removal from blood does not significantly affect the viscosity of the blood. There are five types of leukocytes; polymorphonuclear neutrophils, polymorphonuclear eosinophils, polymorphonuclear basophils, monocytes and lymphocytes. Their primary function is the destruction of infections. Each of these cells is approximately spherical in shape and their diameters and concentrations are:

polymorphonuclear neutrophils:  $9.4\mu\text{m}$ ,  $4.9 \times 10^9/l$

polymorphonuclear eosinophils  $9.4\mu\text{m}$ ,  $170 \times 10^6/l$

polymorphonuclear basophils  $9.4\mu\text{m}$ ,  $50 \times 10^6/l$

monocytes  $7.4\mu\text{m}$ ,  $2.2 \times 10^9/l$

lymphocytes  $9.5\mu\text{m}$ ,  $460 \times 10^6/l$

### Platelets

Platelets are often considered to be a type of leukocyte, being formed from megakaryocyte cells. Their primary function is the stimulation of blood clotting and it is therefore usual to remove platelets from blood samples being used for in-vitro testing. Apart from a slight reduction of viscosity brought about by platelet removal, haemorheological behaviour is not significantly affected as platelet concentration is small, only  $300 \times 10^9/l$ .

### Blood density

The density of blood is very dependent on haematocrit and on temperature. Chmiel and Walitza (1980) give a mean value of blood density of  $1\ 056.17 \pm 3.4\text{kg/m}^3$  for 47 normal healthy blood samples. This mean value is sufficient for the present work, but a more complete description of blood density variation with haematocrit and temperature can be found in Hinghofer-Szalkay (1985).

### 3.3 Plasma Rheology

Plasma is an aqueous solution of a multitude of mainly organic compounds. Typical concentrations of plasma constituents might be:

#### Proteins:

Albumin ( $37\text{kg/m}^3$ )

Globulins:  $\alpha_1$  ( $4\text{kg/m}^3$ )

$\alpha_2$  ( $7\text{kg/m}^3$ )

$\beta$  ( $9\text{kg/m}^3$ )

$\gamma$  ( $13\text{kg/m}^3$ )

Fibrinogen ( $3\text{kg/m}^3$ )

Lipids ( $5\text{kg/m}^3$ )

Others ( $11\text{kg/m}^3$ ) including:

amino acids ( $0.5\text{kg/m}^3$ )

glucose ( $0.8\text{kg/m}^3$ )

Urea ( $0.3\text{kg/m}^3$ )

Lactate ( $0.1\text{kg/m}^3$ )

inorganic ions ( $9.1\text{kg/m}^3$ )

These constituents have some influence, not only on the viscosity of the plasma, but also on the viscosity and yield stress of whole blood, as described below in section 3.4 and more fully by Whitmore (1968). Plasma is highly non-Newtonian when cooled to 10°C below body temperature, but can realistically be considered Newtonian at body temperature in accordance with the findings of Rand et al (1964). Some stated values for the dynamic viscosity of plasma are:  $1.5 \times 10^{-3} \text{Pa s}$  (Rand et al 1964 and Cokelet et al 1963),  $1.16 - 1.35 \times 10^{-3} \text{Pa s}$  (Cokelet 1987),  $1.10 - 1.16 \times 10^{-3} \text{Pa s}$  (Whitmore 1968).

#### Plasma density

Whitmore (1968) states the density of plasma to be  $1.053 \text{kg/m}^3$ , which is in keeping with the findings of Chmiel and Walitza (1980) who give a value of  $1.025.88 \pm 1.15 \text{kg/m}^3$  at 23°C.

### 3.4 Yield Stress

A yield stress is reported by many researchers (Cokelet et al 1963, Whitmore 1968, Merrill et al 1963) to occur in blood when sheared in a static situation, ie sheared from rest. The mechanism for this is possibly due to the formation of rouleaux, the yield stress being a measure of the energy necessary to breakdown the bonding between aggregations of cells experienced by stationary blood. Walburn and Schneck (1976) argue that this is likely not to occur in physiological pulsatile flows, as the time allowed in such regimes is not sufficient for the formation of such aggregations. The value of the yield stress is a much debated parameter and some researchers doubt its existence at all. Chmiel and Walitza (1980) suggested that even in static shear, if

sufficiently accurate viscometers are applied at very low shear rates, then a yield stress would not be detectable. Throughout this work the existence of a yield stress has been assumed because this is a prerequisite of all the constitutive equations considered below, except Walburn and Schneck's. If this assumption is incorrect, then only shear stress predictions at the lowest shear rates ( $< 1s^{-1}$ ) will be erroneous.

Merrill et al (1963) developed a relationship for the prediction of yield stress ( $\tau_y$ ) based on the independent variable of haematocrit:

$$\tau_y^{1/3} = A(H - H_m)/100 \quad [3.1]$$

where:

$$A = (0.8 \times 10^{-3} \pm 0.2 \times 10^{-3} \text{Pa})^{1/3}$$

$H$  = normal haematocrit (usually taken as 45%)

$H_m$  = haematocrit below which yield stress is absent

(Whitmore gives this a value of 5%)

Merrill et al (1963) also suggested that at haematocrit values above 50%, a better correlation could be achieved by using Weltmann and Green's (1943) model:

$$\tau_y = ae^{bH} \quad [3.2]$$

They did not, however pursue this model or put values to the constants "a" and "b" as haematocrits of this magnitude are not common.

Merrill et al (1965b) presented a relationship predicting the effect of haematocrit and fibrinogen on shear stress. A common finding is that when fibrinogen is not present, a yield stress is not apparent.

Documented values of yield stress vary widely from report to report, but some quoted values are:

Whitmore (1968):  $1 \times 10^{-3} \text{Pa} - 6 \times 10^{-3} \text{Pa}$

Merrill et al (1966):  $0 - 14 \times 10^{-3} \text{Pa}$

Charm and Kurland (1965)  $0 - 10 \times 10^{-3} \text{Pa}$

Chmiel and Walitza (1980) 0 (no shear stress)

### 3.5 Experimentally Derived Blood Viscosity Data/Relationships

Several researchers have studied the relationship between shear rate and the prevailing local viscosity of blood, but this relationship is also dependent on so many other rheological factors and influences, such as anticoagulation platelet counts, blood disorders, whether the sample is taken from a smoker or female using oral contraceptives, etc. Most notably those factors which influence blood viscosity are:

- i) Haematocrit
- ii) Temperature
- iii) Protein, fibrinogen, albumin and lipid levels

It is illustrative to look at each of these briefly.

#### Haematocrit

Indisputably the viscosity of whole blood increases with haematocrit. A simple, accurate and widely accepted relationship predicting the variation of viscosity with haematocrit is presented by Begg and Hearns (1966) and Virgilio et al (1964):

$$\text{Log}_{10}(\mu) = m H + c \quad [3.3]$$

where:  $m$  and  $c$  are constants

This relationship certainly agrees with the independent findings of Rand et al (1964) and Lutz and Barras (1983).

Using this relationship as a conversion aid, an increased amount of data is applicable to the study of normal haematocrit blood flow, to which this study has been restricted as far as possible.

### Temperature

Merrill et al (1963) argue that the viscosity of whole blood relative to water ( $\mu_r$ ) is almost linearly proportional to the temperature of the blood, ie:

$$\mu_r = m \theta + c \quad [3.4]$$

where  $\theta$  = temperature of blood ( $^{\circ}\text{C}$ )

m and c are constants

They also suggest that the only mechanism which affects the whole blood's viscosity is the dependence of plasma viscosity on temperature ie, aggregation and flexibility of the erythrocytes is not significantly temperature dependent. Merrill et al (1963) further suggest that the equation applied by Andrade to the prediction of the temperature dependence of water, ie:

$$\mu(\dot{\gamma}) = A(\dot{\gamma})e^{-E/RT} \quad [3.5]$$

where:  $\mu(\dot{\gamma})$  = viscosity at a given shear rate

$A(\dot{\gamma})$  = function of shear rate and blood sample

E = activation energy (J/mole)

R = gas constant

T = absolute temperature

might equally be applied to blood. Neither this, nor equation [3.4] contradict the findings of Schmid-Schönbein et al (1973), Virgilio et al (1964) or Rand et al (1964).

If consideration of blood temperature is made, then in-vitro studies under hyperthermic or hypothermic conditions, which incorporate one or more of the constitutive equations below, become practical. The work described here, however, has been restricted to normothermic conditions.

#### Plasma proteins etc.

The influence of plasma constituents on blood rheology has been studied in great depth and by many researchers. The effect of haematocrit and fibrinogen on the yield stress of blood flow has already been discussed. Tietjen et al (1975) present a study of the influence of plasma globulins plus fibrinogen on the viscosity of blood and infer a linear relationship but correlation is poor. Whitmore (1968) argues that an increase in globulin and fibrinogen levels (above normal physiological concentrations) raises the viscosity of blood because of the increased potential for rouleaux formation, as demonstrated by Fårhaeus (1929). Begg and Hearn (1966) developed an expression of the form:

$$Y = aX_1 + bX_2 + cX_3 + d$$

to determine the effect of the variables haematocrit ( $X_1$ ), fibrinogen ( $X_2$ ) and albumin+globulin ( $X_3$ ), on logarithmic blood viscosity at a given shear rate ( $Y$ ).

Considering all the interest shown over several decades in the effect of plasma proteins on viscosity it is perhaps surprising that of all the constitutive equations examined below, only the model of Walburn and Schneck (1976) considered plasma constituents explicitly.

### 3.6 Blood Models

Blood models can be divided into two general categories, namely those that assume the blood to be homogeneous, and those that assume otherwise.

#### Heterogeneous blood models

As mentioned earlier, when the diameter of a pipe through which blood flows decreases below 0.5mm, blood can no longer be considered as a continuum. Several researchers have proposed heterogeneous models for the description of viscosity (Fårheaus 1929, Fårhaeus and Lindqvist 1931), and to predict the local cell density and plasma slip zone (Hershey and Cho 1966, Gupta et al 1982). These functions can be modelled numerically, but they are not likely to enhance numerical investigations, especially in large vessels, and will introduce as many additional uncertainties as already presented by homogeneous models.

#### Homogeneous models

Blood is heterogeneous, being a concentrated disperse system. The assumption of homogeneity is purely a simplification which aids calculation, but there are flow regimes in which such an assumption is acceptable. Chmiel and Walitza (1980) discuss blood rheology and viscometry with respect to pipe diameter and indicate that, for tubes of diameter greater than 0.5mm, blood may be considered homogeneous. Several viscosity models have evolved which implicitly or explicitly make use of this assumption. The high number of constitutive equations points not only to the importance of establishing mathematically the rheological behaviour of blood, but also to the discord in experimental

findings brought about possibly by the poor recording of exact experimental conditions and assumptions. Furthermore, the variability of blood from sample to sample must account for some of the spread. Some of the most widely accepted constitutive models are:

- i) Power law
- ii) Walburn and Schneck (1976)
- iii) Casson (1959)
- iv) Chmiel and Walitza (1980)
- v) Quemada (1976a,b)

Easthope and Brooks (1980) examined eleven models developed by several researchers, including all those above except for (iv). Here only the best of those models examined by Easthope and Brooks will be discussed:

#### The Power Law

Walburn and Schneck (1976) discuss the popularity of the Casson equation for the prediction of blood viscosity. They point out that the yield stress of blood is measured under static loading conditions, is very small and is mainly due to the formation of rouleaux. They express doubts as to whether a yield stress is manifest in pulsatile flow situations because of the lack of time for rouleaux formation. This argument is born out to some extent in the findings of Cokelet et al (1963). In light of this discussion Walburn and Schneck go on to present an alternative one equation model:

$$\tau = k\dot{\gamma}^n \quad [3.6]$$

or  $\mu_a = k\dot{\gamma}^{n-1}$

This is simply the long established power law equation. They do however, go on to introduce a modified form of this equation, including a yield stress although they do not make use of this:

$$\tau = k\dot{\gamma}^n + \tau_y$$

Their results indicate that the best values of these constants for the one equation model, for blood at 37°C are:

$$k = 0.0134 \times 10^{-3} \text{Pa s}^n$$

$$n = 0.785$$

Hershey and Cho (1966) draw on earlier work which discussed the power law model's insensitivity to temperature. They assigned to the constant "n" the relationship:

$$n = 0.978 - 0.00695H$$

#### Walburn and Schneck (1976)

The one equation model [3.6] with the above constants, did not accurately fit Walburn and Schneck's experimental data, but then no account of haematocrit was taken. Instead of defining different constants for stated haematocrits, Walburn and Schneck re-wrote their model to include haematocrit as a variable in their Best Two Variable Model (BTVM):

$$k = C_1 \exp(C_2 H) \quad [3.7]$$

$$n = 1.0 - C_3 H$$

where, for blood at 37°C:

$$C_1 = 1.48 \times 10^{-3} \text{Pa s}^n$$

$$C_2 = 0.0512$$

$$C_3 = 0.00499$$

$H$  = haematocrit stated as a percentage

This model was reported to be a good statistical fit to experimental data (R-squared value = 0.8789) and compared favourably with that of Sacks et al (1963) who gave the following values to the constants:

$$C_1 = 1.05 \times 10^{-3} \text{Pa s}^n$$

$$C_2 = 0.0054$$

$$C_3 = 0.0045$$

The statistical fit was improved by Walburn and Schneck, still further (to R-squared = .9049) by including plasma proteins into a "Best Three Variable Model" (B3VM):

$$k = C_1 \exp(C_2 H) \times \exp(C_4 (\text{TPMA}/H^2))$$

$$n = 1.0 - C_3 H \quad [3.8]$$

Where, for blood at 37°C:

$$C_1 = 0.797 \times 10^{-3} \text{Pa s}^n$$

$$C_2 = 0.0608$$

$$C_3 = 0.00499$$

$$C_4 = 14.5 \times 10^3 \text{l/kg}$$

$$\text{TPMA} = \text{Total protein Minus Albumin} = 0.0247 \pm 0.00785 \text{kg/l}$$

ref: Ditzel and Kampmann (1971)

$H$  = haematocrit stated as a percentage

In conclusion Walburn and Schneck opt for the use of the "Best Three Variable Model" as the best constitutive equation for the description of whole blood, but do note that each of their independent variables is in fact not independent of the others. All their data pertain to blood samples tested at 37°C. Easthope and Brooks (1980) concluded that Walburn and Schneck's constitutive equation best fitted their data, as compared to all

ten other models they tested. They did, however, re-write the equation (eliminating the TPMA as a variable):

$$\begin{aligned} k &= C_1 \exp(C_2 H) \times \exp(C_{4a}/H^2) \\ n &= 1.0 - C_3 H \end{aligned} \quad [3.9]$$

Values of the four variables of the Walburn and Schneck function presented for Easthope and Brook's population averages for four sample groups of haematocrit adjusted blood at 25°C similar to those of Walburn and Schneck:

$$\begin{aligned} C_1 &= 1.34 \times 10^{-3} - 2.40 \times 10^{-3} \text{Pa s}^n \\ C_2 &= 0.0551 - 0.0613 \\ C_3 &= 0.00433 - 0.00768 \\ C_{4a} &= 340 - 633 \end{aligned}$$

Easthope and Brooks also present standard deviations of each of these parameters for each population. For comparison with other functions, Easthope and Brooks' data for their sample number 29 over the range of shear rates 0.031 - 120s<sup>-1</sup> under steady state has been employed:

$$\begin{aligned} C_1 &= .70 \times 10^{-3} \text{Pa s}^n \\ C_2 &= 0.0366 \\ C_3 &= 0.00389 \\ C_{4a} &= -49.5 \end{aligned}$$

#### Casson equation

$$\sqrt{\tau} = \sqrt{\tau_y} + s\sqrt{Y} \quad [3.10]$$

Several researchers have used this equation as a basis for the description of blood viscosity;

Merrill et al (1965a) Studied pressure - flow relationships in tubes of diameter 0.1 - 1mm. Some interesting arguments presented by them were the dependence of the yield stress on the plasma fibrinogen levels, and their reluctance to accept the concept of a cell depleted slip zone at the tube wall. This might explain the use of tubes of diameter less than 0.5mm contrary to the later findings of Chmiel and Walitza (1980).

Constants used by Merrill et al:

Unspecified temperature and haematocrit

$$\tau_y = 2.25 \times 10^{-3} \text{Pa}$$

$$s = 63.25^{-3} (\text{Pa s})^{1/2}$$

Temperature = 19° C, HCT = 39.3

$$\tau_y = 2.89 \times 10^{-3} \text{Pa}$$

$$s = 72.42^{-3} (\text{Pa s})^{1/2}$$

Temperature = 22.1° C, HCT = 20.1

$$\tau_y = 3.60 \times 10^{-3} \text{Pa}$$

$$s = 52.11^{-3} (\text{Pa s})^{1/2}$$

Charm and Kurland (1965) briefly report the findings of an experimental investigation into the viscosity of blood at 37° C, using three different viscometers. The shear rate ranges of the viscometers were 2 - 230s<sup>-1</sup>, 7.5 - 1 000s<sup>-1</sup> and 1 000 - 10 000s<sup>-1</sup>. Their findings are that the Casson equation can be applied over the entire range of shear rates tested. They also estimate only a 5% error when viscometry results are extrapolated from the range of shear rates 5 - 200s<sup>-1</sup> to 10 000 - 100 000s<sup>-1</sup>

The constants for the Casson equation found by Charm and Kurland are:

$$\begin{aligned} \tau_y &= 0 - 12.96 \times 10^{-3} \text{Pa} && 11.674 \times 10^{-3} \text{Pa mean} \\ s &= 50.596 \times 10^{-3} (\text{Pa s})^{1/2} - 55.972 \times 10^{-3} (\text{Pa s})^{1/2} \\ &&& 52.70 \times 10^{-3} (\text{Pa s})^{1/2} \text{ mean} \end{aligned}$$

Unfortunately they make no mention of the haematocrit of any of their samples, so one must assume a normal mean value of 45HCT. The value they put to yield stress tends very much to err on the high side.

Whitmore (1968) used a model based on the Casson equation:

$$\sqrt{(\tau/\mu_p)} = 1.53\sqrt{\dot{\gamma}} + 2.0 \quad [3.11]$$

in units of Poise and seconds

The equation was used in this form in order that account might be taken of the plasma viscosity. However, Whitmore's equation can be re-arranged to give the Casson equation almost in its standard form:

$$\sqrt{\tau} = 1.53\sqrt{(\mu_p \dot{\gamma})} + 2\sqrt{\mu_p}$$

then  $\tau_y = 4\mu_p$

$$s = 1.53\sqrt{\mu_p}$$

Whitmore assumed a value for plasma viscosity of  $1.2 \times 10^{-3} \text{Pa s}$ , this value is low if compared with the findings of Rand et al (1964) who put the value at around  $1.5 \times 10^{-3} \text{Pa s}$ . However, even using  $1.2 \times 10^{-3} \text{Pa s}$  as the value for  $\mu_p$  leads to the high predicted yield stress of  $4.8 \times 10^{-3} \text{Pa}$ .

Chmiel and Walitza (1980)

Chmiel and Walitza investigated the mechanism by which yield stress is purported to occur and conclude that the yield stresses assumed by other researchers are within the realms of experimental error. Having tested blood viscosity at shear rates as low as  $5 \times 10^{-3} \text{s}^{-1}$ , Chmiel and Walitza also investigate and refute the hypothesis that viscosity variations are due to aggregation. They base this statement on the findings of an experimental investigation into the flow of hardened and unhardened erythrocytes in saline. Their findings show that variable viscosity is a product of the deformation of erythrocytes, deformation being limited at low shear rates because of the "intrinsic rigidity" of the cells and at high shear rates because of the cells approaching maximum deformation. Chmiel and Walitza go on to introduce a seventh degree polynomial equation for the description of blood viscosity with shear:

$$\dot{\gamma} = c\{\tau/a + (\tau/a)^3 + d(\tau/a)^5 + e(\tau/a)^7\} \quad [3.12]$$

Where for haematocrit of 40:

$$a = 0.0114 \text{Pa}$$

$$c = 0.1156 \text{s}^{-1}$$

$$d = -0.032$$

$$e = 1.31 \times 10^{-3}$$

for haematocrit of 44:

$$a = 0.0153 \text{Pa}$$

$$c = 0.128 \text{s}^{-1}$$

$$d = -0.071$$

$$e = 1.716 \times 10^{-3}$$

for haematocrit of 50:

$$a = 0.013\text{Pa}$$

$$c = 0.043\text{s}^{-1}$$

$$d = -0.0326$$

$$e = 0.37 \times 10^{-3}$$

Chmiel and Walitza claim to have achieved good results with this relationship, but its use is limited to shear predictions at very low rates, below  $10\text{s}^{-1}$  as shown in figures 3.3 and 3.4. The usefulness of this function is limited to analytically calculable flow regimes such as simple, laminar tube flow, because the function bases the calculation of shear rate on a known shear stress. The function could not satisfactorily be employed in a CFM study unless complicated and time consuming iterative techniques were used to solve shear stress based on shear rate.

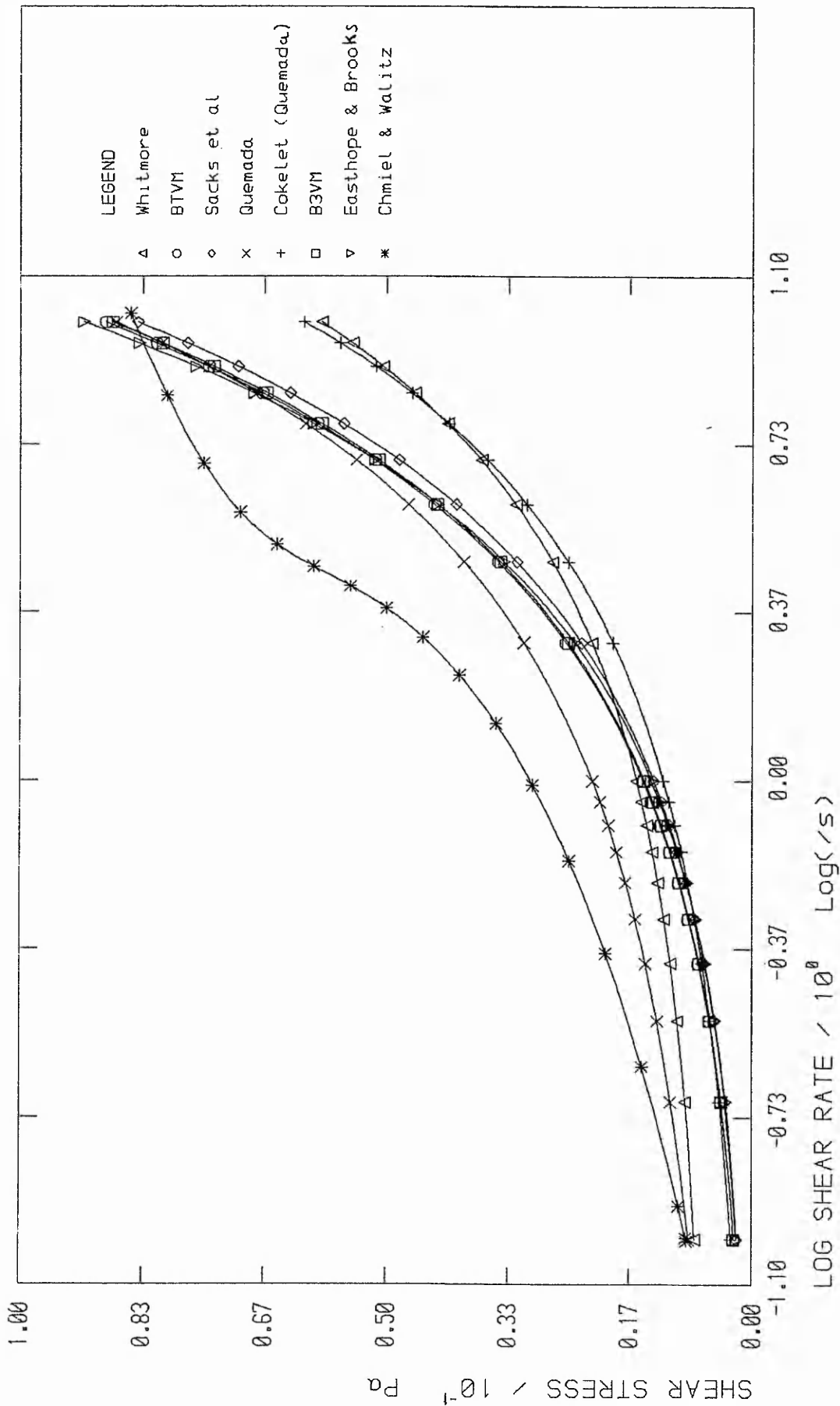
Quemada(1976a and b)

Quemada (1976a and b) discussed the application of a model, devised to predict the viscosity of concentrated disperse systems, to the analysis of blood viscosity based on shear rate and packed red cell volume. Quemada's model which is based on a minimum energy dissipation analysis is more fully discussed, though in terms general to concentrated disperse systems and not blood, in Quemada (1977 and 1978)

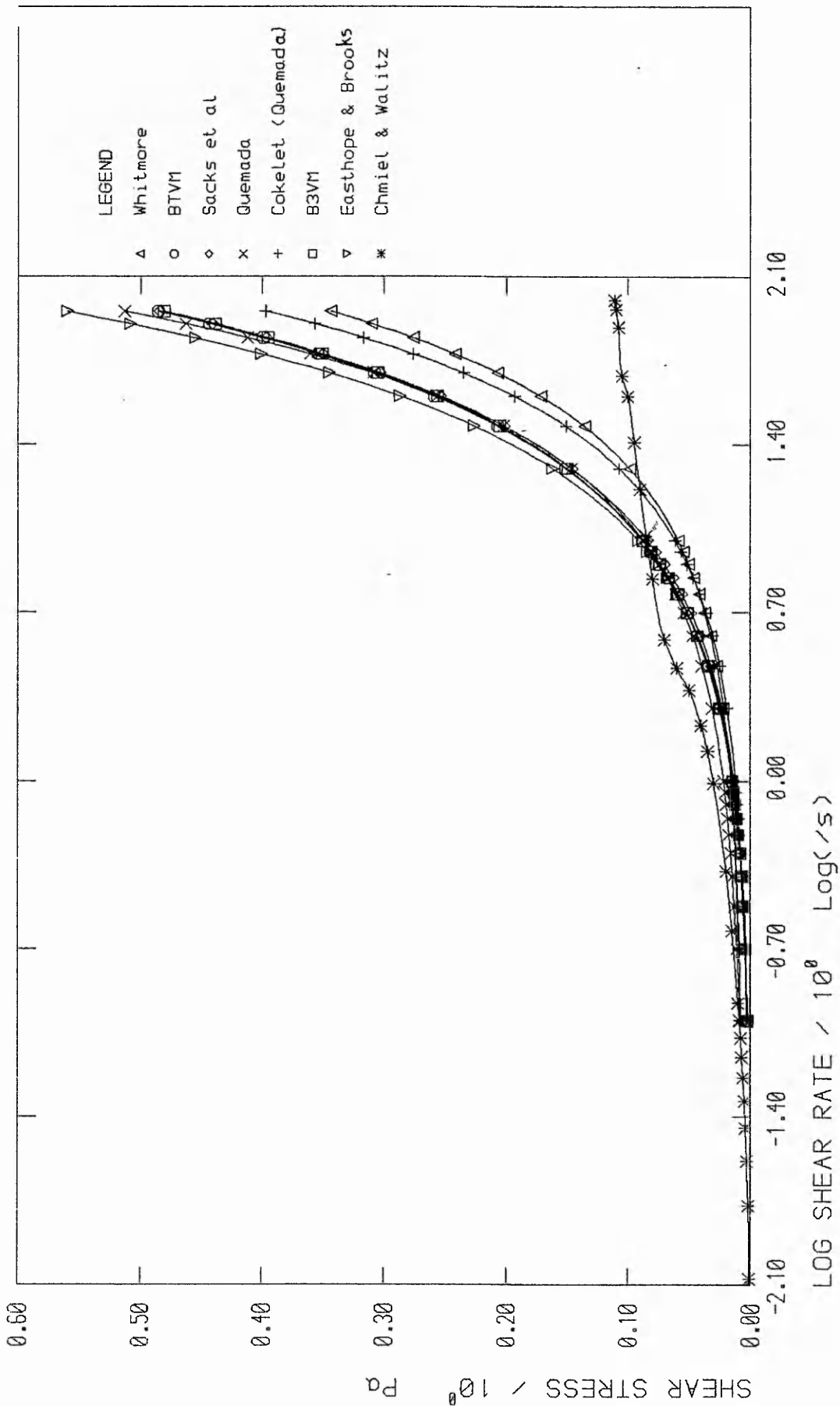
$$\mu_r = \frac{\mu_a}{\mu_p} = (1 - 1/200 kH)^{-2} \quad [3.13]$$

where:

$$k = \frac{\mu_0 + \mu_{\infty} \alpha_0 \sqrt{\dot{\gamma}}}{1 \times 10^{-3} + (\alpha_0 \sqrt{\dot{\gamma}} / 1000)} \quad [3.14]$$



A COMPARISON OF CONSTITUTIVE EQUATIONS: PREDICTED SHEAR STRESS IN BLOOD @ 37 C VS SHEAR RATE



A COMPARISON OF CONSTITUTIVE EQUATIONS: PREDICTED SHEAR STRESS IN BLOOD @ 37 C VS SHEAR RATE

and

$$\dot{\gamma}_c = \alpha_0^{-2} = \text{critical shear rate}$$

Quemada (1976a and b) puts values to the above variables:

for normal whole blood of haematocrit 40, at 37° C

$$\mu_0 = 4.65 \times 10^{-3} \text{ Pa s}$$

$$\mu_{\infty} = 1.84 \times 10^{-3} \text{ Pa s}$$

$$\alpha_0 = 0.67 \text{ s}^{1/2}$$

$$\mu_p = 1.26 \times 10^{-3} \text{ Pa s}$$

for normal whole blood of haematocrit 45, at 37° C

$$\mu_0 = 4.33 \times 10^{-3} \text{ Pa s}$$

$$\mu_{\infty} = 2.07 \times 10^{-3} \text{ Pa s}$$

$$\alpha_0 = 0.73 \text{ s}^{1/2}$$

Quemada notes that when  $\mu_0 > \mu_{\infty}$  a form of the Casson equation is recovered and a yield stress is predicted, though Quemada dismisses the notion of yield stress naming  $\tau_0$  "pseudo-yield stress". He does, however, confirm good agreement with the experimental findings of Merrill et al (1963).

Cokelet (1987) also examined Quemada's equation and gives the following relationships as predictors for the above variables for blood at 37° C:

$$\ln(\mu_0) = 3.874 - 10.41H + 13.8H^2 - 6.738H^3$$

$$\ln(\mu_{\infty}) = 1.3435 - 2.803H + 2.711H^2 - 0.6479H^3$$

$$\ln(\dot{\gamma}_c) = -6.1508 + 27.923H - 25.60H^2 + 3.697H^3$$

Calculating values of these variables for blood at 37° c yields:

for 40 Hct:

$$\mu_0 = 4.426 \times 10^{-3} \text{ Pa s}$$

$$\mu_{\infty} = 1.849 \times 10^{-3} \text{ Pa s}$$

$$\alpha_0 = 0.929 \text{ s}^{1/2}$$

for 45 Hct:

$$\mu_0 = 3.935 \times 10^{-3} \text{ Pa s}$$

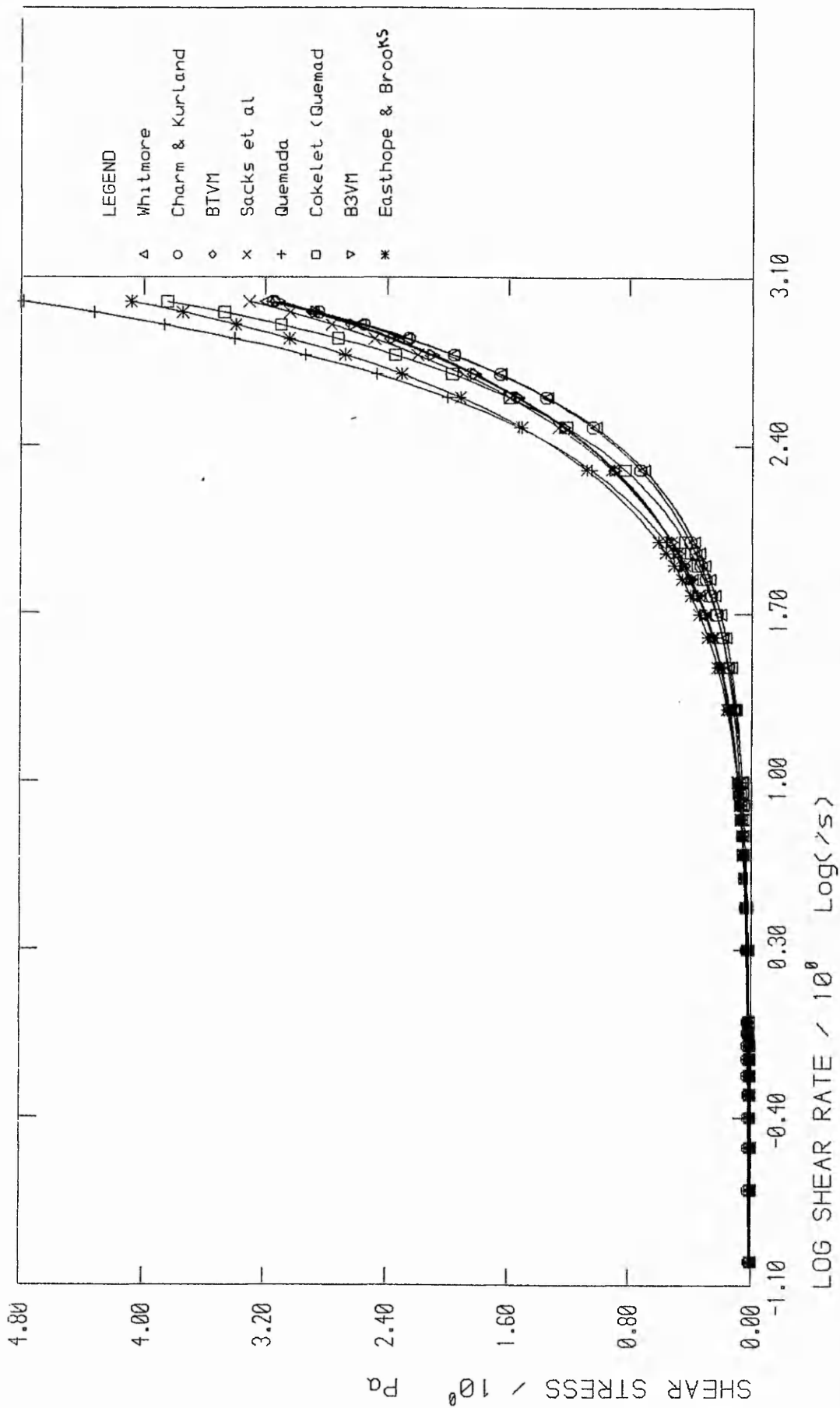
$$\mu_{\infty} = 1.772 \times 10^{-3} \text{ Pa s}$$

$$\alpha_0 = 0.799 \text{ s}^{1/2}$$

### In Conclusion

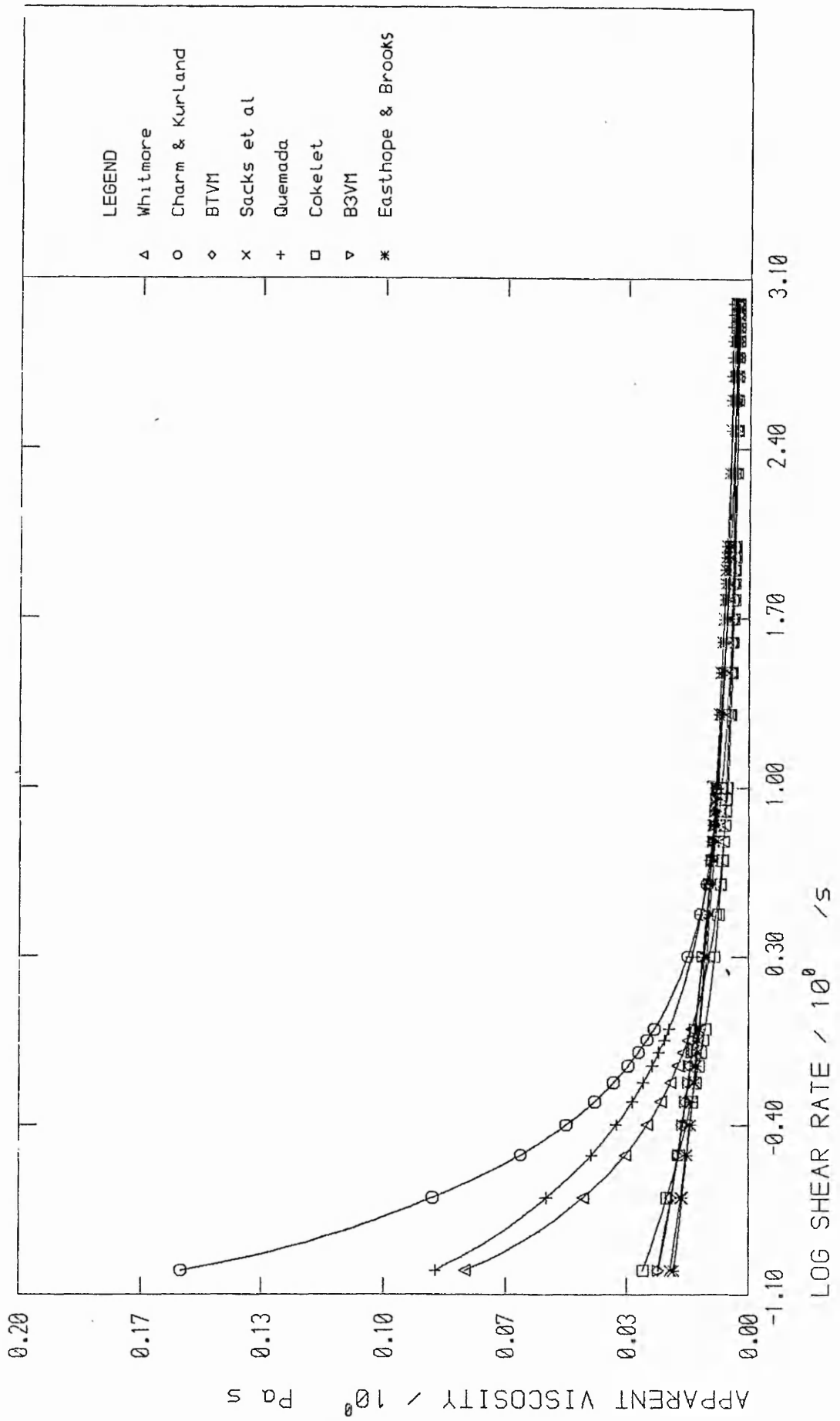
It can be seen from figure 3.5, which shows a comparison of the above constitutive equations in the form of a graph of shear stress against log shear rate for the range of shear rates  $0.1 \text{ s}^{-1}$  to  $1000 \text{ s}^{-1}$  for blood samples of 45% haematocrit, that the spread in shear stress at a given shear rate predicted by the different constitutive equations is very large. The spread is approximately 0% at  $\dot{\gamma} = 0.1 \text{ s}^{-1}$  to 25% at  $1000 \text{ s}^{-1}$ . Figure 3.6 shows the relationship between apparent viscosity and shear rate as predicted by the above constitutive equations for haematocrit of 45%. The variations in predicted values between the different equations is surprisingly large, but the contrast between the relations predicted by the constitutive equations and the Newtonian analogue solution is even more remarkable.

The choice of constitutive equation utilised in a numerical modelling approach must be representative of blood flow, but as seen above the spread is large. Based on figure 3.6 the curve



A COMPARISON OF CONSTITUTIVE EQUATIONS: PREDICTED SHEAR STRESS IN BLOOD @ 37°C VS SHEAR RATE

Figure 3.5



A COMPARISON OF CONSTITUTIVE EQUATIONS PREDICTED APPARENT VISCOSITY OF BLOOD @ 37°C VS SHEAR RATE

which represents the mean was adopted namely that of Whitmore's Casson fit. Further justification for this choice and a more complete discussion is presented in Chapter Four.

CHAPTER FOUR

COMPUTATIONAL MODELLING OF BLOOD AND ANALOGUE FLOW

#### 4.1 Computational Fluid Mechanics

The decision to adopt a computational approach to the analysis of blood flow through heart valve prostheses, in preference to analytical or experimental studies, was based on several factors:

- i) An analytical approach can only be attempted for certain aspects of valve design, eg the reverse flow studies of Gentle (1980) Leefe et al (1986) and then only with very severe restrictions imposed.
- ii) Experimental studies, as discussed in chapter one, are not capable of yielding data comparable to that of CFM studies, and the assumptions necessary about the nature of the flow are just as limiting as those necessary for CFM studies. It was deemed important in this study to be availed not only of those flow parameters obtainable by experimentation, eg velocities, turbulence intensities, pressure drops and streamlines, but also turbulent viscosities, turbulent shear stresses, near-wall velocities and radially variant pressures.
- iii) The opportunity presented by CFM to model the flow of real blood through heart valves was considered important because of the enhanced correlation between design analysis and the clinical situation which would facilitate the forecast of haemolytic and thromboembolic potentials. Experimental flow studies of blood are even more limited than studies involving Newtonian fluids in the amounts of data yielded. Handling problems associated with blood's clotting functions

add to the complexity of experimentation and anticoagulation can affect the overall results.

- iv) In the early stages of prosthesis development a design might be altered several times. If valve performance were to be assessed experimentally then a similar number of test sections would need to be manufactured. In the case of the present design synthesis the manufacture of as many as twenty-six different test sections would have been necessary. The manufacture of such complex sections is very difficult and if dimensional accuracy is to be high, then manufacturing time becomes significant. In comparison, once the computational solution procedure was verified and grid generation coding written, a valve could be modelled geometrically within a few minutes and stationary flow through it could be numerically modelled within four hours real time.
- v) Results analysis is simplified and enhanced by built-in graphics and data handling facilities within CFM codings.

The use of Computational techniques did not, however, eliminate totally the need for experimentation, as a cross check with experimental findings was essential for the verification of computational predictions. Furthermore, computational studies are in all practicality limited to stationary flow, because of the breakdown of the  $k - \epsilon$  turbulence model and the excessive Central Processor Unit (CPU) time necessary to model such non-stationary flow to an acceptable degree of temporal resolution. Pulsatile flow experiments will therefore be necessary in the

conceivable future.

Several CFM studies of heart valve flow have been carried out to date, but most have only considered laminar flow. They will be briefly reviewed as follows:-

Underwood and Mueller (1977)

Present a finite difference study of laminar, Newtonian flow in a geometry which approaches that of a caged disc valve. In their study they recognise the potential contribution that computational fluid mechanics might offer to the assessment of thrombotic and haemolytic potentials. Furthermore they examine recirculation and the maximum shear stresses established due to the interaction of valve components on the flow and also present wall shear stress profiles. Their model is, however, limited considerably by the simplicity of the regime geometry; basically two step blockages in a half cylindrical section. Flow is only analysed in the range of Reynolds' numbers 20 - 1 300.

Underwood and Mueller (1979)

Continue their work from 1977 but with a geometry enhanced by the utilisation of a non-uniform mesh. The flow situations studied are of Newtonian fluid with Reynolds' numbers varying from 50 - 600.

Idelsohn et al (1985)

Present a computational flow study using Finite Element techniques. The geometries used are accurate representations of caged disk and ball valves and a tilting disk valve. They give examples of full field shear stress and velocity vectors and

contours along with pressure gradients across the valve. Their study is also limited to laminar Newtonian flow in the range 100 - 2 000 Reynolds' numbers.

Merchant and Mazumdar (1987)

Have recently addressed the non-Newtonian considerations of blood flow via numerical modelling. Their model was very simple, laminar and orthogonal and used the power law to model the non-Newtonian aspects of blood flow:

$$\tau = k\dot{\gamma}^n$$

Convergence broke down at  $n = .75$  whereas the suggested value for blood flow should be around .66. They concluded that non-Newtonian models only made a difference below 200 Re even though they came up with the almost contradictory predictions of increased thrombotic potential and higher velocities, both in the forward and reverse directions, due to the non-Newtonian flow. They also found that shear stresses throughout were higher in Newtonian flow than in non-Newtonian. Their model is again limited to laminar flow and concern must surely be expressed over their use of such high Reynolds' numbers (up to 6 000) for laminar flow. Furthermore they, themselves, express concern at possible non-convergence.

Thalassoudis et al (1987)

Presented a study of turbulent flow through a Boundary Fitted Coordinate modelled Starr-Edwards valve. Their results are very encouraging, comparing well with experimentally determined data, and they considerably enhance the argument for computational analysis of heart valves. However, this paper again does not consider non-Newtonian flow.

The study described here aims to present a flow situation which more closely represents the in-vivo regime to which a prosthesis would be subjected. This is achieved by combining many of the above modelling complexities; curvilinear geometries, non-Newtonian fluid and turbulence. Further, the flow geometry will be wholly representative of the functional valve, being an integral part of a conduit, and results will be analysed in an attempt to predict thromboembolic and haemolytic potentials.

#### 4.2 A Blood Viscosity Model for CFM

Throughout this work it has been assumed that blood flow is well represented by a homogeneous bulk fluid model. This has restricted the scope of the work to regimes not smaller than 0.5mm, as Chmiel and Walitza (1980) showed that below this diameter continuum models are devalued by the dependence of the plasma slip zone on Haematocrit and flow rate or, in tubes of diameters approximating the erythrocyte diameter, by the Fårhaeus - Linqvist (1931) effect.

As the rheology of blood is that of a plastic fluid a constitutive equation is necessary to describe the shear stress/shear rate relationship, but due to the complexity of blood flow it is not possible to derive any such equation from first principles. Each model then has a certain amount of empirical input. Cokelet (1987) reviews several such equations. Most of the constitutive equations reviewed in chapter three are suitable for application to CFM studies with one notable exception - that of Chmiel and Walitza (1980), which requires foreknowledge of the shear stress in order to calculate the shear

rate. The other equations base their calculation of shear stress on a pre-determined shear rate. The constitutive equation used as a model for blood in this present study was that of Casson (1959):

$$\sqrt{\tau} = \sqrt{\tau_y} + s|\dot{\gamma} \quad [3.10]$$

The reasons for selecting the Casson equation in preference to any of the other constitutive equations were:

i) Ease of application to CFM studies:

As the  $K - \epsilon$  model uses the shear rate term  $\dot{\gamma}$  in the calculation of the turbulent viscosity and provision is already made within PHOENICS to provide  $\dot{\gamma}$ , it is relatively straight forward to utilise this parameter as the basis for the blood viscosity model. The limited number of constants needed by Casson's model, whilst maintaining high accuracy, greatly enhances the ease of its use.

ii) Ease of determination of the empirical constants:

Further to the discussion of blood viscosity models presented in chapter three it became obvious that because of the poor way in which experimental findings and variables are presented in journals etc., it was necessary to use a model that can be verified against the work of several researchers. The model that falls most readily into this category is the Casson equation. This model has been used to fit the experimental findings of several studies, most notably Rand et al (1964) and Charm and Kurland (1965). The model proposed by Quemada (1976a,b) can also be reduced to the form of the Casson equation, which is helpful as most of the data required to form the constants needed by Quemada's

Quemada's model are not usually available in articles presented in journals. The other models discussed in chapter three suffer from too high a complexity, requiring such vague parameters as, for example, TPMA.

iii) Accuracy:

The accuracy of the model itself is high, falling within 5% error over the range of shear rates 0 - 100 000s<sup>-1</sup>, as discussed by Charm and Kurland (1965). The models presented in chapter three predict a large spread of viscosities for a given shear rate, whereas the Casson equation yields the median line.

iv) Good agreement with experimental studies:

A difference of only 4.5% was seen in the predicted pressure gradient when compared with the work of Hershey and Cho (1966) for blood flow of haematocrit 40 at 27°C through small bore tubing.

#### 4.3 The Development of a Computational Model

When applying computational modelling to complex flow regions such as heart valves it is essential to develop the model in a step by step manner. This allows for the verification of every step before proceeding to the next, because necessarily a point is reached beyond which results can not be verified. This was so in the final analysis of shear stress predictions in blood flow through the ball valved conduit. The blood model and shear stress predictions were verified in a simpler (pipe) geometry and

pressure flow characteristics of the ball valve geometry were verified for Newtonian flow cases. In the final analysis when all of these steps are put together, confidence in predictions can only be based on the success of the preceding constituent steps.

#### 4.4 Laminar Flow

The modelling of simple laminar pipe flow aided in the verification of correctness of pressure and momentum predictions (in the form of development lengths and velocity profiles) and in confirming the validity of the shear stress predictor.

Experimental comparisons were made against analytical solutions for the following parameters:-

- i) Velocity profile defined by

$$w = \frac{\Delta P}{4\mu l} (R^2 - r^2) \quad [A1.7]$$

- (ii) Pressure gradient for the Laminar Newtonian flow situation given by Darcy's equation for pipe flow

$$h_f = \frac{\Delta P}{\rho g} = \frac{4f l}{d} \frac{w^2}{2g} \quad [4.1]$$

where  $f$  the friction factor is defined by

$$f = \frac{\tau_w}{1/2 \rho w^2} = \frac{16}{Re_d} \quad [4.2]$$

- (iii) Development length  $X$  utilising Boussinesq's "transition length" formula, where the transition length is defined as the distance along the pipe at which the velocity does not

vary from the final velocity by more than 1%.

$$X/d = 0.065 \text{ Re}_a \quad [4.3]$$

iv) Shear stress, which should obey the radial distribution relationship:

$$\tau = \tau_w \frac{r}{R} \quad [4.4]$$

#### 4.5 Blood Model

Application of the Casson equation to the CFM study was achieved by replacing the fluid's intrinsic (laminar) viscosity with the apparent non-Newtonian viscosity:

$$\mu_L = \mu_a = (s\sqrt{\dot{\gamma}} + \sqrt{\tau_y})^2 / \dot{\gamma} \quad [4.5]$$

where the constants  $s$  and  $\sqrt{\tau_y}$  were varied to suit the particular properties of blood specimen and flow temperature, but generally their allotted values were:

$$s = 0.053001(\text{Pa s})^{1/2}$$

$$\tau_y = 0.0048\text{Pa}$$

In turbulent regimes the effective viscosity was considered to be the sum of "laminar" and "turbulent" viscosities:

$$\mu_{\text{eff}} = \mu_a + \mu_T$$

Verification of the accuracy of blood flow models was carried out by comparison with pressure gradients found experimentally by Hershey and Cho (1966), while velocity profile and shear stress predictions were derived semi-empirically based on the Casson equation and on first principles. Flow parameters in blood flow (even laminar) can not be derived analytically from first principles, as present day knowledge of the shear stress/shear rate relationship in concentrated disperse systems is inadequate.

It was necessary therefore to incorporate into computational and analytical modelling an empirically derived constitutive equation. Working with the Casson equation as the descriptor of apparent viscosity a velocity profile can be developed for the purpose of comparison with CFM results (see Appendix 1 for full derivation):

$$w = \frac{1}{s^2} \left( \tau_y^2(R-r) - \frac{4}{3\tau_y} \sqrt{\frac{\Delta P}{2l}} (R-r)^{3/2} + \frac{\Delta P(R-r)^2}{4l} \right) \quad [A1.11]$$

Shear stress profiles in laminar solutions should still obey the relationship [4.4] above though shear stress profiles in non-Newtonian flow must obviously be non-linear.

#### 4.6 Turbulence Modelling

As discussed earlier, it was necessary to adopt a turbulence model into the computational studies. The  $k - \epsilon$  turbulence model (Launder and Spalding 1974) was chosen because this model is, to date, the most reliable in a wide range of flow regimes. This turbulence model was expected to perform well in the conduit geometry because of its general similarity with the backward facing step geometry which was used as a bench test as reported by Nallasamy (1987). In that work the PHOENICS  $k - \epsilon$  model performed well. Furthermore the experience of Thalassoudis et al (1987) with a similar model showed that it has promise.

The model has its foundations in Boussinesq's Eddy-Viscosity concept which assumes the turbulent shear stresses to be proportional to the mean velocity gradients:

$$\tau = - \overline{u'v'w'}$$

This is translated into the concept of a turbulent viscosity which is wholly flow regime dependent, but which finds application in a

way analogous with laminar or fluid intrinsic viscosity, ie

$$\tau_T = \mu_T \gamma$$

so that

$$\mu_{eff} = \mu_L + \mu_T$$

where:

$\mu_L$  = intrinsic viscosity of the fluid. In the case of complex viscosities  $\mu_L = \mu_a$  and is found from the applied constitutive equation.

$\mu_T = C_\mu C_D \rho k^2 / \epsilon$  assuming  $\rho k^2 / l$  in the Prandtl (1945) - Kolomgorov (1942) equation to be proportional to  $\epsilon$ . The turbulent kinetic energy,  $k$  and the energy dissipation rate,  $\epsilon$ , are calculated at each cell by the generalised differential equations (Jones and Launder 1972):

$$\rho \frac{Dk}{Dt} = \frac{\partial}{\partial y} \left( \frac{\mu_T}{\sigma_k} \frac{\partial k}{\partial y} \right) + \mu_T \left( \frac{\partial u}{\partial y} \right)^2 + \frac{\partial u}{\partial y} - \rho \epsilon \quad [4.6]$$

$$\rho \frac{D\epsilon}{Dt} = \frac{\partial}{\partial y} \left( \frac{\mu_T}{\sigma_\epsilon} \frac{\partial \epsilon}{\partial y} \right) + C_1 \frac{\epsilon}{k} \mu_T \left( \frac{\partial u}{\partial y} \right) + - C_2 \frac{\rho \epsilon^2}{k} \quad [4.7]$$

Throughout this study, the constants have been assigned standard values (Launder and Spalding 1974, Rodi 1980):

$C_\mu$	$C_D$	$\sigma_k$	$\sigma_\epsilon$	$C_1$	$C_2$
0.5478	0.1643	1.0	1.314	1.44	1.92

At the wall the turbulence model is tailored somewhat and the zero slip assumption is applied by way of a wall function. The friction factor at the wall was dictated by either of two selectable in-built functions:

i) Power law function based on Blasius' equation:

$$S_{\phi} = 0.0395/Re_w^{1/4}$$

where  $Re_w$  is as defined below.

This wall function was the simplest and first choice, because of its ease of comparison when checking pressure gradients in a long-hand manner, but proved to be most unsatisfactory yielding errors as great as 30%.

ii) Logarithmic wall function: most commonly used in conjunction with the  $k - \epsilon$  turbulence model. The friction factor is established iteratively by the implementation of the relationship:

$$S_{\phi} = \{\kappa/\ln(1.01 + E(Re_w)S_{\phi}^{1/2})\}^2 \quad [4.8]$$

where for a smooth wall:

$$\kappa, \text{ Von Karmans' constant} = 0.435$$

$$E, \text{ Van Driest's constant} = 9.0$$

In the laminar sub-layer ( $y^+ < 11.5$ ) the above logarithmic wall function is not applicable and the standard laminar descriptor for friction factor is maintained:

$$S_{\phi} = 1/Re_w$$

where:

$S_{\phi}$  = generalised friction factor

$$y^+ = \delta U_{\tau} / \nu$$

$U_{\tau}$  is the friction velocity =  $(\tau/\rho)^{1/2}$

$$Re = w\delta\rho/\mu_L$$

$w$  is the velocity at a point

$\delta$  is the wall-to-cell centre distance

The turbulent kinetic energy and its dissipation rate are dictated

by the relationships:

$$k = \frac{U_{\tau}^2}{(C_{\mu} C_D)^{1/2}} \quad [4.9]$$

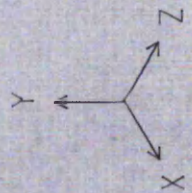
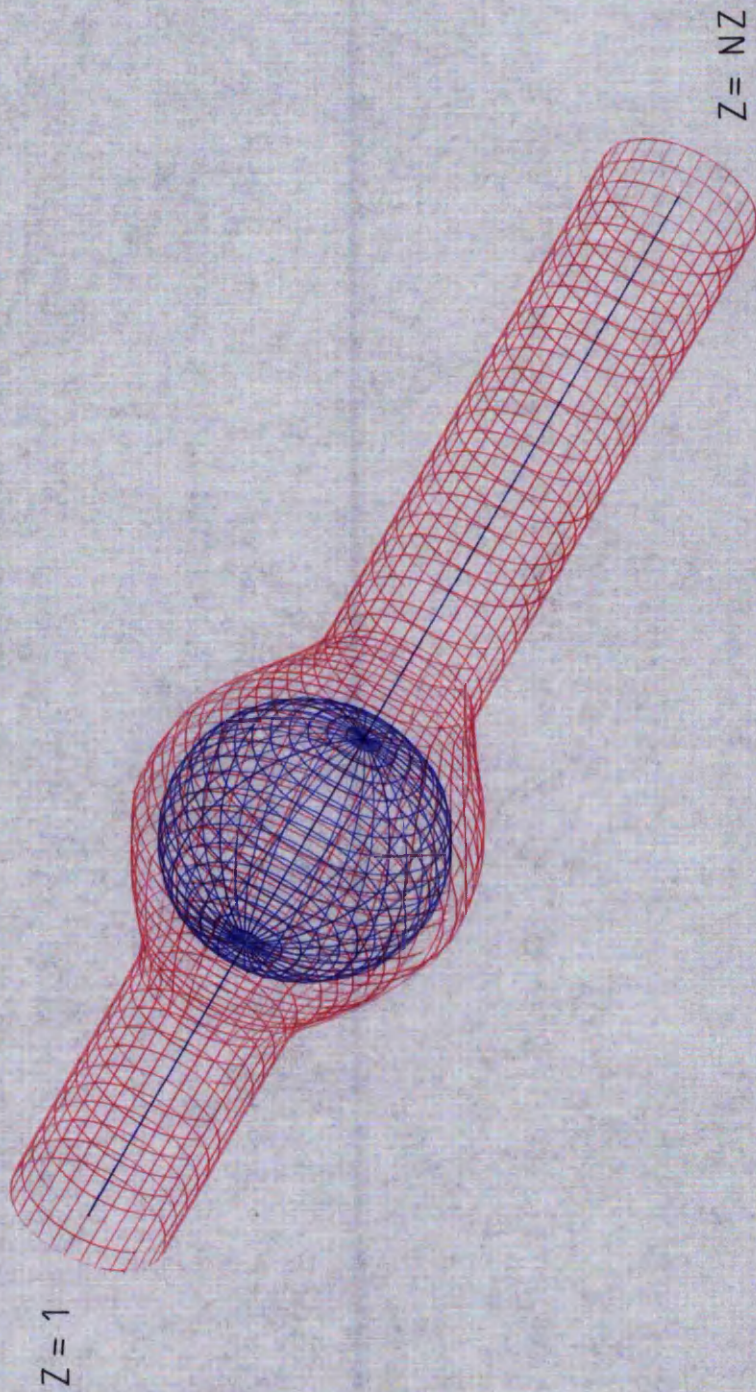
$$\epsilon = U_{\tau}^3 / (\kappa \delta) \quad [4.10]$$

#### 4.7 Geometrical Considerations

Axes for the computational grid were defined as in figure 4.1. Fluid flowed along the Z axis with inlet at Z=1 and outlet at Z=NZ, where NZ was the total number of cells in the Z direction. The radial direction was represented by the Y axis and the circumferential direction by X. NY and NX defined the total number of cells in this axisymmetric polar cylindrical coordinate system.

The original computer modelling of the ball valved conduit was performed on an orthogonal grid, ie a grid that is comprised totally of right, parallel and square cell faces. This method of modelling, although not as accurate in its final predictions, as curvilinear modelling, did yield valid pressure results, though momentum predictions were poor leading to incorrect assessment of shear stress fields. Orthogonal modelling was used by Tansley et al (1986) in an effort to assess the net force on a ball situated in two differing conduit geometries as a compliment to experimental observations of ball instability. However, as discussed in Chapter six, although pressure gradients on an overall scale were acceptable the errors in net force on the ball due to grid interference introduced irreconcilable differences between numerical and experimental observations. It is for

GRID AXIS DEFINITION



reasons of grid interference, ie the inability of even extremely fine orthogonal grids to faithfully reproduce complex curved geometries, that numerical predictions continued in curvilinear geometries, as soon as available.

Grid curvilinearity is achieved in PHOENICS by the use of Body Fitted Coordinates (BFCs); a curvilinear grid system imposed onto a Cartesian base grid. The local velocities are defined to coincide with local cell face orientations and the differential equations are adjusted to allow for geometry considerations. The precise mechanisms of these adjustments may be found in Spalding et al (1986). The main advantages offered by Body Fitted Coordinates are

- (i) an improved representation of modelled geometries,
- (ii) greater accuracy of prediction in geometries incorporating complicated curved surfaces, especially of near-wall characteristics and
- (iii) an enhanced ability to achieve grid independence in complex geometries.

The choice of grid has a marked influence on the correctness of the converged solution, with greater accuracy being afforded, generally, by finer grids. However, one has to play-off this requirement with that for a speedy computational solution, something which is hindered by too many cell centres. Further limitations to the fineness of grid are posed by the requirements of cell spacing at physical boundaries to flow and by in-core storage capabilities of the computer. When the geometry is non-orthogonal, ie when Body Fitted Coordinates are used, the in-core storage capability is stretched even further by the need to

specify every cell corner within the grid. The volume of information needed to specify a flow geometry was increased from  $NX+NY+NZ+3$  regular grid cell centres to  $3(NX+1)(NY+1)(NZ+1)$  BFC cell corners. Further consideration was necessary to ensure as high a degree of orthogonality of cells as is attainable, because without it such solution convergence is unrealisable. Two empirical rules were used during grid generation. Firstly a cell was deemed sufficiently orthogonal if it could be circumscribed, the circle passing through each cell corner. Secondly large numbers of slightly non-orthogonal cells were preferred to fewer cells of high non-orthogonality.

The spacing of cell centres is a factor that not only influences the rate of convergence of a solution, but can also affect the final result. The parameter values predicted at each cell are discretised point values of the finite difference equation solution. If then the cell centre spacing is too large, the linear approximation to the true slope of the finite difference equations will be erroneous. This situation is exacerbated in turbulent solutions as the scale of flow disturbance is much smaller. The solution can therefore be checked to show it is free of this grid dependency by comparing the results against those for a slightly different grid: the results should not vary by more than 1% - 3%.

Launder and Spalding (1974) discuss the importance of wall-cell centre positioning when utilising the logarithmic wall function, more specifically they stress the need to ensure that turbulence, and not viscous effects are dominant at these cell centres. Further, Hedberg et al (1986) cite the range 11.5 - 100 for

dimensionless wall distances ( $y^+$ ) which should be applied at these cell centres, ie  $\delta$  should be chosen so that at the first cell centre:

$$11.5 < y^+ < 100$$

This distance could be estimated analytically, but in practice a monitor was written into PHOENICS's user accessible "GROUND" routine which calculated  $y^+$  at each cell centre for the converged solution.

The assembly of all the above steps into a final analysis yielded shear rates and stresses modelled in blood flow through a ball valved conduit. No verification of the accuracy of results was possible at this stage purely because no experimental techniques were available capable of yielding all the information gathered via CFM modelling.

#### 4.8 Regime Definition

Several methods of defining the grid were considered; re-arranging an existing orthogonal grid by moving only certain extremity points and filling in the in-between points, digitising points from existing drawings or writing a Fortran program to define every point. The last method was adopted for the following reasons:

- i) Increased flexibility; it was possible simply by changing a few values to completely alter the number and spacings of cells. This helped in ensuring grid independence.
- ii) Increased accuracy; as the surfaces of the conduit's inner profile and the ball were already strictly mathematically defined, it seemed obvious to use this knowledge to model

the surfaces.

- iii) Speedier geometry changes; these could be effected by simply changing the mathematical descriptors of the various conduit sections, most notably the outflow tract and near-wall regions.

The Fortran algorithm for defining geometry was relatively straightforward with the exception of the outflow tract profile. As the grids were developed in a series of constant "X" slabs marching forward in the "Z" direction it became necessary to construct a routine to find the height of the conduit wall at the outflow section via the Newton - Raphson Iterative technique. Appendix 2 shows the final form of the grid generation coding. Further orthogonalisation using the "magic" algorithm built into PHOENICS proved to be totally unsatisfactory. Different size versions of a given valve design were generated as scale models of a standard 22mm diameter conduit. Hence all key dimensions in these other size valves were referenced to the standard, ie a blending radius stated as 30mm on a 16mm conduit would in fact be  $30 \times 16 / 22$ mm radius.

#### In conclusion

The above looks briefly at work done by other researchers in the field of numerical flow analysis applied to heart valves.

Discussion continues by pointing out possible flaws in their studies and goes on to suggest possible improvements that might increase correlation between computational studies and in-vivo flow situations. This is achieved primarily by the introduction

of two models:

- i) constitutive equation for the rheological description of blood flow
- ii)  $k - \epsilon$  model for the description of time averaged turbulence properties.

Later, the chapter describes the steps taken in assembling the numerical model geometry and suggests relationships against which numerically derived data could be compared in order to verify correctness of prediction at each stage of model development. Finally, those geometrical factors which affect not only convergence, but ultimately, the final resulting flow field parameters are discussed.

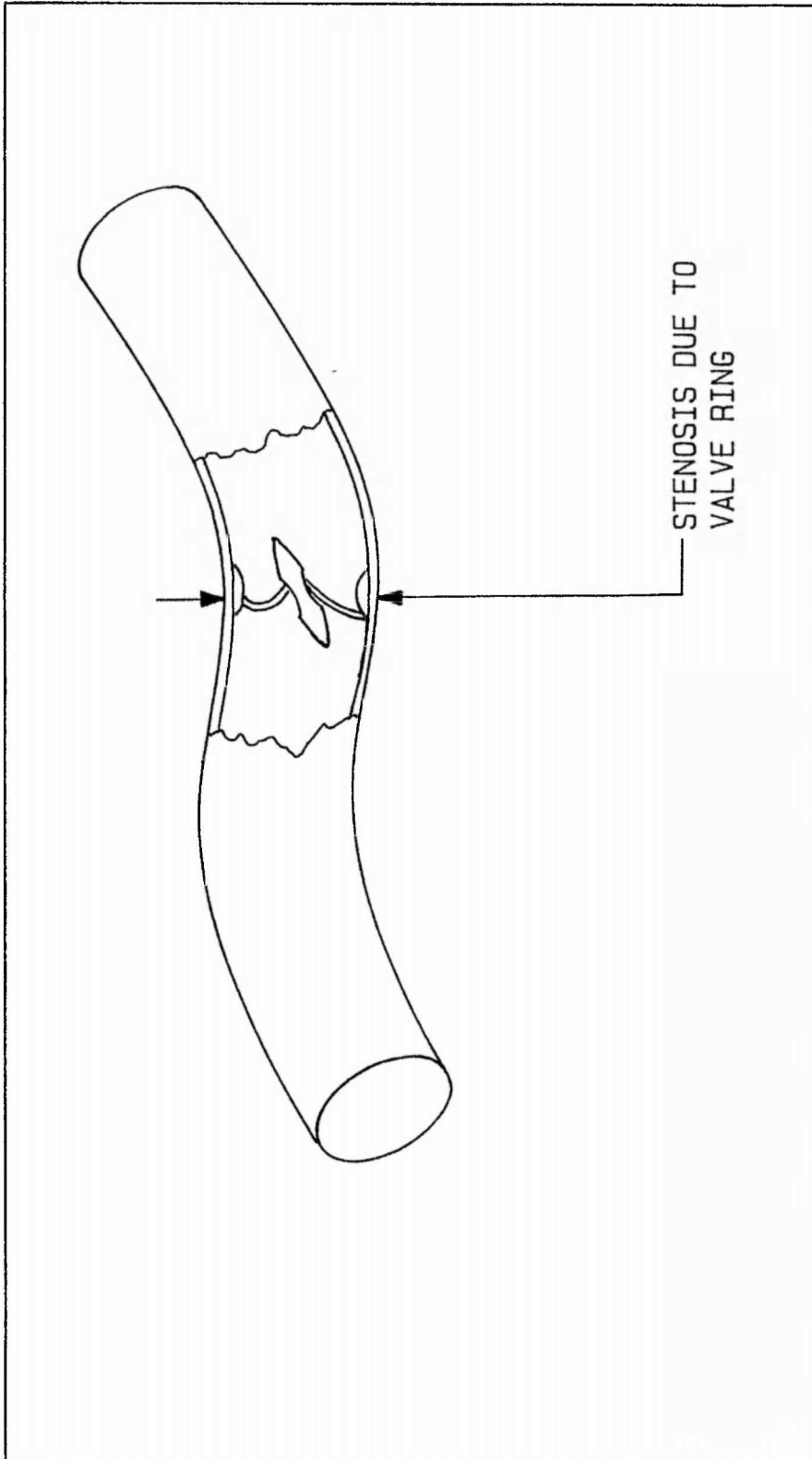
CHAPTER FIVE

INITIAL DEVELOPMENT OF A PROSTHETIC HEART VALVE CONDUIT

## 5.1 Design Philosophy

As outlined in chapter one, prosthetic conduits consist basically of a passive non-return valve incorporated into a section of tubing. To date all commercially available mechanical conduit prostheses have used existing annulus mountable heart valves to occlude reverse flow, which is far from ideal because of the design constraints placed on such valves. These constraints, for example orifice size and valve profile height, dictate valve design and hence limit the maximum attainable haemodynamic characteristics. Many of these design limitations can be relaxed when applied to conduit valves, thus improving the haemodynamic performance of such prostheses. In order to realise the full potential for improved haemodynamics of conduits, several of the less desirable aspects of annulus mountable valves must be addressed:

**Sewing rings:** The mechanical valves mounted into present day conduits were designed to be implanted into a tissue annulus at the site of either an excised mitral valve or aortic valve. Because of this intended usage these valves have sewing rings and although the sewing ring fabric is removed when such a valve is placed into a conduit, the primary orifice or valve ring still remains. This orifice in effect represents a stenosed section of conduit (figure 5.1) and does lead to higher than necessary pressure gradients across the prosthesis. Having such a ring, also induces elevated blood shear stresses which will increase haemolytic potential. Furthermore, at the entrance to the primary orifice where the conduit wall meets the sewing ring base, there is generally an area where haemostasis could occur,



MITRAL DISK VALVE INCORPORATED INTO  
A TYPICAL COMMERCIAL CONDUIT PROSTHESIS

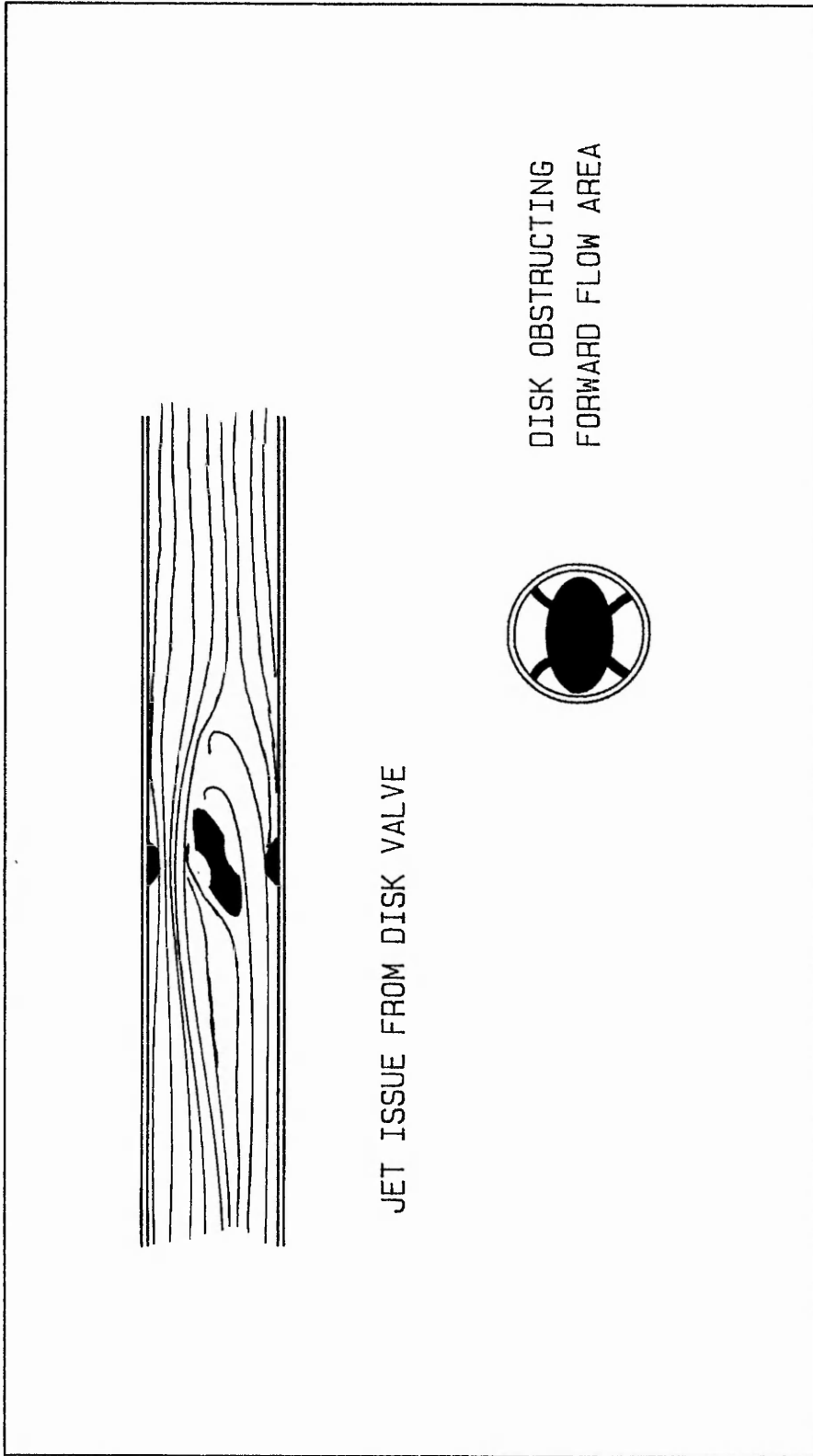
thereby introducing a potential site for thrombus formation.

**Occluder entrapment:** There have still only been relatively few mechanically occluded conduit valves implanted, so the entrapment of occluders by the formation of thrombus on hinging mechanisms in conduits is not well documented, but the potential exists for this mode of dysfunction in conduits, as it does in annulus mounted valves.

**Flow area:** Another undesirable feature of annulus mountable valves is the reduction in flow area due to the obstruction imposed by mounting the occluding mechanism in a simple cylindrical tube. This loss of flow area tends to lead to increased pressure gradients and increased thromboembolic and haemolytic potentials.

**Jet issue:** This is generally of no concern in tissue valves, where the flow issuing from the valve is almost axially aligned, but in valves such as the Björk-Shiley GVP and GVPC pulmonic grafts, blood issuing from the tertiary orifice is at an angle deviated from the axial direction (figure 5.2). This causes impingement on the nearby conduit wall and will elevate the haemolysis rate.

**Valve size:** In annulus mounted valves, size is critical if the valve is to fit correctly. Available sizes are therefore limited to the range of physiologically occurring heart annuli. Conduit valves are mounted in less critical sites and an increase in the dimensions of the valve could be accommodated. The benefits of this would be reduced resistance to blood flow and an enhanced



JET ISSUE FROM CONDUIT MOUNTED  
BJORK - SHILEY TILTING DISK VALVE

freedom in valve design.

Bioprostheses: Tissue valves offer potentially the best haemodynamic characteristics of all mitral or aortic valves when fitted into a conduit. The reasons for this are larger primary orifices, lesser pressure gradients and more axially aligned flow. However, the use of standard sized valves is still limiting. Although the freedom from anticoagulation offered by bioprostheses is very much an advantage, the limited longevity is of primary concern, especially if the conduit is to be used in paediatrics.

The design philosophy adopted for the conduit valve under development at Trent Polytechnic called for a custom made conduit occluder. This radically new approach would have to break away from the constraints outlined above, which are imposed onto current conduits by their use of existing heart valves. Yet if the conduit is to find general acceptability amongst cardiac surgeons then an element of familiarity must be introduced. The valve developed, which stemmed from the work of Gentle (1983), takes the form of a ball retained by a rigid divergent/convergent section integral with the conduit. Flexibility was introduced by the addition, either end, of a Dacron flexible conduit graft. Valve action is simple; the ball seats against the conical inlet section during the reverse pressure phase. During systole, the ball moves forward off its seating, to be restrained by three lobes cast into the convergent outflow tract, in a position allowing flow around the ball.

The major task posed by this design philosophy was the

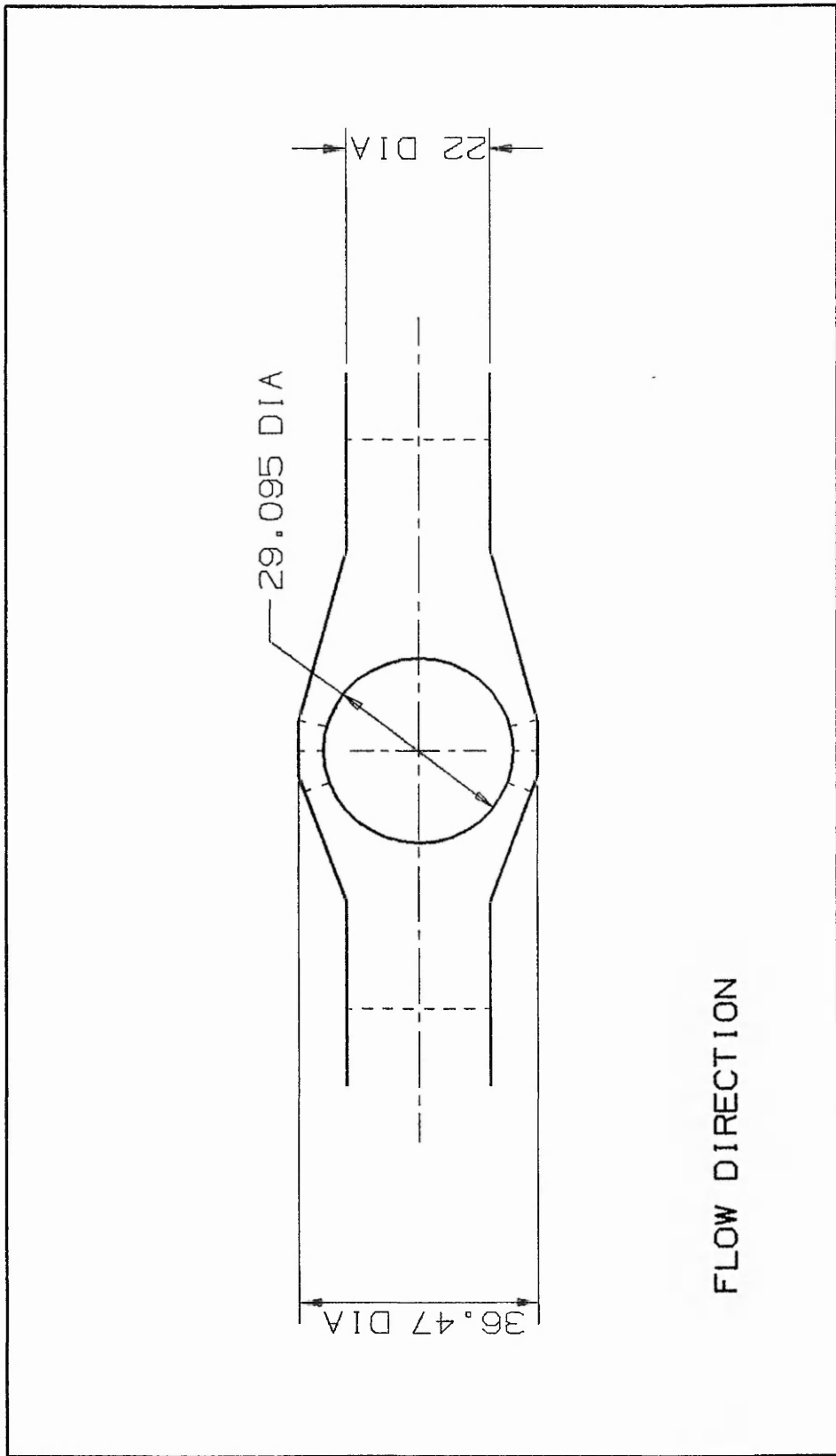
optimisation of haemodynamic characteristics. This entailed the maintenance of a fairly constant fluid velocity throughout the valve by ensuring that the flow area was held constant at five key sections along the conduit:

- i) the upstream cylindrical conduit
- ii) the frustrum between the inlet cone and the ball
- iii) the annulus between the ball and the central cylindrical section
- iv) the frustrum between the outlet cone and the ball
- v) the downstream cylindrical conduit

These areas are marked on the diagram of the first prototype of the valve (SISO) shown in profile by figure 5.3. Gentle (1983) and Benjamin (1986) investigated the effect of inlet section divergence angle on the cross valvular pressure gradient and they arrived at the conclusion that  $40^\circ$  included inlet angle represented the optimum. The outlet section had an included angle of  $30^\circ$ .

A further design feature that might be deemed radical is the intended use of ceramics in the manufacture of the valve. The advantages of using such a material are;

- i) the ease of manufacture compared with materials such as pyrolytic carbon, which requires extensive polishing
- ii) the likely reduction in haemolysis because of the decrease in prosthetic surface presented to the blood, due to tissue ingrowth into the ceramic as discussed by Gentle et al (1981b) and Gentle (1986). Heimke et al (1980) also discuss tissue ingrowth, though in relation to hip prostheses. The



SECTIONS OF CONSTANT AREA IN ORIGINAL (SISO) VALVED CONDUIT PROSTHESIS

need for anticoagulation is likely to be reduced, or even alleviated, as blood should not come into contact with conduit surfaces which are masked by tissue ingrowth.

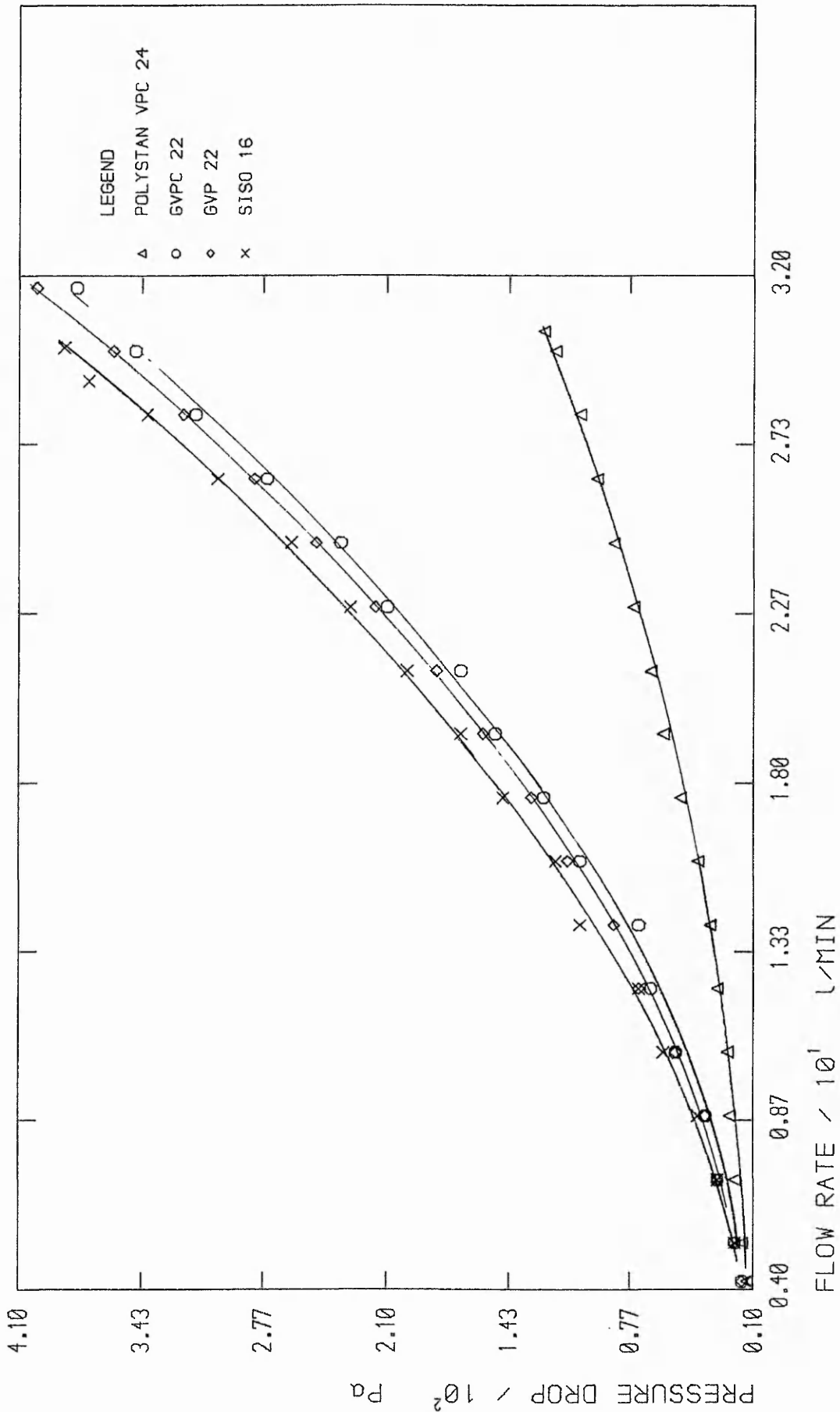
A Silastic ball was selected to occlude reverse flow as this material is well established in this capacity, being used in Starr-Edwards valves. This choice of material might improve the acceptability of the valve by introducing a degree of familiarity. Tissue ingrowth into this material does not occur but, even so, materially induced thrombotic incidents are minimal. Dimensional stability of Silastic can now be guaranteed, the early problems of swelling due to protein absorption having been fully overcome. Further justification for adopting this material is the reduction of closing noise which would be totally unacceptable if, say, a hollow stellite ball were used. Another potential problem reduced by the use of a soft ball might be the stress fracture of the ceramic ball seating due to continual impacting.

## 5.2 Conduit Performance: First Prototype (SISO)

Preliminary tests on the conduit (Gentle 1983 and Benjamin 1986) highlighted a potentially problematic design area for this first prototype conduit, namely that of ball oscillation. This instability was noted at all but the very lowest forward flow rates. These observations are in keeping with the findings of other researchers (Viggers et al 1967, Uglov et al 1978 and 1984) who reported occluder instability in caged ball valves used in the aortic position. Streak photography suggested that oscillations were not the result of vortex shedding. Further

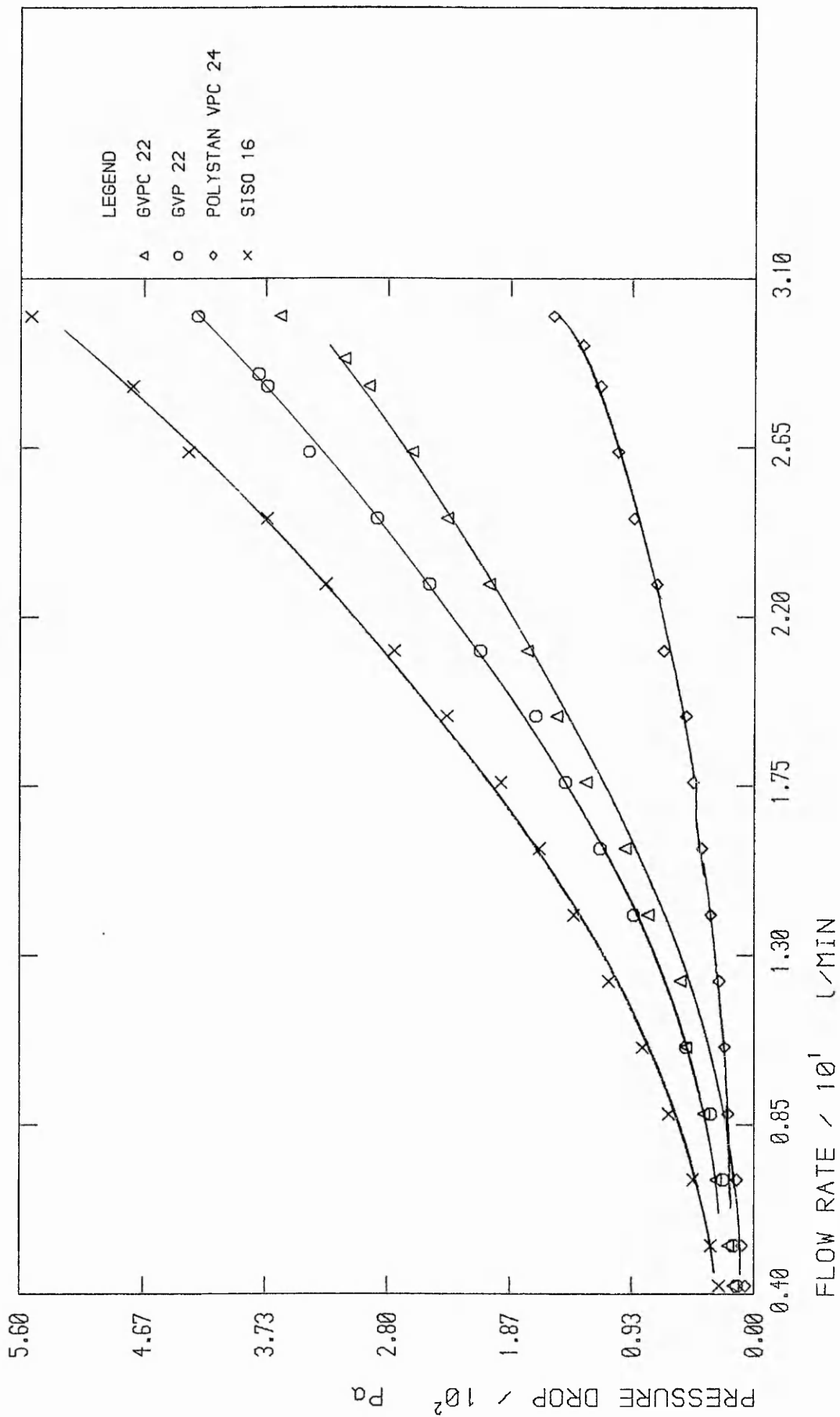
investigation by Benjamin (1986) indicated that the cause was an increase in flow area immediately downstream of the ball where there is a transition from annular flow around the ball in its fully open position to pipe flow along the exit section. Increased flow area led to a decrease in velocity, with a subsequent rise in pressure sufficient to cause a resultant anti-streamwise force on the ball, lifting it clear of the forward restraints and towards the inlet section. This would cause an increased streamwise force which, in turn, would force the ball downstream again for the cycle to repeat itself. An "order of magnitude" calculation using Bernoulli's equation revealed that a sufficient pressure rise was indeed produced. The existence of ball oscillation made the valve clinically unacceptable, as it would cause a marked increase in mechanically induced haemolysis with erythrocytes being crushed between the ball and the conduit wall.

Oscillation problems aside, the pressure/flow characteristics of the 16mm diameter SISO valve were excellent, reaching a maximum of just 386Pa in a flow rate of 30l/min of water, following the testing procedure described in chapter two and with the occluder fixed to its seating. This gradient compared favourably against larger diameter, commercially available conduits when subjected to flows of water and analogue fluids. Benjamin (1986) shows this comparison against two 22mm diameter Björk-Shiley pulmonic conduit prosthesis, one convexo-concave (GVPC) and one spherical disc (GVP), and against a 24mm Polystan VPC porcine valved conduit (figures 5.4 and 5.5). Maximum pressure gradients yielded were 350, 360Pa and 124Pa respectively, under similar water test conditions for a flow rate of 30l/min. Comparison



PRESSURE FLOW CHARACTERISTICS OF VALVED CONDUITS IN WATER

Figure 5.4

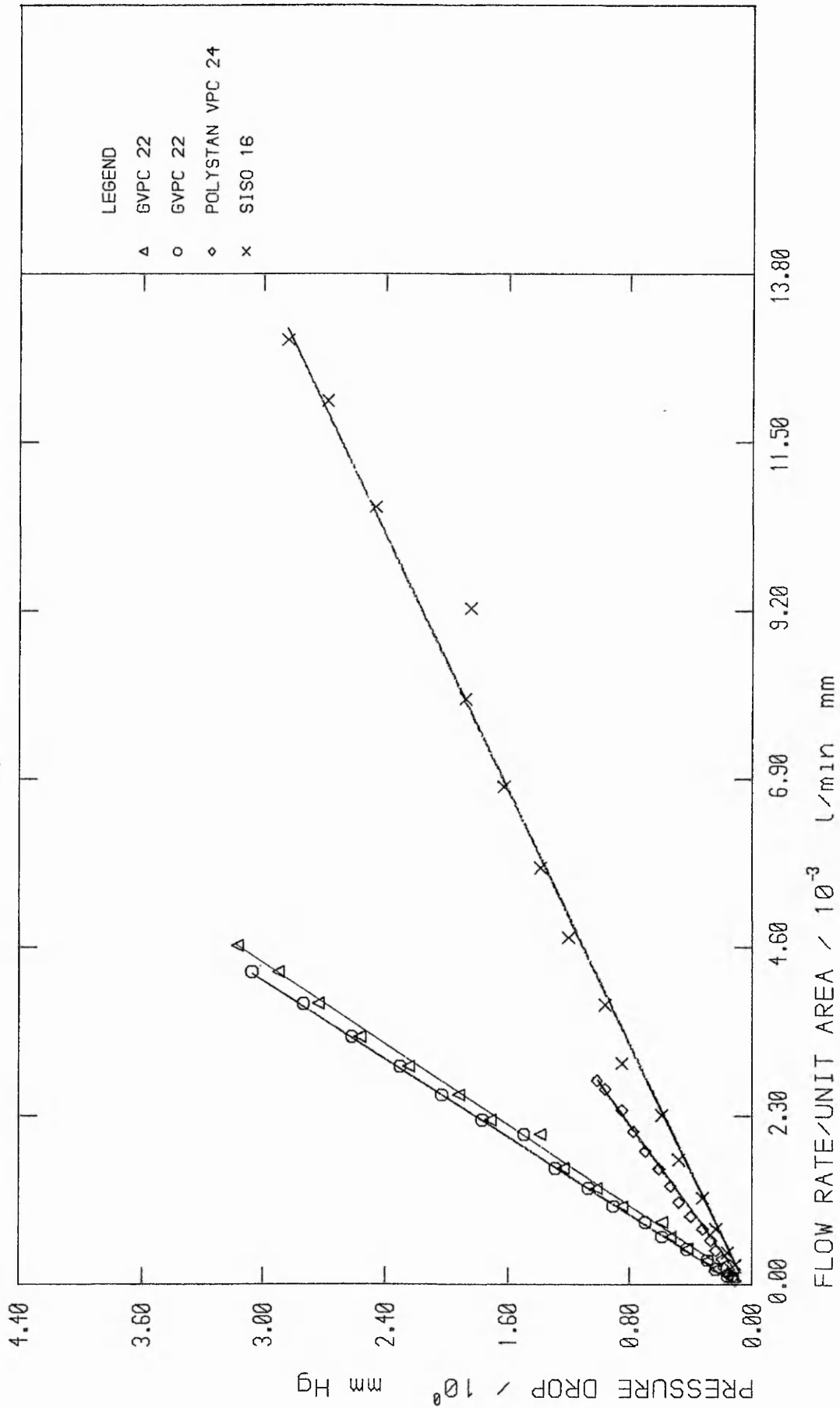


PRESSURE FLOW CHARACTERISTICS OF VALVED CONDUITS IN BLOOD ANALOGUE SOLUTION

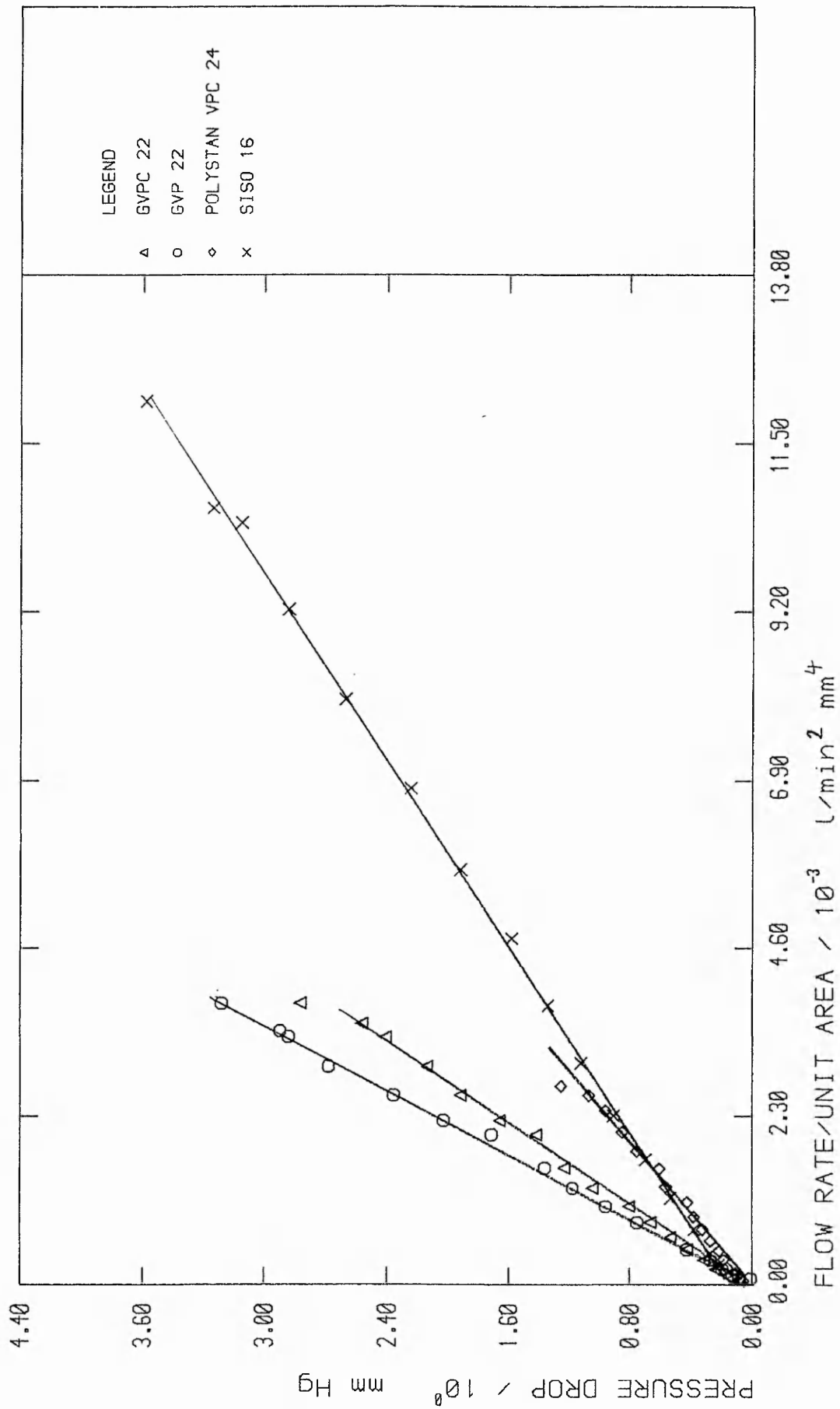
of experimental data was hampered by the differing conduit sizes. However, similarity of pressure/flow characteristics was assessed by comparing the pressure gradient of each valve in water and blood analogue flow for a given flow rate/unit area, in a manner similar to that suggested by Gentle (1977). This comparison, depicted in figures 5.6 and 5.7 plots pressure gradient (mm Hg) versus flow rate/unit area ( $l^2/\text{min}^2 \text{mm}^4$ ) and indicates that the ceramic SISO conduit valve displayed better characteristics than the larger mechanical and bioprosthetic valved conduits. Figures 5.8 and 5.9 show a similar comparison which attempts to account for dynamic similarity by non-dimensionalising pressure into Euler numbers,  $(2\Delta p/\rho w^2)$  and flow rate into Reynolds' numbers ( $w d/\nu$ ). Though over simplistic in its approach, this analysis again points to the ceramic SISO conduit having the best pressure flow characteristics of all the conduits tested by Benjamin.

### 5.3 Conduit Performance: Second Prototype (SICO)

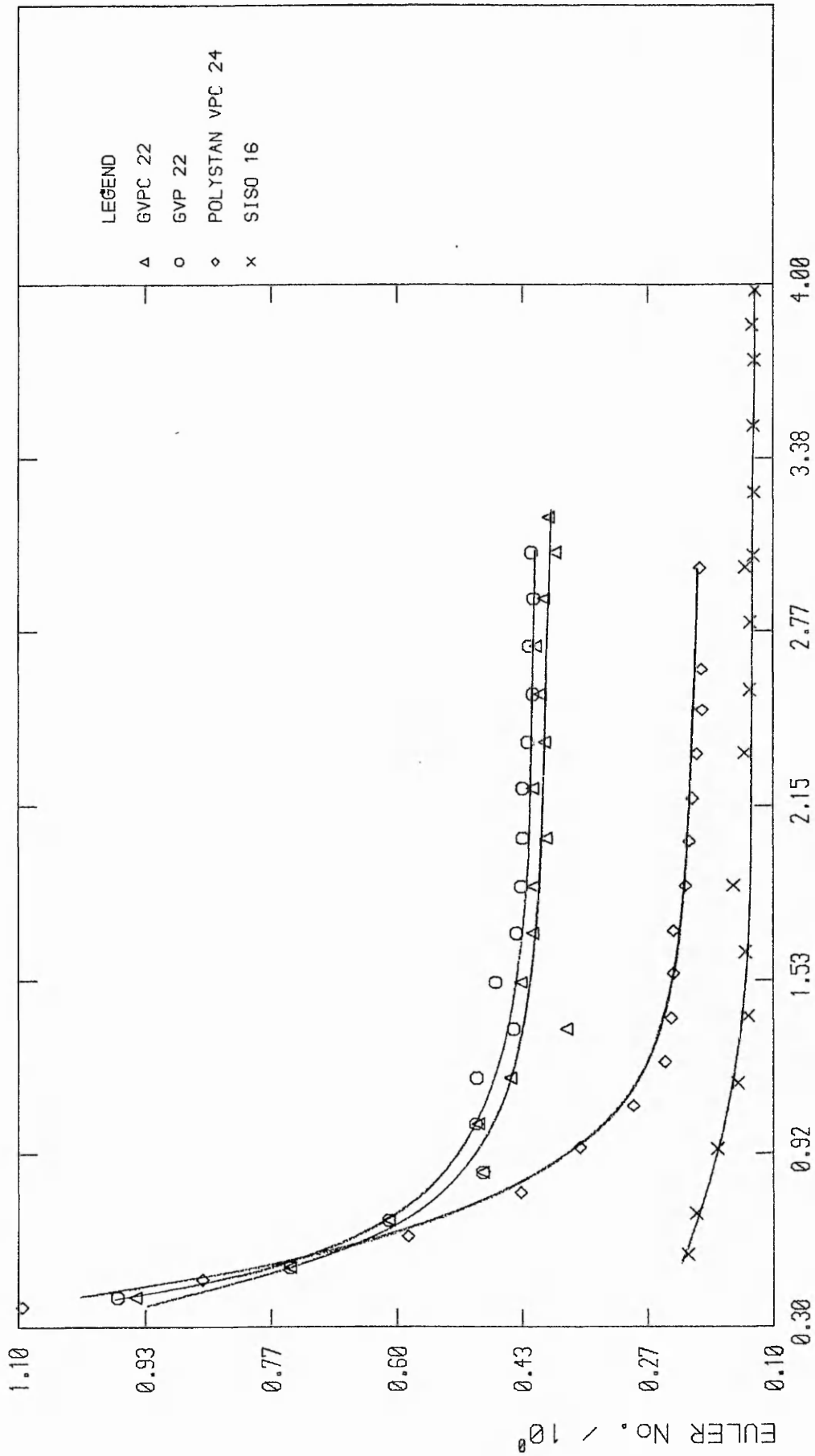
Because of occluder instability a further prototype was developed, manufactured and tested as part of this thesis. The aim was to improve the constancy of flow area around the downstream side of the ball. Since the "flow area" means that part of a given cross-section "seen by" the flow or alternatively the area which is everywhere normal to the velocity but whose outer edge defines the cross-section, it should be apparent that to keep this quantity constant required a prior knowledge of the velocity field that the new profiled downstream section would produce. This could not be attained independently, so calculation had to proceed on conservatively assumed velocity



PRESSURE PER UNIT AREA FLOW RATE OF CONDUITS IN WATER

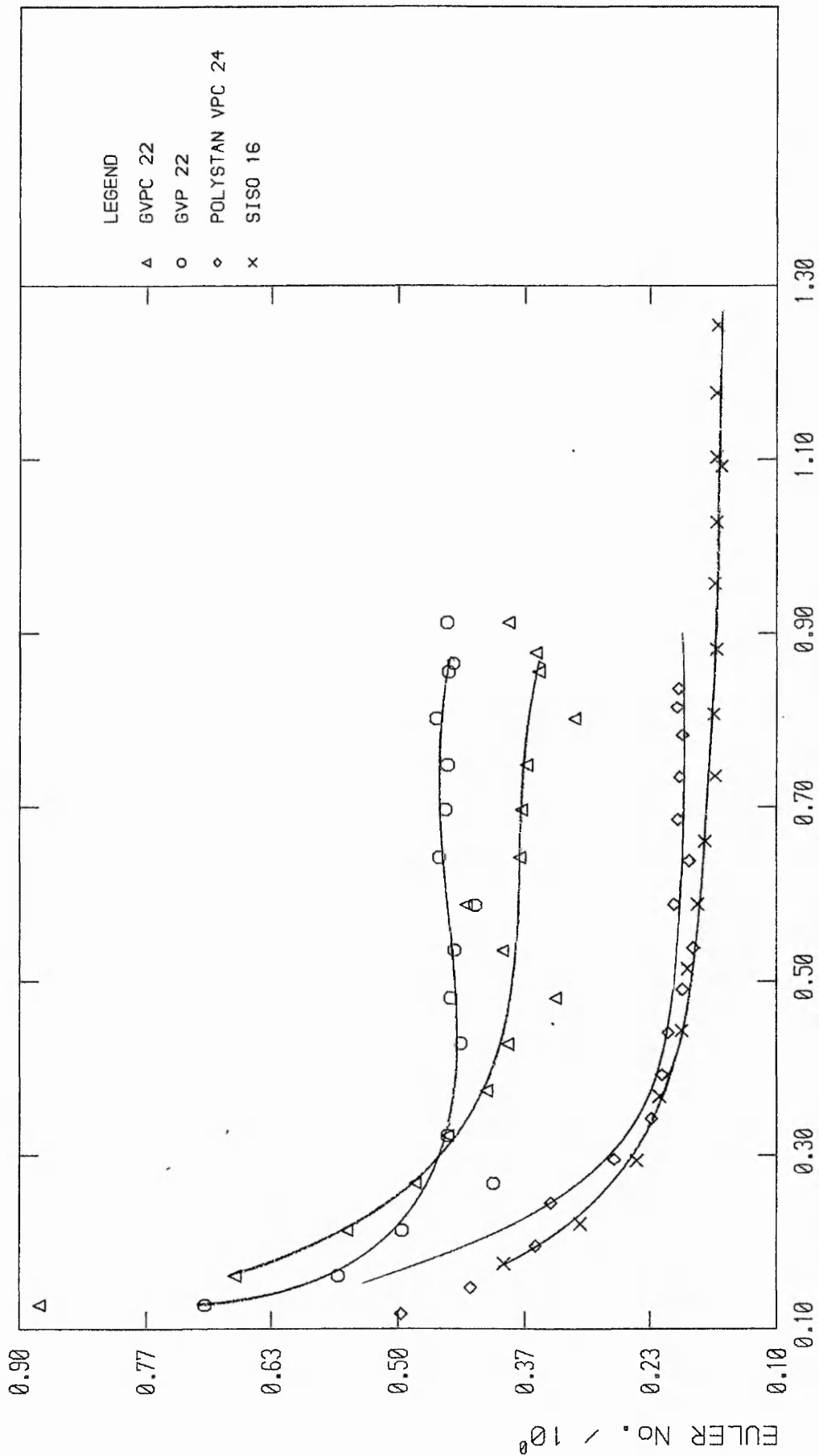


PRESSURE PER UNIT AREA FLOW RATE OF  
CONDUITS IN BLOOD ANALOGUE SOLUTION



REYNOLDS' No. / 10<sup>4</sup>

DIMENSIONLESS PRESSURE FLOW CHARACTERISTICS  
OF VALVED CONDUITS IN WATER



DIMENSIONLESS PRESSURE FLOW CHARACTERISTICS OF VALVED CONDUITS IN BLOOD ANALOGUE SOLUTION

Figure 5.9

directions. The flow area was defined as normal to the ball surface (hence conical in form) and the velocity was taken as everywhere normal to the flow area. Referring to figure 5.10, it can be seen that flow area was given by:

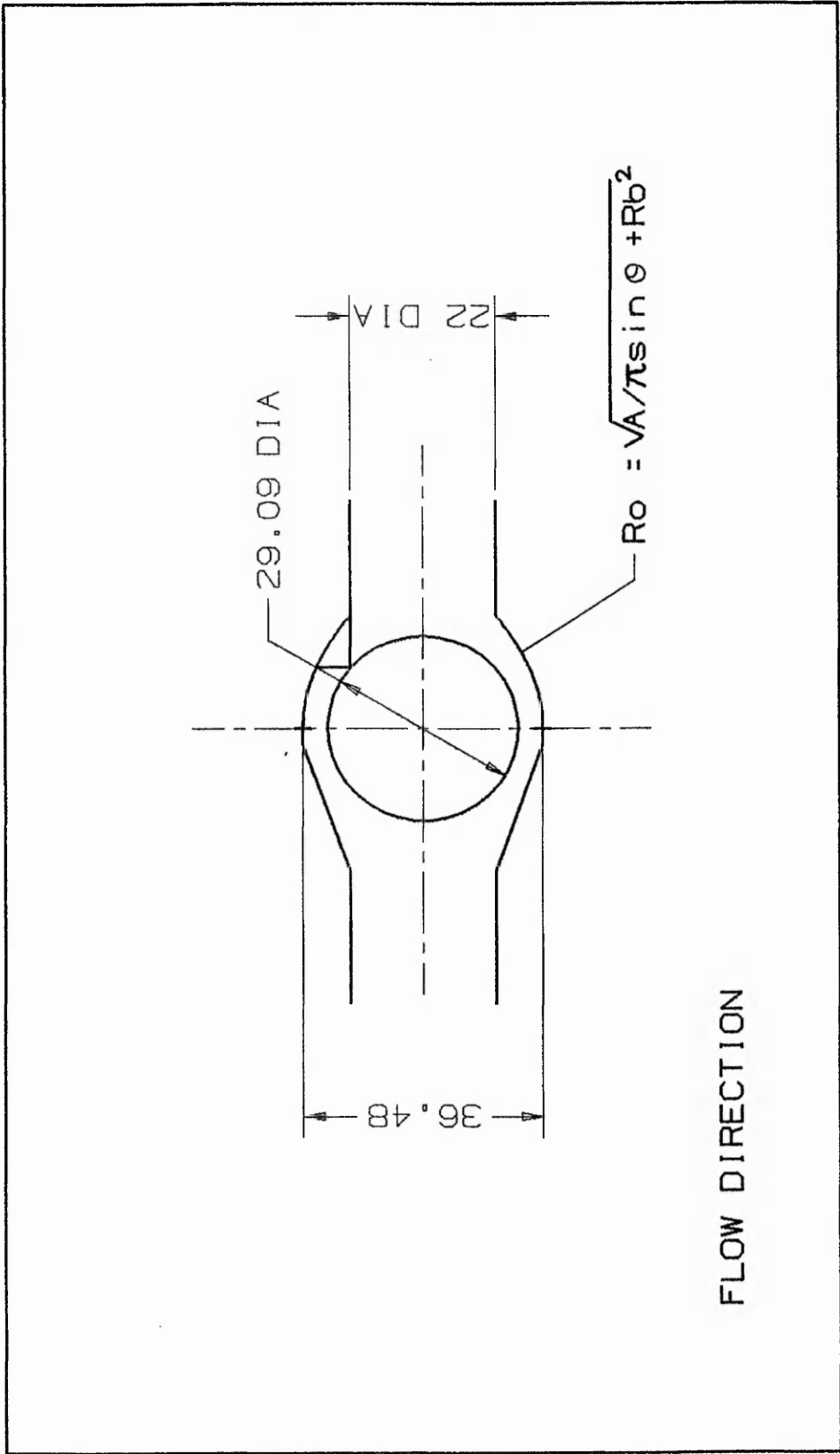
$$A = \int_{R_b}^{R_o} 2\pi r \sin\theta \, dr$$

and hence

$$R_o = \sqrt{(A/\pi \sin\theta) + R_b^2} \quad [5.1]$$

where A is kept constant and equal to the area of the inlet pipe. The locus of  $R_o$  fixed the downstream conduit profile until it intersected with the cylindrical outflow pipe. An estimate was made of the error of the "constant flow area" assumption by taking a revised assessment of the flow direction as being everywhere parallel to the bisector of the angle between the tangents to the ball and the conduit inner surface (ie the flow was somewhere between tangential to the ball and tangential to the conduit surface). The assumed flow area was thus determined to be no worse than 1.2% in error and was such as to produce a reduced area, resulting in slightly lower pressure and hence further counteracting the cause of oscillation. A prototype was manufactured and tested under steady flow conditions using water. It was also decided to provide pressure tappings the same distances upstream and downstream of the inlet section as for the original design in order to investigate the effect of the modification on pressure drop characteristics.

Tests of the improved prototype over the entire range of flowrates to which the original was subjected and found to be

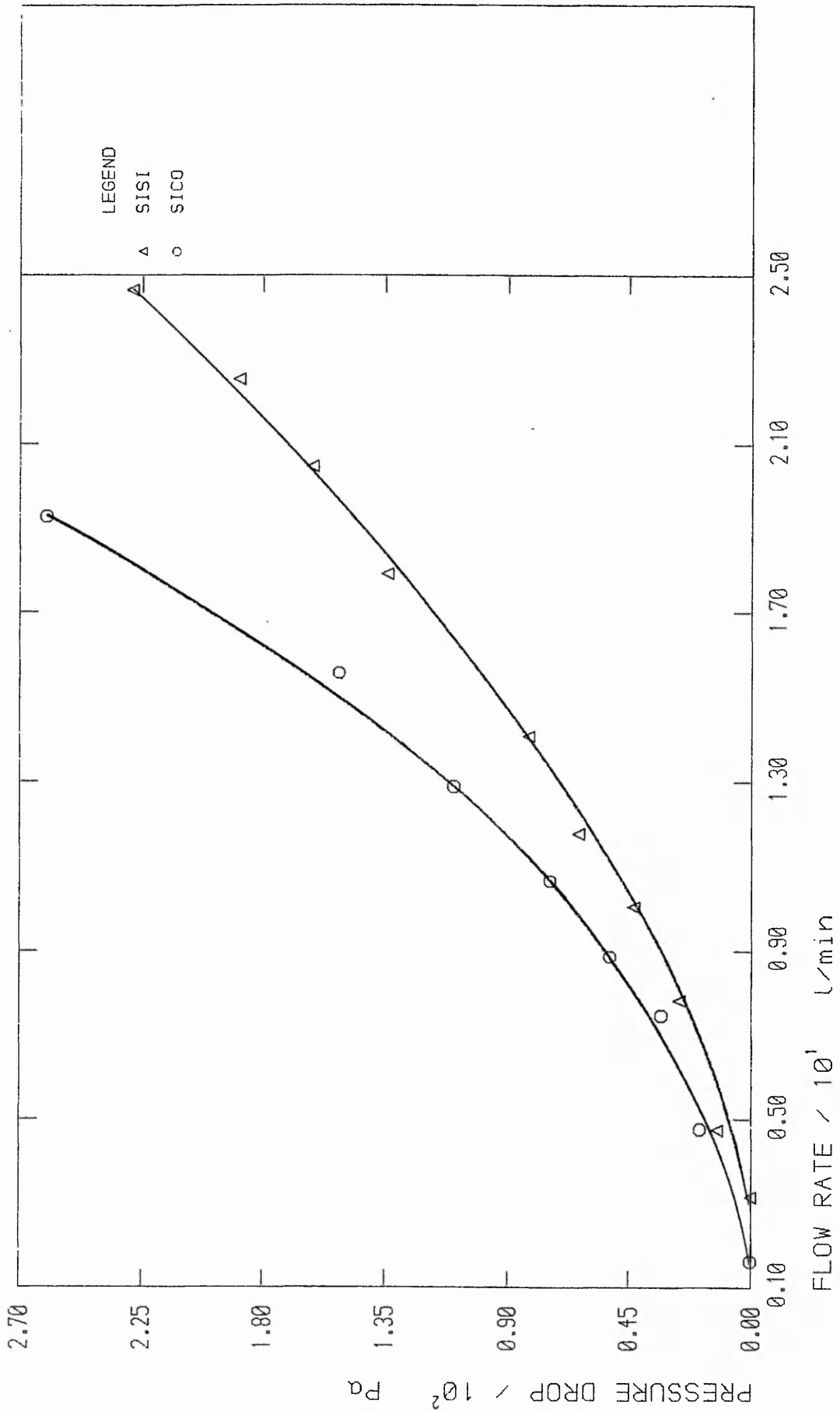


RE-MODELLED OUTFLOW SECTION OF THE SECOND (SICO) PROTOTYPE VALVE

unstable showed that there was no tendency for the ball occluder to oscillate nor to lift off the forward restraints. Figure 5.11 shows the pressure drop measurements for the two valves (SISO and SICO) tested in a range of water flow rates.

Trends in pressure drops across the original and re-shaped valves were seen to be similar when modelled physically and numerically but showed the pressure drop across the re-shaped valve to be approximately twice the pressure drop across the original valve. The values of pressure gradient for the remodelled valve, although higher were still acceptable when compared with the pressure gradients of the Björk-Shiley conduits discussed earlier. Putting these values into context, the pressure gradients might be considered high for this type of conduit, which naturally exhibit enhanced fluid dynamics, but are low compared with annulus mounted valves where typical gradients are of the order of 1 000Pa during peak systole (Yoganathan et al 1979c, Bruss et al 1983, Reif and Huffstutler 1984, Knott et al 1986).

Nevertheless, as this pressure loss is not recovered downstream, it represents a loss in energy or reduction in forward flow efficiency of the valve. The cause could well be separation due to the abrupt direction change where the outflow pipe leaves the valve body. Ways of ameliorating this situation are considered later in the thesis, in chapter seven.



A COMPARISON OF PRESSURE FLOW CHARACTERISTICS BETWEEN THE TWO CERAMIC VALVE PROTOTYPES

### In conclusion

It has been demonstrated that the problem of instability is closely connected with pressure distribution around the occluder and that this can successfully be designed out by careful selection of the conduit profile surrounding the occluder. Further work was clearly necessary to optimise the outlet flow section to one which maintained the reduced pressure gradients without introducing occluder instability. The work also demonstrated the potential improved hydrodynamic efficiency afforded by a custom made valved conduit.

CHAPTER SIX

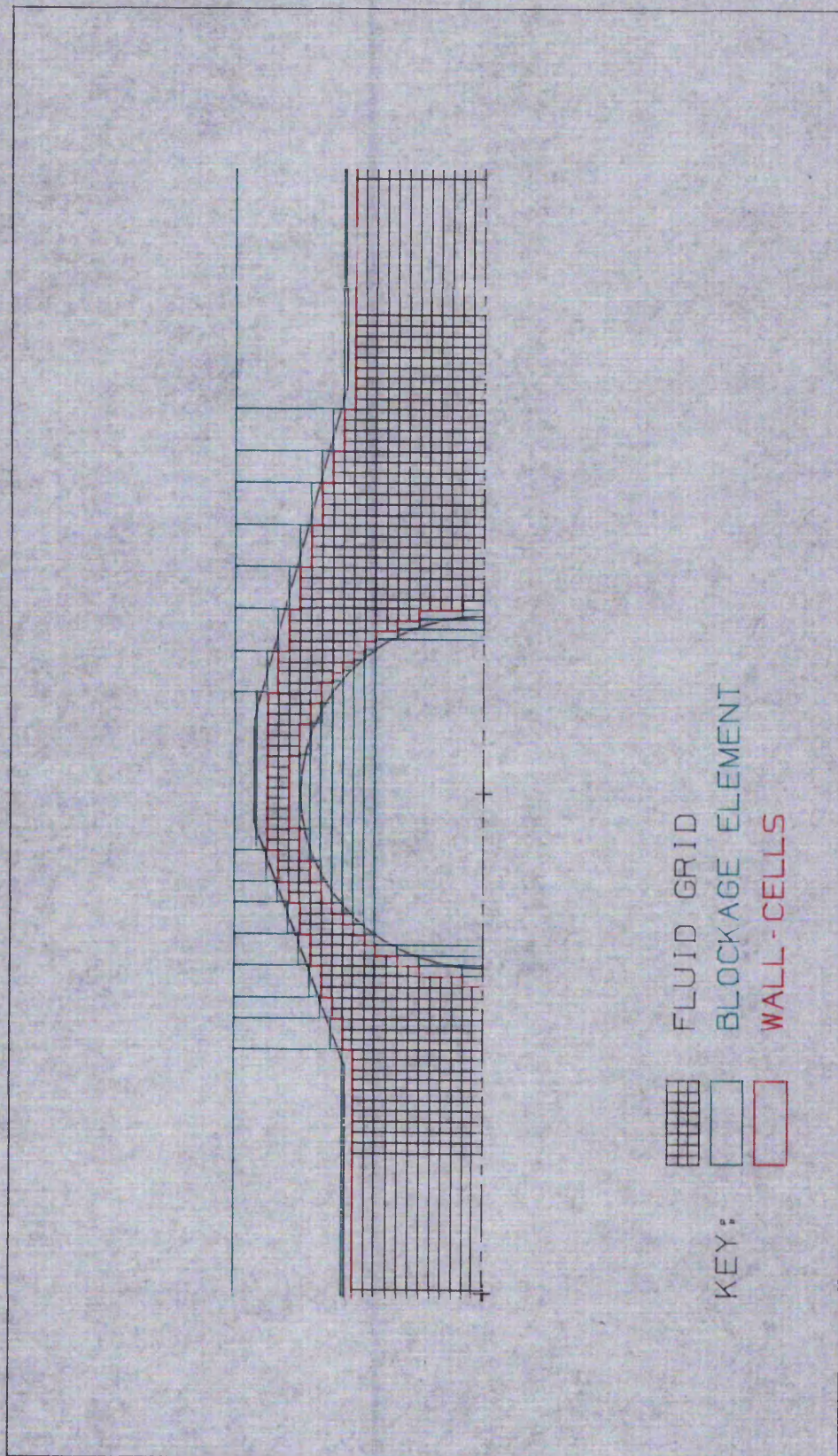
RESULTS - AN ANALYSIS OF PHOENICS

## 6.1 Introduction

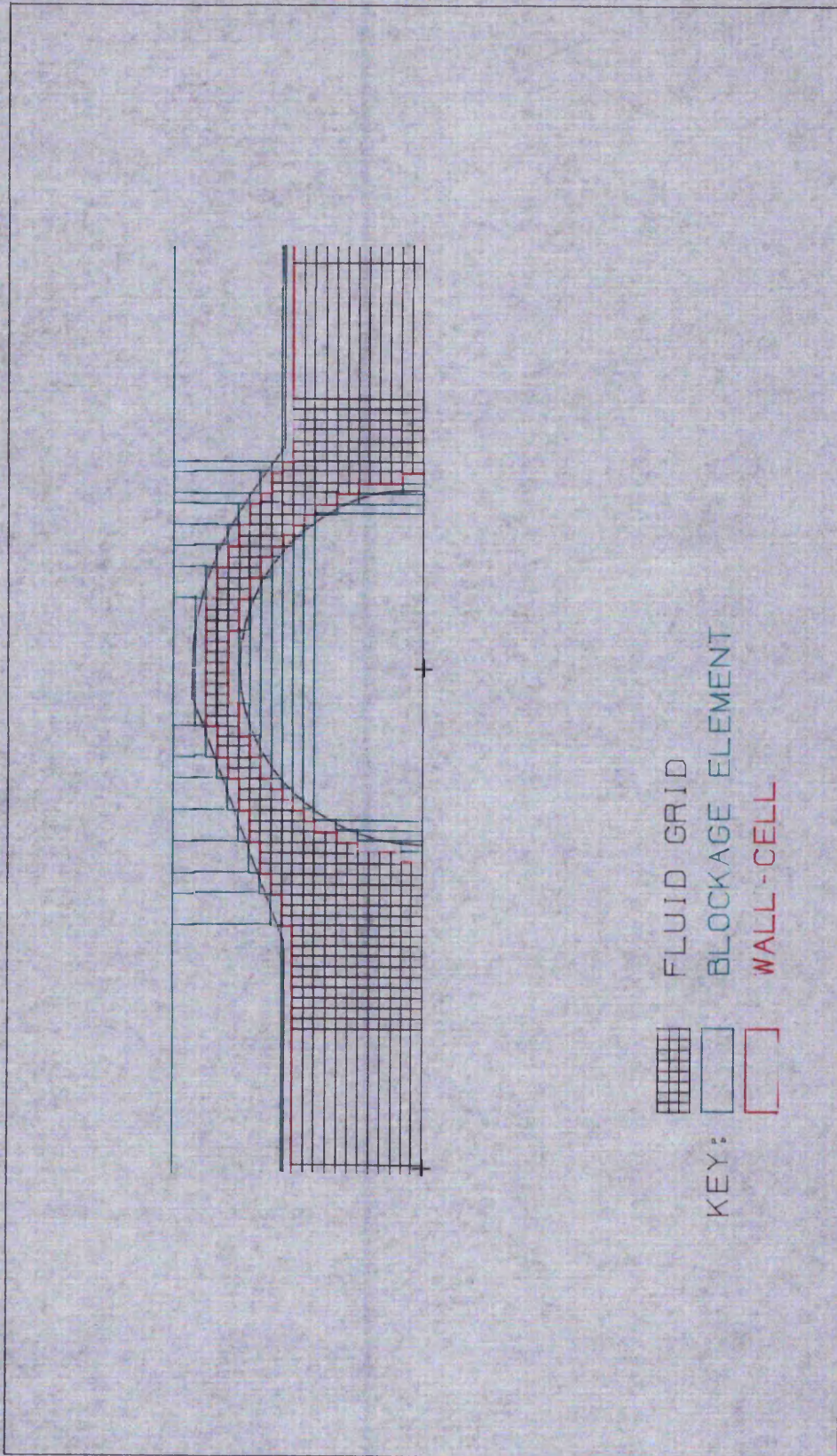
Before examining the flow characteristics of a certain geometry, it was important to establish a level of confidence in the solution procedure as applied to that geometry. To this end a battery of tests was conducted which examined all aspects of computational predictions, stemming from an examination of individual solved parameters under very restricted conditions such as laminar and turbulent velocity fields in simple pipe geometries. As described in chapter four, such predictions are of limited use but were necessary steps in establishing an overall model for examination of principles, such as momentum, in the finalised geometries.

Orthogonal modelling was carried out before the general availability, to PHOENICS of Body Fitted Coordinate modelling. A three-dimensional grid was fitted to the conduit dimensions. Figure 6.1 illustrates the diametral half-plane model of the original section, and figure 6.2 the re-modelled outflow section.

The restraining struts were omitted for ease of modelling, whilst the ball was specified as fixed in space at the fully open position. A uniform inlet velocity of 0.625m/s was specified, corresponding to a volumetric flowrate of 7.54l/min and a Reynolds number based on conduit inner diameter of 10 000, accordingly, a turbulent solution was modelled. A long inlet section was specified to allow for the development of a reasonable velocity profile. Fluid properties were taken as those of water since the instability problem was observed during tests in water. The downstream pressure was set to zero and the pressure drop across the valve was taken as the average value at



SISO VALVE SUPERIMPOSED ONTO AN ORTHOGONAL GRID: RADIAL HALF PLANE



SICO VALVE SUPERIMPOSED ONTO AN ORTHOGONAL  
 GRID: RADIAL HALF PLANE

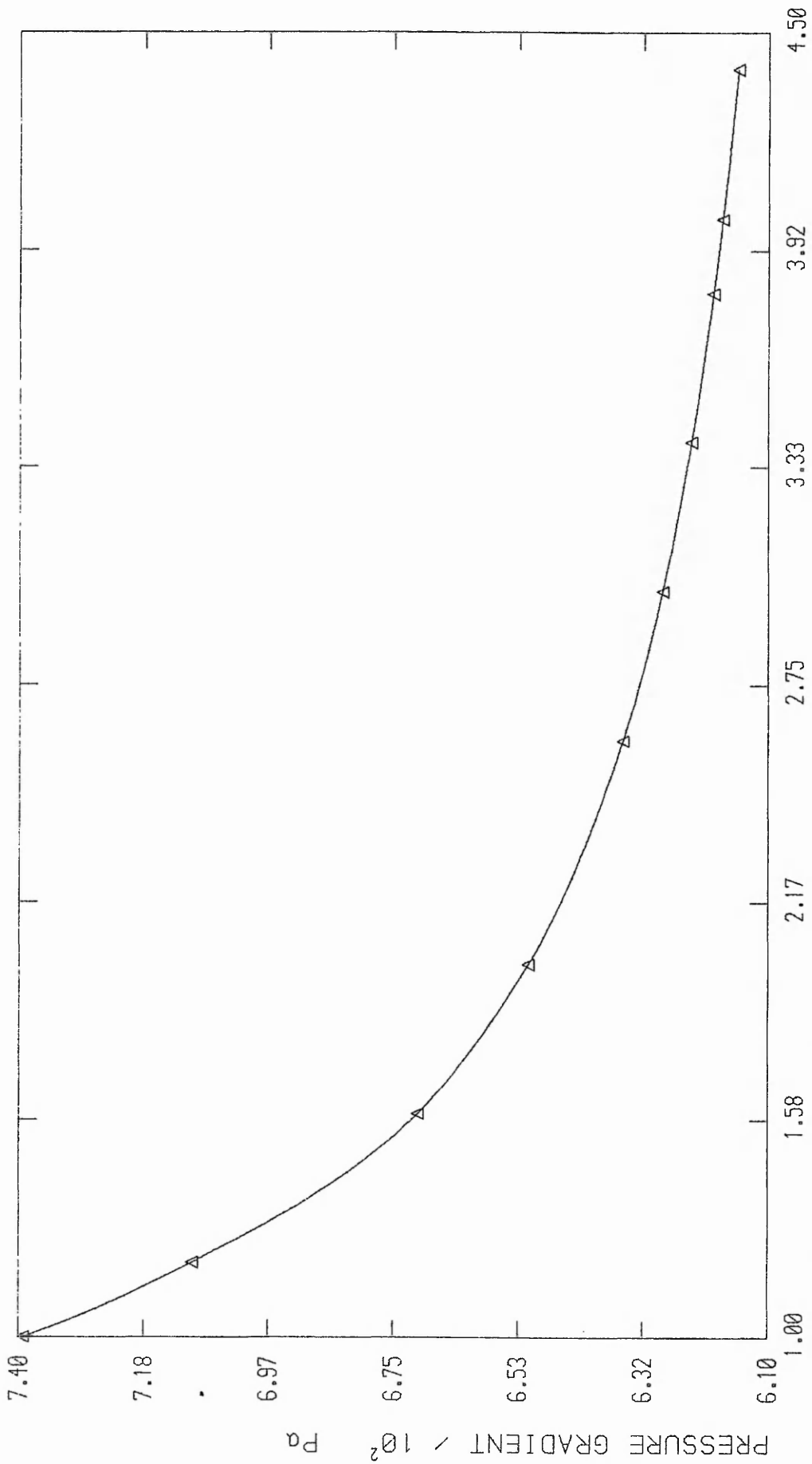
the valve entry section. Flow was assumed axisymmetric.

When they became available, Body Fitted Coordinates (BFC's) were employed. This more readily facilitated the achievement of grid independence. Flow geometries were no longer dependent on cell densities, ie. the need to use high numbers of small cells in order to define, say, a circular profile was abolished by the ability to define curvilinear profiles. This then allowed for complete grid dependency analysis.

## 6.2 Grid Dependency

Several steps were necessary in order to achieve complete grid independence in non-orthogonal geometries. Firstly and most simplistically, the density of cells within the geometry was varied between the limits of 10 - 110/radius, in a manner which quickly yielded grid independent solutions in simple pipe modelling. Grid independence was not attainable via this method in the more complex geometries.

Revising the method, the geometry was divided into three areas: the near-outer-wall, near-ball-surface and central flow regions. Whilst maintaining the dimensions of the two near-wall regions, the density of cells was varied within the central flow region between 10 - 50 cells and the parameters important to this study, namely pressure, shear stress, shear rate and velocities were monitored. Independence of grid density within this region was deemed to be completely satisfied at a density of 45 nodes, as prescribed by figure 6.3 which plots predicted pressure gradient against cell density for the central region, and shows minimal



No. OF CELLS /  $10^1$

GRID INDEPENDENCE CHECK:  
 PRESSURE GRADIENT VS NUMBER OF HALF-RADIAL CELLS

differences above a cell density of 40. Figures 6.4 - 6.7 show the variations at the centreline in pressure and shear stress, and at the conduit wall, in shear rate and shear stress. Each of these figures shows minimal difference in predictions above a cell density of 34. However, the cell density which yields full independence, ie 45, represents a higher cell density than could effectively be employed, bearing in mind the constraints of computational time. To reduce this problem a cell density of 30/radius was utilised, thus saving large amounts of computer time, and introducing only small errors (1 - 3% in the above solved parameters).

The final step in ensuring grid independence was to examine the effect of wall-cell centre distance ( $\delta$ ) on the flow solution. For a given flow rate grid dependency based on this dimension could be readily established. However, the dependency itself varied with flow rate as can be seen in figures 6.8 and 6.9 which plot streamwise force on the ball and pressure gradients through the same valve geometry experiencing two differing flow rates; 7l/min and 21l/min. Therefore it became necessary to establish solution dependency not only based on geometrical considerations at the wall, but also on flow conditions. This was instituted by the monitoring of the dimensionless wall distance ( $y^+$ ) defined as:

$$y^+ = \delta U_{\tau} / \nu$$

Figure 6.10 shows that grid independence was realised when  $y^+$  at the centre of the wall-cells was maintained in excess of 11.5. Figures 6.11 and 6.12 show the  $y^+$  values for the flow study carried out with a flow rate of 7l/min. From these figures it is apparent that a satisfactory wall cell dimension was not

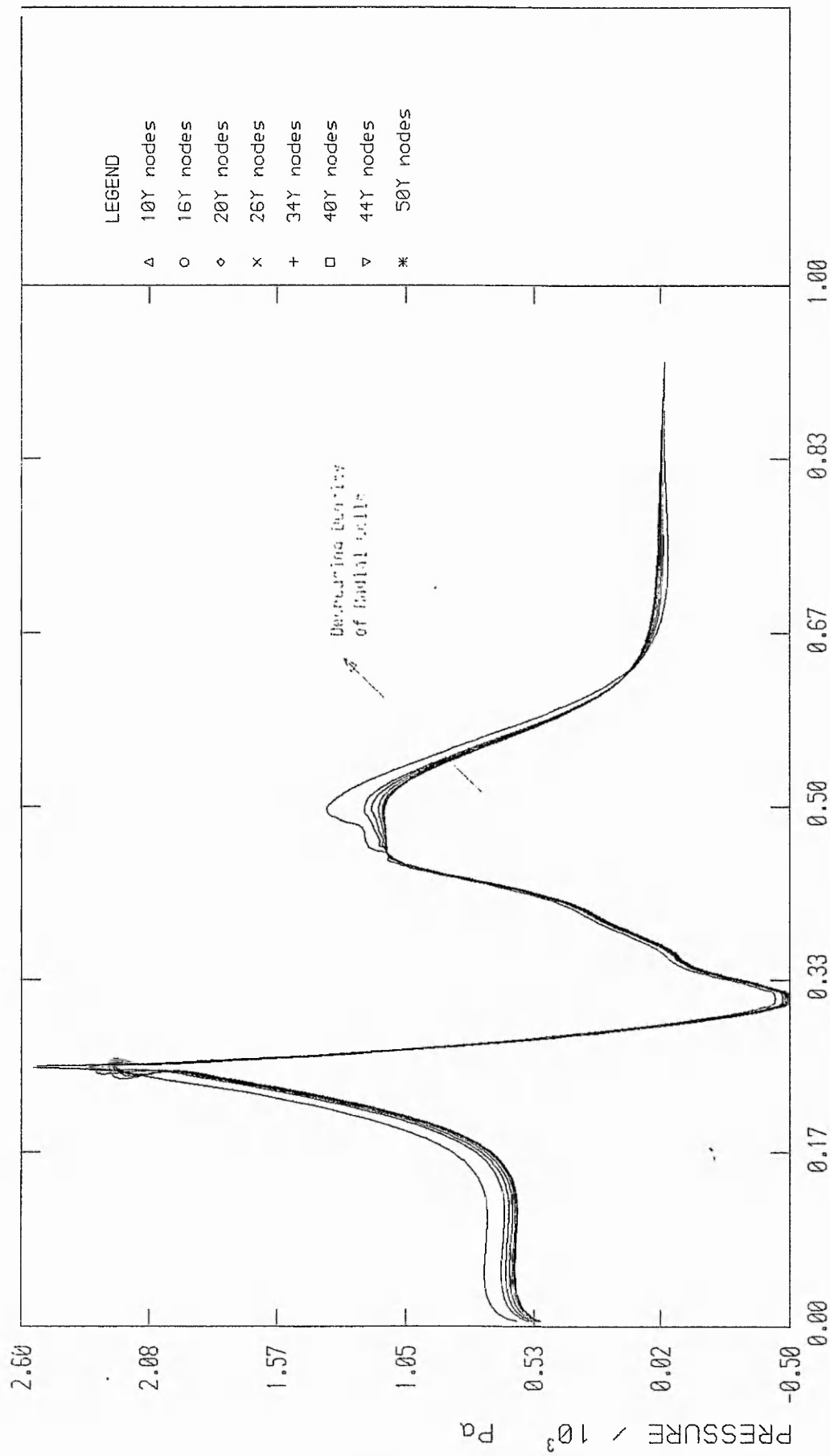
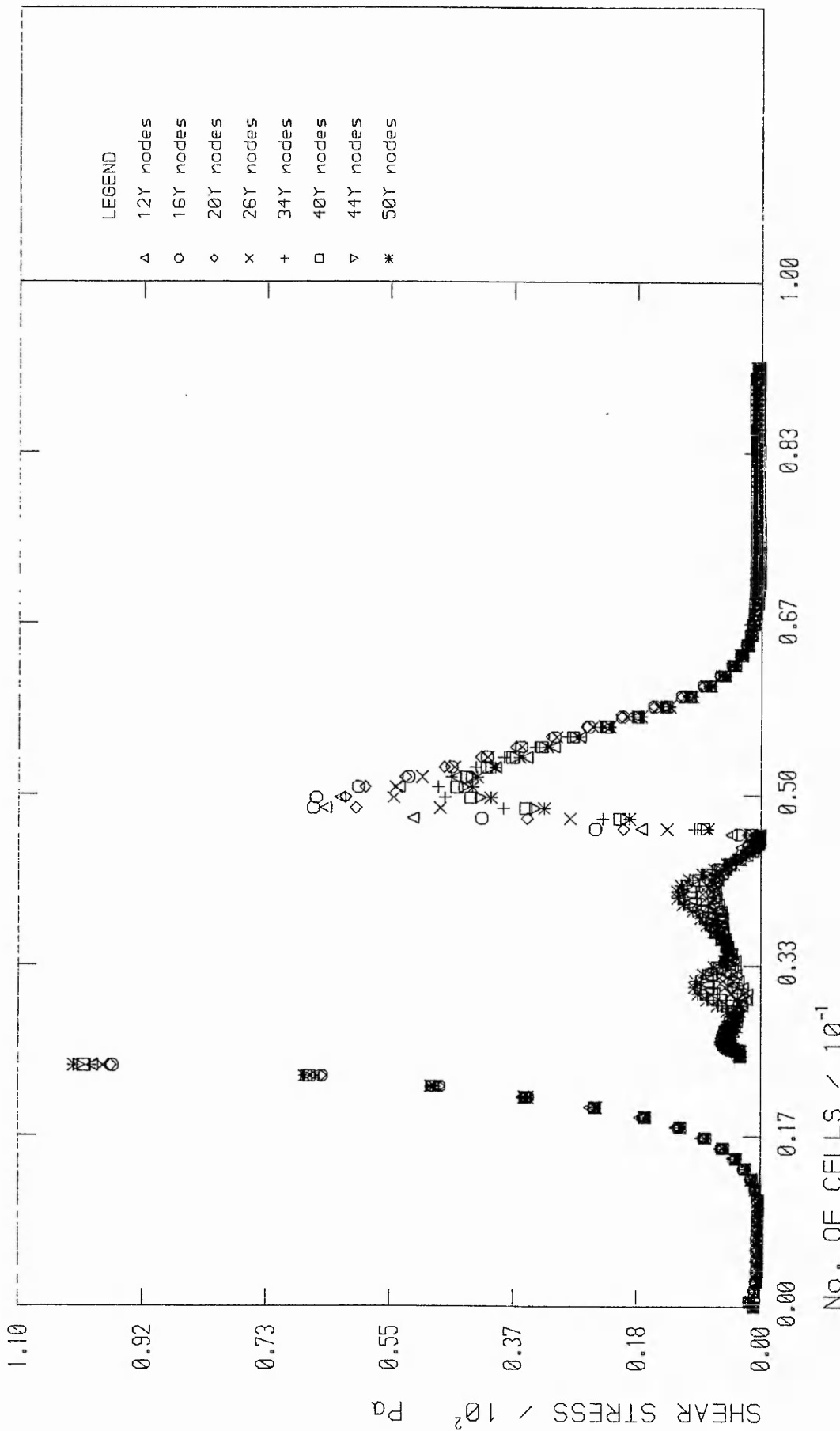
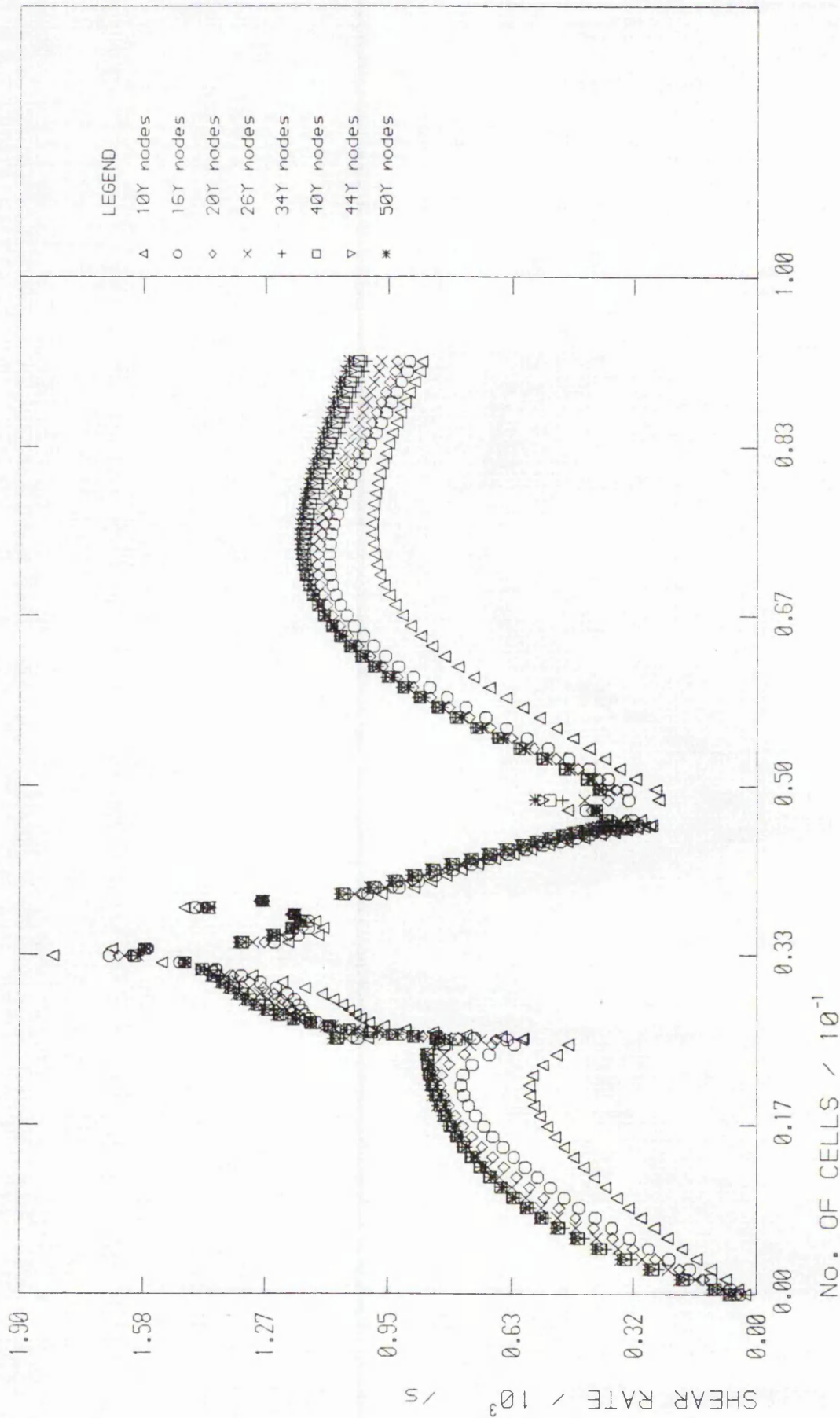


Figure 6.4

GRID INDEPENDENCE CHECK: CENTRELINE  
 PRESSURE VS NUMBER OF HALF-RADIAL CELLS

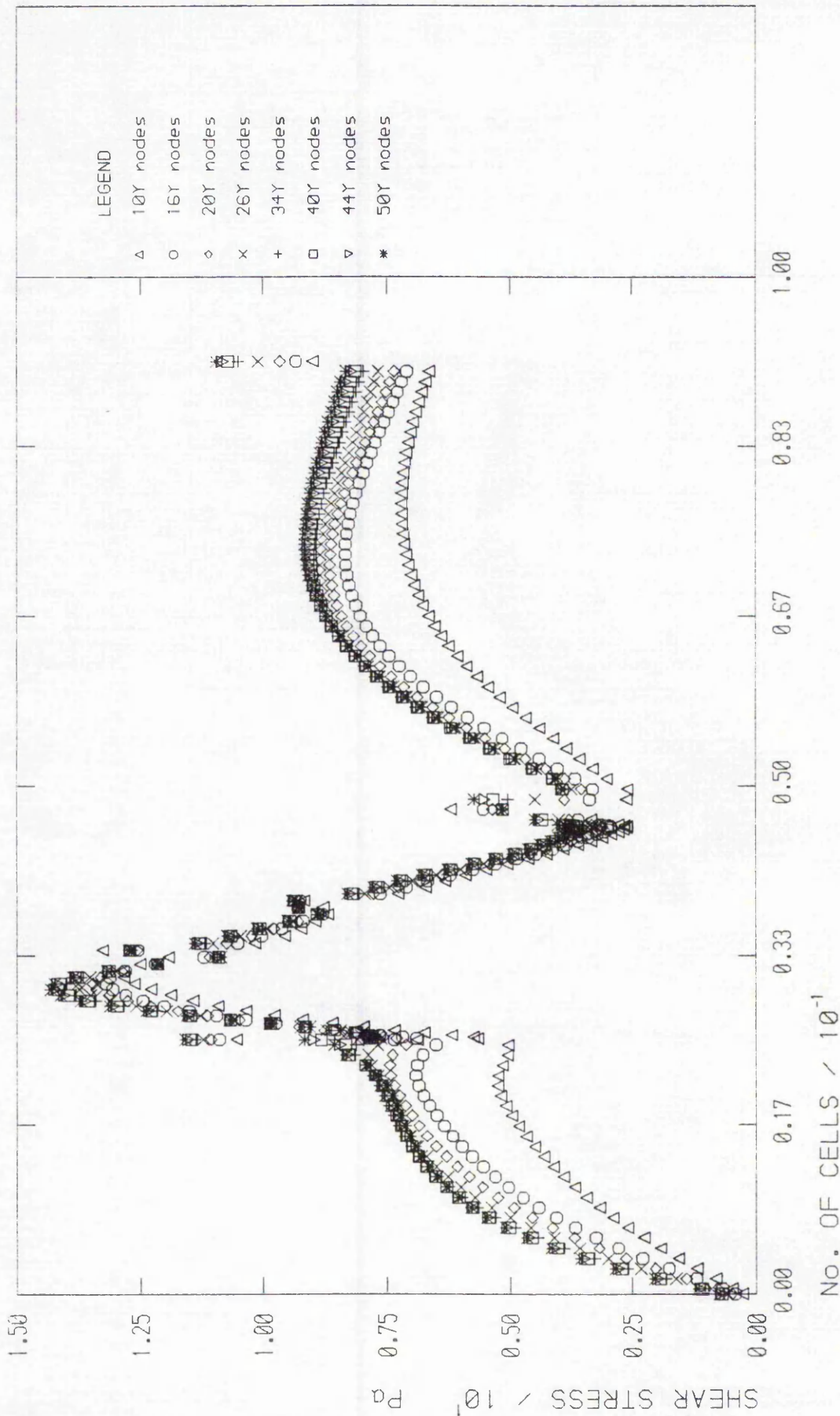


GRID INDEPENDENCE CHECK: CENTRELINE  
 SHEAR STRESS VS NUMBER OF HALF-RADIAL CELLS

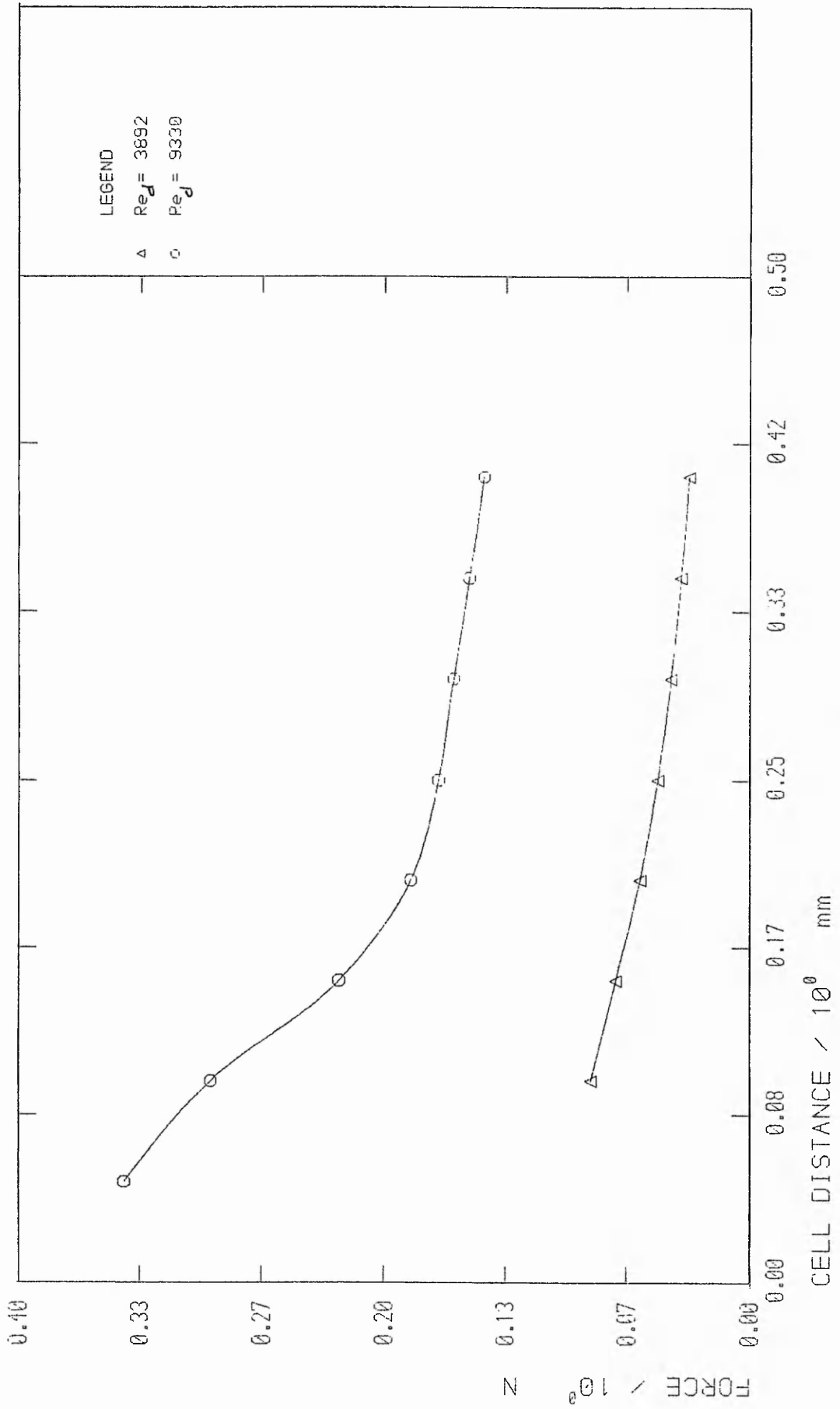


GRID INDEPENDENCE CHECK: SHEAR RATE AT CONDUIT WALL VS NUMBER OF HALF-RADIAL CELLS

Figure 6.6

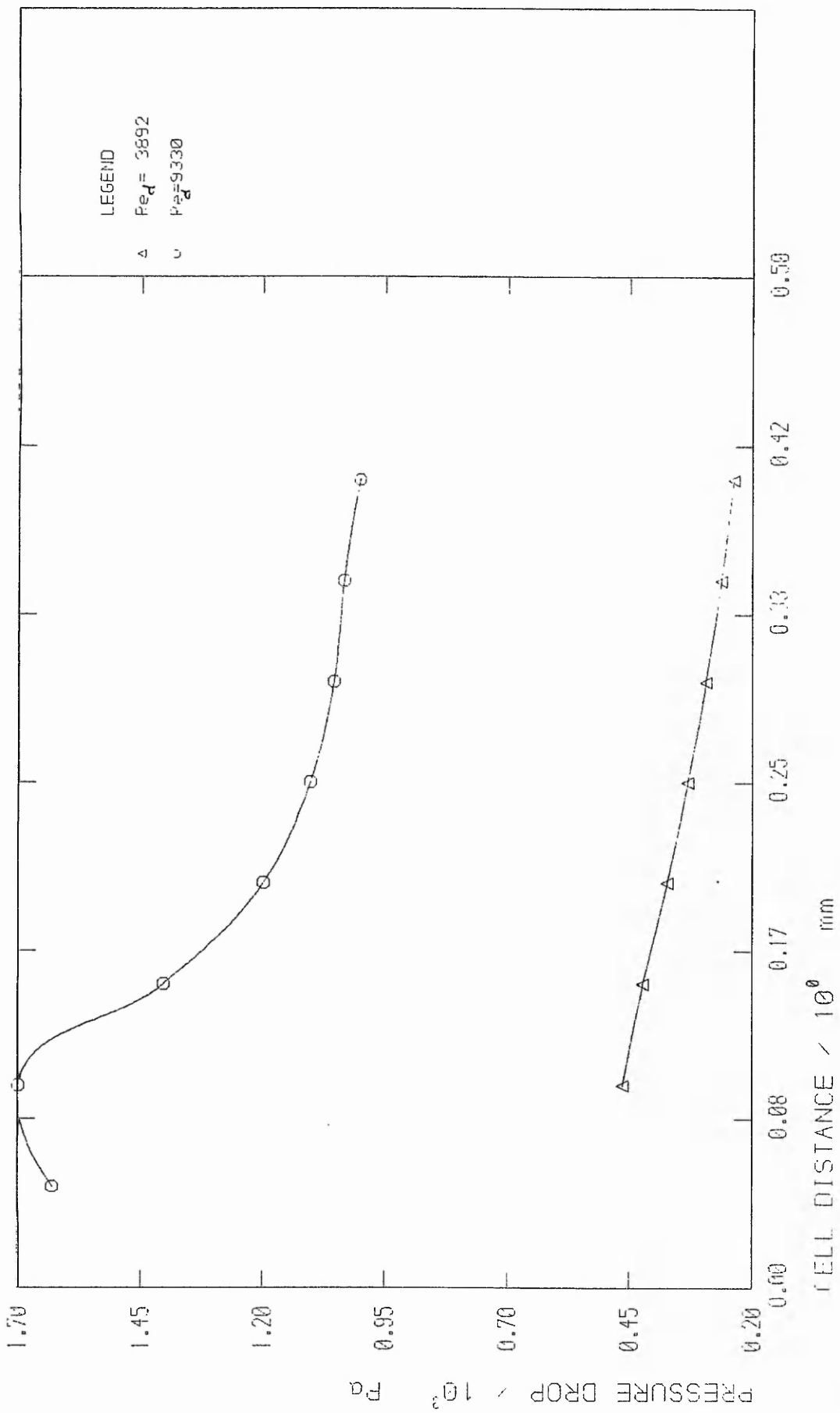


GRID INDEPENDENCE CHECK: SHEAR STRESS AT THE CONDUIT WALL VS NUMBER OF HALF-RADIAL CELLS

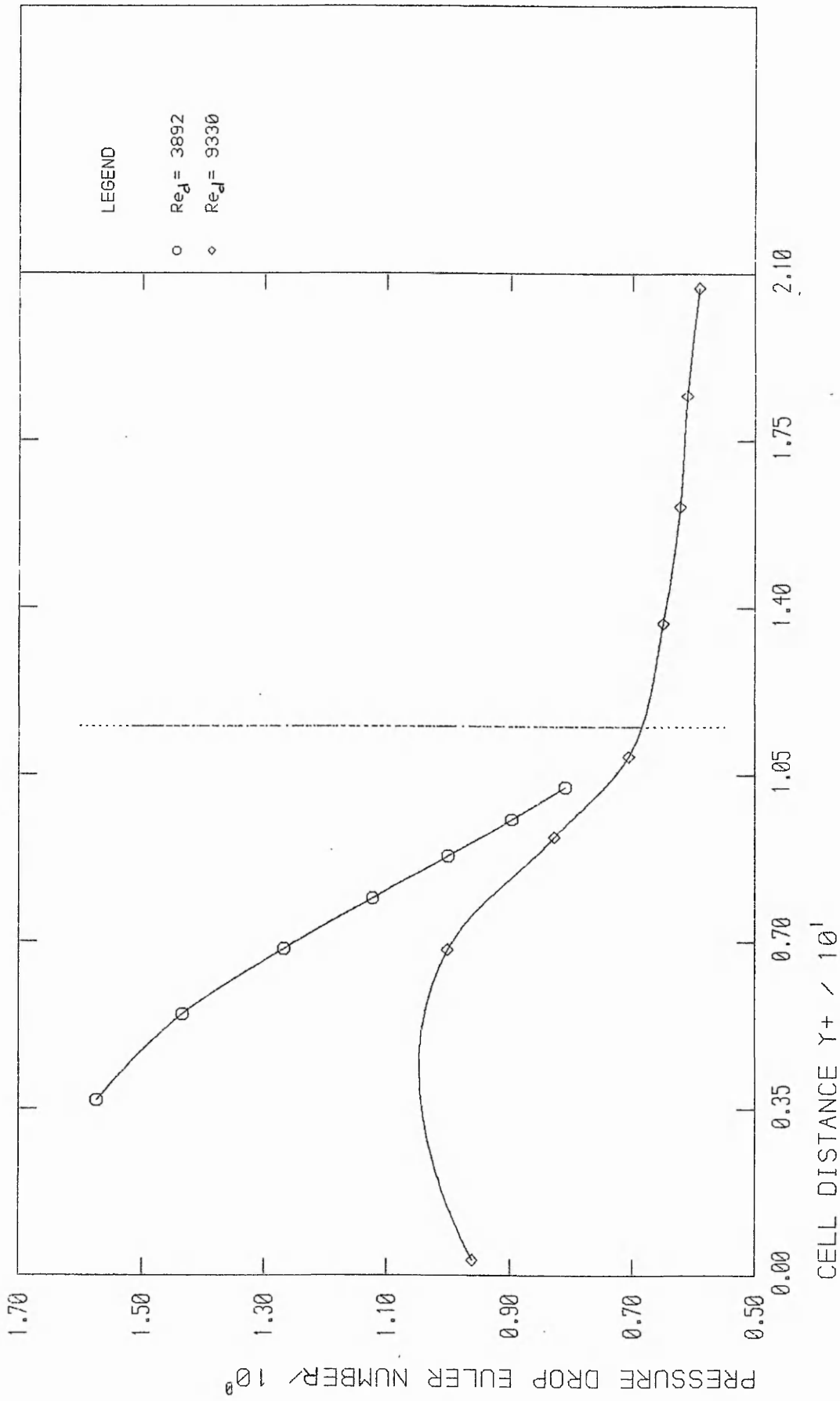


ANALYSIS OF FIRST CELL CENTRE POSITIONING: FORCE ON THE OCCLUDED BALL VS WALL-CELL CENTRE DISTANCE

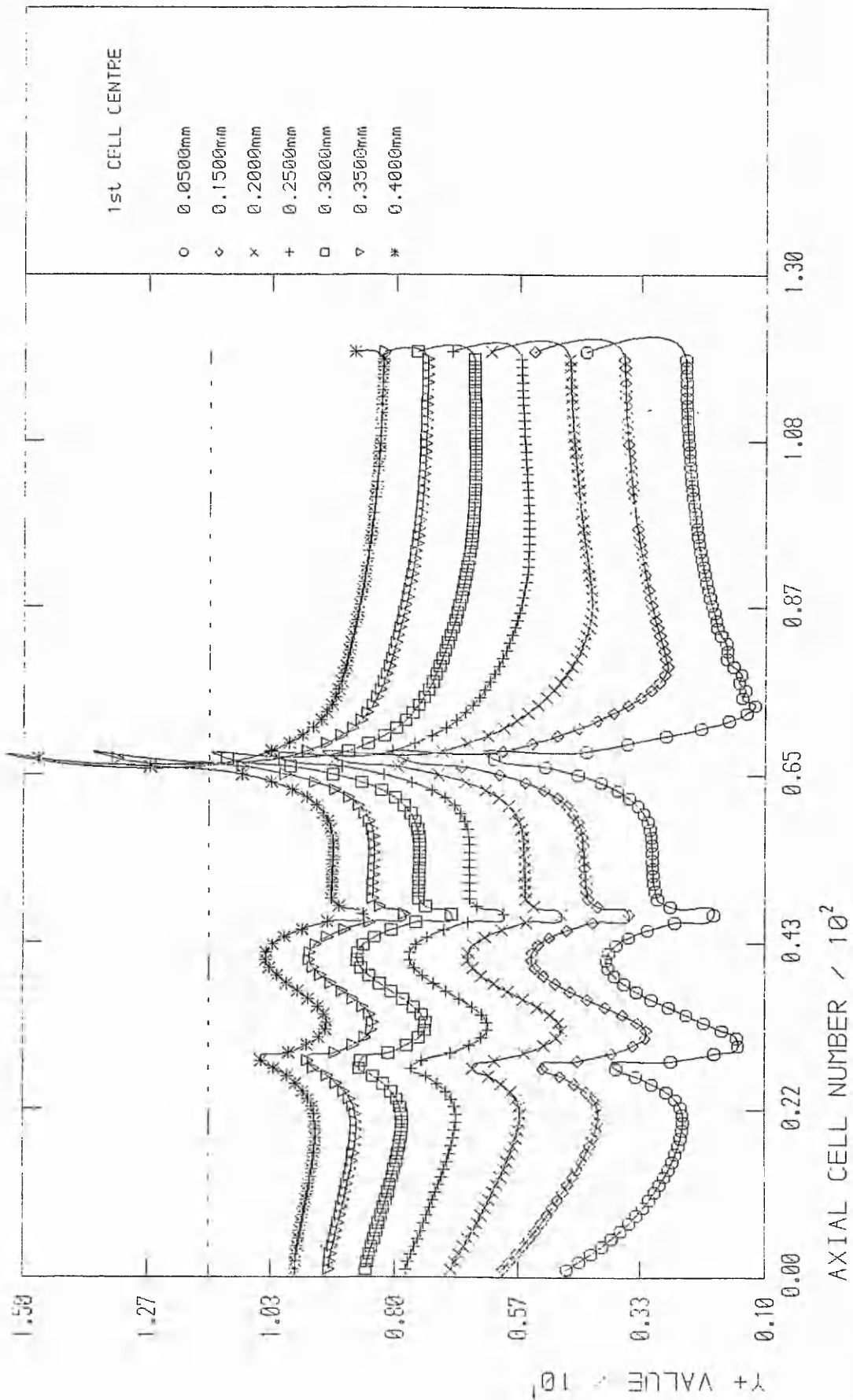
Figure 6.8



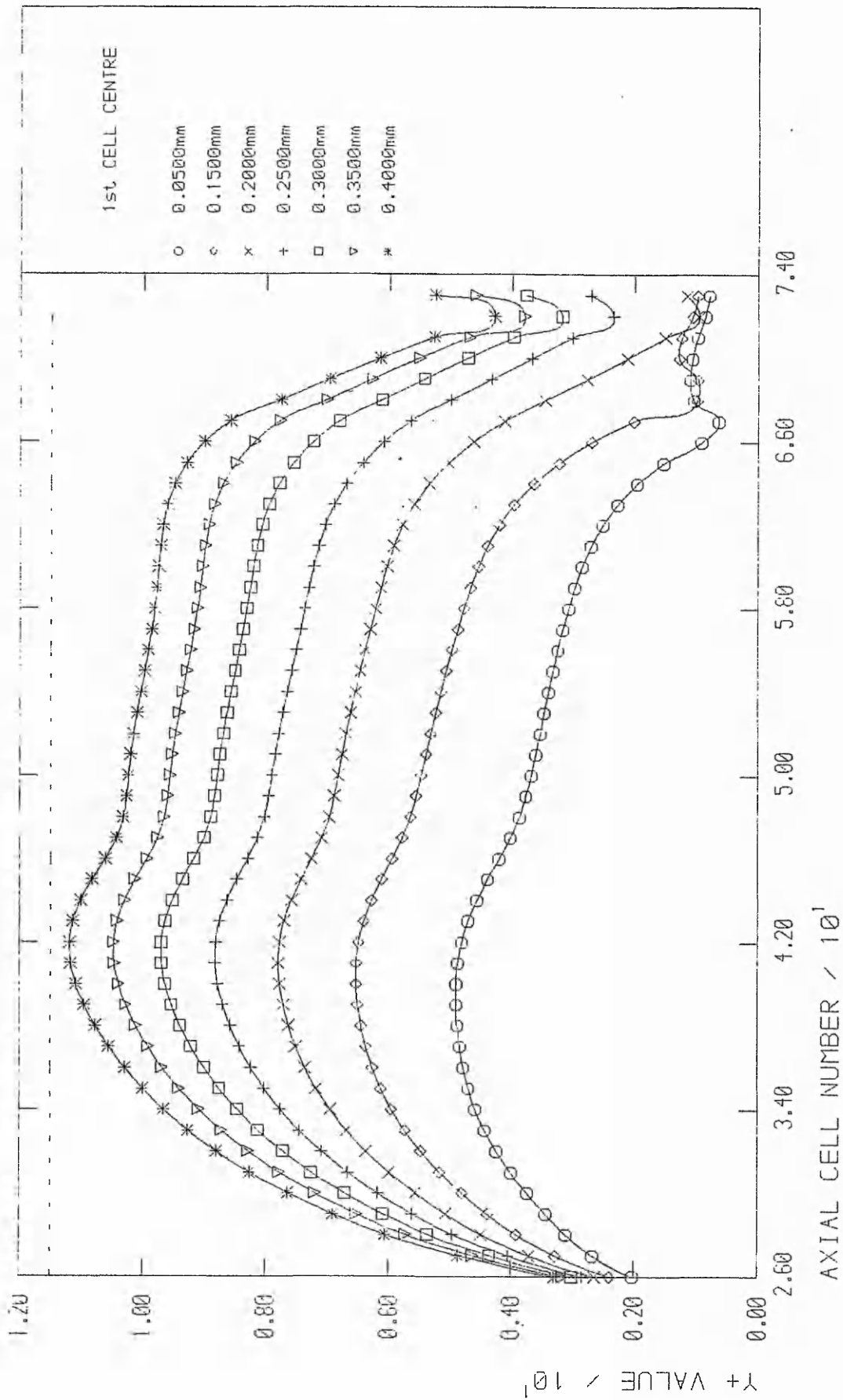
ANALYSIS OF FIRST CELL CENTRE POSITIONING:  
 PRESSURE GRADIENT BALL VS FIRST CELL CENTRE DISTANCE.



ANALYSIS OF FIRST CELL CENTRE POSITIONING: DIMENSIONLESS PRESSURE GRADIENT VS DIMENSIONLESS FIRST CELL CENTRE DISTANCE



SOLUTION DEPENDENCE ON WALL CELL DIMENSIONS:  
 Y+ AT CONDUIT SURFACE VERSUS CELL NUMBER, FLOW RATE = 7L/min



SOLUTION DEPENDENCE ON WALL CELL DIMENSIONS:

Y+ AT BALL SURFACE VERSUS CELL NUMBER, FLOW RATE = 70  $\mu$ m/s

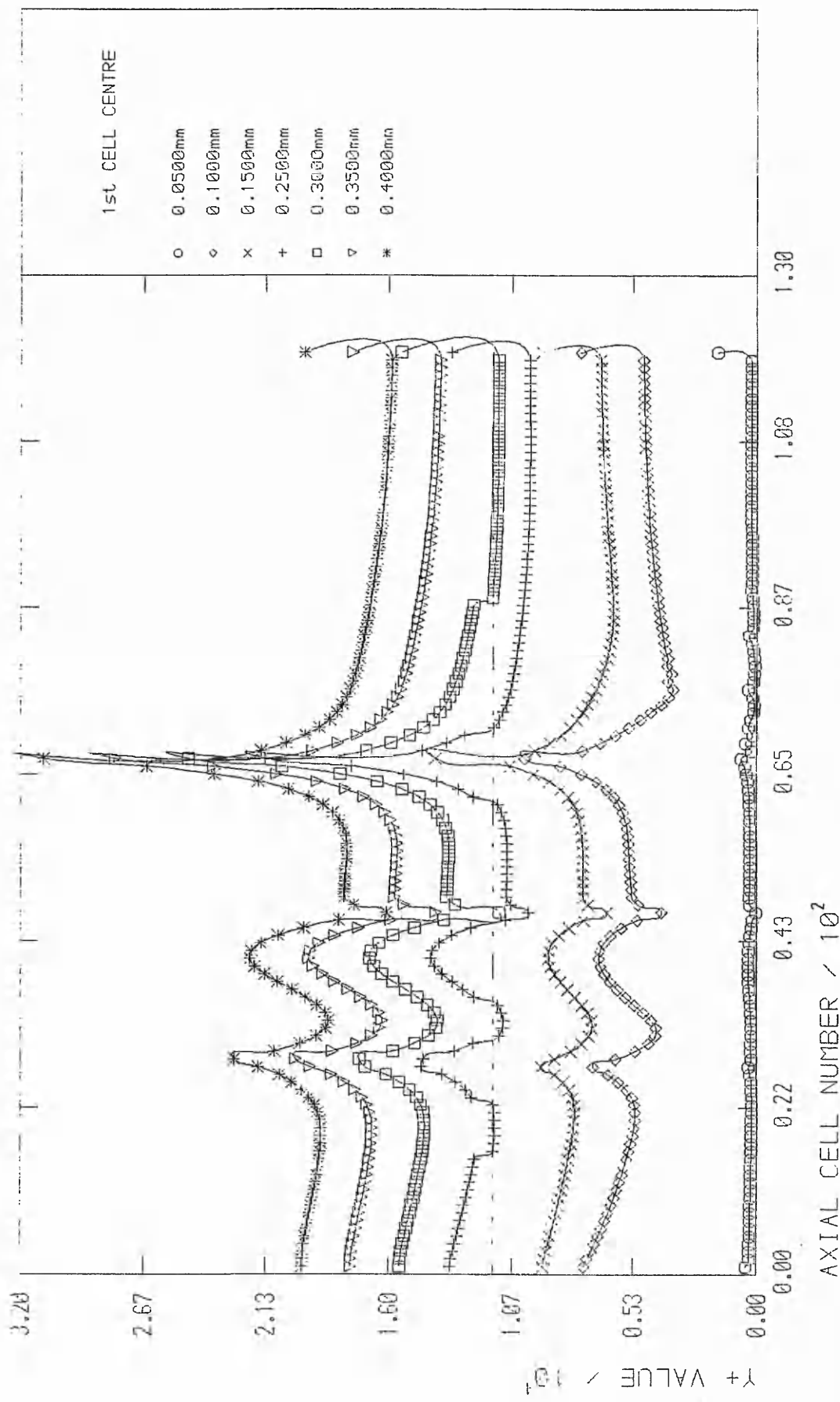
established as  $y^+$  for each value of  $\delta$  fell below 11.5, even with  $\delta$  set equal to 0.4mm. In a flow rate of 21l/min acceptable  $y^+$  values were established at and above  $\delta = 0.25$ mm (figures 6.13 and 6.14). Further figures show that with  $\delta$  maintained at 0.4mm, flow conditions at the conduit wall and ball surface remain acceptable for all flow rates to which the valve sections were subjected; SISO (figures 6.15 and 6.16), SICO (figures 6.17 and 6.18), LRRSICO (figures 6.19 and 6.20). The conclusion that grid independence could not be established when  $y^+$  at the wall-cell centres did not exceed 11.5 is in accordance with the findings of Rosten and Spalding (1986) and Thalassoudis et al (1987), described earlier in chapter four. This non-dimensional wall distance takes into consideration not only the physical location of the cell centre, but also the localised flow rate, being of the form of a localised Reynolds' number. The dimensionless wall-cell centre distance was monitored by the run-time 'GROUND' routine by introducing the relationship:

$$y^+ = \frac{k^{1/2} C_{\mu} C_D^{1/4} \delta}{\nu}$$

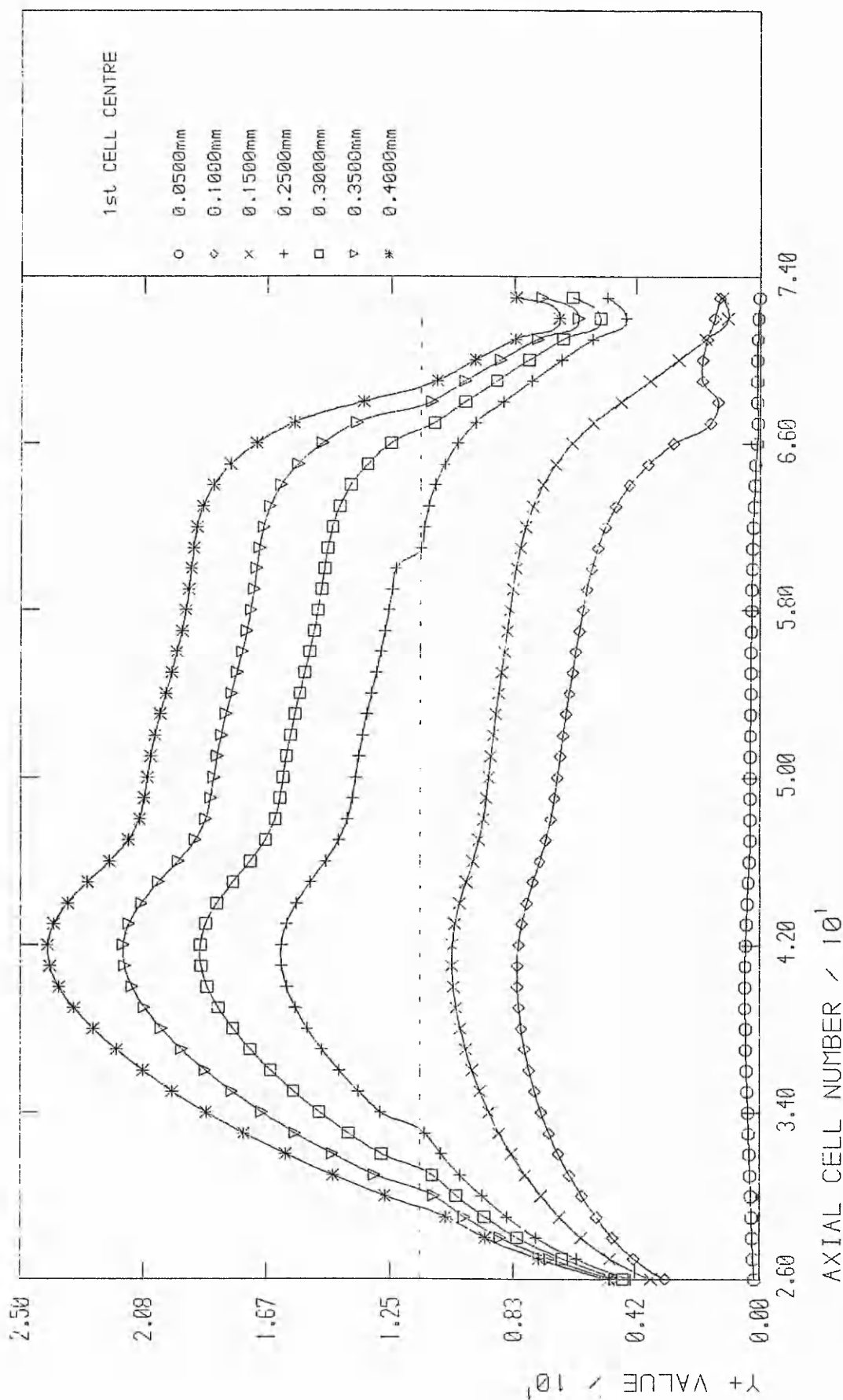
which is derived by substituting in to the definition for  $y^+$  the relationship for  $U_{\tau}$  taken from the descriptor of  $k$  at the wall in equation [4.9], ie

$$\text{from [4.9] } U_{\tau} = C_{\mu} C_D^{1/4} k^{1/2}$$

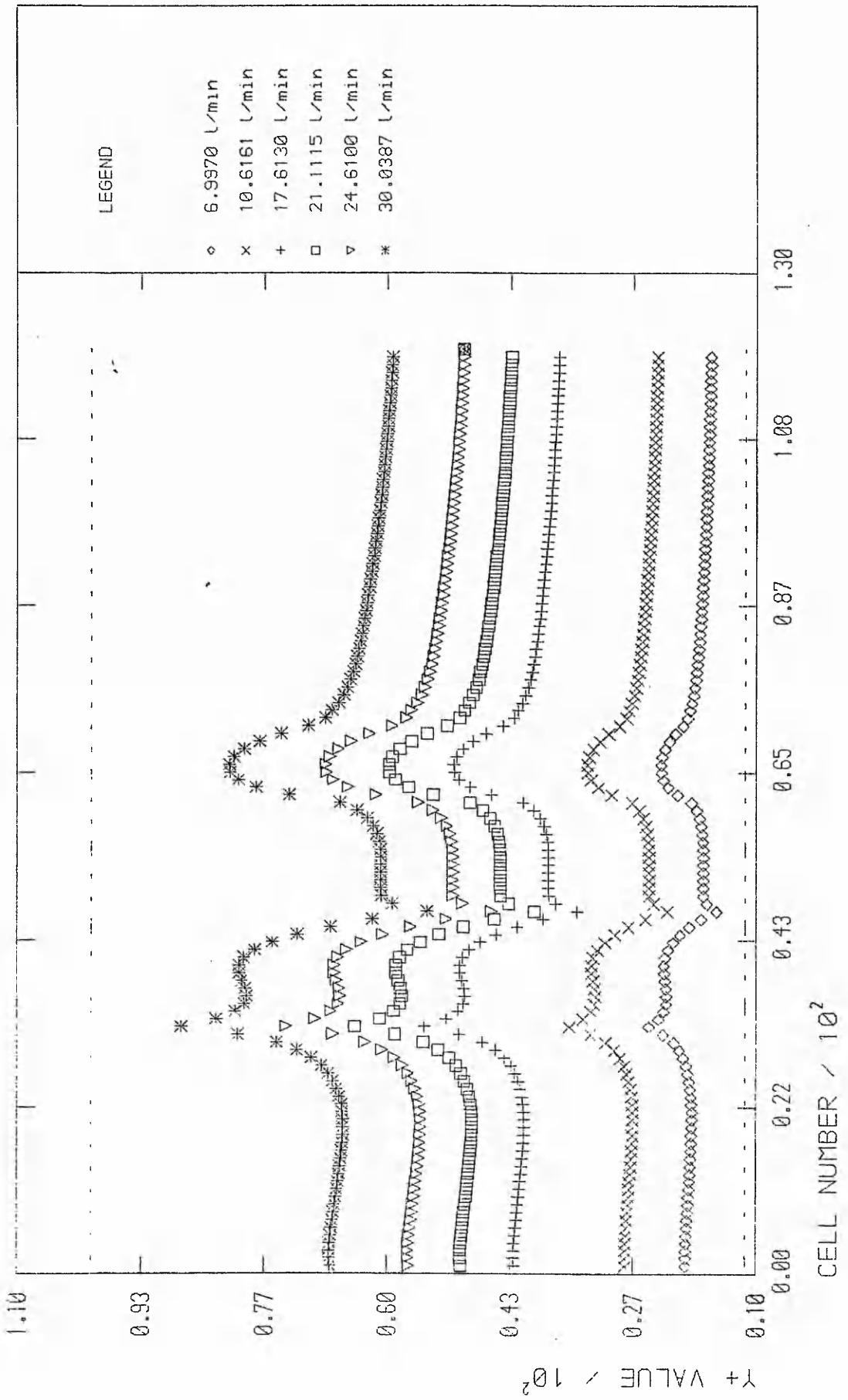
is substituted into  $y^+ = \delta U_{\tau} / \nu$



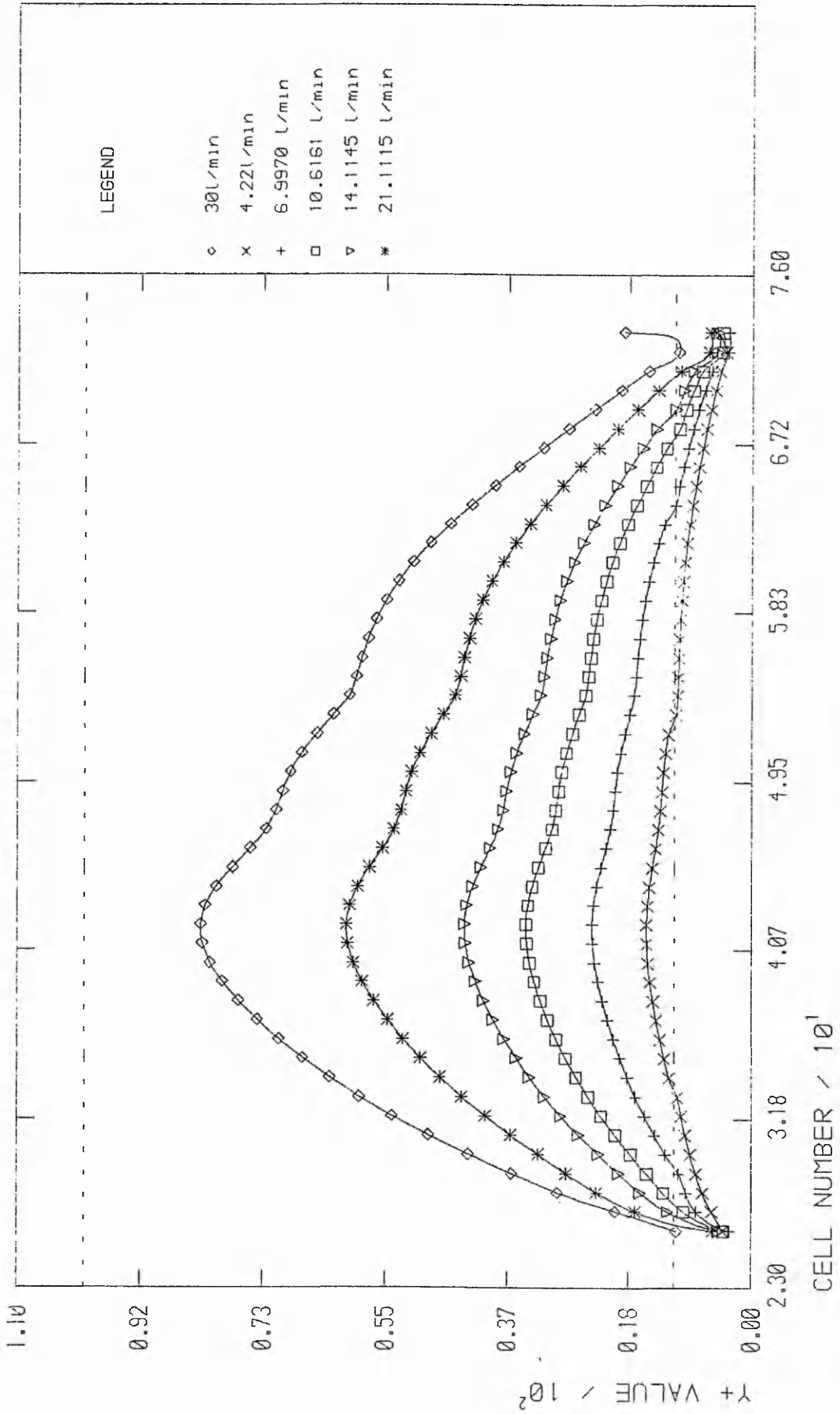
SOLUTION DEPENDENCE ON WALL CELL DIMENSIONS:  
 Y+ AT CONDUIT SURFACE VERSUS CELL NUMBER, FLOW RATE = 21L/min



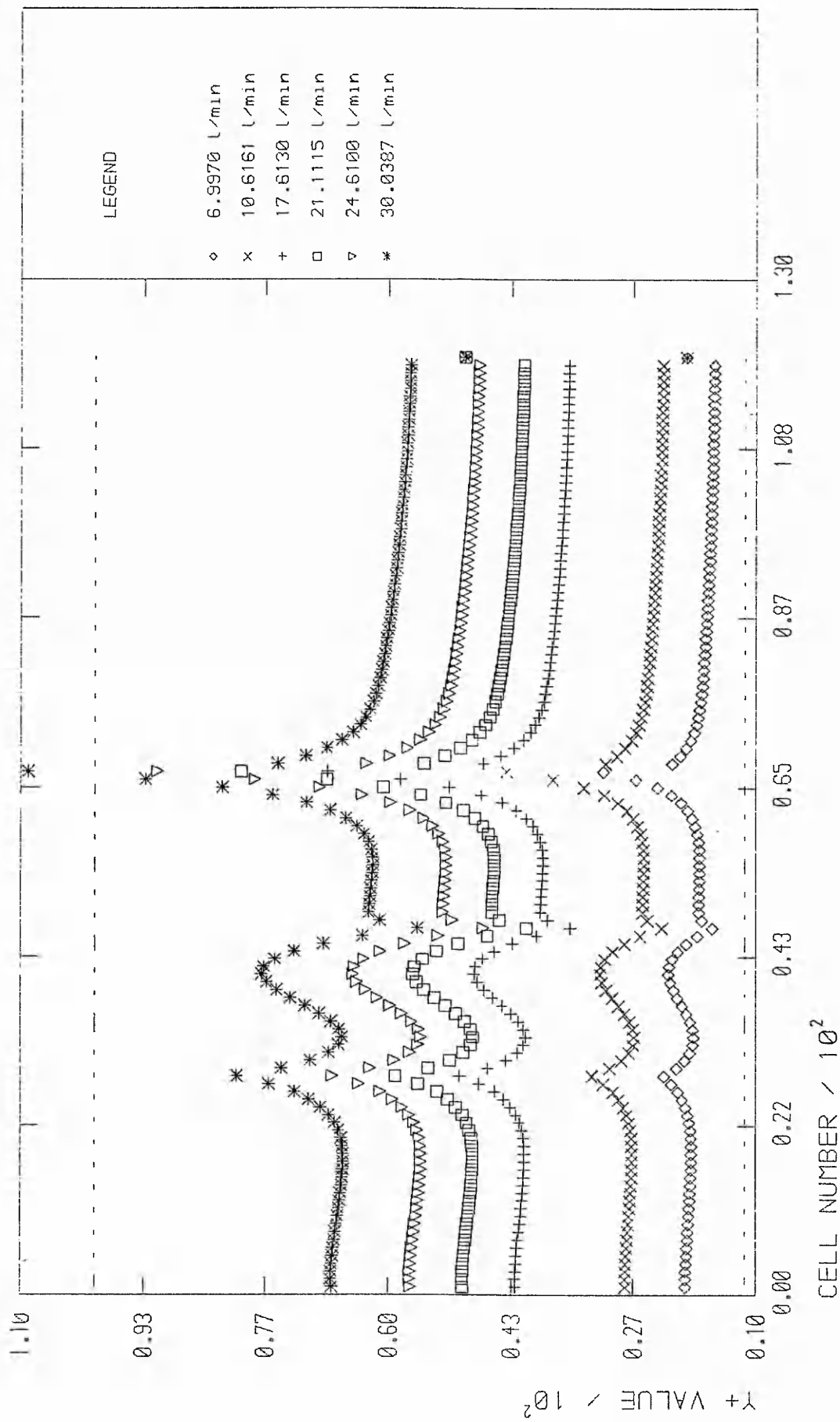
SOLUTION DEPENDENCE ON WALL CELL DIMENSIONS:  
 Y+ AT BALL SURFACE VERSUS CELL NUMBER, FLOW RATE = 21L/min



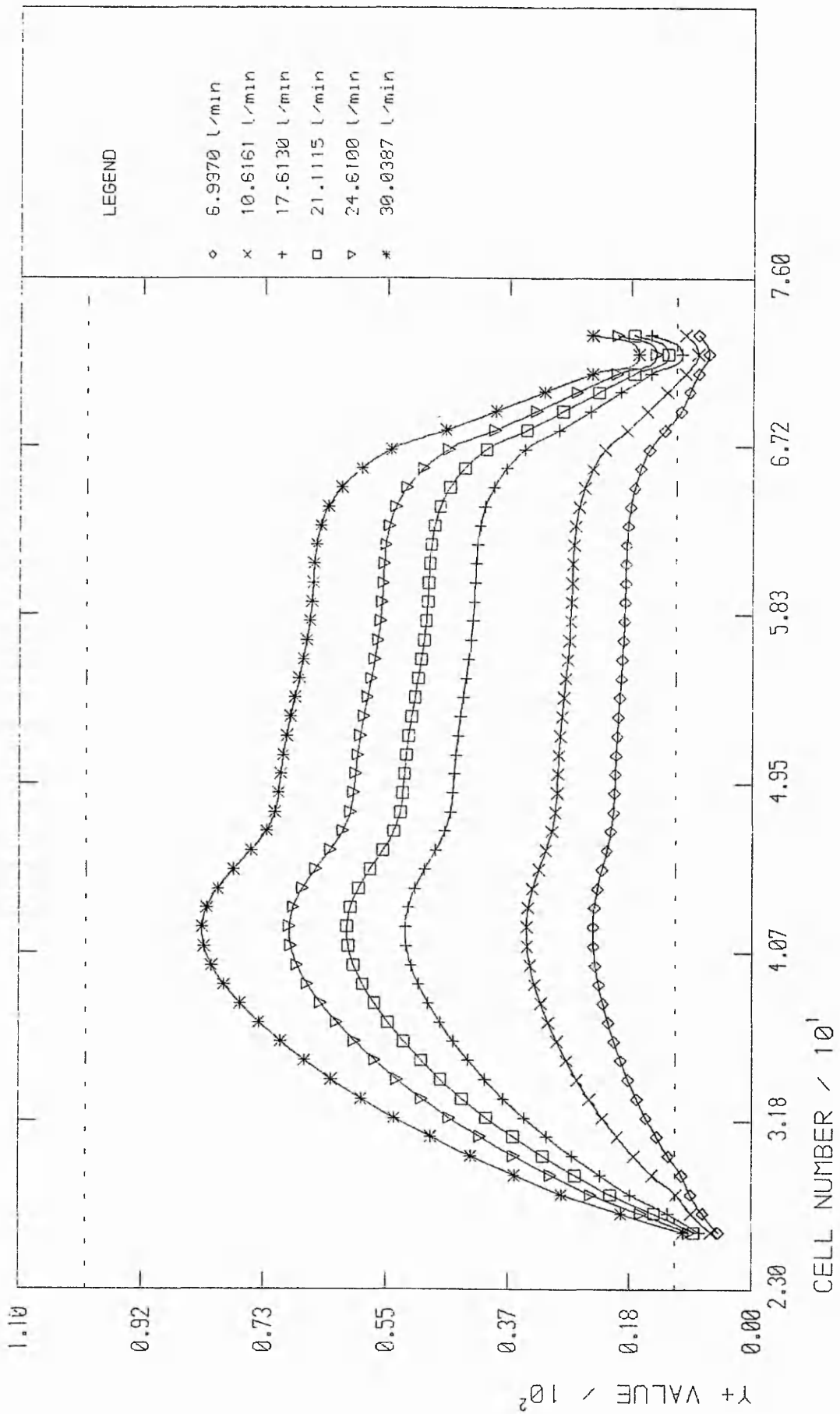
CELL NUMBER VERSUS Y+ FOR VARYING FLOW RATES:  
CONDUIT WALL OF ORIGINAL VALVE GEOMETRY



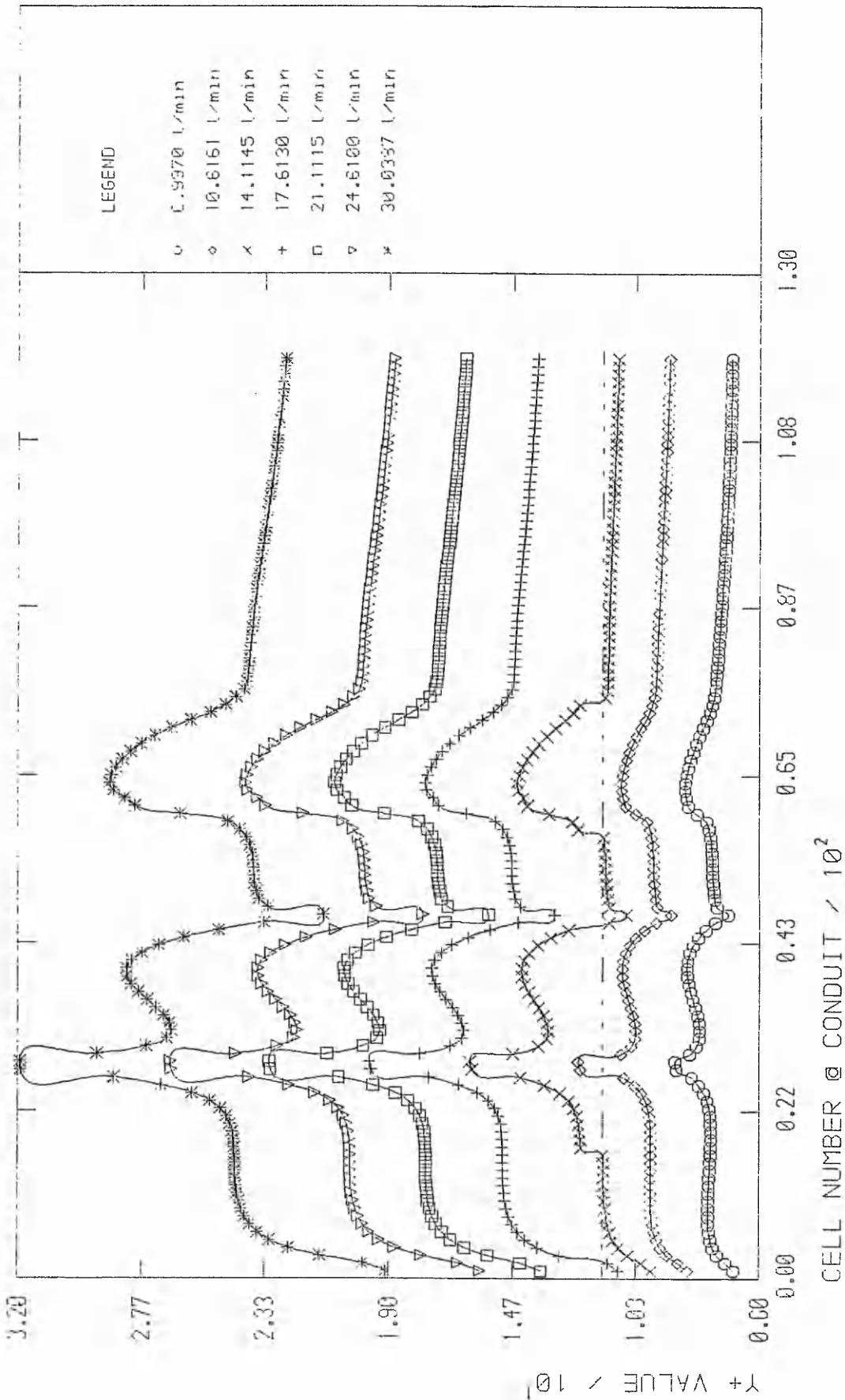
CELL NUMBER VERSUS Y+ FOR VARYING FLOW RATES:  
BALL SURFACE OF ORIGINAL VALVE GEOMETRY



CELL NUMBER VERSUS Y+ FOR VARYING FLOW RATES:  
CONDUIT WALL OF SECOND PROTOTYPE VALVE GEOMETRY (SICO)

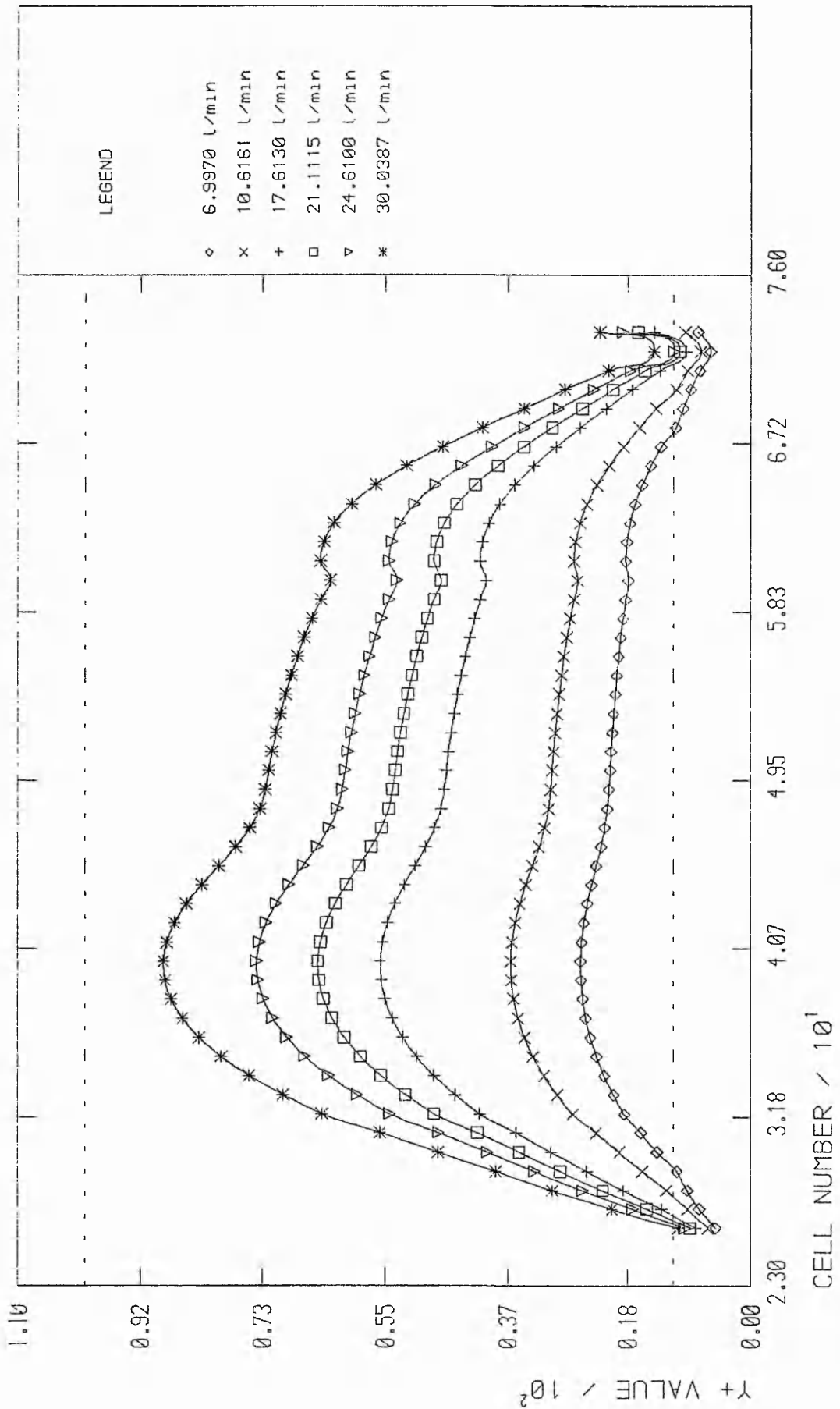


CELL NUMBER VERSUS Y+ FOR VARYING FLOW RATES:  
BALL SURFACE OF SECOND PROTOTYPE VALVE GEOMETRY (SICO)



DIMENSIONLESS FIRST CELL CENTRE DISTANCE FOR VARYING BLOOD FLOW RATES IN FINALISED CONDUIT DESIGN (LRRSICO) WITH 30mm BLENDING RADIUS

Figure 6.19



CELL NUMBER VERSUS Y+ FOR VARYING FLOW RATES:  
BALL SURFACE OF THIRD PROTOTYPE VALVE GEOMETRY (LRRSICO)

### 6.3 Momentum in Orthogonally Modelled Grids - Simple pipe

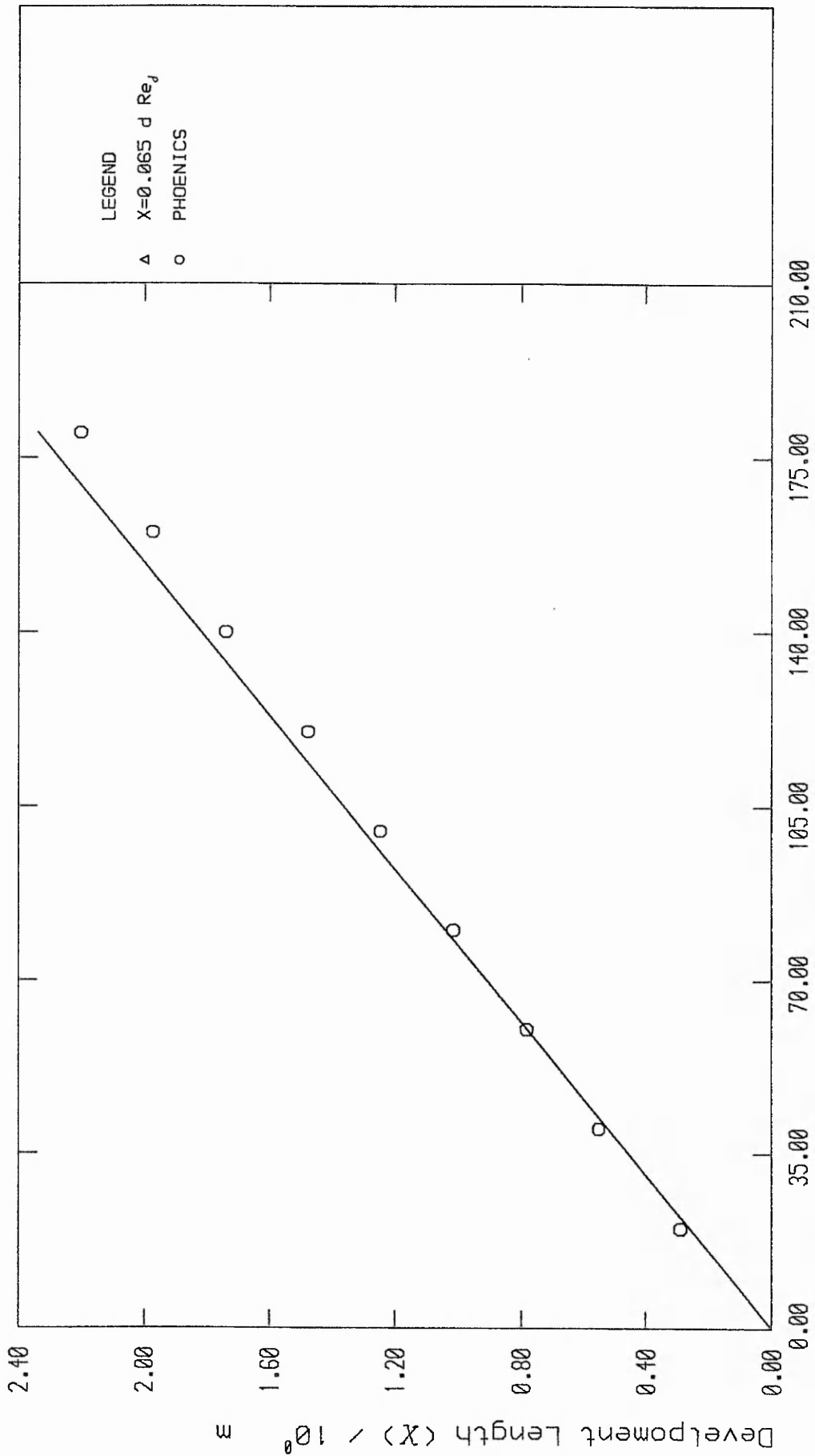
A series of predictions in laminar flow regimes were made in a simple pipe geometry, varying Reynolds' number in steps of 200 from a lower value of 200 up to 1 800, after which the laminar/turbulent transition threatens the validity of prediction. Several parameters were examined to validate each step of construction of the final and complex modelling regime.

The development length was found by manual examination of the CFM result files. The maximum error (of -5.8%) in the prediction of development length by PHOENICS is at  $Re_d = 1\ 800$ . PHOENICS tended to predict a shorter development length than Boussinesq at Reynolds' numbers above  $Re_d = 600$  (see figure 6.21). The best fit of the development length data yielded the relationship:

$$X/d = 0.0596 Re_d + 0.062 \quad [6.1]$$

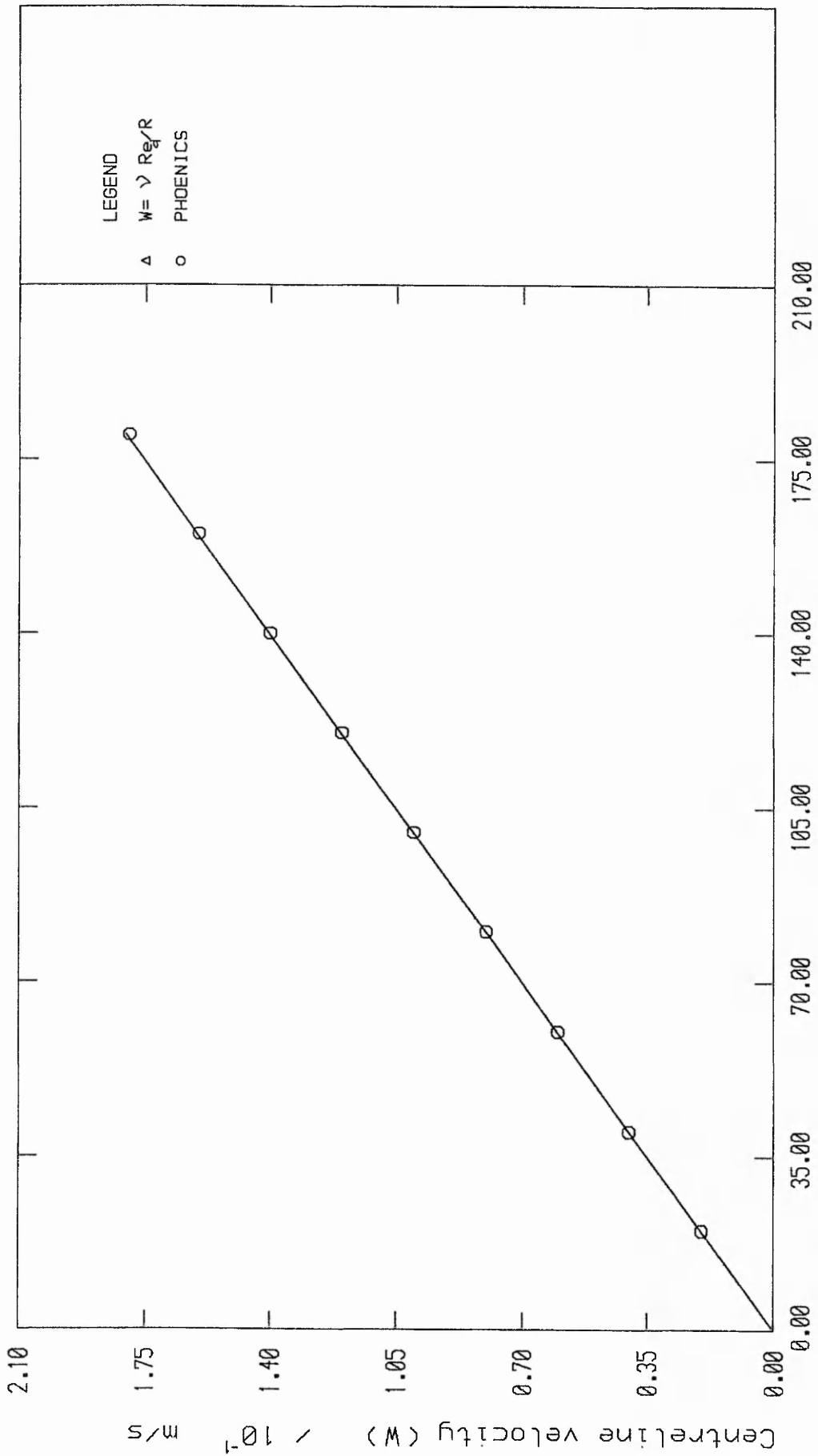
This is directly comparable with Boussinesq's equation [4.3].

The error in the predicted maximum velocity was negligible (0.28% - 0.66%) over the above range of Reynolds' numbers (see figure 6.22), though interpolation was necessary to arrive at the centreline velocity as the closest predicted velocity was half the boundary cell width above the centreline. The predicted turbulent velocity profile was as expected, and is plotted in figure 6.23. To verify the correctness of predictions of turbulent velocity a similar series of tests was conducted to those of the laminar flow study. Based on Darcy's equation and using Blasius' descriptor for wall friction, PHOENICS predictions for pressure gradient were typically +3.9% in error and  $w_{max}/w_{ave}$  yielded a value of 1.215, only +2.8% below the



Reynold's Number (Re) / 10<sup>1</sup>

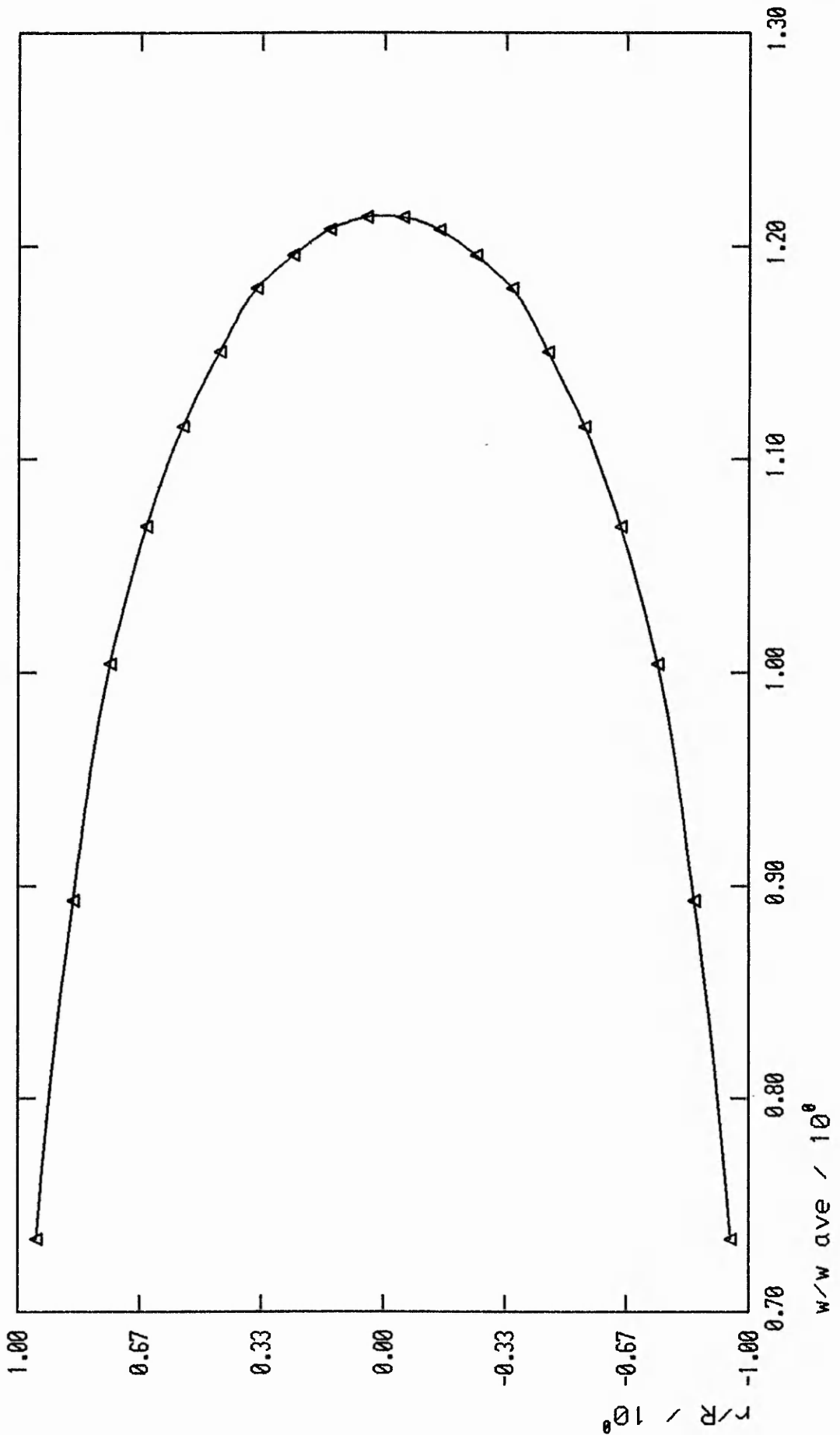
PHOENICS AND ANALYTICAL DEVELOPMENT LENGTH PREDICTIONS  
 FOR LAMINAR, NEWTONIAN PIPE FLOW



Reynold's Number ( $Re_d$ ) /  $10^1$

PHOENICS AND ANALYTICAL MAXIMUM VELOCITY PREDICTIONS FOR LAMINAR, NEWTONIAN PIPE FLOW

Figure 6.22



NORMALISED VELOCITY PROFILE IN FULLY DEVELOPED TURBULENT PIPE FLOW

Figure 6.23

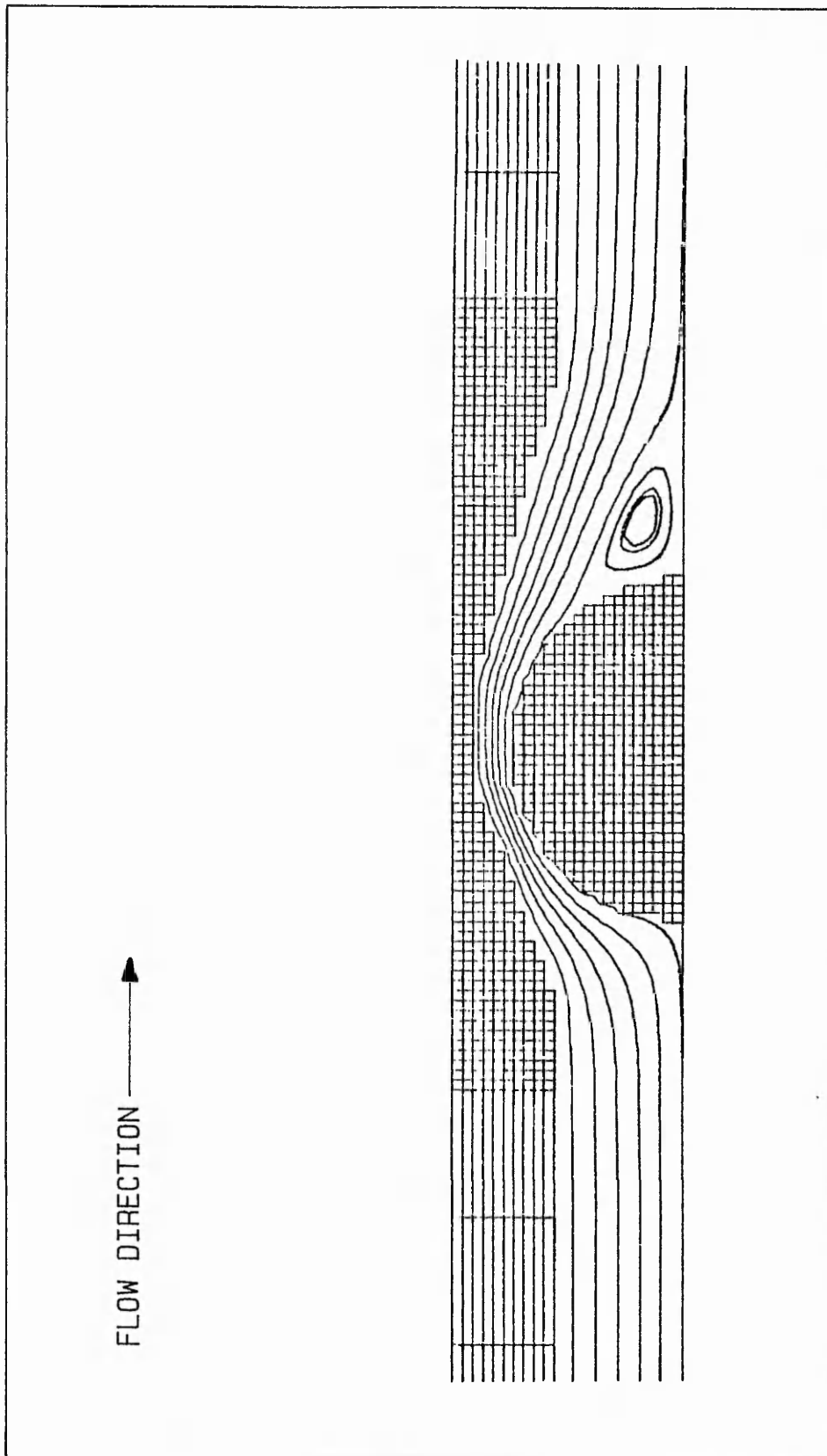
lower value of the expected range 1.2195 - 1.25.

#### 6.4 Momentum in Orthogonally Modelled Grids - Valve Geometry

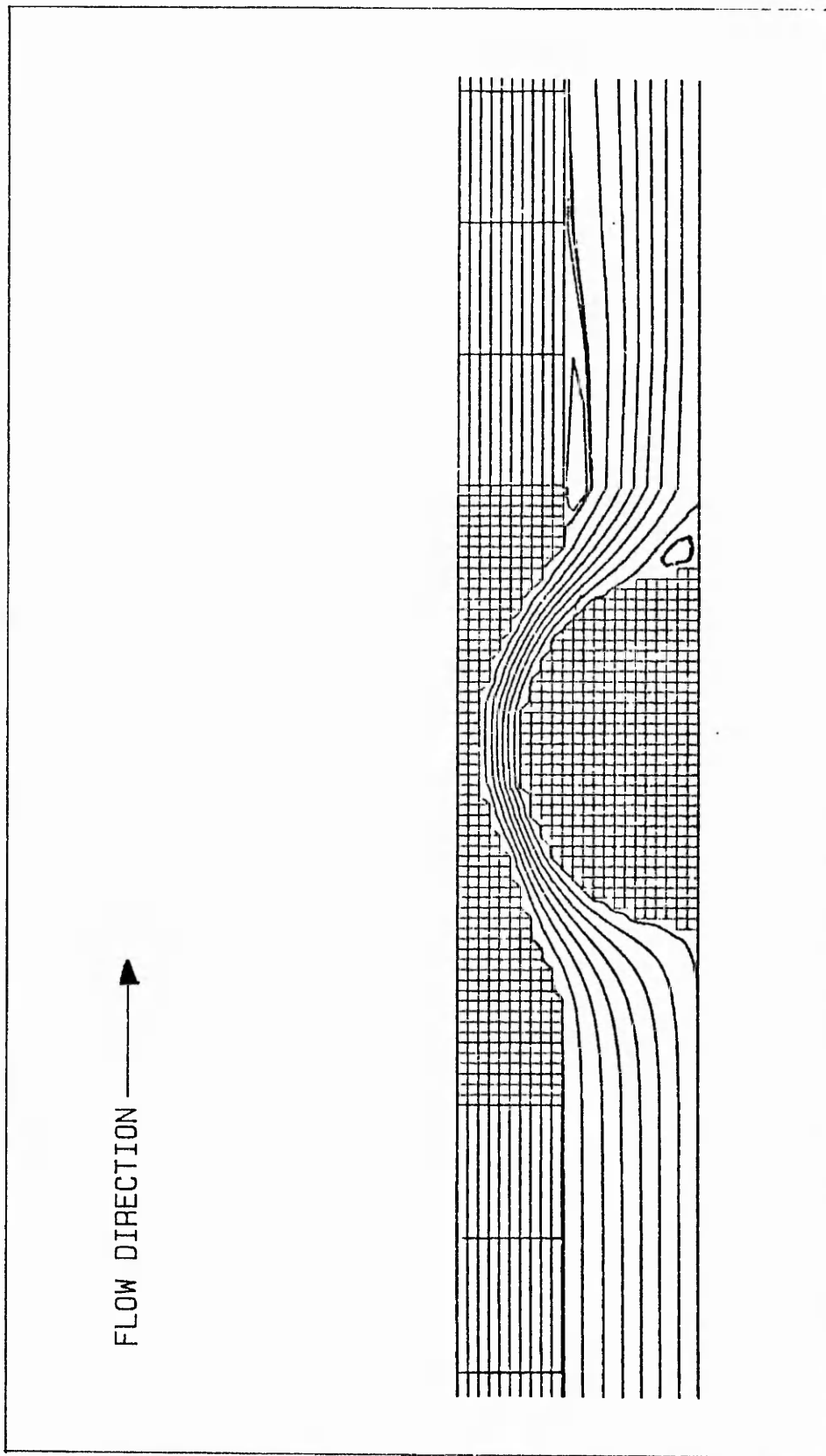
The solution in orthogonal grids yielded reasonable pressure gradients but convergence was slow and therefore time consuming. Grid independence was difficult to achieve because the spacing and size of cells directly affected the profile of the flow geometry and excessive time would need to be expended in order to repeatedly re-fit the valve geometry to a continually varying grid. The non-realisation of a satisfactorily grid independent regime affected momentum predictions in two ways: discontinuity of the flow occurred at steps on the ball surface and outer wall profile, as seen in the streamlines of figures 6.24 and 6.25. Also zones of recirculation were predicted behind the ball and, although plausible, such recirculation was not apparent in reality. This problem was later demonstrated to be dependent upon the positioning of the wall-cell centres. More specifically if the dimensionless distance of the wall-cell centres did not exceed 11.5 (ie. if  $y^+ > 11.5$  at  $\delta$ ) momentum prediction was poor.

#### 6.5 Momentum Predictions in Curvilinear Grids

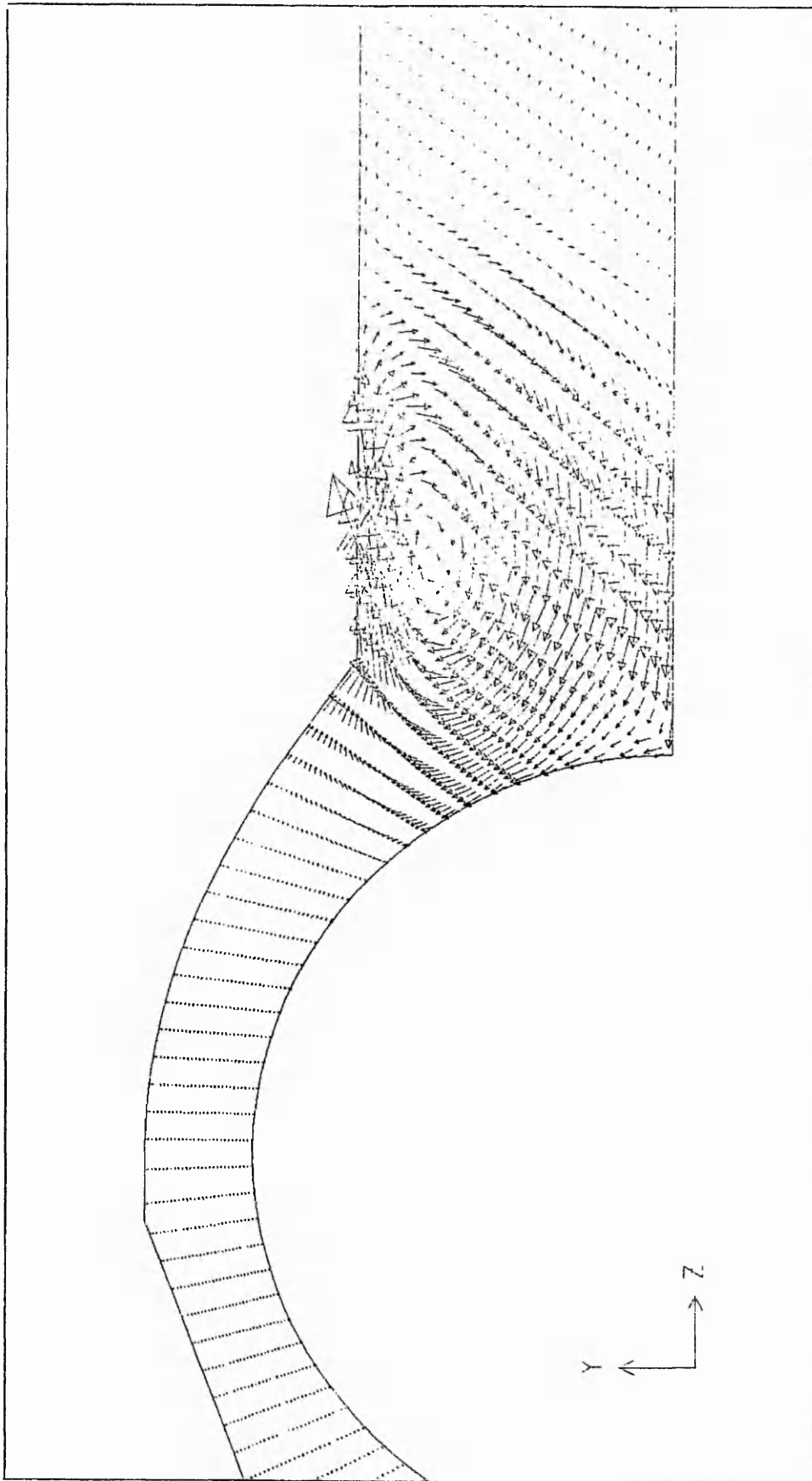
A more complete analysis of momentum predictions was possible for Body Fitted Coordinate grid geometries due to the reasons outlined above. The major question raised by the first series of tests was whether or not predictions of recirculation were correct, as prescribed in orthogonally modelled solutions. Figures 6.26 - 6.29 show vector diagrams of velocity fields



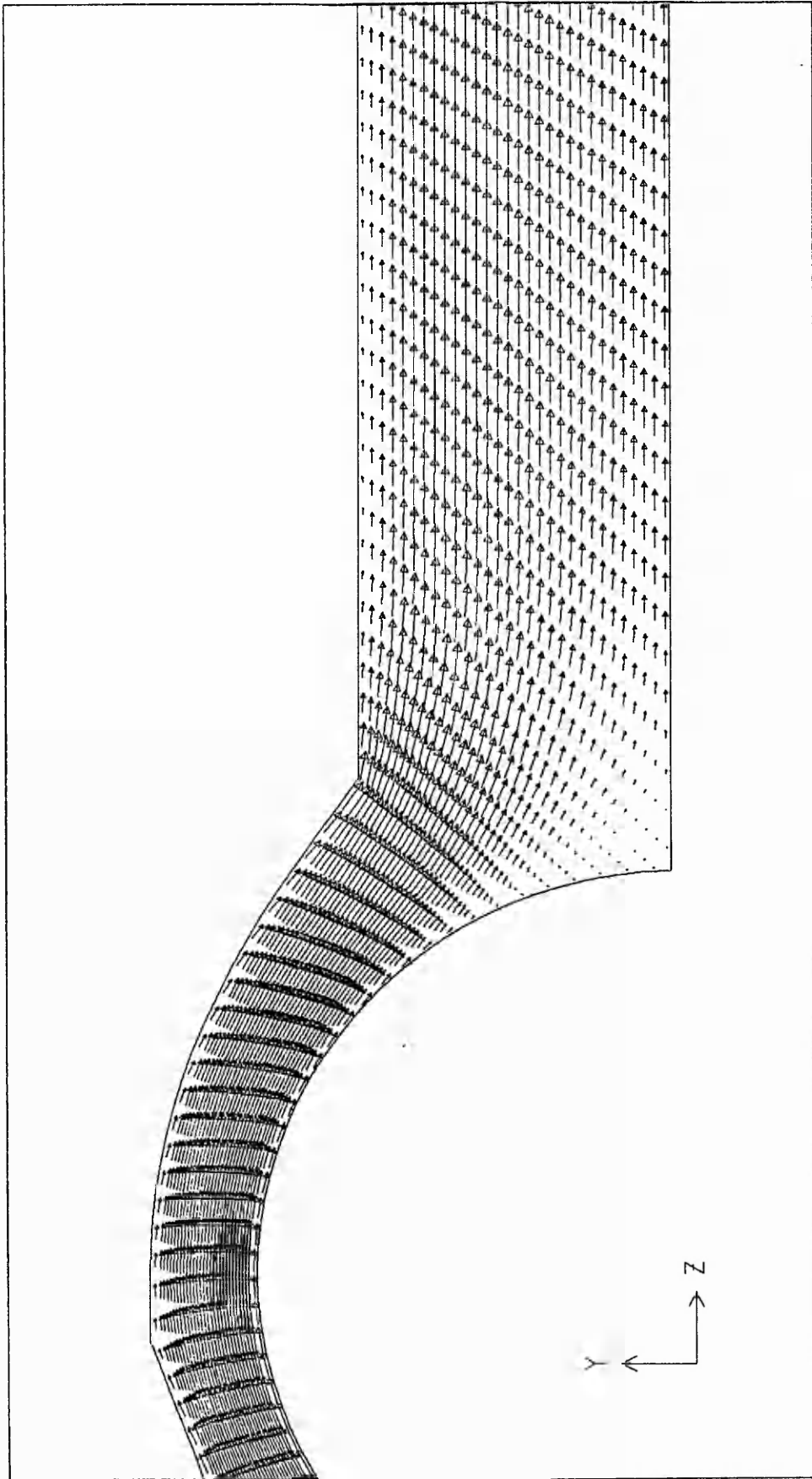
STREAMLINES FOR FLOW THROUGH SISO  
VALVE MODELLED ONTO AN ORTHOGONAL GRID



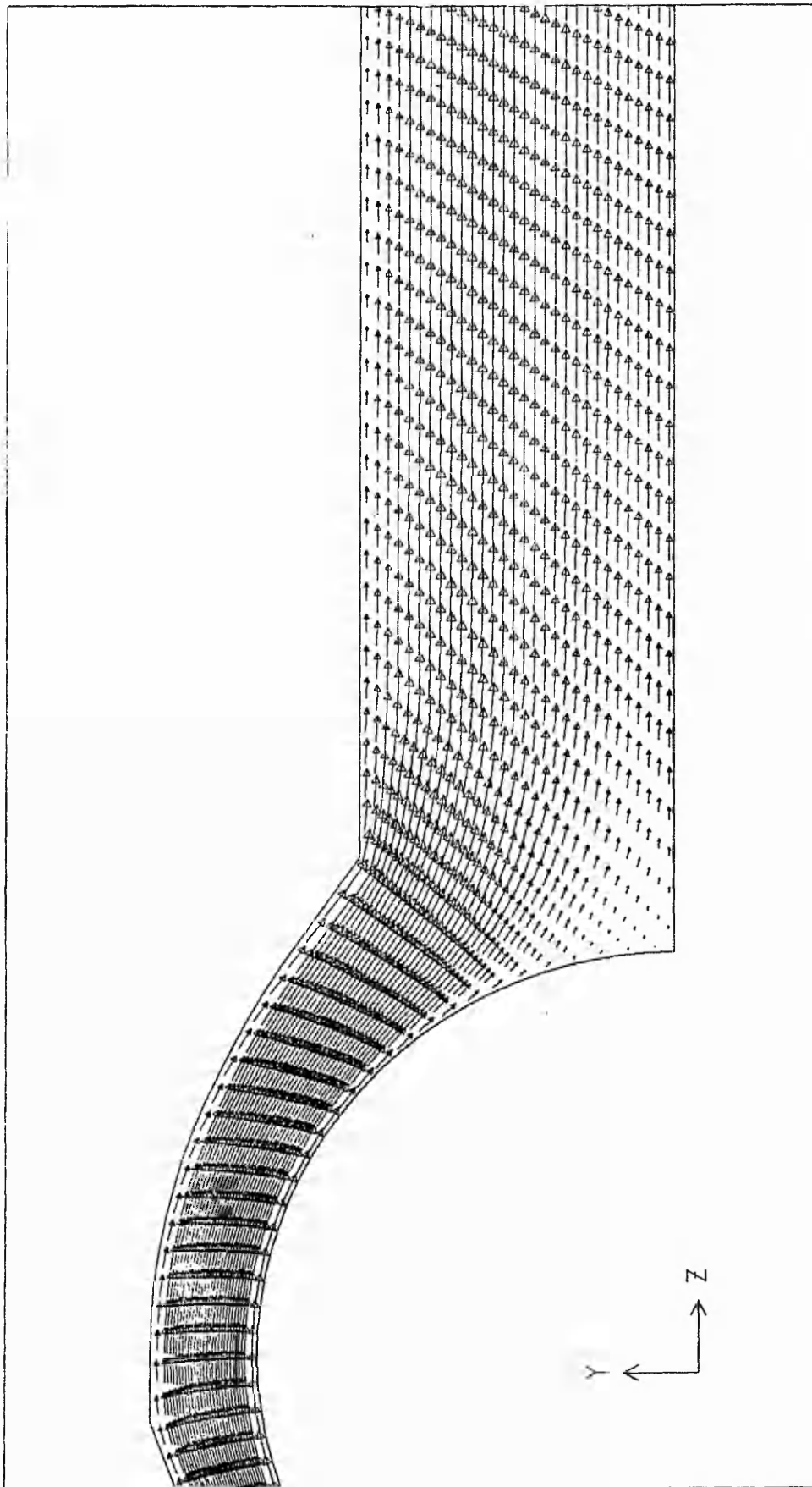
STREAMLINES FOR FLOW THROUGH SICO VALVE MODELLED ONTO AN ORTHOGONAL GRID



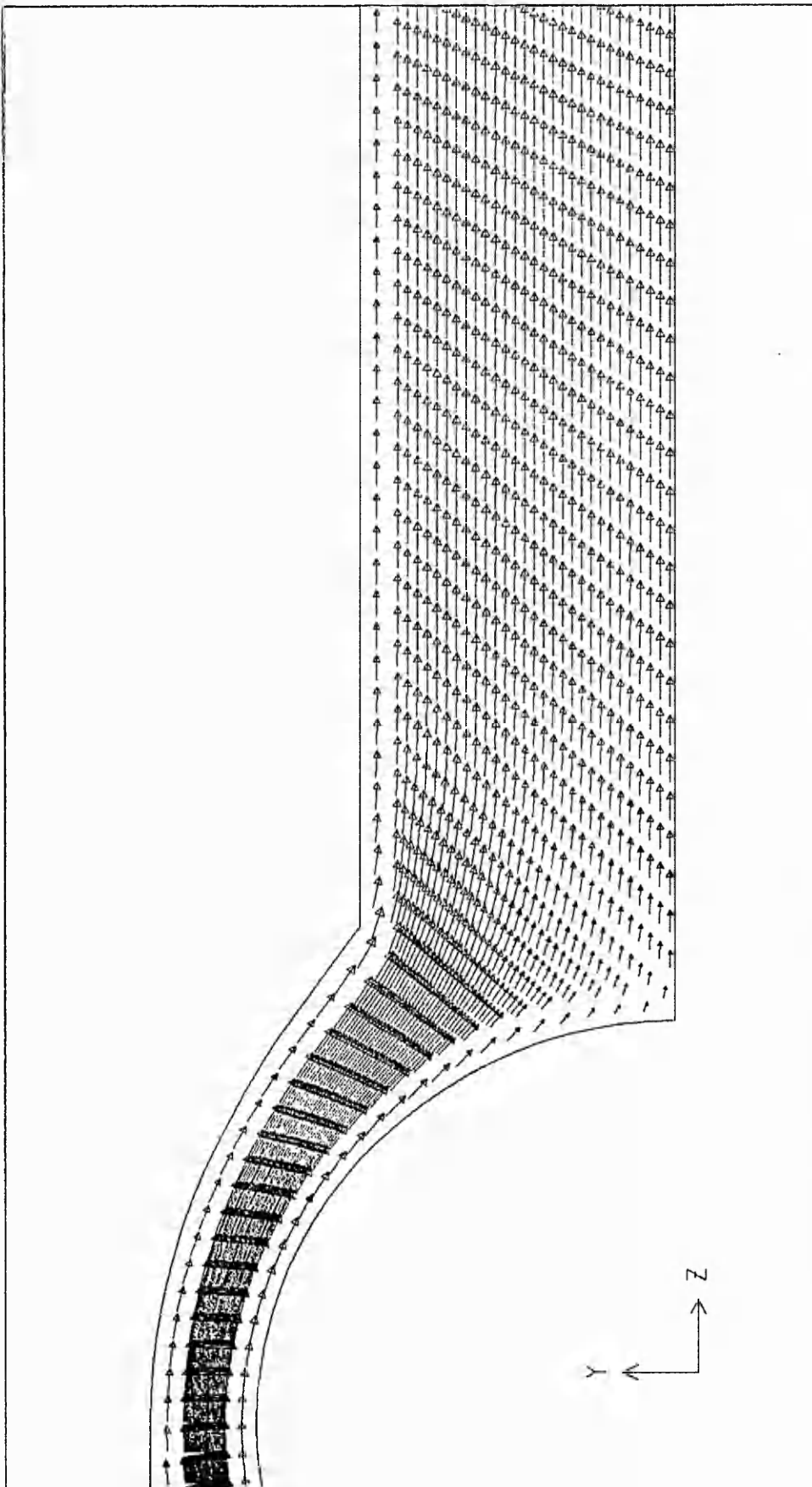
VELOCITY VECTORS IN SICO VALVE  
 $y^+$  AT BALL SURFACE CELL CENTRES = 3.18



VELOCITY VECTORS IN SICO VALVE  
Y+ AT BALL SURFACE CELL CENTRES = 6.82



VELOCITY VECTORS IN SICO VALVE  
Y+ AT BALL SURFACE CELL CENTRES = 9.1



VELOCITY VECTORS IN SICO VALVE  
Y+ AT BALL SURFACE CELL CENTRES = 20.71

predicted by BFC procedures. Clearly the amount of recirculation is considerably dependent upon the choice of cell centre distance, particularly at the ball surface. In consideration of the findings of the grid independence tests discussed above, velocity fields in figures 6.26 - 6.28, where average  $y^+$  values at cell centres along the ball surface were 3.18, 6.82 and 9.19 respectively, can clearly be invalidated in favour of the velocity field predicted in figure 6.29, where  $y^+$  is 20.71. Furthermore, flow fields observed experimentally using flow visualisation techniques also discount the existence of recirculation (see chapter five). Although this finding was surprising, as recirculation would occur behind the ball in an infinite flow field, other research programmes have presented similar conclusions; Smith et al. (1975), Hasenkamp et al. (1987), but comparison is limited because of differences in test sections and distances downstream where velocities were quoted. Recirculation is also obviously very dependent upon the geometry into which the ball is placed (Modi and Akutsu 1980). A further limitation to the prediction of momentum parameters was encountered in the breakdown of the  $k - \epsilon$  model, which invalidated modelling in flow of Reynolds' numbers below 3 000. This observation is similar to that of Edwards (1988) who discusses deviation from expected parameter values at Reynolds' numbers of 4 000.

The entire solution for momentum was dependent upon the correct prediction of shear rate, as shear rate was used both in the generation term of the  $k - \epsilon$  model and by the constitutive equation in the formulation of apparent viscosity. However, the shear rate generator built into PHOENICS proved unsatisfactory

when applied to curvilinear geometries as only an incomplete two dimensional shear rate term was provided:

$$\dot{\gamma} = a \frac{\partial w^2}{\partial x} + b \left( \frac{\partial w}{\partial x} \frac{\partial w}{\partial y} \right) + c \frac{\partial w^2}{\partial y}$$

where a,b, and c are geometrical constants (Rosten and Spalding 1986)

This term severely under predicted the shear rate, especially in the regions where flow deviated furthest from the Z-wise direction. As a consequence the viscosity of the blood was over predicted, leading to excessive pressure gradients across the valve. Moreover, the use of such a shear term reduced the validity of Computational Fluid Mechanics as a flow analysis technique, since it is less valid than the assumption of isotropic turbulence made in LDA work. The solution to the problem was to introduce a "psuedo second phase". Into the second phase velocities were placed the Cartesian resolutes of the first phase velocities. The shear rate calculations were then based on the second phase velocities and were conducted in the same manner as would be the first phase in an orthogonal geometry (utilising the full three dimensional generation term):

$$\dot{\gamma} = 2 \left( \left( \frac{\partial u}{\partial x} \right)^2 + \left( \frac{\partial v}{\partial y} \right)^2 + \left( \frac{\partial w}{\partial z} \right)^2 \right) + \left( \frac{\partial u}{\partial y} + \frac{\partial v}{\partial x} \right)^2 + \left( \frac{\partial u}{\partial z} + \frac{\partial v}{\partial x} \right)^2 + \left( \frac{\partial w}{\partial y} + \frac{\partial v}{\partial z} \right)^2$$

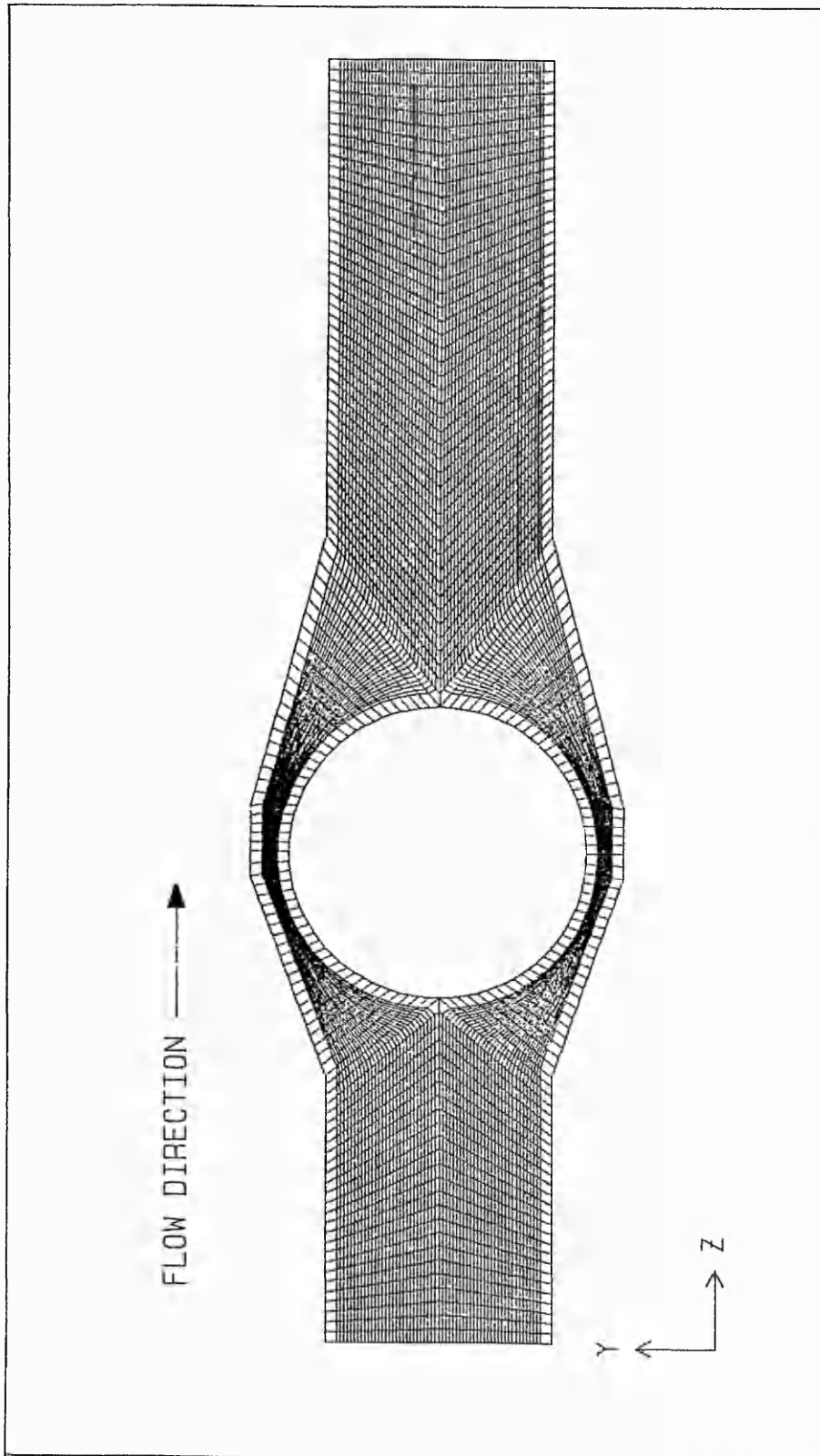
Where flow was only two dimensional, the third dimensional terms were disregarded, leaving a complete two dimensional term for incompressible flow.

## 6.6 Convergence, Convection/Diffusion and Continuity

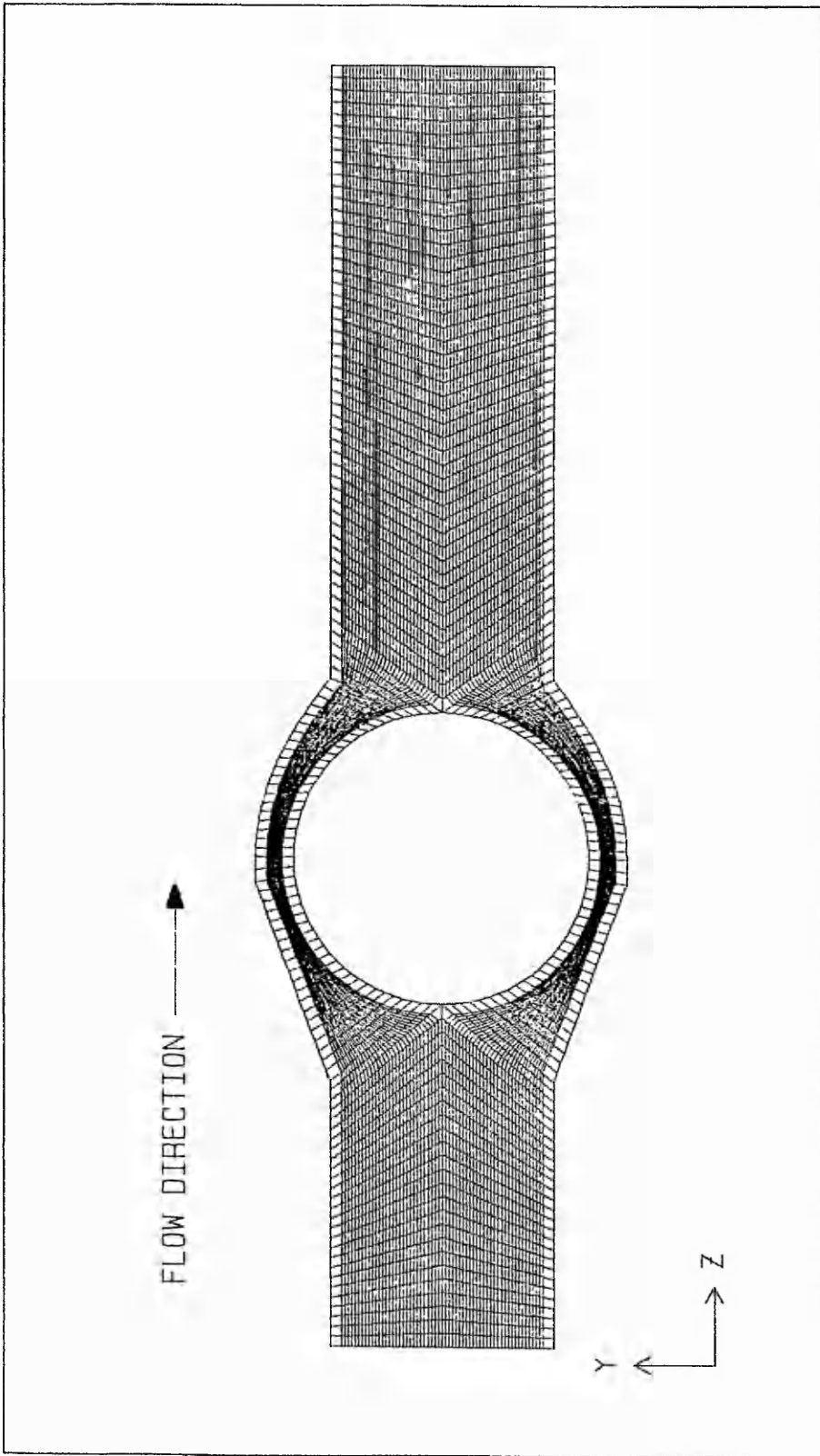
Other factors which affected momentum were convergence, convective/diffusive links and continuity.

In simple orthogonal geometries convergence was not difficult to achieve and high under relaxation values could be assigned to each of the solved variables. In more complex geometries convergence was less readily achieved and relaxation was necessarily high leading to excessive computer time usage. Further difficulties were encountered when BFC's were used to model the flow field. Convergence under these circumstances was very dependent upon the shape of each and every cell, and high non-orthogonality in any cell could lead to non-convergence. Convergence also proved increasingly difficult to attain with decreasing wall-cell dimension. Figures 6.10, 6.13 and 6.14 show the effect of non-convergence of a solution as seen for  $\delta=0.05\text{mm}$ . Necessarily, a great deal of time was expended in order to devise grids capable of yielding convergent solutions and the resulting geometries are shown in figures 6.30 - 6.32 which represent the SISO, SICO and LRRSICO (with 30mm radius) conduits respectively. PHOENICS does incorporate Laplacian solvers which are designed to orthogonalise pre-defined grids, but these proved to be totally inadequate.

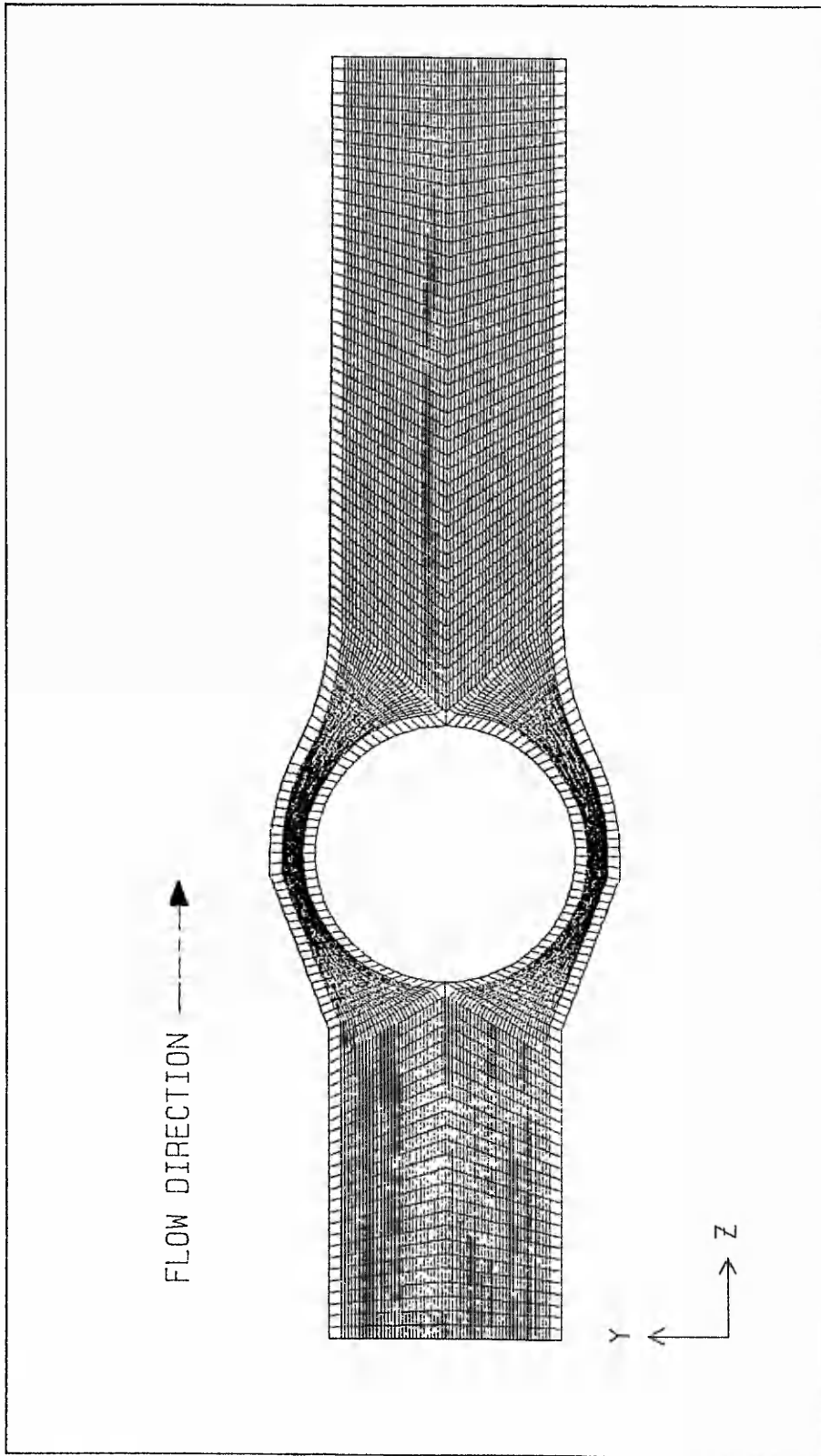
Neither continuity nor the final solution were affected by the ratio of diffusion:convection. Values of full field parameters did not differ considerably if diffusive links were activated. For example, streamwise force on the ball was not altered by more than 1.8%, nor pressure gradients by more than 3% if the cell-to-



SISO VALVE GEOMETRY SUPERIMPOSED  
ONTO A CURVILINEAR GRID



SICO VALVE GEOMETRY SUPERIMPOSED  
ONTO A CURVILINEAR GRID



LRRSICO VALVE GEOMETRY WITH 30mm BLENDING RADIUS SUPERIMPOSED  
ONTO A CURVILINEAR GRID

cell diffusion was altered from 0 to 50%. The diffusive links were disabled as momentum will be almost totally dependent on convection at the values of Reynolds' numbers considered in this study (>3 000).

Continuity checks, which were based on comparisons between residuals of the volume fraction 'R' at inlet and outlet sections, proved satisfactory in all converged solutions.

Finalised boundary conditions used in modelling (as seen in the 'Q1' input file in Appendix 3), based on the above findings were:

INLET:  $k_{in} = 0.25 w^2 \times 0.018$

$$\epsilon = k_{in}^{1.5} \times 0.1643/l$$

where:  $l$ , the mixing length =  $0.09 \times$  Radius

$Re = 3\ 000 - 40\ 000$  based on conduit diameter and bulk flow properties

OUTLET:  $P = 0.00$  (fixed)

CONDUIT WALL AND BALL SURFACE:

$k$  and  $\epsilon$  based on logarithmic wall functions.

$\delta = 0.4\text{mm}$  giving values of  $y^+$  above 11.5 at wall-cell centres for inlet Reynolds' numbers greater than 3 000.

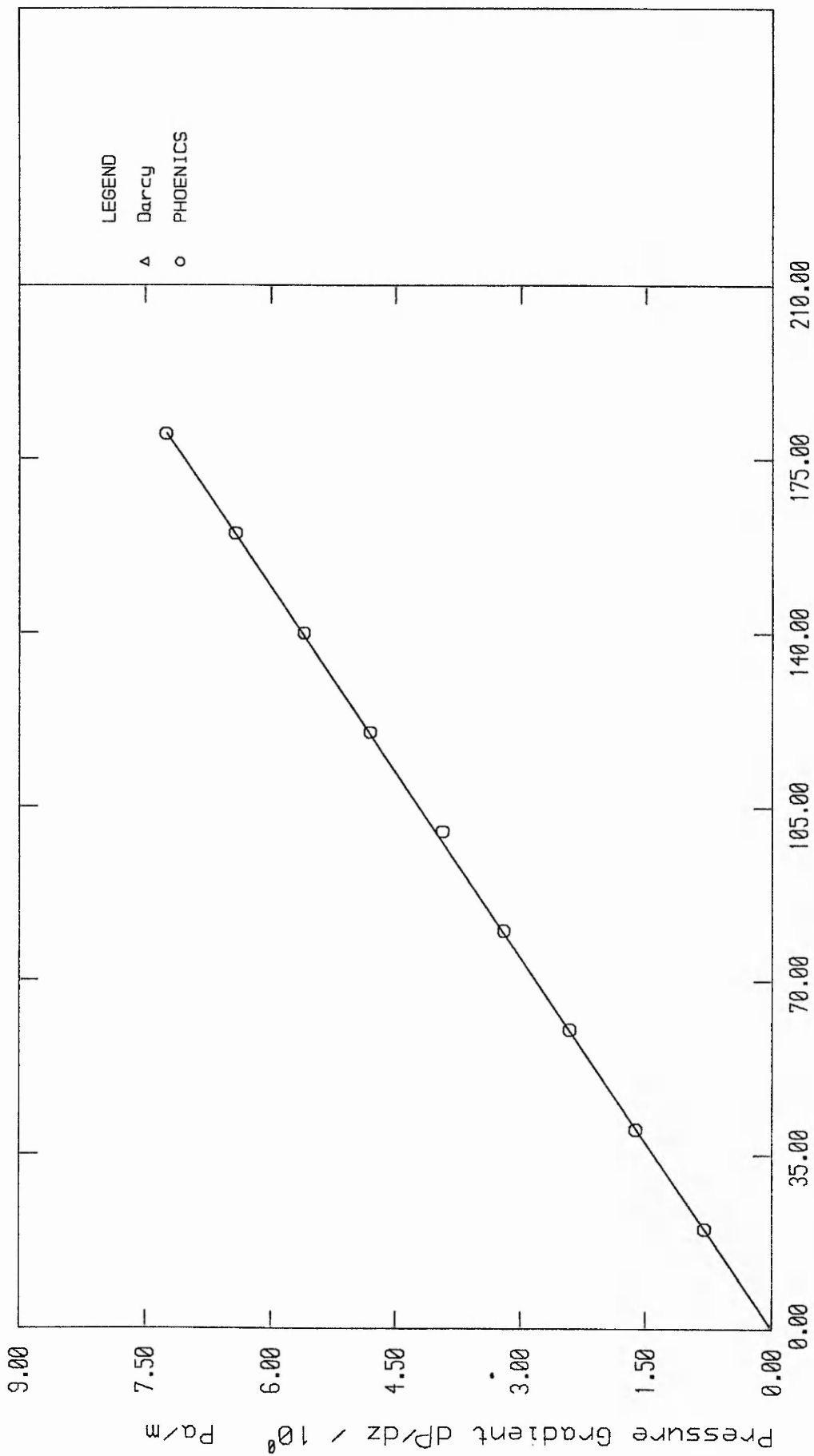
Convergence was deemed complete when the residual of each solved parameter was reduced below  $1 \times 10^{-6}$ . Generally the least converged parameter was  $\epsilon$ , the residual value of which tended to

be 100 orders of magnitude higher than for pressure and 10 orders of magnitude above the other remaining residuals. The full field residuals for  $\epsilon$  were kept high by high values at the boundaries. A further check on convergence ensured that no parameter value varied by more than 0.1% at each cell centre. Convergence in the finalised valve geometry typically needed 150 - 200 sweeps on a 1.5 MIP Vax 11/785 computer following a restart from a similar solution (eg. similar valve profile with same flow rate, or same valve with lower flow rate).

### 6.7 Pressure Predictions

The pressure gradients predicted by PHOENICS in laminar pipe flow (see figure 6.33) do not vary significantly from those yielded analytically via the application of Darcy's equation. A constant error of -0.57% was predicted except at Reynolds' number of 1 000 where the error was -2.2%. Turbulent pipe flow was equally accurately predicted with errors typically of +3.9%

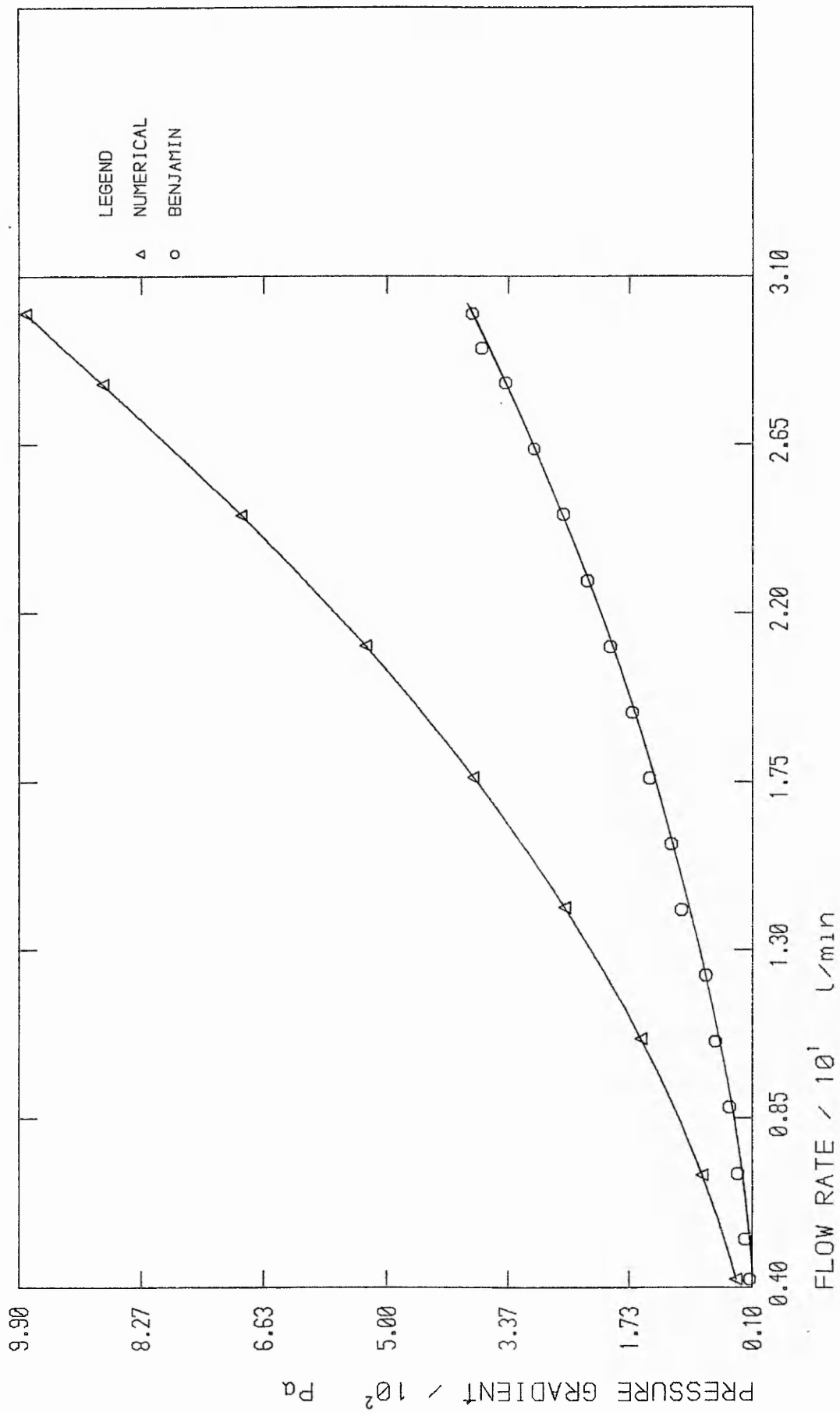
First analysis of valve pressure gradient predictions yielded computationally, however, showed large differences with experimental findings, ie. the predicted pressure gradient was almost thrice that observed experimentally (figure 6.34). Some difference was to be expected in line with the findings of Swanson (1984) who discussed variations in pressure gradient measurements between different researchers. The thrust of Swanson's report was to highlight the influence of test section design on pressure measurements. He quoted that in some cases experimentally measured pressure gradients were five times greater than those of other researchers, for the same valve and



Reynold's Number ( $Re_f$ ) /  $10^1$

PHOENICS AND ANALYTICAL PRESSURE GRADIENT PREDICTIONS FOR LAMINAR, NEWTONIAN PIPE FLOW

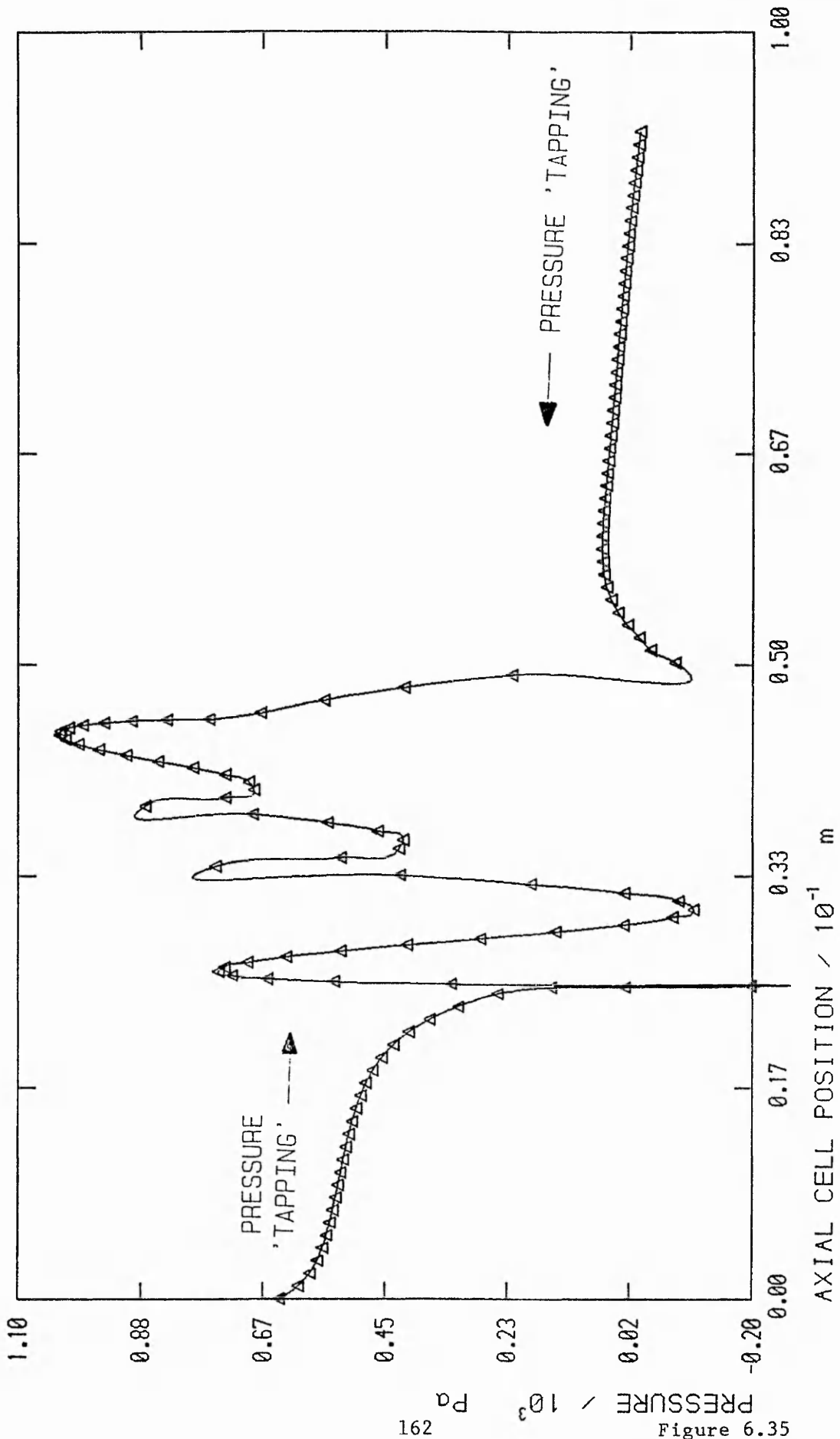
Figure 6.33



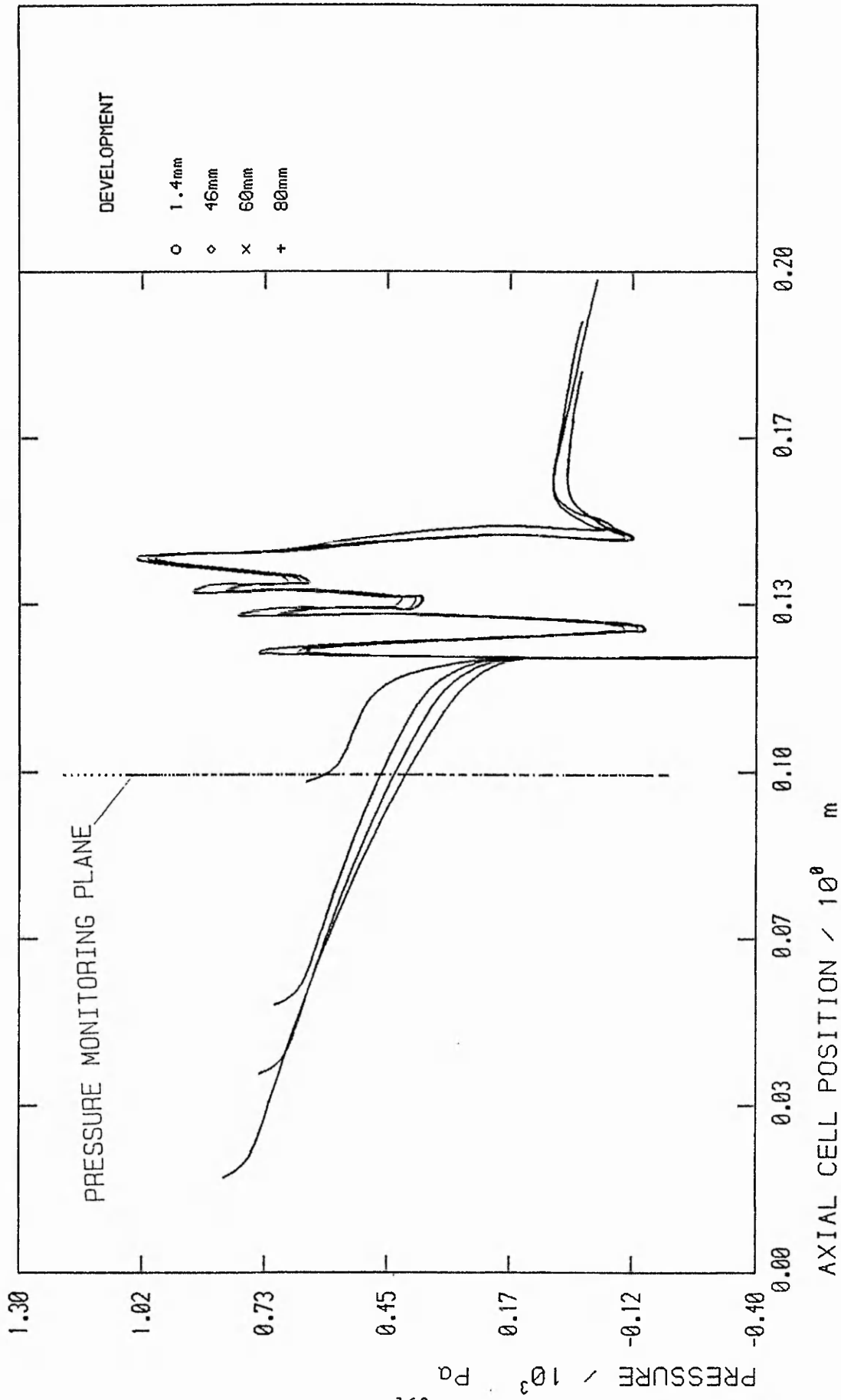
COMPARISON BETWEEN NUMERICAL AND EXPERIMENTAL PRESSURE GRADIENTS FOR THE SISO VALVE IN VARYING WATER FLOW RATES

Figure 6.34

flow rate, but in different test sections. This discussion emphasised the need to numerically model in a geometry which closely represents the experimental situation if comparison was to be made with experimental findings. So far in the numerical work the location of pressure tappings had only been made approximately the same as the experimental tappings. In fact the computational pressure 'tappings' had unwisely been located at the inflow and outflow planes where large losses were experienced. This situation was rectified by removing the pressure monitoring by several cell dimensions downstream and upstream respectively and, instead of taking a mean radial pressure at each section, pressure was monitored only at the wall, in a similar manner to the experimental situation (figure 6.35). This improved the situation considerably, but predicted pressure gradients were still 200% greater than those yielded experimentally. Further study examined the effect of inlet and outlet conditions on pressure gradients between given planes as earlier numerical geometries included only a short inflow development section, whereas flow into the conduit was fully developed in the experimental situation. Pressure gradient was monitored at two planes fixed with respect to the divergent/convergent section of the conduit, and of similar location to the pressure tappings used experimentally. The length of parallel sided inlet and outlet conduit to be modelled was increased and the pressure profile along the wall was monitored. The results, shown by figure 6.36, demonstrate the profound influence development length has on valvular pressure gradient and the lesser influence of exhaust length. The final analysis showed the original differences to be reconcilable because pressure gradients are the same experimentally and



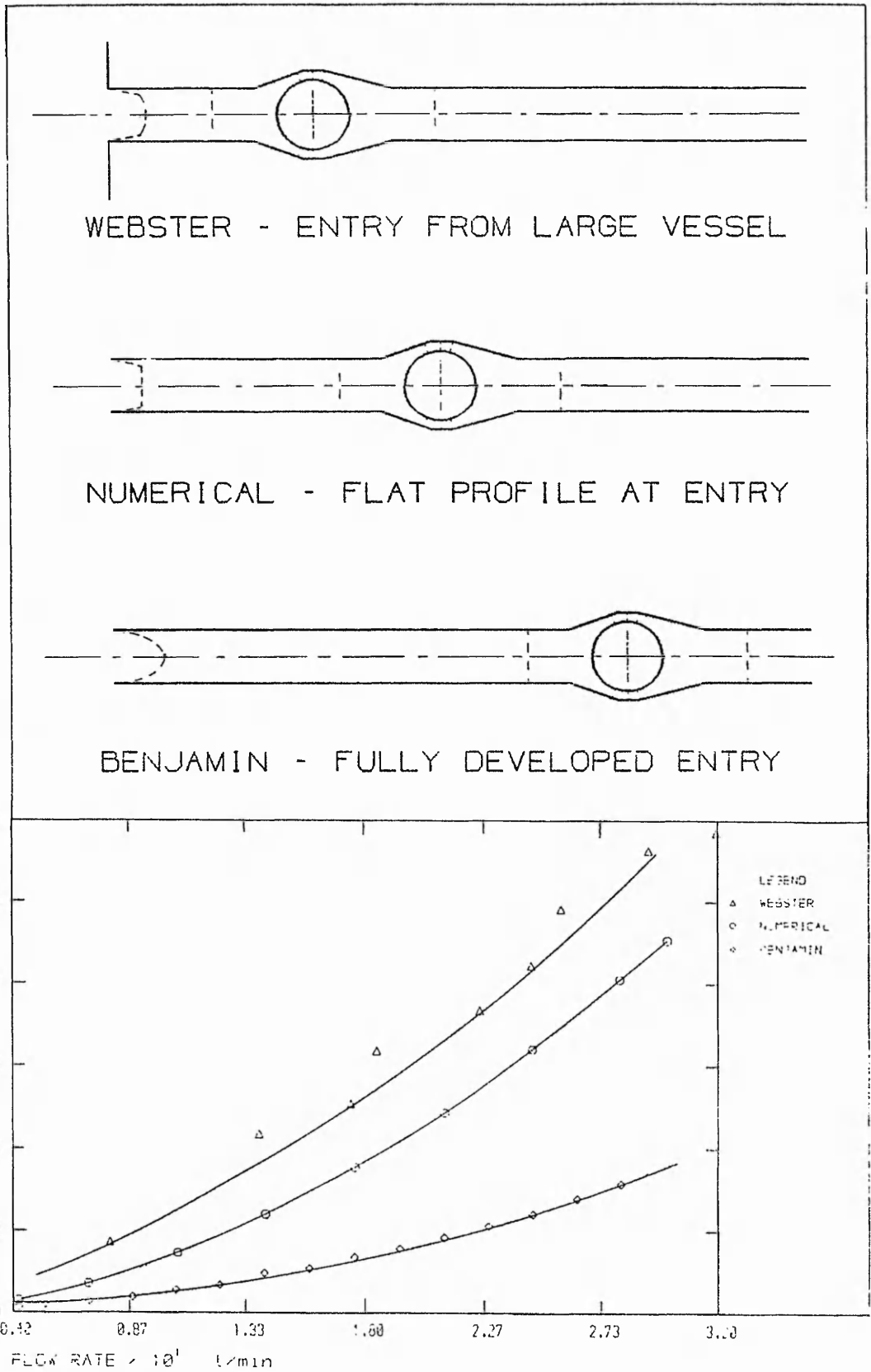
AXIAL VARIATION IN PRESSURE AT THE CONDUIT WALL  
FOR WATER FLOW RATE OF 21.1 l/min



AXIAL VARIATION IN PRESSURE AT THE CONDUIT WALL  
FOR WATER FLOW RATE OF 21.1 l/min

numerically when similar inlet sections and pressure monitoring devices are used numerically. Further evidence of the effect of inlet configuration can be seen in Webster (1982) who used a short development length which took flow from a large receiver, in a geometry which is closer to that originally modelled numerically. Webster's results were immediately comparable with the numerical ones (figure 6.37). Figure 6.37 shows a comparison between recorded pressure gradients for the varying flow geometries discussed. This analysis of reliance on inlet conditions, although it validates the numerical modelling, is disturbing in so far as it highlights the dangers of comparing the findings of different research programmes. It does, however, emphasise the need for comparison of pressure/flow characteristics of valves in identical experimental situations. Further, this finding emphasises the need to establish numerical geometries, identical to the experimental situation if comparison is to be attempted.

Increasing the lengths of inlet and outlet section modelled numerically led to excessive computational time requirements, brought about by the need to define a significantly higher number of grid points (62 radial points for one axial cell width) in order to maintain the same aspect ratio. Hence, modelling continued utilising the short inlet/outlet grid geometry, even though this did not correspond to the experimental reality. However, this in no way depreciated the value of numerical comparisons between valve designs, though it did hamper comparison with established experimental data. Furthermore, it actually increased correlation with the in-vivo situation for an implanted conduit, where flow would not be able to develop before



ANALYSIS OF THE EFFECT OF ENTRY LENGTH ON PRESSURE GRADIENTS FOR THE SISO VALVE IN VARYING WATER FLOW RATES

reaching the valve inlet and would probably stem from a large vessel (ventricle).

## 6.8 Shear Stress and Shear Rate

Shear stress in simple laminar flow was found from the relationship:

$$\tau = \mu_L \dot{\gamma}$$

Figure 6.38 gives a representative laminar sample shear stress gradient at  $Re_d = 1\ 200$ . The difference between the gradients of the CFM and analytically yielded slopes is an error of 0.63%. The shear stresses at both inner and outer boundaries show greater, though still acceptable, errors of -2.9% and +2.7% respectively. These increased errors are due to the shear rate being assessed over a reduced cell width at the boundaries.

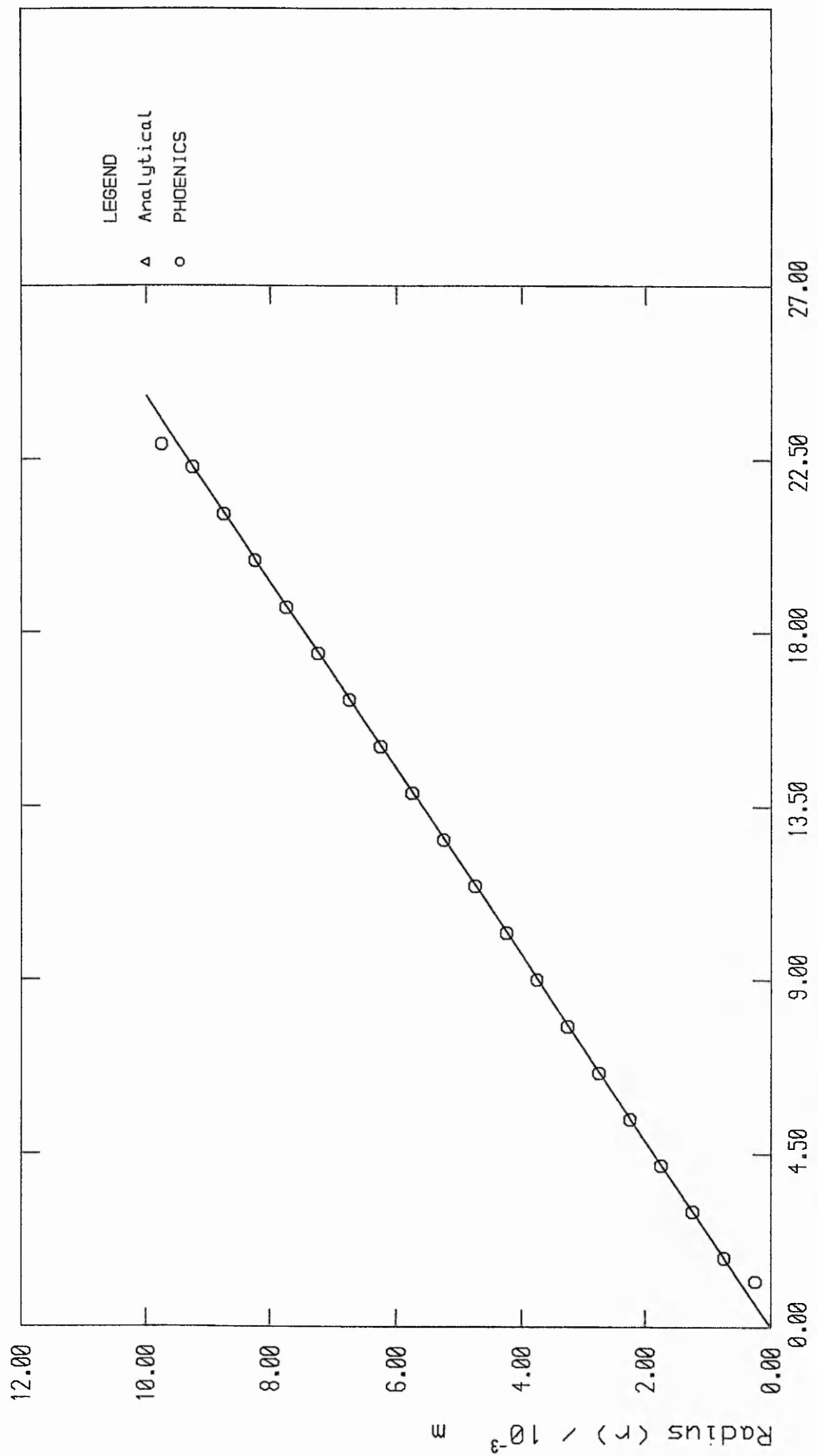
Verification of correct prediction of shear stresses, and therefore shear rates, was by comparison against the work of Laufer (1954). Laufer showed that the radial shear stress profile for fully developed turbulent flow satisfies the relationship:

$$uv = \nu \frac{dw}{dr} + \frac{r}{R} U_{\tau}^2 \quad [6.2]$$

where  $U_{\tau}^2$  is deduced from:

$$\frac{1}{\rho} \frac{\partial P}{\partial z} = -\frac{2}{R} U_{\tau}^2 \quad [6.3]$$

The values for the shear rate term ( $dw/dr$ ) and the pressure



Shear stress (τ) / 10<sup>-3</sup> Pa

PHOENICS AND ANALYTICAL SHEAR STRESS GRADIENT PREDICTIONS FOR LAMINAR, NEWTONIAN PIPE FLOW OF REYNOLD'S = 1200

gradient ( $\partial P/\partial z$ ) were substituted from PHOENICS predicted values. Figure 6.39 shows that PHOENICS predictions were accurate, with regression of the PHOENICS values for shear stress against Laufer's yielding an  $R^2$  value of 83.4%. This correlation would be increased if Laufer's equation had accounted for the sublayer transition (full statistical analysis is given in Appendix 4). Small deviation is seen, however, at the centre-most cells as experienced in laminar flow. Larger differences are seen at the wall cells where the near-wall  $k - \epsilon$  model is active. However, the transition at the sub layer is close to that expected, though sublayer dimensions are over predicted by as much as 20%.

### 6.9 Prediction of Occluder Instability

In the original orthogonal modelling of heart valve flow, a post-processing routine was written to calculate the axial sum of pressure and shear forces on the ball from the pressure and velocity distributions around it.

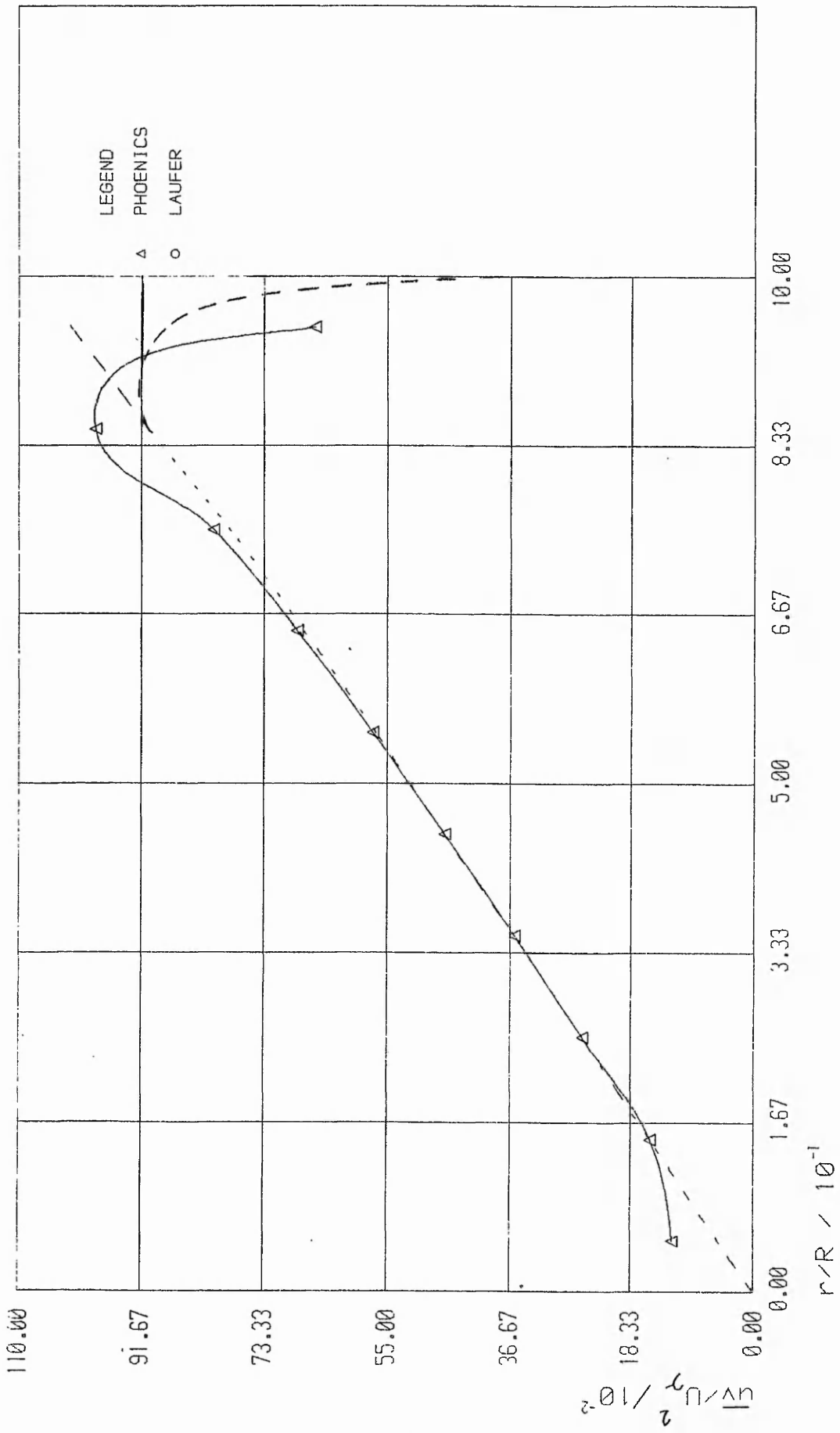
Pressure force ( $F_p$ )

$$F_p = \sum P \delta A_p \quad [6.4]$$

and the viscous drag force on the ball ( $F_v$ ):

$$F_v = \int_{z=0}^{z=2Rb} 2\pi \mu r \frac{dw}{dy} \delta z \quad [6.5]$$

Assessment of the two force terms yielded by numerical solution was hampered by grid interference; throughout the range of flow rates in the original (SISO) valve a net resultant streamwise force on the ball was predicted. This would ensure the valve



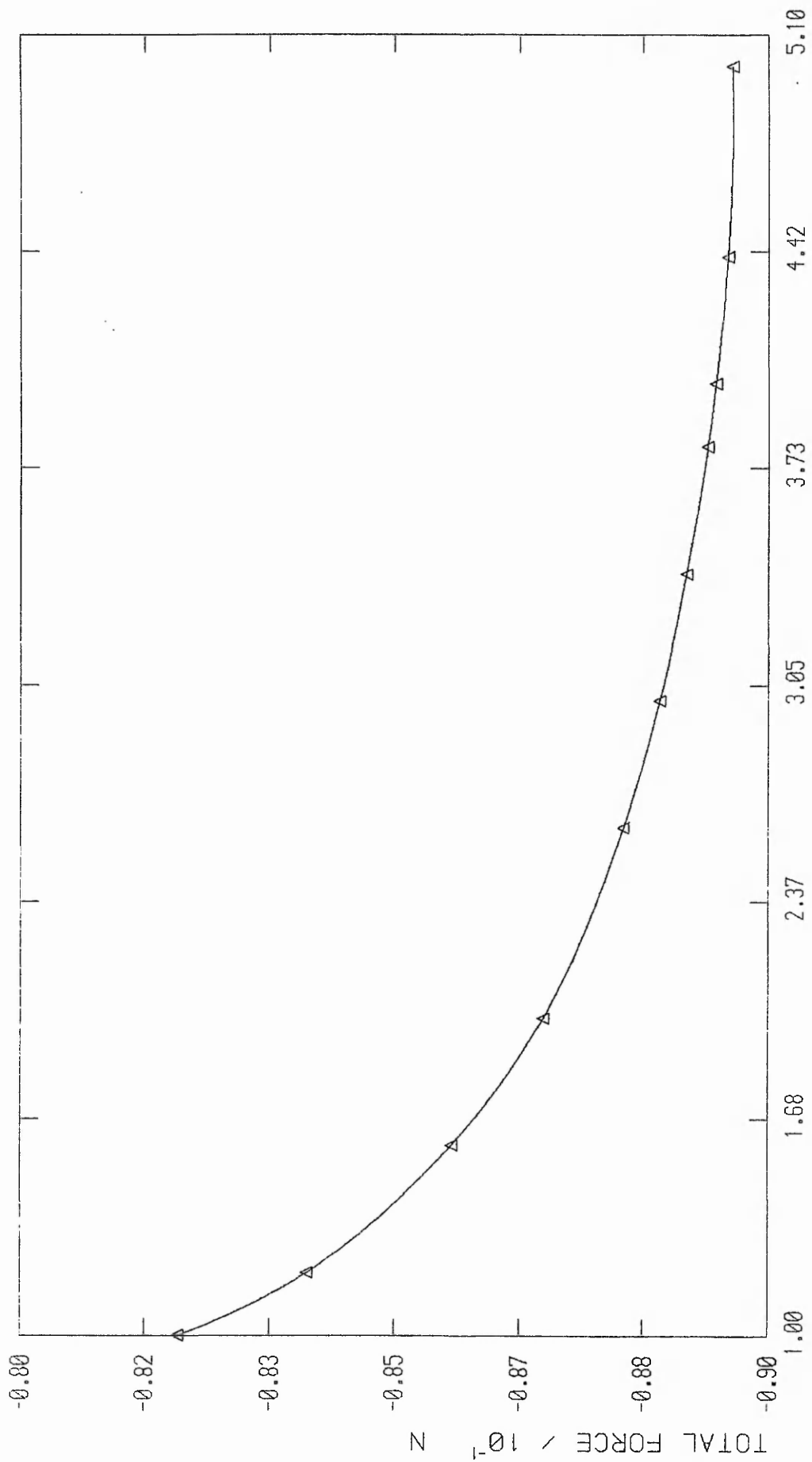
NON-DIMENSIONALISED SHEAR STRESS PLOTTED AGAINST NORMALISED RADIUS TO SHOW COMPARISON BETWEEN PHOENICS AND LAUFER (1954)

Figure 6.39

remaining in the fully open state. Whereas experimentally the ball was seen to be marginally unstable in flow rates of water above 5l/min. However, this discrepancy was resolved when it was realised that grid-based modelling had led to prediction of impingement on the upstream facing walls of the ball. Therefore an unwanted increase in the pressure force in the streamwise direction had obviously occurred. The magnitude of streamwise force predicted in the original section was 38.9mN, and in the second prototype (SICO); 78.88mN.

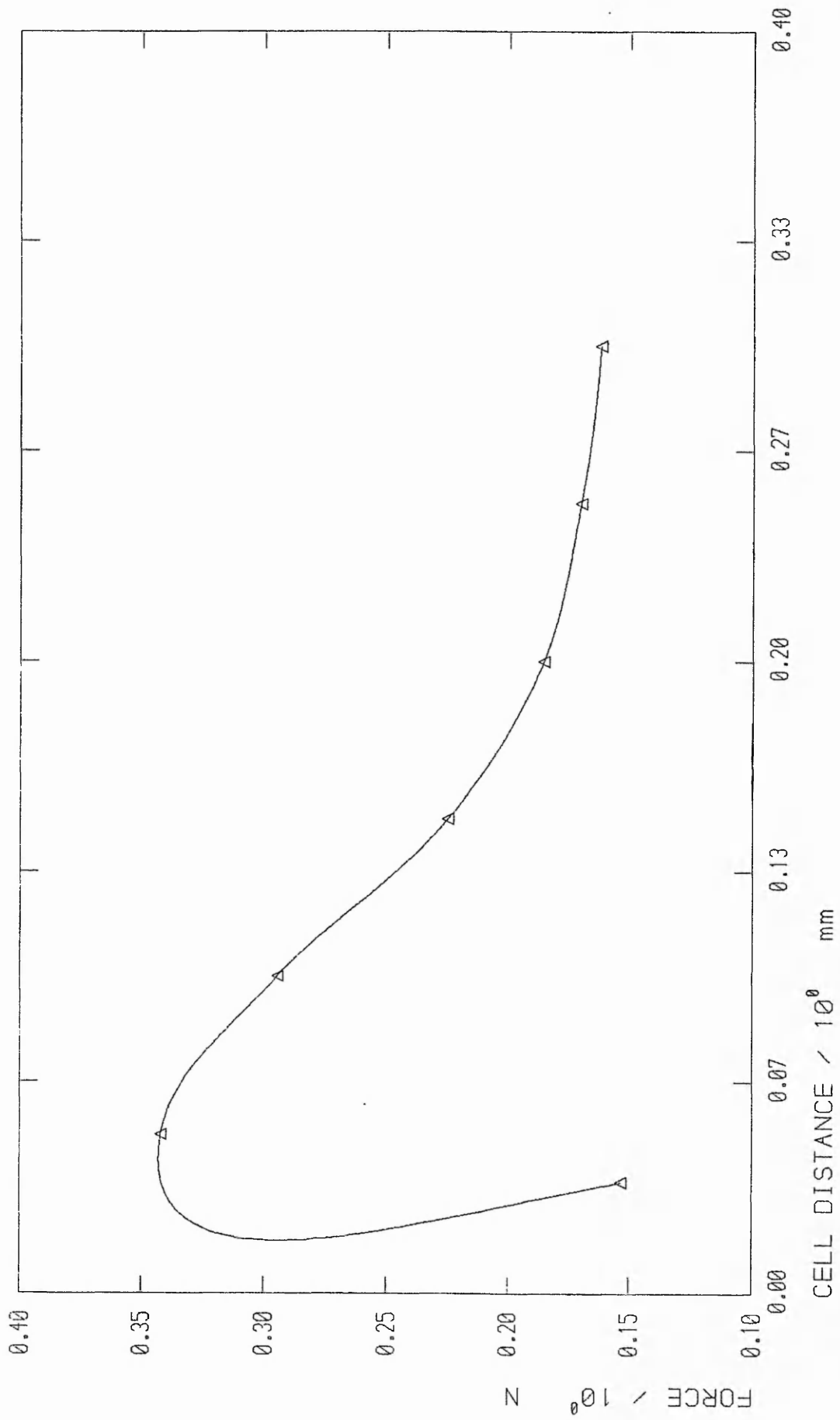
The problem disappeared when analysis of force on the ball was applied in non-orthogonal regimes. Instead of post-processing to gain information regarding the force on the ball, a routine was written into the 'Ground' program based on the equations [6.4] and [6.5]. Care was necessary to ensure that shear stresses were derived from the Cartesian resolutives of velocity axially along the ball surface and not the velocities parallel to the 'North faces' of the cells. Results obtained by such modelling in the original valve did in fact predict anti-streamwise net force on the ball down to the lower limits of flow rates modelled.

However it was not possible to model the lower flow rates where ball stability was transitional due to the breakdown of the  $k - \epsilon$  model. Further, predicted ball stability in the second prototype valve (SICO) was confirmed experimentally. Predicted force on the ball was highly grid dependent but was shown, by figures 6.40 and 6.41, to yield satisfactory results for the geometries employed.



No. OF CELLS /  $10^1$

GRID INDEPENDENCE CHECK:  
FORCE ON THE BALL VS NUMBER OF HALF-RADIAL CELLS



ANALYSIS OF FIRST CELL CENTRE POSITIONING:  
 FORCE ON THE OCCLUDER BALL VS FIRST CELL CENTRE DISTANCE

## 6.10 Blood Model

In simple laminar blood flow, the predicted radial shear stress distribution varied linearly with displacement from the centreline. The error in computationally predicted wall shear stress, as compared with that predicted semi-empirically by equation A1.4 was negligible - only 0.47%, with PHOENICS yielding the relationship:

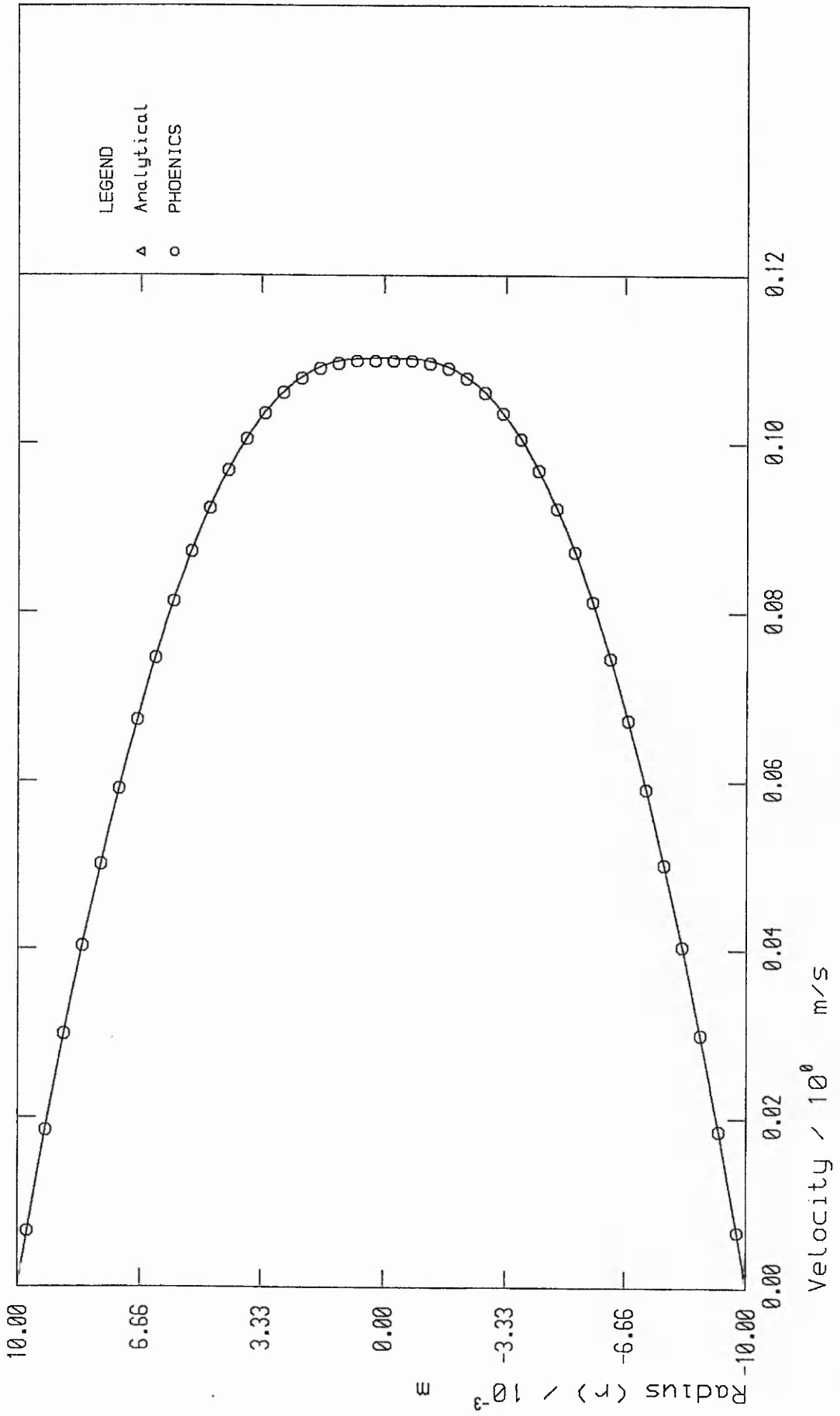
$$\tau = 0.99526 \frac{\Delta p r}{2l}$$

for flow modelled by the Casson equation, in a pipe of 20mm diameter. The velocity profile generated computationally was accurate to within 0.5% error of the semi-empirically predicted form of equation [A1.11], as shown by figure 6.42. This result confirms that the apparent viscosity was in fact being correctly amended with regard to local shear rates. The blood model was therefore guaranteed to be effective in all flow regimes including turbulent (dependent upon correct prediction of the generation term  $\gamma$  by the turbulence model) as viscosity alterations in turbulent flow are regime-dependent and not fluid-dependent. ie:

$$\mu_{eff} = \mu_L + \mu_T \quad \text{where } \mu_L = \mu_a$$

### In Conclusion

The above observations verify that PHOENICS was correctly predicting all hydrodynamic/haemodynamic properties and that the solution was independent of the final geometries chosen. Numerical modelling was now at a stage where it could usefully be employed as a design tool.



PHOENICS AND ANALYTICAL VELOCITY GRADIENT PREDICTIONS FOR LAMINAR, NON-NEWTONIAN PIPE FLOW  $dp/dx=23 \text{ Pa/m}$

Figure 6.42

CHAPTER SEVEN

CONDUIT RE-DESIGN

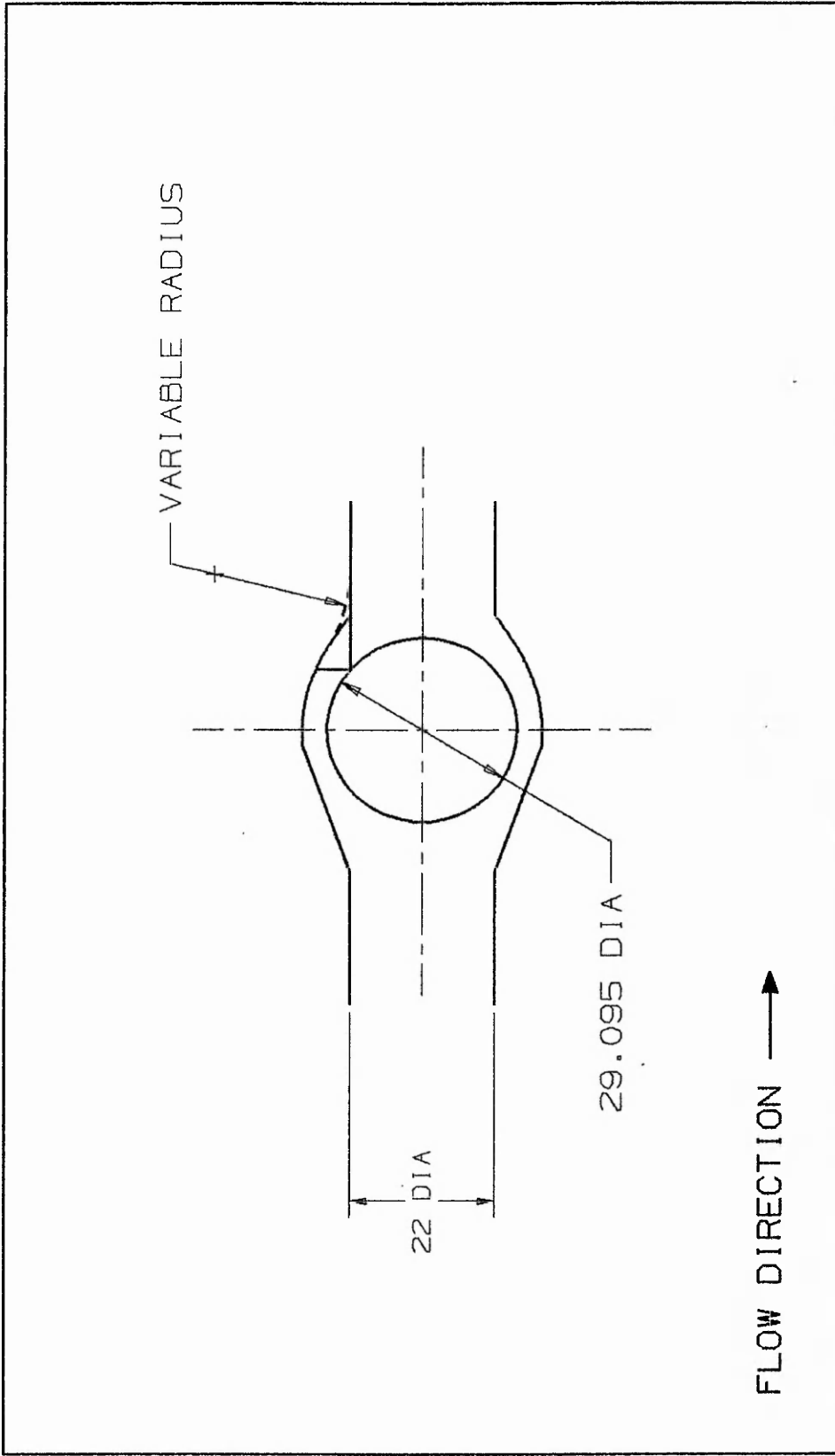
## 7.1 Introduction

Based on the analysis of the first two prototypes, design optimisation became a compromise between minimisation of the pressure gradient and maintenance of the required stability of the ball occluder during forward flow. Further factors influenced by valve profile are shear stress and, therefore, haemolytic potential. Particularly noticeable is the marked decrease in peak shear stresses over the conduit wall, at the point where the convergent section meets the outlet cylindrical conduit, due to increased blending radius.

## 7.2 Best Valve Profile

The initial criteria used in the re-design of the ball occluded heart valve conduit were the minimisation of pressure gradient and maintenance of occluder stability, ie ensuring a net streamwise force on the ball. Preliminary numerical modelling was carried out using water as the flow medium, and several design changes were assessed:

The first approach to ensure conduit stability, namely that of introducing a constant flow area behind the ball, resulted in unacceptably high pressure gradients across the valve, as described in chapter five. Analysis suggested that the optimum profile of outflow tract lay somewhere between the straight profile and the constant area profile. Accordingly, the valve was re-designed by adding a radius to blend the corner between the outflow tract profile and the constant diameter exit section of the conduit (see figure 7.1). The addition of this radius had

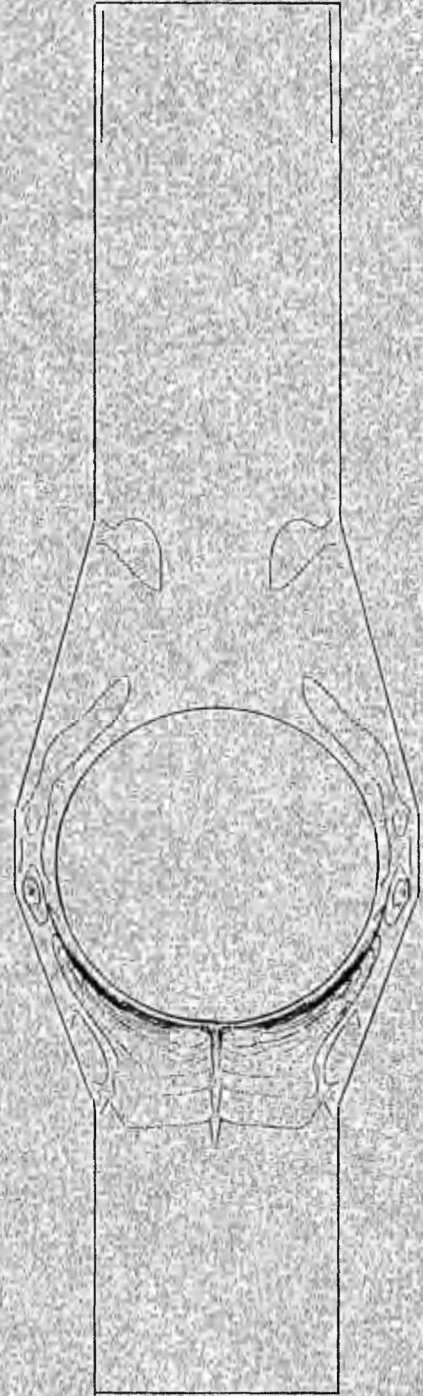


ADDITION OF BLENDING RADIUS TO OUTFLOW SECTION OF VALVES

a two-fold purpose in so far as it introduced a readily variable means of altering the flow area (and therefore outflow pressure), and reduced shear stresses at what would otherwise be a sharp corner. Evidence of reduction in shear stresses at the sharp corners is shown, most graphically, by figures 7.2 to 7.4 which depict full-field contours of total shear stresses. Figure 7.2 shows stresses in the SICO valve, figure 7.3 shows elevated stresses at the sharper cornered SICO valve, and figure 7.4 highlights reduction of these stresses by the addition of a 45mm blending radius. The variation of pressure with blending radius is shown in figure 7.5 for several section designs, from which it is obvious that pressure gradient decreases with blending radius (a straight outflow profile was considered to be a radius of infinite dimension). Figure 7.6 shows streamwise force on the ball for the same geometries. Sadly it became apparent that as radius increased the ball stability reduced, ie pressure and stability optimisation were mutually opposed.

A further study considered the influence of inlet profile on pressure gradient and occluder stability. The inlet profile was modelled in a similar manner to the outlet, this valve nominated Curved Inlet/Curved Outlet (CICO) is shown in figure 7.7. However, this re-design lead to a 5% increased pressure gradient across the valve (CICO). Stability also suffered, see figures 7.5 and 7.6. Further work could have been carried out on the optimisation of the inlet section by the addition of a blending radius, but as shear stresses due to the sharp corner of the straight divergent section were insignificant when compared with other stresses in the valves (see later and figures 7.8 - 7.11), the straight inlet section was maintained.

SHEAR STRESS CONTOURS  
WATER FLOW RATE = 21.1 l/min  
ORIGINAL VALVE

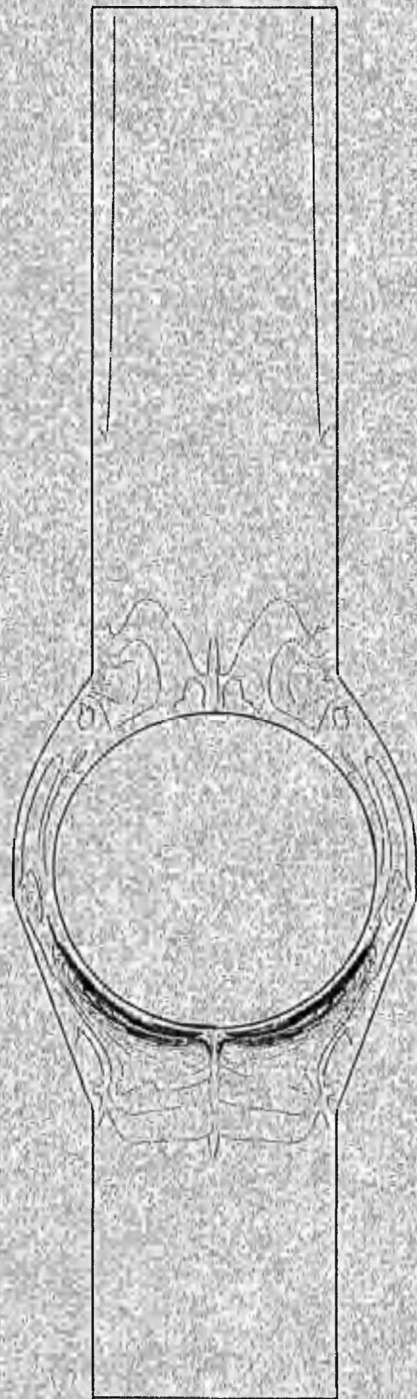


11 16 50 77 54 82 69 98



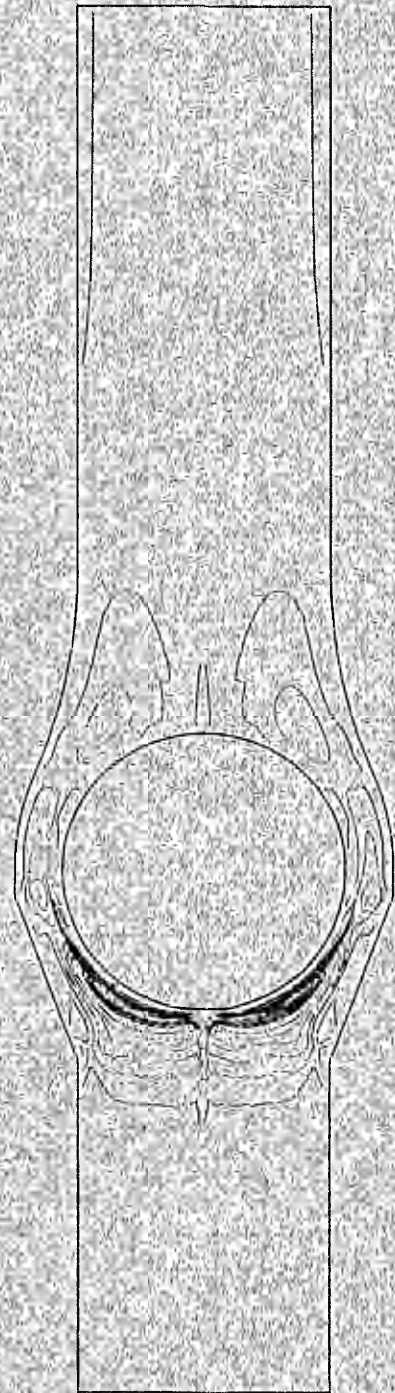
Figure 7.2

SHEAR STRESS CONTOURS  
WATER FLOW RATE = 21.1 l/min  
SECOND PROTOTYPE (S1C0)



Z  
Y

SHEAR STRESS CONTOURS  
WATER FLOW RATE = 21.1 l/min  
BLENDING RADIUS = 4.5mm



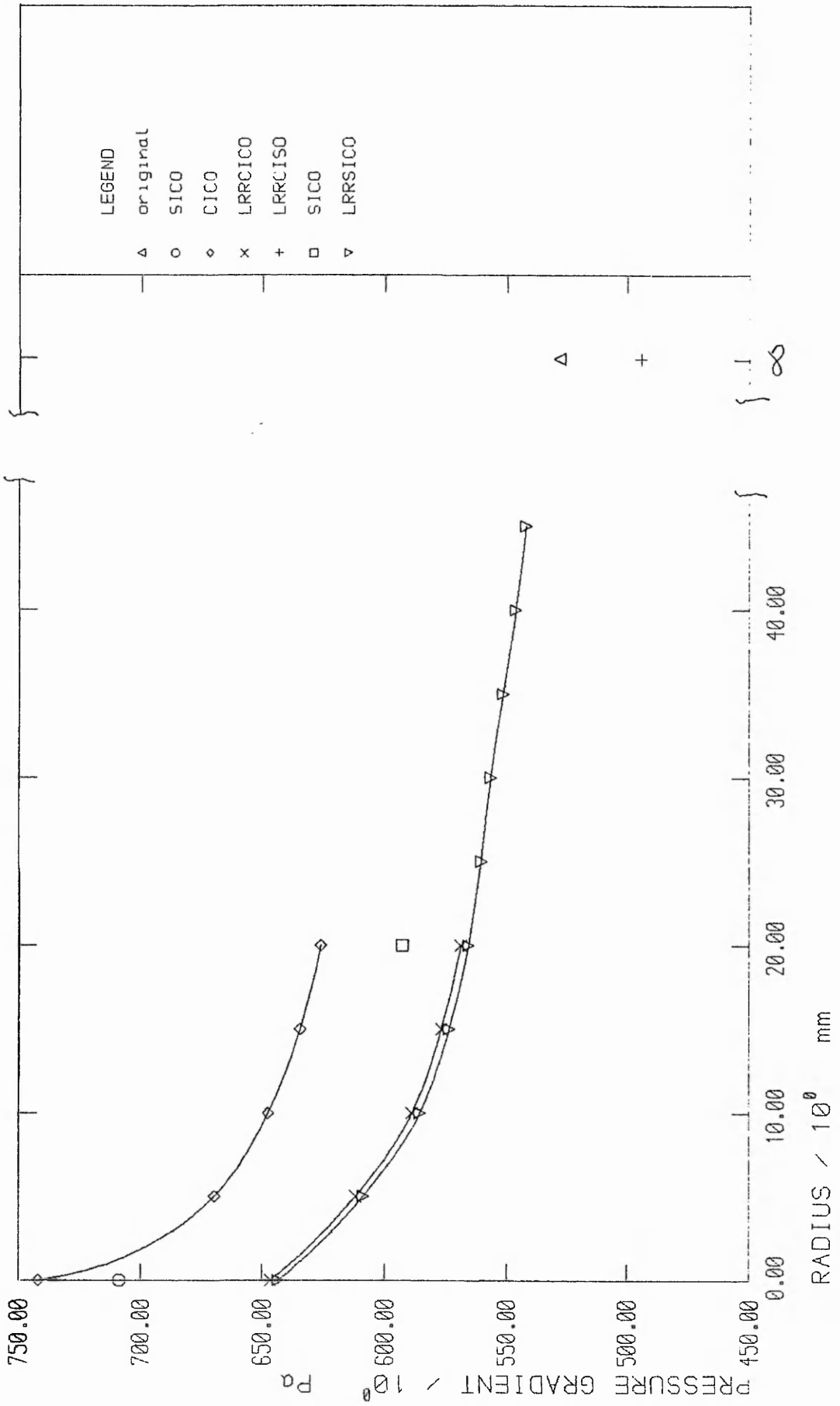
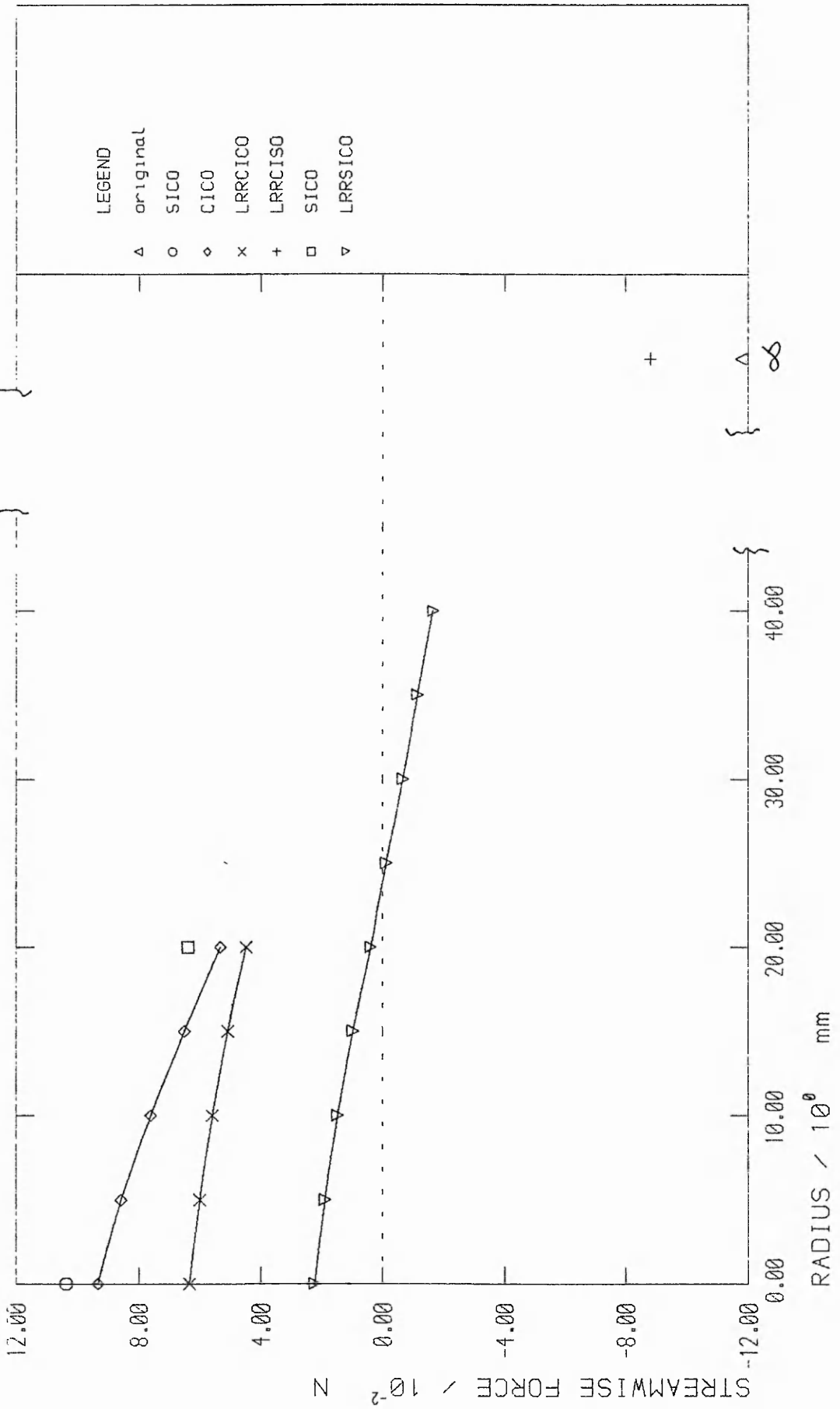
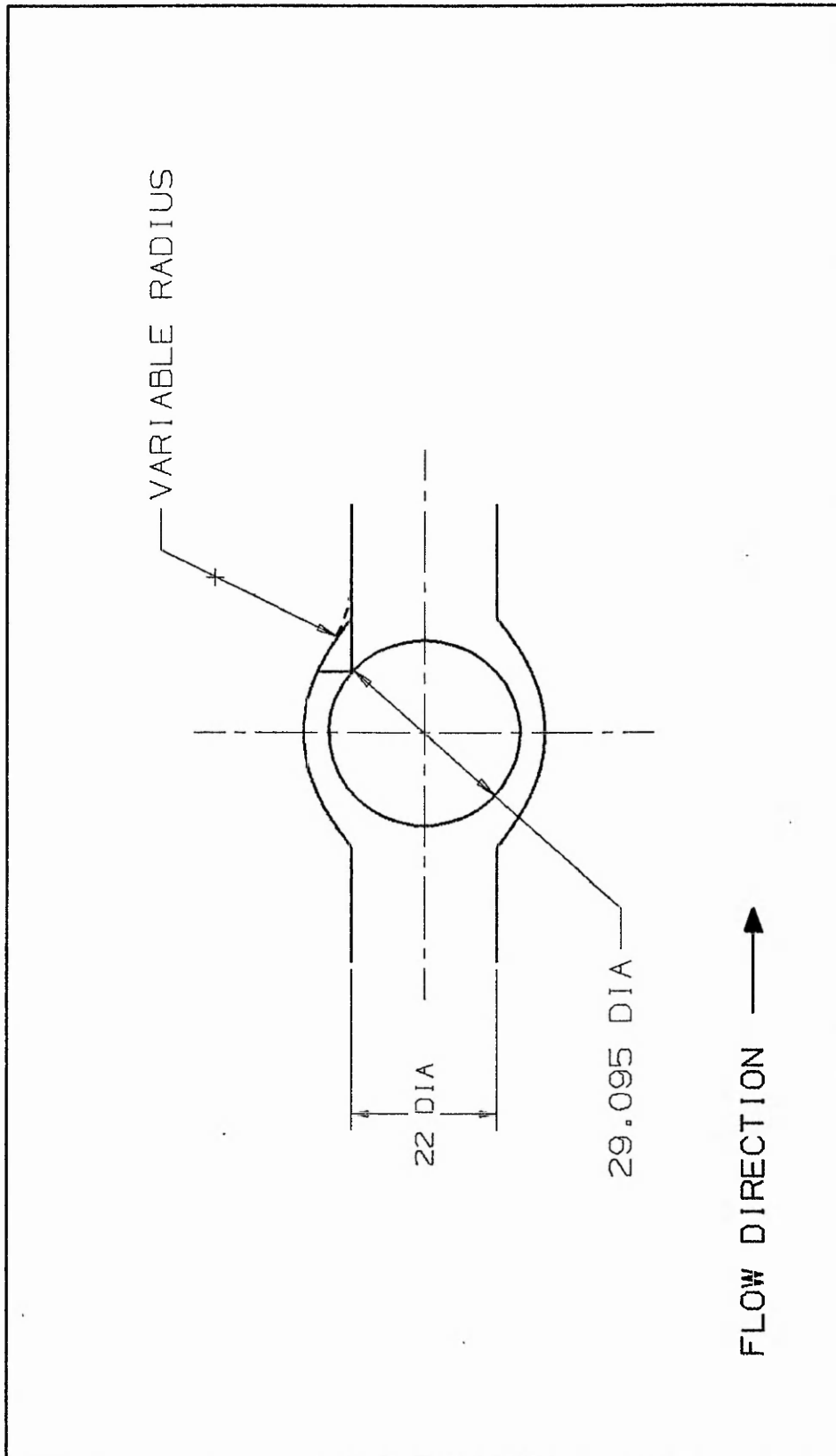


Figure 7.5

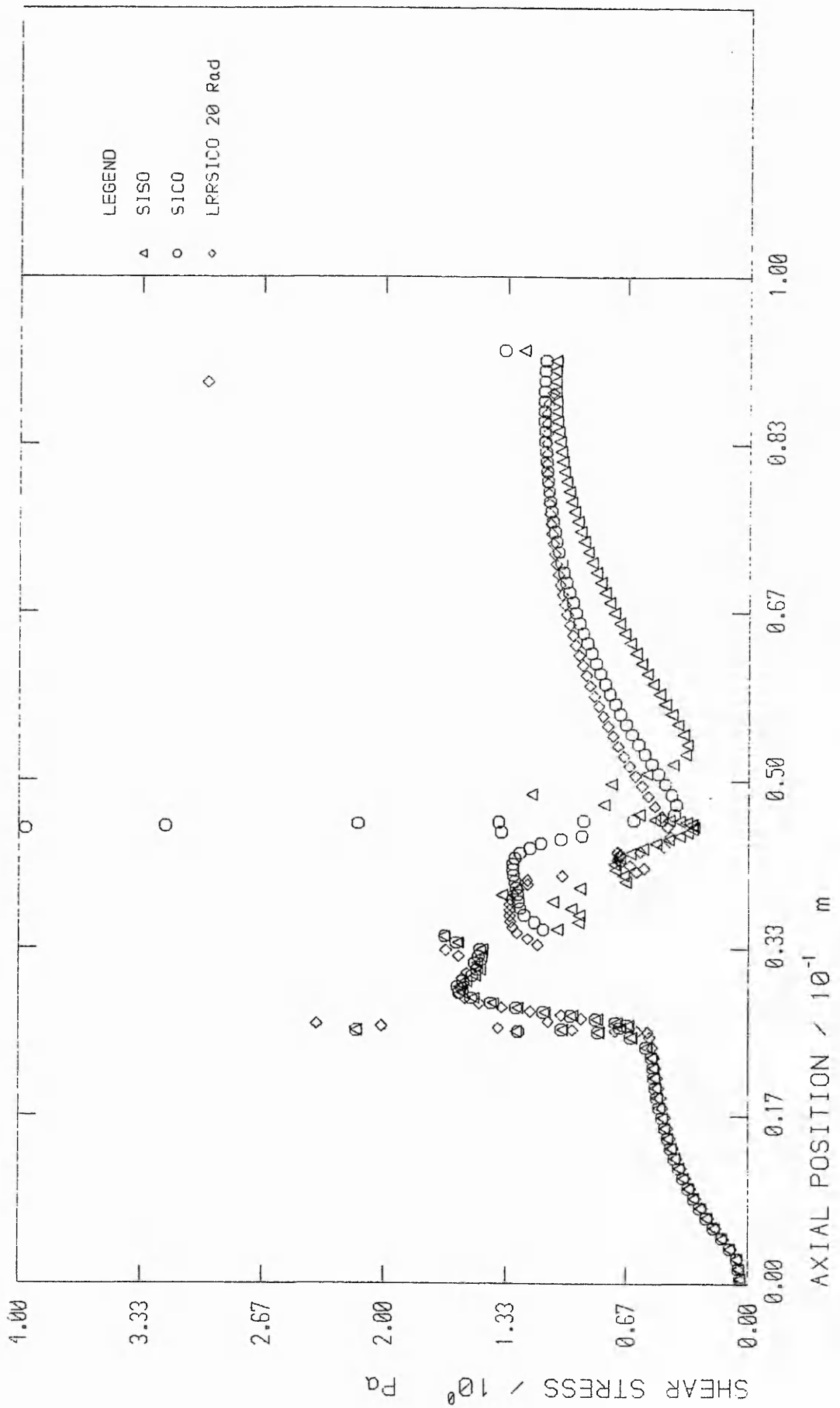
PRESSURE VERSUS OUTLET BLENDING RADIUS  
FOR THE PROTOTYPE CERAMIC VALVES AT 21.1 l/min



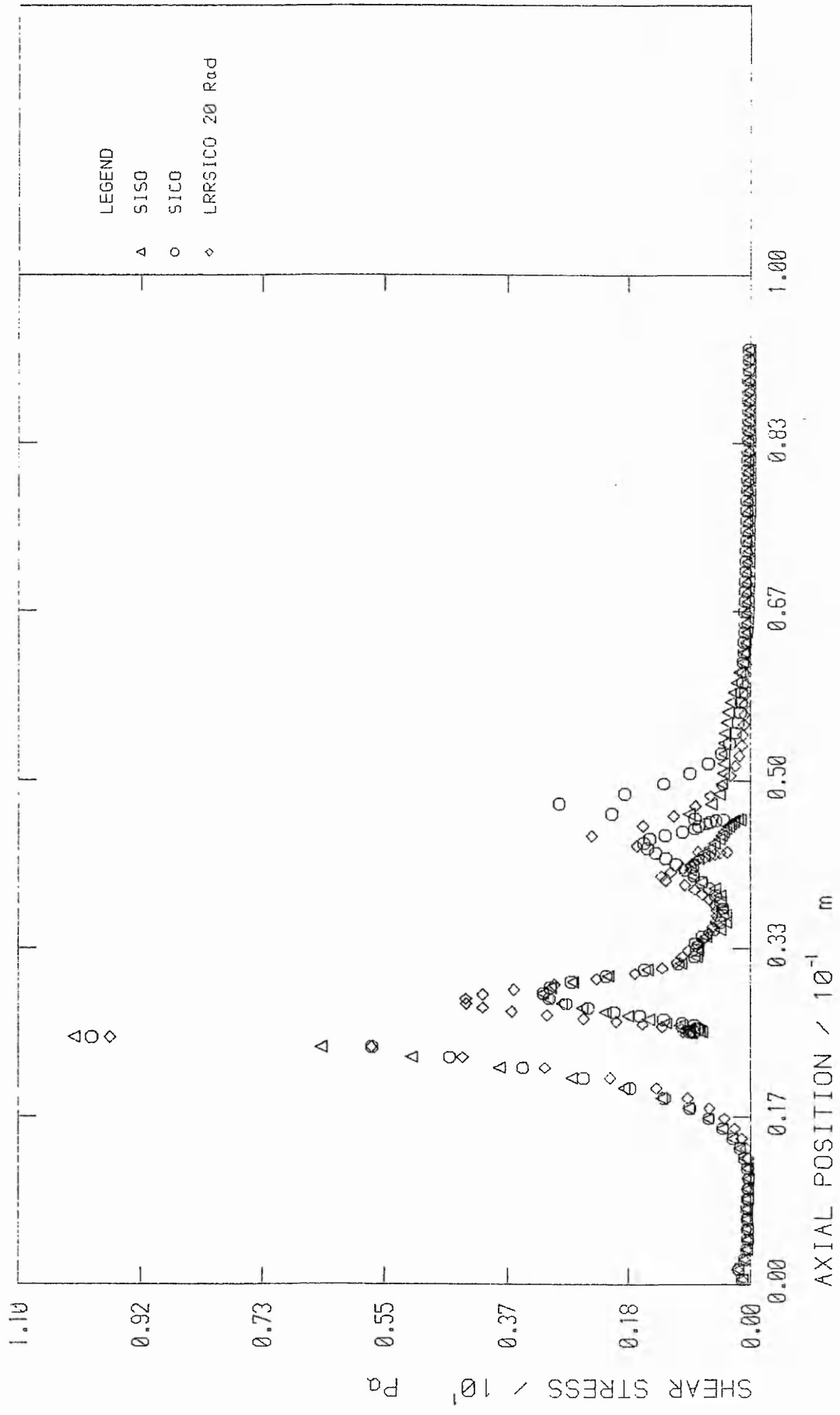
FORCE ON THE BALL VERSUS OUTLET BLENDING RADIUS FOR THE PROTOTYPE CERAMIC VALVES AT 21.1 l/min



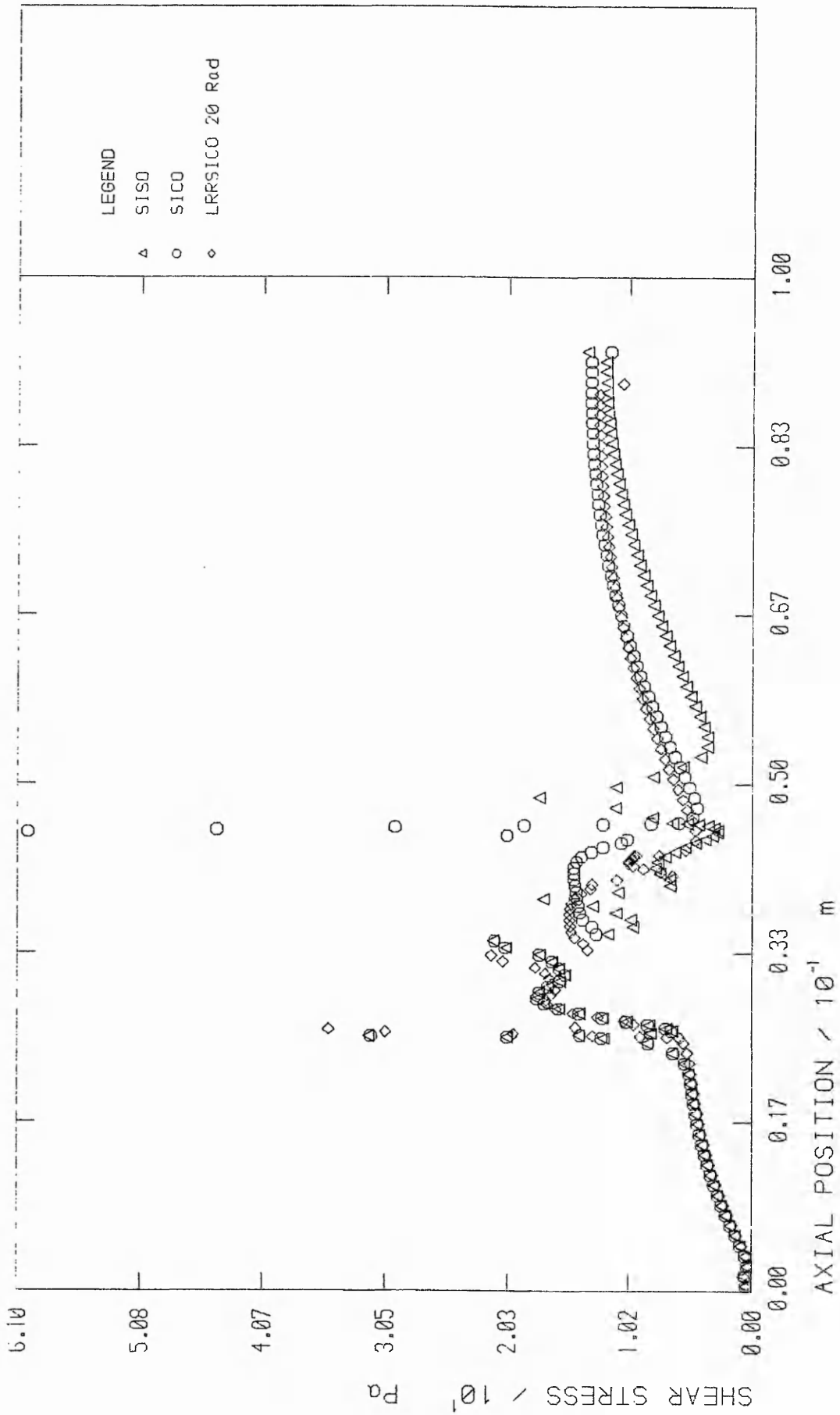
CONDUIT FEATURING SIMILAR INFLOW AND  
OUTFLOW PROFILES (CICO)



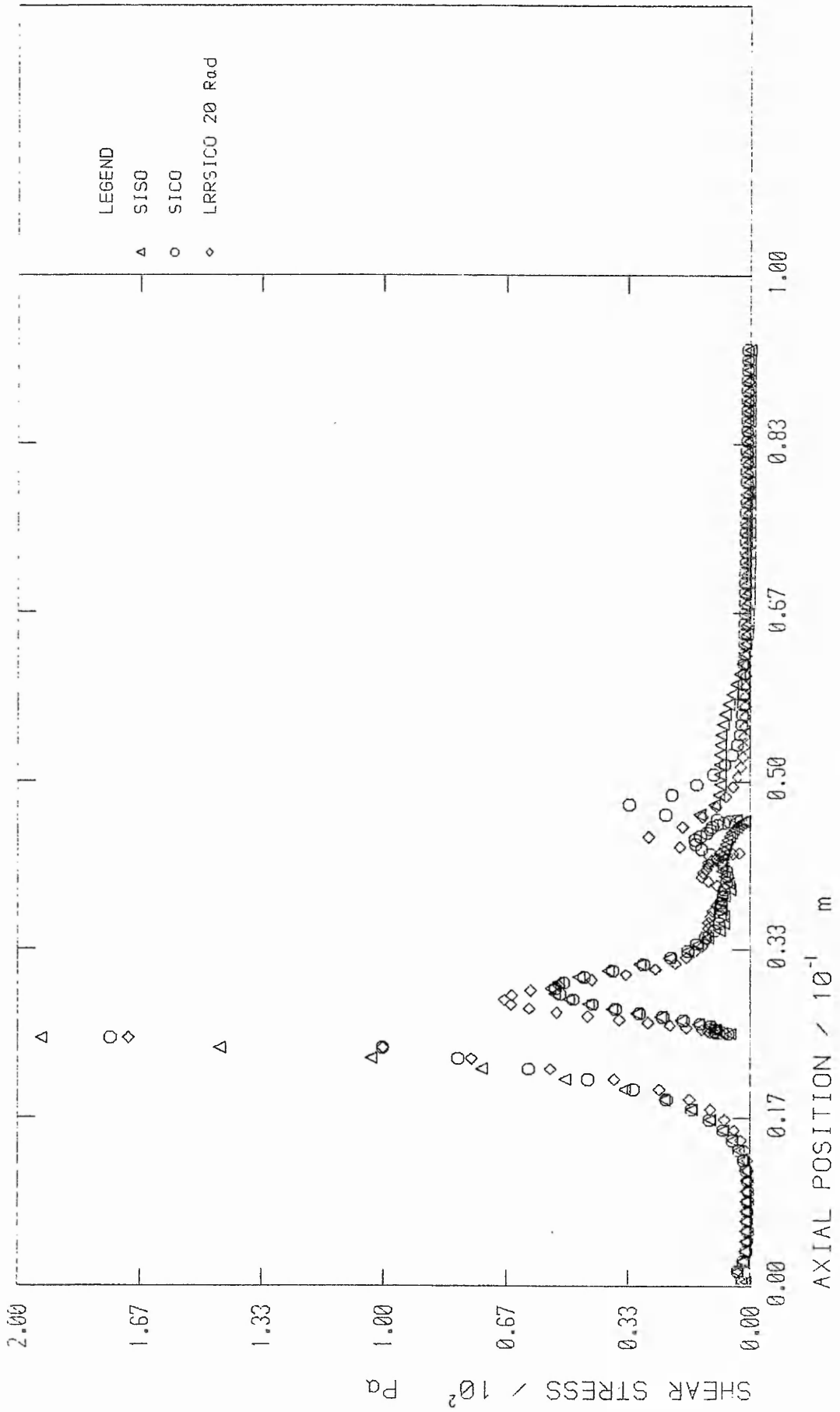
COMPARISON BETWEEN THREE PROTOTYPE CONDUIT DESIGNS:  
 SHEAR STRESS AT CONDUIT WALL, FLOW = 7 L/min



COMPARISON BETWEEN THREE PROTOTYPE CONDUIT DESIGNS:  
 SHEAR STRESS AT CENTRELINER AND BALL SURFACE FLOW = 7L/min



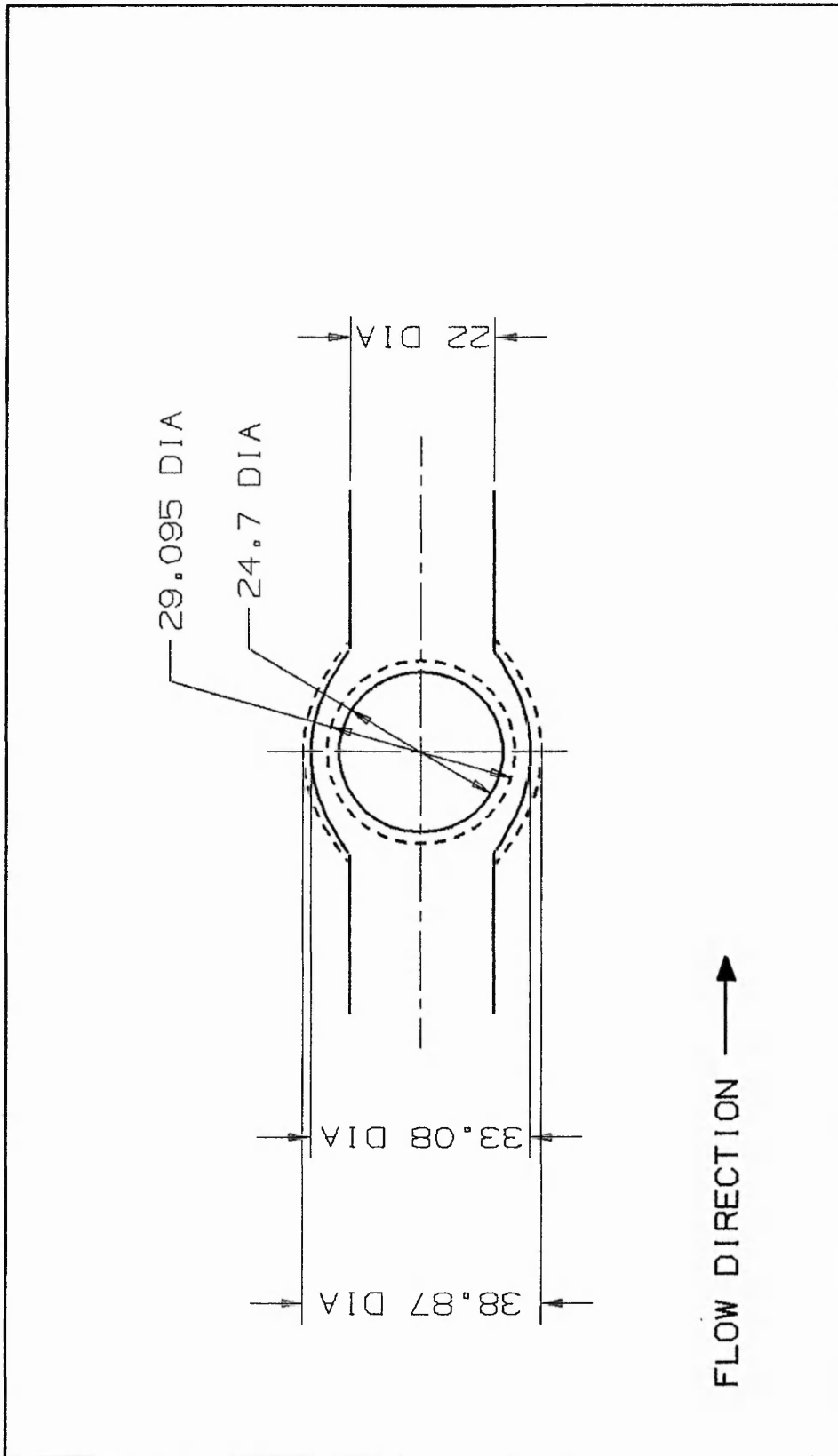
COMPARISON BETWEEN THREE PROTOTYPE CONDUIT DESIGNS:  
SHEAR STRESS AT CONDUIT WALL, FLOW = 30L/min



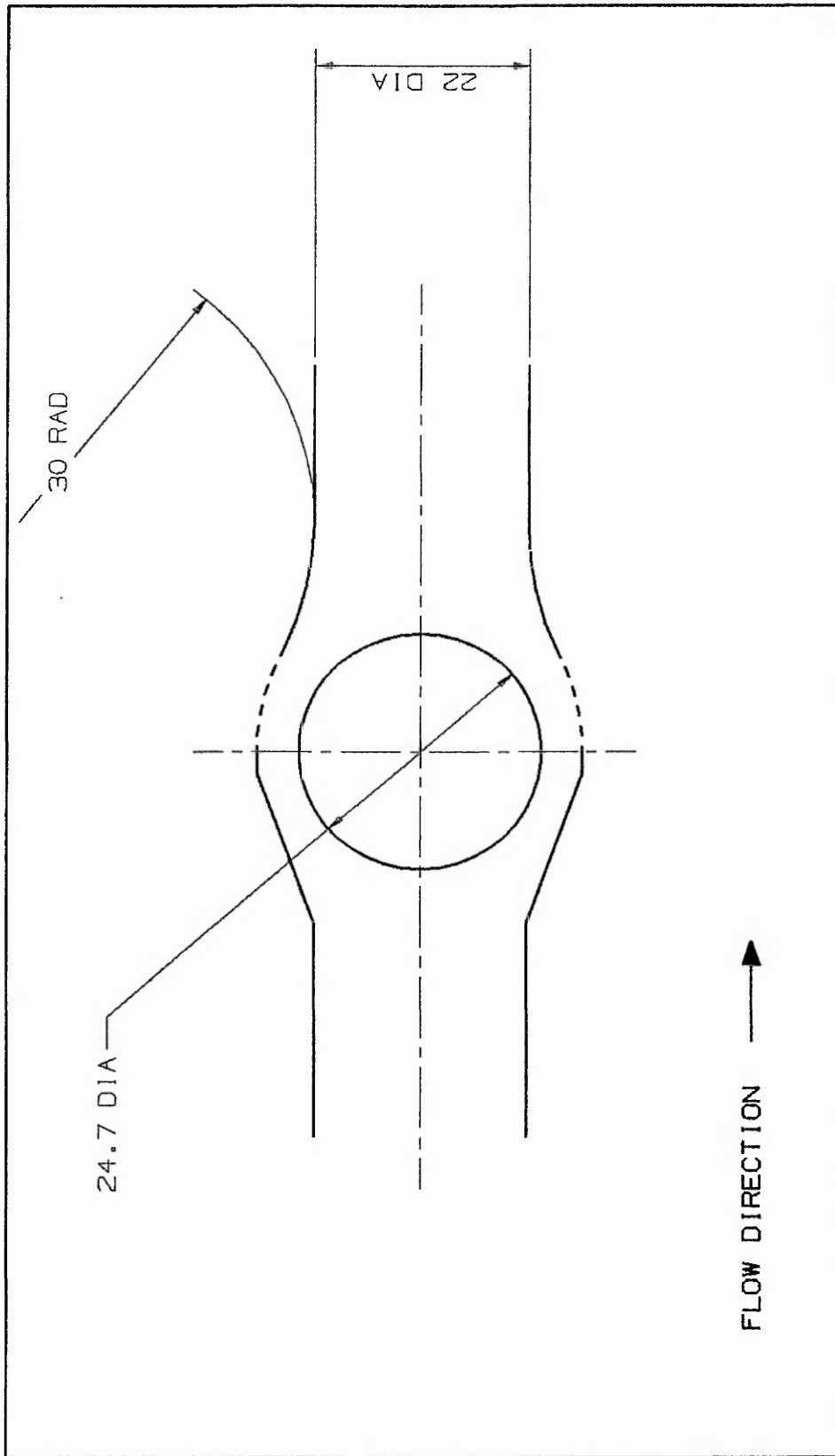
COMPARISON BETWEEN THREE PROTOTYPE CONDUIT DESIGNS:  
 SHEAR STRESS AT CENTRELINE AND BALL SURFACE FLOW = 30L/min

The final attempt at a major geometry improvement was to reduce the ratio of conduit radius to ball radius (see figure 7.12) ie reduce ball size for a given conduit diameter. This was done on the premise that energy loss would be reduced if flow remained more axially aligned. The result was not only reduced external valve dimensions for a given flow area, but also improved pressure/flow characteristics as seen in a comparison between the pressure gradients of the series of valves nominated "Low Radius Ratio" (LRR) and the other valves in figure 7.5. The ratio of primary orifice to ball diameter was chosen to match that of the Starr-Edwards ball-and-cage prostheses in an attempt to introduce similarity with proven valves. The included angle of divergence at the inlet section was maintained at  $40^\circ$ , as this had already proved satisfactory in hydrodynamic terms and in the avoidance of the ball "self-locking" into its seating, a problem which is introduced with smaller angles.

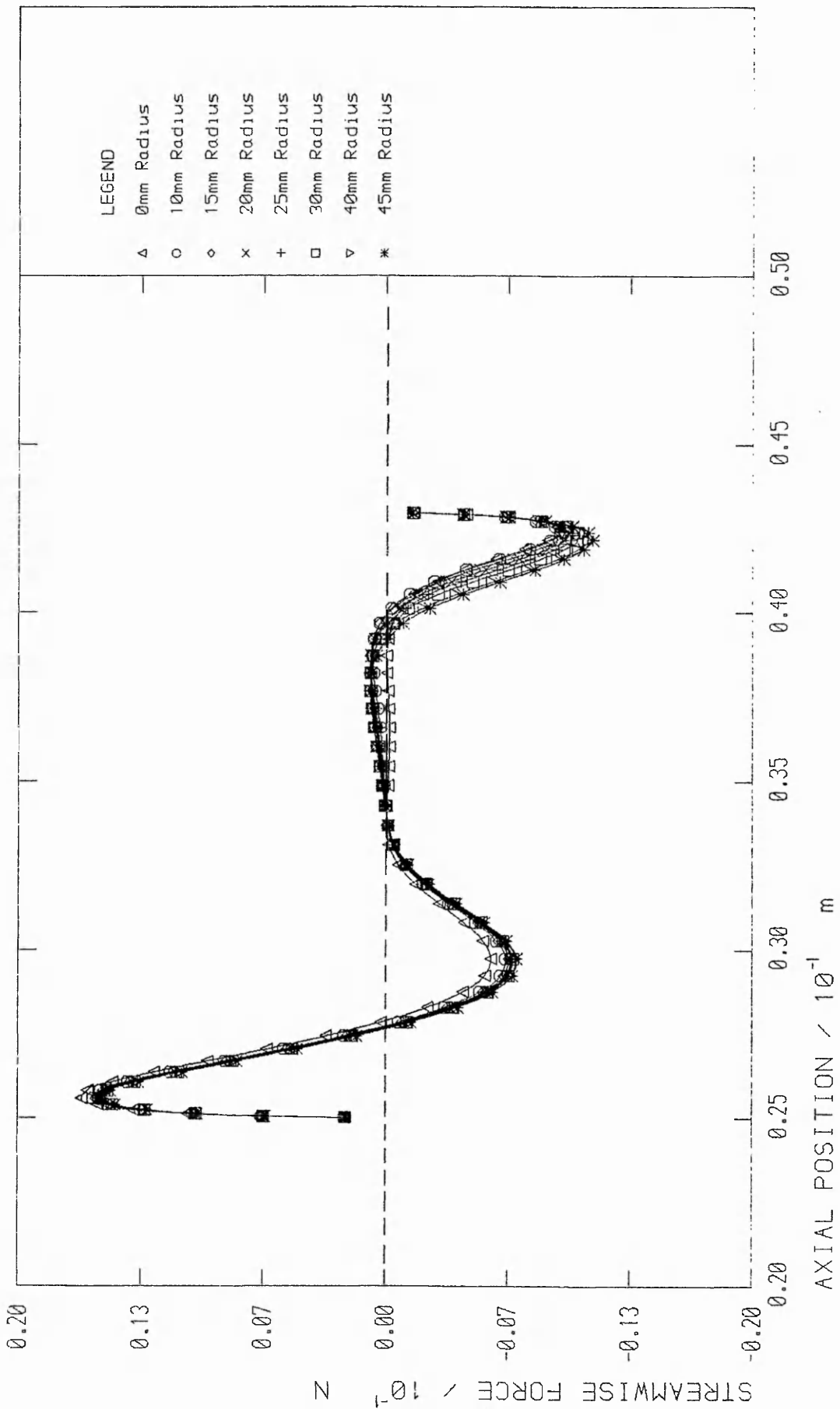
The above features were combined into a third prototype valve nominated LRRSICO, the features of which were; a straight inlet section, curved outlet section with a blending radius at the site where the convergent profile meets the parallel conical outflow conduit, and a reduced conduit-to-ball radius ratio (see figure 7.13). Figures 7.5 and 7.6 show the overall characteristics of this valve design with variation of blending radius dimension. Detailed information of flow parameter variation on a cell to cell basis is shown in further graphs. Figure 7.14 details the increase in anti-streamwise force behind the ball with increasing blending radius, The reduction of valve pressure gradient and increase in pressure behind the ball, which ultimately reduces stability is highlighted in figure 7.15. Figure 7.16 plots the



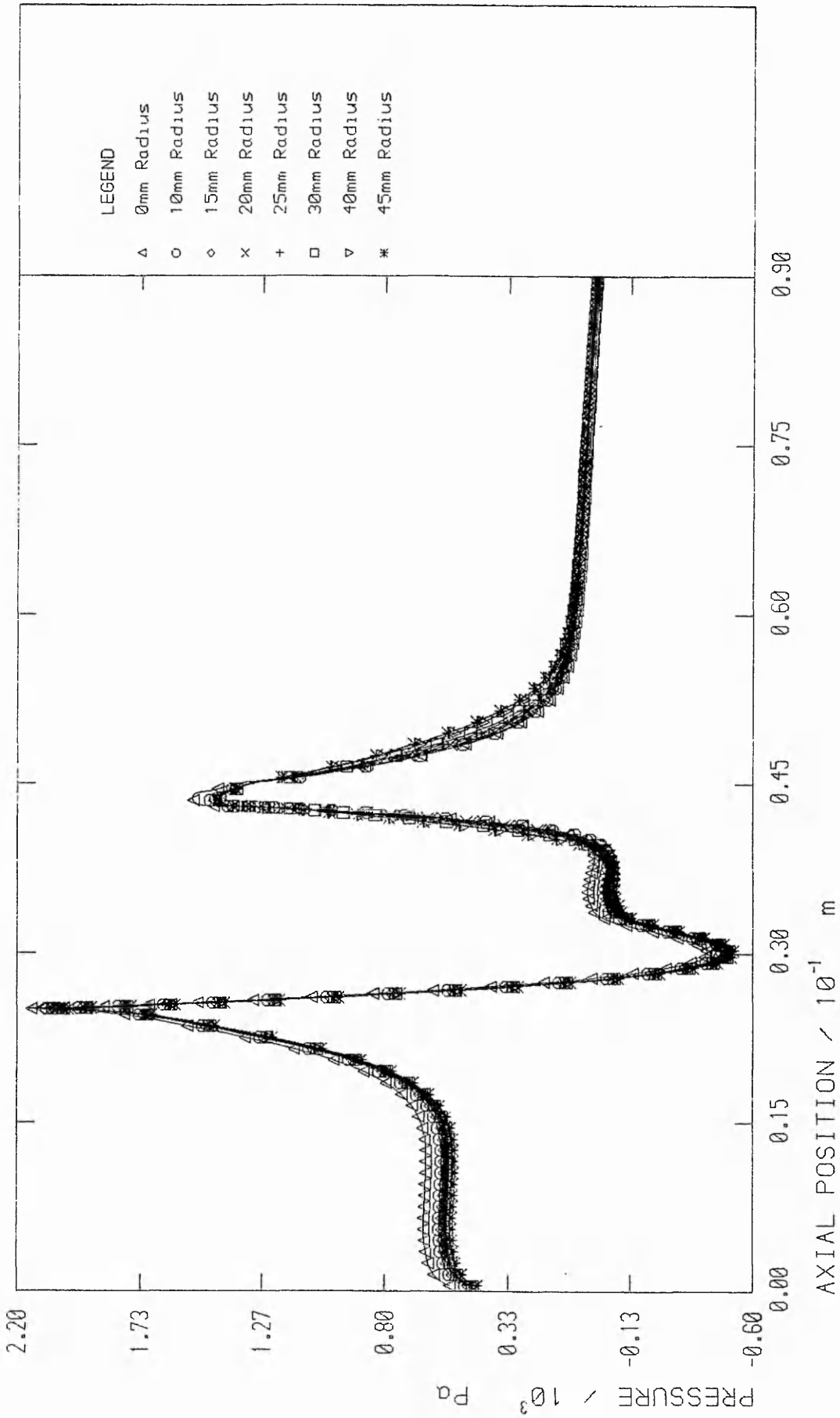
REDUCTION OF OCCLUDER DIMENSION WITH RESPECT TO CONDUIT DIAMETER (LAR SERIES)



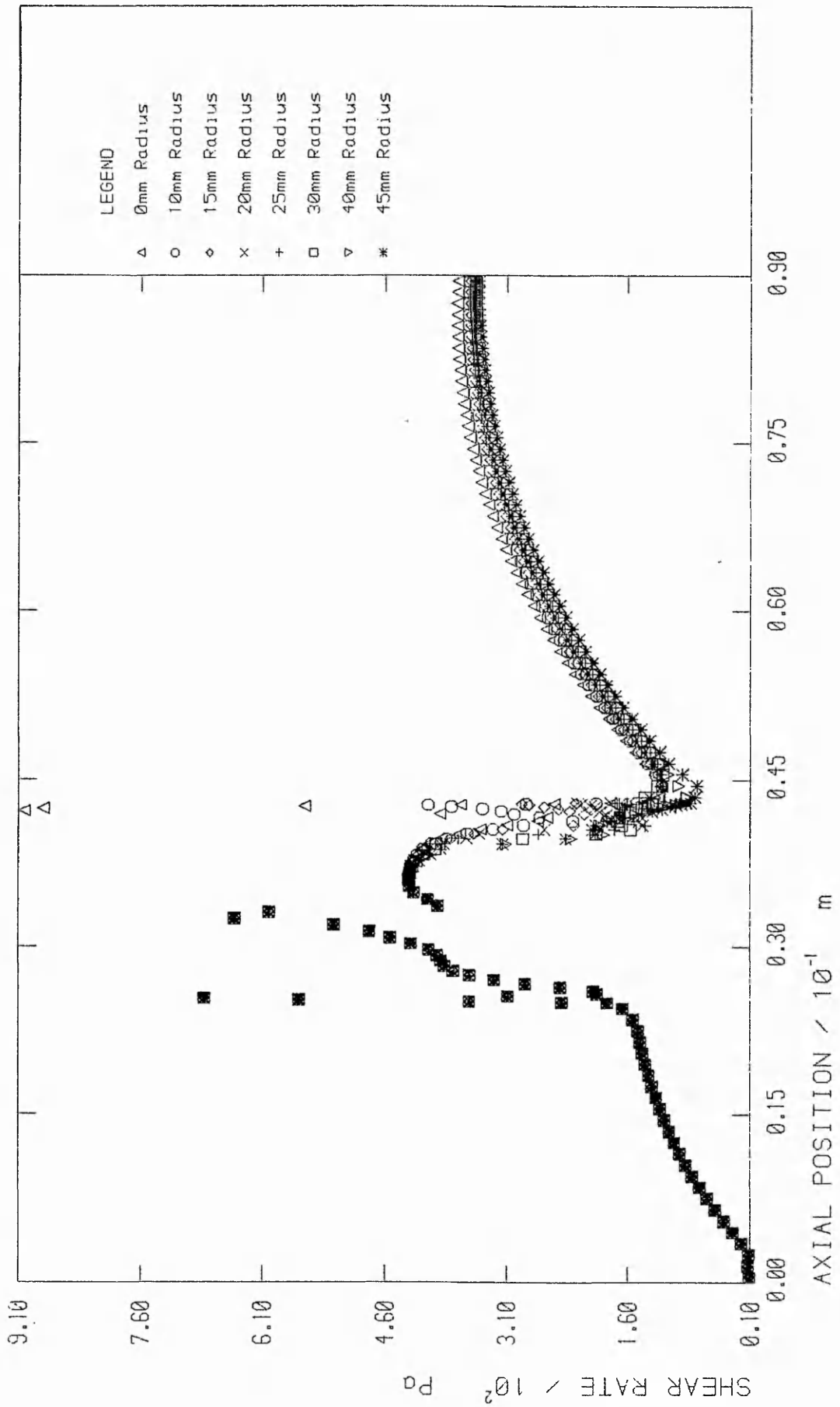
FINALISED CONDUIT DESIGN NOMINATED  
LRRSICO WITH 30mm BLENDING RADIUS



THE INFLUENCE OF BLENDING RADIUS ON CONDUIT PERFORMANCE  
 AXIAL POSITION VERSUS STREAMWISE FORCE ON THE BALL



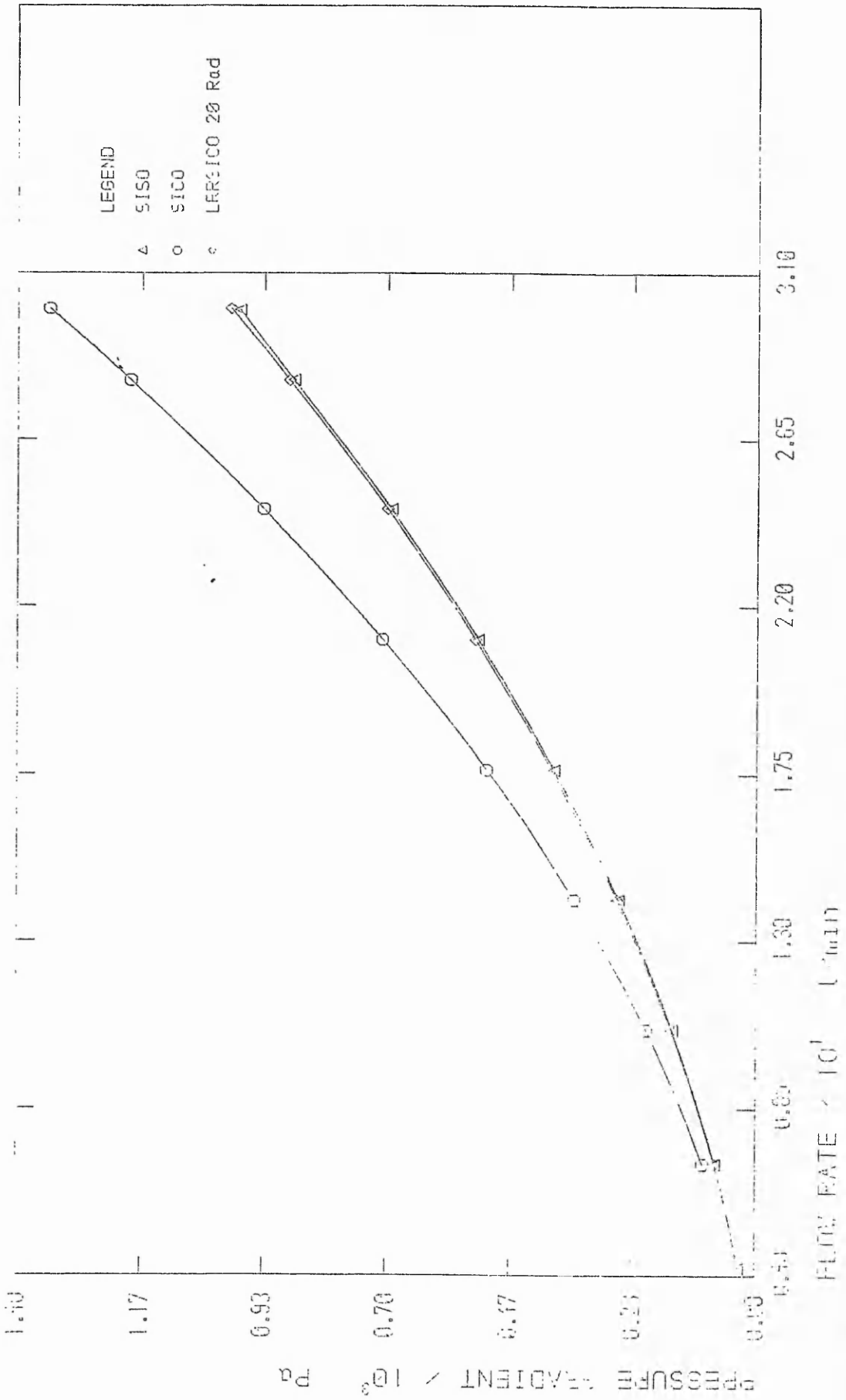
THE INFLUENCE OF BLENDING RADIUS ON CONDUIT PERFORMANCE  
 AXIAL POSITION VERSUS PRESSURE AT CENTRELINE



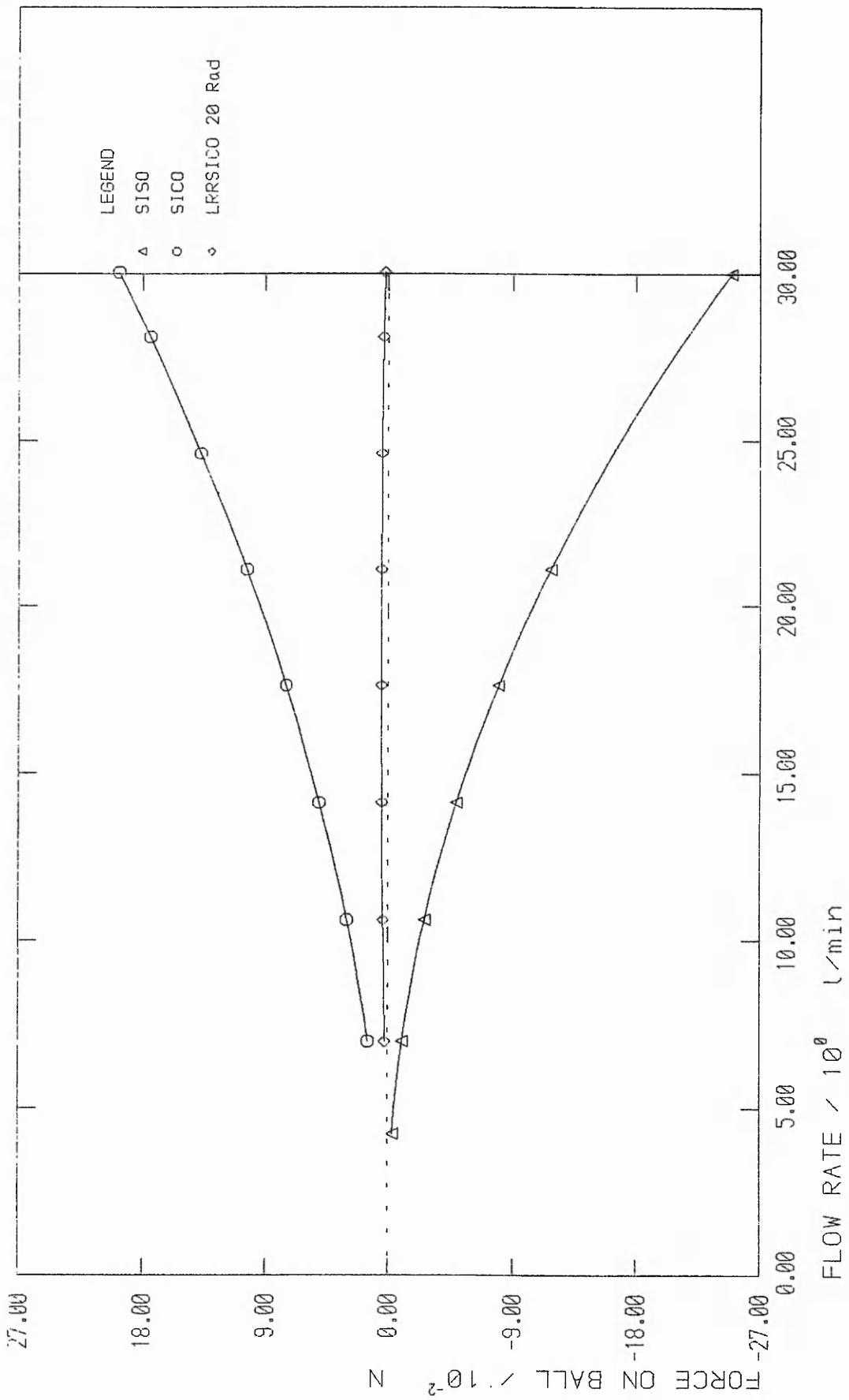
THE INFLUENCE OF BLENDING RADIUS ON CONDUIT PERFORMANCE  
 AXIAL POSITION VERSUS SHEAR RATE AT CONDUIT WALL

reduction in shear rate at the conduit wall with increasing radius, and shows that the region most affected is that in proximity with the blending radius.

Based on the predicted onset of occluder instability in water flow, seen in figure 7.6, the blending radius adopted was 20mm. The characteristics of this valve are compared against the first two prototypes in figures 7.17 - 7.21. Pressure/flow characteristics (figure 7.17) of the LRRSICO valve with a 20mm blending radius almost match those of the original prototype (which remained unsurpassed). However, unlike the SISO valve, occluder oscillation was not induced by higher flow rates due to a greatly reduced area of high pressure behind the ball (figures 7.18 and 7.19). The overall effect of these changes on the streamwise force experienced by the ball is shown in figure 7.20 which depicts the sum of pressure and shear forces at each cell centre along the ball surface. The magnitude of negative force behind the ball is reduced in line with that of the more stable SICO valve, but the magnitude of positive force is less due to a reduced streamwise shear force component. Figure 7.21 shows that these tendencies are similar in higher flow rates. Throughout the studies the non-dimensional wall distance ( $y^+$ ) values at the wall cells were monitored (figures 7.22 and 7.23). This ensured compliance with established modelling guidelines (see chapter six) but also gave a measure of turbulence at the prosthetic surface. Ideally kinetic energy of turbulence at prosthetic surfaces should be minimised. This is seen (in figure 7.22) to occur with increasing blending radius.

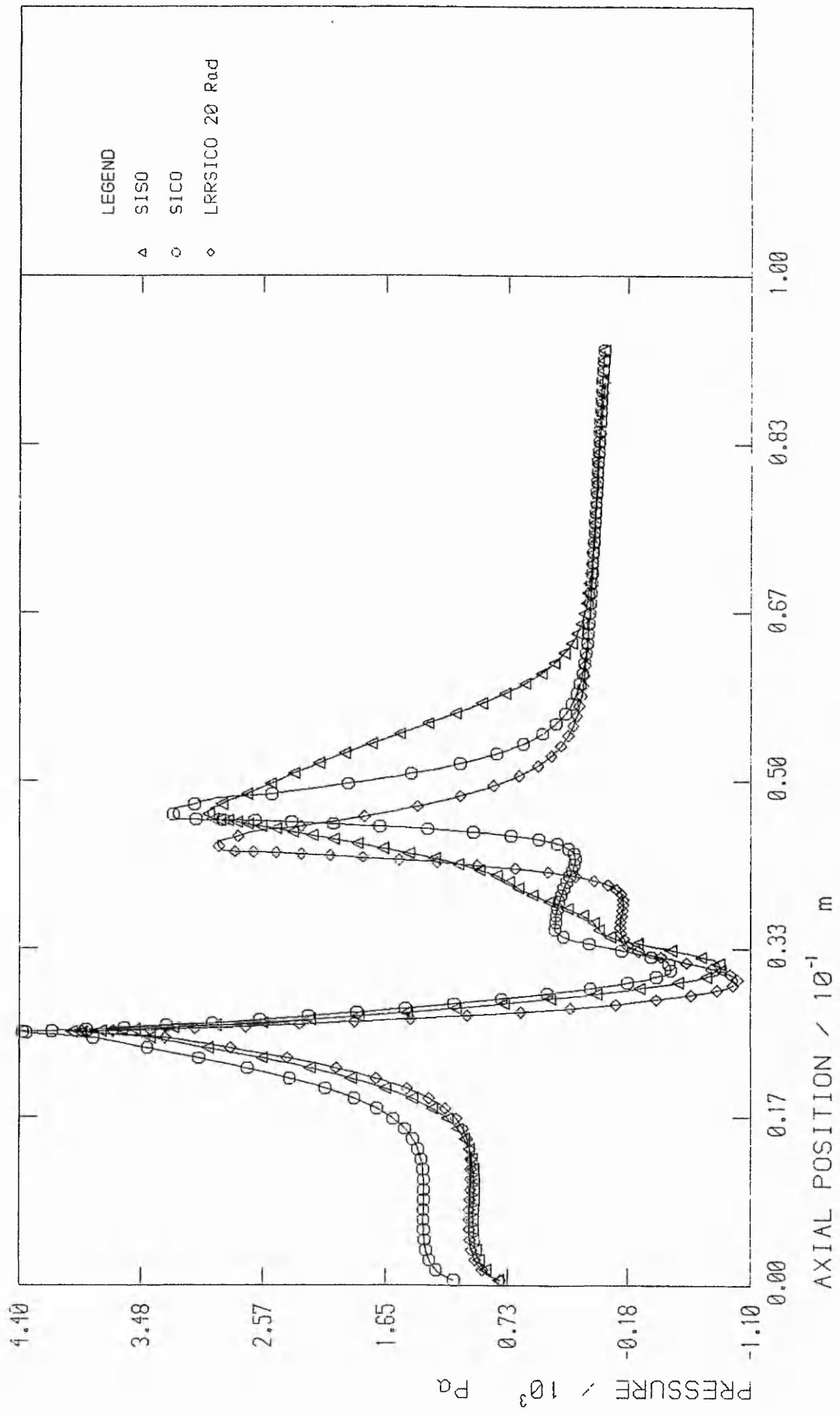


COMPARISON OF PRESSURE GRADIENT VERSUS FLOW RATE OF WATER  
 FOR THREE VALVE PRESSURE GRADIENT CIRCUIT DESIGNS:



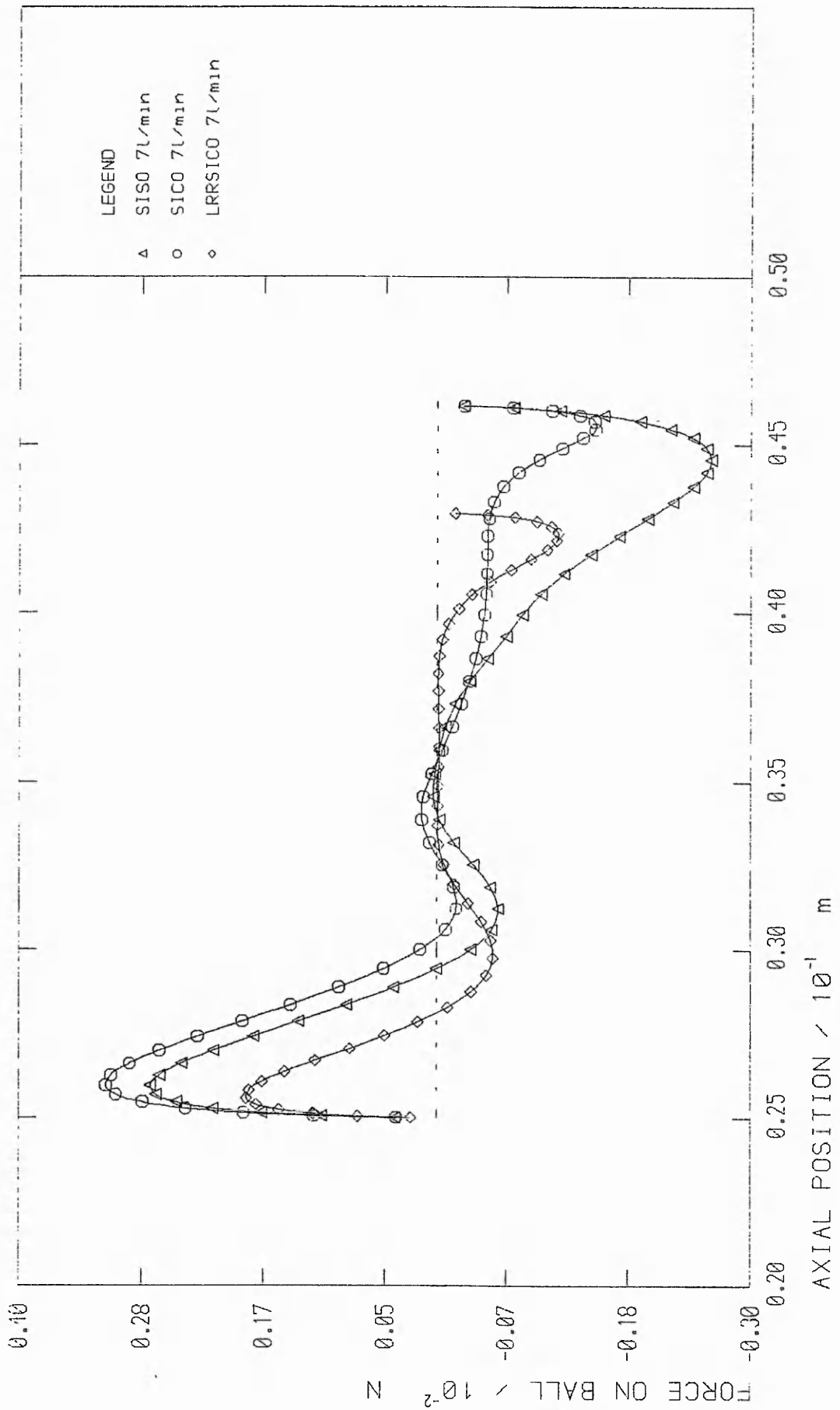
A COMPARISON BETWEEN THREE PROTOTYPE CONDUIT DESIGNS:  
 FORCE ON THE BALL VERSUS FLOW RATE OF WATER

Figure 7.18

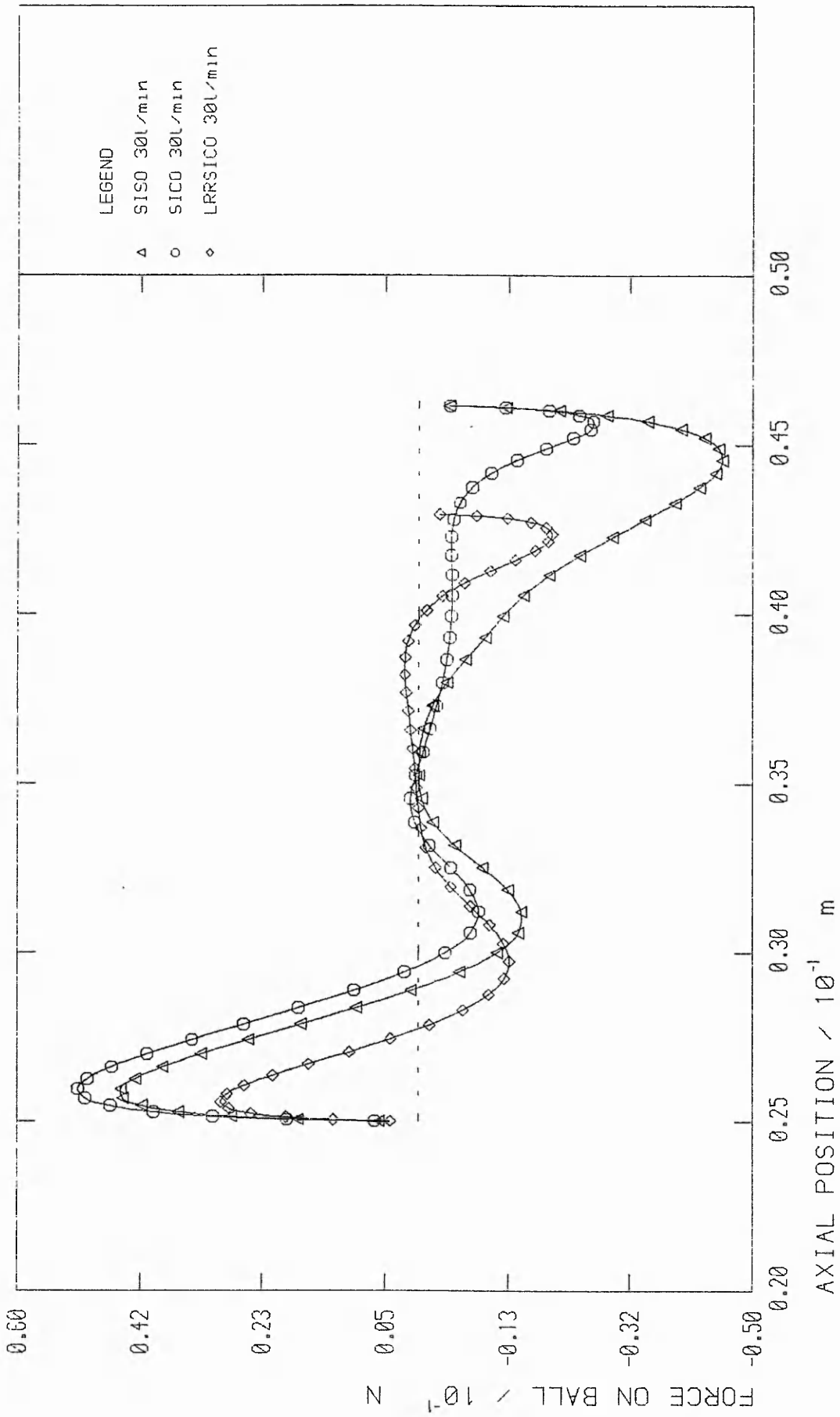


COMPARISON BETWEEN THREE PROTOTYPE CONDUIT DESIGNS  
 PRESSURE PROFILE ON THE BALL SURFACE AND CENTRELINE FLOW = 30L/min

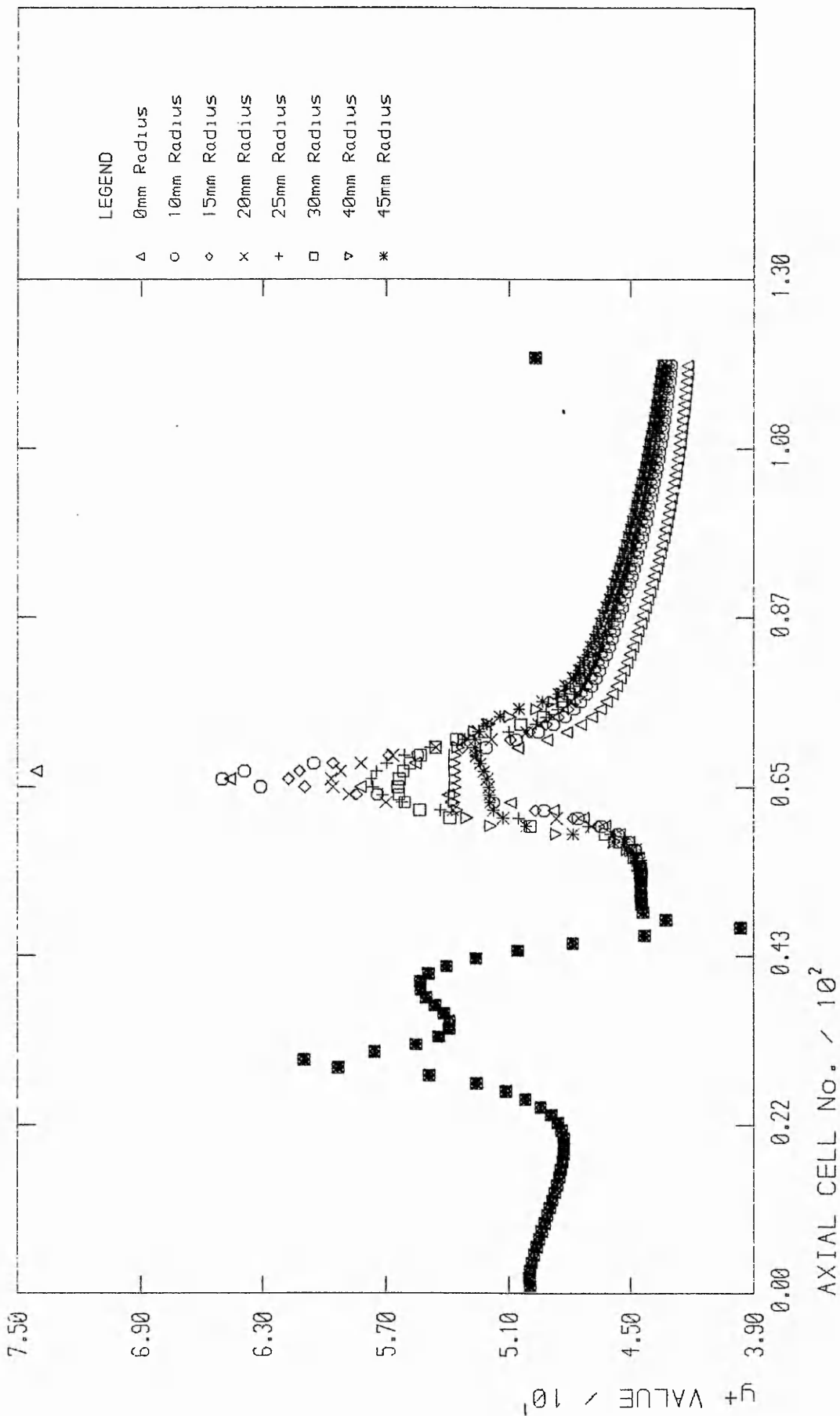
Figure 7.19



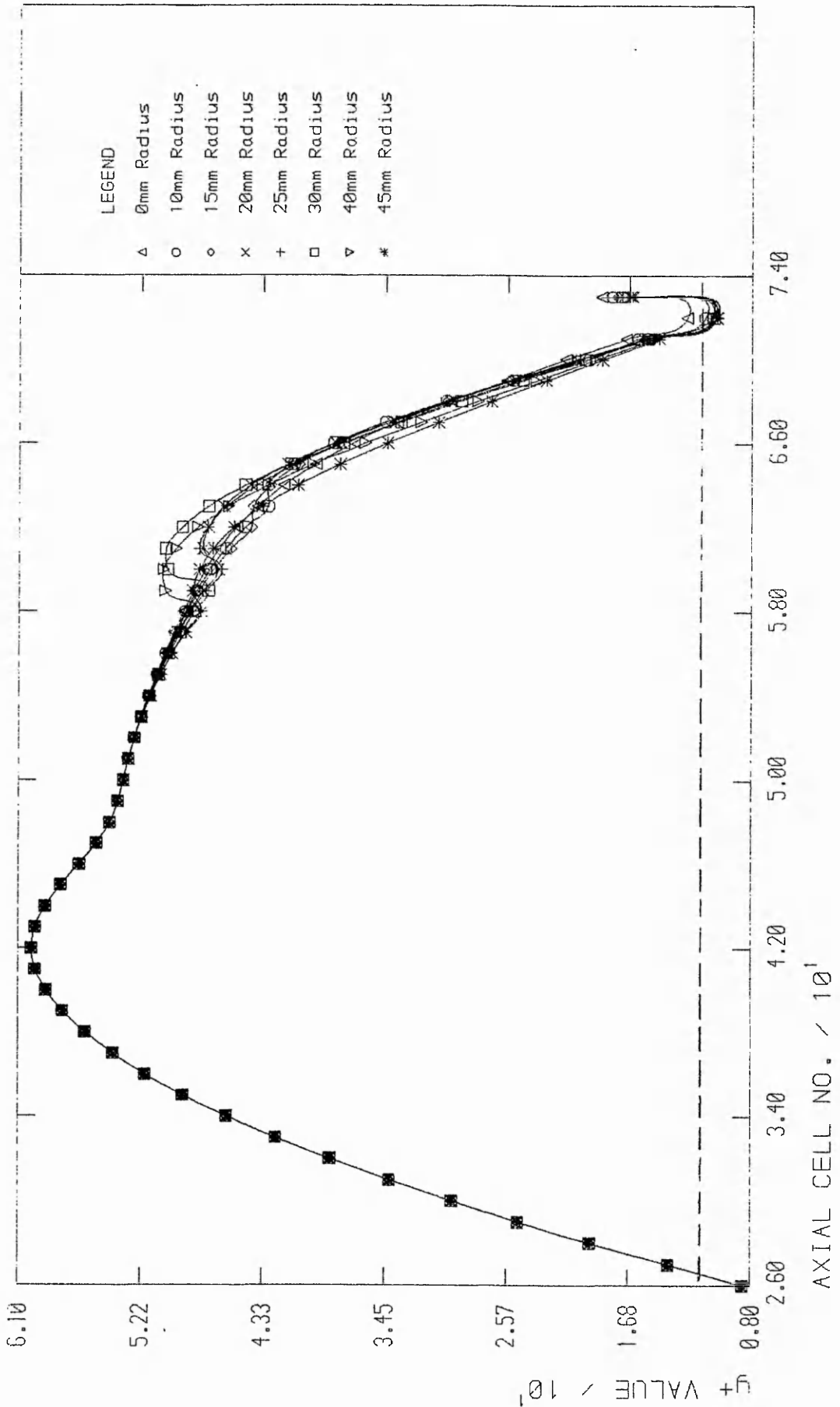
COMPARISON BETWEEN THREE PROTOTYPE CONDUIT DESIGNS:  
 STREAMWISE FORCE PROFILE ON THE BALL SURFACE FOR FLOW = 7l/min



COMPARISON BETWEEN THREE PROTOTYPE CONDUIT DESIGNS:  
 STREAMWISE FORCE PROFILE ON THE BALL SURFACE FOR FLOW = 300 L/min



THE INFLUENCE OF BLENDING RADIUS ON CONDUIT PERFORMANCE  
CONDUIT WALL CELL VERSUS DIMENSIONLESS WALL DISTANCE

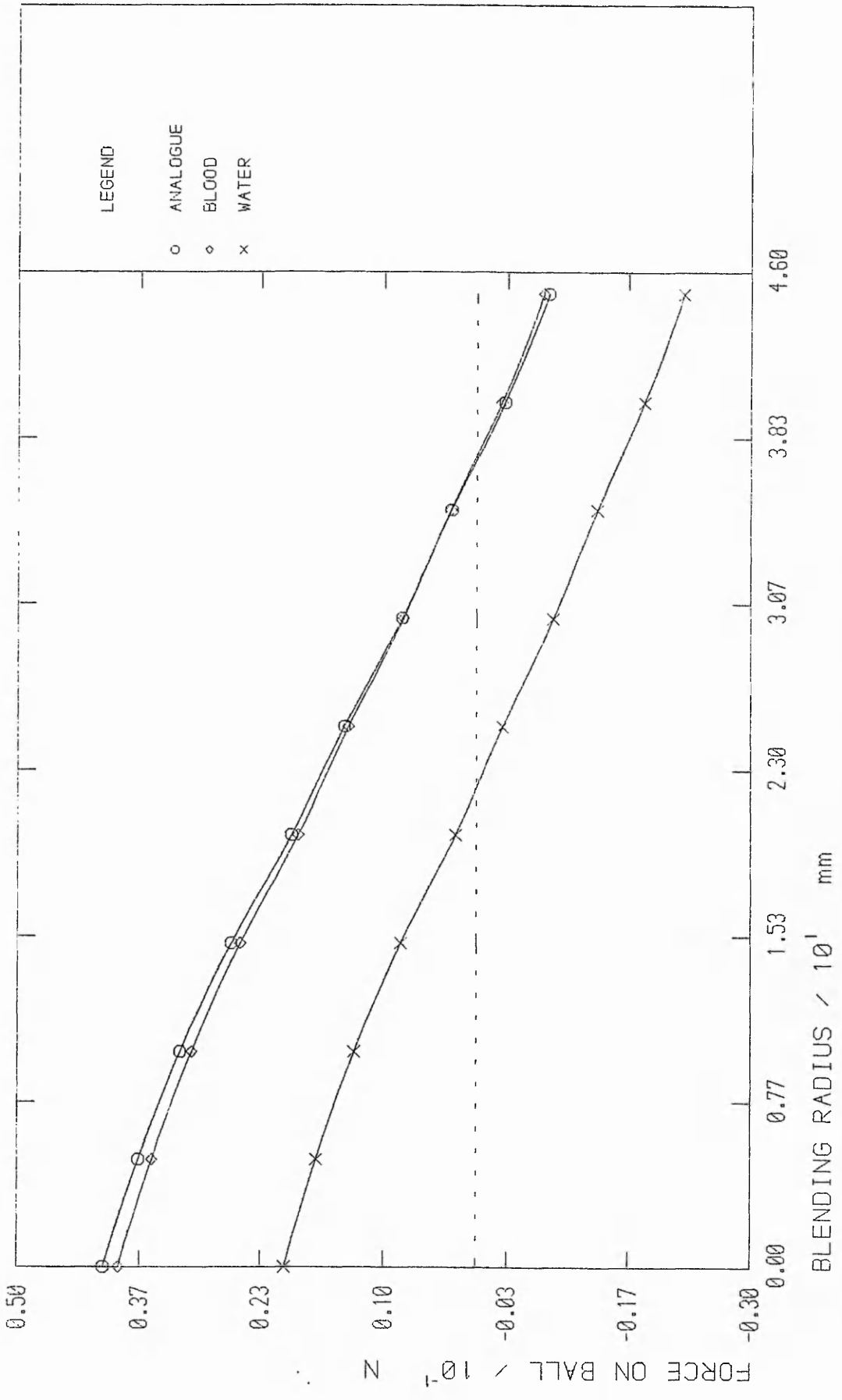


THE INFLUENCE OF BLENDING RADIUS ON CONDUIT PERFORMANCE  
CENTRELINE AXIAL CELL VERSUS DIMENSIONLESS WALL DISTANCE

### 7.3 Finalisation of Design for Blood Flow

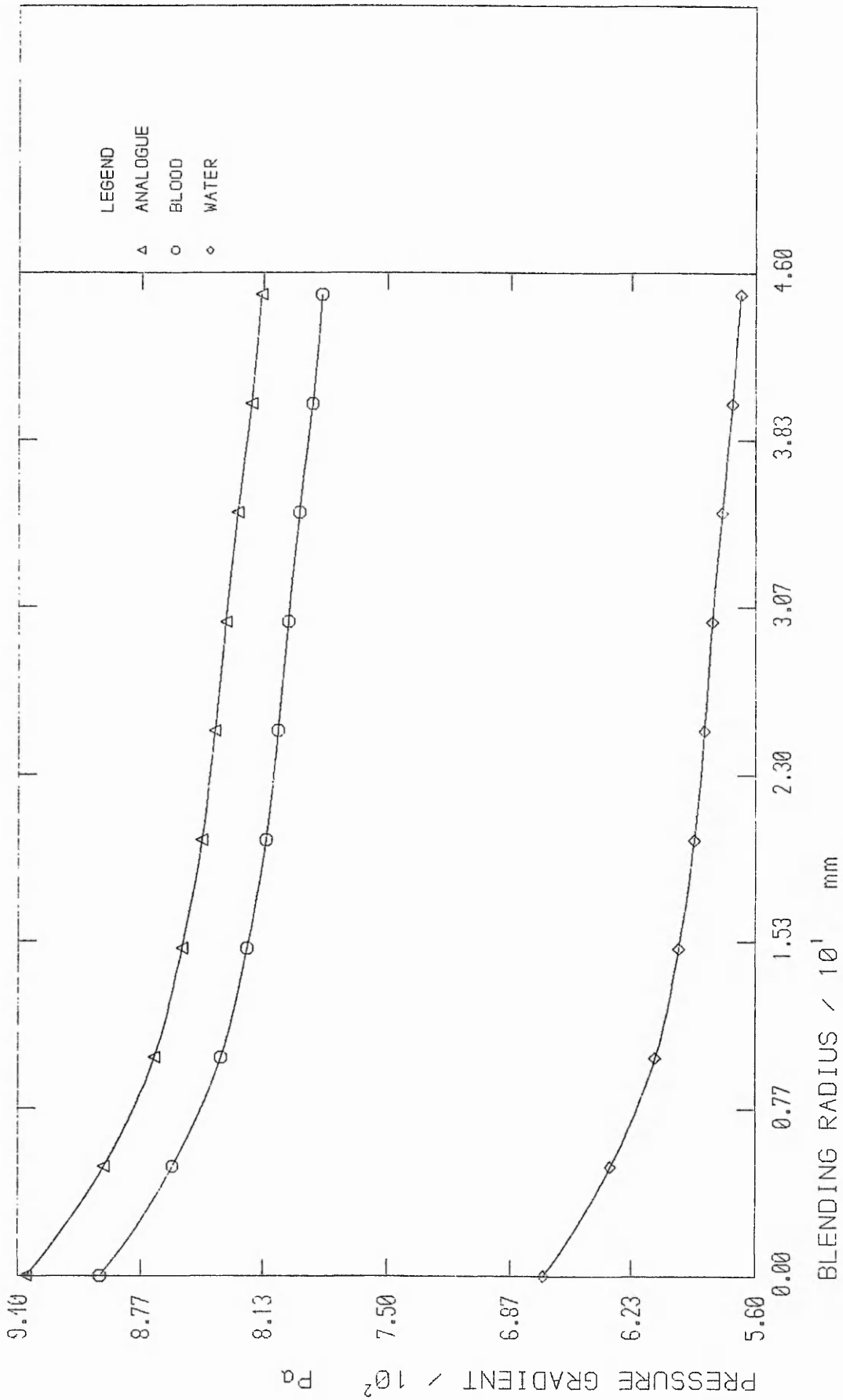
Studies of analogue and blood flow through the LRRSICO valve geometry indicated that occluder instability would not occur until the blending radius was increased to 37mm, as shown in figure 7.24. This is contrary to observations made in water flow. Furthermore, figure 7.25 shows pressure gradients in the more viscous fluids to be elevated by 30%. Ramifications of these findings are that if a valve were designed based on water flow, then not only would the pressure gradient across the valve have been under estimated, but also the optimal blood flow geometry would not have been realised. Based on the results of these studies, the valve was re-designed to incorporate a 30mm radius in preference to 20mm, still allowing some factor of safety to avoid occluder instability if the valve were implanted into a patient whose blood viscosity was naturally low for some reason, such as anaemia.

If blood analogue solution had been used in the computer study instead of real blood the same optimum valve geometry would have been established. Differences in valve performance when subjected to flows of blood and analogue solution would only have been slight. For example, pressure gradient predictions for analogue flows would have varied from those of blood by only 5%, as evident from figure 7.25. Maximum shear stresses occurred at the point of impingement on the ball surface and were unaltered by blending radius. This parameter would have been predicted 6.9% too high in analogue solutions (figures 7.26 - 7.28). This finding is contrary to observations made in simple pipe geometries, but in accord with the findings of Merchant and



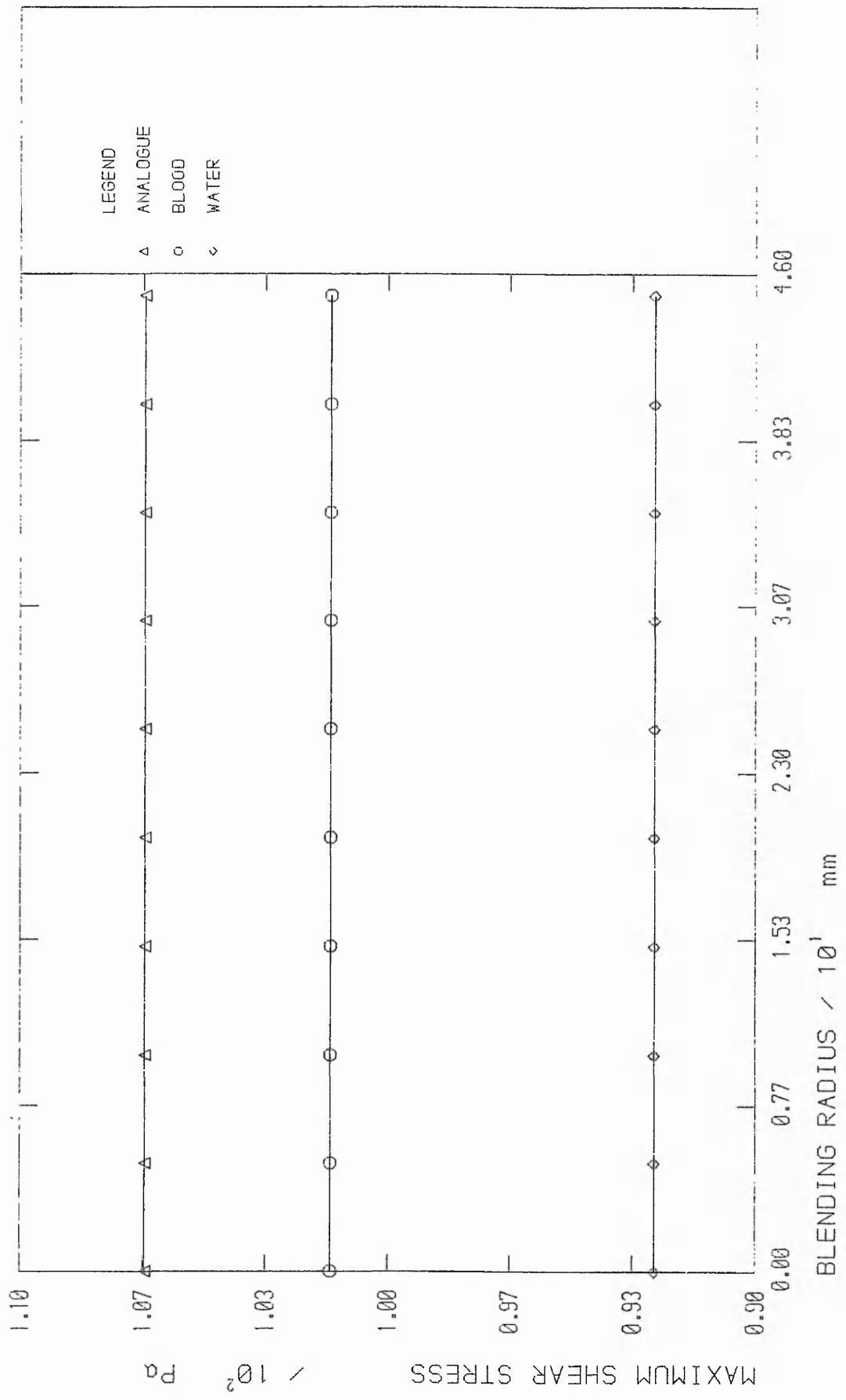
FLOW CHARACTERISTICS OF FINAL PROTOTYPE VALVE WITH ALTERNATIVE BLENDING RADII AND IN VARIOUS FLOW MEDIA

Figure 7.24

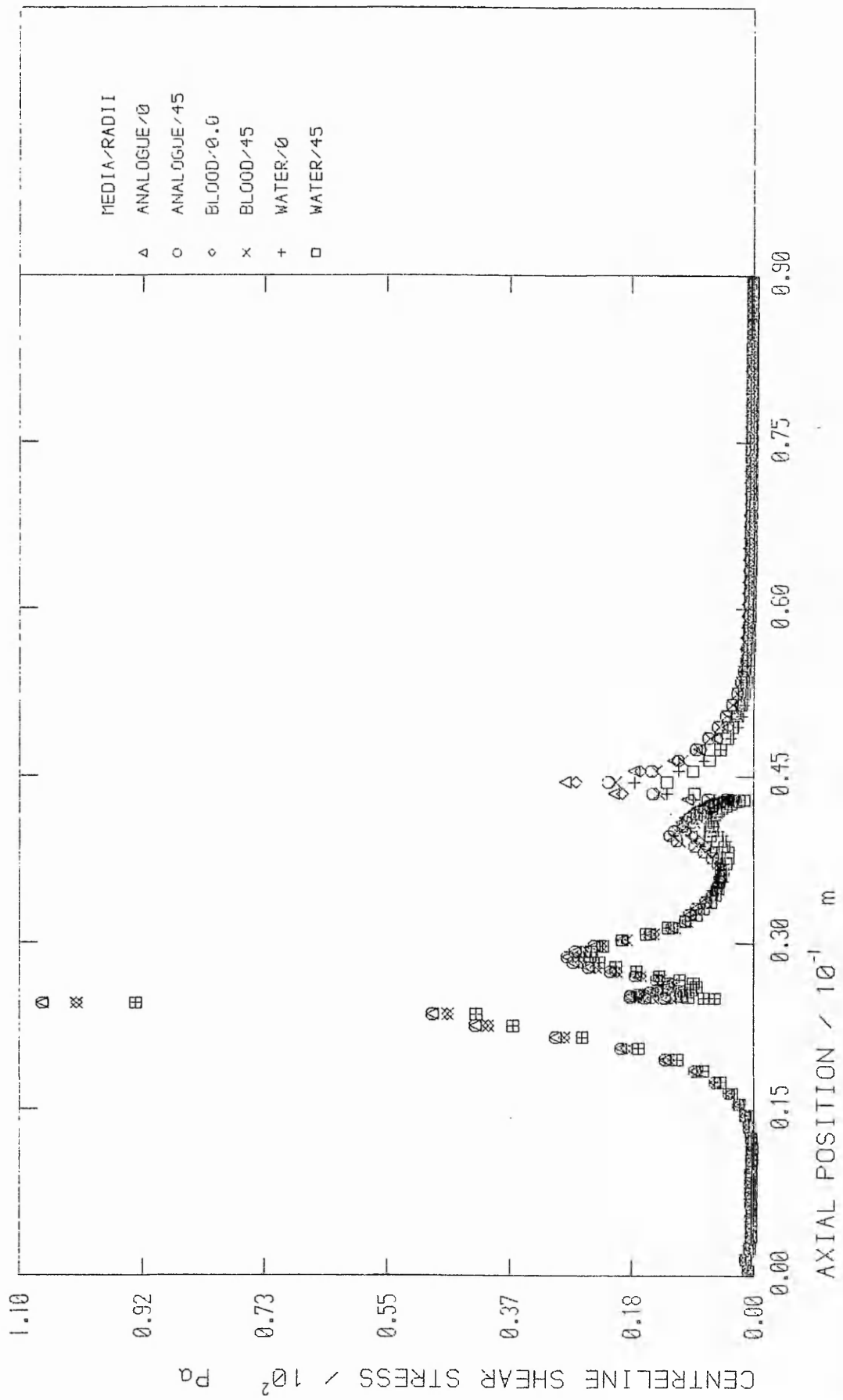


FLOW CHARACTERISTICS OF FINAL PROTOTYPE VALVE WITH ALTERNATIVE BLENDING RADII AND IN VARIOUS FLOW MEDIA

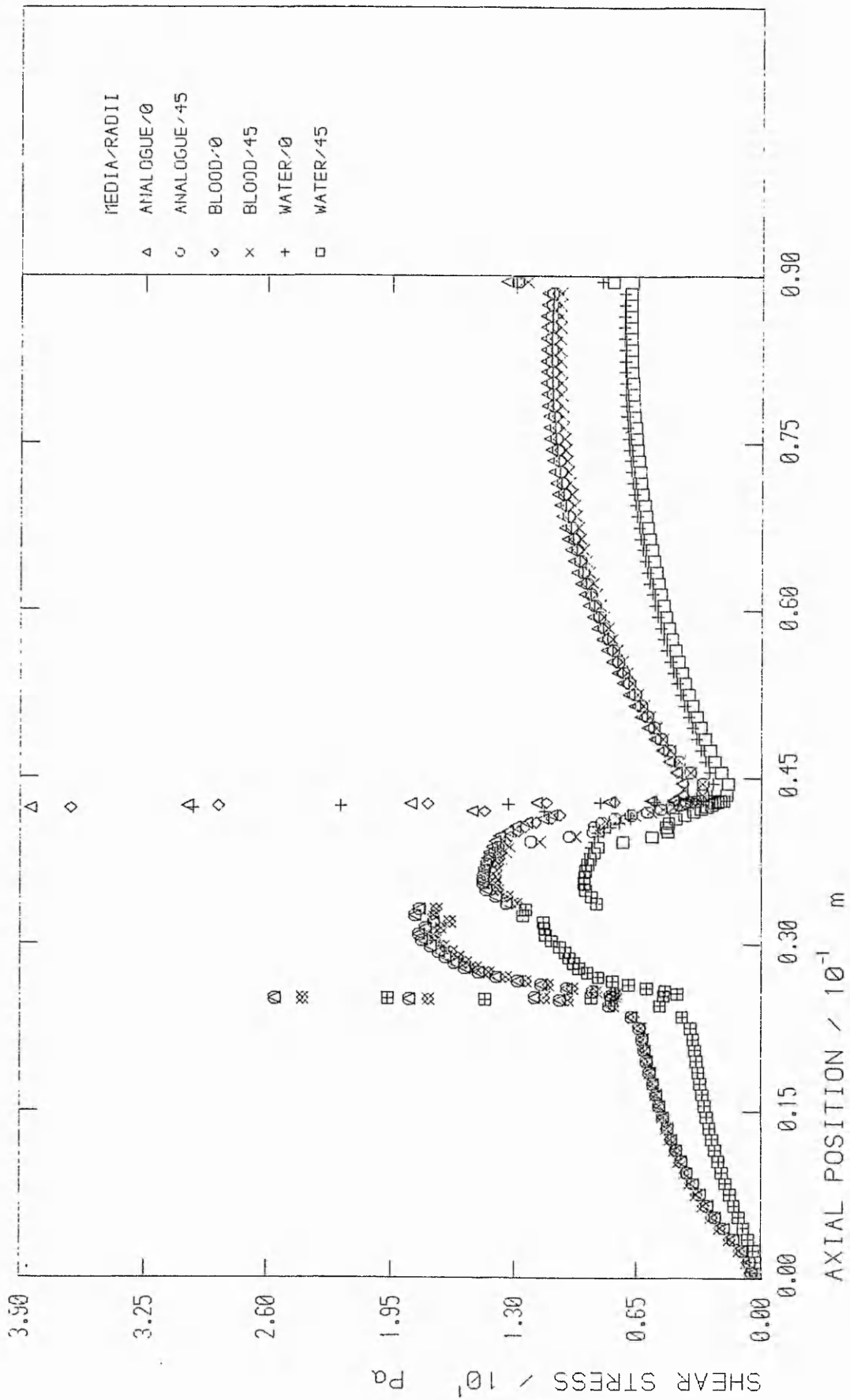
Figure 7.25



FLOW CHARACTERISTIC OF FINAL PROTOTYPE VALVE WITH ALTERNATIVE BLENDING RADII AND IN VARIOUS FLOW MEDIA



THE EFFECT OF BLENDING RADIUS AND MEDIA ON FLOW IN FINAL (LRRSICO) VALVE: SHEAR STRESS ALONG CENTRELINE AND BALL SURFACE



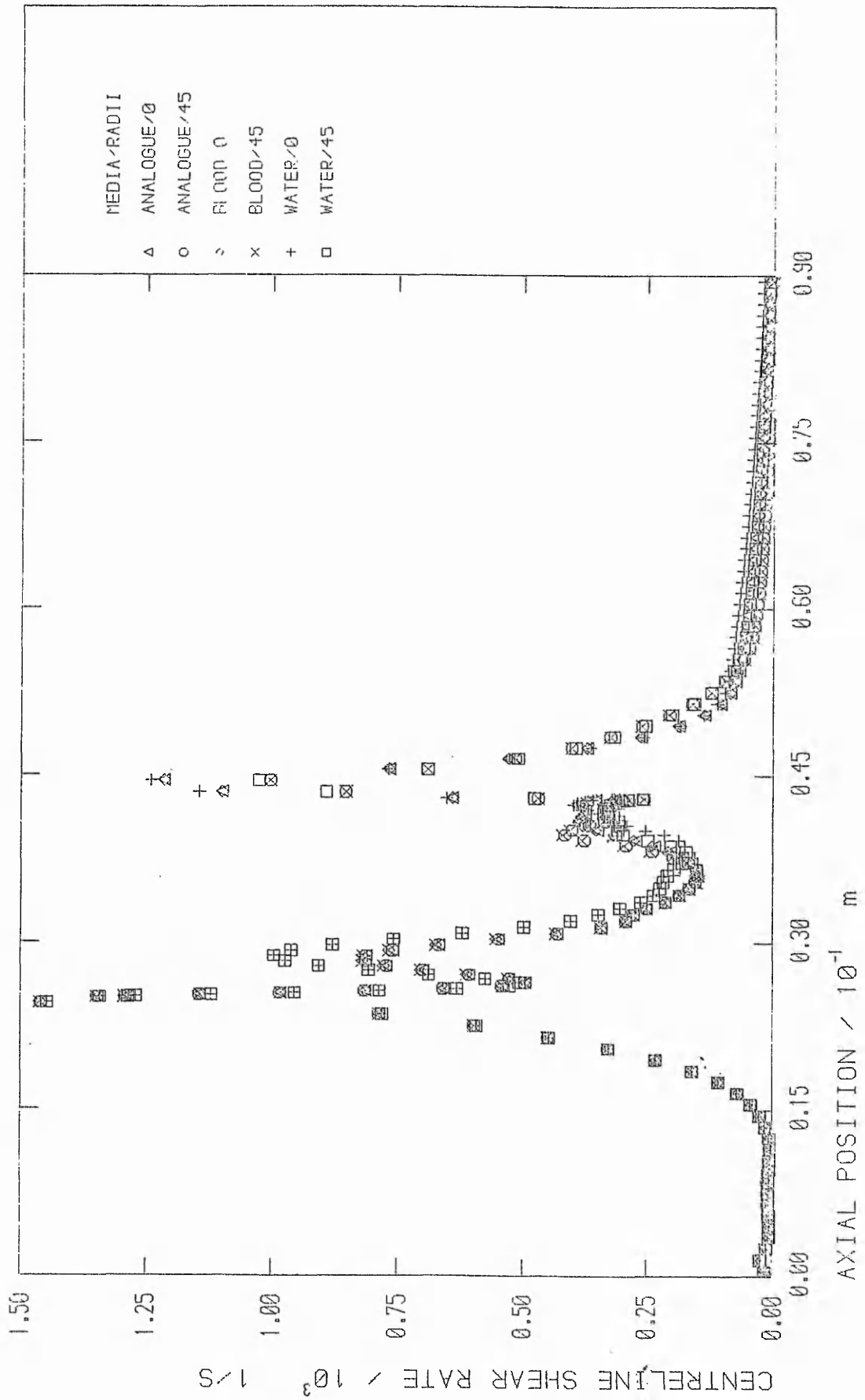
THE EFFECT OF BLENDING RADIUS AND MEDIA ON FLOW IN FINAL (LRRSICO) VALVE: SHEAR STRESS VERSUS AXIAL CELL POSITION ALONG CONDUIT WALL

Mazumdar (1986). Differences in shear rates and the levels of turbulence for the two fluids were minimal (figures 7.29 - 7.32).

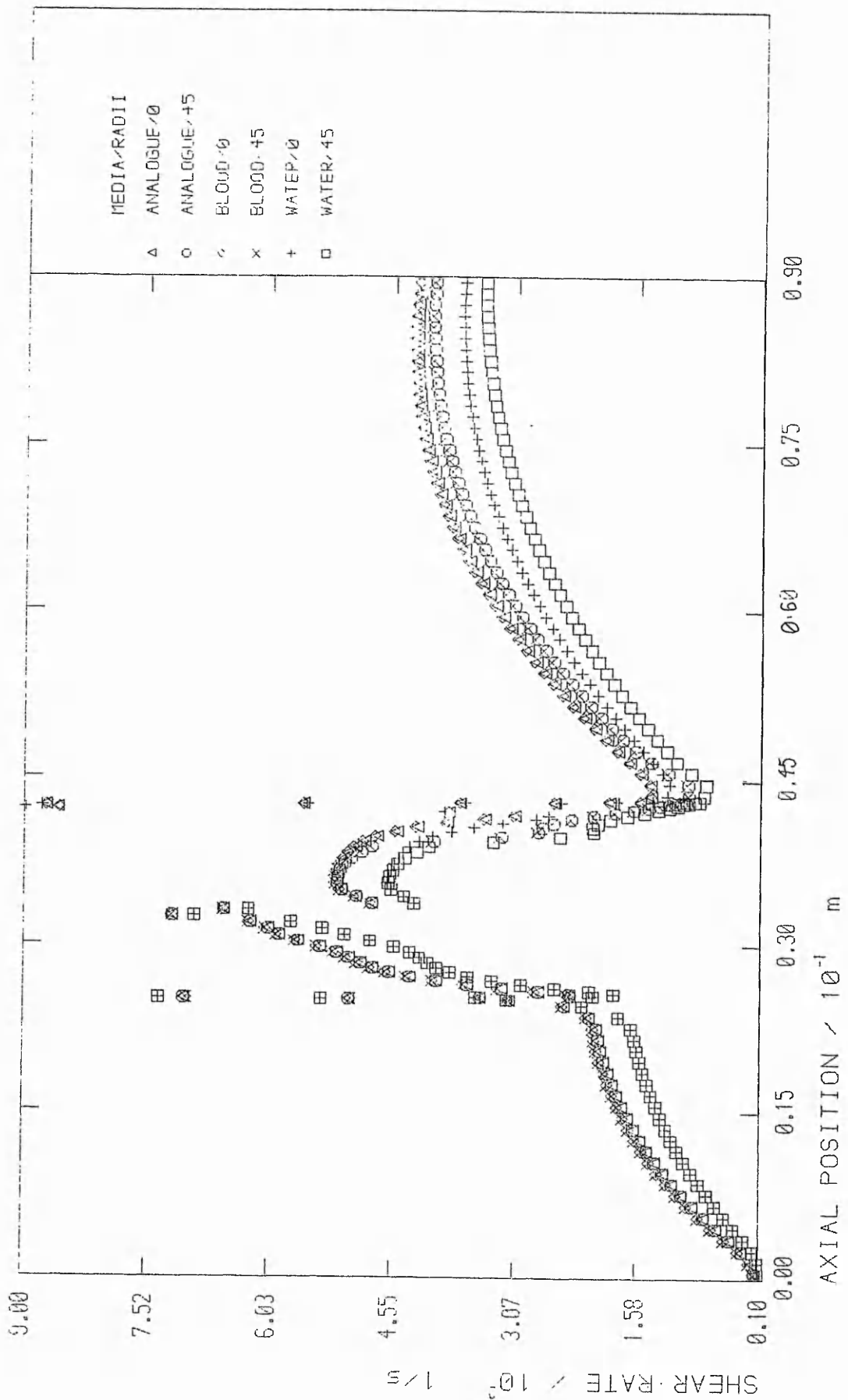
#### 7.4 Assessment of Final Design

Final valve assessment comprised two series of computational tests. First, a size 16 valve was subjected to flow rates of blood and analogue solution varying from 7l/min up to a maximum 30l/min. Second, blood flow at 21.1l/min was modelled through the range of valve sizes 10mm - 24mm. Size variation was achieved by allowing for a sizing factor in the Fortran algorithm which generated the grid geometry, each valve being a directly scaled model of the 22mm diameter valve. The volumetric flow rate of 21.1l/min was maintained through each size variant by increasing inflow velocity with decreasing conduit diameter. The dimensionless wall distance ( $y^+$ ) to the first cells was held similar by decreasing the wall-cell dimensions proportional to conduit size. A full analysis of all flow rates through the eight size variants was not attempted as this would have taken an excessive amount of CPU time.

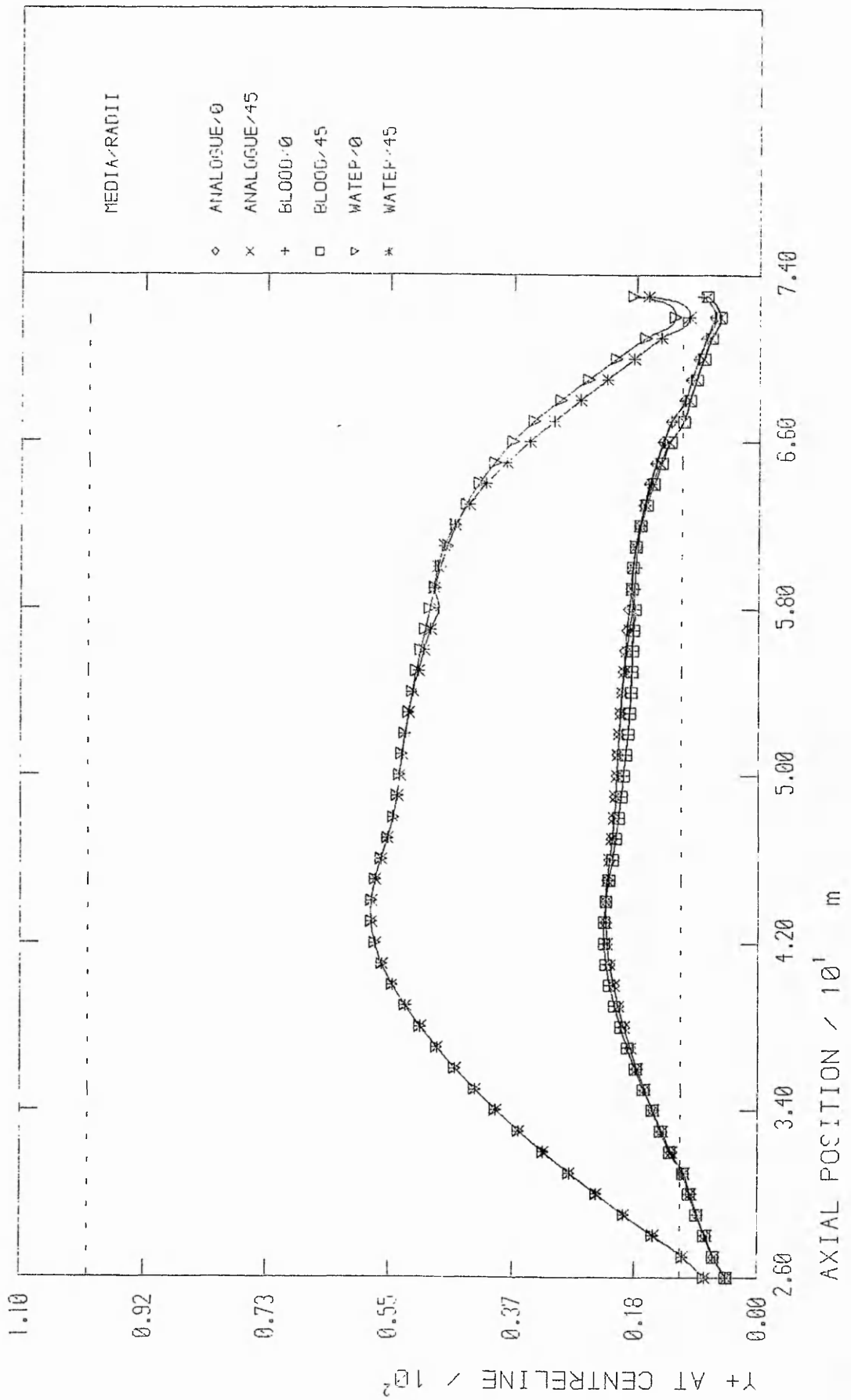
Figure 7.33 shows a rapid decrease in valvular pressure gradient with increasing valve size. For blood flow the maximum gradient measured in the 10mm diameter valve was 4 600Pa (34.5 mmHg), and the minimum gradient across the 24mm conduit was only 170Pa (1.27mmHg). Pressure gradients experienced by the 16mm valve ranged from a maximum 1 477Pa (11mmHg), in a flow rate of 30l/min, down to 160Pa (1.2mmHg) for 7l/min flow rate (figure 7.34). These pressure/flow characteristics are excellent when compared with annulus mounted mechanical valves. Yoganathan et



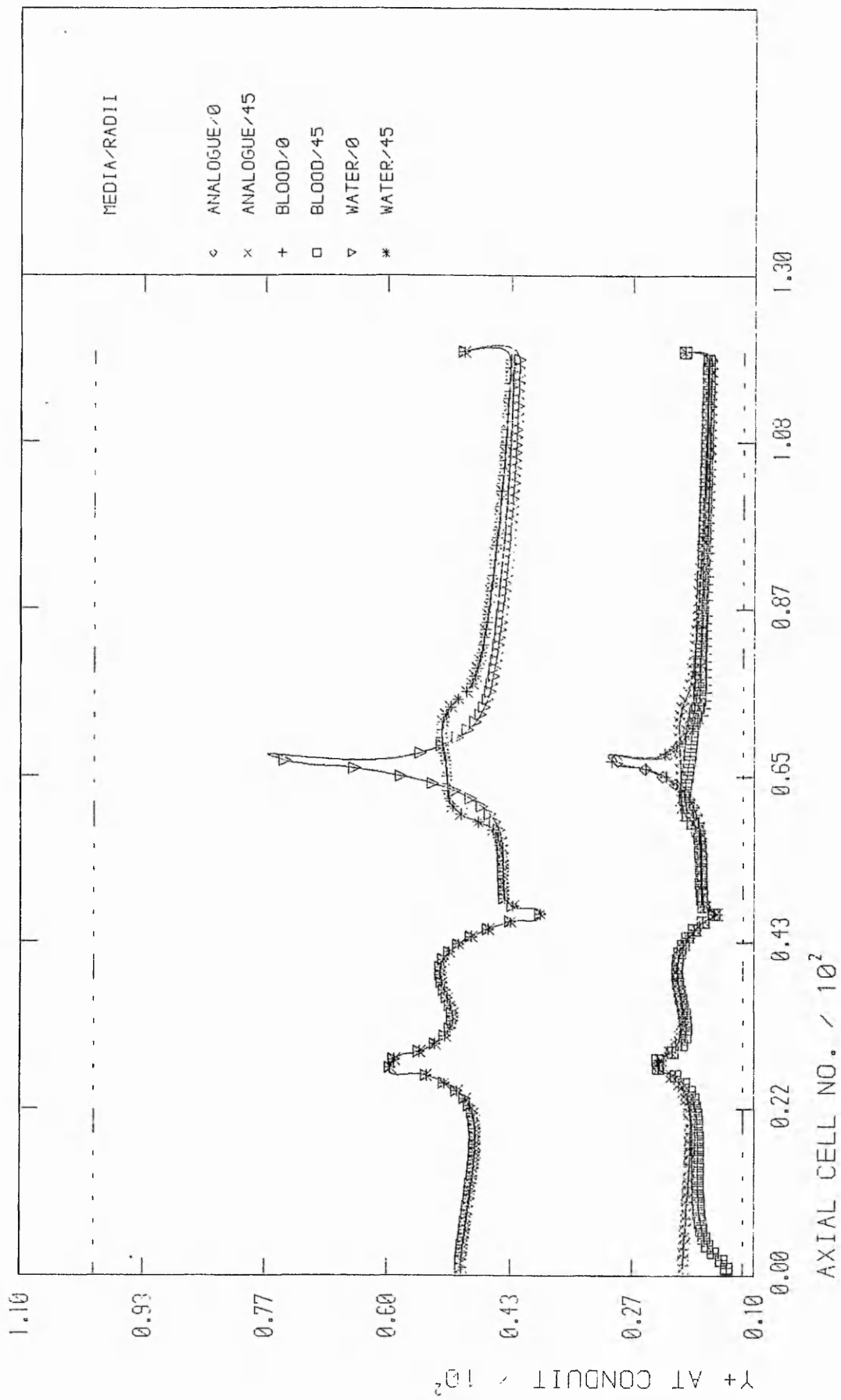
THE EFFECT OF BLENDING RADIUS AND MEDIA ON FLOW IN FINAL (LFRSICO) VALVE: SHEAR RATE ALONG CENTRELINE AND BALL SURFACE



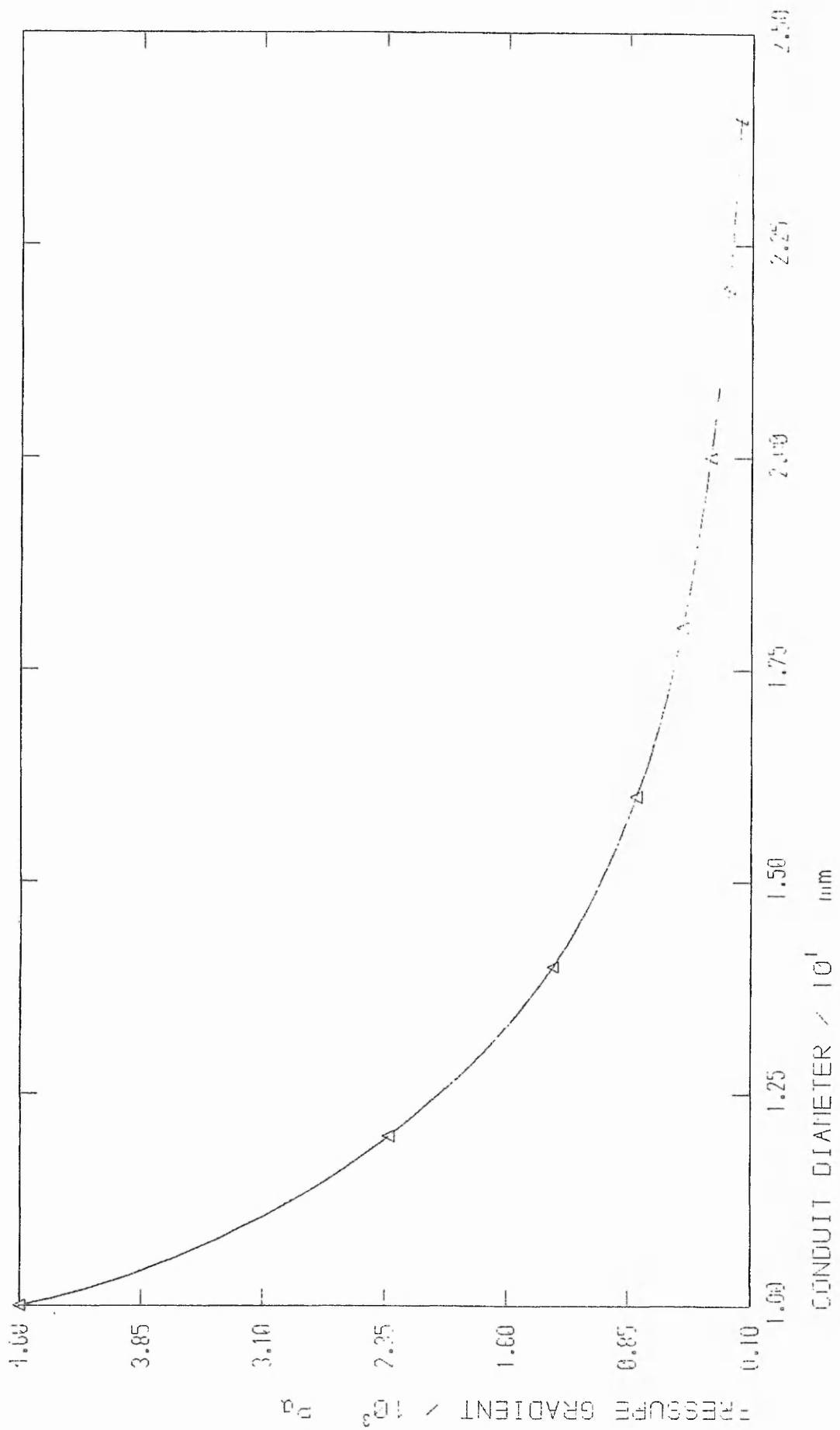
THE EFFECT OF BLENDING RADIUS AND MEDIA ON FLOW IN FINAL (LRRSICO) VALVE: SHEAR RATE AT CONDUIT WALL VS AXIAL POSITION OF CELL



THE EFFECT OF BLENDING RADIUS AND MEDIA ON FLOW IN FINAL (LRRSICO) VALVE: A CHECK ON DIMENSIONLESS CELL CENTRE DISTANCE AT BALL SURFACE

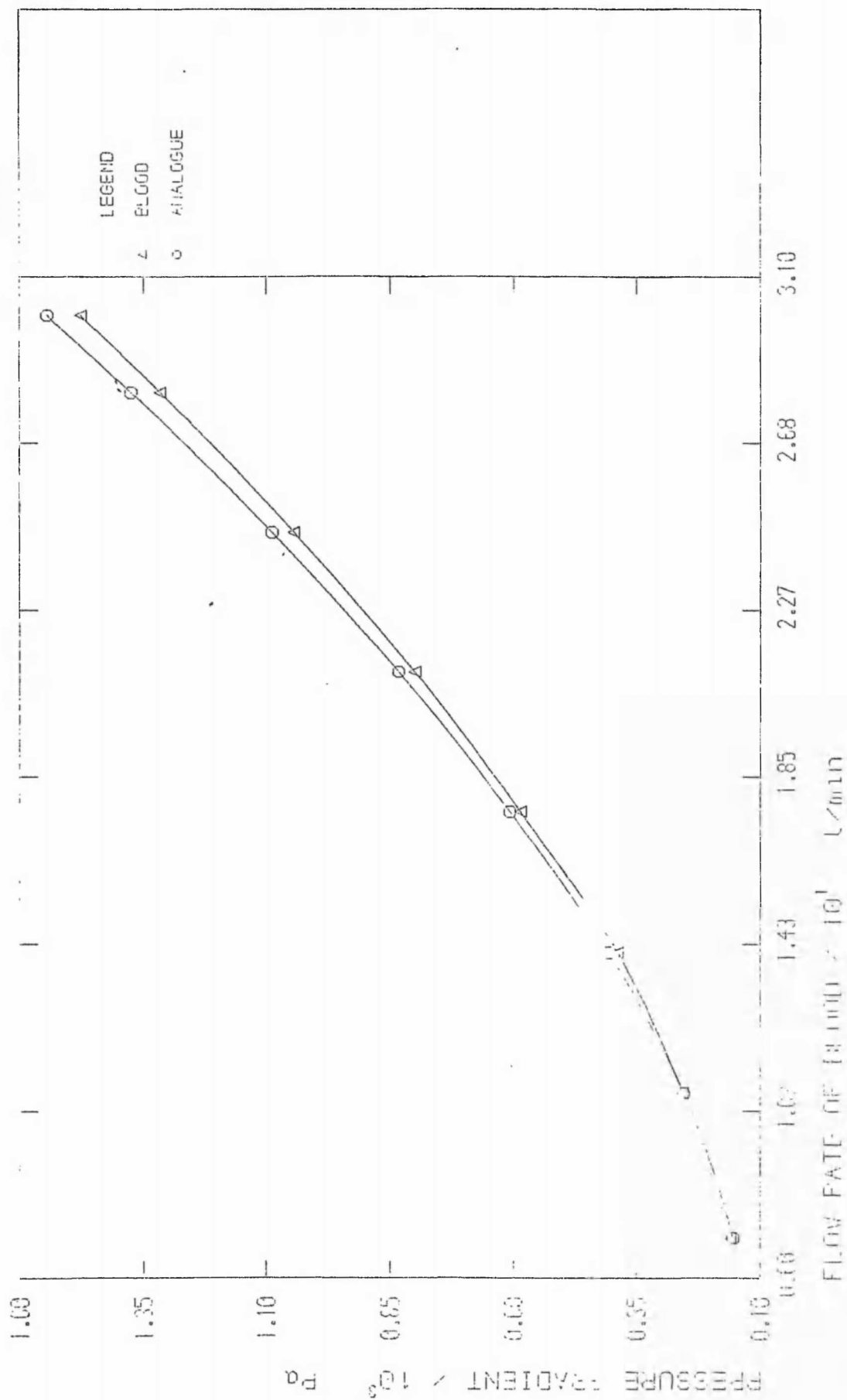


THE EFFECT OF BLENDING RADIUS AND MEDIA ON FLOW IN FINAL (LRRSICO) VALVE: A CHECK ON DIMENSIONLESS CELL CENTRE DISTANCE AT CONDUIT WALL



PRESSURE GRADIENT VERSUS CONDUIT SIZE OF FINALISED (LFR5110) VALVE WITH 30mm BLENDING RADIUS

Figure 7.33



PRESSURE GRADIENTS IN FINALISED (LRS10) VALVE WITH 30mm BLENDING RADIUS

Figure 7.34

al (1979c) quote pressure gradients for 21.1l/min flow rate of 1 480Pa in a Smeloff-Cutter A-5 and 760Pa in a Björk-Shiley mitral valve. Bruss et al (1983) compared four different disk valves of 27mm sewing ring diameter and found that pressure gradients at 21.l/min range from 394Pa to 667Pa. The above compare with 832Pa in the much smaller 16mm (LRRSICO) conduit.

A more complete comparison should have been afforded by applying the Gorlin - Gorlin (1951) equation to yield a constant of proportionality between pressure gradient and flow per unit area, as suggested by Gentle (1977). However, this type of analysis should strictly only be used to yield comparisons of valve performance when pressure/flow data is taken from valves mounted in similar experimental conditions, as discussed in chapter six, but reasonable comparison can be made against the findings of Gentle (1977) whose work is analytically based.

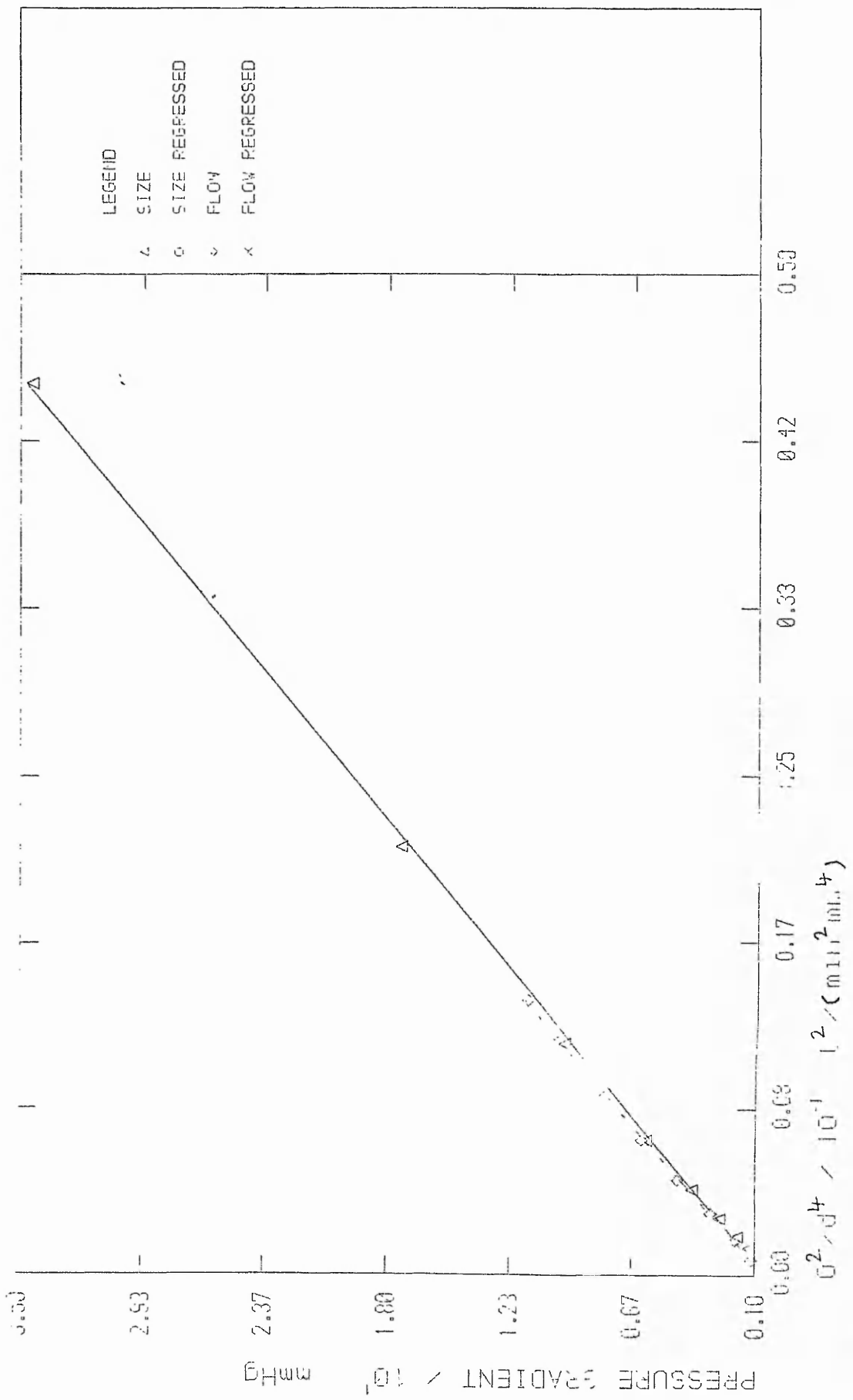
For each blood flow test series conducted on the LRRSICO prosthesis values of pressure gradient (mmHg) were plotted against the square of flow rate/unit area ( $l^2/min^2 mm^4$ ). The results are shown in figure 7.35. Linear regression revealed, for the constant size tests, a relationship:

$$\Delta P = 0.626 + 805Q^2/d^4$$

and for the tests involving various sizes subjected to a constant flow rate:

$$\Delta P = 0.602 + 767Q^2/d^4$$

Accuracy of fit was high (figure 7.35) with  $R^2$  values of 99.9% in each case. A more complete analysis is presented in Appendix 5. These relationships, with a slope of circa 800 represent an average 226% efficiency with respect to an ideal annulus-mounted



GORLIN-GORLIN ANALYSIS OF PRESSURE/FLOW CHARACTERISTICS IN FINALISED LRESICO VALVE WITH 30mm BLENDING RADIUS

Figure 7.35

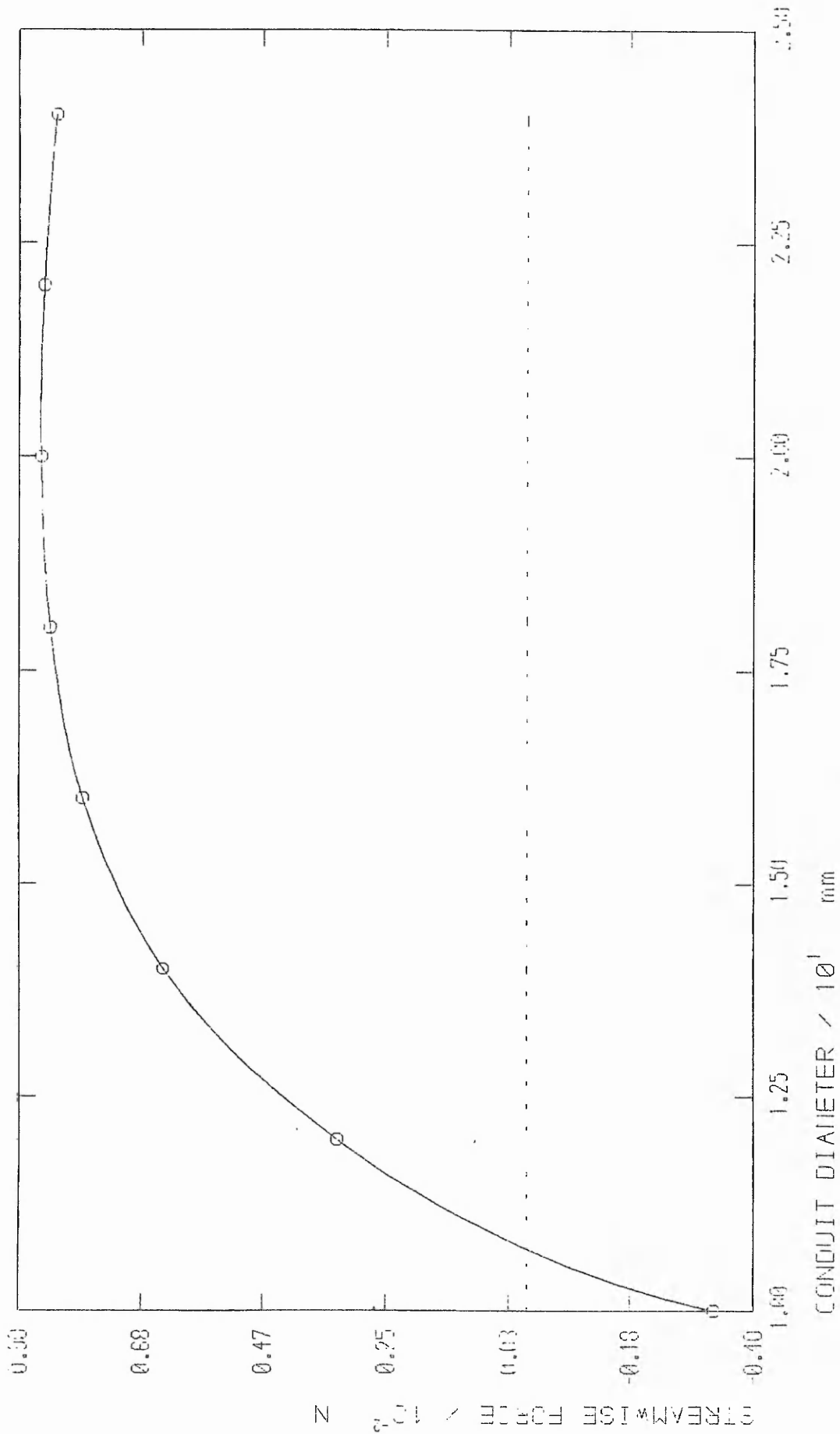
orifice with slope 1 775. Gentle (1977) presents efficiencies, derived from a similar comparison, for several annulus mounted mechanical valves. The Starr-Edwards valve exhibited the highest efficiency of 56%, followed by Edinburgh (42%), Björk-Shiley (32%) and Beall (31%). This would suggest, though with reservations because of rig differences, that the LRRSICO valve exhibits pressure/flow characteristics enhanced beyond those of an ideal orifice. Shanebrook and Levine (1979) present values for the constant of proportionality, as defined above, for five conduit types. Their quoted values range from 4 900 - 25 000 representing 36.2% to 14% efficiencies. Such high values might lead to concern over the construction of their conduits, or of their pressure drop data, however, it is probable that results were severely influenced by the experimental configuration adopted; namely one of placing a conduit into an apicoaortic shunt situation. In such a configuration higher pressure gradients will be expected due to short development lengths upstream of the valve, and also due to inlet being from a large vessel (the ventricle). Down stream conditions are also more severe, with flow exhausting into a vessel perpendicularly orientated, and with its own flow. Similarity with Benjamin's (1986) findings are good when allowances are made for differences in experimental flow conditions. Adjustment because of rig differences would bring the numerical pressure/flow characteristics of the LRRSICO valve in line with those of Benjamin rendering a value for the constant of proportionality of approximately 320, based on this valves similarity with the SISO valve (shown in figure 7.5). Comparison of pressure/flow characteristics for the LRRSICO conduit with Benjamin's constants of proportionality, shown in chapter five, again confirms the

superior performance of the finalised (LRRSICO with 30mm radius) valve.

Examination of streamwise forces on the occluder revealed that only in excessively high flow per unit area does instability occur, eg for flow rates above 21.1l/min in valve sizes below 11mm diameter, as depicted in figure 7.36, or in flows well above the physiological maximum of 30l/min through valves of 16mm diameter and above (figure 7.37). The validity of the data points representing the two lesser flow rates in figure 7.37 must be called into question, deviating as they do from the expected shape of the line. Examination of figure 7.38 points to a probable breakdown of the  $k - \epsilon$  model at the wall due to localised Reynolds' numbers at the ball surface being below the acceptable minimum, ie  $y^+ < 11.5$ .

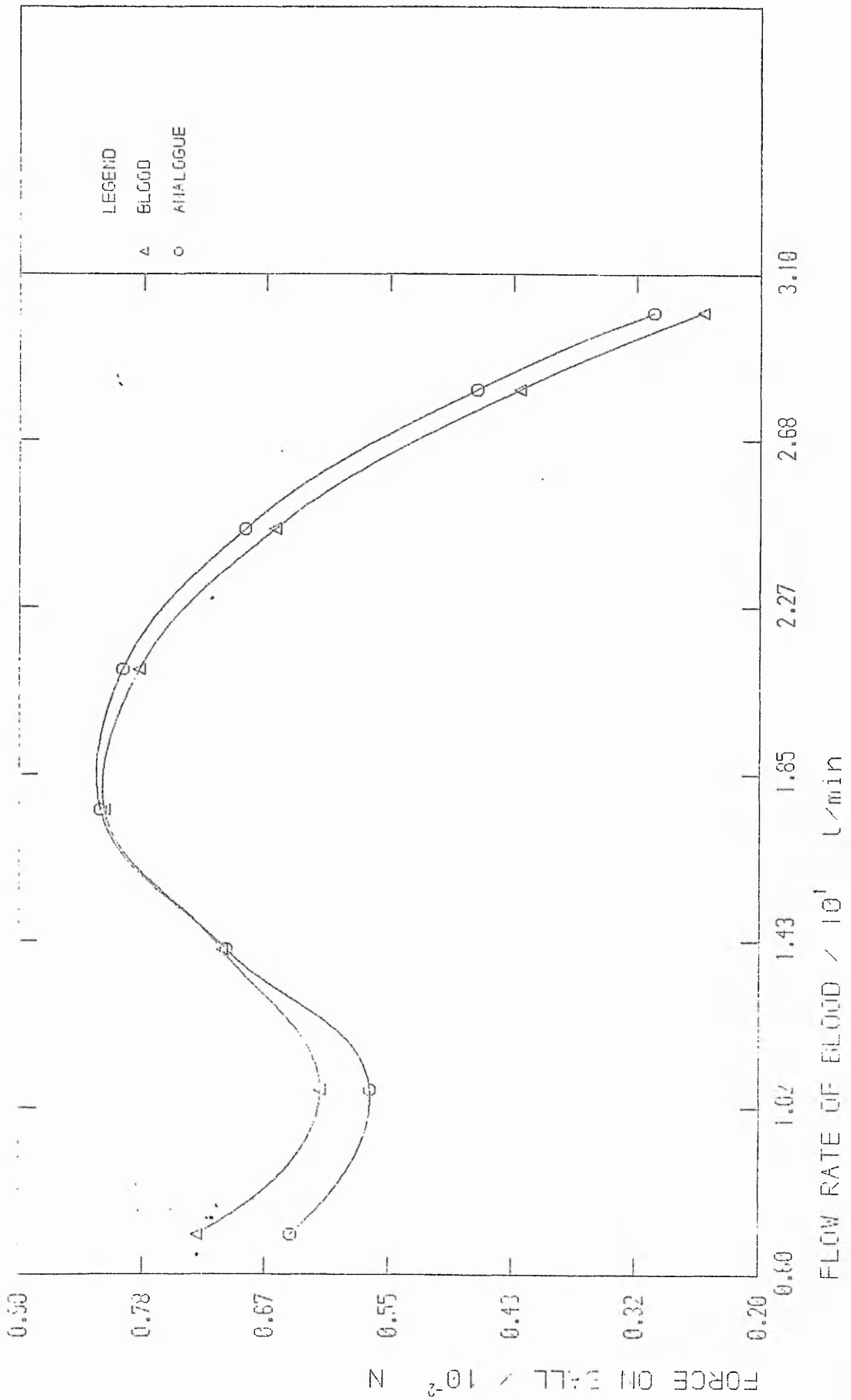
Shear stress levels within the valve have been contained well within the threshold for haemolysis due to in-bulk shear, in all situations other than for excessively high flow rates in the smallest valve sizes (see figure 7.39). In valves of 16mm diameter and above, critical stresses in-bulk will not occur in physiological flow rates (figure 7.40). Figures 7.41 and 7.42 show shear stress profiles along the conduit and ball surfaces. These and figure 7.43 which plots full-field shear stress contours, clearly demonstrate that such maxima only occur in isolated areas, such as the impingement point on the ball surface, and points of change in conduit surface direction.

The mechanism which induces haemolysis near to prosthetic surfaces needs only a fraction of the shear stress levels needed

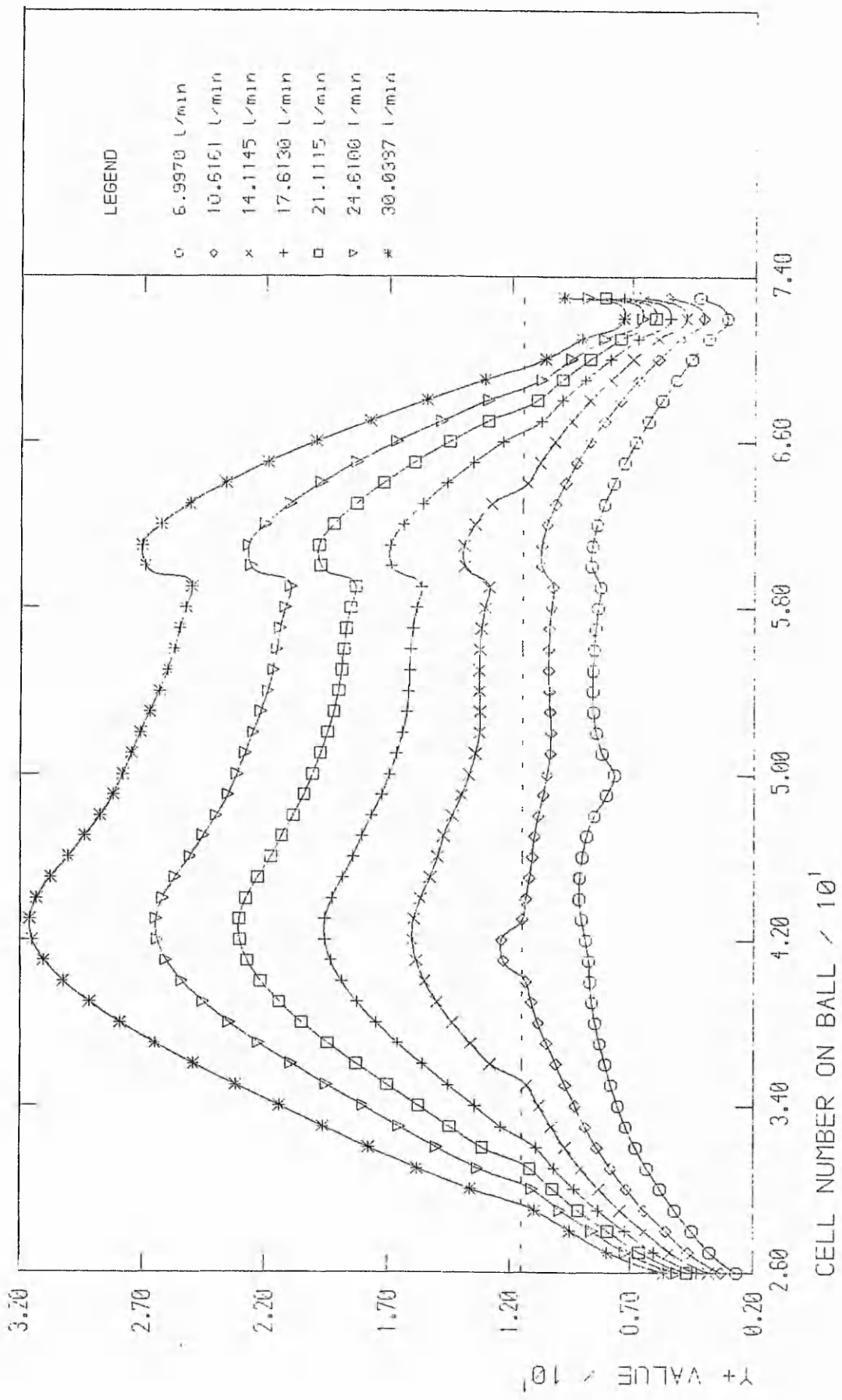


FORCE ON BALL VERSUS CONDUIT SIZE OF FINALISED (LEKSID) VALVE WITH 30mm BLENDING RADIUS

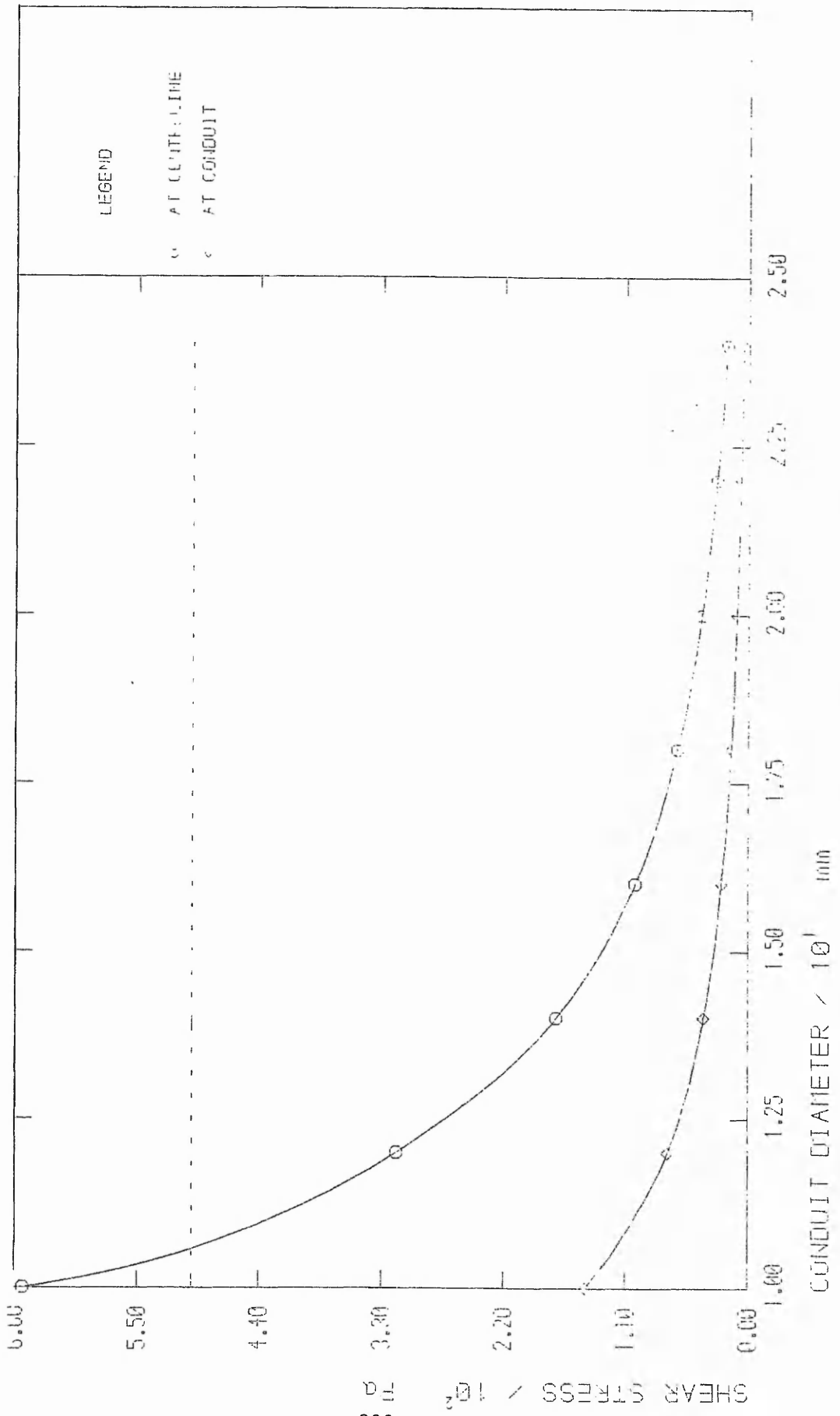
Figure 7.36



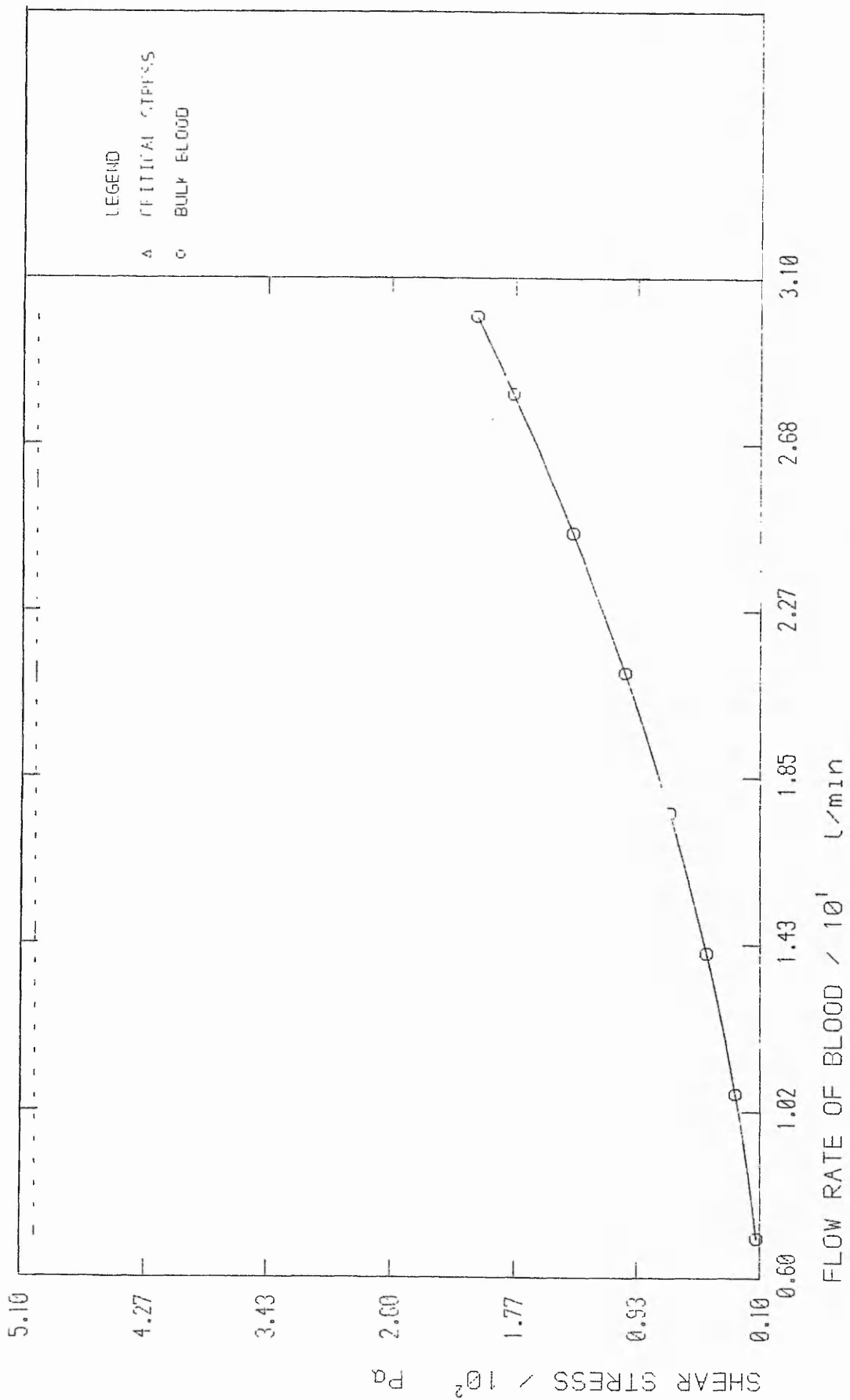
FLOW RATE VERSUS STREAMWISE FORCE ON THE BALL IN FINALISED (LFRSICO) VALVE WITH 30mm BLENDING RADIUS



DIMENSIONLESS FIRST CELL CENTRE DISTANCE FOR VARYING BLOOD FLOW RATES IN FINALISED CONDUIT DESIGN (LRRSICO) WITH 30mm BLENDING RADIUS

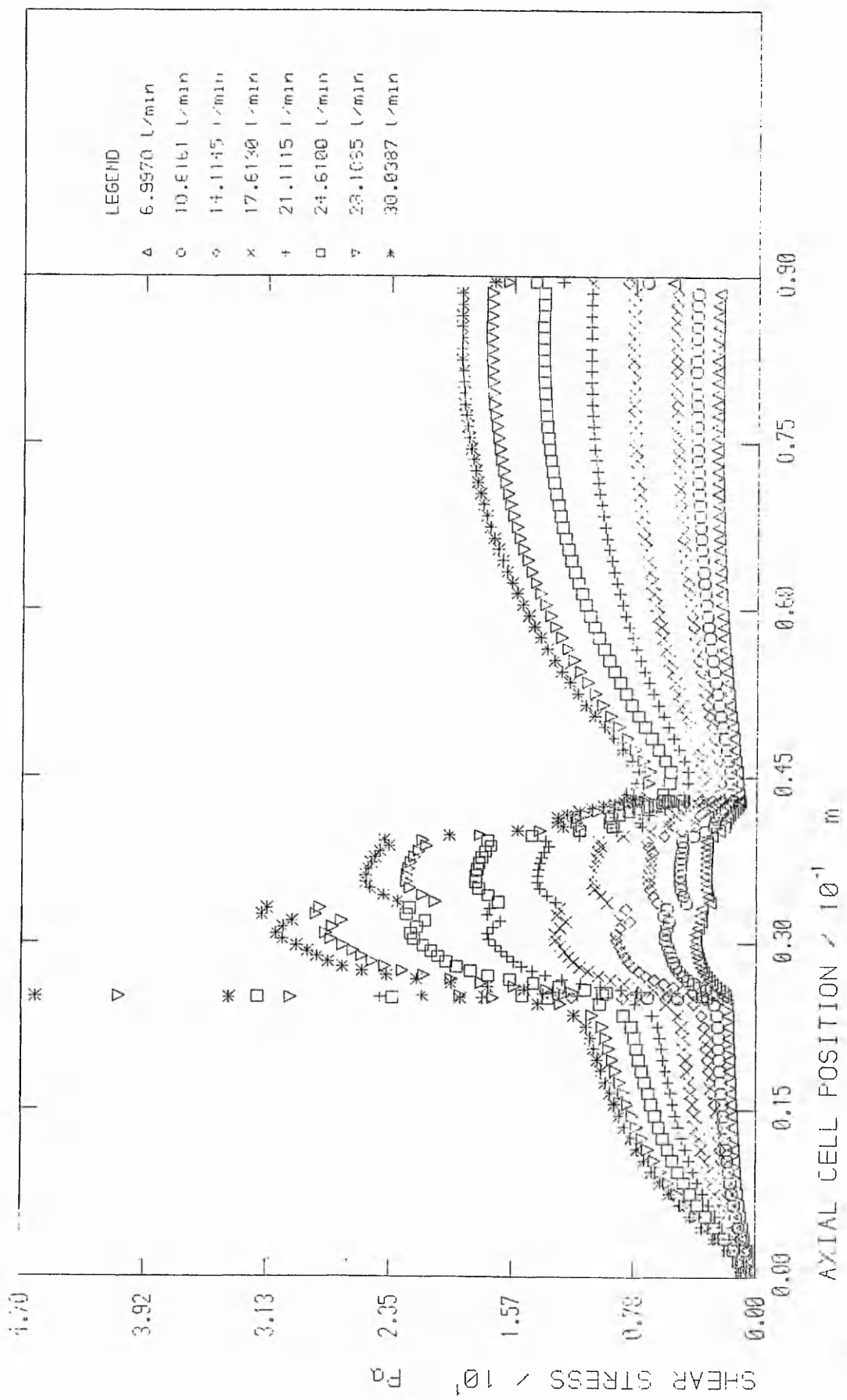


MAXIMUM SHEAR STRESS VERSUS CONDUIT SIZE OF FINALISED (LRF510) VALVE WITH 30mm BLENDING RADIUS



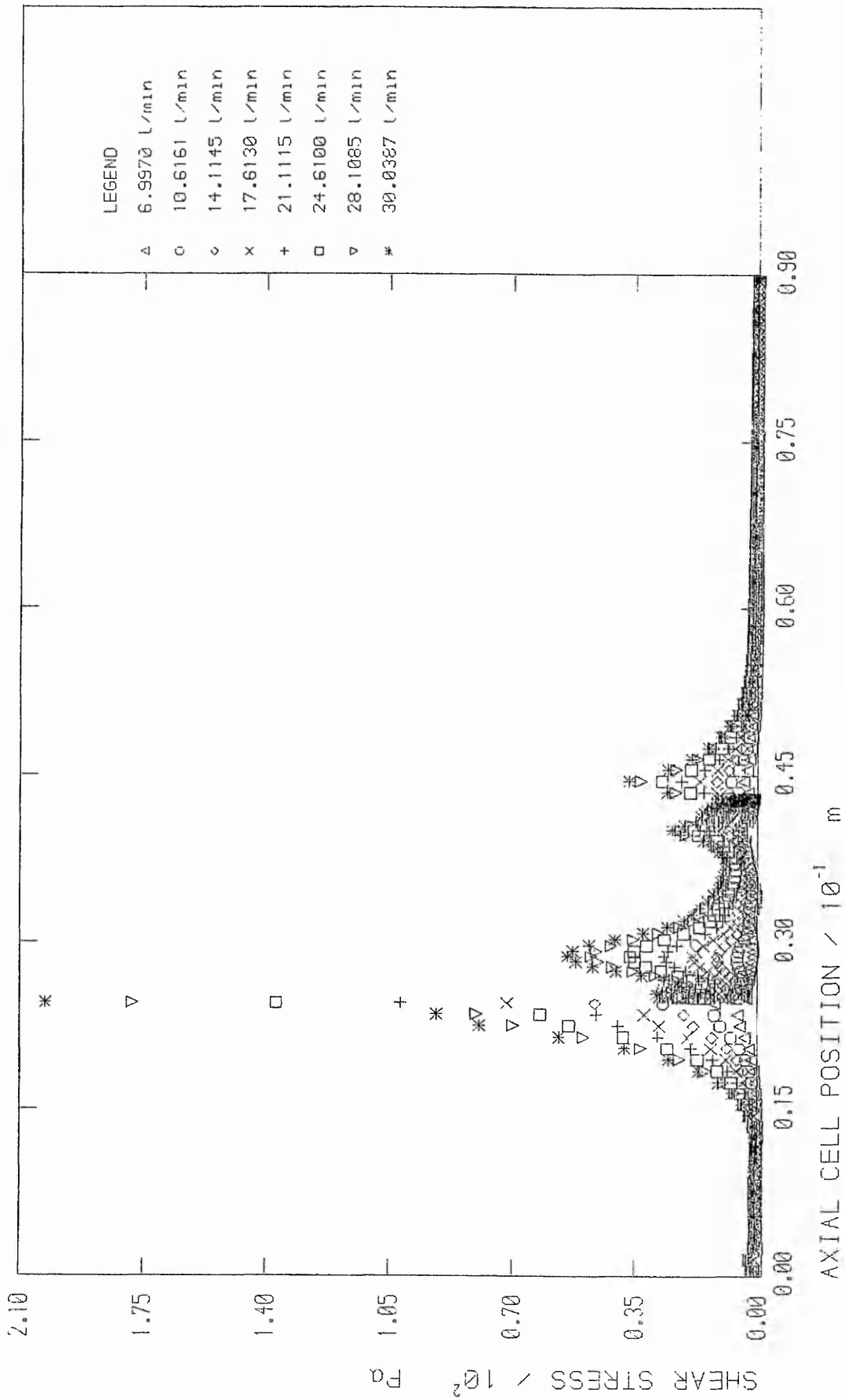
FLOW RATE VERSUS MAXIMUM SHEAR STRESS (AT IMPINGEMENT ON THE BALL) IN FINALISED (LRRSICO) VALVE WITH 30mm BLENDING RADIUS

Figure 7.40



SHEAR STRESS DISTRIBUTION ON CONDUIT WALL FOR VARYING BLOOD FLOW RATES IN FINALISED (LRRSICO) VALVE WITH 30mm BLEEDING RADIUS

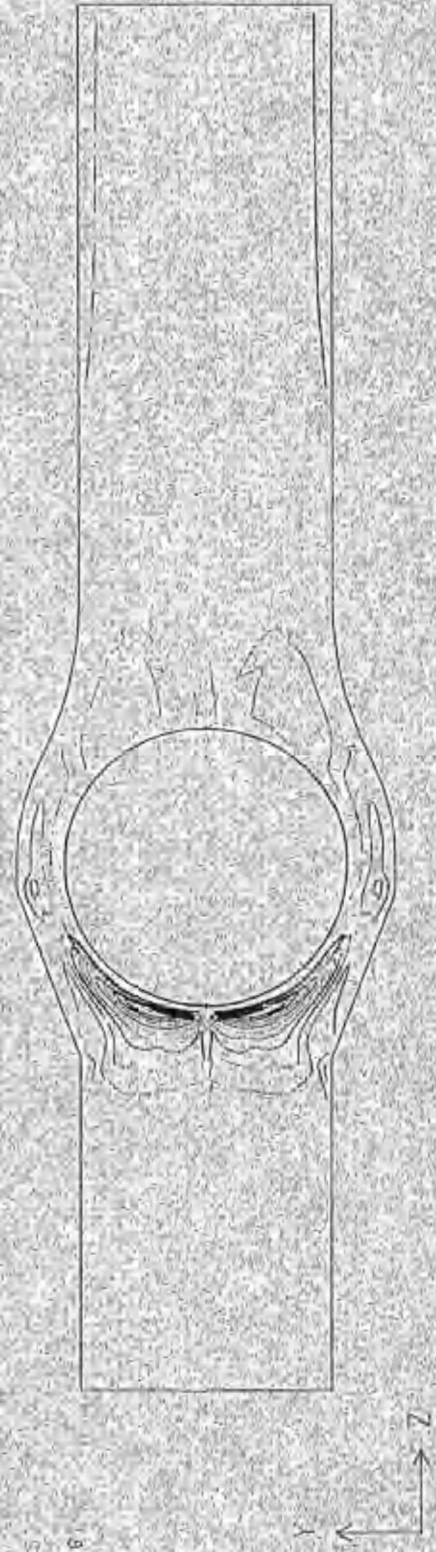
Figure 7.41



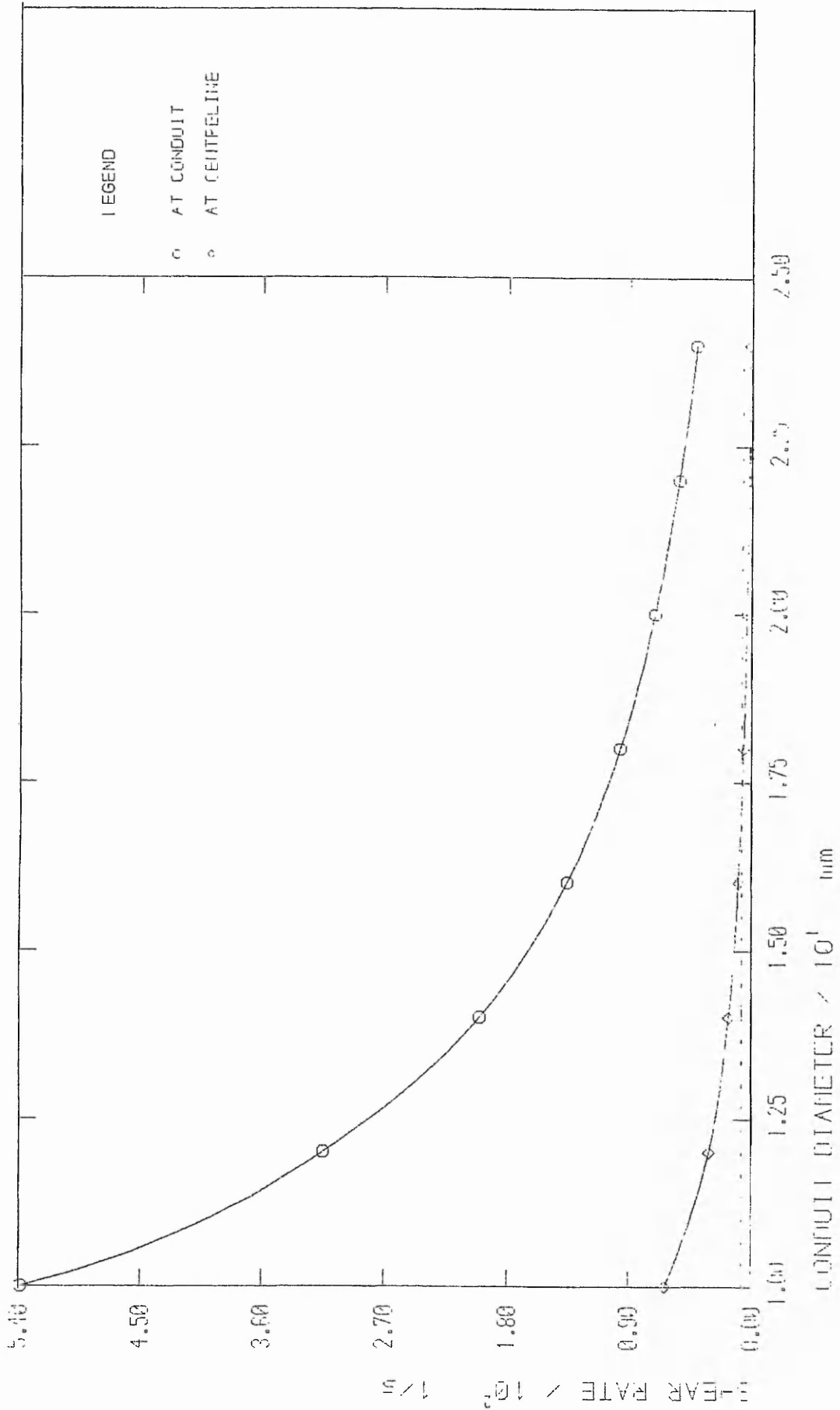
SHEAR STRESS DISTRIBUTION ON BALL AND CENTRELINE FOR VARYING BLOOD FLOW RATES IN FINALISED (LRRSICO) VALVE WITH 30mm BLENDING RADIUS

Figure 7.42

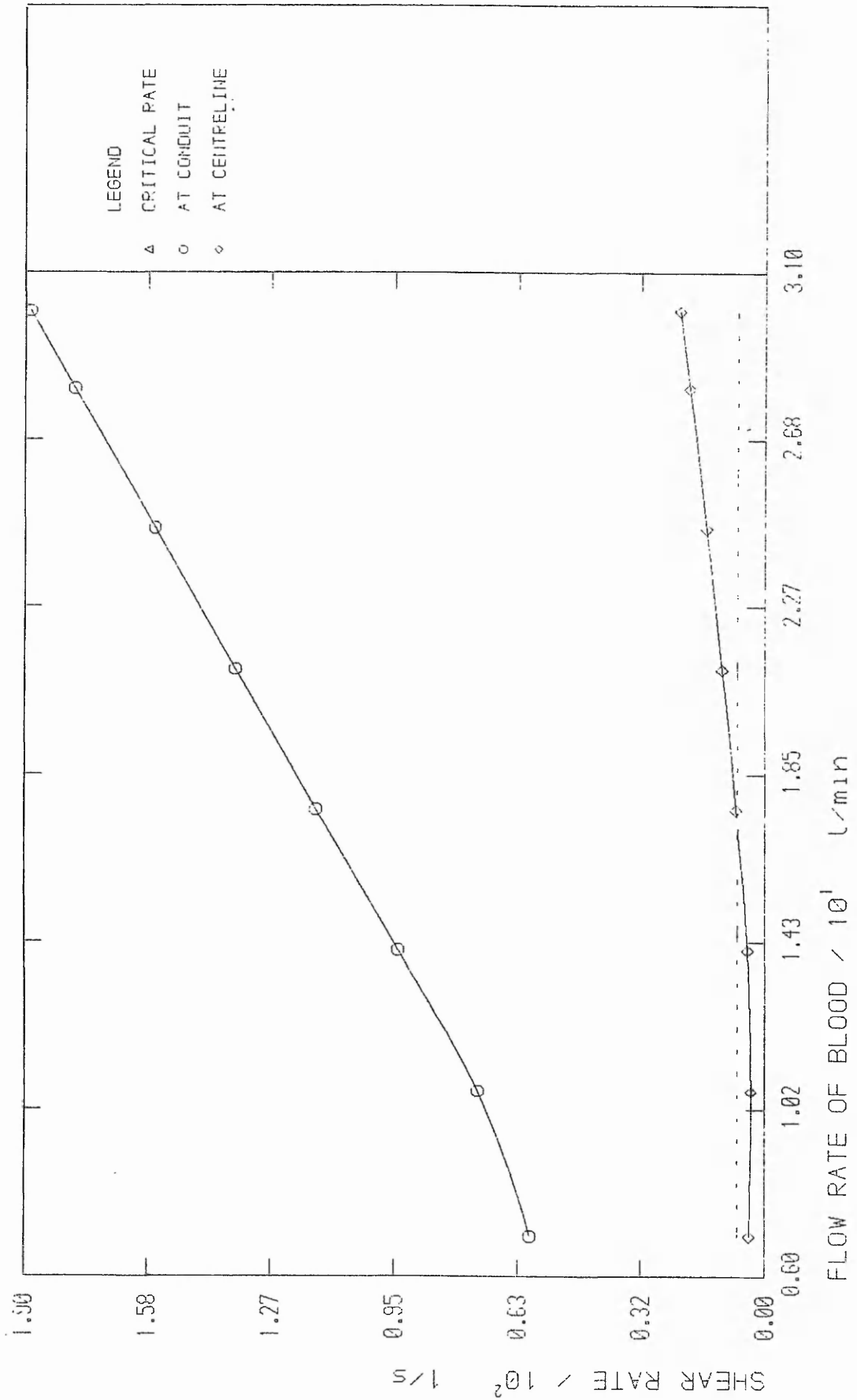
TOTAL SHEAR STRESS CONTOURS FOR BLOOD FLOW  
THROUGH 20mm LRRSICO CONDUIT WITH 30mm BLENDING RADIUS



to cause lysis in-bulk, being of the order of 150Pa or even lower. The precise thresholds for such damage are not only ill-defined but also material dependent, and so reduction of near-wall shear stress and turbulent activity must be performed as well as possible, even below suggested thresholds. The near-wall characteristics portrayed by the finalised (LRRSICO) valve are very good, with shear stresses along the conduit wall being generally below 20Pa, though they are elevated to around 30Pa in the divergent/convergent section, similar to stresses predicted by Merchant and Mazumdar (1986). Confidence is therefore high that this valve would exhibit only a limited haemolytic potential at the conduit wall, particularly as it is aided further by the choice of the ceramic valve body material. Shear stresses at the ball surface are, on average, 20 - 30Pa higher than at the conduit wall, but stresses here are still generally below threshold values and give no cause for concern regarding haemolysis. Minimum shear rates at the junction of the blending radius with the parallel outflow conduit section are shown, by figure 7.44, to approach critically low values in the larger valve sizes, especially when subject to lower flow rates. Such low shear rates might indicate possible thromboembolic problems at this site, though this is unlikely in an area so exposed to mainstream and reversing flow. In-vivo trials would be necessary to confirm this. Thromboembolic complications are unlikely to be brought about by the low shear rates experienced at the centreline (figure 7.45), being located midstream and away from prosthetic surfaces. At the ball surface, thromboembolic complications are unlikely as shear rates are higher and the occluder is free to rotate at random in the flow, each elemental area of surface experiencing continually varying flow patterns.



MINIMUM SHEAR RATE VERSUS CONDUIT SIZE OF FINALISED (CR510) VALVE WITH 30mm BLENDING RADIUS



FLOW RATE VERSUS MINIMUM SHEAR RATES  
 IN FINALISED (LRRSICO) VALVE WITH 30mm BLENDING RADIUS

Figure 7.45

## 7.5 Recommendations as to Application

Based on the above discussion it is possible to draw up suggested guidelines, though simplistic, as to which size of valve should be implemented in a particular case:

As the normal application for this type of prosthesis would be in corrective paediatric surgery, then as a general rule the largest possible valve should be implanted to accommodate later body growth. However, the possible thromboembolic complications in the blending radius area might be exacerbated by the relatively low flow rates in a child. A lower threshold value for flow per unit area is therefore suggested to be  $1.3 \times 10^{-3} \text{ l}/(\text{min}^2 \text{ mm}^4)$ . This might limit the maximum suitable size for a particular recipient.

Minimum suitable size for this valve, unlike most other valves, is not realistically limited by pressure gradient which is so low as to be non-crucial. Limitation is set mainly by occluder instability, which is likely to occur when flow per unit area exceeds  $30 \times 10^{-3} \text{ l}/(\text{min}^2 \text{ mm}^4)$ .

CHAPTER EIGHT

DISCUSSIONS

## 8.1 Functionality of CFM

The decision to use a proprietary finite difference package (PHOENICS) in the study of conduit heart valve flow, rather than write a new one, was through necessity. Several research programmes in the past have written "in-house" CFM codes, but these required a considerable input of time and effort by several members of a team. They also required extensive knowledge of techniques such as matrix handling and solving, as well as a considerable understanding of the physics of flow. The present research programme was conceived as being a small programme involving only one person. Its aims were not to develop solution coding, as this had been done several times before, but were:

- i) to employ CFM as a tool to extract information not previously obtained by computational or experimental heart valve flow studies, and
- ii) to develop additional coding for insertion into PHOENICS enabling its use in the design of valved conduits, by modelling in a situation most closely representing the in-vivo valve situation.

This approach to computational analysis did not require such in-depth understanding of the physics of flow, nor an excessive number of man hours in the writing of coding. However, it did require extensive customising of the proprietary coding because PHOENICS was written as a general purpose CFM code to be applied in a multitude of flow situations, and was not specifically suited to blood flow modelling. Suiting PHOENICS to the precise

needs of this particular application ie turbulent, non-Newtonian, blood flow enclosed by curved boundaries in itself required a considerable amount of coding to be written. It was also necessary to keep abreast of the latest developments of PHOENICS which is continually growing in complexity, such as the introduction of curvilinear grids. A further programming complication was the need to introduction of a constitutive equation into the coding, as PHOENICS does not cater for non-Newtonian flows as standard. All these additions were aided by the inherent flexibility of PHOENICS which is built in an almost modular form, and although it does not allow access to core matrix handling coding, it does facilitate amendment to all flow parameters and solution routines.

PHOENICS itself functioned very well once the necessary changes had been made, and no findings contradicted experimental observations. Furthermore, even the highly complicated characteristic of streamwise force on the ball occluder was seen to be correctly predicted. This, and the fact that pressure gradients across such complex flow geometries were correctly predicted, leads to a high confidence in the numerical modelling technique. Correct prediction of velocity profiles in turbulent flow and in laminar non-Newtonian flow add to this confidence. Nevertheless, more work should be carried out to verify computational methods as applied to non-Newtonian flow. Comparisons against the work of other research programmes, for example the team in Adelaide (Merchant, Mazumdar, Thalassoudis and Noye) increase confidence in the modelling and the results.

The major advance that CFM is capable of making is an improved

ability to assess thromboembolic and haemolytic potentials, because of the ease with which shear rates and shear stresses are found. The improved correlation between in-vivo situations and the test situation afforded by CFM is also a significant advantage over experimental techniques.

## 8.2 Effectiveness of the Blood Model

The use of the Casson equation for the description of blood viscosity variation with local shear rate, although time consuming in its selection and implementation, was not a difficult addition to make to the solution procedure. This model functioned exactly as envisaged, as demonstrated by complete verification of velocity profiles generated in laminar flow and by point-by-point inspection of the turbulent flow field values for shear rate and intrinsic viscosity. However, differences in haemodynamic and hydrodynamic characteristics predicted numerically using blood and blood analogue were not extensive (figures 7.25 - 7.32). However, this could not have been foreseen, bearing in mind the profound differences in flow characteristics between these two media in laminar flow situations as shown in table 8.1.

### Table 8.1 A comparison of flow properties in a pipe

This table shows a comparison between values of haemodynamic/hydrodynamic variables, as predicted numerically for laminar flow through a smooth walled pipe of 20mm diameter. The analogue fluid modelled was a 30% aqueous glycerol solution of density  $1170\text{kg/m}^3$  and dynamic viscosity  $3.323 \times 10^{-6}\text{Pa s}$ . The

"blood" flow was modelled on the Casson equation for the data presented by Charm and Kurland (1965) and Rand et al (1964).

<u>Parameter</u>	<u>Analogue</u>	<u>Rand et al</u>	<u>Charm &amp; Kurland</u>	<u>Units</u>
dP/dz	47.617	68.00	63.02	Pa/m
$\mu_{\max}$	3.587	3.133	3.316	mPa s
$\dot{\gamma}_{\max}$	68.28	71.83	71.78	s <sup>-1</sup>
$\dot{\gamma}_{\min}$	3.569	0.5119	0.5339	s <sup>-1</sup>
$\tau_{\max}$	0.2269	0.3281	0.2995	Pa
$\tau_{\min}$	0.01186	0.02214	0.02011	Pa
$v_{\max}/v$	1.996	1.841	1.842	

The maximum differences described in table 8.1 between flow parameters in blood analogue solution, with respect to blood were approximately:

Pressure gradient = -27%

shear rates:  $\dot{\gamma}_{\max}$  = -5%,  $\dot{\gamma}_{\min}$  = +580%

shear stresses:  $\tau_{\max}$  = -26%,  $\tau_{\min}$  = +91%

Predictions of similar parameters yielded by turbulent flow studies were:

Pressure gradient = +5%

shear rates:  $\dot{\gamma}_{\max}$  = -5%,  $\dot{\gamma}_{\min}$  = +114%

shear stresses:  $\tau_{\max}$  = 7%,  $\tau_{\min}$  = +165.5%

The differences in flow parameter appear to point to blood

flowing more easily in turbulent flow than analogue flows, due to a generally lower viscosity at the high shear rates. The situation is reversed in laminar flow where a much greater proportion of the central flow region is taken up by plug flow, because in axially aligned laminar flow the shear rates at the pipe centre are close to zero.

In the final analysis, the use of blood flow was not critical to the design synthesis of the valve, as optimum valve profile would have been prescribed if modelling were conducted in either blood or blood analogue solution, (as described in 7.3). However, no previous works have applied a constitutive equation to the design of a valve, and only one previous work was found which had a non-Newtonian fluid in numerical analysis. Therefore, this work was essential, increasing understanding of analogue flow and establishing a base against which other work may be compared. Furthermore, it leads the way to the time dependent flow analysis required for pulsatile flow and small vessel flow where non-Newtonian aspects might be more important, or to the possible eventual modelling of clotting function and thrombus growth. However, the above table suggests that flow studies carried out in blood analogue solutions are likely to underestimate the thromboembolic potential of a valve. This is because minimum shear rate will be over predicted by as much as 165.5%. This finding this is not as crucial as the figures suggest, because this difference between the flow characteristics of blood and analogue solutions occur midstream and away from prosthetic surfaces and regions of stasis. Obviously water flow does not accurately represent blood flow and, if used as a flow medium in design synthesis, would have lead to the selection of a non-

optimal valve geometry.

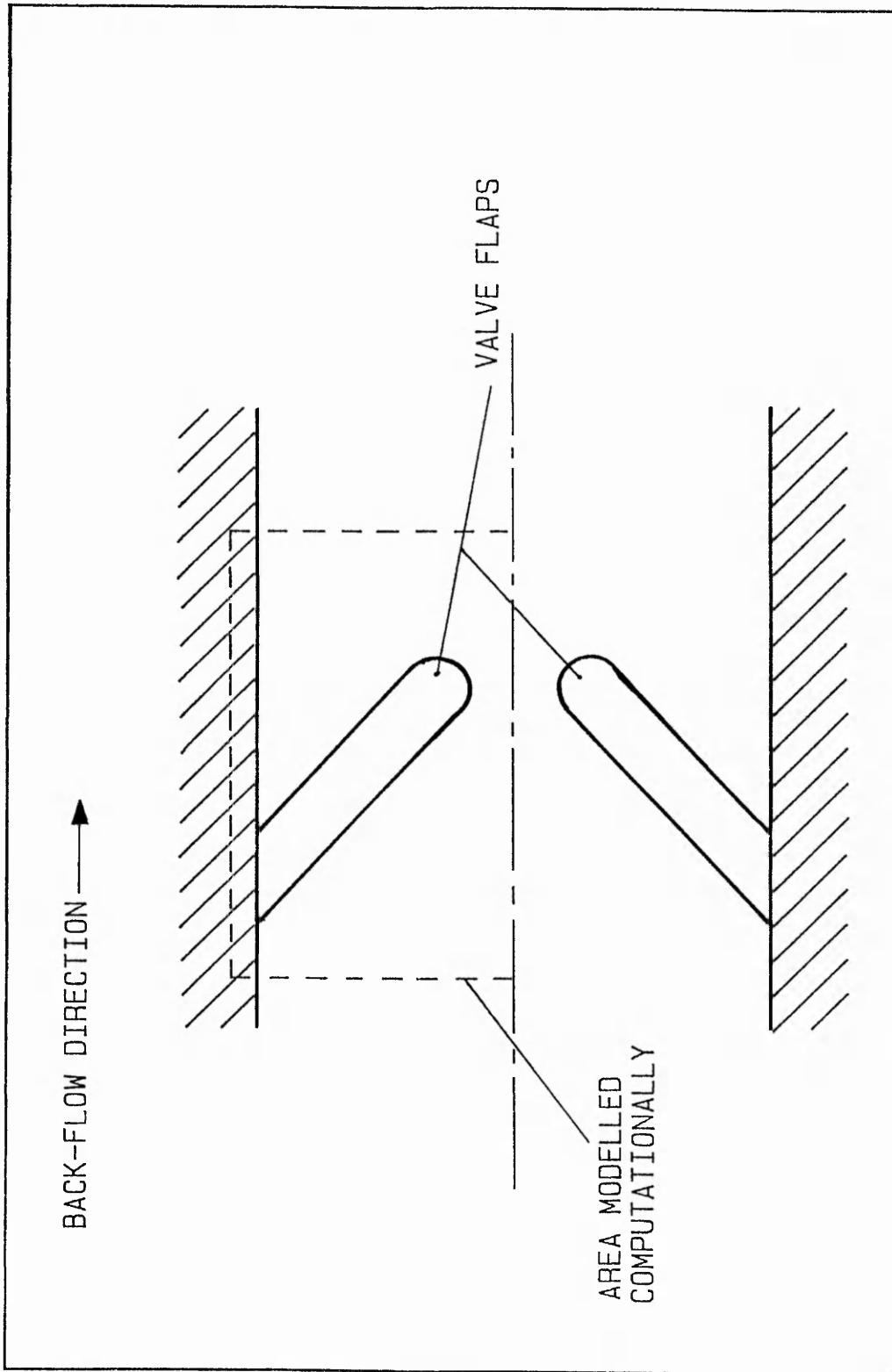
### 8.3 A Further Example of CFM Applied to Heart Valves - Backflow

This example, based on Leefe et al (1986), demonstrates another area where numerical modelling might have advantages over experimental investigation, namely in the study of flow in very small geometries. The study aimed to predict laminarisation of flow in a regime defined to be steady backflow through a gap between the twin flaps of a Gentle (1981b) mitral valve. The question the study attempted to answer was whether an increased gap would aid washing action because of an increase in flow rate leading to turbulence. This question had been approached analytically by Reif et al (1980) and Gentle (1982). Both authors had also presented experimental pressure/flow characteristics for reverse flow and compared their gradients of logarithmic friction factor/Reynolds number with a similar gradient exhibited by pipe flows, in order to draw conclusions about the nature of flow through the gap between the valve flaps. Gentle attempted to justify the use of a large gap, arguing that a turbulent backflow would aid washing action on the proximal side of the flap, whereas Reif tried to justify designing for minimal backflow. The need, analytically, to assume a fully developed velocity profile, appears to have been one of the major limitations. This assumption would tend to overlook the increased wall velocities likely to occur in the undeveloped flow and would lead to increased estimates of friction factor. LDA could not be applied to this geometry to test the assumption due to the difficulties of measuring in such small dimensions (in Gentle's valve the gap was 0.5mm). However, using numerical

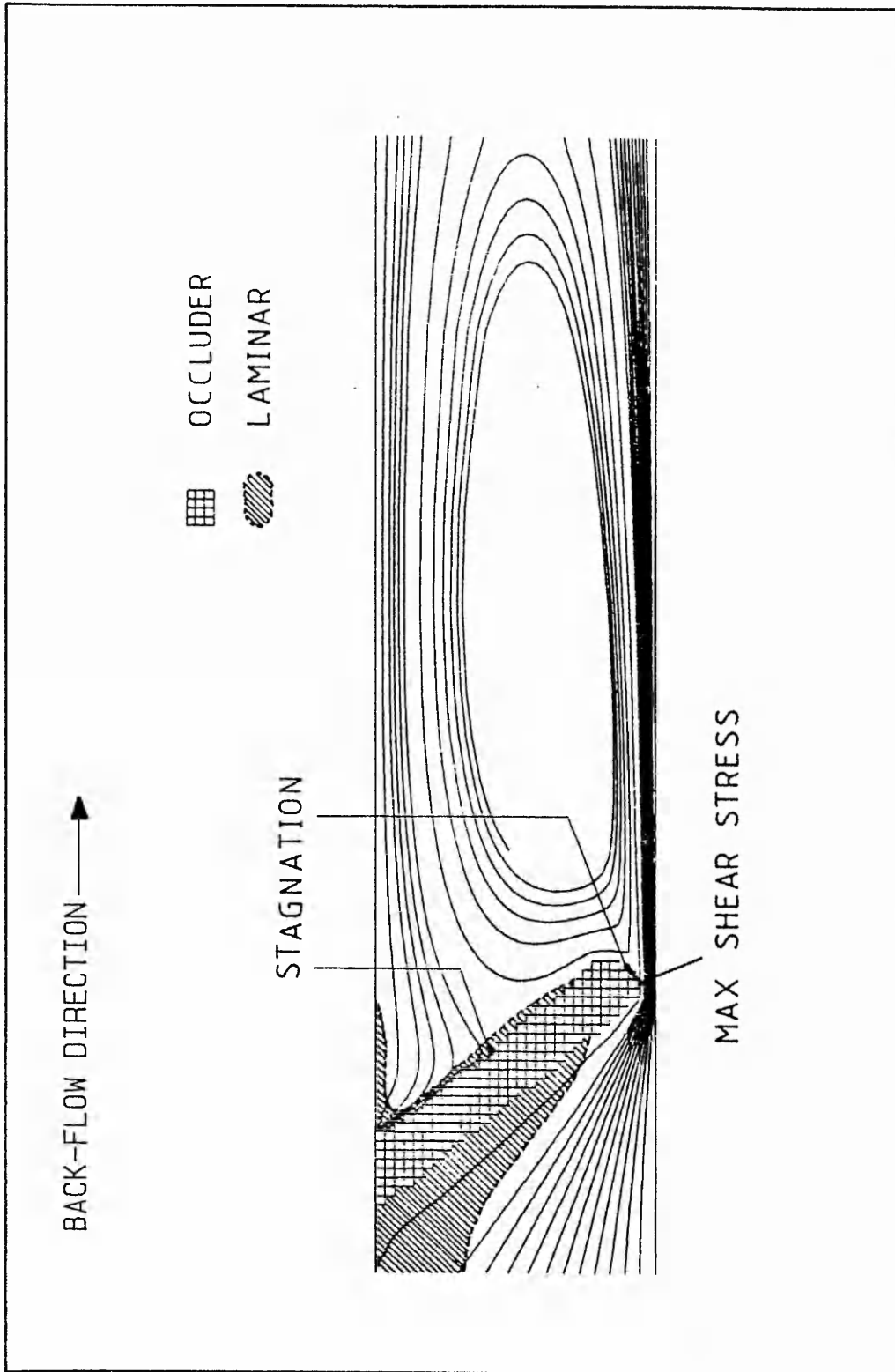
modelling based on the geometry featured in figure 8.1, it became readily possible to analyse flow in such regimes, to establish undeveloped velocity profiles and pressure gradients and also to predict the onset of turbulence (figure 8.2), the shear stresses within the fluid (figure 8.3) and the extent of washing action. From this study it was demonstrated that shear stresses in Gentle's original valve were dangerously high leading to an increased likelihood of haemolysis during the reverse pressure phase of the cardiac cycle. Furthermore, better guidelines for the design for backflow between twin flaps were proposed.

#### 8.4 Performance of the Final Conduit Design

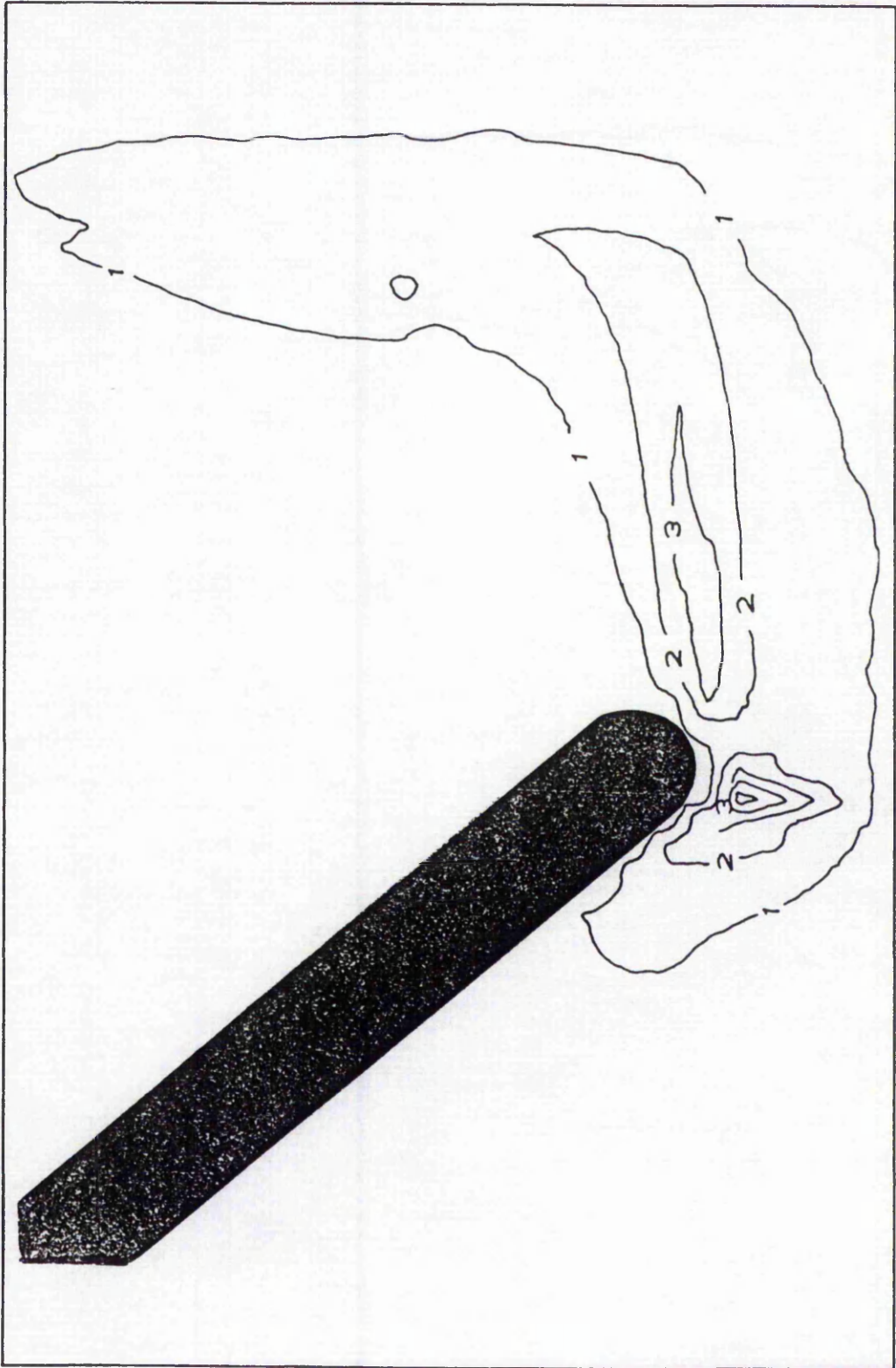
The potential for improvement of conduit design has largely been realised by the "purpose-built" approach. Excellent pressure/flow characteristics were demonstrated, with a 226% flow efficiency as compared with an ideal orifice. This forward flow efficiency is a great improvement, not only with respect to existing orifice mounted valves but also in comparison with commercial conduits incorporating a mitral or aortic mechanical/xenograft valve. Occluder instability has been overcome without significantly affecting the pressure/flow characteristics exhibited by the original SISO valve. Non-critical shear rates and shear stresses predicted for the final conduit design suggest that thromboembolism and haemolysis are unlikely to be exhibited by this valve. Though such analysis is dependent on critical values being correctly established, these still need confirming in further animal/clinical trials.



SCHEMA OF COMPUTATIONAL GEOMETRY FOR BACK-FLOW STUDY IN TWIN FLAP VALVE



PREDICTION OF LAMINARISATION IN  
 BACKFLOW THROUGH TWIN FLAP MITRAL VALVE



CONTOURS OF SHEAR STRESS FOR BACKFLOW THROUGH A TWIN FLAP MITRAL VALVE

## 8.5 Confidence in Computational Predictions

The apparently poor agreement between experimental and numerical pressure gradient predictions was initially a cause for concern. However, further analysis proved this not to be significant, as by re-modelling the numerical regime to match the experimental situation exactly, numerically yielded pressure gradients were made to coincide with experimental results with high accuracy. Moreover, the original differences in pressure gradients between the numerical and experimental results were less than differences already reported between experimental results found in different research programmes. Swanson (1984) indicates that such discrepancies are to be expected and that re-modelling was a valid process.

Confidence was greatly improved by the correct prediction of streamwise force on the occluder. This parameter, which is most complex in its make up, relies on pressure, velocity (and therefore turbulence properties) as well as shear components and geometrical factors, so the fact that this was correctly predicted points to all its component parameters being calculated correctly. Good agreement was also seen with the work of Merchant and Mazumdar (1986) for non-Newtonian flow. Furthermore, the constitutive equation incorporated into the numerical solution was shown to be functioning exactly as expected in laminar and turbulent flow.

## 8.6 Continuation of CFM Study of Heart Valves

Future computational study of heart valve conduits must surely aim towards the replacement of many expensive and time consuming animal trials through an ability to accurately model and assess the in-vivo situation at the design stage of valve development. This step would, however, be dependent on an improved knowledge of haemolytic and thromboembolic occurrences and their relationships with haemodynamic parameters, such as shear stress shear rate and near wall turbulence.

Such further work should include a complete LDA verification of numerically predicted flow velocities, and a complete experimental pressure/flow characteristic appraisal for valve sections identical to the geometries modelled numerically. Further improvements to the numerical modelling would be gained by experimentally justifying the  $k - \epsilon$  model at key locations in the flow regime. This would again entail a LDA study, to assess the optimum values of empirical constants used in the turbulence model. It might be that these constants could not be universally applied throughout the regime, but might need alteration in specific areas. The model could also be improved by enhancing its ability to work at low Reynolds' numbers, something which could be achieved by selecting any one of a number of low Reynolds' numbers models discussed by Nallasamy (1987). Improvements could be even further enhanced by an ability to model in pulsatile flow, although this might introduce a need to vary the turbulence model constants with time. Other turbulence models (see Nallasamy) offer potentially improved near-wall predictions which

in turn would allow for even better grid definition, since at present the closest cell centre to the wall was 0.4mm into the flow. Great improvements to computational modelling, including an ability to confidently study pulsatile flows, could alternatively be afforded by the direct solution of the Navier Stokes equations. Though this would be dependent on a large increase in computer storage ability and computational speed, it might be made possible in the future by transputers.

To date, non-continuum models of blood flow which might account for, say, the Fåhræus/Lindqvist effect or clotting functions, as described by Dintenfass (1962, 1964a,b) have not been attempted. It is true that such non-continuum models would introduce a great number of unknown quantities, all of which would need establishing first, but such modelling might represent a great improvement in small vessel flow, or time dependent flow especially if the rate and extents of thrombus formation could be predicted at sites of haemostasis.

#### 8.7 Further work on the Ceramic Conduit Designs

Further work on the conduit must now surely be aimed at preparing the design for manufacture. This would entail experimental assessment of pulsatile flow characteristics, clinical acceptability, testing of the material, and detailed manufacturing process specification.

Closing functions for the prototype conduits intuitively seem to be good, with the occluder quickly closing onto the seating ring when flow is reversed, but extensive experimentation is necessary

in pulsatile flow conditions to ensure this, and possibly to assess the influence of geometrical factors, such as inlet divergence angle. An assessment of cyclic energy losses is also necessary. The seal formed between the occluder and the seating ring was excellent and the ball was seen to remain in the seated position against the action of gravity for several hours with only a very small reverse static pressure.

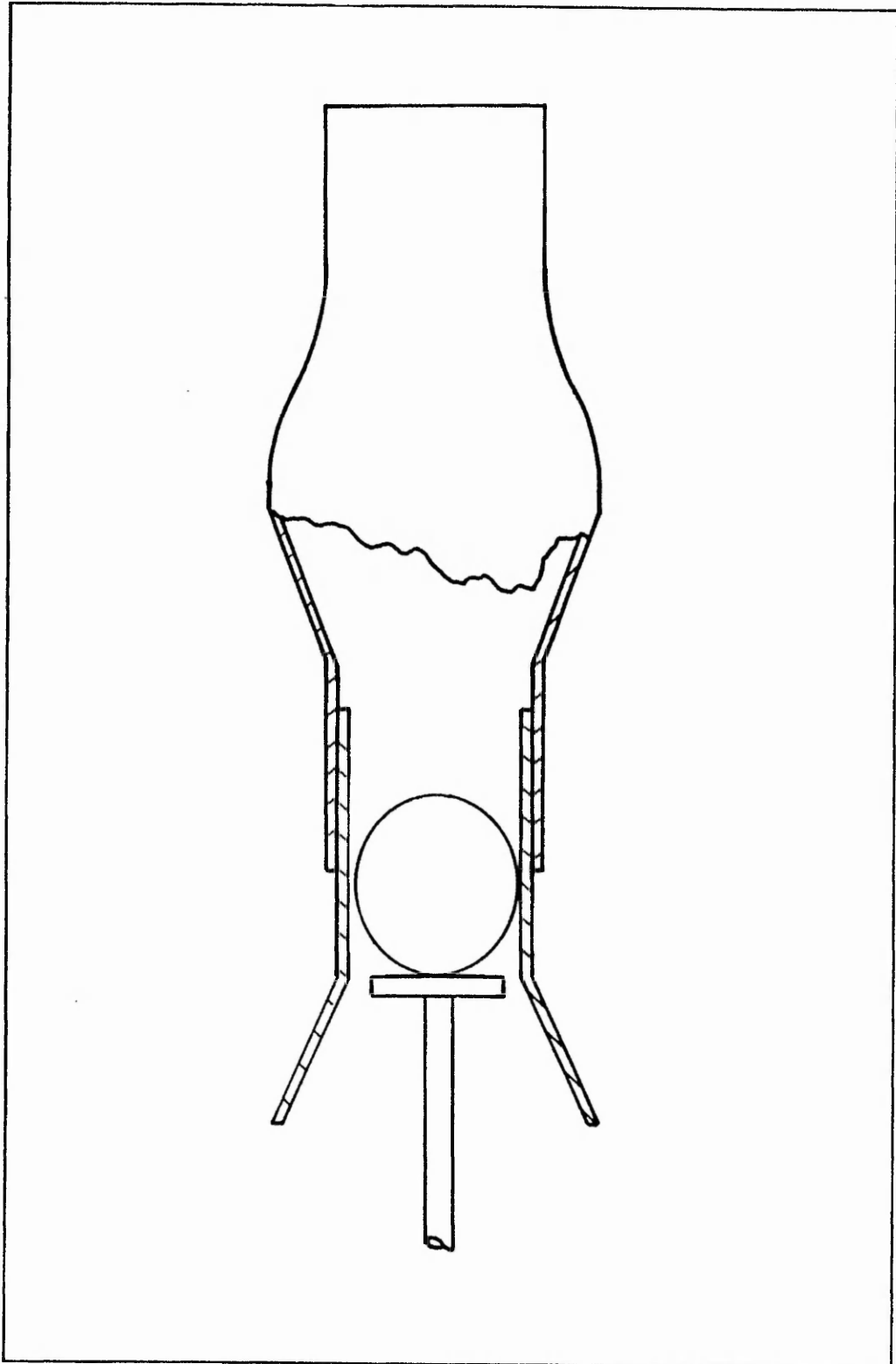
Accelerated wear tests need to be conducted on the ball because Silastic has not been used in conjunction with ceramics before, in this type of application. However, the applicability of such test results would be dependent on the expected ingrowth of body cells into the material, something which is itself affected by material density and surface finish. It therefore would be necessary to conduct ingrowth tests, similar to Gott ring tests, to establish the rate and extent of ingrowth.

It is aimed to manufacture the final LRRSICO valved conduit with a 30mm blending radius design. Preliminary tests have shown the valve profile to be suitable for slip casting using 99.9% pure alumina. Two alumina powders of 5-10 $\mu$ m average particle size have been tested\* to establish their castability to the required form. Casting of the first of these materials was much less controllable than the for second which could readily be slip cast to 2mm wall thickness without the need to deflocculate the slurry. It is proposed that the manufacturing process will proceed along two paths:

*\*BACO RA 10 and ALCOA A17 NE*

- i) Prototype manufacture/feasibility study: the valve will be slip cast in two parts, split along the radial plane at the centreline of the forward flow occluder position. The casting will be part sintered and machined to ensure dimensional accuracy, and to allow holes for sewing Dacron conduit to the inlet and outlet sections. Following full sintering, final assembly will include insertion of the ball, positioning of the forward restraining struts and adhesive joining of the two halves.
  
- ii) Production valve manufacture: this will entail the manufacture of dies and isostatic pressing of the alumina powder into a final, dimensionally accurate, single piece conduit, the form of which will include the forward restraining struts as an integral feature of the outflow tract wall. Drilling will be necessary to allow the joining of the flexible Dacron graft conduit at inlet and outlet. Final assembly of the ball into the conduit will probably be carried out with the ball being forced down a thin sectioned stainless steel tube, lubricated possibly with heparin, which is inserted into the conduit inlet section (figure 8.4).

It is envisaged that dimensional accuracy of the valve would be checked using non-destructive radioactive and/or ultrasonic metrological techniques.



POSSIBLE METHOD OF ASSEMBLING THE BALL  
INTO FINAL, SINGLE-PIECE LRSICO VALVE

CHAPTER NINE

CONCLUSIONS

The two main aims of this research program were two fold:

- i) to assess the usefulness of finite difference Computational Fluid Dynamics in the analysis of heart valve function, whilst;
- ii) using CFM as a design tool for the optimisation of a purpose built valved heart conduit.

These aims required the development of solution algorithms and techniques for inclusion into a proprietary finite difference code. It was also necessary to specify flow geometries which not only accurately represented the several valve conduits designed, but which allowed for accurate prediction of haemodynamic/hydrodynamic function.

For any technique to be of value its employment must represent some advantage. In fluid dynamic terms this could be a capability for use where other techniques cannot be applied, it could be an ability to render improved results over the other techniques, or to yield parameters that other applicable techniques cannot. It might be argued, in certain applications, that numerical flow analysis can satisfy all three of these categories. However, in this study CFM predictions were not seen to surpass state-of-the-art experimental techniques in quality of velocity or pressure gradient prediction. Nevertheless, the study did demonstrate that CFM analysis can be applied to geometries inaccessible to experimental techniques, (examples being near-wall and in the modelling of in-vivo regimes) and that CFM will yield information that is not satisfactorily obtainable

when in-vitro techniques are applied to heart valve assessment.

In numerical analysis the choice of grid type onto which the valve was modelled, whether orthogonal or curvilinear, was of great significance. The present work, which examined flow around ball valves, has shown that the advantages of using non-orthogonal grids, mainly those of computer storage savings, are outweighed by several disadvantages, namely;

- i) difficulties in obtaining grid independence
- ii) limited physical similarity between the geometry superimposed onto the grid
- iii) poor predictions of momentum.

In curvilinear geometries where grid independence was established, momentum predictions were seen to be good, but no better than could be obtained experimentally. Pressure prediction, though reliable, was not easily made to agree with experimentally observed gradients because of the differences between the experimental and numerical geometries. This problem does not limit CFM any more than in-vitro study, as large differences in measured pressure gradients are cited for similar valves in different experimental situations.

Computational fluid dynamics was shown to have advantages over experimentation when applied to flow areas inaccessible to experimental techniques, some examples being near to the conduit walls or occluder surface in the conduit flow; in small geometries as in the back flow example presented in the discussion, or in assessments of in-vivo flow with real blood. None of these situations is readily approached experimentally

because of the influence of the walls, the refraction of interrogating beams, interaction on the flow by intrusive probes, poor resolution of probing techniques, or because of ethical restraints in the case of in-vivo study. Analytical methods can be shown to be not only simplistic, but questionable in the majority of complex flow situations.

Computational fluid mechanics was shown to excel in its prediction of shear components, allowing easy generation of full field shear stresses and shear rate information. This facility greatly enhanced in-depth study of haemolytic and thromboembolic potentials. It is in such analysis that CFM is most likely to make its greatest contribution to heart valve assessment and design, because such data cannot be readily be found by any other method. Moreover, because of the ease and speed with which CFM can be applied to differing valve geometries, the technique has real value in the design process, allowing valve prototypes to be assessed much more rapidly than would be possible in-vitro.

However, there will always be a need for experimentation to account for unforeseen problems, such as ball oscillation as experienced in the original SISO valve, which would probably have gone unnoticed in a purely numerical study. Furthermore, experimentation is necessary at present, in the study of pulsatile flow which presents difficulties to CFM in the movement of the boundaries (ie the occluder) and because of the breakdown of the turbulence model in non-steady flow. Computer run time and storage capacity would also remain a problem even if these other difficulties could be resolved.

The need to use a turbulence model is the major limitation in CFM, even when, what is arguably the best turbulence model ( $k - \epsilon$ ) is used. This calls into doubt the ability of CFM to correctly predict fields in pulsatile flow (which is why this study is purely steady flow). Furthermore it can cause solution non-convergence or inaccuracies in momentum predictions if extreme caution is not applied when defining the most critical flow region near the wall, where viscous, and not turbulence effects are dominant. For these reasons it became necessary to closely monitor the dimensionless wall distance ( $y^+$ ) at the first cell centre, because if this value fell below 11.5 then momentum predictions were poor.

Further difficulties encountered in the use of CFM were:

- i) in devising the computational geometries for modelling the valve conduits. This stemmed from the failure of numerical modelling to obtain convergence in highly non-orthogonal cells, and because of the dependence of solution on the wall-cell centre positioning.
- ii) the introduction into the solution procedure, a constitutive equation for the description of blood flow characteristics.
- iii) The need to re-write the generation term (for  $\gamma$ ) of the  $k - \epsilon$  model because of the poor way in which it was calculated by PHOENICS. Only a poor 2-dimensional term was available for use in PHOENICS when curvilinear geometries were modelled, this term severely under-predicted shear rate in flow which deviated a long way from the axial. The effect

of this was the over-prediction of intrinsic viscosity, and under-prediction of kinetic energy of turbulence and turbulence dissipation, and therefore poor predictions of momentum fields in general.

The findings that only limited differences in turbulent flow parameters were predicted between the two different fluids: blood analogue solution and blood (modelled via Casson's constitutive equation) were surprising as laminar flows exhibited much greater differences in analytical and numerical analysis. However, large the differences in predicted minimum shear rates for the two fluids pointed to analogue solution flow studies underestimating the likely thromboembolic potential of a prosthetic valve.

Furthermore, only one previous research program had numerically compared the two fluids, and the model used for blood flow was not particularly precise leaving room to question the results. Modelling in a blood, was then, by no means a wasted exercise as it established a reliable benchmark against which analogue flows could be compared. However, it is fair to conclude that the optimisation of valve geometry would not have suffered as a consequence of using analogue solution instead of blood as the medium.

Once the complete numerical model had been assembled (including geometry, generation term and blood viscosity predictor), design was greatly aided by the implementation of CFM. The time needed to generate and test a valve design was very short (around 4 hours real-time), this facilitated the testing of many more valve sections than would be

feasible if an experimental approach were adopted. Furthermore, CFM allowed for a more complete analysis of valve flow characteristics, allowing for predictions of maxima and minima of shear stresses and rate in the critical regions near to prosthetic surfaces, as well as in bulk, this enhanced the assessment of likely thromboembolic complication and blood lysis. The outcome of the design synthesis was a purpose built valved conduit which exhibited considerably enhanced pressure/flow characteristics, as compared with existing valves whilst guaranteeing occluder stability, and which was likely to exhibit exceptionally low thromboembolic and haemolytic potentials. It was also possible to lay down guidelines regarding suitable implantation sites and patients.

## REFERENCES

- Abujelula, M.T. and Lilley, D.G. 1984. Limitations and empirical extensions of the  $k - \epsilon$  model as applied to turbulent confined swirling flows. *Chemical Engineering Communications*, 31, 223-236
- Akutsu, T. and Modi, V.J. 1982. Fluid dynamics of several mechanical prosthetic heart valves using Laser Doppler Anemometry. In: *Proceedings IX Annual Meeting of the European Society for Artificial Organs*, Brussels, Belgium, 107-110
- Anadere, I., Chmiel, H., Hess, H. and Thurston, G.B. 1979. Clinical blood rheology. *Biorheology*, 16, 171-178
- Aston, S.J. and Mulder, D.G. 1971. Cardiac valve replacement: a seven year follow up. *Journal of Thoracic and Cardiovascular Surgery*, 61, 547-555
- Autret, A., Grandotto, M. and Dekeyser, I. 1987. Finite element computation of a turbulent flow over a two-dimensional backward-facing step. *International Journal for Numerical Methods in Fluids*, 7, 89-102
- Bacher, R.P. and Williams, M.C. 1970. Hemolysis in capillary flow. *Journal of Laboratory and Clinical Medicine*, 76, 485-496
- Begg, T.B. and Hearn, J.B. 1966. Components in blood viscosity: The relative contribution of haematocrit, plasma, fibrinogen and other proteins. *Clinical Science*, 31, 87-93
- Beissinger, R.L. and Williams, M.C. 1984. A dual Mechanism for low-stress Hemolysis in laminar blood flow. *Journal of the American Institute of Chemical Engineers*, 30, (4), 569-577
- Benjamin, E.L. 1986. *Steady flow investigations of valved heart conduits*. M.Phil. thesis, Trent Polytechnic, Nottingham, UK.
- Bicen, A.F. 1982. Refraction correction for LDA measurements in flows with curved optical boundaries. *Technology and Science of Informatics quarterly*, 8, (2), 10-12
- Blackshear, P.L. 1972. Mechanical hemolysis in flowing blood. In: Fung, Y.C., Perrone, N. and Anliker, M. (eds.), *Biomechanics: its foundation and objectives*. Prentice-Hall, New Jersey, USA, 501-528
- Blackshear, P.L. and Blackshear, G.L. 1987. Mechanical hemolysis. In: Skalak, R. and Chien, S. (eds.), *Handbook of Bioengineering*, McGraw-Hill, chapter 15
- Bruss, K.-H., Reul, H., Van Glise, J. and Knott, E. 1983. Pressure drop and velocity fields at four mechanical heart valve prostheses: Björk-Shiley standard, Björk-Shiley concave-convex, Hall-Kaster and St. Jude medical. *Life Support Systems*, 1, 3-22

- Casci, C., Fumero, R. and Montevecchi, F. 1977. Prosthetic heart valves. In: Hwang, N.H.C. and Normann, N.A. (eds.), *Cardiovascular flow dynamics and measurements*, University Park Press, Baltimore, USA, 851-875
- Casson, N. 1959. A flow equation for pigment-oil suspensions of the printing ink type. In: Mill, C.C. (ed.), *Rheology of Disperse Systems*, Pergamon Press, London, 84-102
- Chandran, K.B., Khalighi, B. and Chen, C.J. 1985a. Experimental study of physiological pulsatile flow past valve prostheses in a model of human aorta - I. Caged ball valves. *Journal of Biomechanics*, 18, (10), 763-772
- Chandran, K.B., Khalighi, B. and Chen, C.J. 1985b. Experimental study of physiological pulsatile flow past valve prostheses in a model of human aorta - II. Tilting disc valves and the effect of orientaton. *Journal of Biomechanics*, 18, (10), 773-780
- Charm, S. and Kurland, G. 1965. Viscometry of human blood for shear rates of 0-100,000 sec<sup>-1</sup>. *Nature*, 206, 617-618
- Chien, S. 1971. Present state of blood rheology. *Hemodilution. Theoretical basis and clinical application. International symposium, Rottach-Egern*, Karger, Basel, 1-45
- Chmiel, H. and Walitza, E. 1980. *On the rheology of blood and synovial fluids*, Research Studies Press, John Wiley and Sons, Chichester.
- Clayton, B.R. and Massey B.S. 1967. Flow visualisation in water: a review of techniques. *Journal of Scientific instrumentation*, 44, 2-11
- Cokelet, G.R., Merrill, E.W., Gilliland, E.R. and Shin, H. 1963. The rheology of human blood-measurement near and at zero shear rate. *Transactions of the Society of Rheology*, 7, 303-317
- Cokelet, G.R. 1987. The Rheology and tube flow of blood. In: Skalak, R. and Chien, S. (eds.), *Handbook of Bioengineering*, McGraw-Hill, chapter 14
- Copley, A.L. 1967, A.L., Luchini, B.W. and Whelan, E.W. 1967. On the role of fibrinogen-fibrin complexes in erythrocyte aggregation and flow properties of blood. *Biorheology*. 4, 87
- Dintenfass, L. 1962. Thixotropy of blood and proneness to thrombus formation. *Circulation Research*, 11, 233-239
- Dintenfass, L. 1964a. Viscosity and clotting of blood in venous thrombosis and coronary occlusions. *Circulation Research*, 14, (1) 1-16
- Dintenfass, L. 1964b. Rheological approach to thrombosis and atherosclerosis. *Angiology*, 15, 333-343

- Ditzel, J. and Kampmann, J. 1971. Whole-blood viscosity, hematocrit and plasma protein in normal subjects at different ages. *Acta Physiologica Scandinavica*, 81, 264-268
- Duff, W.R. 1970. *Fluid dynamics of prosthetic heart valves*. Ph.D. thesis, Purdue University, USA
- Easthope, P.L. and Brooks, D.E. 1980. A comparison of rheological constitutive functions for whole human blood. *Biorheology*, 17, 235-247
- Edwards, R.J. 1988. *Heat transfer in annular ducts fitted with longitudinal fins with and without swirl*. Ph.D. thesis, Trent Polytechnic, Nottingham
- Fåhræus, R. 1929. The suspension stability of the blood. *Physiological Reviews*, 9, (2), 241-274
- Fåhræus, R. and Lindqvist, T. 1931. The viscosity of blood in narrow capillary tubes. *American Journal of Physiology*, 96, 562-568
- Figliola, R.S. and Mueller, T.J. 1981. On the hemolytic and thrombogenic potential of occluder prosthetic heart valves from in-vitro measurements. *Transactions of the ASME Journal of Biomechanical Engineering*, 103, 83-89
- Fry, D.L. 1968. Acute vascular endothelial changes associated with increased blood velocity gradients. *Circulation Research*, 12, 165-197
- Fry, D.L. 1969. Certain histological and chemical responses of the vascular interface to acutely induced stress in the aorta of dog. *Circulation Research*, 24, 93-108
- Gartling, D.K. 1986. Finite element methods for non-Newtonian flows. *Sandia National laboratories USA*, report number SAND 85-1704 E 1.99: DE86 007410
- Gentle, C.R. 1977. A limit to hydraulic design of heart valve prostheses. *Engineering in Medicine*, 6, (1), 17-21
- Gentle, C.R. 1980. A porous ceramic mitral valve prosthesis. In: Hastings, G.W. and Williams, D.F. (eds.), *Mechanical Properties of Biomaterials*, John Wiley and sons, New York
- Gentle, C.R., Arundel, P.A., Hamilton, D.I. and Swales, P.D. 1981a. Development of a twin-flap porous mitral valve prosthesis. *Journal of Biomedical Engineering*, 3, 3-8
- Gentle, C.R., Juden, H. and Swales, P.D. 1981b. Testing of an all-ceramic mitral valve prosthesis. In: *Proceedings of the XIII meeting of the European Society for Artificial Organs*, Copenhagen, Denmark, 352-355

- Gentle, C.R. 1982. Characterisation of leakage flow in cardiac valve prostheses. *Proceedings of the IX Annual Meeting of the European Society for artificial Organs*, Brussels, Belgium, 102-106
- Gentle, C.R. 1983. Minimization of pressure drop across heart valve conduits: a preliminary study. *Life Support Systems*, 1, 263-270
- Gentle, C.R. 1986. The use of ceramics in prosthetic heart valves. In: *Proceedings of the Heart valve Engineering seminar, Institute of Mechanical Engineers*, London, 31-33
- Giersiepen, M., Reul, H., Knoch, M. and Rau, G. 1986. Pressure drop and velocity fields at mechanical heart valves. In: *Proceedings XIII Annual Meeting of the European Society for Artificial Organs, Life Support Systems*, 4 Supplement 2, 166-168
- Gorlin, R. and Gorlin, S.G. 1951. Hydraulic formula for calculation of the area of the stenotic mitral valve, other cardiac valves, and central circulatory shunts. I. *American Heart Journal*, 41, (1), 1-29
- Gupta, B.B., Nigam, K.M. and Jaffrin, M.Y. 1982. A three-layer semi-empirical model for flow of blood and other particulate suspensions through narrow tubes. *Transactions of the ASME Journal of Biomedical Engineering*, 104, 129-135
- Hampshire R.G. 1984. Flow visualisation with stroboscopic illumination to provide an unambiguous record of direction. *Journal of Physics E: Science Instrumentation*, 17, 741-743
- Hasenkamp, J.M., Westphal, D., Reul, H., Gormsen, J., Giersiepen, M., Stodkilde-Jorgensen, H. and Paulsen, P.K. 1987. Three-dimensional visualisation of axial velocity profiles downstream of six different mechanical aortic valve prostheses, measured with a hot-film anemometer in a steady state flow model. *Journal of Biomechanics*, 20, (4), 353-364
- Hedberg, P.K., Rosten, H.I. and Spalding, D.B. 1986. *The PHOENICS equations (TR/99)*, CHAM Limited, London
- Heimke, G., Griss, P., Jentshura, G. and Werner E. 1980. Bio-inert and bio-active ceramics in orthopaedic surgery. In: Hastings, G.W. and Williams, D.F. (eds.), *Mechanical properties of Biomaterials*, John Wiley and sons, Chapter 15
- Hellums, J.D., and Brown, C.H., 1975. Blood cell damage by mechanical forces. In: Hwang, N.H.C. and Normann, N.A. (eds.), *Cardiovascular flow dynamics and measurements*, University Park Press, Baltimore, USA, 799-823

- Hershey, D. and Cho, S.J. 1966. Blood flow in rigid tubes: thickness and slip velocity of plasma film at the wall. *Journal of Applied Physiology*, 21, 27-32
- Hinghofer-Szalkay, H. 1985. Volume and density changes of biological fluids with temperature. *Journal of Applied Physiology*, 59, 1 686-1 689
- Idelsohn, S.R., Costa, L.E. and Ponso, R. 1985. A comparative study of blood flow through prosthetic heart valves using the finite element method. *Journal of Biomechanics*, 18, (2), 97-115
- Johnson, S.A. 1970. Platelets in hemostasis. In: Seegers, W.H. (ed.), *Blood clotting enzymology*, Academic Press, London 379-420
- Jones, W.P. and Launder, B.E. 1972. The prediction of laminarization with a two-equation model of turbulence. *International Journal of Heat and Mass Transfer*, 15, 301-314
- Knott, E., Reul, H. and Steinseifer, U. 1986. Pressure drop, energy loss and closure volume of prosthetic heart valves in aortic and mitral position under pulsatile flow conditions. In: *Proceedings of XIII Annual meeting of the European Society for Artificial Organs, Life Support Systems*, 4, Supplement 2, 139-141
- Kolomgorov A.N. 1942. Equations of turbulent motion of an incompressible fluid. *Izvestiya, Akademiya Nauk SSSR, Seria Fizicheskaya*, 6, 56-58
- Lampert, R.H. and Williams, M.C. 1978. Effect of surface materials on shear-induced hemolysis. *Journal of Biomedical Materials Research*, 6, 499-532
- Launder, B.E. and Spalding, D.B. 1972. *Mathematical models of turbulence*, Academic Press, London
- Launder, B.E. and Spalding, D.B. 1974. The numerical computation of turbulent flows. *Computer Methods in Applied Mechanics and Engineering*, 3, 269-289
- Laufer, J. 1954. The structure of turbulence in fully developed pipe flow. *National Advisory Committee for Aeronautics, USA, Report Number 1174*
- Leefe, S.E. and Gentle C.R. 1987. Theoretical evaluation of energy loss methods in the analysis of prosthetic heart valves. *Journal of Biomedical Engineering*, 9, 121-127
- Leefe, S.E., Edwards, R.J., Tansley, G.D. and Gentle, C.R. 1986. Investigation into leakage design in prosthetic heart valves. In: *Proceedings of the 26th. Annual Meeting of the Biological Engineering Society*, Glasgow

- Leverett, L.B., Hellums, J.D., Alfrey, C.P. and Lynch, E.C. 1972. Red blood cell damage by shear stress. *Biophysical Journal*, 12, 257-273
- Lourenco, L. and Krothapalli, A. 1987. The role of photographic parameters in laser speckle or particle image displacement velocimetry. *Experiments in Fluids*, 5, 29-32
- Lutz, T.W. and Barras, J.-P. 1983. Rheological behaviour of human blood and plasma at steady flow and oscillatory flow. *VASA*, 12, (2), 121-125
- Mann, K.A., Deutsch, S., Tarbell, J.M., Geselowitz, D.B., Rosenberg, G. and Pierce, W.S. 1987. An experimental study of Newtonian and non-Newtonian flow dynamics in a ventricular assist device. *Transactions of the ASME Journal of Biomechanical Engineering*, 109, 139-147
- Merchant, G.J. and Mazumdar, J. 1986. A numerical model for non-Newtonian blood flow through a disk-type prosthetic heart valve. *Automedica*, 7, (3), 159-177
- Merrill, E.W., Gilliland, E.R., Cokelet, G., Shin, H., Britten, A. and Wells, R.E. 1963. Rheology of human blood, near and at zero flow. Effects of temperature and hematocrit level. *Biophysical Journal*, 3, 199-213
- Merrill, E.W., Benis, A.M., Gilliland, E.R., Sherwood, T.K. and Salzman, E.W. 1965a. Pressure-flow relations of human blood in hollow fibers at low flow rates. *Journal of Applied Physiology*, 20, 954-967
- Merrill, E.W., Gilliland, E.R., Lee, T.S. and Salzman, E.W. 1966. Blood rheology: effect of fibrinogen deduced by addition. *Circulation Research*, 18, 437-446
- Merrill, E.W., Margetts, W.G., Cokelet, G.R., Britten, A., Salzman, E.W., Pennell, R.B. and Melin, M. 1965b. Influence of plasma proteins on the rheology of human blood. In: Copley, A.L. (ed.), *Proceedings of the 4<sup>th</sup> International Conference on Rheology, 4. Symposium on Biorheology*, Interscience, New York, USA, 601-611
- Mehta, U. and Lomax, H. 1982. Reynolds averaged Navier Stokes computation of transonic flows: the state of the art. In: Nixon, D. (ed.), *Progress in astronautics and aeronautics, transonic aerodynamics*, American Institution of Aeronautics and Astronautics, 81, 297-375
- Meynart, R. and Lourenco, L.M. 1984. Laser speckle velocimetry in fluid dynamics applications. In: *Lecture series in digital image processing in fluid dynamics*, March 5-9, Von Karman Institute for Fluid Dynamics, Brussels, Belgium

- Modi, V.J. and Akutsu, T. 1980. Flow Visualisation studies with Starr-Edwards heart valve prosthesis. In: Merzkirch, W. (ed.), *Flow Visualization II, Proceedings of the 2<sup>nd</sup> International symposium on flow visualization*, Bochum, West Germany, 593-597
- Monroe, J.M., Lijana, R.C. and Williams, M.C. 1980. Hemolytic properties of special materials exposed to a shear flow, and plasma changes with shear. *Biomaterials, Medical Devices, and Artificial Organs*, 8, (2), 103-144
- Morain, J.G. 1982. *Turbulence modelling for Computational Aerodynamics*. American Institute of Aeronautics and Astronautics, paper 82-0164
- Nallasamy, M. 1987. Turbulence models and their applications to the prediction of internal flows: a review. *Computers and Fluids*, 15, (2), 151-194
- Narducci, C., Russo, L., Battaglia, L., Angelica, G., Giovannini, E. and D'Alessandro, L.C. 1986. Dysfunction of double disc valvular prosthesis: report on 5 cases. In: *Proceedings XIII Annual Meeting of the European Society for Artificial Organs Life Support Systems*, 4 Supplement 2, 160-162
- Nunez, L., Iglesias, A. and Sotillo, J. 1980. Entrapment of leaflets of St. Jude Medical cardiac valve prosthesis by miniscule thrombosis. Report of two cases. *Annals of Thoracic Surgery*, 29, 566-569
- Prandtl, L. 1945. Über ein neues formalsystem für die ausgebildete turbulenz, *nachrichten von Der Akademie der Wissenschaft in Göttingen*
- Quemada, D. 1976a. Hémorhéologie - Une nouvelle méthode de caractérisation de la viscosité sanguine. *Comptes Rendus Hebdomadaires des seances. Academie des Sciences, Paris série D*, 282, (21), 1905-1908
- Quemada, D. 1976b. Hémorhéologie - Contraintes et vitesses de cisaillement associées à la destruction des agrégats de globules rouges sanguins: un abord viscosimétrique. *Comptes Rendus Hebdomadaires des seances. Academie des Sciences, Paris série D*, 283, (1), 119-122
- Quemada, D. 1977. Rheology of concentrated disperse systems and minimum energy dissipation principle I. Viscosity-concentration relationship. *Rheologica Acta*, 16, 82-94
- Quemada, D. 1978. Rheology of concentrated disperse systems II. A model for non-Newtonian shear viscosity in steady flows. *Rheologica Acta*, 17, 632-642

- Rand, P.W., Lacombe, E., Hunt, H.E. and Austin, W.H. 1964. Viscosity of normal human blood under normothermic and hypothermic conditions. *Journal of Applied Physiology*, 19, 117-121
- Reif, T.H., Cocolin, G. and Huffstutler, M.C. 1980. A note on the leakage of the new Omniscience/tm pivoting disk prosthetic heart valve. *Transactions of the ASME Journal of Biomedical Engineering*, 102, 342-344
- Reif, T.H. and Huffstutler, M.C. 1984. A comparative flow study of the Omniscience and the Björk-Shiley cardiac valve prostheses. *International Journal of Artificial Organs*, 7, (5), 277-282
- Reul, H., Talukder, N. and Muller, E.W. 1981. Fluid Mechanics of the natural mitral valve. *Journal of Biomechanics*, 14, (5), 361-372
- Rodi, W. 1980. Turbulence models and their application in hydraulics. A state-of-the-art paper. *International Association for Hydraulic Research*, Delft, Holland
- Rooney, J.A. 1970. Hemolysis near an ultrasonically pulsating gas bubble. *Science*, Washington, 169, 869-871
- Roshcke, E.J., Harrison, E.C. and Blankenhorn, D.H. 1975. Fluid shear stresses during the opening sequence of prosthetic heart valves. In: *Proceedings of the 28th annual Conference on Engineering in Medicine and Biology*, pp D5.4
- Roshcke, E.J., Harrison, E.C., Carl, J.R., Parnassus, W. and Moachanin, J. 1977. Evaluation of recovered heart valves. In: *proceedings of the 12th meeting of the Association for the Advancement of Medical Instrumentation*, San Francisco
- Rosten, H.I. and Spalding, D.B. 1986. *PHOENICS - Beginners guide and user manual (TR/100)*, CHAM Limited, London
- Ross, J.C., Hufnagel, J., Freis, C., Harvey, W. and Partenope. 1954. The hemodynamic alterations produced by a plastic valvular prosthesis for severe aortic insufficiency in man. *Journal of Clinical Investigations*, 33, 891
- Sacks, A.H., Raman, K.R., Burnell, J.A. and Tickner, E.G. 1963. *Vidya*, report No. 119
- Schmid-Schönbein, H, Klose, H.J., Volger, E. and Weiss, J. 1973. Hypothermia and blood flow behavior. *Research and Experimental Medicine*, 161, 58-68
- Shanebrook, J.R. and Levine, M.L. 1979. Hemodynamics of left ventricular apex-aortic valved conduits. *Cardiovascular diseases, Bulletin of the Texas Heart Institute*, 6, (4), 425-438

- Shapiro, S.I. and Williams A.R. 1970. Hemolysis in simpler shear flows. *Journal of the American Institute of Chemical Engineers*, 16, 575-580
- Smith, C.R., Sand, M.E. and Bendick, P.J. 1975. Measurement of prosthetic valve flow behavior in a steady flow simulator using an LDV. *ASME conference of applied Mechanics, Symposium on Biomechanics*, paper 75-APMB-8
- Solen, K.A., Whiffen, J.D. and Lightfoot, E.N. 1978. The effect of shear, specific surfaces, and air interface on the development of emboli and hemolysis. *Journal of Biomedical Materials Research*, 12, 381-399
- Solen, K.A., Whiffen, J.D. and Lightfoot, E.N. 1981. Plasma glucose concentrations and the development of blood emboli and hemolysis. *Journal of Laboratory and Clinical Medicine*, 98, (2), 206-216
- Spalding, D.B. 1981. A general purpose computer program for multi-dimensional one and two-phase flow. *Mathematics and Computers in Simulation*, 23, 267-278
- Stern, M. 1985. Laser Doppler Velocimetry in blood and multiply scattering fluids: theory. *Applied Optics*, 24, (13), 1968-1986
- Swanson, W.M. and Clark, R.E. 1980. Streaming birefringent flow qualitative evaluation of prosthetic heart valves. In: Merzkirch, W. (ed.), *Flow Visualization II, Proceedings of the 2<sup>nd</sup> International symposium on flow visualization*, Bochum, West Germany, 605-609
- Swanson, W.M. 1984. Comparison of in-vitro valve pressure drop results from different investigators. *Medical Instrumentation*, 18, (2), 115-117
- Tansley, G.D., Edwards, R.J., Leefe, S.E. and Gentle, C.R. 1986. Ball occluder instability during forward flow through prosthetic heart valve conduits. In: *Proceedings of XIII Annual meeting of the European Society for Artificial Organs Life Support Systems*, 4 Supplement 2, 169-171
- Thalassoudis, K., Mazumdar, J., Noye, B.J. and Craig, I.H. 1987. Numerical study of turbulent flow through a caged-ball prosthetic heart valve using a boundary-fitted co-ordinate system. *Medical and Biological Engineering and Computing*, 26, 173-180
- Tietjen, G.W., Chien, S., Leroy, C., Gavras, I., Gavras, H. and Gump, F.E. 1975. Blood viscosity, plasma proteins and Raynaud syndrome. *Archives of Surgery*, 110, 1 343-1 346

- Tiederman, W.G., Steinle, M.J. and Phillips, W.M. 1986. Two-component laser velocimeter measurements downstream of heart valve prostheses in pulsatile flow. *Transactions of the ASME Journal of Biomechanical Engineering*, 108, 59-64
- Tillmann, W., Reul, H., Herold, M., Bruss, K.-H. and Van Glise, J. 1984. In-vitro wall shear measurements at aortic valve prostheses. *Journal of Biomechanics*, 17, (4), 263-279
- Uglov, F.G., Zubtsovskii, V.N., Dobrova, N.B., Bushmarin, O.N., Orlovskii, P.I., Saraev, Y.N. and Perinov, Y.A. 1978. Distribution of pressure on the surface of the closing elements of artificial heart valves. *Biomedical Engineering*, 12, (2), 61-65
- Uglov, F.G., Orlovskii, P.I., Murasalova, F.A., Evdokimov, S.V., Bushmarin, O.N. and Yakovenko, V.V. 1984. Investigation of self-induced vibrations of the ball closing an artificial aortic valve. *Biomedical Engineering*, 18, 48-50
- Underwood, F.N. and Mueller, T.J. 1977. Numerical study of the steady axisymmetric flow through a disk-type prosthetic heart valve in a constant diameter chamber. *Transactions of the ASME, Journal of Biomechanical Engineering*, 99, 91-97
- Underwood, F.N. and Mueller, T.J. 1979. Numerical study of the steady axisymmetric flow through a disk-type prosthetic heart valve in an aortic shaped chamber. *Transactions of the ASME, Journal of Biomechanical Engineering*, 101, 198-204
- Viggers, R.F., Robel, S.B. and Sauvage, L.R. 1967. A hydraulic figure of merit for heart valve prostheses. *Journal of Biomedical Materials Research*, 1, 103-112
- Virgilio, R.W., Long, D.M., Mundth, E.D. and McClenathan, J.E. 1964. The effect of temperature and hematocrit on the viscosity of blood. *Surgery*, 55, (6), 825-830
- Walburn, F.J. and Schneck, D.J. 1976. A constitutive equation for whole human blood. *Biorheology*, 13, 201-210
- Webster, K.A. 1982. *Steady flow testing of a prototype heart valve prosthesis*, B.Sc. thesis, Trent Polytechnic, Nottingham
- Weiting, D.W. 1969. *Dynamic flow characteristics of heart valves*. Ph.D. thesis, Texas University, USA
- Weltmann, R. and Green, H. 1943. Rheological properties of colloidal solutions, pigment suspensions and oil mixtures. *Journal of Applied Physics*, 14, 569-576
- Whitmore, R.L. 1963. Hemorheology and hemodynamics. *Biorheology*, 1, 201-220

Whitmore, R.L. 1968. *Rheology of the Circulation*, Pergamon Press, Oxford

Wielogorski, J.W., Davy, W.T.J. and Regan, R.J. 1976. The influence of surface rugosity on hemolysis occurring in tubing. *Biomedical Engineering*, 11, 91-94

Williams, A.R., Hughes, D.E., Nyborg, W.L. 1970. Hemolysis near a transversely oscillating wire. *Science*, Washington, 169, 871-873

Woo, Y.-R., Williams, F.P. and Yoganathan, A.P. 1983. In-vitro fluid dynamic characteristics of the Abiomed Trileaflet heart valve prosthesis. *Transactions of the ASME, Journal of Biomedical Engineering*, 105, 338-345

Yoganathan, A.P., Reamer, H.H., Harrison, E.C. and Corcoran, W.H. 1979a. Laser-Doppler anemometer to study velocity fields in the vicinity of prosthetic heart valves. *Medical and Biological Engineering and Computing*, 17, 38-44

Yoganathan, A.P., Reamer, H.H., Harrison, E.C. and Carl, J.R. 1979b. In vitro velocity measurements in the near vicinity of the Björk-Shiley aortic prosthesis using a laser-Doppler anemometer. *Medical and Biological Engineering and Computing*, 17, 435-459

Yoganathan, A.P., Corcoran, W.H. and Harrison, E.C. 1979c. Pressure drops across prosthetic aortic heart valves under steady and pulsatile flow - in vitro measurements. *Journal of Biomechanics*, 12, 153-164

## APPENDIX ONE

### DERIVATION OF NEWTONIAN AND NON-NEWTONIAN VELOCITY PROFILES

## A1.1 Newtonian Velocity Profile - Analytical

Consider a two dimensional element of in-compressible fluid in a horizontal pipe under weightless conditions (Figure A1.1).

The net force acting on the cylinder is

$$\Delta F = \Delta P \pi r^2 \quad [A1.1]$$

The viscous drag force will be:

$$F_v = 2\tau \pi r l \quad [A1.2]$$

For steady fully developed flow in equilibrium:

$$\Delta P \pi r^2 = 2\tau \pi r l \quad [A1.3]$$

Then:

$$\tau = \Delta P r / 2l \quad [A1.4]$$

This gives the shear stress in the fluid at any radius 'r' and the shear stress at the wall ' $\tau_w$ ' by the substitution of 'R' for 'r', also, as the shear stress is a linear relationship with respect to radius and a maximum at the wall (for pipe flow) then:

$$\tau = \tau_w \frac{r}{R} \quad [A1.5]$$

From the definition of dynamic viscosity ( $\mu$ )

$$\mu = \tau / \dot{\gamma}$$

Where one dimensional shear rate

$$\dot{\gamma} = - dw/dr \quad [A1.6]$$

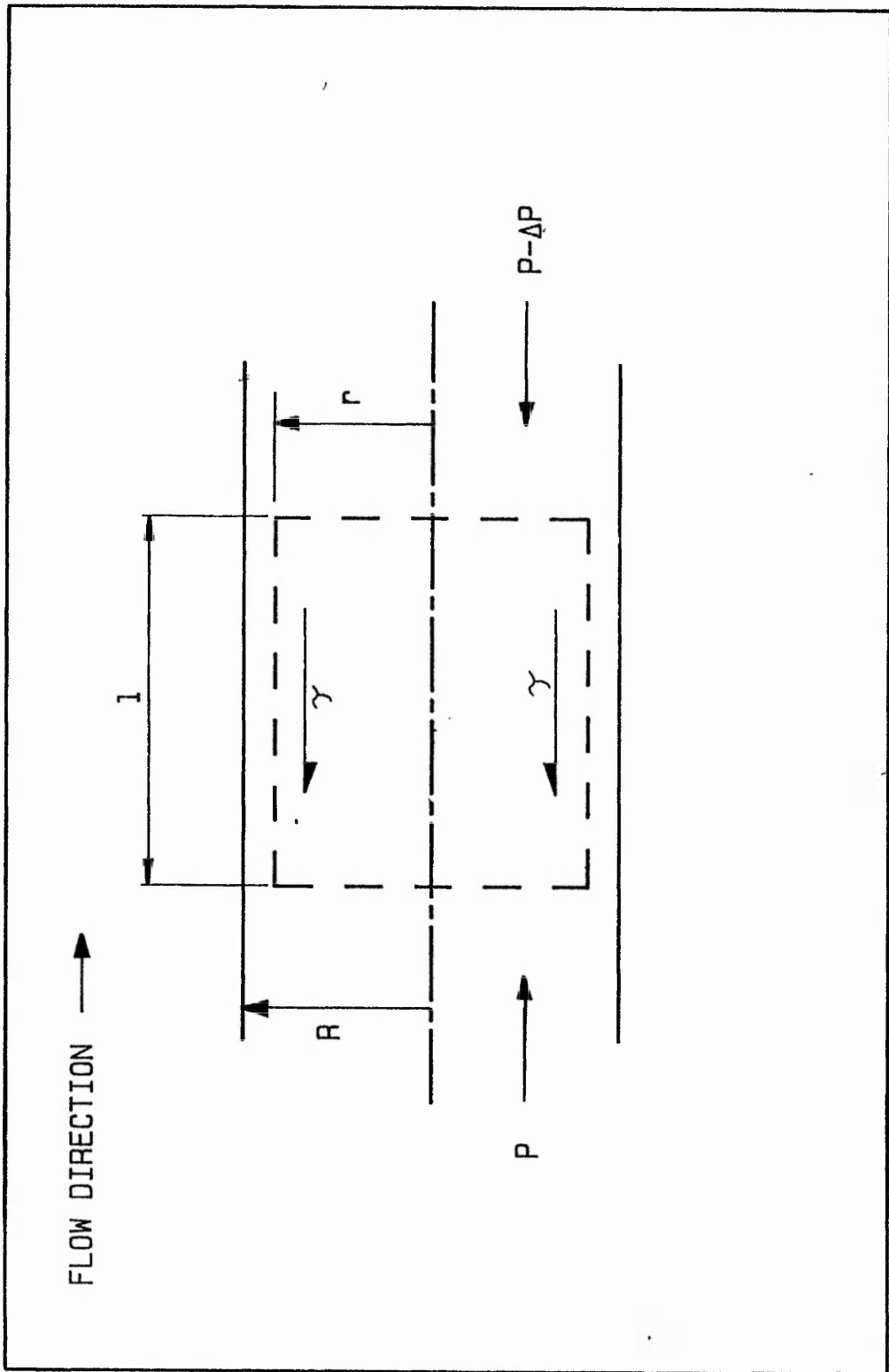
A relationship for velocity can be arrived at by separating and integrating:

$$dw = - \int \frac{\Delta P}{2\mu l} r dr$$

$$w = -(\Delta P / 4\mu l) r^2$$

putting in the boundary conditions (at  $r = R$ ,  $w = 0$ ) gives:

$$w = \frac{\Delta P}{4\mu l} (R^2 - r^2) \quad [A1.7]$$



ELEMENT OF FLUID IN FULLY DEVELOPED LAMINAR PIPE FLOW

## A1.2 Non-Newtonian Velocity Profile

Shear stress in simple laminar flow is found from the relationship

$$\tau = \mu_L \dot{\gamma}$$

where:

$\mu_L$  is the Newtonian viscosity  
for incompressible fluids:

$$\dot{\gamma}^2 = 2 \left( \left( \frac{1}{r} \frac{\partial u}{\partial \theta} \right)^2 + \left( \frac{\partial v}{\partial r} \right)^2 + \left( \frac{\partial w}{\partial z} \right)^2 \right) +$$

$$\left( \frac{\partial u}{\partial r} + \frac{1}{r} \frac{\partial v}{\partial \theta} \right)^2 + \left( \frac{\partial w}{\partial r} + \frac{\partial v}{\partial z} \right)^2 + \left( \frac{\partial u}{\partial z} + \frac{1}{r} \frac{\partial w}{\partial \theta} \right)^2 \quad [A1.8]$$

The complex blood viscosity  $\mu_a$  in the computational study replaces the laminar viscosity, thus:

$$\mu_L = \mu_a = \tau / \dot{\gamma}$$

Working with the Casson equation as the descriptor of apparent viscosity a velocity profile can be developed:

$$\tau = (s\sqrt{\dot{\gamma}} + \sqrt{\tau_y})^2 \quad [3.7]$$

from steady laminar pipe flow:

$$\tau = \Delta Pr / 2l \quad [A1.9]$$

substituting gives

$$\frac{\Delta Pr}{2l} = s^{-1} (\sqrt{\dot{\gamma}} + \sqrt{\tau_y})^2$$

or

$$\dot{\gamma} = (-\sqrt{\tau_y} \pm \sqrt{(\Delta Pr / 2l) / s})^2$$

as  $\dot{\gamma} = -dw/dr$ , then separating variables and multiplying out gives:

$$-dw = \{ \tau_y \pm 2\sqrt{\tau_y (\Delta Pr / 2l)} + \Delta Pr / 2l \} 1/s^2 dr$$

or

$$w = \int_0^R \frac{-1}{s^2} \left( \tau_y \pm 2\sqrt{\tau_y \frac{\Delta Pr}{2l}} + \frac{\Delta Pr}{2l} \right) dr$$

$$= \frac{-1}{s^2} \left( \tau_y r \pm \frac{4}{3} \sqrt{\tau_y \frac{\Delta Pr}{2l}} r^{3/2} + \frac{\Delta Pr^2}{4l} \right) + A \quad [A1.10]$$

finding the constant of integration by applying a known boundary condition:

$$\text{at } r = R, w = 0$$

then:

$$A = \frac{1}{s^2} \left( \tau_y R \pm \frac{4}{3} \sqrt{\frac{\tau_y \Delta P}{2l}} R^{3/2} + \frac{\Delta P}{4l} R^2 \right)$$

therefore:

$$w = \frac{1}{s^2} \left( \tau_y (R-r) \pm \frac{4}{3} \sqrt{\frac{\tau_y \Delta P}{2l}} (R-r)^{3/2} + \frac{\Delta P (R-r)^2}{4l} \right)$$

The correct root of this equation is not obvious but was found to be the negative root following the analysis of CFM results.

finally then:

$$w = \frac{1}{s^2} \left( \tau_y (R-r) - \frac{4}{3} \sqrt{\frac{\tau_y \Delta P}{2l}} (R-r)^{3/2} + \frac{\Delta P (R-r)^2}{4l} \right) \quad [A1.11]$$

APPENDIX TWO

LRR SERIES GRID GENERATION CODING

This interactive Fortran program would read the required geometry for each LRR series valve, calculate each of the  $(NX+1) \times (NY+1) \times (NZ+1)$  points of the curvilinear grid. Output from the program was in the format suitable for input to PHOENICS via the 'readco' command. Geometry generation is based on the 22mm diameter conduit, and size variation is achieved by multiplication by a conversion factor.

```

DIMENSION XC(10,40,200), YC(10,40,200), ZC(10,40,200)
DIMENSION T(200),CSUBL(200), BSUBL(200), ZCSUBL(200)
DIMENSION ZBSUBL(200)
DOUBLE PRECISION Rb,Rc,Rs,A,Ro,C,D,pi,Dtop,Dout,IRAD,Dwl,DCON
DOUBLE PRECISION ZFRAC1,ZFRAC2,Ti,Tn,Z,RES,Din
DOUBLE PRECISION ANG,YRAD,DRAD,ZRAD,YYCTR,ZYCTR,CONV
INTEGER NX,NY,NZ,NO,NC,NW,ITER,Nb,I,J,K,Ct,NL,NU,NS,NE,NP
INTEGER NR, NT, IOF, OOF, NCON, NSUBL
CHARACTER ST, SO
OPEN(UNIT=31,STATUS='UNKNOWN',FILE='3DHV.DAT')

```

```

C
C   USER INPUT SECTION
C
C   NX is the number of CELLS in the X direction = 90 degrees/NX
C   NY is the number of CELLS in the Y direction (as per phoenics)
C   NZ is the number of CELLS in the Z direction (as per phoenics)
C   NO is the nuber of the cell at the ball centre line
C   Nb is the number of ball surface cells
C
WRITE(5,15)
15  FORMAT(1X,'IS INLET PROFILE STRAIGHT? (Y/N)')
    READ(6,20) ST
20  FORMAT (A1)
    WRITE(5,16)
16  FORMAT(1X,'IS OUTLET PROFILE STRAIGHT? (Y/N)')
    READ (6,20) SO
    WRITE(5,30)
30  FORMAT(1X,'INPUT NX, NY, NZ')
    READ(6,*) NX,NY,NZ
    WRITE(5,40)
40  FORMAT(1X,'INPUT RADIUS (mm), ZFRAC1 (mm), ZFRAC2 (mm)')
    READ(6,*) IRAD, ZFRAC1,ZFRAC2
    ZFRAC1=ZFRAC1/1000
    ZFRAC2=ZFRAC2/1000
    WRITE(5,55)
55  FORMAT(1X,'INPUT BALL-CENTRE CELL, No. OF CELLS ON BALL')
    READ(6,*) NO,NB
    WRITE(5,60)

```

```

60     FORMAT(1X,'INPUT X-DIRECTION ANGLE (degrees)')
      READ(5,*)ANG
      WRITE(5,10)
10     FORMAT(1X,'INPUT No. OF OFFSET NODES: INLET, OUTLET')
      READ(6,*) IOF, OOF
      WRITE(5,32)
32     FORMAT(1X,'INPUT FIRST THICKNESSES ON BALL (mE-4)')
      READ(6,*)BSUBL(1)
      WRITE(5,33)
33     FORMAT(1X,'INPUT FIRST THICKNESSES AT CONDUIT (mE-4)')
      READ(6,*)CSUBL(1)
      WRITE(5,34)
34     FORMAT(1X,'INPUT CONDUIT RADIUS (mm)')
      READ(6,*) Rc
      BSUBL(1)=BSUBL(1)/10000
      CSUBL(1)=CSUBL(1)/10000
      Rc=Rc/1000

C
C     CONSTANTS SECTION
C
C     A is the conduit area and Rb is the ball radius
      pi=3.1415926
      A=Rc**2*pi
      CONV=Rc/11.0E-3
      Rb=0.01235*CONV
      NX=NX+1
      NY=NY+1
      NZ=NZ+1
      NB=NB/2
      NSUBL=1
      DO 2 K= 1,NZ
      BSUBL(K)=BSUBL(1)
      CSUBL(K)=CSUBL(1)
2     CONTINUE
C
C     TO GENERATE Z-WISE NODES (Z INCREASING FROM 1 TO NZ)
C
C     For inlet at centreline
C
      NF=NO-NB
      NE=NO+NB
      DO 25 K=1,NF
      ZC(1,1,K)=ZFRAC1*(K-1)
25    CONTINUE
C
C     For the inlet face of the ball

```

```

C
ZC(1,1,NO)=ZC(1,1,NF)+Rb
DO 50 K=NF+1,NO-1
ZC(1,1,K)=ZC(1,1,NO)-Rb*SIN(Pi*(NO-K)/(2*NB))
50 CONTINUE
C
C For the back face of the ball
C
DO 75 K=NO,NE
ZC(1,1,K)=ZC(1,1,NO)+Rb*SIN(Pi*(K-NO)/(2*NB))
75 CONTINUE
C
C For outlet at centreline
C
DO 100 K=NE+1,NZ
ZC(1,1,K)=ZC(1,1,NE)+ZFRAC2*(K-NE)
100 CONTINUE
C
C For inlet conduit wall
C
Dwl=ZC(1,1,NO)-(2.232069E-3*CONV)
IF(ST.EQ.'Y') Din=ZC(1,1,NO)-(16.98356E-3*CONV)
IF(ST.EQ.'N') Din=ZC(1,1,NO)-(15.51564E-3*CONV)
NC=NF+IOF
DO 125 K=1,NO
IF(Dwl.GE.ZC(1,1,K).AND.Dwl.LE.ZC(1,1,K+1)) NW=K+1
125 CONTINUE
DO 150 K=1,NC-1
ZC(1,NY,K)=(Din/(NC-1))*(K-1)
150 CONTINUE
C
C For divergent section
C
IF(ST.EQ.'N') GOTO 165
DO 160 K=NC,NW
ZC(1,NY,K)=Din+((K-NC)*(Dwl-Din)/(NW-NC))
YC(1,NY,K)=Rc+((K-NC)*(5.53853E-3*CONV)/(NW-NC))
160 CONTINUE
DO 162 K=NW+1,NO
ZC(1,NY,K)=Dwl+((K-NW)*(ZC(1,1,NO)-Dwl)/(NO-NW))
YC(1,NY,K)=16.53852E-3*CONV
162 CONTINUE
GOTO 212
165 DO 175 K=NC,NO
Ti=(35.3352+((K-NC)*(90-35.3352)/(NO-NC)))*2*Pi/360
Ro=(A/(Pi*DSIN(Ti))+Rb**2)**.5

```

```

ZC(1,NY,K)=ZC(1,1,NO)-Ro*DCOS(Ti)
YC(1,NY,K)=Ro*DSIN(Ti)
175 CONTINUE
C
C For convergent outlet section
C
212 Dcon=ZC(1,1,NO)+4.6296E-3*CONV
IF(SO.EQ.'Y') Dout=ZC(1,1,NO)+(30.06641E-3*CONV)
IF(SO.EQ.'N') Dout=ZC(1,1,NO)+(15.51564E-3*conv)
NP=NE-OOF
ZC(1,NY,NP)=Dout
DO 250 K=NO,NP
ZC(1,NY,K)=ZC(1,1,NO)+(Dout-ZC(1,1,NO))*(K-NO)/(NP-NO)
IF(Dcon.GE.ZC(1,1,K).AND.Dcon.LE.ZC(1,1,K+1)) NCON=K+1
250 CONTINUE
IF(SO.EQ.'Y') ZC(1,NY,NCON)=Dcon
C
C For conduit outlet
C
DO 275 K=NP+1,NZ
ZC(1,NY,K)=Dout+((K-NP)*(ZC(1,1,NZ)-Dout)/(NZ-NP))
275 CONTINUE
C
C TO GENERATE Y-WISE NODES
C
C Profile of the ball and centre line (inlet)
C
DO 285 K=1,NF
YC(1,1,K)=0.0
285 CONTINUE
DO 300 K=NF+1,NO-1
YC(1,1,K)=(Rb**2-(ZC(1,1,NO)-ZC(1,1,K))**2)**.5
300 CONTINUE
C
C inlet Conduit wall
C
DO 325 K=1,NC-1
YC(1,NY,K)=Rc
325 CONTINUE
C
C To generate the profile of the ball and centre line (outlet)
C
330 DO 400 K=NO,NE-1
YC(1,1,K)=(Rb**2-(ZC(1,1,K)-ZC(1,1,NO))**2)**.5
400 CONTINUE

```

```

DO 425 K=NE,NZ
YC(1,1,K)=0.0
425 CONTINUE
C
C   To generate the outflow tract and conduit wall:
C
C   for straight outlet profile
IF(SO.EQ.'Y') GOTO 675
C
C   via Newton_Raphson iteration for theta based on Z
C
T(NO-1)=pi/2
DO 650 K=NO,NP
ITER=0
Ti=T(K-1)
550 Ro=(A/(Pi*DSIN(Ti))+Rb**2)**.5
C=Ro*DCOS(Ti)-(ZC(1,NY,K)-ZC(1,1,NO))
D=(A/(2*pi*Ro*(DTAN(Ti)**2)))+(Ro*DSIN(Ti))
Tn=Ti+(C/D)
RES=Tn-Ti
IF((DABS(Tn-Ti)).LT.1E-16) GOTO 600
Ti=Tn
ITER=ITER+1
GOTO 550
600 ITER=ITER+1
T(K)=Tn
YC(1,NY,K)=Ro*DSIN(Tn)
625 FORMAT(1x,'Z=',D14.7,' Y=',D14.7,' Theta=',D14.7,' Ro=',D14.7)
WRITE(6,*)
650 CONTINUE
GOTO 710
675 DO 690 K=NO+1,NCON
ZC(1,NY,K)=ZC(1,1,NO)+(Dcon-ZC(1,1,NO))*(K-NO)/(NCON-NO)
YC(1,NY,K)=16.53852E-3*CONV
690 CONTINUE
DO 700 K=NCON+1,NP
ZC(1,NY,K)=Dcon+((K-NCON)*(Dout-Dcon)/(NP-Ncon))
YC(1,NY,K)=(16.53852E-3*CONV)+((NCON-K)*
1 (5.53852E-3*CONV)/(NP-NCON))
700 CONTINUE
C
C   Outlet Conduit wall
C
710 DO 725 K=NP+1,NZ
YC(1,NY,K)=Rc
725 CONTINUE

```

C  
C  
C

To add blending radius at exit from convergent section

```
IF(IRAD.EQ.0) GOTO 799
IF(IRAD.EQ.5) GOTO 730
IF(IRAD.EQ.10) GOTO 740
IF(IRAD.EQ.15) GOTO 750
IF(IRAD.EQ.20) GOTO 760
IF(IRAD.EQ.25) GOTO 762
IF(IRAD.EQ.30) GOTO 764
IF(IRAD.EQ.35) GOTO 766
IF(IRAD.EQ.40) GOTO 768
IF(IRAD.EQ.45) GOTO 769
730  YRAD=16.0E-3*CONV
      ZRAD=ZC(1,1,NO)+(16.96194E-3*CONV)
      DRAD=ZRAD-(2.63495E-3*CONV)
      GOTO 770
740  YRAD=21.0E-3*CONV
      ZRAD=ZC(1,1,NO)+(18.36702E-3*CONV)
      DRAD=ZRAD-(5.13290E-3*CONV)
      GOTO 770
750  YRAD=26.0E-3*CONV
      ZRAD=ZC(1,1,NO)+(19.71856E-3*CONV)
      DRAD=ZRAD-(7.40829E-3*CONV)
      GOTO 770
760  YRAD=31.0E-3*CONV
      ZRAD=ZC(1,1,NO)+(21.00906E-3*CONV)
      DRAD=ZRAD-(10.26579E-3*CONV)
      GOTO 770
762  YRAD=36.0E-3*CONV
      ZRAD=ZC(1,1,NO)+(22.24108E-3*CONV)
      DRAD=ZRAD-(11.38148E-3*CONV)
      GOTO 770
764  YRAD=41.0E-3*CONV
      ZRAD=ZC(1,1,NO)+(23.41892E-3*CONV)
      DRAD=ZRAD-(13.13019E-3*CONV)
      GOTO 770
766  YRAD=46.0E-3*CONV
      ZRAD=ZC(1,1,NO)+(24.54724E-3*CONV)
      DRAD=ZRAD-(14.75082E-3*CONV)
      GOTO 770
768  YRAD=51.0E-3*CONV
      ZRAD=ZC(1,1,NO)+(25.63064E-3*CONV)
      DRAD=ZRAD-(16.26468E-3*CONV)
      GOTO 770
769  YRAD=56.0E-3*CONV
```

```

ZRAD=ZC(1,1,NO)+(26.67348E-3*CONV)
DRAD=ZRAD-(17.68767E-3*CONV)
770 DO 780 K=NO,NZ
IF(DRAD.GE.ZC(1,NY,K).AND.DRAD.LE.ZC(1,NY,K+1)) NR=K
IF(ZRAD.GE.ZC(1,NY,K).AND.ZRAD.LE.ZC(1,NY,K+1)) NT=K
780 CONTINUE
ZC(1,NY,NR)=DRAD
ZC(1,NY,NT)=ZRAD
IRAD=IRAD*CONV/1000
DO 790 K=NR,NT
ZC(1,NY,K)=DRAD+((ZRAD-DRAD)*(K-NR)/(NT-NR))
YC(1,NY,K)=YRAD-(IRAD**2-(ZRAD-ZC(1,NY,K))**2)**.5
790 CONTINUE
ZC(1,NY,NT+1)=ZC(1,NY,NT)+0.5*ZFRAC2
C
C TO GENERATE THE INTERMEDIATE Y VALUES (Y = 2 TO NY-1)
C
799 CONTINUE
DO 802 K=1,NF-1
BSUBL(K)=YC(1,NY,K)/NY
802 CONTINUE
DO 803 K=NE+1,NZ
BSUBL(K)=YC(1,NY,K)/NY
803 CONTINUE
DO 801 K=1,NZ
ZCSUBL(K)=(ZC(1,NY,K)-ZC(1,1,K))*CSUBL(K)/(YC(1,NY,K)
1 -YC(1,1,K))
ZBSUBL(K)=(ZC(1,NY,K)-ZC(1,1,K))*BSUBL(K)/(YC(1,NY,K)
1 -YC(1,1,K))
801 CONTINUE
DO 820 K=1,NZ
ZYCTR=(ZC(1,NY,K)-ZC(1,1,K))-(ZCSUBL(K)+ZBSUBL(K))
YYCTR=(YC(1,NY,K)-YC(1,1,K))-(CSUBL(K)+BSUBL(K))
C DO 800 J=1,NSUBL+1
YC(1,2,K)=YC(1,1,K)+BSUBL(K)
ZC(1,2,K)=ZC(1,1,K)+(ZBSUBL(K)/NSUBL)
YC(1,NY-1,K)=YC(1,NY,K)-CSUBL(K)
ZC(1,J,K)=ZC(1,NY,K)-ZCSUBL(K)
DO 820 J=3,NY-2
ZC(1,J,K)=ZC(1,1,K)+ZBSUBL(K)+(ZYCTR*(J-2)/(NY-3))
YC(1,J,K)=YC(1,1,K)+BSUBL(K)+(YYCTR*(J-2)/(NY-3))
820 CONTINUE
C
C TO INTRODUCE THREE-DIMENSIONALITY IN X-PLANE
C
DX=(ANG/(NX-1))*2*Pi/360

```

```

DO 900 K=1,NZ
DO 900 J=1,NY
DO 900 I=2,NX
ZC(I,J,K)=ZC(1,J,K)
YC(I,J,K)=YC(1,J,K)*COS(DX*(I-1))
XC(I,J,K)=YC(1,J,K)*SIN(DX*(I-1))
900 CONTINUE
C
C TO OUTPUT TO DISK THE GENERATED GRID FILE NAMED: 3DHV.DAT
C
WRITE(31,1200) NX, NY, NZ
DO 1100 K=1,NZ
WRITE(31,1225) ((XC(I,J,K),J=1,NY),I=1,NX)
WRITE(31,1225) ((YC(I,J,K),J=1,NY),I=1,NX)
WRITE(31,1225) ((ZC(I,J,K),J=1,NY),I=1,NX)
1100 CONTINUE
WRITE(31,1125)
1125 FORMAT('FILENAME=3DHV.DAT')
1200 FORMAT(3I5)
1225 FORMAT(5(1PE13.6))
CLOSE(31)
CLOSE(32)
END

```

**APPENDIX THREE**

**PHOENICS (Q1) INPUT FILE**

The file below is typical of the PHOENICS input file for valve flow in BFC grids. The lines of the file which are indented by two or more characters are comments and would not be operated on by PHOENICS. Of these comment fields the lines indented by only two characters are lines that were operated on in earlier runs or runs using different fluids, but which have been indented so as not to be active in the present run. The italics comment fields have been added afterwards in order to aid understanding as part of the thesis.

This particular input file was to model the flow of 21.1l/min of blood through the finalised 'LRRSICO' valve with a 30mm blending radius. The run was re-started from a previous run, the results of which were held within a file named 'B17.DAT'. Convective links were disabled and the  $k - \epsilon$  turbulence model, suitable wall and inlet and outlet conditions were specified in group 13. The number of sweeps was set to 300 but convergence was completed in a lesser number of sweeps. A second run was carried out after convergence, this allowed the outputting of data to plot files.

```
TALK=F;RUN( 1, 2);VDU= 2
  GROUP 1. Run title
TEXT(21l/min BLOOD LRRSICO30 CONDUIT DIA = 16mm)
REAL(WIN,REYNO,RAD,DIA,MU,YIELD,SLOPE,TKEIN,EPIN,GMIXL)
REAL(QIN,ANGLE,SUBL,BLEND)
INTEGER(PLT)
BLEND=30.0
RAD=12.0E-3
DIA=RAD*2
WIN=1.75*(8E-3**2/RAD**2)
  MU=3.323E-3
  MU=1.002E-3
SLOPE=0.053001          Viscosity not constant
YIELD=0.004800         but set via ENUL=GRND7
ANGLE=5.0
QIN=RAD**2*3.1415926*WIN*60000
  GROUP 2. Transience; time-step specification
  GROUP 3. X-direction grid specification
NX=1
  GROUP 4. Y-direction grid specification
NY=30
SUBL=0.8
  GROUP 5. Z-direction grid specification
PARAB=F.               Elliptic solver employed
NZ=120
  GROUP 6. Body-fitted coordinates or grid distortion
```

```

BFC=T;NONORT=T
READCO(B21)           Grid definition read..
RSTGEO=F             (each time as a data file)
SAVGEO=F            (and grid is not stored)
  GROUP 7. Variables stored, solved & named
  solve for pressure (whole-field) and velocity.
SOLVE(V1,W1)         variables solved for
SOLUTN(P1,Y,Y,Y,N,N,N) Pressure solved whole-field
VISL=17,NAME(17)=ENUL
VIST=18,NAME(18)=ENUT
NAME(19)=GAMA
NAME(20)=TAUL
NAME(21)=TAUT
NAME(22)=TTAU
} variables named
STORE(ENUL,ENUT,VCRT,WCRT,V2,W2,GAMA,TAUL,TAUT,TTAU)
  GROUP 8. Terms (in differential equations) & devices
DIFCUT=0.0          no convection - all difusion
  GROUP 9. Properties of the medium (or media)
TURMOD(KEMODL)      activate k - ε model
RHO1=1107.3
RHO1=1056.17        the density of blood
RHO1=998.2
  GROUP 10. Inter-phase-transfer processes and properties
  GROUP 11. Initialization of variable or porosity fields
INIADD=F.
NAMFI=B17
  ** Calculation of KE (where fric=0.018)...
TKEIN=0.25*(WIN**2)*0.018 initial guess at k field
  ** Calculation of EP (where lmix=0.09 x h)...
GMIXL=0.09*RAD
EPIN=(TKEIN**1.5)*0.1643/GMIXL initial guess at ε field
  ** Initial values
FIINIT(P1)=0.1
FIINIT(V1)=WIN/100
FIINIT(W1)=WIN
FIINIT(ENUL)=MU/RHO1
FIINIT(KE)=TKEIN
FIINIT(EP)=EPIN
FIINIT(ENUT)=MU/RHO1
FIINIT(P1)=READFI
FIINIT(V1)=READFI
FIINIT(W1)=READFI
FIINIT(ENUL)=READFI
FIINIT(KE)=READFI
FIINIT(EP)=READFI
FIINIT(ENUT)=READFI
} values read from existing field

```

```

GROUP 12. Convection and diffusion adjustments
GROUP 13. Boundary conditions and special sources
  Inlet conditions
  PATCH(INLET,LOW,1,NX,1,NY,1,1,1,1)
  COVAL(INLET,P1,FIXFLU,WIN*RHO1);COVAL(INLET,W1,ONLYMS,WIN)
  COVAL(INLET,KE,ONLYMS,TKEIN);COVAL(INLET,EP,ONLYMS,EPIN)
  Outlet conditions
  PATCH(OUTLET,HIGH,1,NX,1,NY,NZ,NZ,1,1);COVAL(OUTLET,P1,FIXVAL,0.0)
  Ball surface friction
  PATCH(BALL,SWALL,1,NX,1,1,26,73,1,1)
  COVAL(BALL,V1,0.0,0.0)
  COVAL(BALL,W1,GRND2,0.0)
  COVAL(BALL,KE,GRND2,GRND2);COVAL(BALL,EP,GRND2,GRND2)
  Conduit wall surface friction
  PATCH(COND,NWALL,1,NX,NY,NY,1,NZ,1,1)
  COVAL(COND,V1,0.0,0.0)
  COVAL(COND,W1,GRND2,0.0)
  COVAL(COND,KE,GRND2,GRND2);COVAL(COND,EP,GRND2,GRND2)
  ENUL=GRND7,VISL=17 Use Casson, written in 'GROUND'
  GROUP 14. Downstream pressure for PARAB=.TRUE.
  GROUP 15. Termination of sweeps
  LSWEEP=300 Number of iterations
  GROUP 16. Termination of iterations
  GROUP 17. Under-relaxation devices
  RELAX(P1,LINRLX,0.5) Under relaxation terms
  RELAX(V1,FALSDT,0.3)
  RELAX(W1,FALSDT,0.3)
  RELAX(KE,FALSDT,0.3)
  RELAX(EP,FALSDT,0.3)
  GROUP 18. Limit on variables or increments to them
  GROUP 19. Data communicated by satellite to GROUND
  ** If plots are required set PLT = 1
  PLT=0
  RG(1)=RHO1
  RG(2)=MU
  RG(4)=SLOPE
  RG(5)=YIELD
  RG(6)=QIN
  RG(7)=ANGLE
  RG(8)=SUBL
  RG(9)=BLEND
  IG(1)=PLT
  GENK=T activate shear rate generator
  GROUP 20. Preliminary print-out
  GROUP 21. Print-out of variables
  OUTPUT(P1,Y,Y,Y,Y,Y)

```

```
OUTPUT(V2,N,N,N,N,N,N)
OUTPUT(W2,N,N,N,N,N,N)
OUTPUT(VCRT,N,N,N,N,N,N)
OUTPUT(WCRT,N,N,N,N,N,N)
INIFLD=F.
```

} *output to results file*

GROUP 22. Spot-value print-out

```
TSTSWP=1
NPRINT=LSWEEP
IPLTL=LSWEEP
IXMON=1;IYMON=1;IZMON=71
```

GROUP 23. Field print-out and plot control

```
NXPRIN=NX,NYPRIN=NY,NZPRIN=NZ
NPLT=1
NCOLCO=70
NUMCLS=7
```

GROUP 24. Dumps for restarts

```
NSAVE=B21
NOWIPE=T.
```

*file for tokenised results  
values default as above*

```
AUTOPS=T.
RESTRT(ALL)
```

*re-start from previous run*

```
STOP
NAMFI=B21
```

*start of second run*

```
FIINIT(P1)=READFI
FIINIT(V1)=READFI
FIINIT(W1)=READFI
FIINIT(ENUL)=READFI
FIINIT(KE)=READFI
FIINIT(EP)=READFI
FIINIT(ENUT)=READFI
```

```
LSWEEP=5
IG(1)=1
```

*send data to plot files*

```
NXPRIN=NX,NYPRIN=1,NZPRIN=1
```

```
RESTRT(ALL)
```

```
STOP
```

APPENDIX FOUR

STATISTICAL ANALYSIS OF RADIAL SHEAR  
STRESS VARIATION FOR TURBULENT PIPE FLOW

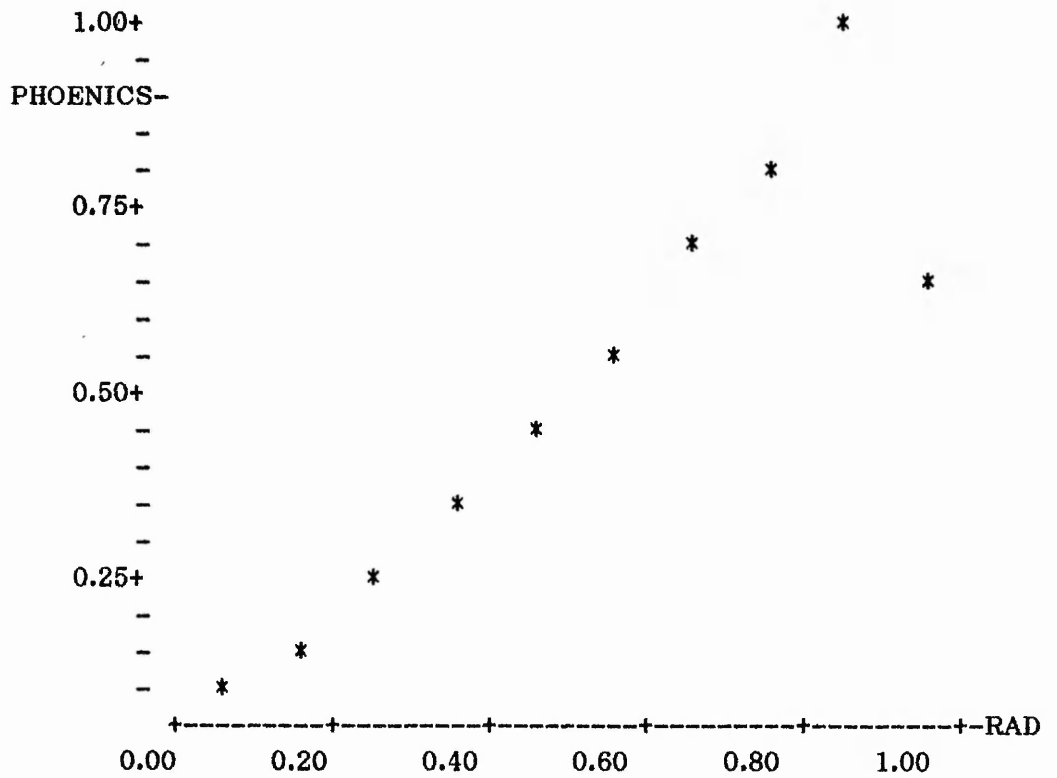
#### A4.1 Statistical Analysis of Radial Shear Stress

The Minitab statistical package was used to analyse the shear stress profile across a radial section, in turbulent pipe flow predicted by PHOENICS. This relationship was compared with experimental results presented by Laufer (1954). Pipe diameter was 20mm. The final analysis shows a very high correlation between PHOENICS and Laufer.

#### A4.2 Table of Data

PHOENICS	LAUFER	RADIUS
0.65764	1.02163	0.95
0.98576	0.90585	0.85
0.80790	0.78379	0.75
0.68390	0.67386	0.65
0.57146	0.56778	0.55
0.46415	0.46540	0.45
0.35961	0.35978	0.35
0.25656	0.25667	0.25
0.15408	0.15387	0.15
0.12087	0.05254	0.05

**A4.3 Plot of PHOENICS Non-dimensionalised Shear Stress Versus Normalised Radius**



**A4.4 Regression of PHOENICS Shear Stress against Normalised Radius**

The regression equation is  
 $PHOENICS = 0.0671 + 0.878 RAD$

Predictor	Coef	Stdev	t-ratio
Constant	0.06712	0.07155	0.94
RAD	0.8782	0.1241	7.08

$s = 0.1127$        $R-sq = 86.2\%$        $R-sq(adj) = 84.5\%$

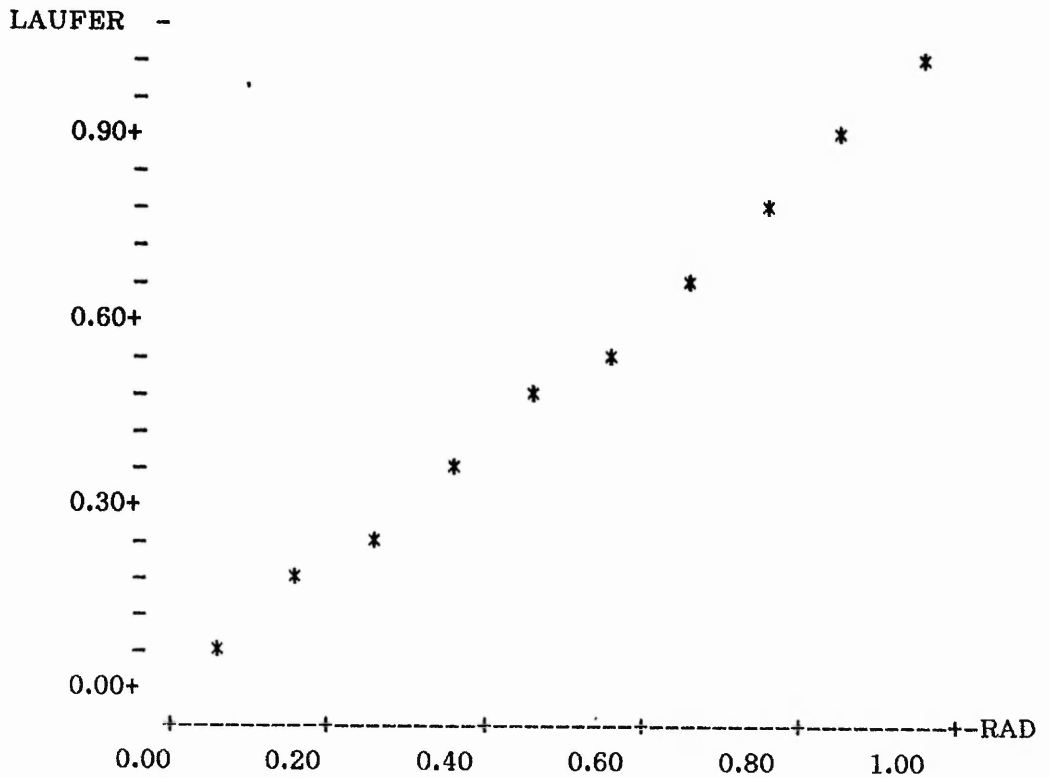
Analysis of Variance

SOURCE	DF	SS	MS
Regression	1	0.63620	0.63620
Error	8	0.10161	0.01270
Total	9	0.73782	

Obs.	RAD	PHOENICS	Fit	Stdev.Fit	Residual	St.Resid
1	0.950	0.6576	0.9014	0.0662	-0.2437	-2.67R
2	0.850	0.9858	0.8135	0.0562	0.1722	1.76
3	0.750	0.8079	0.7257	0.0472	0.0822	0.80
4	0.650	0.6839	0.6379	0.0402	0.0460	0.44
5	0.550	0.5715	0.5501	0.0362	0.0214	0.20
6	0.450	0.4642	0.4623	0.0362	0.0019	0.02
7	0.350	0.3596	0.3745	0.0402	-0.0149	-0.14
8	0.250	0.2566	0.2867	0.0472	-0.0301	-0.29
9	0.150	0.1541	0.1988	0.0562	-0.0448	-0.46
0	0.050	0.1209	0.1110	0.0662	0.0098	0.11

R denotes an obs. with a large st. resid.

A4.5 Plot of Laufer's Non-dimensionalised Shear Stress against .Normalised Radius



#### A4.6 Regression of Laufer's Shear Stress against Normalised Radius

The regression equation is

$$\text{LAUFER} = -0.0112 + 1.07 \text{ RAD}$$

Predictor	Coef	Stdev	t-ratio
Constant	-0.011213	0.006108	-1.84
RAD	1.07066	0.01059	101.07

s = 0.009622      R-sq = 99.9%      R-sq(adj) = 99.9%

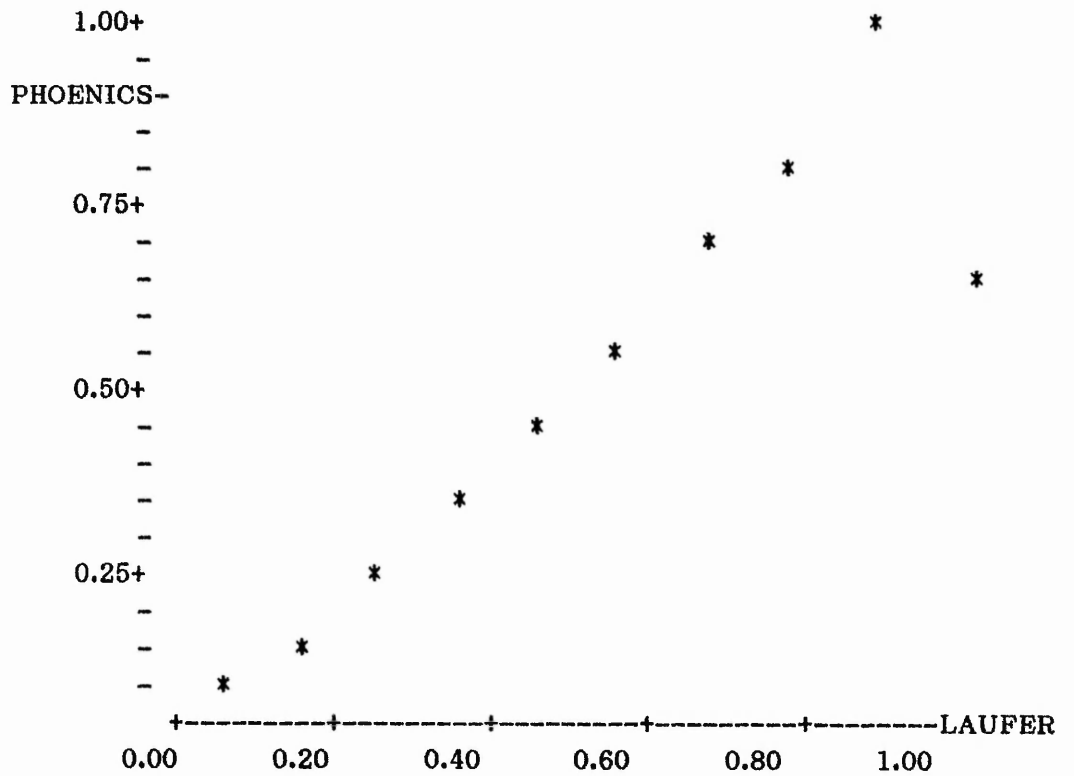
#### Analysis of Variance

SOURCE	DF	SS	MS
Regression	1	0.94571	0.94571
Error	8	0.00074	0.00009
Total	9	0.94645	

Obs.	RAD	LAUFER	Fit	Stdev.Fit	Residual	St.Resid
1	0.950	1.02163	1.00591	0.00566	0.01572	2.02R
2	0.850	0.90585	0.89885	0.00480	0.00700	0.84
3	0.750	0.78379	0.79178	0.00403	-0.00799	-0.91
4	0.650	0.67386	0.68472	0.00343	-0.01086	-1.21
5	0.550	0.56778	0.57765	0.00309	-0.00987	-1.08
6	0.450	0.46540	0.47058	0.00309	-0.00518	-0.57
7	0.350	0.35978	0.36352	0.00343	-0.00374	-0.42
8	0.250	0.25667	0.25645	0.00403	0.00022	0.02
9	0.150	0.15387	0.14939	0.00480	0.00448	0.54
10	0.050	0.05254	0.04232	0.00566	0.01022	1.31

R denotes an obs. with a large st. resid.

A4.7 Plot of Shear Stress: PHOENICS Versus Laufer



A4.8 Regression of PHOENICS Versus Laufer's Shear Stresses

The regression equation is  

$$\text{PHOENICS} = 0.0789 + 0.815 \text{ LAUFER}$$

Predictor	Coef	Stdev	t-ratio
Constant	0.07889	0.07283	1.08
LAUFER	0.8153	0.1198	6.80

$s = 0.1166$        $R\text{-sq} = 85.3\%$        $R\text{-sq}(\text{adj}) = 83.4\%$

Analysis of Variance

SOURCE	DF	SS	MS
Regression	1	0.62908	0.62908
Error	8	0.10873	0.01359
Total	9	0.73782	

Obs.	LAUFER	PHOENICS	Fit	Stdev.Fit	Residual	St.Resid
1	1.02	0.6576	0.9118	0.0701	-0.2542	-2.73R
2	0.91	0.9858	0.8174	0.0588	0.1683	1.67
3	0.78	0.8079	0.7179	0.0482	0.0900	0.85
4	0.67	0.6839	0.6283	0.0410	0.0556	0.51
5	0.57	0.5715	0.5418	0.0372	0.0297	0.27
6	0.47	0.4642	0.4583	0.0375	-0.0058	0.05
7	0.36	0.3596	0.3722	0.0418	-0.0126	-0.12
8	0.26	0.2566	0.2881	0.0489	-0.0316	-0.30
9	0.15	0.1541	0.2043	0.0577	-0.0503	-0.50
10	0.05	0.1209	0.1217	0.0675	-0.0009	-0.01

R denotes an obs. with a large st. resid.

APPENDIX FIVE

GORLIN - GORLIN ANALYSIS APPLIED TO THE LRRSICO CONDUIT

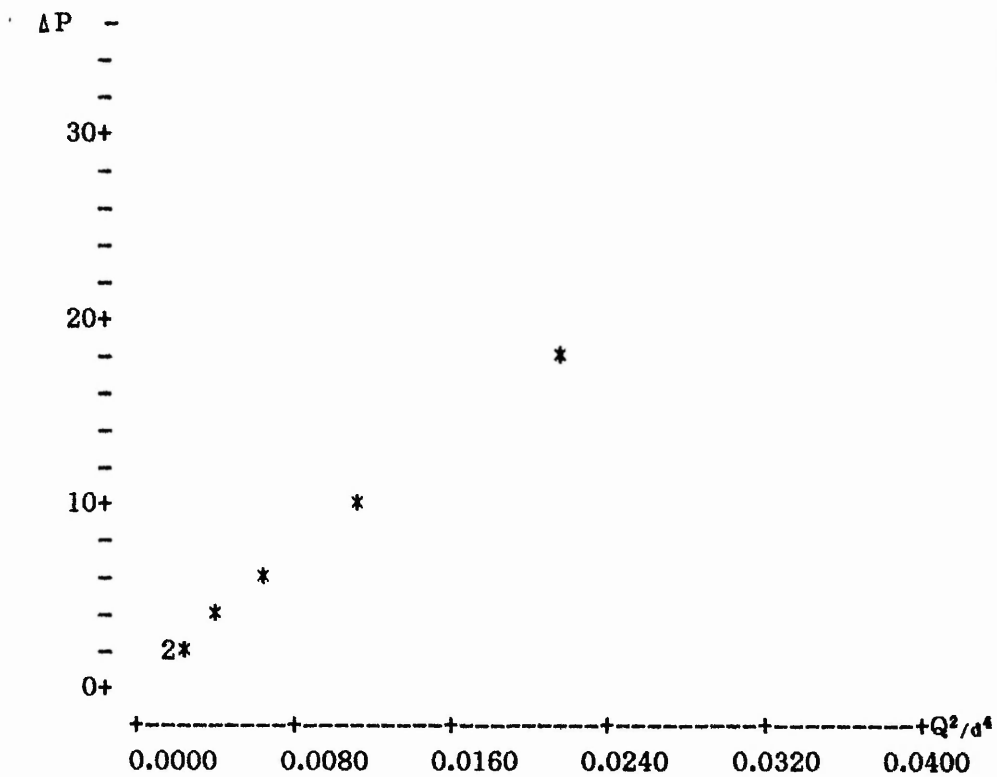
### A5.1 Statistical Analysis

The Minitab statistical package was used to analyse the relationship between values of pressure gradient (mmHg) and flow rate/unit area ( $\text{P}/\text{min}^2 \text{mm}^4$ ) predicted by PHOENICS. This analysis was carried out for two test series; the first held the size of conduit constant, at 16mm diameter, whilst varying the flow rate of blood through the conduit, the second test series maintained a constant blood flow rate of 21.1l/min through varying valve sizes. The regression constants are used to classify haemodynamic performance of the conduit.

### A5.2 Table of Data For Pressure gradient Versus Flow Rate/Unit Area: Varying Valve Size for 21.1l/min Flow Rate

ROW	$\Delta P$	$Q^2/d^4$
1	34.4478	0.0445210
2	17.4419	0.0214704
3	9.8351	0.0115892
4	6.0002	0.0067934
5	3.8873	0.0042411
6	2.6427	0.0027826
7	1.8167	0.0019005
8	1.2872	0.0013419

**A5.3 Plot of pressure Gradient Versus Flow Rate/Unit Area for a constant 21.1 l/min Flow through Varying Valve Size**



**A5.4 Regression of Pressure gradient Versus Flow Rate/Unit Area For Varying Conduit Size and 21.1/min Flow Rate**

The regression equation is

$$\Delta P = 0.602 + 767 Q^2/d^4$$

Predictor	Coef	Stdev	t-ratio
Constant	0.6015	0.1433	4.20
Q <sup>2</sup> /d <sup>4</sup>	766.553	7.866	97.45

s = 0.3082      R-sq = 99.9%      R-sq(adj) = 99.9%

**Analysis of Variance**

SOURCE	DF	SS	MS
Regression	1	902.03	902.03
Error	6	0.57	0.09
Total	7	902.60	

Obs.	Q <sup>2</sup> /d <sup>4</sup>	ΔP	Fit	Stdev.Fit	Residual	St.Resid
1	0.0445	34.448	34.729	0.279	-0.281	-2.16RX
2	0.0215	17.442	17.060	0.133	0.382	1.37
3	0.0116	9.835	9.485	0.109	0.350	1.21
4	0.0068	6.000	5.809	0.116	0.191	0.67
5	0.0042	3.887	3.853	0.124	0.035	0.12
6	0.0028	2.643	2.735	0.130	-0.092	-0.33
7	0.0019	1.817	2.058	0.134	-0.242	-0.87
8	0.0013	1.287	1.630	0.137	-0.343	-1.24

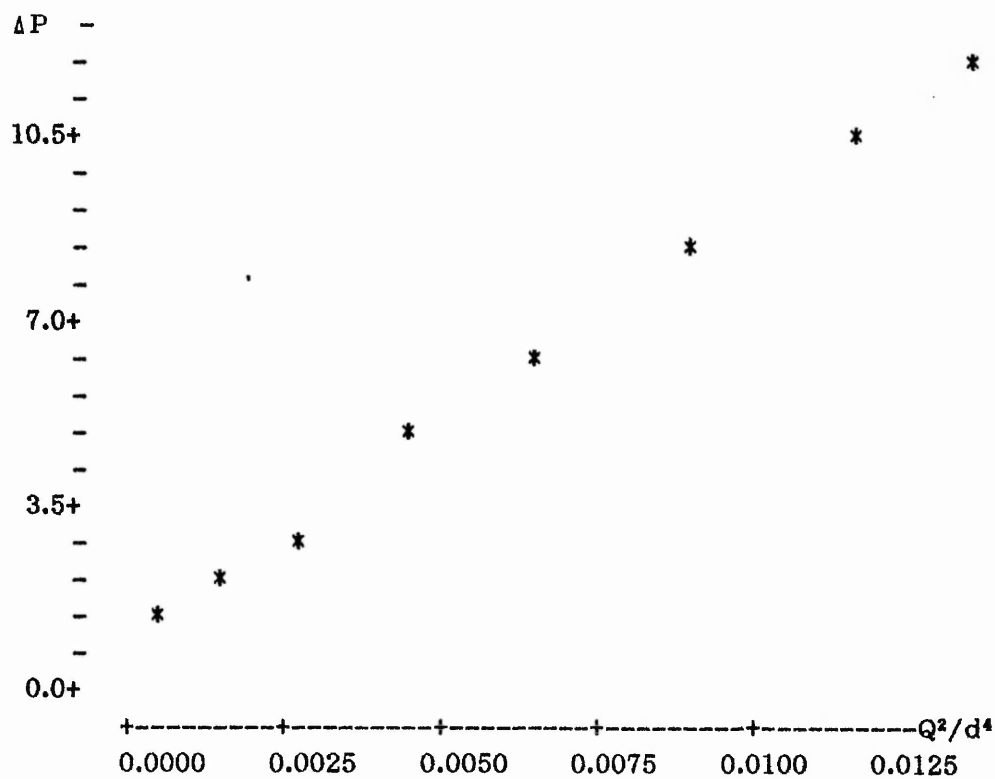
R denotes an obs. with a large st. resid.

X denotes an obs. whose X value gives it large influence.

A5.5 Table of Data for Pressure Gradient Versus Flow Rate/Unit Area for Varying Flow rates in 16mm Conduit

ROW	$\Delta P$	$Q^2/d^4$
1	1.1614	0.0007470
2	1.9056	0.0017197
3	3.0416	0.0030398
4	4.5541	0.0047335
5	6.2413	0.0068008
6	8.1599	0.0092415
7	10.3032	0.0120558
8	11.5791	0.0137684

A5.6 Plot of Pressure Gradient Versus Flow Rate/Unit Area for Varying Flow rates in 16mm Conduit



**A5.7 Regression of Pressure Gradient Versus Flow Rate/Unit Area for Varying Flow rates in 16mm Conduit**

The regression equation is  
 $\Delta P = 0.626 + 805 Q^2/d^4$

Predictor	Coef	Stdev	t-ratio
Constant	0.62585	0.07025	8.91
$Q^2/d^4$	804.879	8.870	90.74

$s = 0.1130$        $R\text{-sq} = 99.9\%$        $R\text{-sq(adj)} = 99.9\%$

**Analysis of Variance**

SOURCE	DF	SS	MS
Regression	1	105.17	105.17
Error	6	0.08	0.01
Total	7	105.25	

Obs.	$Q^2/d^4$	$\Delta P$	Fit	Stdev.Fit	Residual	St.Resid
1	0.0007	1.1614	1.2271	0.0649	-0.0657	-0.71
2	0.0017	1.9056	2.0100	0.0583	-0.1044	-1.08
3	0.0030	3.0416	3.0725	0.0505	-0.0309	-0.31
4	0.0047	4.5541	4.4357	0.0430	0.1184	1.13
5	0.0068	6.2413	6.0997	0.0400	0.1416	1.34
6	0.0092	8.1599	8.0641	0.0467	0.0958	0.93
7	0.0121	10.3032	10.3293	0.0634	-0.0261	-0.28
8	0.0138	11.5791	11.7077	0.0758	-0.1286	-1.53

APPENDIX SIX

ALTERATIONS TO 'GROUND' AND 'GREX1' CODING

**A6.1 Changes to GROUND Fortran Coding to Incorporate Constitutive Equation**

```
C      INCREASE STORAGE SIZE
C
      COMMON F(800000)
      NFDIM=800000
C
C      OUTPUT CODE GENERATION NAME
C
      CALL WRIT40('GROUND STATION IS TURBULENT.GRND JULY 87 ')
C
C      SET DUMMY PARAMETERS AND ASSIGN VARIABLES
C
      PARAMETER(MY=70,MX=3)
      DIMENSION GENUL(MY,MX),GENUT(MY,MX),GAMMA(MY,MX)
      DIMENSION GTAUL(MY,MX),GTAUT(MY,MX),GTTAU(MY,MX)
      DIMENSION GP1(MY,MX), GDWDY(MY,MX), GSAREA(MY,MX)
      DIMENSION GA(3), GB(3), GC(3), GFT(150), GKE(MY,MX)
      DIMENSION GYPLUS(MY,MX), GYWC(MY,MX), GNYP(MY,MX)
      REAL GRHO1,GMU,GSLOPE,GYIELD,GQIN,TOTP1,TOTP2,GDP,GFP
      REAL GFS, GTHETA, GANGLE, GFTSUM, GZG, GSUBL, GBLEND
      INTEGER OPN, GPLT, WRT, SWRT
      EQUIVALENCE(GRHO1,RG(1))
      EQUIVALENCE(GMU,RG(2))
      EQUIVALENCE(GSLOPE,RG(4))
      EQUIVALENCE(GYIELD,RG(5))
      EQUIVALENCE(GQIN,RG(6))
      EQUIVALENCE(GANGLE,RG(7))
      EQUIVALENCE(GSUBL,RG(8))
      EQUIVALENCE(GBLEND,RG(9))
      EQUIVALENCE(GPLT,IG(1))

      DATA OPN,WRT,TOTP1,TOTP2,SWRT/0,0,0.0,0.0,0/
      DATA GFP,GFS,GFTSUM/0.0,0.0,0.0/
C
C      ASSIGN INTERNAL VARIABLE STORAGE
C
      CALL MAKE(EASP1)
      CALL MAKE(EASP6)
      CALL MAKE(ZGNZ)
C
C      OPEN FILES FOR PLOT DATA IF PLOTTED FLAG IS NOT SET
C      AND IF PLOTS ARE CALLED FOR. THEN SET FLAG
```

C

```
IF (GPLT.NE.1) GOTO 112
TYPE *,'PLT = 1    => PLOTS CALLED FOR'
IF(OPN.NE.0) GOTO 112
OPEN(UNIT=30,STATUS='UNKNOWN',FILE='CENTAU.PA4',
1ACCESS='APPEND')
OPEN(UNIT=31,STATUS='UNKNOWN',FILE='WALLTAU.PA4',
2ACCESS='APPEND')
OPEN(UNIT=32,STATUS='UNKNOWN',FILE='CENGAMA.PA4',
3ACCESS='APPEND')
OPEN(UNIT=33,STATUS='UNKNOWN',FILE='WALLGAMA.PA4',
4ACCESS='APPEND')
OPEN(UNIT=34,STATUS='UNKNOWN',FILE='CENP1.PA4',
5ACCESS='APPEND')
OPEN(UNIT=35,STATUS='UNKNOWN',FILE='DPDQ.PA4',
6ACCESS='APPEND')
OPEN(UNIT=36,STATUS='UNKNOWN',FILE='DFDQ.PA4',
7ACCESS='APPEND')
OPEN(UNIT=37,STATUS='UNKNOWN',FILE='CENF.PA4',
8ACCESS='APPEND')
OPEN(UNIT=39,STATUS='UNKNOWN',FILE='CENYPLUS.PA4',
9ACCESS='APPEND')
OPEN(UNIT=40,STATUS='UNKNOWN',FILE='WALLYPLUS.PA4',
1ACCESS='APPEND')
OPN=1
GOTO 113
112 TYPE *,'PLT = 0    => NOT CREATING PLOT FILES'
113 CONTINUE
```

C

C

RETRIEVE VISCOSITIES, SHEAR RATE AND TURBULENCE PROPERTIES

C

```
CALL GETYX(VIST,GENUT,MY,MX)
CALL GETYX(VISL,GENUL,MY,MX)
CALL GETYX(EASP1,GAMMA,MY,MX)
CALL GETYX(KE,GKE,MY,MX)
CALL GETYX(EASP6,GDWDY,MY,MX)
```

C

C

CHECK CALL FOR NOWTONIAN OR NON-NEWTONIAN FLUID  
AND CALCULATE VISCOSITY AND SHERA STRESSES

C

C

```
DO 961 IX=1,NX
DO 961 IY=1,NY
GAMMA(IY,IX)=GAMMA(IY,IX)**.5
GTAUT(IY,IX)=GAMMA(IY,IX)*GENUT(IY,IX)*GRHO1
IF(ENUL.EQ.GRND7) GOTO 9611
IF(ENUL.EQ.GRND5) GOTO 9612
```

```

9611  GTAUL(IY,IX)=((GSLOPE*GAMMA(IY,IX)**.5)+GYIELD**.5)**2
C     TYPE *,'GAMMA=',GAMMA(IY,IX),'GTAUL=',GTAUL(IY,IX)
      GOTO 9613
9612  GTAUL(IY,IX)=GMU*GAMMA(IY,IX)
9613  GENUL(IY,IX)=GTAUL(IY,IX)/(GRHO1*GAMMA(IY,IX))
      GTTAU(IY,IX)=GTAUL(IY,IX)+GTAUT(IY,IX)
C
C     CALCULATE Y PLUS VALUES
C
      CALL GTIZYX(13,IZ,GYWC,1,IX)
      GYPLUS(1,IX)=GKE(1,IX)**0.5*0.54772*GYWC(1,IX)/GENUL(1,IX)
      GNYP(1,IX)=2*50*GENUL(1,IX)/(GKE(1,IX)**.5*0.54772)
      GYPLUS(NY,IX)=GKE(NY,IX)**0.5*0.54772*GYWC(NY,IX)/GENUL(NY,IX)
      GNYP(NY,IX)=2*50*GENUL(NY,IX)/(GKE(NY,IX)**.5*0.54772)
961  CONTINUE
C
C     SET CALCULATED VALUES BACK INTO THE SOLVER
C
      CALL SETYX(AUX(VISL),GENUL,MY,MX)
      CALL SETYX(C4,GAMMA,MY,MX)
      CALL SETYX(C5,GTAUL,MY,MX)
      CALL SETYX(C6,GTAUT,MY,MX)
      CALL SETYX(C7,GTTAU,MY,MX)
C
C     TO OUTPUT DATA TO PA4 FILES FOR PLOTTING:
C     SET UP HEADERS
C
      IF(GPLT.NE.1) GOTO 19699
      CALL GETYX(P1,GP1,MY,MX)
      IF(ISWEEP.NE.LSWEEP-1) GOTO 19699
      IF(WRT.NE.0) GOTO 19621
      WRITE(30,19611) GQIN,NZ
      WRITE(31,19611) GQIN,NZ
      WRITE(32,19611) GQIN,NZ
      WRITE(33,19611) GQIN,NZ
      WRITE(34,19611) GQIN,NZ
      WRITE(37,19611) GQIN,NZ
      WRITE(39,19611) GQIN,NZ
      WRITE(40,19611) GQIN,NZ
      WRT=1
19611  FORMAT(F8.4,' Rad blend*',/, 'X,1,1',/,I3)
19621  CONTINUE
19622  FORMAT(1X,E12.5,2X,E12.5)
19623  FORMAT(1X,F9.5,2X,F10.5)
19628  FORMAT(1X,F9.5,2X,E12.5)
C

```

```

C      CALCULATE GEOMETRICAL POSITIONS OF CELL CENTRES
C
      CALL GETPT(1,1,IZ,GA(1),GA(2),GA(3))
      CALL GETPT(1,1,IZ+1,GB(1),GB(2),GB(3))
      CALL SUB(GB,GA,GC)
      GZG=(GC(3)/2)+GA(3)
C
C      WRITE SHEAR COMPONENTS, Y PLUS AND PRESSURE TO PLOT FILES
C
      WRITE(30,19622)GZG,GTTAU(1,1)
      WRITE(31,19622)GZG,GTTAU(NY,1)
      WRITE(32,19622)GZG,GAMMA(1,1)
      WRITE(33,19622)GZG,GAMMA(NY,1)
      WRITE(34,19622)GZG,GP1(1,1)
      WRITE(40,9619) IZ, GYPLUS(NY,1)
9619  FORMAT(1X,I3,3X,F10.6)
C
C      CALCULATE AREAS, LOCATE OCCLUDER AND CALCULATE FORCE
C      ON THE OCCLUDER AND SEND TO PLOT FILES
C
      IF(ABS(GC(2)).GT.0) GOTO 19624
      GOTO 19625
19624  CALL GTIZYX(8,IZ,GSAREA,MY,MX)
      WRITE(39,9619) IZ, GYPLUS(1,1)
      GSAREA(1,1)=GSAREA(1,1)*360/GANGLE
      GTHETA=ATAN(GC(2)/GC(3))
      GFS=(1*GDWDY(1,1)*(GENUL(1,1)+GENUT(1,1))*GRHO1*
      1GSAREA(1,1))*COS(GTHETA)
      GFP=(3.1415926*GP1(1,1)*(GB(2)**2-GA(2)**2))
      GFT(IZ)=GFP+GFS
      WRITE(37,19622)GZG,GFT(IZ)
      GFTSUM=GFTSUM+GFT(IZ)
19625  CONTINUE
      IF(IZ.EQ.NZ-1) WRITE(36,19628) GQIN, GFTSUM
      IF(IZ.NE.1) GOTO 19626
      DO 19626 IY=1,NY
      TOTP1=TOTP1+GP1(IY,1)
19626  CONTINUE
      IF(IZ.NE.NZ) GOTO 19627
      DO 19627 IY=1,NY
      TOTP2=TOTP2+GP1(IY,1)
19627  CONTINUE
      GDP=(TOTP1-TOTP2)/NY
      IF(SWRT.NE.0) GOTO 19630
      WRITE(35,19623) GQIN, GDP
      SWRT=1

```

19630 CONTINUE  
19699 CONTINUE  
RETURN

## A6.2 Changes to GREX1.FOR Coding

Grexl.for was altered to account for full generation term, 2-dimensionally as below, or 3-dimensionally if the comment fields are activated.

```
COMMON/LGE1/L1(25)
LOGICAL L1
LOGICAL STORE,SOLVE,PRINT
C   CALL FN33(IN(103),1E-20)
   CALL GETCAR
   DO 19410 NN=1,NPHI
C   IF(NAME(NN).EQ.'UCRT') IUCRT=NN
   IF(NAME(NN).EQ.'VCRT') IVCRT=NN
   IF(NAME(NN).EQ.'WCRT') IWCRT=NN
   19410 CONTINUE
C   CALL FN0(U2,IUCRT)
   CALL FN0(V2,IVCRT)
   CALL FN0(W2,IWCRT)
C   L1(U2)=T
   L1(V2)=T
   L1(W2)=T
   CALL FNGENK(EASP1,2)
   CALL FNDWDY(EASP6,W2)
C   L1(U2)=F
   L1(V2)=F
   L1(W2)=F
   CALL GETCAR
```

**APPENDIX SEVEN**

**PUBLISHED PAPERS AND PRESENTATIONS**

#### A7.1 Papers Published in Chronological Order

Tansley, G.D., Edwards, R.J., Leefe, S.E. and Gentle, C.R. 1986. Ball occluder instability during forward flow through prosthetic heart valve conduits. In: *Proceedings of XIII Annual meeting of the European Society for Artificial Organs Life Support Systems*, 4 suppl. 2, 169-171

Leefe, S.E., Edwards, R.J., Tansley, G.D. and Gentle, C.R. 1986. Investigation into leakage design in prosthetic heart valves. In: *Proceedings of the 26th. Annual Meeting of the Biological Engineering Society*, Glasgow

Leefe, S.L., Tansley, G.D. and Gentle, C.R. 1986. Pulsatile flow testing of prosthetic heart valve conduits. In: *Heart Valve Engineering*, Mechanical Engineering Press, London, 15-19

Tansley, G.D., Edwards, R.E. and Gentle, C.R. 1988. The role of computational fluid mechanics in the analysis of prosthetic heart valve flow. *Accepted for publication in Medical and Biological Engineering and Computing*

#### A7.2 Presented - unpublished

Tansley, G.D. 1987. The prediction of haemodynamic characteristics of prosthetic heart valve flow using PHOENICS. *Presented at the PHOENICS users meeting, Queens College, Oxford, UK*

# BALL OCCLUDER INSTABILITY DURING FORWARD FLOW THROUGH PROSTHETIC HEART VALVE CONDUITS

G.D. Tansley, R.J. Edwards, S.E. Leefe, C.R. Gentle

Department of Mechanical Engineering, Trent Polytechnic, Nottingham, UK

Preliminary tests on a ball occluder heart valve conduit (1,2) have highlighted a potentially problematic design area. The valve consists of a conical inlet section against which the ball seats during the reverse pressure phase and a downstream tapered section with three rigid struts which restrain the occluder during forward flow. However, axial oscillation of the ball was noted at all but the very lowest forward flow rates. This is in keeping with the findings of other researchers (3,4,5). Streak photography has revealed that this was not the result of vortex shedding. Further investigation by Benjamin (2) has suggested that the cause was an increase in flow area immediately downstream of the ball centre where there is a transition from annular flow around the ball to pipe flow down the exit section, producing a decrease in velocity and a rise in pressure sufficient to cause a resultant backwards force on the ball, lifting it clear of the struts and towards the inlet section. This would cause a back-pressure which, in turn, would force the ball downstream again for the cycle to repeat itself. An "order of magnitude" calculation using Bernoulli's equation revealed that a sufficient pressure rise was indeed produced. A new outlet section was designed to provide constant flow area with the ball in the fully open position and was found to have cured ball vibration. In addition, a numerical simulation of flow through the improved conduit was developed and checked against the prototype by comparing predicted and measured overall pressure drops. This model confirmed the absence of a net upstream force on the ball in the fully open position.

## Methods

Based on the considerations outlined above, a further prototype was developed, manufactured and tested. The aim was to maintain a constant flow area around the downstream side of the ball. Since the "flow area" means that part of a given cross-section "seen by" the flow or alternatively the area of the surface which is everywhere normal to the velocity but whose outer edge defines the cross-section, it should be apparent that to keep this quantity constant required a prior knowledge of the velocity field that the new profiled downstream section would produce. Since this could not be attained, calculation had to proceed on conservatively assumed velocity directions. The flow area was defined as normal to the ball surface (hence conical in form) and the velocity taken as everywhere normal to the flow area. Referring to figure 1, it can be seen that flow area was given by

$$A = \int_{R_b}^{R_o} 2 \pi r \sin \theta \, dr$$

and hence

$$R_o = \sqrt{A/(\pi \sin \theta) + R_b^2}$$

where A is kept constant and equal to the area of the inlet pipe. The locus of  $R_o$  fixed the downstream conduit profile until it intersected with the cylindrical outflow pipe. An estimate was made of the error of the "constant flow area" assumption by taking a revised assessment of the flow direction as being everywhere parallel to the bisector of the angle between the tangents to the ball and the conduit inner surface (i.e. the flow was somewhere between tangential to the ball and tangential to the conduit surface). The

assumed flow area was thus determined to be no worse than 1.2% in error and was such as to produce a reduced area, resulting in slightly lower pressure and hence further counteracting the cause of the problem. A prototype was manufactured and tested under steady flow conditions using water. It was also decided to provide pressure tapings the same distances upstream and downstream of the inlet section as for the original design in order to investigate the effect of the modification on pressure drop characteristics.

The new design was also modelled mathematically using the "Phoenix" finite difference procedure running on a Vax 11/785 mainframe computer. This was for two reasons. Firstly, a check was required that the pressure distribution was no longer such as to produce a net backwards force. Secondly, if the pressure drop predicted by "Phoenix" for a given flow rate agreed with that determined experimentally for the conduit, then one could simply run the program to test subsequent design modifications without the necessity of building a prototype for each, until the design was finalised. A three-dimensional grid was fitted to the conduit dimensions. Figure 2 illustrates a typical diametral half-plane. The restraining struts were omitted for ease of modelling, whilst the ball was specified as fixed in space at the fully open position. A uniform inlet velocity of 0.625 m/s was specified, corresponding to a volumetric flowrate of 7.54 l/min and a Reynolds number based on conduit inner diameter of 10 000, which was within the test range. Accordingly, a turbulent solution was produced. A long inlet section was specified to allow for the development of a reasonable velocity profile. Fluid properties were taken as those of water since the instability problem was observed during tests in water. A downstream pressure of zero was specified so that the pressure drop across the valve could be read directly as the pressure at the valve entry section. The output file contained a list of pressures and two velocity components, axial and radial, for each grid cell of a diametral half-plane. Circumferential velocity was not required since the flow was assumed axi-symmetric. A program was written to calculate the net pressure and shear forces on the ball from the pressure and velocity distributions around it. Clearly, the resultant ball force was the sum of the two.

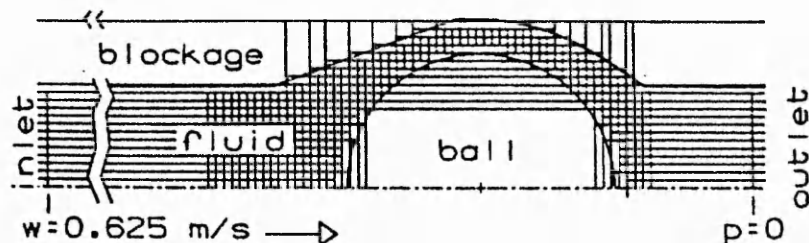


Figure 2

### Results

Tests of the improved prototype over the entire range of flowrates to which the original was subjected and found to be unstable showed that there was no tendency for the ball occluder to oscillate nor lift off the restraining struts. Figure 3 shows the pressure drop measurements for the two valves.

### Discussion

The primary object of the investigation was to establish the cause of ball occluder instability and to effect its cure. Clearly this has been achieved. However, the pressure drop experiments have indicated that the re-profiled downstream section has resulted in a reduction in forward flow efficiency of

the valve. The cause could well be separation at the abrupt direction change where the outflow pipe meets the valve body. Clearly, this can be prevented by further streamlining - either a blending radius or a small Venturi throat. Further scope for improvement is offered by the incorporation of a similar design procedure for the inlet section, based on maintaining a constant flow area around the upstream side of the fully-open ball, improving the streamlining here and thus reducing separation losses and ensuring that a sensibly predictable pressure pattern is maintained throughout. Closing function would not be jeopardised since backward displacement of the ball would immediately result in the reduction of the upstream flow area causing increased velocity and decreased pressure upstream, thus assisting closure.

Whilst the foregoing is encouraging for the conduit designer, unfortunately it is of little comfort to the manufacturer of prosthetic heart valves for straightforward replacement operations, since here there is no scope for profiling the heart or the major vessels. Indeed, the aortic root would seem to be a case in point, where flow between the orifice and occluder is at high velocity which drops downstream where flow is into the sinuses of Valsalva, which constitute a significant enlargement.

### Conclusion

It has been demonstrated that the problem of instability is closely connected with pressure distribution around the occluder and that the designer can successfully guard against this by careful selection of the conduit profile surrounding the occluder. However, there remains a potential problem with the use of caged-occluder type prostheses for straightforward valve replacement, where the downstream area cannot be shaped.

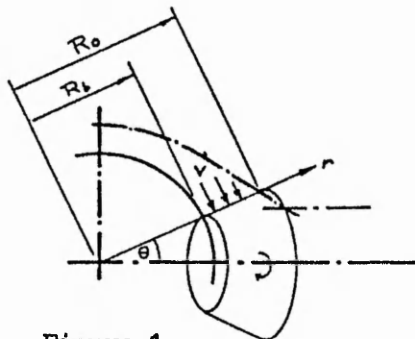


Figure 1

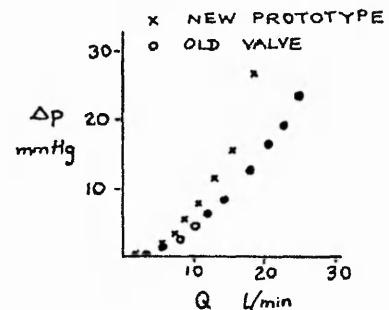


Figure 3

### References

1. Gentle, C.R. (1983) Minimization of pressure drop across heart valve conduits: a preliminary study. Life Support Systems, 1, 263.
2. Benjamin, E.L. (Unpublished) Steady flow investigations of valved heart conduits. MSc Thesis, Trent Polytechnic, Nottingham, pp51-52,72-88.
3. Uglov, F.G. et al (1978) Distribution of pressure on the surface of the closing elements of artificial heart valves. Biomedical Engineering, 12, 61.
4. Uglov, F.G. et al (1984) Investigation of self-induced vibrations of the ball closing an artificial aortic valve. Biomedical Engineering, 18, 45.
5. Viggers, R.F., Robel, S.B. and Sauvage, L.R. (1967) A hydraulic figure of merit for heart valve prostheses. Journal of Biomedical Materials Research, 1, 103.

### Address for reprints

Dr. C.R. Gentle, Department of Mechanical Engineering, Trent Polytechnic, Burton Street, Nottingham NG1 4BU, UK

TITLE: INVESTIGATION INTO LEAKAGE DESIGN IN PROSTHETIC HEART VALVES

ABBREVIATED TITLE: Valve leakage flow

AUTHORS: S.E. LEEFE, R.J. EDWARDS, G.D. TANSLEY, C.R. GENTLE

## ABSTRACT

The design of pivoting or tilting occluder prosthetic heart valves deliberately incorporates a degree of leakage in the "shut" position in order to effect a washing action, thus preventing clot formation. It has been suggested that experimentally determined relationships between friction factor and Reynolds number for leakage flow demonstrate turbulence and that this could represent a means of improving the washing action.

This paper presents a physical argument augmented by numerical simulation using the "Phoenix" finite difference code to offer an alternative explanation for the form of the friction factor versus Reynolds number curve. Some shortcomings of designing for a turbulent leakage flow are highlighted and guidelines are recommended on the suitable choice of leakage gap dimensions.

## INTRODUCTION

The design of pivoting or tilting occluder prosthetic heart valves has, over recent years, deliberately incorporated a degree of leakage flow in the "closed" position. This is intended to inhibit thrombus formation both by preventing the blood from becoming stagnant and, principally, by forcing a high pressure jet through the leakage gap, thus effecting a scouring action.

Leakage flow has been studied by Rief et al (1980) and Gentle (1982), with a view, in each case, to demonstrating the superior characteristics of one valve over another, although the criteria for comparison differ. Rief et al were apparently seeking to minimise leakage, whilst Gentle was concerned with characterising the flow regime on the grounds that turbulent leakage flow would produce a more effective washing action than laminar. Both studies presented experimental data in terms of pressure drop versus flow rate and both used the gradient of a logarithmic plot of friction factor versus Reynolds number to draw conclusions as to the nature of the flow, by comparison with the expected values for fully-developed pipe flow. It is apparent, however, that there was poor quantitative agreement between such predicted curves and the experimental data. Rief et al seemed aware of this point and offered a plausible explanation in terms of the irregular pattern of leakage flow. Indeed, Parsons (1982) presented a similar explanation for his findings on the Bjork-Shiley valve's leakage behaviour, which could go some way towards accounting for Gentle's results with this valve.

All of the valves studied produced curves whose gradients were less than predicted and one had a measured friction factor an order of magnitude larger than expected. The explanation offered, namely that the high friction factor was caused by surface roughness, is questionable when considering the curves for fully turbulent flow in rough pipes. These ambiguities are clearly apparent when experimental data are superimposed on the Moody chart, figure 1.

Since the data for Gentle's twin-flap valve shows the furthest departure from theoretical predictions, and since no other plausible explanation for this discrepancy has been offered elsewhere, this paper will concern itself only with this valve. Its purpose is to offer an alternative explanation for the form of the non-dimensional plots of experimental data. This explanation, in turn, calls into question the idea of designing for turbulent leakage and suggests a basis for the rational selection of leakage gap dimensions. The work also forms part of the development programme for an all-ceramic twin-flap mitral valve (Gentle, 1980, Gentle, Arundel et al, 1981 and Gentle, Juden et al, 1981).

## ANALYSIS

The accepted equations describing fully-developed laminar or turbulent flow in smooth pipes are:

$$f = \frac{24}{Re} \quad \text{and} \quad f = \frac{0.079}{Re^{0.25}} \quad - (1)$$

respectively, where  $f$  is the friction factor, defined by:

$$f = \frac{\tau_w}{\frac{1}{2} \rho \bar{u}^2} \quad - (2)$$

and the Reynolds number:

$$Re = \frac{2\bar{u}\delta}{\nu} \quad - (3)$$

is based on the hydraulic diameter, which, for a slit, is  $2\delta$ , where  $\delta$  is the slit width. Here,  $\tau_w$  is the wall shear stress,  $\rho$  is the fluid density,  $\nu$  is its kinematic viscosity and  $\bar{u}$  is the mean velocity. In each case the equation arises by considering a fully-developed velocity profile, parabolic for laminar and  $1/7$ th power law for turbulent. The problem with using these to characterise leakage flow through a closed prosthetic heart valve is that the axial path length is so short that the conditions could only be described as entry flow, and therefore it is unreasonable to assume that the velocity profile through the gap is the same as it would be for fully-developed conditions. This will have twofold significance. Firstly, the profile will be changing throughout the length and secondly, it will be flatter than the fully-developed profile for the same flowrate and will, therefore, give rise to a greater wall velocity gradient, hence friction factor.

For simplicity, we will concentrate on the effect of this "fuller" profile and assume that its shape lies somewhere between the totally flat and the fully-developed and remains unchanged throughout the

length of the leakage gap. Three further assumptions are made, as follows:-

- 1) Since the leakage gap is a thin slit whose breadth is some 30 times its width, a "parallel plate" analysis is more appropriate than a "circular pipe" analysis. Plate separation is taken as  $\delta$ .
- 2) Velocity profile is defined, to the centreline, as:

$$\frac{u}{u_m} = \left\{ \frac{y}{(\delta/2)} \right\}^{\frac{1}{n}} \quad - (4)$$

where  $u_m$  is the maximum (centreline) velocity and  $y$  is the distance from the wall. Here, the value of  $n$  defines the shape of the velocity profile: the larger its value the "fuller" the profile. For fully developed turbulent flow,  $n=7$ .

- 3) The non-dimensional relationship:

$$\frac{u}{u^*} = K_1 \left\{ \frac{u^* y}{\nu} \right\}^{\frac{1}{n}} \quad - (5)$$

holds, where  $u^*$  is the "friction velocity",  $\sqrt{\tau_w/\rho}$   $K_1$  is taken as a constant over the relevant range of Reynolds number (although it is, in fact, a weak function of  $Re$ ).

We now follow the scheme of Duncan et al (1970) with appropriate modifications for parallel plate theory. Equation (5) evaluated at the centreline yields:

$$\frac{u_m}{u^*} = K_1 \left\{ \frac{u^* \delta}{2\nu} \right\}^{\frac{1}{n}} \quad - (6)$$

whilst the definition of mean velocity,  $\bar{u}$ , together with the assumed velocity profile of equation (4), gives:

$$\frac{\bar{u}}{u_m} = \frac{n}{(n+1)} \quad - (7)$$

Equations (6) and (7) combine to give:

$$u^* = \left( \frac{2\nu}{\delta} \right) \left( \frac{n+1}{n K_1} \right) \bar{u}^n \quad - (8)$$

and substituting the definitions of friction factor and Reynolds number (equations (2) and (3)) yields the result:

$$F = K Re^{-\frac{2}{(n+1)}} \quad \text{where } K = 2 \left( \frac{n+1}{n K_1} \right)^{\frac{n+1}{n}} \frac{2n}{(n+1)} \quad - (9)$$

Thus, the gradient of the  $\log(f)$  vs  $\log(Re)$  curve is  $-2/(n+1)$ , so that a "fuller" profile (larger  $n$ ) results in a shallower gradient.

Regression analysis of Gentle's data yields:

$$f = 0.2998 Re^{-0.1131} \quad - (10)$$

so that, for the twin-flap valve we have:

$$n = 16.7 \quad \text{and} \quad K_1 = 3.15$$

Combining equations (4) and (7) yields:

$$\frac{u}{u} = \left(1 + \frac{1}{n}\right) \left\{ \frac{y}{(\delta/2)} \right\}^{\frac{1}{n}} \quad - (11)$$

The velocity profile defined by equation (11) with  $n=16,7$  is shown together with that for  $n=7$  (fully developed turbulent) for the same mean velocity, in figure 2. It is apparent that this profile is significantly flatter, and hence has a steeper wall velocity gradient resulting in the elevated friction factor observed in practice. Further, the flat profile resulting from the fact that the flow is not fully-developed, explains the shallow gradient of Gentle's curve.

The high friction factor can also be explained by considering that the closed valve constitutes a converging duct, for which the momentum theorem yields:

$$\tau_w = -\frac{\delta}{2} \frac{d}{dz} \left( p + \frac{1}{2} \rho \bar{u}^2 + \rho gh \right) \quad - (12)$$

where  $p$  is the static pressure,  $h$  the elevation and  $z$  the flow direction. Thus, to assume  $f$  is proportional to  $\Delta P$  is to neglect the velocity and elevation terms. Order-of-magnitude calculation shows the velocity term is comparable with the pressure term. Thus

for the analysis to be valid,  $\bar{u}$  must be assumed constant throughout the slit, i.e. that the slit is of constant width. This constrains us to a short length around the flap base where  $\bar{u}$  is already large and so the pressure is significantly lower than its assumed inlet value. Thus, the quoted pressure drop, hence friction factor, is too large.

#### NUMERICAL MODELLING

Leakage flow was modelled using the "Phoenics" finite difference package. Since quantitative information was required only for flow through the leakage gap itself, a 2-dimensional model was employed. Since flow is symmetrical, only a half-plane was modelled. The flowrate was set at 2.5 litres/min ( $4.2 \times 10^{-5}$  m<sup>3</sup>/s). A converged solution was obtained whose results are summarised on the streamline plot of figure 3. There is turbulence as the jet emerges. Whilst the highly elliptic nature of the flow field has produced considerable upstream turbulence, flow over most of the flap surface, except for a small region at its base, is laminar. Two stagnation points are apparent on the occluder surface: one on the downstream face and the other just distal to the flow separation point at the base. This, significantly, coincides with a small local laminar region. The maximum shear stress in the gap is calculated as 2.2 kN/m<sup>2</sup>.

## DISCUSSION.

As demonstrated above, flow through the gap itself, albeit not fully-developed, does appear to be turbulent, with the accompanying advantages, but consideration of where on the occluder surface this turbulence lies reveals that it is primarily in regions which are best washed in forward flow anyway (see figure 4). Indeed, Gentle, Juden et al (1981) report that the hinges have been deliberately placed so as to ensure adequate washing action between the flaps when open. However, the two places at which there is stasis when the valve is shut are precisely the same points most likely to provide stagnation during forward flow, namely the base where the dividing streamline impinges and the flap tip where separation will occur.

As reported above, the maximum shear stress was 2.2 kN/m<sup>2</sup>. The pressure drop for this flowrate was approximately 9 kN/m<sup>2</sup>, since this was central to the reported test range. Rough calculation shows that a more typical physiological pressure differential of 17 kN/m<sup>2</sup> would yield a wall shear stress of 4.2 kN/m<sup>2</sup> for the twin-flap valve, as compared with 0.62kN/m<sup>2</sup> for the Bjork-Shiley valve (for the same pressure drop) estimated from the equation:

$$\tau_w = \frac{\delta}{2} \frac{\Delta p}{l} \quad - (13)$$

where  $l$  is the leakage gap length in the flow direction. Blackshear (1972) states that short-duration shear stress over 4 kN/m<sup>2</sup> will cause haemolysis, probably by cell membrane rupture, whilst there is

a second mechanism requiring a shear stress level of about 0.1 kN/m<sup>2</sup> sustained for several seconds. Opinion is divided as to whether the resulting cell damage is caused by mechanical tearing of long thin processes drawn out when cells anchor to the wall, or by laminar shear stress in the bulk flow. The former mechanism is thought to be the principal mode of haemolysis at prosthetic surfaces and is extremely dependent on surface treatment. Clearly then, despite the choice of porous alumina to encourage tissue growth to reduce the chance of haemolysis at the surface, the values of shear stress produced merely by the choice of leakage gap are unacceptably high for clinical use.

Finally, to produce turbulent leakage, the gap must be wide, producing large backflow. For example, quoted flow for a back pressure of 20 kN/m<sup>2</sup> is 3.95 litres/min ( $6.6 \times 10^{-5}$  m<sup>3</sup>/s). Assuming a typical mean forward flow of 25 litres/min ( $4.2 \times 10^{-4}$  m<sup>3</sup>/s), a regurgitant fraction well over 15% is readily produced.

#### LEAKAGE GAP DIMENSIONS

Evidently, a wide leakage gap can have serious consequences, so design criteria are required. Obviously, it is of prime importance to ensure that any planned washing action scours the surface regions where thrombus formation is most likely. A lower limit on leakage flow might be suggested by that necessary to prevent cell adhesion to the occluder surface, but, as previously mentioned, the nature of the surface is the significant factor here. However, since it is

agreed that the washing action of leakage flow is desirable, it seems sensible not to limit this to a minimum, but rather to fix gap width around an upper limit set by consideration of haemolysis or regurgitation. Such a criterion might be the 4 kN/m<sup>2</sup> shear stress for haemolysis by cell membrane rupture. This, however, is likely to produce a large gap and hence excessive regurgitation. Also, Blackshear's comments concerning the mechanisms of haemolysis at prosthetic surfaces indicate that the 4 kN/m<sup>2</sup> shear stress criterion may be too high in these circumstances. Since the 0.1 kN/m<sup>2</sup> shear stress condition applies to situations in which this level is sustained for several seconds, it does not appear relevant for pulsatile cardiac flow, and anyhow, would lead to leakage gaps only a few microns wide.

This leaves the acceptable regurgitant fraction as the criterion for an upper limit. Unfortunately, since the known physiological parameter is the pressure difference across the closed valve, calculation of regurgitant flow presupposes a knowledge of the Q- p relationship. We have seen that although correlation with fully-developed predictions is poor, it is better for Reynolds numbers well into the laminar regime -- possibly good enough for a rough design calculation. Thus, for slit flow:

$$\delta = \left( \frac{12\mu l Q}{w \Delta p} \right)^{\frac{1}{3}} \quad \text{--(14)}$$

where  $\mu$  is the dynamic viscosity, Q is the volumetric flowrate and w is the leakage gap breadth, dictated by valve geometry. Equation (14) could yield an estimate of  $\delta$  required to produce an acceptable

leakage flow for a given pressure drop. We may also check whether the Reynolds number:

$$Re = \frac{2 \rho Q}{\mu w} \quad - (15)$$

is sufficiently low. Equation (13) could then produce a rough check on the shear stress level.

#### CONCLUSION

In order to obtain a turbulent washing action, one must risk excessive regurgitation, high shear stress and consequent mechanical haemolysis. Even then the turbulence is not necessarily produced where washing is most needed. It seems more sensible, therefore, to design for laminar flow through a well-placed leakage gap in a valve made from a suitable material. This has been seen to provide adequate protection against thrombus formation and haemolysis in clinical use.

## REFERENCES

Blackshear, P.L. (1972). Mechanical hemolysis in flowing blood, in: Y.C. Fung, N. Perrone and M. Anliker (eds.), Biomechanics -- Its Foundations and Objectives, Prentice-Hall, Englewood Cliffs, N.J.

Duncan, W.J., Thom, A.S. and Young, A.D. (1970). Mechanics of Fluids, Edward Arnold, London, pp.311-313.

Gentle, C.R. (1980). A porous ceramic mitral valve prosthesis, in: G.W. Hastings and D.F. Williams (eds.), Mechanical Properties of Biomaterials, John Wiley & Sons, New York.

Gentle, C.R. (1982). Characterisation of leakage flow in cardiac valve prostheses. Proceedings of ESAO, vol IX, 102-106.

Gentle, C.R., Arundel, P.A., Hamilton, D.I. and Swales, P.D. (1981). Development of a twin-flap porous ceramic mitral valve prosthesis. J. Biomed. Eng., 3, 3-8.

Gentle, C.R., Juden, H. and Swales, P.D. (1981). Testing of an all-ceramic mitral valve prosthesis. Proceedings of ESAO, vol VIII, 352-355.

Parsons, R.W.T. (1981). Leakage flow testing of artificial heart valves. Undergraduate project thesis, Trent Polytechnic, Nottingham.

Rief, T.H., Cocolin, G. and Huffstutler, M.C. (1980). A note on the leakage of the new Omniscience/tm pivoting disk prosthetic heart valve. J. Biomech. Eng. Trans. ASME, 102, 342-344.

FIGURE CAPTIONS

Figure 1. Experimental leakage flow data superimposed on Moody chart for fully-developed pipe flow.

Figure 2. Predicted and estimated velocity profiles in the leakage gap.

Figure 3. Summary of numerical model results for the twin-flap valve.

Figure 4. Forward flow through the twin-flap valve.

AUTHORS' AFFILIATIONS

S.E. LEEFE BA (Oxon)

R.J. EDWARDS BSc (Hons)

G.D. TANSLEY BSc (Hons)

C.R. GENTLE PhD, BSc, DIC, ARCS, MBES, MESAO

Department of Mechanical Engineering, Trent Polytechnic,  
Burton St., Nottingham NG1 4BU, UK.

Queries to: Dr. C.R. Gentle

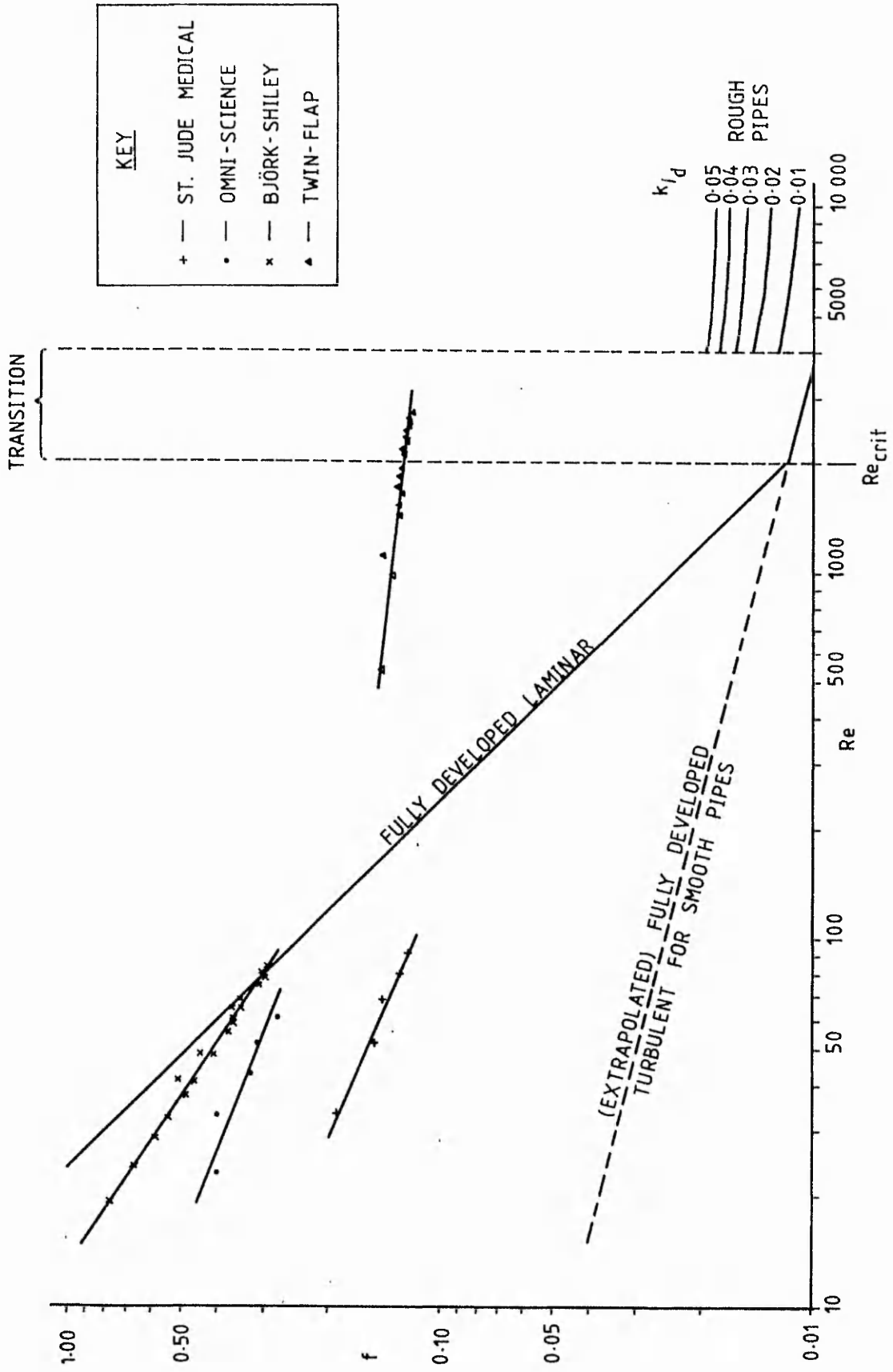


FIGURE 1

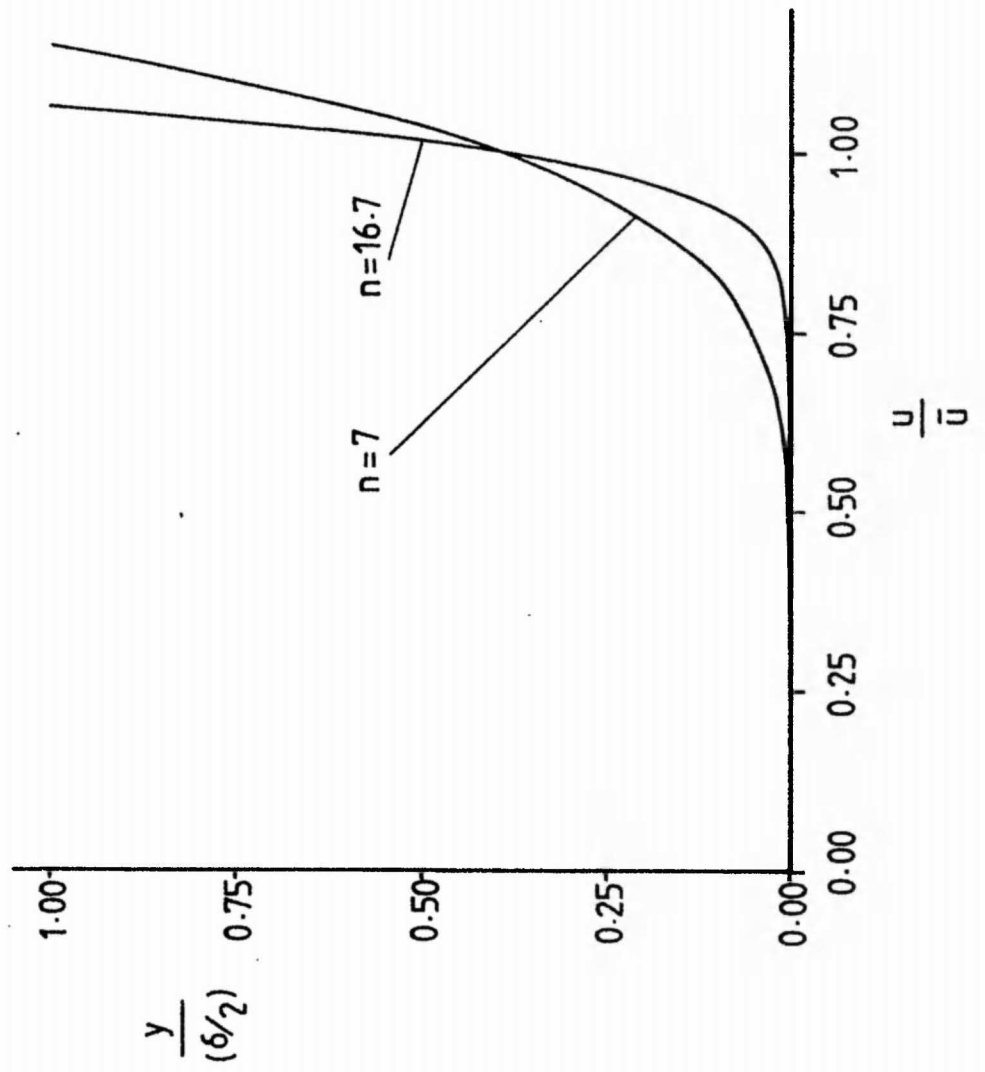
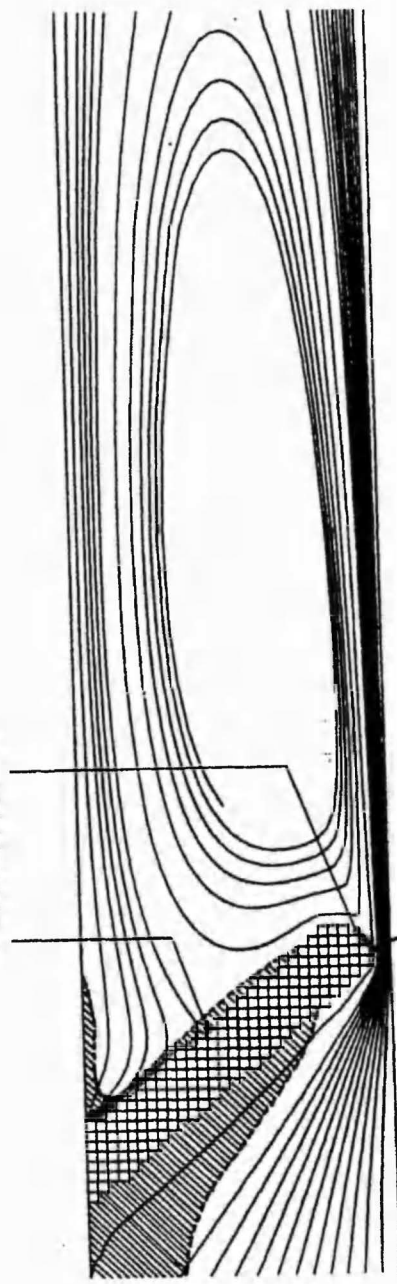


FIGURE 2

OCCLUDER  
LAMINAR



STAGNATION



MAX SHEAR STRESS

FIGURE 3

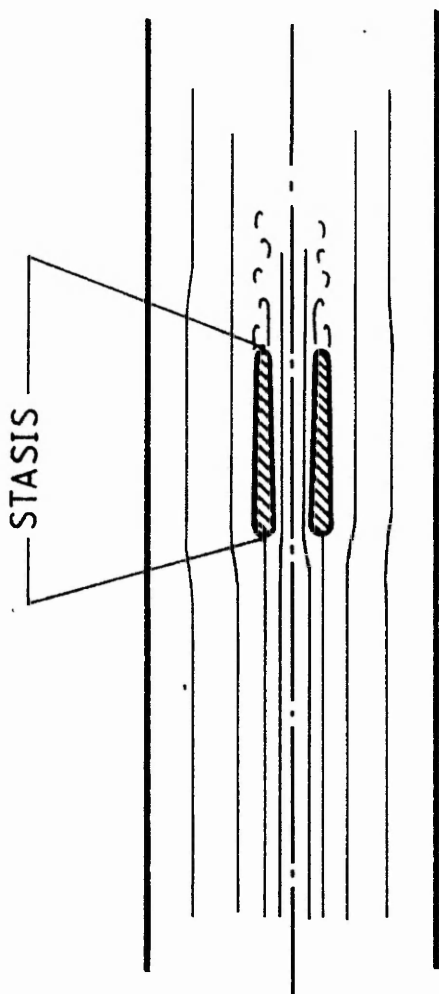


FIGURE 4

# Pulsatile flow testing of prosthetic heart valve conduits

S E LEEFE, G D TANSLEY and C R GENTLE

Department of Mechanical Engineering, Trent Polytechnic, Nottingham, UK

**SYNOPSIS** A pulse duplicator for testing prosthetic heart valve conduits is described. The model left ventricle permits the testing of a conduit either as a straightforward valve replacement or as an apico-aortic shunt. Drive is provided by a microcomputer-controlled servomotor, operating a piston forcing an hydraulic fluid into a chamber surrounding the model ventricle, thus providing direct programmable control of ventricular volume throughout the cycle. Pressure and flow signals are digitised, stored and processed in a microcomputer to yield performance data in terms of energy loss.

The first phase of the research programme concerns the testing of existing conduit designs. The second will incorporate particle image velocimetry for flow visualisation to highlight regions of stasis and high shear rate. These findings, in conjunction with the results of the tests outlined above, will form the basis for the development of a new valved conduit.

## 1 INTRODUCTION

Artificial heart valves have been the subject of extensive testing and development work over the years. Consequently, there is a large array of prostheses available to the surgeon and the choice of replacement valve can be determined by referring to fairly exhaustive *in vitro* and clinical performance data as well as considering cost. Unfortunately, the choice of prosthesis for conduit operations is not so scientific. Not only is there a far more restricted choice available, but the extent of published performance data is limited. Indeed, the authors know of no references containing pulsatile flow test results for prosthetic heart valve conduits. This results from a lack of development work, which is surprising, given the scope for improvement afforded by the absence of geometrical constraints which the surrounding vessels impose on the design of valves for straightforward replacement. Instead, the strategy has been to incorporate a valve, which has been designed to separate two chambers, into a length of conduit tubing. Clearly, this is a different fluid mechanical situation and, as such, is unlikely to be optimal. This approach also unnecessarily restricts the type of valve which can be employed in a conduit. For example, if a Starr-Edwards valve were to be sewn into straight tubing, in the open position the ball occluder would still occupy nearly all of the cross-section: a downstream enlargement is essential for its efficient operation. Thus we can see that a pulsatile flow test facility for valved conduits is necessary both to provide the surgeon with performance data and to enable development work to proceed.

Since valved conduits are employed in a variety of ways it is logical to test their performance in different modes of usage. For this reason the pulse duplicator allows a conduit to be tested as an apico-aortic shunt by providing the model ventricle with an optional second outflow.

The fluid circuit compliance and resistance can be adjusted to model either pulmonary or systemic load conditions. Great flexibility is also afforded by the use of computer-generated driving waveforms for ventricular volume. One is not constrained to a sinusoidal function, although, should one wish to use this as a suitable standardised basis for testing, one is at liberty to vary its amplitude and frequency virtually continuously. One can employ a physiological-type waveform, vary its amplitude and frequency, alter the ratio of filling to emptying time or even study the effect of arrhythmia. By designing versatility into the pulse duplicator one has a valuable research tool.

## 2 DESCRIPTION OF APPARATUS

### 2.1 Fluid circuit

The heart is essentially a positive displacement pump. Changes in ventricular volume determine the flow of blood into or out of the chamber and pressures throughout the system are a function of the load impedance. This standpoint justifies the pulse duplicator design. See Figures 1 and 2. A flexible membrane, semi-elliptical in cross-section, cast in cold cure clear silicone rubber (MDX-4-4210, Dow Corning) models the ventricle walls. This sits inside a cylindrical acrylic enclosure and is sealed from above by a plate containing inlet and outlet ducts. A pipe carries hydraulic fluid from a master cylinder to the chamber surrounding the membrane. As this fluid is pumped into the enclosure it squeezes the membrane, emulating the squeezing action of ventricular systole. Further, the volume pumped in equals the reduction of 'ventricular' volume, so, by controlling piston position or velocity, one may directly control ventricular volume or its rate of change. There is a hole through the base of the membrane and the cylindrical container. This is normally plugged but may be used as a second outflow for testing a conduit as an apico-aortic shunt. For

the basic pulsatile flow testing the conduit is attached in the aortic position. Compliance is provided by a pressure chamber into which air may be pumped through a car tyre valve. Resistance is provided by a simple screw clamp. All interconnecting tubing is of 22 mm bore clear plastic. (Since all the conduits obtained for testing are of nominal 22 mm diameter this choice of bore is used throughout the circuit.) Downstream of the impedance elements, the flow drains into an open reservoir which feeds the return to the pulse duplicator's atrial chamber. A Bjork-Shiley mitral valve separates the atrium from the ventricle. All circuit elements are fitted with standardised flange connectors for ease of interchangeability. Interconnecting pipe lengths are terminated in the same connectors, the tubing sliding over an external taper so that the bore remains constant throughout the joint. See Figure 3. Most conduits are flexible and somewhat porous. This raises two problems: firstly, how to secure them into position in the test apparatus and secondly, how to prevent leakage through the conduit walls. Both these difficulties may be overcome by mounting the conduit inside a length of 25 mm bore plastic tubing, securing it by sewing o-rings to both ends of the conduit and locating them in grooves machined into the tubing. See Figure 4. The stiffness of the tubing holds the conduit in position, whilst the o-rings provide axial location within the sheathing and prevent leakage of the fluid which seeps through the conduit walls.

The original working fluid was a buffered Ringer's solution (as used by Juden (1)), but this had to be abandoned since it caused unacceptable zero drift of the electromagnetic flowmeter probe. Eventually, a solution of 50g/dm<sup>3</sup> of sodium chloride in distilled water was mixed with glycerol in the ratio 70:30 by volume, giving a conductive working fluid, compatible with the flowmeter, with a kinematic viscosity (at 19.5°C) of  $3.00 \times 10^{-6} \text{ m}^2/\text{s}$ , which is comparable to that of blood, and a density of  $1.10 \times 10^{-3} \text{ kg/m}^3$ .

## 2.2 Drive System

Mechanical power to the pulse duplicator is derived from a linear motion reciprocating pump comprising a piston and cylinder arrangement. The choice of drive system was governed by two factors: smoothness of operation and availability of existing resources. These considerations led to the use of analogue command of a servo-motor to control piston velocity. Figure 5 shows a schematic diagram of the control system. Drive is taken from a low-friction nut running on a lead screw which is coupled to a d.c. servo-motor with integral tachogenerator for velocity feedback (M670 TE, by McLennon Servo). Velocity control is provided by a servo-amplifier (EM 200, McLennon Servo) taking its command signal from a 14-bit digital-to-analogue converter (RS 7534, Radio Spares). The signal is generated by a dedicated single board computer (1087/05E, Antronics Ltd) using sampled waveform data stored sequentially in EPROM. The system is capable of pumping at a maximum ejection rate of 1 dm<sup>3</sup>/s at pulse rates between 30 and 200/min. Thus, within these limitations, any waveform may be output by selecting an appropriately programmed EPROM. One such option is a 'physiological' waveform derived from a graph of left ventricular volume versus time for a typical healthy subject, presented in Strand (2). This was reproduced as a 25-term

Fourier series, from which was derived a smooth and continuous curve of the rate of change of ventricular volume. (The volume curve and its inverted derivative are shown in Figure 6.) This was sampled at 1024 equally spaced points and the values stored in EPROM to generate the piston velocity control signal.

A further feature of the control system is the 'reset' function, which stops the piston dead. This can be effected manually or on receipt of signals from opto-sensors at the lead screw's extremities, preventing the possibility of mechanical damage caused by the nut running into either end. There is also a manual override so that the nut can be re-positioned after a reset. Finally, trigger signals are available to initiate and stop a data acquisition cycle and to operate a laser or a camera for flow visualisation studies.

## 2.3 Data acquisition system

For reasons discussed by Leefe and Gentle (3), conduit performance is to be assessed in terms of 'energy loss'. This requires the continuous measurement, throughout a cycle, of two pressures (or one differential) and one volumetric flowrate. For tests on a conduit used as an apico-aortic shunt, three pressures (or two differentials) and two flows are needed. Instrumentation is comprised of pressure transducers (22 A-005-G IC-Sensors, Computer Controls Ltd), an electromagnetic flowmeter (SP2202 Research Blood Flowmeter with SP4005 22 mm i.d. cannulating probe supplied by Gould Medical) and a turbine flowmeter (B / 5/8 / 8, A.O.T Systems). The pressure transducers were calibrated statically, whilst the flowmeters were calibrated for steady flows in the range -30 to +30 dm<sup>3</sup>/min in the working fluid. The data acquisition system is based around an eight channel, programmable gain, 12-bit analogue-to-digital converter (ADC) unit (U-A/D, U-Microsystems Ltd) under the control of a dedicated Apple IIe microcomputer. For rapid sampling the ADC gain needs to be kept constant, but the electromagnetic flowmeter signal is two orders of magnitude larger than the pressure transducer signals. Also, the turbine flowmeter's output is a small a.c. signal whose frequency is proportional to flow. Further, some of the signals are negative-going, but the ADC unit is unipolar. For these reasons a signal conditioning unit was built which also includes a facility for auto-calibration under computer control. Signal sampling is at the rate of ten kHz (with five channels this is two kHz per channel) so that data for a typical one second cycle, stored in bit-form occupies about 20 kilobytes of RAM. Data acquisition must, therefore, be controlled from an assembly language subroutine, since BASIC is too slow and floating point numerical data is wasteful of memory. The acquisition cycle is initiated and terminated by trigger pulse inputs generated by the drive system's computer. At the end of a cycle, data is retrieved from memory, one channel at a time, converted into values of process variables by means of calibration equations and stored on disc for subsequent plotting, manipulation and analysis. The system is shown schematically in Figure 7.

## 3 PROGRAMME OF WORK

The aim of the programme of research into prosthetic heart valve conduits, being undertaken at

Trent Polytechnic, is to develop a prototype which demonstrably improves on existing designs. To this end, a base of performance data is being established for comparison. This primarily entails the calculation of 'energy loss' per pulse for each conduit in the aortic position, with a given ventricular forcing function. Performance may also be evaluated for the conduit used as an apico-aortic shunt for the relief of a given degree of aortic valve stenosis, by calculating the 'energy loss' for a system in which the aortic outflow tract incorporates, for example, a 70 per cent occlusion representing the stenosed valve, and the conduit provides a second outflow tract.

The proposed idea for prototype development is a variant of the caged ball valve idea, in which there is a rigid, ceramic valve-bearing section attached at either end to flexible conduit tubing. The central section would consist of an inlet tract, sealed, under adverse pressure gradient, by a spherical occluder, which, under forward flow conditions, would move out into a diverging section, where it would be restrained from sealing the outflow duct by three struts, integral to the converging outlet section. See Figure 8. Preliminary steady flow tests on a rigid mock-up (4) have indicated that considerable improvements in forward flow pressure drop over existing designs are possible, although attention is needed with regard to the problem of ball instability. An investigation into this problem (5), however, has pinpointed the cause. Development work will be augmented both by the use of numerical flow simulation with the 'Phoenix' finite difference package and flow visualisation studies on transparent prototypes, using particle image velocimetry, to highlight regions of stasis and high shear rate. This technique relies upon the exposure of small

particles (typically five microns) to double pulsed ruby laser radiation, for the creation of two laterally displaced image matrices on a photographic negative. Local velocity vectors are derived by analysing the Young's fringes produced by the pointwise interrogation of a contact printed positive transparency in laser light. The magnitude of the velocity vector is inversely proportional to the fringe spacing, whilst its direction is gleaned from the fringe direction.

#### REFERENCES

- (1) JUDEN, H. Wear studies of prosthetic heart valves, PhD Thesis, Trent Polytechnic, 1983.
- (2) STRAND, F.L. Physiology: a regulatory systems approach, Macmillan, 1983, p233.
- (3) LEEFE, S.E., GENTLE, C.R. A theoretical evaluation of energy loss methods in the analysis of prosthetic heart valves. Submitted August 1986 to: Journal of Biomedical Engineering.
- (4) GENTLE, C.R. Minimization of pressure drop across heart valve conduits: a preliminary study. Life Support Systems, 1983, 1, 263-270.
- (5) TANSLEY, G.D., EDWARDS, R.J., LEEFE, S.E., GENTLE, C.R. An investigation into ball occluder instability in prosthetic heart valve conduits. Presented at 13th annual meeting of the European Society for Artificial Organs, Avignon, France, September 18-20, 1986.

22	HYDRAULIC FLUID INLET/OUTLET	COPPER		1	
21	BASE PLATE	PERSPEX		1	
20	SECURING RING	BRASS		1	
19	SECURING COLLAR	BRASS		1	
18	PLUG	PERSPEX	POLISH	1	
17	O-RING, 1/16" SECTION	RUBBER		1	
16	C'S'K SCREW, 8 BA x 1/4"	BRASS		14	
15	C'S'K SCREW, 4 BA x 3/8"	BRASS		6	
14	WASHER	FIBRE		1	
13	VENT PLUG, M3 x 6	STEEL		1	
12	FLEXIBLE MEMBRANE	RUBBER		1	
11	PRESSURE TAPPING TUBE	COPPER		1	
10	O-RING, 1/16" SECTION	RUBBER		1	
9	OUTLET STUB PIPE	PERSPEX		1	
8	SECURING COLLAR	PERSPEX	POLISH	1	
7	INLET STUB PIPE	PERSPEX	POLISH	2	
6	GRUB SCREW, M4 x 4			1	
5	INLET/OUTLET MANIFOLD	PERSPEX	POLISH	1	
4	22mm DIA BJÖRK-SHILEY VALVE			1	
3	C'S'K SCREW, 8 BA 3/8	BRASS		27	
2	VALVE RING	PERSPEX	POLISH	1	
1	PUMP BODY	PERSPEX	POLISH	1	
REF.	PART No.	NAME OF PART	MATERIAL	FINISH	No OFF
DRN	S.F.L.	SCALE 1:1	MODEL HEART PUMP		DRG No.
APPO.	SHEET	GENERAL ARRANGEMENT			
DATE 3-6-85	SHEET No.	TRENT POLYTECHNIC			

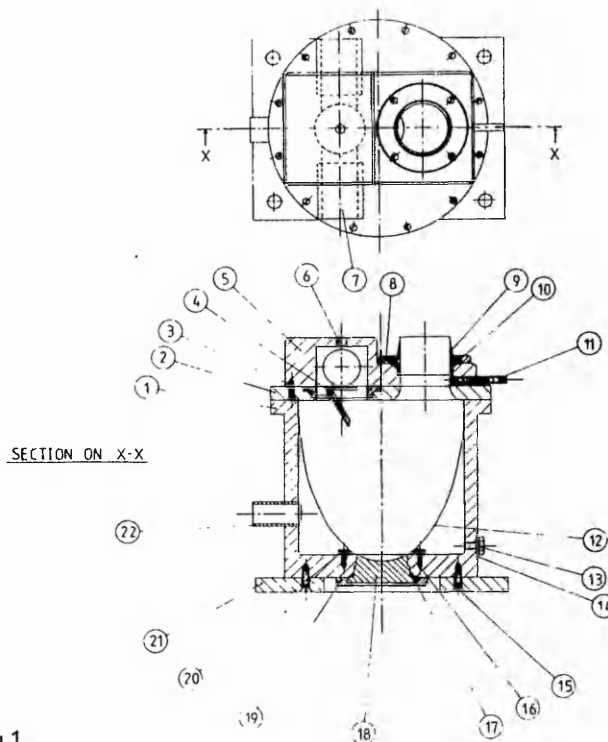


Fig 1

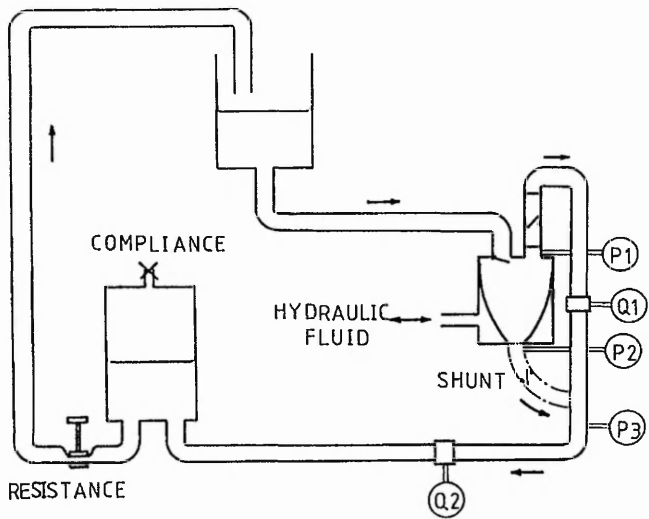


Fig 2

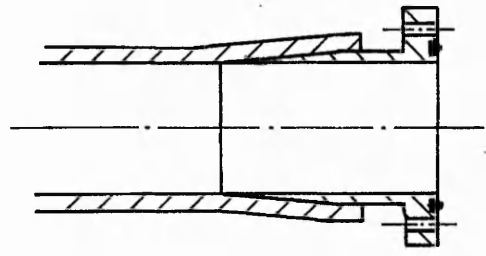


Fig 3

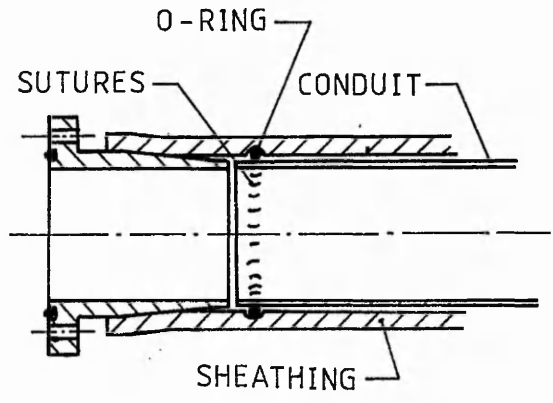


Fig 4

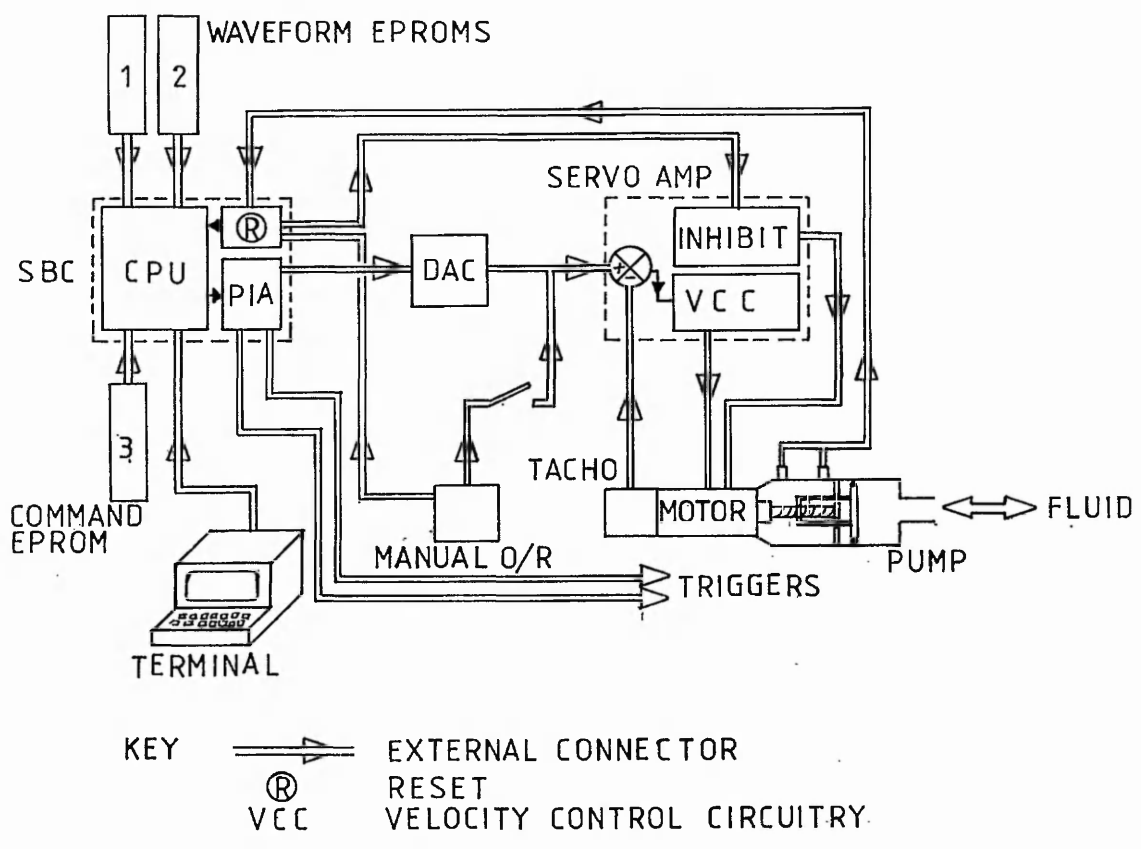


Fig 5

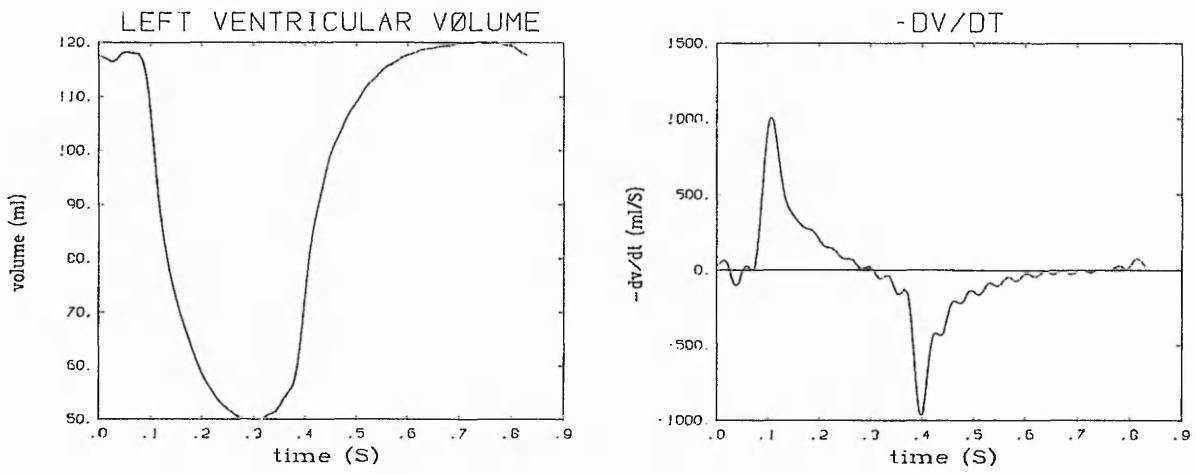


Fig 6

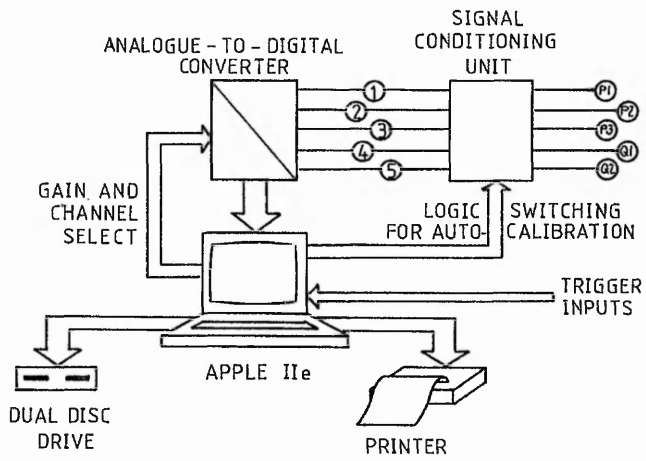


Fig 7

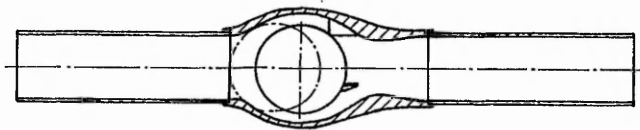


Fig 8

THE ROLE OF COMPUTATIONAL FLUID MECHANICS IN  
THE ANALYSIS OF PROSTHETIC HEART VALVE FLOW

G.D. TANSLEY, R.J. EDWARDS and C.R. GENTLE

The Department of Mechanical Engineering, Trent Polytechnic, Nottingham

ABSTRACT

This paper aims to present the strengths and weaknesses of Computational Fluid Mechanics (CFM) as compared to existing in-vitro haemodynamic techniques such as LDA, hot wire anemometry and static pressure measurement and to discuss the application of CFM to the analysis of prosthetic heart valve flow. It presents a brief summary of existing methods used in analysing in-vitro heart valve flow (along with CFM), the special problems inherent in each method and the quantities each is capable of giving. The analysis then goes on to present examples of information yielded by CFM. It also contains a brief discussion of the data requirements for the analysis of heart valve performance and the clinical relevance of fluid dynamic occurrences.

The conclusion drawn is that CFM has a major role to play in the analysis of prosthetic heart valve flow and design because of the improved availability of data afforded and the increased correlation between CFM and clinical flow regimes, due to the ability to consider realistic models of blood.

## INTRODUCTION

The dependence of haemolysis and thrombosis on prosthetic heart valve flow is well established and many in-vitro studies have been conducted over the last three decades with the aim of fully describing the mechanisms of such occurrences. It has become obvious that there are several mechanisms by which haemolysis is induced via prosthetic valve flow, but those of relevance to the fluid dynamics realm are shear stress related; similarly thrombosis is a stasis or shear rate related problem. It is therefore necessary that designers of heart valves have adequate shear stress and shear rate data pertaining to blood flow through each valve. Unfortunately there are difficulties associated with obtaining these data; none of the presently applied in-vitro techniques is capable of rendering shear stress directly, having to rely on assumptions about the nature of the turbulence, namely isotropy. This reduces correlation between the flow occurrences studied in-vitro and the clinical situation. Correlation is further reduced by the need to model in blood analogue fluids, assuming that their flow behaviour closely approximates that of blood. Theoretically, CFM should be able to overcome these problems by predicting directly the shear stresses and rates for fluids of complex viscosity such as blood. Presently this sort of modelling is uncommon and although CFM is starting to find acceptance, much of the data presented (eg velocity profiles) could equally well have been obtained by Laser Doppler Anemometry. This may be due in part to the fact that CFM blood flow packages have until now been developed from scratch every time. This is difficult, slow and often inefficient. However, proprietary packages such as PHOENICS (Spalding 1981) are now available which are capable of handling blood flow through heart valves realistically. Some encouraging preliminary results have already been obtained in the current research programme using PHOENICS (Tansley et al. 1986 and Leefe et al. 1986) and so it seems an opportune moment to review how CFM can best be applied to valve prostheses and how it compares with existing techniques for assessing the haemodynamic faults associated with proposed valve models.

## THE BACKGROUND TO CFM

Due to the complex nature of the Navier-Stokes' partial differential equations describing fluid flow, a purely analytical solution is only possible for simple configurations in laminar, steady, fully developed regimes. As such flow situations do not occur in the cardiovascular system close to the heart, or indeed in prosthetic valve flow, which can be either undeveloped laminar or turbulent, the use of analytical methods in heart valve design is very restricted. Hence a numerical approach must be adopted if relevant flows are to be analysed non-experimentally. In its simplest form, computational analysis will be based on the solution of the parabolised Navier-Stokes equations, yielding information about boundary layer type flows (Lauder and Spalding 1974); if the flow has areas of streamwise separation, the full, elliptic form of the Navier-Stokes equations must be invoked.

Computational numerical methods in the form of finite difference or finite element approximation procedures offer solutions to differential equations and have been of immense value for some time in the fields of mechanical stress and vibration analysis. Unfortunately, standard computational numerical methods cannot be applied to the solution of turbulent fluid flow because the requirements of excessive storage space and run time make it impractical on existing computers. This is due to the nature of turbulent flow: inherently three dimensional, non-linear and with a very high spatial and temporal density of occurrence of important turbulent processes (ie processes taking place in short distances and time periods). The reasons for the onset of turbulence are complex, but generally turbulence occurs when flow is sufficiently disturbed at relatively high Reynolds' numbers, though this is very geometry dependent. In order to overcome the problems of solving turbulent flow, time-averaged properties of turbulence are considered, thus eliminating the necessity for an extremely fine grid, but this requires a model to describe the transport of momentum by the turbulent motions. Numerous attempts to describe turbulence physically in terms of calculable properties have been made and can be classified into two concepts; turbulent (eddy) viscosity and turbulent stress. Here we will concentrate only on the most widely used and accepted model which utilises the turbulent viscosity concept and is known as the  $k - \epsilon$  model (Jones and Lauder 1972). This two equation procedure calculates two quantities:  $k$ , the kinetic energy and  $\epsilon$ , its dissipation rate, to yield a time averaged description of turbulence. The apparent or local turbulent viscosity  $\mu_t$  is then found from:

$$\mu_t = C_\mu \rho \frac{k^2}{\epsilon}$$

where:  $C_\mu$  is a constant of turbulence  
 $\rho$  is the density of the working fluid.

An effective viscosity  $\mu_{eff}$  can then be obtained from:

$$\mu_{eff} = \mu_L + \mu_t$$

where  $\mu_L$  is the laminar viscosity of the fluid.

This facilitates the calculation of turbulent stresses from:

$$\tau = \mu_{eff} dv/dx$$

When the flow is purely laminar, the turbulence model is suppressed and the laminar form of the Navier-Stokes equations are solved, then simply:

$$\mu_{\text{eff}} = \mu_L$$

To obtain  $k$  and  $\epsilon$ , empirical constants are required by the model and these have been established in free turbulent flows. Such constants were the failure of earlier models, due to their values varying so greatly for differing flow situations. Launder and Spalding (1974) reported the establishment of a universally applicable  $k$  and  $\epsilon$  model of reasonable accuracy both in near wall and free stream analysis. However, Abujelula and Lilley (1984) discussed the limitations of the empirical constants of the  $k - \epsilon$  model and concluded that modifications were required in certain flows but that, in general, realistic predictions could be obtained with the standard model. However, modelling turbulence in unsteady (pulsatile) flow situations is highly complex with much to be completed before standard models can be applied with confidence. At the present time empirically derived modifications to existing models relating to a particular flow geometry will have to be made in order to numerically describe transient flow. Morain (1982) and Metha and Lomax (1982) provide some insight into the current state of the art in turbulence modelling and conclude that current research is working towards a catalogue of models which have been established in particular areas of fluid flow. Bearing in mind that serious research in the modelling of turbulence has only taken place over the last sixteen years and that there is a vast amount yet to do, it is still a matter of speculation as to whether a uniquely acceptable turbulence model will exist before the availability of computers with sufficient storage capability to make turbulence modelling redundant.

Because of the special requirements of turbulence models in solution algorithms, finite difference techniques are utilised significantly more than finite element methods. In particular, finite element methods need parameter values at nodal points within individual elements, whereas such values are assumed constant within the volume domain in finite difference methods. However, recent developments in finite element techniques have enabled their application to the modelling of both turbulent flows (Autret et al. 1987) and non-Newtonian flows (Gartling 1986). Although finite element solution algorithms generally obtain convergence more slowly than finite difference methods, they have been favoured in the majority of mathematically modelled fields. The primary reason for this is the inherent obtrusiveness of the traditional finite difference grid in non-orthogonal geometries (figure 1.a) which is responsible for large inaccuracies at discontinuities in the solution domain. It was such inadequacies in finite difference grids which gave birth to finite elements, in order to analyse stress fields in airframes (figure 1.c shows a typical finite element grid). Considerable effort has been made to enable non-interfering grid generation but it has only been in the last five years that such grids have become commercially available in finite difference solution algorithms, in the form of Body Fitted Co-ordinates (figure 1.b). This significant break-through has importance in areas of research such as prosthetics where the vast majority of geometries are non-orthogonal. State-of-the-art finite difference codes can now boast flexibility in grid generation as well as a choice of turbulence models. Such solution procedures are becoming common place in aircraft and automotive aerodynamics, petroleum research, weather prediction and nuclear engineering.

## ANALYSIS OF THE FLUID DYNAMIC PROBLEM

The associations between poor haemodynamics and clinical complications have been well discussed over the last thirty years or so, since Ross et al. (1954) first reported on haemolysis caused by prosthetic heart valves. It is therefore only necessary to briefly outline the clinical complications that are related to fluid flow and are consequently of interest when assessing flow analysis techniques such as LDA or CFM. Five clinical conditions dependent on bulk blood flow (ie not material or mechanically related etc.) have been identified as being potential causes of failure of heart valve prostheses, these can be broadly classified as:

- 1] Haemolysis due to high in-bulk shear stress
- 2] Shear stress related haemolysis at the blood/prosthesis interface
- 3] Damage to endothelial linings due to jet impingement
- 4] Valve dysfunction due to thrombus formation at hinge points
- 5] Thrombo-embolism

These will be considered individually.

- 1] To predict the destruction of erythrocytes in bulk flow we need to establish the dependence of haemolysis on the magnitude and duration of high in-bulk shear stress. Leverett et al. (1972) summarise the findings of various researchers - Rooney (1970), Blackshear (1972), Williams et al. (1970), Shapiro and Williams (1970), etc. and estimate, graphically, a relationship between the threshold shear and exposure time. Later, Hellums and Brown (1975) concluded that levels of shear stress sufficient to cause in-bulk haemolysis are present in normally functioning prosthetic valves. This statement was based on a discussion of data presented by Roschke et al. (1975) who gave conservative estimates of shear stress based on wall shear stresses in boundary layer flow. Hellums and Brown use as their threshold for haemolysis a stress magnitude and duration of  $500 \text{ N/m}^2$  and  $1 \times 10^{-3}$  seconds respectively, this, they argue is representative of the 'flight time' of a blood cell through a valve prosthesis.
- 2] There is no doubt that haemolysis occurs at the wall of a prosthesis in shear stresses much lower than those needed in the above case (below  $150 \text{ N/m}^2$ ). However, the precise mechanics of this haemolysis are not fully understood. There have been several approaches to the investigation of surface induced haemolysis including analysis of: the role of surface roughness (Bacher and Williams 1970), haemolysis at wall contact (Solen et al. 1978, 1981), and the material forming the prosthetic surface (Lampert and Williams 1972, Monroe et al. 1980, Solen et al. 1978) and the surface/volume ratio (Beissinger and Williams 1984). One cause of surface induced haemolysis, argues Blackshear (1972), is that additional stresses are encountered by erythrocytes as they adhere to and are subsequently torn from the prosthetic surface. This is not a problem that can be solved by a fluid dynamic analysis and therefore will not be discussed here. What is of fluid dynamic interest is the reduction of this occurrence brought about by decreasing shear stresses near to the wall: Blackshear (1972)

suggests that high shear stresses near to a prosthetic surface lead to the increased probability of cell contact with the wall and hence an increase in haemolysis via this mechanism. This is exacerbated by the excitation of clotting agents due to limited releases by erythrocytes in the elevated stress regions - see for reference: Blackshear (1972) and Johnson (1970) and for a more complete reference: Blackshear and Blackshear (1987).

- 3] Several studies - eg. Figliola and Mueller (1981) and Fry (1968, 1969), have discussed the possibility of damage to the endothelial lining of the aorta due to the implantation of prosthetic heart valves. This damage is reported by Fry (1968,1969) to occur in shear stresses as low as  $40\text{N/m}^2$ . The phenomenon is highly dependent upon the direction of blood issuing through the orifices of a prosthetic heart valve, particularly around a ball or disc occluder or through the minor orifice of a tilting disc valve, but is especially sensitive to the magnitude and duration of the shear stress impingent on the wall. Dewey et al. (1981) and Nerem et al. (1984) discuss changes in endothelial cell orientation and regeneration for stresses as low as  $0.5\text{N/m}^2$ . More significant to this paper is the work of Vaishnav et al. (1983) who examine the erosion of canine endothelium under conditions of varying shear stress and present an empirical equation to describe the relationship between apparent erosion stress and time.
- 4] Possibly a more important cause of valve unacceptability is dysfunction due to occluder immobilisation by the formation of thrombus at critical sites, especially the hinge points of twin flap or tilting disk valves. There is ample clinical documentation of the occurrence of such problems (refs : Narducci et al. (1986), Nunez et al. (1980), Aston and Mulder (1971), etc.). Clots are known to form in areas of haemostasis or low shear, the mechanisms being discussed by Dintenfass (1964) who presents data on the time related aspects of clotting under differing shear rate conditions. Dintenfass (1964) also presents, as it were, a critical lower shear rate (of order of magnitude of  $7\text{ sec}^{-1}$ ) where clotting due to the low shear mechanism is accelerated by as much as one thousand fold. Thrombosis can also be caused by higher shear rates as the aggregation of cells takes place in eddies and in an environment of the contents of damaged erythrocytes (in a similar manner to that discussed earlier). These mechanisms are further exacerbated by the complex, non-Newtonian viscosity of blood, which as it starts to slow down, is further slowed by the increase of viscosity - see Whitmore (1968) for a more complete discussion of blood viscosity.
- 5] This final category of bulk fluid related prosthetic heart valve failure is caused by the same mechanisms as the previous, ie low shear rates at stasis points or higher rates close by, but the sites may be different, and valve dysfunction does not necessarily occur. Thrombus can form both upstream and downstream of the valve, as well as at the occluder and may be apparent at any point where low shear rates occur - some possibilities being close to the sewing ring, upstream of the occluder and shielded from a washing action by the occluder, or at the apex of a ball valve cage. Thrombosis in itself in these areas is not of great concern (if stenosis does not ensue because of it), but the mobilisation of the thrombus leading to thrombo-embolism at a downstream site cannot be tolerated.

It must be reiterated that the aim of the above discussion is not to provide a definitive work on the mechanisms of haemolysis and thrombosis, but simply to establish the need to know the magnitudes of shear stress and shear rate that exist in any valve flow condition. One may then avoid known critical values, and thus reduce the thrombotic and haemolytic potentials of a prosthesis at the design stage. Having established the importance of haemodynamic parameters on clinical conditions one must then ascertain the actual values of these parameters in a particular valve. This must be done by in-vitro experimentation and hence it involves modelling of the flow region and of the blood itself. Since this modelling leads to many problems of flow analysis, the next section will consider critically the techniques available.

## IN-VITRO FLOW ANALYSIS TECHNIQUES

There are several in-vitro techniques available capable of yielding information about a valve's haemodynamics. Each has its own special difficulties and advantages and each can give only certain data, but by using several techniques in a complementary manner, most (but by no means all) aspects of a valve's flow behaviour can be established. The techniques commonly applied to the study of heart valve flow are:

- 1] Laser Doppler Anemometry - this can yield full field velocity vectors (except near wall) if crossed beams are used, turbulence intensities (scalar), Reynolds stress in boundary layers.
- 2] Ultrasound Doppler - this technique can yield velocity information and shear stress in blood and can be employed both in-vivo and in-vitro
- 3] Hot Wire/ Hot Film Anemometry - this yields Velocity vectors and turbulence intensities in boundary layer flow regimes.
- 4] Pitot tube measurements - these yield Velocity vectors in streamwise dominant flow.
- 5] Flow visualisation Studies - yield streamline tracings and, with certain techniques, a quantitative indication of velocity.
- 6] Static Pressure Measurements - yield the pressure drop across a valve or section and pressure recovery data. When used in conjunction with flow metering, energy losses can be indicated.
- 7] Flow metering - yields a measure of bulk fluid flow, but no indication of localised flow rates, energy losses can also be assessed (see above)

Taking each in turn:

### 1] LASER DOPPLER ANEMOMETRY (LDA)

The Technique: A laser beam is split and brought together again (see figure 2), both path lengths being the same. As the paths cross an interference pattern is created (as in figure 3), any particle crossing this pattern will reflect a "doppler burst" of light (figure 4) which is detected by a photo-multiplier. By measuring the time period between the peaks of the burst the velocity of the particle can be deduced.

The Advantages: This technique is well established and non-intrusive, ie it will not disturb the flow field. The spatial resolution, ie the data yielded per unit area, is high. Absolute velocities are measured alleviating the need for calibration. LDA lends itself very well to automation via computer control for the establishment of both velocities and turbulence intensities and will yield velocities free from directional ambiguity. LDA can also be used in a pulsed mode for the analysis of pulsatile flow fields.

The Disadvantages: Setting up an LDA system can be very time consuming, as can its application, especially in the pulsed mode. The technique cannot be used to map fluid velocities in opaque media and therefore cannot be used in conjunction with blood. The

geometry of the test section can cause untold problems because of inaccessibility both of the control volume and of the photo-multiplier. Distortion of the control volume by refractive index mismatching can occur, leading either to measuring in the wrong place or, even worse, a distortion of the control volume and consequently a velocity offset. This technique also suffers because of its inability to obtain data close to walls and blockages.

## 2] ULTRASOUND DOPPLER

The Technique: Like LDA this method of analysing velocities relies on the doppler principle: as particles (in this case normally blood) cross the reference beam a doppler shift is introduced in the reflected beam. The magnitude of this shift is proportional to the velocity of the particles. Ultrasound doppler differs from LDA in that the beam is not of laser light, but of ultrasound waves, to which soft body tissues and blood are translucent.

The Advantages: The ability of Ultrasound Doppler to see through body tissues allows the positioning of the control volume in places such as the ascending aorta or within the ventricles and thus yielding information about heart valve flow. The use of Ultrasound Doppler in-vitro allows the measurement of velocity and shear stresses in blood filled test sections thus eliminating the need to model using blood analogue solutions (Mann et al. 1987)

The Disadvantages: The need to assume isotropy of turbulence is possibly the major drawback of the technique. In-vivo there is no solution to this problem, but in-vitro a three beam set up could do away with the need for this assumption. The size of the control volume is large and difficult to control due to the spreading out of the ultrasound waves, this means that a lot of the smaller scale turbulence information can not be assessed.

## 3] HOT WIRE/HOT FILM ANEMOMETRY

The Technique: An electrical current is caused to flow through and heat a wire, cross wires or film probe of high electrical resistivity which is placed into a moving fluid. The conduction of heat away from the probe is dependent upon the velocity of fluid passing over it and the current drawn is proportional to the cooling effect on the probe. Consequently, by monitoring the current necessary to maintain a constant probe temperature, the velocity of the fluid passing over it can be deduced following calibration against a known fluid velocity. A more complete discussion of hot film anemometry applied to blood flow can be found in works by Paulsen et al. (1983 and 1987) and Tillmann et al. (1984).

The Advantages: Hot wire/hot film anemometry is very well established and relatively cheap to install, it is a very simple technique to use and can be used in opaque media.

The Disadvantages: The use of probe based anemometry necessarily complicates the test section geometry because of the need to place a probe into the flow. The wires of a hot wire probe are of very fine gauge and therefore cannot be used in a two phase flow containing large solid particles, as these would break the probe wires, this can be overcome by using a hot film probe. Probably the factor that most restricts hot wire and hot film anemometry is the

intrusive nature of the probes themselves. This makes meaningless any velocity data recovered from recirculative flow because of the interaction of the probe and mount with the flow. The probes because of their size have a limited spatial resolution of application and cannot be used in very close proximity to walls and obstructions though film can be wall mounted to yield information about boundary layer flow.

#### 4] PITOT TUBE MEASUREMENTS

The Technique: Static and dynamic pressures are obtained by a probe, with perpendicularly opposed pressure tapings, placed into the flow field. The difference between these two pressures is proportional to  $1/2 \rho v^2$  - knowing the density of the fluid, the velocity can be determined.

The Advantages: A very simple technique yielding velocities and static pressures, its cost is very low and analysis of results is straight forward.

The Disadvantages: Pitot tube measurements can only be applied successfully to streamwise dominant flow and have limited spatial resolution, due to the dimensions of the probe, this also limits near-wall measurements. Flow sections are necessarily complicated to allow for probe intrusion.

#### 5] FLOW VISUALISATION STUDIES

The Techniques: There are several flow visualisation techniques. These basically all consist of small tracer particles (powders, emulsions, gas bubbles or beads) being added to the bulk fluid. As the tracers pass through an illuminated section the paths they prescribe are captured on a recording medium - generally photographic film or video. The data yielded is generally only qualitative, showing streamlines, but by using stroboscopic lighting with unequal ratios of illumination and extinction and then by mapping the length of streak obtained in a known film exposure time, a quantitative description of the velocity field can be gained. A recent development in flow visualisation techniques is Particle Image Velocimetry (PIV), where a high concentration of very small particles (10 $\mu$ m diameter) is used to seed the flow. Multiple exposures of the particles passing through a thin sheet of laser light are taken in rapid succession. Velocity vectors are yielded by the interrogation, by laser, of the contact printed positive transparency of the particle images. Velocity vector magnitude is inversely proportional to the Young's fringe spacing set up by the interrogation and vector direction is perpendicular to the lay of the fringes.

The Advantages: The technique can be as complicated or simple as the operator requires (at the expense of data) and can be very inexpensive using readily available materials. Geometrical constraints are not so stringent as for LDA and initiation and use are not time consuming. None of the different forms of the technique are intrusive and all give full flow field information. Using the right mode of flow visualisation, varying amounts of quantitative data can be obtained.

The Disadvantages: Most flow visualisation techniques are only qualitative and therefore only give limited understanding of a flow regime. Quantitative flow visualisation techniques require a large input of time in the analysis of photographic recordings and the installation of PIV for the analysis of turbulent flow is very expensive and not an established technique.

## 6] STATIC PRESSURE MEASUREMENTS

The Technique: A small pressure tapping is made in the side of the test section wall, generally one before the valve and one after. A pressure measuring device ('U'-tube, variable reluctance transducer or similar) is connected to the taps to measure either differential pressures across the valve, or gauge pressures above atmospheric. Energy loss measurements are effected by gathering Pressure drops and Flow Rates throughout a series of complete heart cycles, although recent analysis (Leefe and Gentle 1986) has shown that this is by no means as simple as is currently supposed.

The Advantages: This form of measurement is very simple and cheap to achieve and has for a long time been used almost as the definitive classifier of valve haemodynamic performance.

The Disadvantages: Static pressure measured in the above way is very prone to inaccuracies because of the assumption that the pressure distribution will be the same throughout the radial plane. This is not the case in flows where streamlines are strongly curved - the flow regime that is dominant in most cases of heart valve flow.

## 7] FLOW METERING

The Methods: There are two very popular flow meter types applied to flow rate metering in prosthetic heart valve flow; electro-magnetic and turbine. The electro-magnetic meter works by the Hall effect where an electrically conducting fluid passing through a field of magnetic flux induces an EMF. The magnitude of this induced voltage is directly proportional to the flow velocity. The turbine flow meter relies on the movement of a turbine inserted into the flow. The movement of the turbine causes a small current to be developed in an attached generator indicating flow rate.

The Advantages: Both methods of measuring flow rate are relatively inexpensive and easily applied in-vitro. Signal conditioning and analysis are straight forward and quick, accuracy can be high but is dependent on conditions such as flow symmetry and working fluid.

The Disadvantages: Turbine meters can be slow to react to small variations in flow rate due to their inertia and consequently can lag behind the fluid, or completely miss small fluctuations. Electro-magnetic flow meters do not suffer from inertia problems as there are no moving parts, but deviations of the flow profile away from symmetry will cause errors. This also occurs, though much less significantly, in turbine meters. Electro-magnetic flow meters can also be affected by electrical noise and by the choice of working fluid and vessel material.

The above methods of flow analysis are all applied to in-vitro models of heart valve flow with varying degrees of success. However, in-vitro modelling itself suffers from several problems, most notably:

1] that of using blood as a flow medium because of the obvious handling difficulties, even with anticoagulation or with the platelets removed, and because its opaque nature prevents the use of the most popular flow study methods.

2] If blood is not to be used, but is to be replaced by an analogue solution there is a reduction in the correlation of in-vitro fluid behaviour to that in-vivo because of the complex viscosity of blood. This, argue Chmiel and Walitza (1980), is significant in complex flow geometries. Moreover analysis even of a regime as simple as fully developed laminar pipeflow can point to the introduction of significant errors due to the use of analogue solutions. It is shown in table 1, displaying data generated by the CFM technique described later, that a valve will have generally poorer haemodynamic characteristics, (ie. higher thrombotic and haemolytic potentials) than will be predicted in analogue flow experiments.

TABLE 1

A comparison of flow properties in a pipe. The analogue fluid used was a 30% aqueous glycerol solution of density  $1170 \text{ kg/m}^3$  and dynamic viscosity  $3.006 \times 10^{-6} \text{ m}^2/\text{s}$ . The 'blood' flow is modelled on the Casson equation for the data presented by Charm and Kurland and Rand et al. (see below).

<u>Parameter</u>	<u>Analogue</u>	<u>Rand et al.</u>	<u>Charm and Kurland</u>	<u>Units</u>
$dp/dx$	47.617	68.00	63.02	Pa/m
$\mu_{max}$	3.587	3.133	3.316	mPa s
$\dot{\gamma}_{max}$	68.28	71.83	71.78	$\text{s}^{-1}$
$\dot{\gamma}_{min}$	3.569	0.5119	0.5339	$\text{s}^{-1}$
$\tau_{max}$	0.2269	0.3281	0.2995	Pa
$\tau_{min}$	0.01186	0.02214	0.02011	Pa
$v_{max}/v$	1.996	1.841	1.842	

## MODELLING BLOOD FLOW USING CFM

Many of the above difficulties seem to be surmountable by the application of CFM. There are no problems relating to the accessibility of test equipment or control volumes, no difficulties of modelling posed by opaque fluids (since no actual visualisation is required) and hence there is no need to model in a fluid other than blood, unless trying to verify hydraulic test data or save computer time by only studying a simple model. CFM can yield full field information about any flow parameter; those that can be yielded by other techniques - velocities, turbulence intensities, pressure drops and streamlines and those that cannot - turbulent viscosities and hence reliable measures of turbulent shear stresses, near-wall velocities and pressures throughout a radial section. Several CFM studies have been carried out to date, but most have only considered laminar flow (Underwood and Meuller 1977 and 1979, Idelsohn et al. 1985, Peskin 1982), though a recent paper by Thalassoudis et al. (1987) presented a study of turbulent flow through a Boundary Fitted Coordinate modelled Starr-Edwards valve. However, as yet no study has addressed the non-Newtonian aspect of blood flow. Graphical data can be produced, once the flow solution has been arrived at and areas containing values of particular interest, such as high shear stress and stasis, can be highlighted. Depending on the package used, however, this can be difficult. Flow sections can readily be altered as part of the design process and flow data can be retrieved without actually manufacturing a physical model.

As the rheology of blood is that of a Plastic fluid a constitutive equation is necessary to describe the shear stress/shear rate relationship, but due to the complexity of blood flow it is not possible to derive any such equation from first principles, each then has a certain amount of empirical input; Cokelet (1987) reviews several such equations. Most of the constitutive equations are suitable for application to CFM studies with one notable exception - that of Chmiel and Walitza (1980), which requires foreknowledge of the shear stress in order to calculate the shear rate. The other equations base their calculation of shear stress on a pre-determined shear rate. The equation used by the authors in this present study was that of Casson (1959):

$$|\tau| = |(a_0) + |(a_1\dot{\gamma})|$$

Where:  $\tau$  = shear stress

$\dot{\gamma}$  = shear rate

$a_0$  and  $a_1$  are empirical constants found by fitting the Casson equation to observed blood flow data. Taking an average of each of these constants presented by Charm and Kurland (1965) for blood at 37°C from a range of donors, puts the values at  $a_0 = 10.726 \times 10^{-3} \text{Pa}$  and  $a_1 = 52.367 \times 10^{-3} \text{Pa s}$ . By way of comparison, fitting data presented by Rand et al. (1964) gives slightly different values of the constants;  $a_0 = 12.0341 \times 10^{-3} \text{Pa}$  and  $a_1 = 54.636 \times 10^{-3} \text{Pa s}$  (to yield S.I. units) for blood of 40HCT at 37°C.

The  $\dot{\gamma}$  term will usually be available in CFM codes as it is the generation term used in the turbulence model. The complex blood viscosity  $\mu_a$  replaces the laminar viscosity, thus:

$$\mu_L = \mu_a = \tau / \dot{\gamma}$$

and so the blood viscosity is activated both in laminar modelling and turbulent modelling where:

$$\mu_{eff} = \mu_L + \mu_T$$

The reasons for selecting the Casson equation in preference to any of the other constitutive equations were:

- 1] Ease of application to CFM studies
- 2] Ease of determination of the empirical constants
- 3] Accuracy is high - within 5% error over the range of shear rates 0 - 100 000 s<sup>-1</sup> (Charm and Kurland 1965)
- 4] Good agreement with experimental studies (error of 4.5% compared with the work of Hershey and Cho (1966))

Throughout the studies blood was assumed to be a continuum, suggested by the findings of Chmiel and Walitza (1980), as the studies have been restricted to flow regimes of dimensions not less than 0.5mm. This assumption would need modification if, for example, capillary flow was being modelled.

#### The Disadvantages of CFM

Undoubtedly the major disadvantage of CFM is the inadequacy of current turbulence models. Although significant progress has been made in this area and good results are being recorded in turbulent flow, until turbulent phenomena can be solved in the primary state, CFM cannot offer a totally accurate solution in all flow situations. Of particular concern is the applicability of any of the current state-of-the-art turbulence models to unsteady flow. This is a major limitation in heart valve work. Although a solution could be attempted for such flow the authors would not be able to quantify any level of certainty on the results of such an analysis and have therefore restricted study to steady state problems. Related problems are the large amounts of computer storage necessary and the time taken for a complete solution to be reached, even with the simplifying application of turbulence models. The expense of installing and maintaining a CFM package may be prohibitive and the cheaper micro computer options are only of limited value when modelling large three dimensional flow fields. Most 'bought-in' CFM packages do not accommodate the use of such model complexities as non-Newtonian fluids or distensible boundaries and time must necessarily be expended in writing algorithms to allow for these. The need to incorporate such algorithms might restrict the choice of suitable packages.

#### A CASE STUDY TO ILLUSTRATE THE USE OF CFM

The aim of this case study is to describe one particular flow situation where the advantages of CFM over experimental methods can be best appreciated. The study is concerned with an analysis of leakage flow through a Gentle twin flap mitral valve (Gentle et al. 1981).

As part of this valve's development an enlarged gap was introduced between the closed flaps. The intention was to allow a controlled volume of blood to flow in the reverse direction, through this gap and thus effect a washing action, reducing the likelihood of clot formation. This

washing action would be further enhanced, argues Gentle (1982), if the blood flowing through the gap was turbulent. The gap design criterion was initially based analytically on Reynolds' numbers and skin friction factor. This proved not to be a suitable criterion, as discussed by Leefe et al. (1986), who also discussed the many severely restricting assumptions necessary to simplify the problem down to an analytically approachable one and the poor correlation between the analytical model and experimentation.

If this flow were to be analysed experimentally one might be justified in assuming two dimensionality because of the geometry of the gap, and so a two beam, frequency shifted LDA system should yield satisfactory shear stress data in analogue flows. If the LDA measurement were to be made on the valve itself and not on a two dimensional mock up then correcting lenses would be necessary if measurements were required away from the axis of the valve, or complicated control volume displacement and intersect angle correction calculations would be necessary. Further experimental restrictions would be presented by the relatively poor spacial resolution of LDA (as compared with CFM), bearing in mind that the gap is only 0.5mm wide. One further limitation to the experimental procedure is the need to use a blood analogue solution, which must surely limit the degree of confidence in predictions of the shear stress and shear rates. If Ultra sound Doppler was employed instead of LDA, the latter problem might be overcome, but spatial resolution of measurement would be likely to suffer further, and the choice of materials from which the test section could be manufactured would be severely restricted by the need for 'ultrasound transparency'. Hot film anemometry would not be useful because of the recirculating nature of the flow.

In the computationally modelled version of Leefe et al., the problem was considered two-dimensionally for simplicity and to reduce the requirements for computer time and storage, but in principle it could equally well have been considered three-dimensionally. The flow region is well suited to application of the standard  $k - \epsilon$  model so high accuracy was expected confidently even though some reduction of accuracy was expected at the wall. The assumption of steady flow was not severely limiting because backflow of this nature is essentially much closer to being steady than forward flow. Furthermore the same assumption would probably have been made for the experimental study.

The results of this CFM study are presented graphically, Figure 5 presents a schema of the two-dimensional flow region. Figure 6 shows computationally predicted streamlines for leakage flow through twin flap mitral valve. Figures 7 and 8 present shear stress plots in alternative forms; either as vectors or contours. Finally figure 9 shows graphically the prediction of the onset of turbulence. The analysis of these results highlights the severe limitations of analytical approaches to the investigation of leakage flow. Also highlighted in this study was the unexpectedly high haemolytic potential of the valve in the leakage flow mode.

## DISCUSSION AND CONCLUSION

When applied to prosthetic heart valve evaluation no in-vitro technique is capable of yielding all the data necessary to describe fully a flow field. Not even when several of these techniques are used together can full field shear stresses be obtained. Furthermore, in-vitro modelling in itself is not wholly suited to the analysis of blood flow due to problems relating to the opaqueness of blood and its clotting function.

The use of Computational Fluid Mechanics alleviates these modelling problems and permits the evaluation of blood flow, unaffected by blood's opaque nature or by clotting, as no physical modelling is necessary. The greatest advantage CFM has over the in-vitro techniques is the ability to predict full field attributes, especially shear stresses and turbulent viscosities. CFM, however, is not without its limitations, the major one being the need for turbulence modelling because of the limited capabilities of existing digital computers. This is the single largest cause of error in predictions and can restrict the application of the technique to certain flow regimes, most notably to steady flow analysis. Further limitations of CFM are the expense in terms of finance, computer time and storage and the expertise needed to write 'in-house' CFM codes or modifications for 'bought-in' packages, for example to allow the study of non-Newtonian fluid flow or distensibility.

The major advance CFM is capable of making to heart valve research is a greater correlation between modelled flow and the understanding of clinical complications, than is possible with in-vitro modelling. This is brought about by the ability of CFM to yield values for the critical flow attributes, turbulent viscosity and Reynold's stresses, without the need for inference from scalar factors such as turbulence intensity. CFM can be based on a closer representation of the clinical flow regime than is generally possible using in-vitro modelling because of the problems associated with physically modelling in blood. This also improves the correlation with in-vivo flow as the non-Newtonian viscosity of blood plays a very important role in regions of haemostasis and consequently has a bearing on thrombotic complications.

In conclusion, the authors believe there is great potential for improvements in prosthetic valve haemodynamics via the application of existing CFM techniques along with the complementary in-vitro analysis methods. However, in realising the problems posed currently by the need for turbulence models, one must look forward to the time when a universally applicable turbulence model is developed, or the capabilities of computers are so improved as to make such models redundant.

## REFERENCES

- Abujelula, M.T. and Lilley, D.G. 1984. Limitations and empirical extensions of the  $k - \epsilon$  model as applied to turbulent confined swirling flows. *Chemical Engineering Communications*, **31**, 223-236
- Aston, S.C. and Mulder, D.G. 1971. Cardiac valve replacement: a seven year follow up. *Journal of Thoracic and Cardiovascular Surgery*, **61**, 547-555
- Autret, A, Grandotto, M and Dekeyser, I. 1987. Finite element computation of a turbulent flow over a two-dimensional backward-facing step. *International Journal for Numerical Methods in Fluids*, **7**, 89-102
- Bacher, R.P. and Williams, M.C. 1970. Hemolysis in capillary flow. *Journal of Laboratory and Clinical Medicine*, **76**, 485-496
- Beissinger, R.L. and Williams, M.C. 1984. A dual Mechanism for low-stress Hemolysis in laminar blood flow. *Journal of the American Institute of Chemical Engineers*, **30**, (4), 569-577
- Blackshear P.L. 1972. Mechanical hemolysis in flowing blood. in: Fung, Y.C., Perrone, N. and Anliker, M. (eds.), *Biomechanics: its foundation and objectives*, Prentice-Hall, New Jersey, USA, 501-528
- Blackshear, P.L. and Blackshear G.L. 1987. Mechanical hemolysis in: Skalak, R. and Chien, S. (eds.), *Handbook of Bioengineering*, McGraw-Hill, chapter 15
- Casson, N. 1959. A flow equation for pigment-oil suspensions of the printing ink type. in: Mill, C.C. (ed.), *Rheology of Disperse Systems*, Pergamon Press, New York. Ch 5.
- Charm, S and Kurland, G. 1965. Viscometry of human blood for shear rates of 0 - 100 000  $\text{sec}^{-1}$ . *Nature*, **206**, 617-618
- Chmiel, H. and Walitza, E. 1980. On the rheology of blood and synovial fluid. *Research Studies Press (John Wiley and Sons)*, Chichester
- Cokelet G.R. 1987. The rheology and tube flow of blood. in: Skalak, R. and Chien, S. (eds.), *Handbook of Bioengineering*, McGraw-Hill, chapter 14
- Dewey, C.F, Bussolari, S.R., Gimbrone, M.A. and Davies, P.F. 1981. The dynamic response of vascular endothelial cells to fluid shear stress. *ASME Transactions: Journal of Biomechanical Engineering*, **103**, 177-185
- Dintenfass, L. 1964. Rheological approach to thrombosis and atherosclerosis. *Angiology*, **15**, 333-343
- Figliola, R.S. and Mueller, T.J. 1981. On the hemolytic and thrombogenic potential of occluder prosthetic heart valves from in-vitro measurements. *ASME Transactions: Journal of Biomechanical Engineering*, **103**, 83-89
- Fry, D.L. 1968. Acute vascular endothelial changes associated with increased blood velocity gradients. *Circulation Research*, **12**, 165-197

- Fry, D.L. 1969. Certain histological and chemical responses of the vascular interface to acutely induced stress in the aorta of dog. *Circulation Research*, **24**, 93-108
- Gartling, D.K. 1986. Finite element methods for non-Newtonian Flows. Scandia National Laboratories, USA, report number SAND-85-1704, [DE 86 007410/GAR]
- Gentle, C.R. 1982. Characterisation of leakage flow in cardiac valve prostheses. in: *Proceedings of the IX meeting of the European Society for Artificial Organs*, 102-106
- Gentle, C.R., Juden, H. and Swales, P.D. 1981. Testing of an all-ceramic mitral valve prosthesis. in: *Proceedings of the European Society for Artificial Organs*, **8**, 352-355
- Hellums, J.D., and Brown, C.H., 1975. Blood cell damage by mechanical Forces. in: Hwang, H.N.C. and Normann, N.A. (eds.), *Cardiovascular flow Dynamics and Measurements*, University Park Press, Baltimore, USA., 799-823
- Hershey, D. and Cho, S.J. 1966. Blood flow in rigid tubes: thickness and slip velocity of plasma film at the wall. *Journal of Applied Physiology*, **21**, 27-32
- Idelsohn, S.R., Costa, L.E. and Ponso, R. 1985. A comparative computational study of blood flow through prosthetic heart valves using the finite element method. *Journal of Biomechanics*, **18**, 97-115
- Johnson, S.A. 1970. Platelets in hemostasis. in: Seegers, W.H. (ed.) *Blood clotting enzymology*, Academic Press, 379-420
- Jones, W.P. and Launder, B.E. 1972. The prediction of laminarisation with a 2 - equation model of turbulence. *International Journal of Heat and Mass Transfer*, **15**, 301-314
- Lampert, R.H. and Williams, M.C. 1972. Effect of surface materials on shear-induced hemolysis. *Journal of Biomedical Materials Research*, **6**, 499-532
- Launder, B.E. and Spalding, D.B. 1974. The numerical computation of turbulent flows. *Computer Methods in Applied Mechanics and Engineering*, **3**, 269-289
- Leefe, S.E and Gentle C.R. 1987. Theoretical evaluation of energy loss methods in the analysis of prosthetic heart valves. *Journal of Biomedical Engineering*, **9**, (2), 121-127
- Leefe, S.E., Edwards, R.J., Tansley, G.D. and Gentle, C.R. 1986. Investigation into leakage design in prosthetic heart valves in: *Proceedings of the 26th. Annual Meeting of the Biological Engineering Society*, Glasgow
- Leverett, L.B., Hellums, J.D., Alfrey, C.P. and Lynch, E.C. 1972. Red blood cell damage by shear stress. *Biophysical Journal*, **12**, 257-273

- Mann, K.A., Deutsch, S., Tarbell, J.M., Geselowitz, D.B., Rosenberg, G. and Pierce, W.S. 1987. An experimental study of Newtonian and non-Newtonian flow dynamics in a ventricular assist device. *ASME Transactions: Journal of Biomechanical Engineering*, **109**, 139-147
- Monroe, J.M., Lijana, R.C. and Williams, M.C. 1980. Hemolytic properties of special materials exposed to a shear flow and plasma changes with shear. *Biomaterials, Medical Devices and Artificial Organs*, **8**, 103-144
- Morain, J.G. 1982. Turbulence modelling for Computational Aerodynamics. *American Institute of Aeronautics and Astronautics*, paper 82-0164
- Mehta, U. and Lomax, H. 1982. Reynolds averaged Navier Stokes computation of transonic flows: the state of the art. in: Nixon, D. (ed.) *Progress in astronautics and aeronautics, transonic aerodynamics*, American Institution of Aeronautics and Astronautics, **81**, 297-375
- Narducci, C., Russo, L., Battaglia, L., Angelica, G., Giovannini, E. and D'Alessandro, L.C. 1986. Dysfunction of double disc valvular prosthesis: report on 5 cases. in: *Proceedings XIII Annual Meeting of the European Society for Artificial Organs*, 160-162
- Nerem, R.M., Levesque, M.J. and Sato, M. 1984. Vascular dynamics and the endothelium. *Frontiers in Biomechanics, symposium on frontiers of applied mechanics and biomechanics*, San Diego, 324-341
- Nunez, L., Iglesias, A. and Sotillo J. 1980. Entrapment of leaflets of St. Jude Medical cardiac valve prosthesis by miniscule thrombosis. Report of two cases. *Annals of Thoracic Surgery*, **29**, 566-569
- Paulsen, P.K. and Hasenkam, J.M. 1983. Three-dimensional visualization of velocity profiles in the ascending aorta in dogs, measured with a hot-film anemometer. *J. Biomech.*, **16**, (3), 201-210
- Paulsen, P.K., Hasenkam, J.M., Nygaard, H. and Gormsen, J. 1987. Analysis of the dynamic properties of a hot-film anemometer system for blood velocity measurements in humans. *Medical and Biological Engineering and Computing*, **25**, 195-200
- Peskin, C.S. 1982. The fluid dynamics of heart valves: experimental, theoretical and computational methods. *Annual Review of Fluid Mechanics*, **14**, 235-259
- Rand, P.W., Lacombe, E., Hunt, H.E. and Austin, W.H. 1964. Viscosity of normal blood under normothermic and hypothermic conditions. *Journal of Applied Physiology*, **19**, 117-121
- Rooney, J.A. 1970. Hemolysis near an ultrasonically pulsating gas bubble. *Science (Washington)*, **196**, 869-871
- Roschke, E.J., Harrison, E.C. and Blankenhorn, D.H. 1975. Fluid shear stress during the opening sequence of prosthetic heart valves. Proc. 28th. Ann. Conf. Engr. Med. Bio. PP D5.4

Ross, J.C., Hufnagel, J., Freis, C., Harvey, W. and Partenope. 1954. The hemodynamic alterations produced by a plastic valvular prosthesis for severe aortic insufficiency in man. *Journal of Clinical Investigations*, **33**, 891-900

Shapiro, S.I. and Williams A.R. 1970. Hemolysis in simpler shear flows. *Journal of the American Institute of Chemical Engineers*, **16**, 575-580

Solen, K.A., Whiffen, J.D. and Lightfoot, E.N. 1978. The effect of shear, specific surface, and air interface on the development of blood emboli and hemolysis. *Journal of Biomedical Materials Research*, **12**, 381-399

Solen, K.A., Whiffen, J.D. and Lightfoot, E.N. 1981. Plasma glucose concentrations and the development of blood emboli and hemolysis. *Journal of Laboratory and Clinical Medicine*, **98**, (2), 206-216

Spalding, D.B. 1981. A general purpose computer program for multi-dimensional one and two-phase flow. *Mathematics and Computers in Simulation*, **23**, 267-278

Tansley, G.D., Edwards, R.J., Leefe, S.E. and Gentle, C.R. 1986. Ball occluder instability during forward flow through prosthetic heart valve conduits. In: *Proceedings of XIII Annual meeting of the European Society for Artificial Organs*, 169-171

Tillmann, W., Reul, H., Herold, M., Bruss, K.H., and Van Gilse, J. 1984. In-vitro wall shear measurements at aortic valve prostheses. *Journal of Biomechanics*, **4**, 263-279

Thalassoudis, K., Mazumdar, J. and Noye, B.J. 1987. Numerical study of turbulent blood flow through a caged-ball prosthetic heart valve using a boundary-fitted co-ordinate system. *Medical and Biological Engineering and Computing*, **26**, 173-180

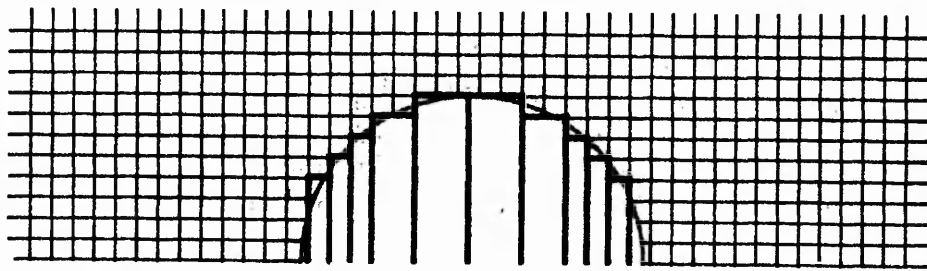
Underwood, F.N. and Mueller, T.J. 1977. Numerical study of the steady axisymmetric flow through a disk-type prosthetic heart valve in a constant diameter chamber. *ASME Transactions: Journal of Biomechanical Engineering*, **99**, 91-97

Underwood, F.N. and Mueller, T.J. 1979. Numerical study of the steady axisymmetric flow through a disk-type prosthetic heart valve in an aortic shaped chamber. *ASME Transactions: Journal of Biomechanical Engineering*, **101**, 198-204

Vaishnav, R.N., Patel, D.J., Atabek, H.B., Deshpande, M.D., Plowman, F. and Vossoughi, J. 1983. Determination of the local erosion stress of the canine endothelium using a jet impingement method. *ASME Transactions: Journal of Biomechanical Engineering*, **105**, 77-83

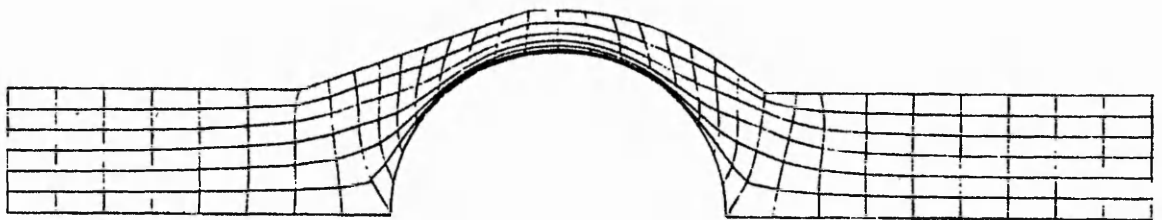
Whitmore R.L. 1968. *Rheology of the Circulation*. Pergamon Press, Oxford.

Williams, A.R., Hughes, D.E., Nyborg, W.L. 1970. Hemolysis near a transversely oscillating wire. *Science (Washington)*, **196**, 871-873  
Blackshear 1972 - Publisher is Prentice Hall, New Jersey, USA.



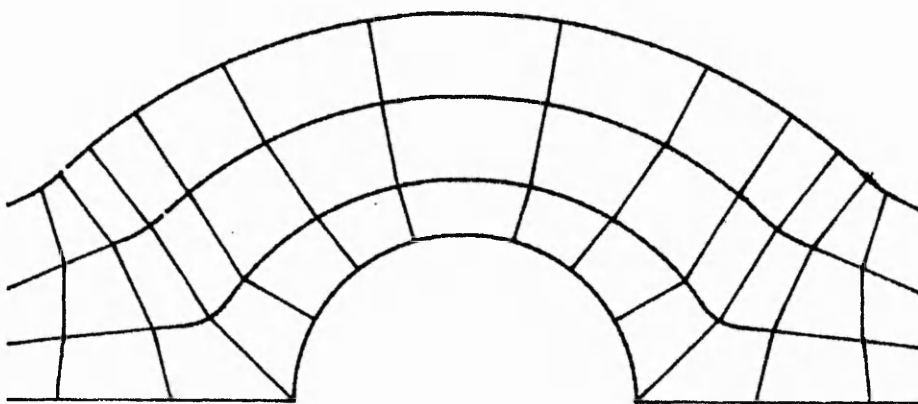
A

ORTHOGONAL FINITE DIFFERENCE GRID



B

NON-ORTHOGONAL FINITE DIFFERENCE GRID  
(BFC GRID)



C

FINITE ELEMENT GRID

FIG1 EXAMPLES OF FINITE ELEMENT  
AND FINITE DIFFERENCE GRIDS

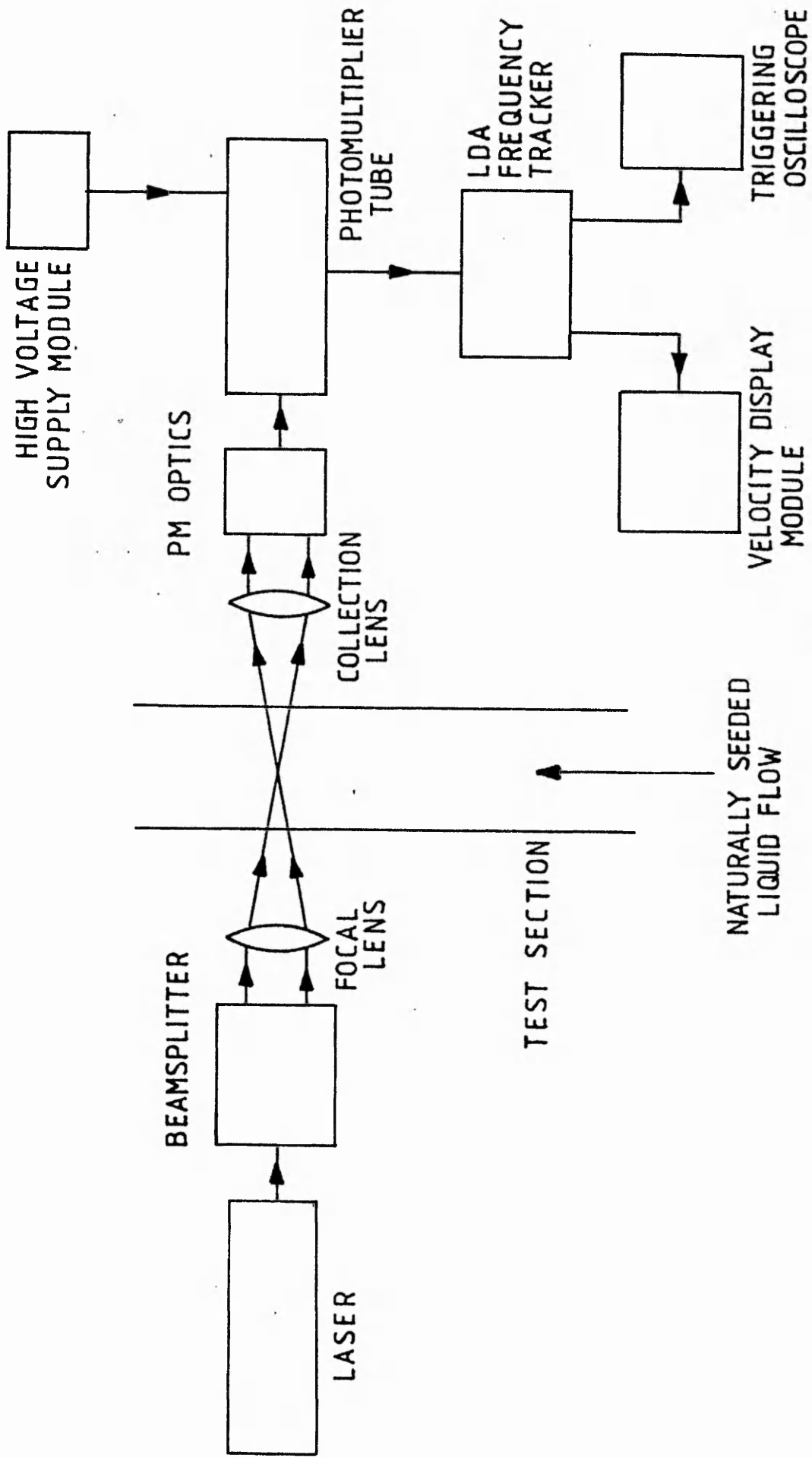


FIG 2 SCHEMATIC OF AN LDA SYSTEM

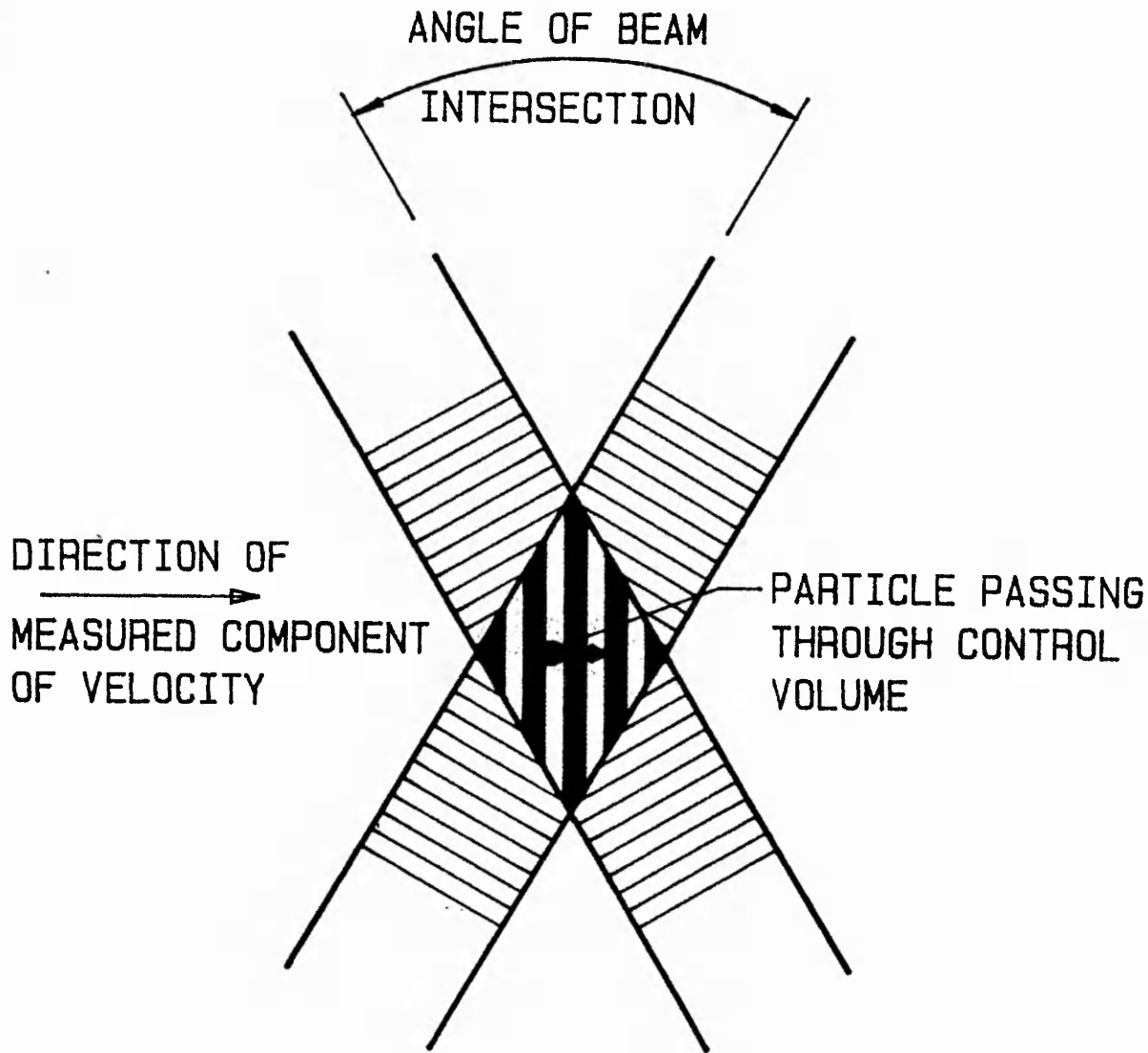
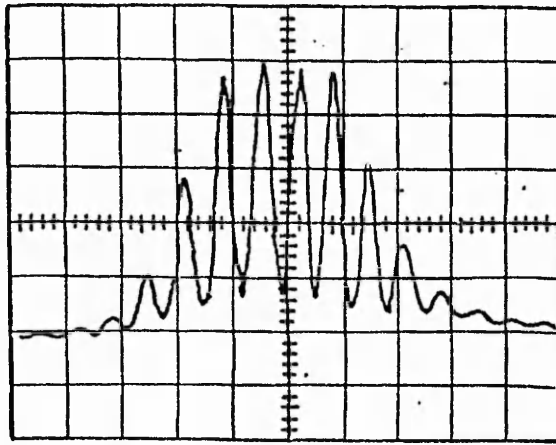
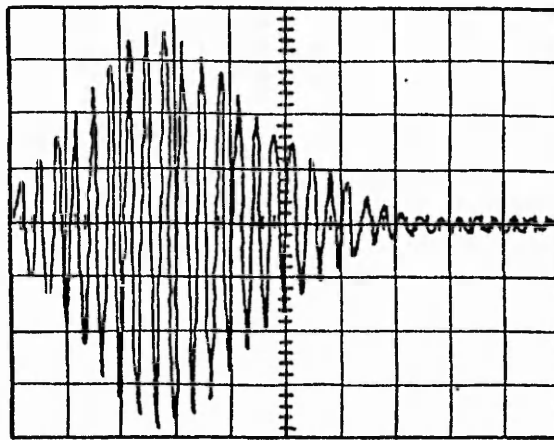


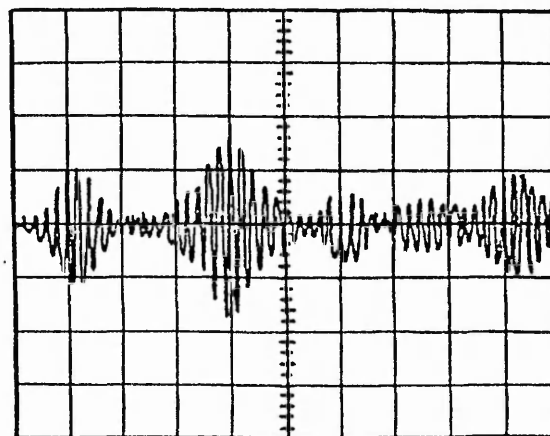
FIG 3 LDA CONTROL VOLUME FRINGE PATTERN



Doppler Burst - Detector Signal



Doppler Burst - Band-pass  
Filtered Signal



Multiple-particle Signal

FIG 4 TYPES OF LDA SIGNAL

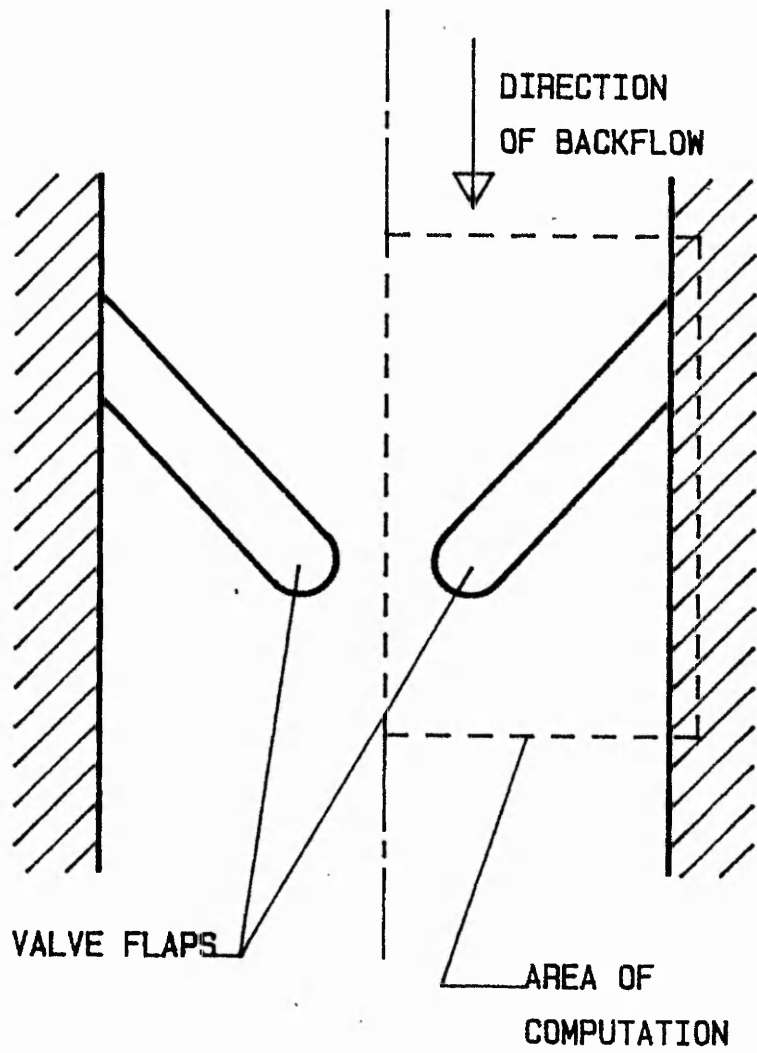


**FIG.5 SCHEMATIC OF SOLUTION REGION  
APPLIED TO A GENTLE TWIN FLAP  
CERAMIC VALVE**

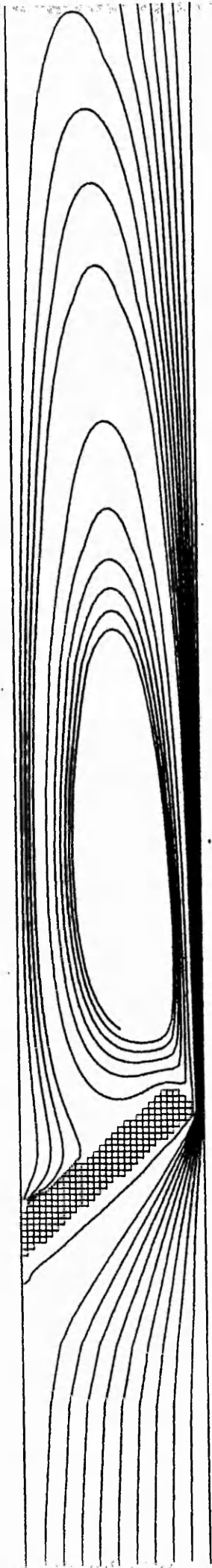


FIG 6 STREAMLINE PLOT OF A TWIN FLAP CERAMIC VALVE IN BACK FLOW

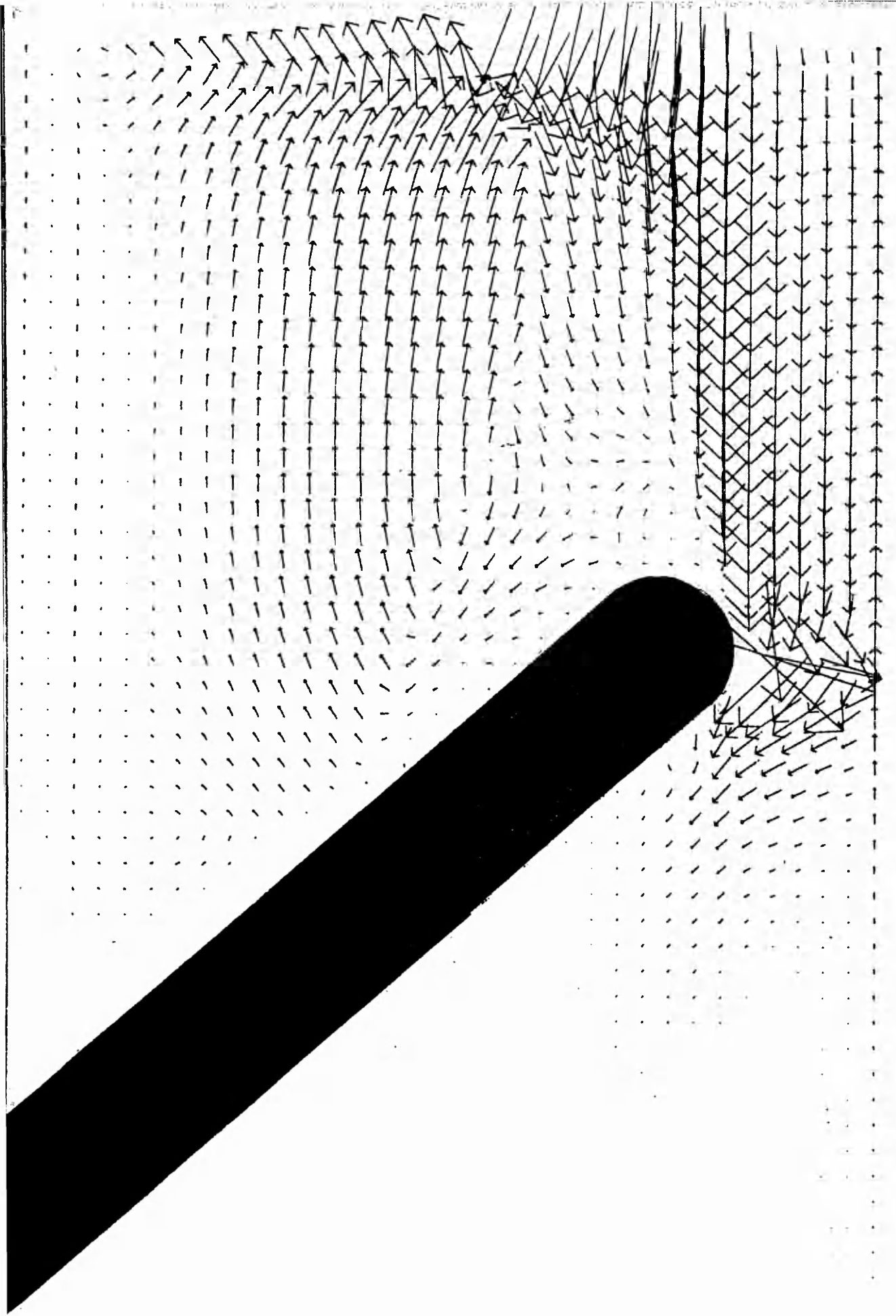


FIG 7 SHEAR STRESS VECTOR PLOT OF A TWIN FLAP CERAMIC VALVE IN BACK FLOW

CONTOUR KEY $N/m^2$	
1	0.00584498
2	0.01753494
3	0.02922490
4	0.04091486
5	0.05260483

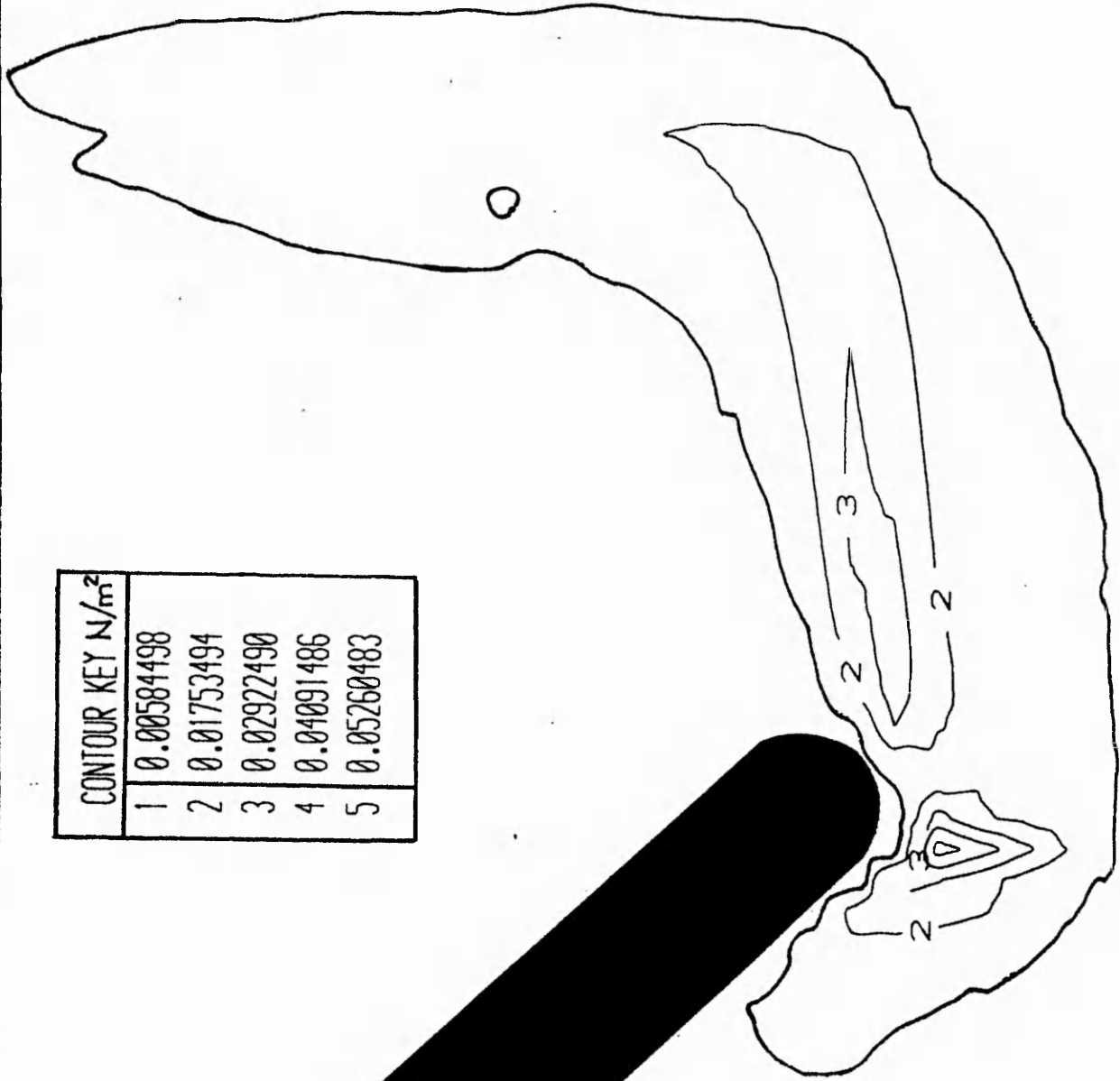


FIG 8 SHEAR STRESS CONTOUR PLOT

OCCLUDER

LAMINAR

STAGNATION

MAX SHEAR STRESS

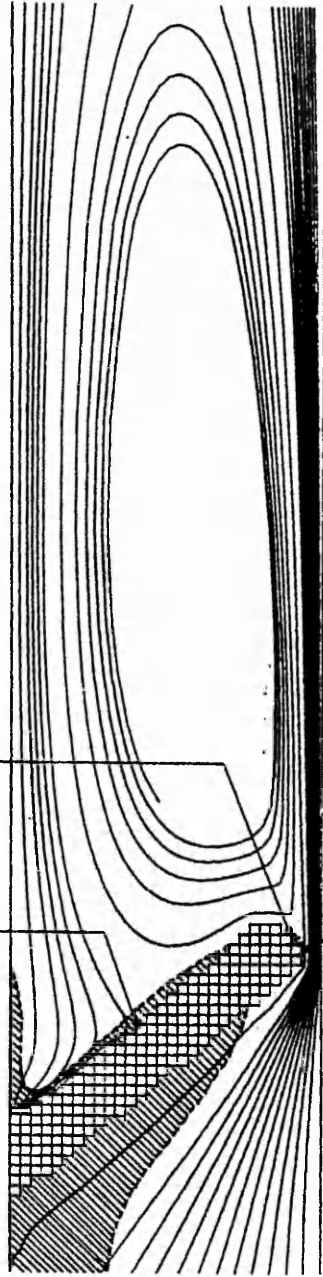


FIG 9 LAMINAR and STAGNATION REGIONS

The Prediction of haemodynamic characteristics of  
prosthetic heart valve flow using PHOENICS

G. D. Tansley

Department of Mechanical Engineering, Trent Polytechnic, Nottingham

This paper stems from current research projects at Trent Polytechnic aimed at optimizing the designs of a heart valve conduit and twin flap mitral valve.

ABSTRACT

The clinical acceptability of heart valve prostheses is inextricably linked to the valve's haemodynamic characteristics. More specifically, the problems of haemolysis (the destruction of red blood corpuscles) have been reported by several researchers to be a product of high shear stresses induced in the blood by the implantation of a prosthetic valve. Thrombosis, ie the formation of clots has been attributed to the existence of haemostasis or areas of low shear rate in regions in close proximity to a prosthesis.

Unfortunately, shear stresses and rates are two haemodynamic characteristics which are most difficult, if not impossible, to ascertain with any degree of confidence, due to the limitations of in-vitro modelling and current flow measurement techniques. It is for these reasons that the PHOENICS code has been applied to the analysis of heart valve blood flow and prosthesis design. PHOENICS is eminently suited to the prediction of blood flow, needing only the slightest modifications to the 'ground' file to introduce the non-Newtonian effects of blood which is modelled on the Casson equation:

$$\sqrt{\tau} = s\sqrt{\dot{\gamma}} + c$$

where: the constants 's' and 'c' are dependents of the blood temperature and composition, etc.

' $\dot{\gamma}$ ' is found in 'ground' via the function 'FNGENK' and ' $\tau/\dot{\gamma}$ ' is used to modify 'ENUL'.

## INTRODUCTION

### Valve implantation

#### 1] What are heart valves?

Basically heart valves are passive non-return valves:

- A] Natural they are bicuspid or tricuspid and are formed of living tissue.
- B] Mechanical they consist of a sewing ring surrounding a primary orifice which is mechanically occluded, commonly by a tilting disc, twin flaps, or a caged ball or disc.
- C] Bioprosthetic valves are made from porcine or bovine materials and given a form similar to the natural valve, but usually a stent is included to support the valve.
- D] Conduits - these consist of a section of flexible tubing, into which a mechanical or bioprosthetic valve is mounted.

#### 2] Implantation sites

There are four sites in the heart where natural valves are situated (see fig. 1). In general however, only the valves in the left heart are replaced, ie the Aortic and Mitral valves. The right heart valves (tricuspid and pulmonic) which suffer only 1/5<sup>th</sup> the pressure seen in the left heart are not so problematic so their replacement is rare.

Conduits are implanted typically as Apeco-Aortic shunts, ie between the apex of the heart and the descending aorta (fig. 2).

#### 3] Reasons for implantation

- A] To replace stenosed natural valves (valves in which the primary flow orifice has become partially blocked - causing an excessive pressure drop across the valve). This condition can lead the heart becoming considerably enlarged (hypertrophy) which can be fatal, and also to a poor quality of life - as circulation is restricted.
- B] To replace regurgitant valves (valves that allow excessive backflow). Severe regurgitation can lead to the failure of upstream valves and to the damage of the lungs due to an increase of pressure in the circulation of the right heart.
- C] As Apeco-aortic shunts, conduits are used to by-pass partially blocked aortas, this improves the circulation of blood to the abdomen.

## PROSTHETIC HEART VALVE FAILURE

There are many reasons why heart valves fail in service: mechanical failure, calcification and tearing of bioprosthetic material etc. Here, however, only failures due to haemodynamic factors are of interest. These can be divided into 5 categories:

### 1] Haemolysis in bulk fluid

This is the destruction of red blood corpuscles due to high shear stresses in the bulk of the flow. To avoid this condition, which can lead to Anaemia and death, a valve should not induce shear stresses higher than  $500 \text{ N/m}^2$  (fig. 3) this is the Haemolysis threshold in valve flow (Hellums and Brown 1975).

### 2] Haemolysis at the blood/prosthesis interface

blood cells are much more prone to damage at the prosthetic surface due to adhesion to the surface. Haemolysis can occur at shear stresses as low as  $150 \text{ N/m}^2$ . To reduce this problem shear stresses induced close to the valve's prosthetic surfaces should be minimised.

### 3] Damage to endothelial lining due to jet impingement

The lining of the Aorta is prone to damage by the impingement of jets of blood issuing from a valve. Directionality of the jets is important and so is the level of stress (damage occurs at values as low as  $40 \text{ N/m}^2$ ).

### 4] Valve dysfunction due to thrombus formation at hinge points

Thrombus forms in areas of haemostasis, these areas are likely to occur near to hinge points. The thrombus formed can cause total or partial restriction to occluder movement. At shear rates below  $7 \text{ s}^{-1}$  thrombus formation is accelerated (Dintenfass 1964).

### 5] Thrombo-embolism

Thrombo-embolism is also caused by haemostasis. The sites of thrombus formation might not be critical but the passage of thrombus downstream leading to embolism is potentially fatal.

summarizing:

It is important to establish the magnitudes of shear stresses and Shear rates and the areas in which critical values may occur as these yield a quantitative measure of a valve's thrombo-embolic and haemolytic potential.

## THE RHEOLOGY OF BLOOD

The above problems are increased by the rheological behaviour of blood, the shear rate/viscosity relationship of which is that of a plastic fluid.

Blood may be considered a continuum whilst flowing through tubes of a diameter greater than .5mm (Chmiel and Walitza 1980) and several descriptive equations have been formulated to describe the flow of blood under these conditions. (Cokelet 1987 reviews these equations.) In this current work the Casson equation was employed because:

- 1] The casson equation is easily applied to PHOENICS
- 2] The constants are easily determined
- 3] Accuracy is good - within 5% error over the range of shear rates 0 - 100 000 s<sup>-1</sup> (Charm and Kurland 1965)
- 4] Good agreement with experimental flows (an error of 4.5% in pressure was predicted in the current work based on the experimental work of Hershey and Cho 1966)

The Casson Equation:

$$\sqrt{\tau} = s\sqrt{\dot{\gamma}} + c$$

Where 'c' and 's' are constants dependent on the blood haematocrit and temperature etc.

Using Normal blood of haematocrit 45 at body temperature (37 Celcius):

$$s \approx 0.053$$

$$c \approx 0.107$$

Though these values may vary due to the samples of blood tested.

Whitmore(1968) re-writes the Casson equation taking into account the viscosity of plasma( $\mu_0$ ), which it is fair to assume, is Newtonian at body temperature:

$$\sqrt{\tau/\mu_0} = 1.53\sqrt{\dot{\gamma}} + 2.0$$

Using PHOENICS to Compare Newtonian fluids with Blood models for a regime as simple as laminar pipe flow indicates that if Newtonian fluids were used to assess key flow parameters such as shear stress, serious under prediction of the thrombo-embotic and heamolytic potentials of valves would result (fig. 4).

In analogue fluid:

Minimum shear rate is under predicted by 600%

Maximum shear stress is under predicted by 28%

## IN-VITRO MEASUREMENT OF FLOW CHARACTERISTICS

Presented below is a brief summary of current experimental techniques which are applied to the analysis of blood flow and specific difficulties which limits their usefulness:

TECHNIQUE	MEASUREMENTS	LIMITATIONS
L.D.A.	Full field velocities	except near walls
	Turbulence Intensities	needs 3 beam set up Reynolds' shear stress or assumed 3rd dimension

Access is often restricted and lengthy corrections for the beam intersect angle are necessary in complex geometries. The flow media must be transparent to the illuminating source - this restricts measurement in blood.

ULTRASOUND DOPPLER	Full field velocities	very limited resolution In-vivo severe access restrictions
-----------------------	-----------------------	---

Ultrasound Doppler anemometry is capable of yielding real-time in-vivo velocity fields, obviously modelling is not necessary and blood is the fluid used, but 3 dimensional measurements are not possible in-vivo so that turbulence intensities and Reynolds' shear stresses are of very limited use. In-vitro Ultrasound Doppler measurements suffer from a poor resolution and the need for three beams.

HOT WIRE/FILM ANEMOMETRY	Velocity vectors	not near wall and with limited resolution and access
	Turbulence Intensities	in axially aligned flows only

Anemometry of this kind is not well suited to application in recirculating flows because of its intrusive nature and directional ambiguity. Probes are susceptible to damage by particles in the fluid.

PITOT TUBE	Velocities	only in axially aligned flow and with limited resolution
------------	------------	--

Pitot tubes can be blocked by blood corpuscles and access in heart valve flows is often limited for intrusive techniques.



## PHOENICS PREDICTIONS

The Casson equation was used in the 'Ground' file to modify the laminar Viscosity 'ENUL', by setting:

$$ENUL = \tau/\dot{\gamma}$$

where the local shear rate used ( $\dot{\gamma}$ ) was the square root of the local variables of the array set up by the statement 'GENK = T.' in 'Satlit'

Verification was by way of checks on those parameters which could be assessed analytically:

- 1] The shear stress distribution in laminar flow regimes (fig. 5 )
- 2] Velocity profiles in laminar flow (fig. 6)
- 3] Shear stress profiles in turbulent flow: (fig. 7)

Having verified that the shear stresses (and therefore shear rates) were being correctly predicted the Blood flow model was verified against experimental findings of Hershey and Cho (1966), though only the pressure gradient could be compared.

By way of a case study, an analysis of leakage design in the Gentle twin flap mitral valve (Gentle et al. 1981) is given below:

A certain amount of backflow is designed into this valve to alleviate haemostasis when the valve is closed, thus preventing clot formation. It was intended by Gentle that the backflow should be turbulent to enhance the washing action.

Results of analysis by PHOENICS confirmed that the backflow was turbulent (fig. 8).

but a maximum shear stress of 2.2kN/m<sup>2</sup> existed - this would lead to haemolysis and unfortunately the areas of stagnation in backflow corresponded to those in forward flow (fig. 9) - see Leefe et al.(1986).

Figure 10 shows a contour plot of shear stress under a reduced backflow pressure - the stress magnitude key is in kN/m<sup>2</sup>.

## CONCLUSIONS

When applied to prosthetic heart valve evaluation, no in-vitro technique is capable of yielding all the data necessary to describe fully a flow field. Not even when several of these techniques are used together can full field shear stresses be obtained. Furthermore, in-vitro modelling in itself is not wholly suited to the analysis of blood flow due to problems relating to the opaqueness of blood and its clotting function.

The use of Computational Fluid Mechanics alleviates these modelling problems and permits the evaluation of blood flow, unaffected by blood's opaque nature or by clotting. The greatest advantage CFM has over the in-vitro techniques is the ability to predict full field attributes, especially shear stresses and shear rates, these are the quantities which best predict a valve's likely clinical performance. Hence a greater correlation, between the fluid dynamic testing of a valve and it's in service situation, is achieved by the application of CEM than is possible with in-vitro modelling.

## ACKNOWLEDGEMENTS

The support of Mr G. D. Tansley as a Research Student by the Science and Engineering Research Council.

Many thanks to Dr C. R. Gentle for his supervisory role and for the loan of material.

## REFERENCES

Charm, S. and Kurland, G. 1965. Viscometry of human blood for shear rates of 0 - 100 000  $\text{sec}^{-1}$

Chmiel, H. and Walitza, E. 1980. On the rheology of blood and synovial fluid. *Research Studies Press (John Wiley and Son), Chichester*

Cokelet, G.R. 1987. *The rheology and tube flow of blood. In: Skalak, R. and Chein, S. (eds.) The handbook of bioengineering, McGraw-Hill*

Dintenfass, L. 1964. Rheological approach to thrombosis and atherosclerosis. *Angiology*, (15), 333-343

Gentle, C.R., Juden, H. and Swales, P.D. 1981. Testing of an all-ceramic mitral valve prosthesis. in: *Proceedings of the European Society for Artificial Organs*, (8), 352-355

Hellums, J.D., and Brown, C.H., 1975. Blood cell damage by mechanical Forces. in: Hwang, H.N.C. and Normann. N.A. (eds.), *Cardiovascular flow dynamics and measurements*, 799-823

Hershey, D. and Cho, S.J. 1966. Blood flow in rigid tubes: thickness and slip velocity of plasma film at the wall. *Journal of Applied Physiology*, 21, 27-32

Leefe, S.E., Edwards, R.J., Tansley, G.D. and Gentle, C.R. 1986. *Investigation into leakage design in prosthetic heart valves in: Proceedings of the 26th. Annual Meeting of the Biological Engineering Society, Glasgow, to be published by Pergamon Press*

Whitmore R.L. 1968. *Rheology of the Circulation*, Pergamon Press, Oxford

# THE HUMAN HEART

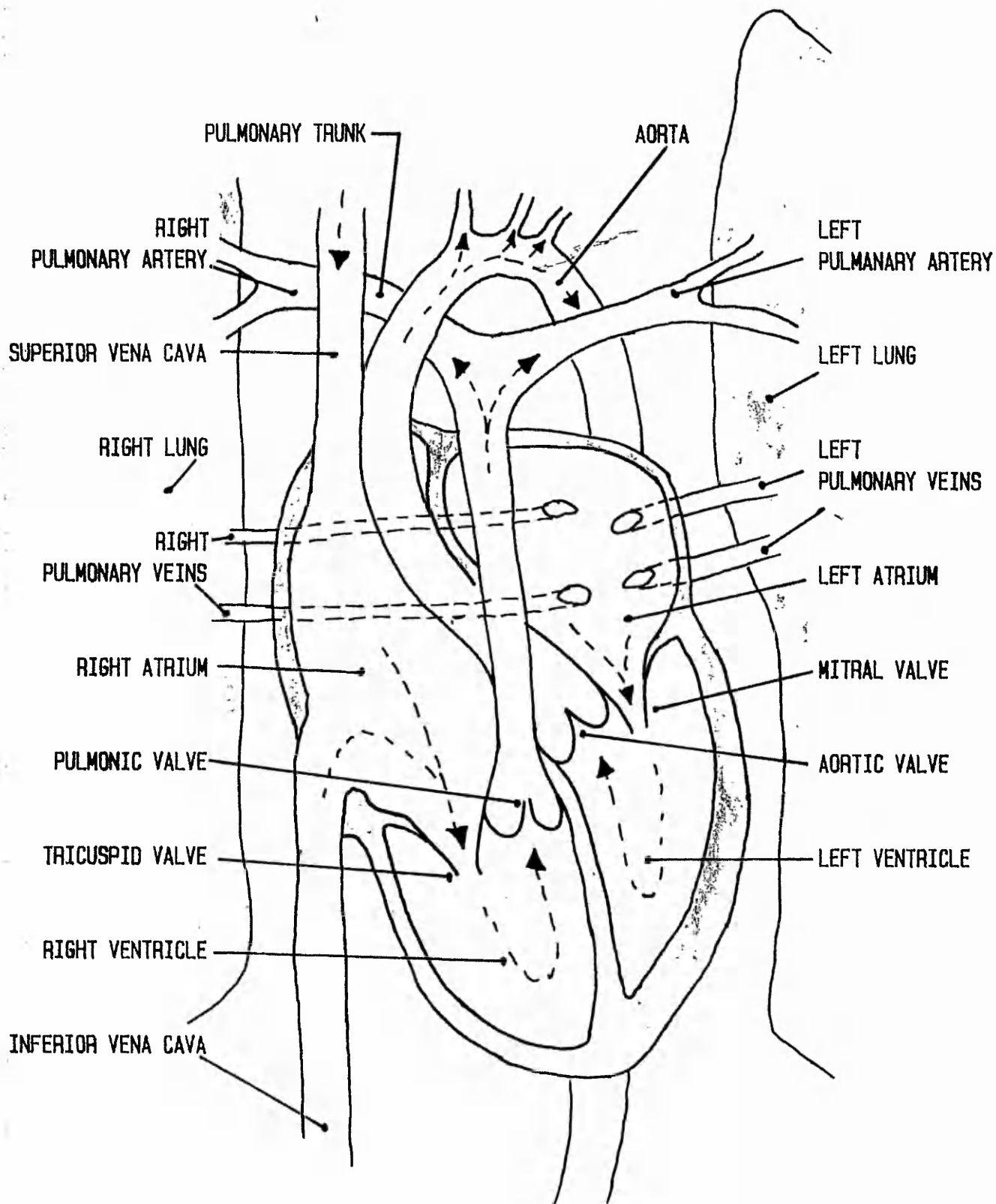


FIGURE 1

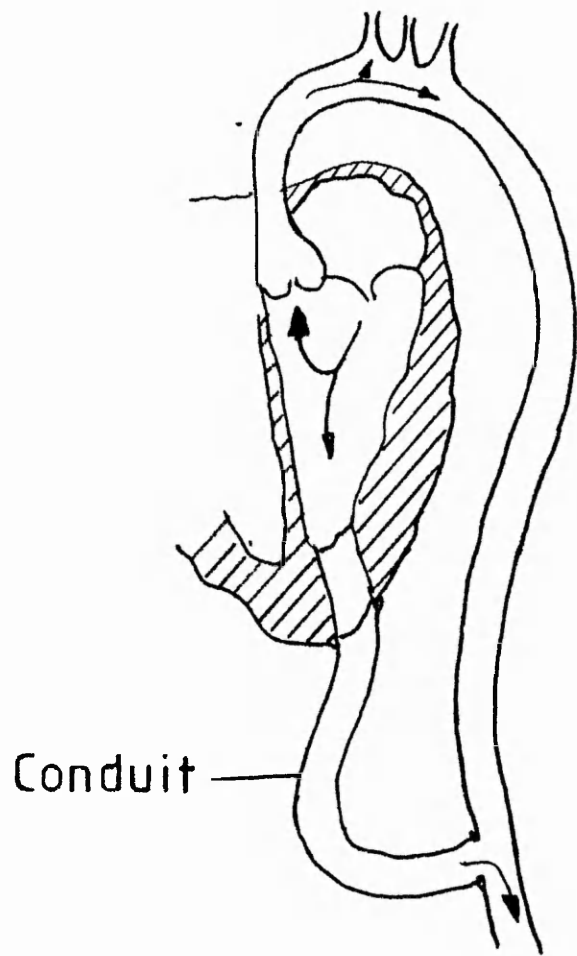
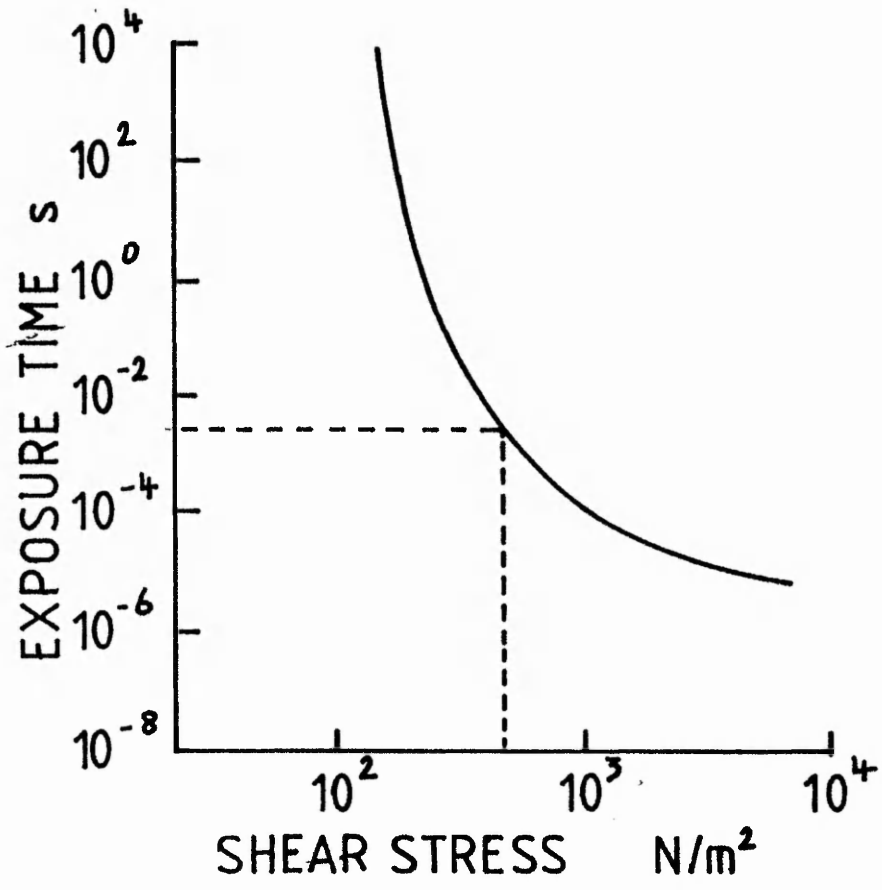


FIGURE 2



HAEMOLYSIS THRESHOLD

FIGURE 3

# A COMPARISON BETWEEN BLOOD AND NEWTONIAN FLUID FLOW

PARAMETER	ANALOGUE	RAND	CHARM
$dp/dz$	47.617	68.00	63.02
$\mu_{\max}$	00.3587	00.3313	00.3316
$\dot{\gamma}_{\max}$	68.28	71.83	71.78
$\dot{\gamma}_{\min}$	03.569	00.5119	00.5339
$\tau_{\max}$	00.2269	00.3281	00.2995
$\tau_{\min}$	00.01186	00.02011	00.02214
$\frac{\omega_{\max}}{\bar{\omega}}$	01.996	01.841	01.842

$$\text{RAND : } \sqrt{\tau} = 0.0546\sqrt{\dot{\gamma}} + 0.110$$

$$\text{CHARM : } \sqrt{\tau} = 0.0524\sqrt{\dot{\gamma}} + 0.104$$

FIGURE 4

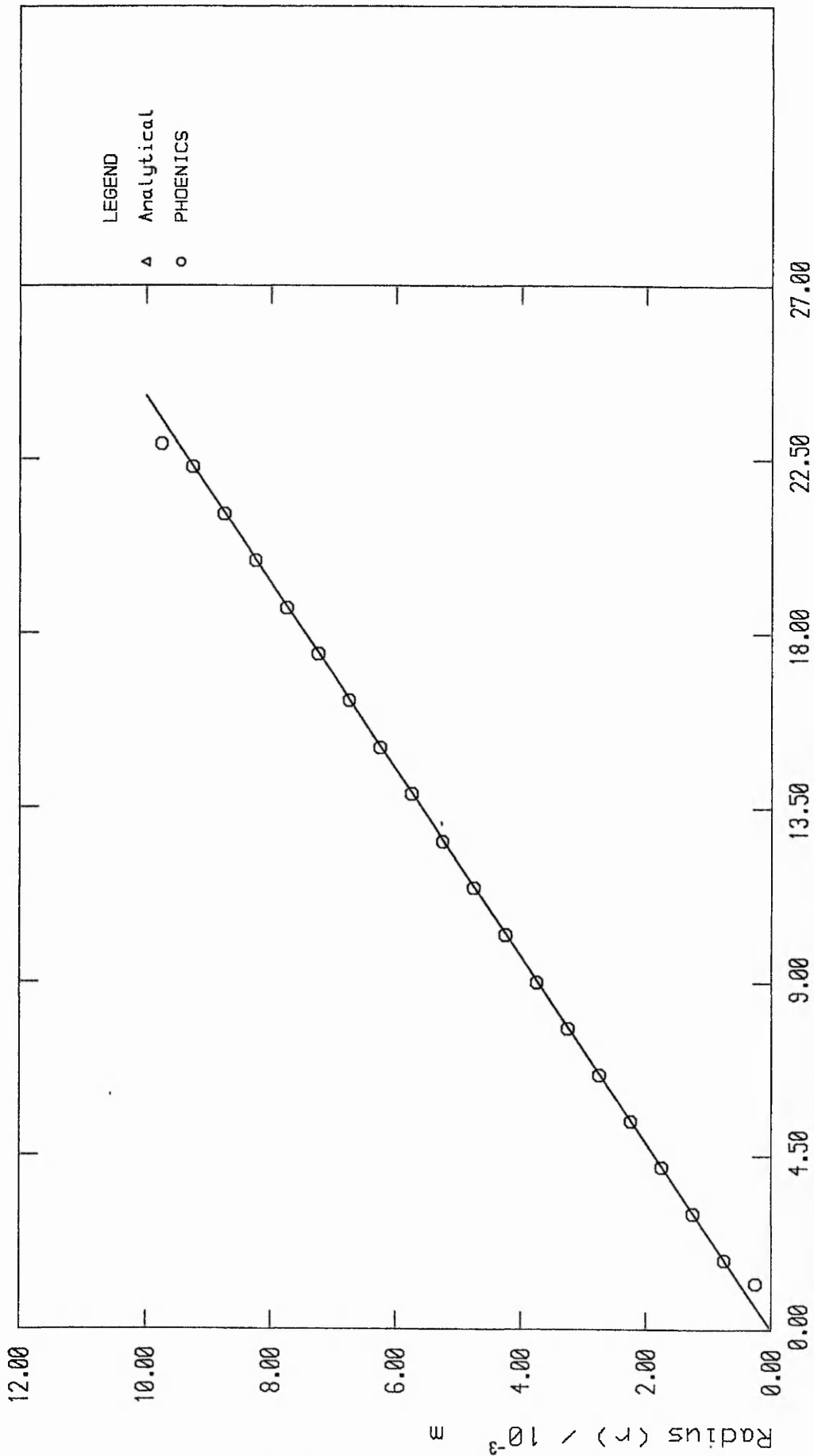


FIGURE 5

Shear stress  $(\tau) / 10^{-3} \text{ Pa}$

PHOENICS AND ANALYTICAL SHEAR STRESS GRADIENT PREDICTIONS  
 FOR LAMINAR, NEWTONIAN PIPE FLOW OF REYNOLD'S = 1200

CFM (PHOENICS) VELOCITY GRADIENT PREDICTIONS  
 FOR LAMINAR, ANALOGUE AND BLOOD PIPE FLOW Q=CONSTANT

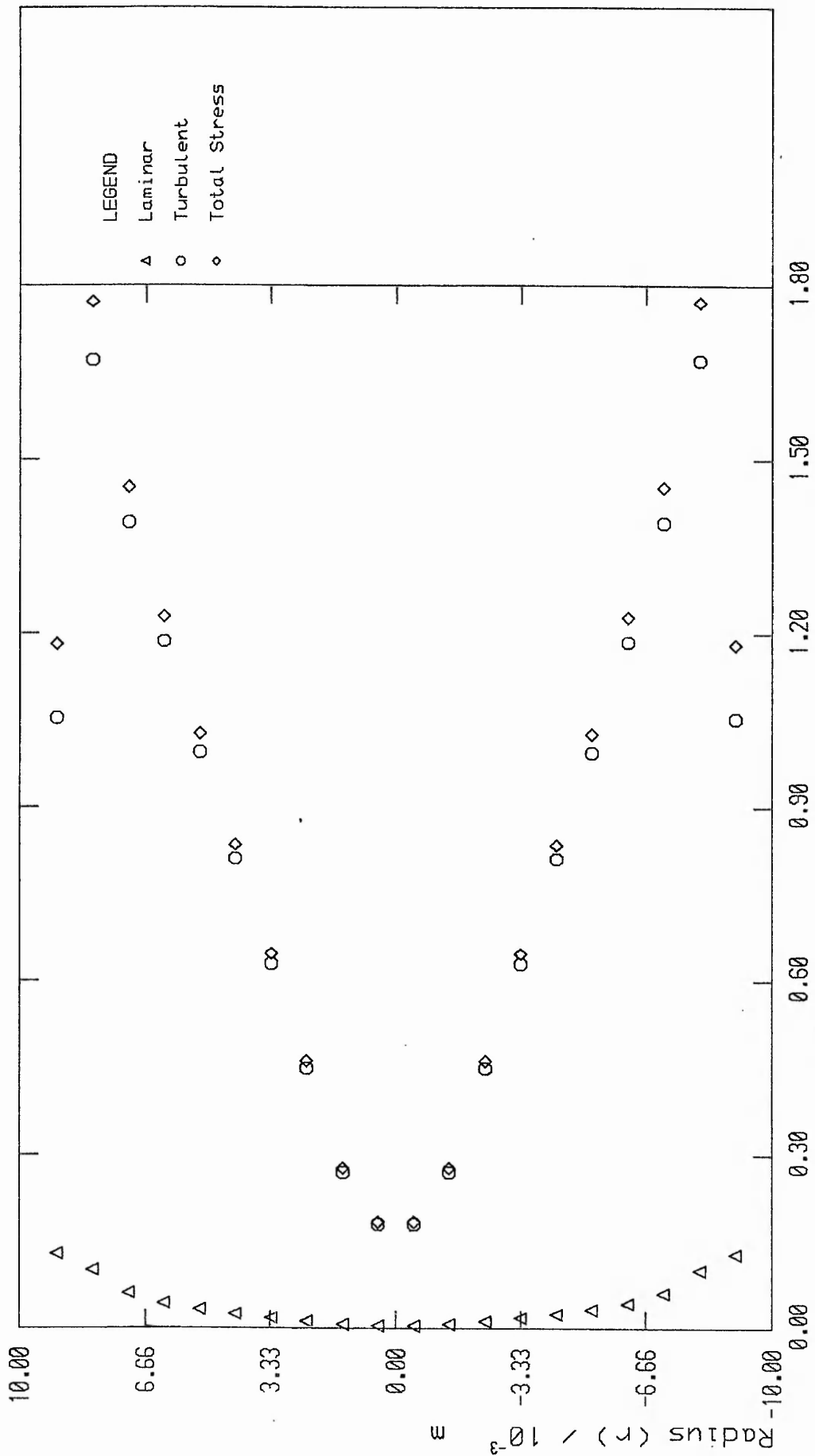


FIGURE 7

PHOENICS PREDICTIONS OF SHEAR STRESS FOR  
TURBULENT, NEWTONIAN PIPE FLOW (Re = 12000)

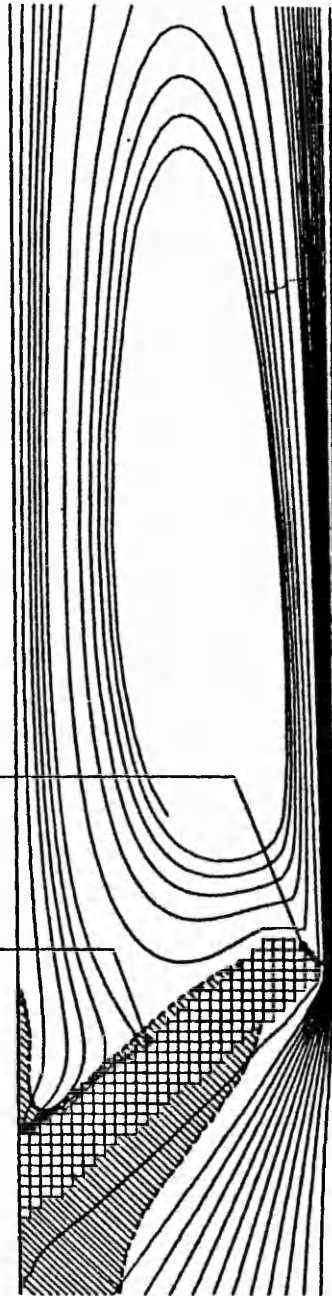
OCCLUDER



LAMINAR



STAGNATION



MAX SHEAR STRESS

FIGURE 8

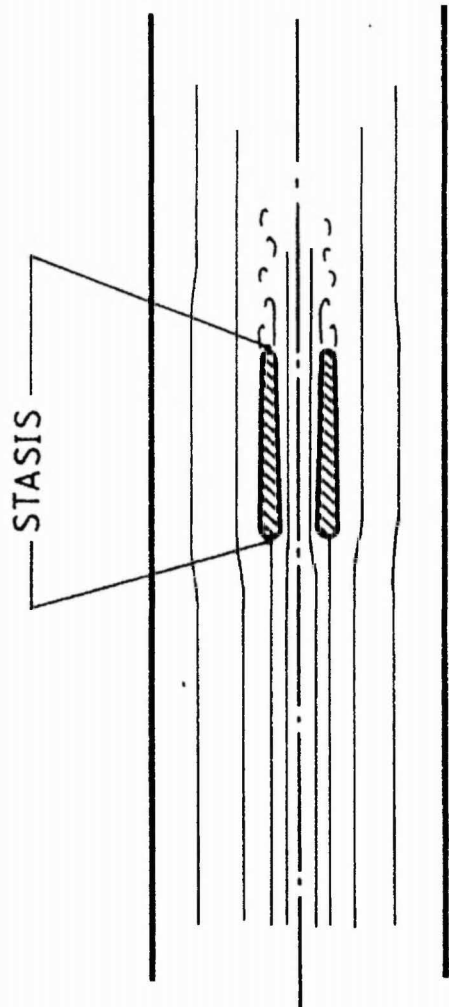
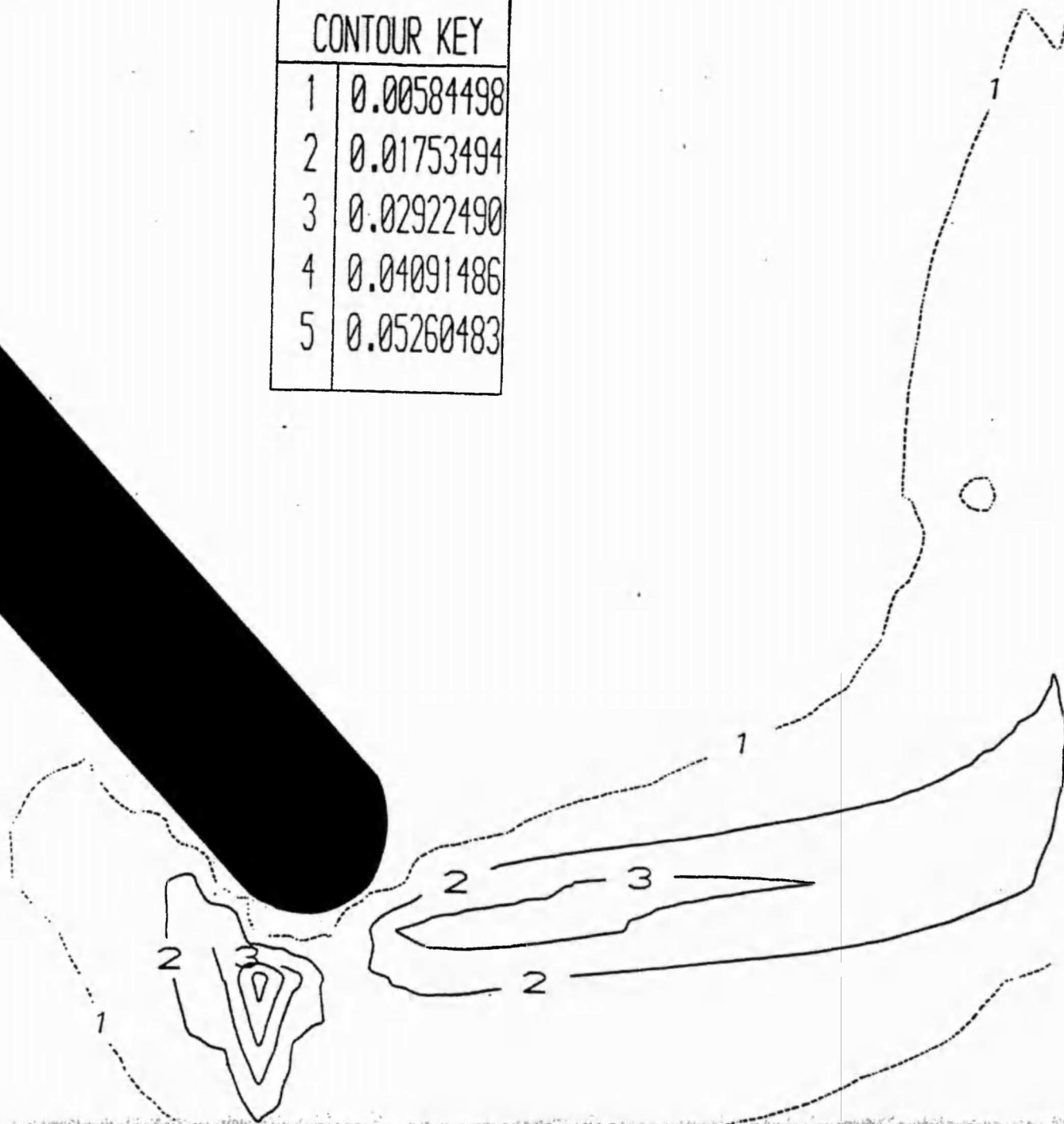


FIGURE 9

### CONTOUR KEY

1	0.00584498
2	0.01753494
3	0.02922490
4	0.04091486
5	0.05260483



F FIGURE 1 00